Functional characterization of the SARS-CoV-2 spike protein and syncytia formation

Maaran Michael Rajah

▶ **To cite this version:**

Maaran Michael Rajah. Functional characterization of the SARS-CoV-2 spike protein and syncytia formation. Virology. Université Paris Cité, 2021. English. ⟨NNT : 2021UNIP7367⟩. ⟨tel-04167010⟩

HAL Id: tel-04167010

https://theses.hal.science/tel-04167010v1

Submitted on 20 Jul 2023

HAL is a multi-disciplinary open access archive for the deposit and dissemination of scientific research documents, whether they are published or not. The documents may come from teaching and research institutions in France or abroad, or from public or private research centers.

L'archive ouverte pluridisciplinaire **HAL**, est destinée au dépôt et à la diffusion de documents scientifiques de niveau recherche, publiés ou non, émanant des établissements d'enseignement et de recherche français ou étrangers, des laboratoires publics ou privés.

HAL Authorization

Université de Paris

École doctorale Bio Sorbonne Paris Cité (BioSPC ED n°562)

Unité Virus et Immunité (Institut Pasteur)

Functional characterization of SARS-CoV-2 spike protein and syncytia formation

Maaran Michael RAJAH

Thèse de doctorat Microbiologie

Dirigée Par Pr Olivier Schwartz

Présentée et soutenue publiquement le 10 décembre 2021

Devant un jury composé de:

Pr. Pierre-Emmanuel CECCALDI, PU, Université de Paris	Président
Dr. Nathalie ARHEL, DR, Université de Montpellier	Rapportrice
Pr. François-Loïc COSSET, PU, Université de Lyon	Rapporteur
Pr. Mauro GIACCA, PU, King's College London	Examinateur
Dr Nadine LAGUETTE, DR, Université de Montpellier	Examinatrice
Dr. Claudine PIQUE, DR, Université de Paris	Examinatrice
Dr. Nadia NAFFAKH, DR, Université de Paris	Examinatrice
Pr. Olivier SCHWARTZ, PU, Université de Paris	Directeur de thèse

Université de Paris

École doctorale Bio Sorbonne Paris Cité (BioSPC ED n°562)

Unité Virus et Immunité (Institut Pasteur)

Functional characterization of SARS-COV-2 spike protein and syncytia formation

Maaran Michael RAJAH

Thèse de doctorat Microbiologie

Dirigée Par Pr Olivier Schwartz

Présentée et soutenue publiquement le 10 décembre 2021

Devant un jury composé de:

Pr. Pierre-Emmanuel CECCALDI, PU, Université de Paris	Président
Dr. Nathalie ARHEL, DR, Université de Montpellier	Rapportrice
Pr. François-Loïc COSSET, PU, Université de Lyon	Rapporteur
Pr. Mauro GIACCA, PU, King's College London	Examinateur
Dr Nadine LAGUETTE, DR, Université de Montpellier	Examinatrice
Dr. Claudine PIQUE, DR, Université de Paris	Examinatrice
Dr. Nadia NAFFAKH, DR, Université de Paris	Examinatrice
Pr. Olivier SCHWARTZ, PU, Université de Paris	Directeur de thèse

Title (English): Functional characterization of the SARS-CoV-2 spike protein and syncytia formation

Abstract (English):

The SARS-CoV-2 spike (S) protein is a highly antigenic viral fusogen that triggers viral entry upon interaction with cellular receptors and proteases. The S protein also facilitates the formation of syncytia which are large multinucleated cells formed through the fusion of individual cells. Several coronaviruses including the currently pandemic SARS-CoV-2 form syncytia. Severe cases of COVID-19 are associated with extensive lung damage and the presence of infected syncytial pneumocytes. Syncytia may represent a pathological substrate that contributes to viral dissemination, immune evasion, cytopathicity and the inflammatory response. Here we characterized the role of the SARS-CoV-2 S protein in mediating fusion.

We show that SARS-CoV-2 induce syncytia when the S protein expressed on the cell surface interacts with the angiotensin-converting enzyme 2 (ACE2) receptor on the surface of neighbouring cells. The transmembrane protease serine 2 (TMPRSS2) protease further augments syncytia formation. Viral infection triggers the production of interferon (IFN) and subsequent expression of a wide array of interferon-stimulated-genes, including interferon-induced transmembrane (IFITM) proteins. IFITMs restrict the cellular entry of a broad spectrum of enveloped viruses, possibly by altering the biomechanically properties of the plasma membrane in ways that are unfavorable to fusion. We found that IFITMs effectively restrict SARS-CoV-2 S protein-mediated syncytia formation. However, this restriction is effectively reverted by the TMPRSS2 protease.

As the pandemic progressed, the ancestral Wuhan strain has been replaced by SARS-CoV-2 variants containing several mutations within the S protein. We characterized the Alpha, Beta and Delta variant S proteins in terms of the syncytia formation potential. We report that they induce more fusion than the early D614G variant and the ancestral strain. The fusogenicity of the variants partly correlates with their ACE2 binding potential. The individual mutations associated with the variants differentially modulate syncytia formation. Mutations P681H, D1118H, and D215G augment cell-cell fusion while the antibody escape mutation E484K, K417N and Δ242-244 are restrictive. IFITMs effectively limit syncytia formation induced by variant S proteins.

We also investigated the syncytia formatting potential of the commonly circulating coronaviruses. We found that hCoV-HKU1 S protein induces syncytia only when adjacent cells express catalytically active TMPRSS2. Human IFITM1 restricted HKU1 S mediated syncytia formation. However, mouse IFITM1 increased fusion. Interestingly, while TMPRSS2 accelerates syncytia formation by SARS-CoV-2 and counteracted the restrictive effects of IFITMs, it does not interfere with the restriction of HKU1-S fusion by IFITM1.

In summary, we have characterized the mechanisms of S protein-mediated syncytia formation and its regulation by components of the humoral and innate immune response. Our results provide preliminary insights into the cytopathic effect and pathology induced by SARS-CoV-2

Keywords: SARS-CoV-2, HKU1, Coronavirus, Syncytia, IFITMs, Spike

Titre (Français) : Caractérisation fonctionnelle de la protéine S du SARS-CoV-2 et de la formation de syncytia

Résumé (Français):

La protéine de spicule (S) du SARS-CoV-2 est un fusogène viral hautement antigénique qui déclenche l'entrée virale lors de l'interaction avec les récepteurs et protéases cellulaires. La protéine S facilite également la formation de syncytia qui sont de grandes cellules multinucléées formées par la fusion de cellules individuelles. Plusieurs coronavirus, dont le SARS-CoV-2 actuellement pandémique, forment des syncytia. Les cas graves de COVID-19 sont associés à des lésions pulmonaires étendues et à la présence de pneumocytes syncytiaux infectés. Les syncytia peuvent contribuer à la dissémination virale, à l'évasion immunitaire, à la cytopathie et à la réponse inflammatoire. Ici, nous avons caractérisé le rôle de la protéine S du SARS-CoV-2 dans la médiation de la fusion.

Nous montrons que le SARS-CoV-2 induit des syncytia lorsque la protéine S exprimée à la surface cellulaire interagit avec le récepteur de l'enzyme de conversion de l'angiotensine 2 (ACE2) à la surface des cellules voisines. La protéase transmembranaire sérine 2 (TMPRSS2) augmente aussi la formation de syncytia. L'infection virale déclenche la production d'interféron (IFN) et l'expression subséquente d'un large éventail de gènes, y compris les protéines transmembranaires induites par l'interféron (IFITM). Les IFITM restreignent l'entrée cellulaire d'un large spectre de virus enveloppés, possiblement en modifiant les propriétés biomécaniques de la membrane plasmique de manière défavorable à la fusion. Nous avons constaté que les IFITM restreignent efficacement la formation de syncytia médiée par la protéine S du SARS-CoV-2. Cependant, cette restriction est inversée par la protéase TMPRSS2.

Au fur et à mesure de la progression de la pandémie, la souche ancestrale de Wuhan a été remplacée par des variants du SARS-CoV-2 contenant plusieurs mutations au sein de la protéine S. Nous avons caractérisé les protéines variantes S Alpha, Beta et Delta par rapport à leur potentiel de formation de syncytia. Nous démontrons que la protéine S de ces variants induisent plus de fusion que le variant précoce D614G et que la souche ancestrale. La fusogénicité des variants est en partie corrélée à leur potentiel de liaison à l'ACE2. De plus, les mutations individuelles associées aux variants modulent de manière différentielle la formation de syncytia. Les mutations P681H, D1118H et D215G augmentent la fusion cellule-cellule tandis que les mutations d'échappement aux anticorps E484K, K417N et Δ242-244 sont restrictives. Par ailleurs, les IFITM limitent efficacement la formation de syncytia induite par les protéines variantes S.

Nous avons également étudié le potentiel de formation de syncytia des coronavirus communément en circulation. Nous avons constaté que la protéine S du hCoV-HKU1 induit des syncytia uniquement lorsque les cellules adjacentes expriment la TMPRSS2 sous sa forme catalytiquement active. Nous montrons aussi que l'IFITM1 humain restreint la formation de syncytia médié par la protéine S du hCov-HKU1 alors que l'IFITM1 murin augmente la fusion. Fait intéressant, alors que la protéase TMPRSS2 accélère la formation de syncytia médiée par le SARS-CoV-2 et contrecarre les effets restrictifs des IFITM, elle n'interfère pas avec la restriction de la fusion HKU1-S médiée par l'IFITM1.

En résumé, nous avons caractérisé les mécanismes de la formation de syncytia médiée par la protéine S et sa régulation par des composants de la réponse immunitaire humorale et innée. Nos

résultats fournissent ainsi des informations préliminaires sur l'effet cytopathique et la pathologie induite par le SARS-CoV-2.

Mots-Clés: SARS-CoV-2, HKU1, Coronavirus, Syncytia, IFITMs, Spike

Résumé Substantiel (Français):

Fin 2019, plusieurs patients ont présenté une maladie de type pneumonie causée par un agent inconnu à Wuhan, en Chine. L'agent a été identifié comme le nouveau bêta coronavirus SRAS-CoV-2. En date du 12 septembre 2021, le virus s'était propagé dans 193 pays, causant 224 millions d'infections et plus de 4,6 millions de décès. La maladie à coronavirus 2019 (COVID-19) possède un large spectre d'effets et environ 80% des cas sont soit asymptomatiques, soit présentent des symptômes légers ou modérés. Les symptômes les plus courants de la maladie sont la fièvre, les douleurs musculaires, la toux et une respiration difficile. Une manifestation sévère de la COVID-19 provoque un syndrome de détresse respiratoire aiguë (SDRA) avec des lésions pulmonaires étendues et parfois mortelles. La détérioration du tissu pulmonaire est caractérisée par des lésions alvéolaires diffuses, une thrombose micro/macro-vasculaire et une nécrose des pneumocytes. La majeure partie de l'histopathologie décrite dans l'infection SRAS-CoV-2 est probablement liée à la réponse immunitaire; cependant, les effets cytopathiques induits par le virus peuvent également endommager directement le tissu pulmonaire tout en déclenchant une activation immunitaire supplémentaire. Une caractéristique particulière remarquée dans quelques rapports cliniques est la présence de pneumocytes syncytiaux. Cette observation est étayée par plusieurs rapports d'autopsie de patients décédées de la COVID-19 et de modèles de primates non humains qui décrivent également la présence de syncytia dans le tissu pulmonaire infecté.

Les syncytia sont de grandes cellules multinucléées produites par la fusion de deux cellules ou plus. Au cours de la formation des syncytia, la membrane plasmique de différentes cellules fusionne en une seule bicouche lipidique et leur contenu cytoplasmique fusionne. De nombreux processus physiologiques importants dépendent de cellules en cours de syncytialisation.

Cependant, des agents pathogènes comme le SRAS-CoV-2 peuvent également induire des syncytia. La formation non régulée de syncytia induite par un agent pathogène, dans des cellules qui normalement ne fusionnent pas, est susceptible d'être pathologique. Les cellules syncytiales peuvent faciliter l'infection en disséminant le virus par contact de cellule à cellule ou lors de la mort cellulaire et elles peuvent protéger le virus contre les anticorps neutralisants Elles peuvent également internaliser des cellules immunitaires, ce qui conduit remarquablement à la mort des cellules internalisées. Un effondrement syncytial rapide peut être préjudiciable à la réplication virale et déclencher une réponse immunitaire inflammatoire. Dans tous les cas, les syncytia du SRAS-CoV-2 contribuent très probablement à la pathogénicité virale. Ainsi, comprendre le mécanisme et les conséquences de la formation de syncytia médiée par la protéine S du SRAS-CoV-2 peut fournir des informations importantes sur la pathologie induite par le virus.

Le SRAS-CoV-2 est un virus enveloppé à ARN simple brin de polarité positive (ARNsb+) et le virion peut avoir un diamètre de 60 à 140 nm. L'enveloppe virale est constituée d'une bicouche lipidique enrobée de la protéine de spicule (S) trimérique qui dépasse de la surface. La protéine S facilite la fusion du virion avec la cellule hôte en interagissant avec le récepteur ACE2 humain au cours de la première étape de l'infection. La protéine S est un fusogène de classe I (structurellement composé d'hélices) qui facilite la fusion membranaire après avoir subi des réarrangements structurels qui la font passer d'une forme dite de préfusion métastable à un état compétent pour la fusion. Il s'agit d'une protéine glycosylée longue d'environ 1271 acides aminés et composée des sous-unités S1 et S2 séparées par un site de clivage polybasique. Les protéases cellulaires clivent entre ce site S1/S2 ainsi qu'au niveau d'un site S2' afin d'activer la protéine S.

À la suite de rapports identifiant la présence de cellules syncytiales infectées dans les poumons de patients atteints de la COVID-19 sévère, nous nous sommes efforcés de caractériser le mécanisme par lequel le SRAS-CoV-2 induit la formation de syncytia, en plus d'étudier le degré auquel il affecte la pathologie. Nous avons émis l'hypothèse que la fusion cellule-cellule induite par le SRAS-CoV-2 serait analogue à l'entrée virale et nécessiterait donc l'interaction de la protéine S avec les récepteurs de l'hôte et qu'elle pourrait être modulée différemment par divers facteurs de l'hôte.

Nous avons d'abord caractérisé comment les cellules infectées par le SRAS-CoV-2 forment des syncytia en examinant l'interaction entre la protéine S, le récepteur ACE2 humain et la protéase TMPRSS2 humaine. Nous avons également examiné l'impact des protéines transmembranaires induites par l'interféron (IFITM), un groupe de facteurs de restriction altérant la membrane, sur la formation de syncytia induite par le virus. Les IFITM restreignent un large spectre de virus enveloppés, notamment le VIH, le virus de la grippe, Ebola, Marburg, la dengue, le Zika, le virus du Nil occidental, de l'encéphalite japonaise, de la fièvre de la vallée du Rift, ainsi que les membres de la famille des coronavirus. IFITM1 se localise sur la membrane plasmique, tandis que IFITM2 et 3 transitent tous deux à travers la membrane plasmique avant de se localiser dans les compartiments endo-lysosomaux. Les IFITM empêchent les virus de traverser la membrane cellulaire et d'accéder au cytoplasme, éventuellement en altérant la rigidité et la courbure ou la composition de la membrane. Cela permet d'augmenter la barrière énergétique pour la fusion, entravant la fusion virus-cellule au stade de l'hémi-fusion ou de la formation de pores.

Notre étude a révélé que les cellules infectées par le SRAS-CoV-2 expriment la protéine S à leur surface cellulaire et qu'elle peut ainsi interagir avec les récepteurs ACE2 sur les cellules voisines

pour induire la fusion cellule-cellule. La formation de syncytia est augmentée par la présence de la protéase TMPRSS2 et restreinte par IFITM1, 2 et 3. Cependant, TMPRSS2 annule la restriction médiée par IFITM et le mécanisme par lequel TMPRSS2 subvertit les contraintes biophysiques imposées par les IFITM demeure une question en suspens.

Depuis l'émergence de la souche ancestrale de Wuhan, plusieurs nouveaux variants du SRAS-CoV-2 hébergeant une variété de mutations dans leur génome viral sont apparus et se sont propagés dans le monde. L'un des premiers variants décrits était le variant européen D614G, dans lequel une substitution dans la protéine S augmentait l'infectiosité du virus sans altérer la neutralisation par les anticorps. La pandémie a ensuite vu l'émergence et la propagation du variant Alpha (anciennement appelé B.1.1.7) qui a d'abord été identifié au Royaume-Uni, du variant Beta (B.1.351) identifié en Afrique du Sud, du variant Gamma (P.1 & P.2) identifié au Brésil, et plus récemment du variant Delta (B.1.617) identifié en Inde. Ces « variants préoccupants » (‘variants of concern’, VOC) se caractérisent par leur transmissibilité accrue et leur plus grand potentiel à échapper aux anticorps neutralisants, mais leur impact sur la gravité de la maladie est sujet à débat. Les mutations de la protéine S des COV sont particulièrement intéressantes car elles peuvent affecter à la fois l'antigénicité et l'infectivité du virus. En effet, la protéine S des différents variants abrite une variété de mutations qui peuvent conférer différents avantages. Ainsi, notre deuxième objectif était de caractériser la fusogénicité de la protéine S des variants Alpha, Beta et Delta par rapport à la souche européenne précoce D614G et à la souche ancestrale de Wuhan. Nous avons ensuite utilisé une approche mutagène pour caractériser la contribution de chacune des mutations individuelles associées aux variants Alpha et Beta en termes de leur fusogénicité, de leur capacité d'échappement aux anticorps et de leur potentiel de liaison à l'ACE2.

Nous avons constaté que les variants Alpha et Bêta se répliquent de la même manière, mais forment plus de syncytia que les souches D614G et Wuhan, à la fois lors de l'infection et lors de la transfection des spicules. La protéine S du nouveau variant Delta est également plus fusogène que celle du variant D614G. L'affinité des protéines S avec le récepteur ACE2 est d'ailleurs corrélée à leur fusogénicité. Nous avons aussi observé que les mutations associées aux variants P681H, D1118H et D215G augmentent la formation de syncytia, alors que les mutations E484K, K417N et Δ242-244 sont restrictives. De plus, les mutations qui réduisent la formation de syncytia facilitent l'échappement aux anticorps. Nous avons également constaté que les IFITM restreignent de manière similaire la formation de syncytia induite par les spicules. Dans l'ensemble, nous suggérons donc que les variants sont plus syncytogéniques.

Additionnellement, nous avons utilisé notre système rapporteur de la formation de syncytia pour fournir une caractérisation préliminaire de la protéine S du HKU1, un coronavirus humain négligé. Les coronavirus associés au rhume ou « saisonniers » 229E, NL63, OC43 et HKU1 sont endémiques chez l'homme. L'infection chez les individus sains entraîne généralement une pathogénicité légère caractérisée par des symptômes ressemblant au rhume. Cependant, la maladie peut parfois évoluer vers une détresse respiratoire, des exacerbations de l'asthme et une bronchite chronique chez les patients vulnérables, notamment chez les personnes âgées, les enfants et les personnes immunodéprimées. Ces coronavirus sont également répartis dans le monde entier et présentent une saisonnalité, les infections atteignant un pic entre décembre et mai. Parmi les coronavirus du rhume, HKU1 reste particulièrement énigmatique et mal caractérisé dans la littérature scientifique. Nous avons donc caractérisé la fusogénicité de la protéine S de ce virus,

ainsi que ses interactions avec TMPRSS2, les IFITM et LY6E (Lymphocyte antigen 6 complex locus E). Nous constatons que la présence de TMPRSS2 sous sa forme pleinement active est requise pour la fusion médiée par la protéine S de HKU1 et que l'IFITM1 humain est un puissant inhibiteur de cette fusion. En revanche, l'IFITM1 murin se comporte comme un facteur favorisant la fusion médiée par les spicules de HKU1.

Enfin, la formation de syncytia médiée par le SRAS-CoV-2 a été proposée comme un contributeur potentiel à la pathologie globale. Alors que des cellules syncytiales ont été observées dans le tissu pulmonaire de patients décédés de la COVID-19, leur importance relative et leur contribution générale à l'infection virale restent inconnues. En outre, il n'est pas clair si la formation de syncytia est aussi une caractéristique des infections asymptomatiques ou bénignes du SRAS-CoV-2 ou si elle se produit *in vivo* lors d'une infection par les coronavirus du rhume comme HKU1. La littérature récente suggère que les syncytia induits par le SRAS-CoV-2 peuvent représenter une forme d'effet cytopathique, déclencher une réponse inflammatoire ou immunitaire et favoriser la dissémination et la persistance virales. D'un point de vue méthodologique, la formation de syncytia en culture cellulaire peut également être utilisée comme substitut efficace, bien qu'imparfait, pour caractériser les premiers stades de l'entrée du virion via la fusogénicité de la protéine S. Cette technique présente l'avantage supplémentaire d'être adaptée aux environnements de recherche de niveau de biosécurité 2, lorsque la protéine S est exprimée seule, en l'absence de virus infectieux. En somme, notre travail fournit une caractérisation fonctionnelle de la protéine S du SRAS-CoV-2 et de la formation de syncytia.

Finalement, les outils que nous avons développés pourraient également être appliqués à l'étude d'autres coronavirus, tel HKU1. De futures études pourraient faire la lumière sur les interactions moléculaires entre la protéine S, l'ACE2, le TMPRSS2 et les IFITM. L'examen de la motilité et de la dynamique d'interaction de ces protéines sur la membrane plasmique pendant la formation des syncytia devrait contribuer à la compréhension du mécanisme précis par lequel la formation des syncytia est facilitée ou restreinte. De plus, le développement de modèles animaux pour étudier les syncytia induits par le SRAS-CoV-2 *in vivo* serait également une priorité future.

Acknowledgments

Supervision:

First and Foremost, I would like to thank my PhD director and supervisor Pr. Olivier Schwartz for accepting me into his research group and for his mentorship and support over the past several years. Pr. Schwartz was very generous with his time and went well beyond his prescribed duties to ensure that I received a rigorous scientific education while also giving me the freedom to explore my interests. I will forever be grateful for his support and guidance.

I would also like to acknowledge the two postdoctoral researchers who also supervised my research. My work on SARS-CoV-2 and syncytia formation was supervised by Dr. Julian Buchrieser. In addition to be my teacher and supervisor, Julian was an unwavering advocate of my work and a dear friend. I was extremely lucky to have been able to benefit from his scientific and technical knowledge. Finally, I would like to express my sincere gratitude to Dr. Blandine Monel, who supervised my work on Zika virus during the first year of my PhD. The patient and meticulous training provided by Blandine was instrumental to my progress. I will forever appreciate the kindness and generosity she had shown me. I look forward to seeing what the both of you will accomplish, confident in the knowledge that your future students will be in good hands.

I consider myself truly fortunate to have been mentored by three excellent scientists.

Colleagues and collaborators:

I greatly benefited from a collaborative work environment and I would like to thank all the members of the Virus and Immunity Unit (UVI) including Delphine Planas, Mathieu Hubert, Timothée Bruel, Florence Guivel-Benhassine, Nell Saunders, Elodie Bishop, Nicoletta Casartelli and Françoise Porrot for providing a supportive and productive work environment. I would also like to thank the members of Lisa Chakrabarti's team and Hugo Mouquet's group for their collaboration and scientific advice. I would especially like to thank my officemate Ludivine Grzelak for her friendship, kindness and generosity over the past few years.

Defence Committee:

I greatly appreciate the critical evaluation of my dissertation by my defence committee. I would like to specifically thank Dr. Nathalie Arhel and Pr. François-Loïc Cosset for acting as my rapporteurs and for providing valuable input on my manuscript. I would also like to thank my examiners Pr. Pierre-Emmanuel Ceccaldi, Pr. Mauro Giacca, Dr. Nadine Laguette, Dr. Claudine Pique and Dr. Nadia Naffakh.

Funding:

I would like to acknowledge the Pasteur-Paris University (PPU) International Doctoral Program fellowship for the generous funding which made my research possible. I would also like to thank the Institut Pasteur, Department of Virology for the "Bourse de Soudure" finishing fellowship.

Personal:

I would like to thank my loving companion Annie Bernier who followed me to Paris and suffered the lockdowns with me. The value of her patience and support could not be understated and I look forward to our life together. Finally, I would like to thank my loving parents Vigneswararajah Krishnapillai and Dilkusha Vigneswararajah as well as my brother Maaselen Rajah for all the support they had shown me throughout my academic journey. **I dedicate this accomplishment to the four of you.**

List of Abbreviations

3CLpro	chymotrypsin-like protease
9-O-Ac-Sia	9-O acetylated sialic acid
ACE2	angiotensin converting enzyme 2
ARDS	acute respiratory distress syndrome
CH25H	Cholesterol 25-hydroxylase
COVID-19	Coronavirus disease 2019
CTD	C-terminal domain
CTSL/B	cathepsin L/B
DMV	double membrane vesicles
dsRNA	double stranded RNA
E	envelope
ER	Endoplasmic reticulum
ERGIC	ER-Golgi intermediate compartment
ERV	endogenous retroviruses
FAST	fusion-associated small transmembrane
FP	fusion peptide
GPI	glycosylphosphatidylinositol
hCoVs	human coronaviruses
Hel	RNA helicase
HIV	human immunodeficiency virus
HR	heptapeptide repeat sequences
IFITM	interferon-induced transmembrane proteins
IFN	interferon
IRF3	interferon regulatory transcription factor 3
IRSE	interferon-stimulated response element
ISG	interferon-stimulated genes
KLK13	kallikrein 13
LY6E	lymphocyte antigen 6 complex locus E
M	membrane
MERS-CoV	Middle East respiratory syndrome coronavirus
MHC-I	major histocompatibility complex I
Mpro	main protease
N	nucleocapsid
NF-Kb	nuclear factor kappa B
Nrp1	neuropilin-1
nsp	nonstructural proteins
NTD	N-terminal domain
NTPase	nucleotide triphosphate hydrolase
ORF	open reading frame
PAMP	pathogen-associated molecular patterns
PLpro	papain-like protease

pp	polyprotein
PS	phosphatidylserine
RBD	receptor binding domain
RdRp	RNA-dependent RNA polymerase
RIG-I	retinoic acid-inducible gene I
S Protein (S)	Spike Protein
SARS-CoV-1	severe acute respiratory syndrome coronavirus
SARS-CoV-2	severe acute respiratory syndrome coronavirus 2
sgRNA	sub-genomic mRNAs
ssRNA	sense single-stranded RNA
STAT	signal transducer and activator of transcription
TA	transmembrane anchor
TLRs	Toll-like receptors
TMEM16	transmembrane protein 16
TMPRSS2	transmembrane serine protease 2
VOC	variants of concern
vRNA	viral RNA
vRNP	viral ribonucleoprotein
vRTC	viral replication and transcription complex
ZIKV	Zika virus
α-CoV	*alphacoronavirus*
β-CoV	*betacoronavirus*
γ-CoV	*gammacoronavirus*
δ-CoV	*deltacoronavirus*

List of Figures

Chapter 1

Figure 1.1: Suspected natural and intermediated hosts for each of the human coronaviruses.
Figure 1.2 SARS-CoV-2 viral load, symptoms and disease progression after initial exposure.
Figure 1.3 (A) SARS-CoV-2 virion morphology with the viral structural proteins
Figure 1.4 Coronavirus replication cycle.
Figure 1.5 Molecular mechanism of Spike (S) protein-mediated virus-cell or cell-cell fusion.
Figure 1.6 The innate immune response to coronavirus infection.
Figure 1.7 Cellular syncytia in the lungs of COVID19 patients
Figure 1.8 Schematic representation of the diverse activities of the SARS-CoV-2 spike

Chapter 2

Graphical Abstract 1 Syncytia formation by SARS-CoV-2-infected cells
Figure 1 SARS-CoV-2 induced syncytia formation.
Figure 2 Impact of TMPRSS2 and IFITMs on syncytia formation by U2OS-ACE2-infected cells
Figure 3 Impact of TMPRSS2 and IFITMs on the kinetics of fusion by S-expressing 293T cells
Figure 4 Effect of TMPRSS2 and IFITM on S- or ACE2-expressing cells
Figure EV1 ACE2 and IFITM expression in U2OS-ACE2 cell derivatives.
Figure EV2 Im age quantification methodology.
Figure EV3 Expression of IFITM1, IFITM2, and IFITM3 in SARS-CoV-2-infected syncytia.
Figure EV4 Characterization of SARS-CoV-2-induced syncytia in different cell lines
Figure EV5 Characterization of syncytia formation in Vero cells.
Figure EV6 Dose-response analysis of IFITM1 activity and impact of TMPRSS2 on IFITM1, 2, and 3 levels measured by Western blot.

Chapter 3

Graphical Abstract 2 Fusogenicity of SARS-CoV-2 variants and associated S mutations
Figure 1 Replication kinetics of D614G, Alpha, and Beta variants in cell culture.
Figure 2 SARS-CoV-2 variant infection increases formation of syncytia in U2OS-ACE2 and Vero GFP-split cells.
Figure 3 Alpha and Beta SARS-CoV-2 S proteins induce more robust syncytia formation than D614G.
Figure 4 Mutations associated with Alpha and Beta S proteins differentially affect cell–cell fusion.
Figure 5 ACE2 and monoclonal antibody binding to S proteins with Alpha and Beta associated mutations.
Figure 6 Delta SARS-CoV-2 S protein induces more syncytia formation and binds more to ACE2 than D614G.
Figure EV1 Qualitative and quantitative assessment of syncytia formation
Figure EV2 SARS-CoV-2 variant S proteins are expressed equally at the cell surface.
Figure EV3 Impact of IFN-b1 and IFITMs on SARS-CoV-2 variant replication and S protein-mediated cell–cell fusion.
Figure EV4 SARS-CoV-2 variant S protein-associated mutations are expressed equally at the cell surface.
Figure EV5 ACE2 binding curves to SARS-CoV-2 variant S proteins and associated mutations.
Appendix Figure S1 Assessment of viral replication by flow cytometry in cell lines
Appendix Figure S2 Syncytia formation by SARS-CoV-2 variants
Appendix Figure S3 Variant S protein processing by TMPRSS2

Chapter 4

Figure 1 TMP must be present on the target membrane for HKU1 S-mediated syncytia formation
Figure 2 Fully functional TMPRSS2 is require for HKU1 S-mediated fusion
Figure 3 Modulation of HKU1 S mediated fusion by membrane host factors
Supplemental Figure 1

Chapter 5

Figure 5.1 Spike protein mutations associated with Alpha, Beta, Delta and Gamma SARS-CoV-2 variants.
Figure 5.2 The potential consequences of syncytia formation on SARS-CoV-2 pathology.

List of Tables

Chapter 1

Table 1: Qualitative comparison of transmissibility, antibody escape and disease severity (hospitalization risk) of the D614G, Alpha, Beta, Gamma and Delta variants relative to the ancestral Wuhan strain.

Table 2: Widely used SARS-CoV-2 vaccines and efficacy data from phase III trials.

Chapter 3

EV Table 1: Sequencing and qRT-PCR Primers

EV Table 2: Site Directed Mutagenesis Primers

Table of Contents

Abstract (English) **5**
Résumé (Français): **7**
Résumé Substantiel (Français): **11**
Acknowledgments **19**
List of Figures **25**
List of Tables **29**
Table of Contents **31**
Preface **33**
Chapter 1: General Introduction **35**
Part 1: The discovery, emergence and epidemiology of human coronaviruses **37**
1.1.1 The "Common Cold" or "Seasonal" Human Coronaviruses: 229E, NL63, OC43 and HKU1 38
1.1.2 SARS-CoV-1 40
1.1.3 MERS-CoV 41
1.1.4 SARS-CoV-2 42
1.1.4.1 SARS-COV-2 Variants of Concern 44
1.2.1 Transmission 47
1.2.2 COVID-19: Symptoms and Disease 48
1.2.3 Vaccines and Therapeutics 49
1.2.4 SARS-CoV-2 Virion and RNA 51
1.2.5 Coronavirus replication cycle 53
1.2.6 Structural Proteins 56
1.2.6.1 Spike (S) Protein 56
1.2.6.2 Membrane Protein 59
1.2.6.3 Nucleocapsid protein 59
1.2.6.4 Envelope Protein 60
1.2.6.5 The interplay between the structural proteins 61
1.2.7 Non-structural protein 62
1.2.8 Accessory proteins 63
1.2.8 Immune response to SARS-CoV-2 infection 64
1.2.8.1 Adaptive Immune Response 65
1.2.8.2 Innate Immune Response 66
S protein-mediated Fusion **69**
1.3.1 Physiological vs Pathological Syncytia formation 69
1.3.2 Syncytia formation: A histopathological feature of coronavirus infection 72
1.3.3 The Role of the S protein in Syncytia Formation 74
1.3.3.1 The mechanism of S translocation to the plasma membrane 75
1.3.3.2 S protein mediated activation of TMEM16 and phosphatidylserine exposure 76
1.3.3.3 Summary of the mechanism of S protein-mediated syncytia formation 77
1.3.4 Modulation of S-mediated fusion by membrane-altering host factors 79
1.3.4.1 IFITMs 79
1.3.4.2 LY6E 82
1.3.4.3 CH25H 83

Research Objectives 85

Chapter 2: Syncytia Formation by SARS-CoV-2 Infected Cells 87

Synopsis 89

Chapter 3: SARS-CoV-2 Alpha, Beta & Delta variants display enhanced spike-mediated syncytia formation 113

Synopsis 115

Chapter 4: Preliminary characterizations of hCoV-HKU1 S mediated syncytia formation & modulation by host factors 148

4.1 Abstract 151

4.2 Introduction: Human coronavirus HKU1 151

4.3 Results 155

4.3.1 TMPRSS2 must be present on the target membrane for HKU1-S mediated fusion 155

4.3.2 TMPRSS2 must be fully functional for HKU S-mediated fusion 157

4.3.3 The modulation of HKU1-S mediated fusion by membrane ISGs 159

4.4 Discussion 162

4.5 Material and Methods 164

Chapter 5: Discussion & Perspectives 169

5.1 General Discussion & Perspectives 171

5.2 Variants of Concern S proteins and Fusogenicity 174

5.3 Potential consequences of syncytia formation in SARS-CoV-2 pathogenesis 179

5.3.1 Cytopathic effects 180

5.3.2 Immunological and inflammatory consequences 181

5.3.3 Virological consequences 183

5.4 Applications of S-mediated Syncytia formation 184

Conclusion 185

References 189

Appendices 213

Supplemental Chapter: The role of ER-Shaping proteins on Zika Virus replication 215

S1 Short Introduction: Zika Virus 217

S1.1 ZIKV Epidemiology, Transmission and Clinical Features 217

S1.2 Viral Replication and Proteins 218

S1.3 Research question 219

Copyright Permissions 249

Other Articles & Press Releases 268

Preface

This thesis is presented in manuscript format with permission from my supervisor Pr. Olivier Schwartz, as stipulated by the Université de Paris. The following five articles, in which I am either the first or a co-first author, are presented in this thesis.

Chapter 1 and Chapter 5 *:

1) **Rajah MM,** Bernier A, Buchrieser J, Schwartz O. "SARS-CoV-2 Spike-mediated fusion and Syncytia formation" (2021) Journal of Molecular Biology. (*Review Article)* https://doi.org/10.1016/j.jmb.2021.167280.

* Sections of the thesis introduction and discussion were adapted and submitted as an invited review article

Chapter 2:

2) Buchrieser J*, Dufloo J*, Hubert M*, Monel B*, Planas D*, **Rajah MM* (Co-first author),** Planchais C, Porrot F, Guivel-Benhassine F, Van der Werf S, Casartelli N, Mouquet H, Bruel T & Schwartz O "Syncytia formation by SARS-CoV-2-infected cells" (2020) The EMBO Journal, 39(23):e106267. https://doi.org/10.15252/embj.2020106267.

Chapter 3:

3) **Rajah MM**, Hubert M, Bishop E, Saunders N, Robinot R, Grzelak L, Planas D, Dufloo J, Gellenoncourt S, Bongers A, Zivaljic M, Planchais C, Guivel-Benhassine F, Porrot F, Mouquet H, Chakrabarti LA , Buchrieser J, Schwartz O. "SARS-CoV-2 Alpha, Beta and Delta variants display enhanced Spike-mediated Syncytia Formation" (2021) The EMBO Journal 0:e108944. https://doi.org/10.15252/embj.2021108944

Supplemental Chapter (Appendix):

4) **Rajah MM**, Monel B, Schwartz O "The entanglement between flaviviruses and ER-shaping proteins". (2020) PLOS Pathogens, 16(4): e1008389. *(Review Article)* https://doi.org/10.1371/journal.ppat.1008389

5) Monel B*, **Rajah MM** (**Co-first author**)*, Hafirassou ML, Sid-Ahmed S, Burlaud-Gaillard J, Zhu PP, Nevers Q, Buchrieser J, Porrot F, Meunier C, Amraoui S, Chazal M, Salles A, Jouvenet N, Roingeard P, Blackstone C, Amara A, Schwartz O "The Atlastin ER-shaping proteins facilitate Zika virus replication". (2019) Journal of Virology, 93(23): e01047-19. doi: 10.1128/JVI.01047-19

Secondary contributions were made to the following three articles and the title pages are presented in the appendix:

6) Planas D, Veyer D, Baidaliuk A, Staropoli I , Guivel-Benhassine F , **Rajah MM**, et al. "Reduced sensitivity of SARS-CoV-2 variant Delta to antibody neutralization" (2021) Nature**,** 596 (276-280) https://doi.org/10.1038/s41586-021-03777-9

7) Planas D, Bruel T, Grzelak L, Guivel-Benhassine F, Staropoli I, Porrot F, Planchais C , Buchrieser J, **Rajah MM**, et al. "Sensitivity of infectious SARS-CoV-2 B.1.1.7 and B.1.351 variants to neutralizing antibodies" (2021) Nature Medicine, 27 (917-924) https://doi.org/10.1038/s41591-021-01318-5

8) Grzelak L, Temmam S, Planchais C, Demeret C, Tondeur L, Huon C, Guivel-Benhassine F, Staropoli I, Chazal M, Dufloo J, Planas D, Buchrieser J, **Rajah MM**, et al. "A comparison of four serological assays for detecting anti-SARS-CoV-2 antibodies in human serum samples from different populations" (2020) Science Translational Medicine, 12(559): eabc3103. doi: 10.1126/scitranslmed.abc3103

Chapter 1: General Introduction

Preface to Chapter 1:

This chapter serves as literature review on the subject of SARS-CoV-2 and syncytia formation. It was written by Maaran Michael Rajah, with editorial support from Pr. Olivier Schwartz and Dr. Julian Buchrieser. Sections of this introductory chapter were adapted and submitted as an invited review article to the Journal of Molecular Biology [1]. Permission has been granted by the publisher to include the article in this thesis (see appendix).

Rajah MM, Bernier A, Buchrieser J, Schwartz S. The mechanism and consequences of SARS-CoV-2 spike-mediated fusion and syncytia formation, Journal of Molecular Biology (2021), doi: https://doi.org/10.1016/j.jmb.2021.167280**.**

Part 1: The discovery, emergence and epidemiology of human coronaviruses

Coronaviruses are named for the morphology of the virion, where the protruding spike (S) protein gives the virus a "crown-like" (Latin: corona) appearance. Taxonomically, the family Coronaviridae is situated in the order Nidovirales. The general term "coronavirus" now refers to members of the subfamily orthocoronavirinae which is further subdivided into four genra: *alphacoronavirus* (α-CoV), *betacoronavirus* (β-CoV), *deltacoronavirus (*δ-CoV), and *gammacoronavirus* (γ-CoV) [International Committee on the Taxonomy of Viruses (ICTV); 2020]. The α-CoVs and β-CoVs primarily infect mammals, whereas the δ-CoVs and the γ-CoVs are primarily avian viruses; however, some can also infect mammals [2, 3].

Molecular clock analysis examining the viral RNA-dependent RNA polymerase (RdRp) puts the most recent common ancestor of all coronaviruses at ~10,000 years ago. [3]. Within each of the α-CoV, β-CoV, δ-CoV and γ-CoV genre, the most recent common ancestor was estimated to have existed ~4400, ~5300, ~4800 and ~5000 years ago, respectively [3]. These estimates, however, were strongly disputed based on the great diversity of hosts and their longstanding association with the coronaviruses [4]. Once the effects of purifying natural selection was factored into the analysis, the most recent common ancestor was estimated to have existed around 190 to 489 million years ago; suggesting that coronaviruses have an ancient origin [4]. It is widely acknowledged, that such extrapolative studies can only provide biologically plausible hypotheses and not definitive answers [4]. The first scientific description of a coronavirus was in the 1930s when infectious bronchitis virus, an agent of contagious respiratory disease in chickens, was identified and isolated [5]. During this period, coronaviruses were viewed to be primarily of agricultural concern, and it was

not until the 1960s that their potential to infect humans was described. The pandemic potential of coronaviruses would become very clear in the 2000s. The following sections will explore these human coronaviruses (hCoVs) in detail and in order of their discovery and emergence.

1.1.1 The "Common Cold" or "Seasonal" Human Coronaviruses: 229E, NL63, OC43 and HKU1

Human coronaviruses were first described in the mid-1960s when hCoV-229E and hCoV-OC43 were isolated from samples taken from patients presenting with the common cold, using tracheal organ cultures (OC) and tissue culture systems [6-9]. In 2003, another novel hCoV, NL63 was isolated in the Netherlands (NL) from child presenting with fever, coryza and bronchiolitis [10]. This was followed by the isolation of hCoV-HKU1 in Hong Kong from a 71-year old patient suffering from pneumonia upon his return from Shenzhen, China in 2004 [11]. These discoveries make up the group of hCoVs colloquially referred to as the "common cold coronaviruses" since infection usually resulted in mild pathogenicity with cold-like symptoms. Only the most vulnerable patients (children, the elderly and the immunocompromised) are susceptible to the more severe symptoms which includes pneumonia, asthma exacerbations and chronic bronchitis [6]. These hCoVs display seasonality (hence, they are also known seasonal coronaviruses) and increased antibody titers have been documented mainly between December and May [12]. It has also been suggested that infection may occur on cyclical basis every 2 to 3 years [12].

The circumstances surrounding the emergence of these common hCoVs are unclear but they all likely derive from zoonotic sources. It is hypothesized that the two α-CoVs, NL63 and 229E originated from bats whereas the β-CoVs, HKU1 and OC43 likely emerged from rodents (**Figure**

1.1) [2]. This is supported by molecular clock analysis done on α-CoV sequences derived from bats that suggest a common ancestry with NL63, with an evolutionary divergence event occurring 500 to 900 years ago [13]. Another study also identified sequences related to NL63 and 229E in African bats and suggests that NL63 may be a product of a recombinant event that occurred between NL63-like and 229E-like viruses from two different bat species [14]. Similar studies predicted that 229E emerged around 200-300 years ago [15]. The intermediate host of NL63 is not currently known while viruses similar to 229E have been isolated from dromedary camels and alpacas (**Figure 1.1)** [16]. The origins of OC43 and HKU1 are also obscure but it is hypothesized that rodent coronaviruses are the ancestral source of the β -CoV lineage A, to which they both belong [17]. In support of this, the closest relatives of HKU1 are the murine coronaviruses, mouse hepatitis virus (MHV) and rat coronavirus (RCoV) [17]. The intermediate host of hCoV-HKU1 is not known [2], though it is possible that rodents were both the original reservoir and transmitting host. Molecular clock analysis of OC43 suggests a remarkable similarity to bovine coronavirus (BCoV) and dates the most recent common ancestor of the two viruses to 120 years ago, with a relatively recent transmission event [18]. It is plausible that cattle were the intermediate source of transmission to humans (**Figure 1.1)** [2].

The common cold hCoVs are endemic and are distributed globally. NL63 and 229E are responsible for 10-30% of common cold cases and OC43 and HKU1 are associated with 5% and 1% of respiratory infections, respectively [18-20]. Due to their mild pathogenicity and relative obscurity, they drew minimal scientific interest. However, the emergence and rapid geographic expansion of the more lethal hCoVs in the 2000s rekindled interest in their milder relatives. The understanding of coronavirus emergence, evolution, and biology as well as the systems that were developed in

order to study the common cold coronaviruses undoubtedly facilitated the research into the more pathogenic hCoV-SARS-CoV-1, hCoV-MERS-CoV and more recently hCoV-SARS-CoV-2.

1.1.2 SARS-CoV-1

The first significant hCoV pandemic was caused by severe acute respiratory syndrome coronavirus (SARS-CoV-1) in 2003. The virus is believed to have emerged in late 2002 in the Guangdong province in southern China. In 2003 it spread across the world, causing more the 8,000 infection with a 10% mortality rate [21-23]. SARS-CoV-1 likely spilled over to human from civets and racoon dogs sold at live wild animal markets (**Figure 1.1)** [24, 25]. It was found that 13% of live animal traders and more than 50% of traders that specialize in civets had antibodies for SARS-CoV-1, despite not being diagnosed with SARS [26]. Later studies identified SARS-like coronaviruses in bat populations suggesting that bats may be the natural reservoir host (**Figure 1.1)** [27]. SARS-CoV was noticeably different than the previously described hCoVs in terms of disease severity. Clinical symptoms included fevers, chills, coughs and muscle pains with more severe cases presenting with lymphopenia, liver dysfunction and acute respiratory distress [25, 28]. Elderly patients were more susceptible to severe forms of the disease than children and suffered a fatality rate around ~40% [25, 29, 30]. The treatment for SARS-CoV at that time included β-interferon, assisted ventilation and anti-inflammatory drugs while research into candidate vaccines was underway [25, 30]. In their excellent overview of the SARS-CoV pandemic published in December 2003, Stadler and colleagues stressed the importance of continuing with therapeutic and vaccine research, fearing that the decline of the SARS-CoV-1

would exhaust the economic incentives to fund research that may be necessary to address future coronavirus pandemics [25]. Their observation would prove to be prescient.

1.1.3 MERS-CoV

A decade after the emergence of SARS-CoV-1, Middle East respiratory syndrome coronavirus (MERS-CoV) was isolated from a deceased patient who presented with acute pneumonia and renal failure in Saudi Arabia [31]. The virus would go on to cause more than 2200 infections and 800 deaths as it spread to 27 countries [32]. The majority of cases were localized in Saudi Arabia and surrounding countries, with the 2015 epidemic in South Korea being the notable exception [32]. Similar to many of the other coronaviruses, it is postulated that bats are the reservoir species for MERS-CoV (**Figure 1.1)** [33-35]. Dromedary camels were the intermediate host prior to human transmission (**Figure 1.1)** [36, 37]. Clinically, infection results febrile illnesses (fever, cough, shortness of breath) and severe cases can lead to acute respiratory distress syndrome (ARDS) and multiorgan dysfunction syndrome [32]. Therapeutic and treatment options were similar to SARS-CoV-1 infections [38]. The case fatality rate for MERS-CoV infection was also high at 30% [32]. In retrospect, the emergence and spread of SARS-CoV-1 and MERS-CoV was clear evidence of the pandemic potential of coronaviruses. This potential would be fully realized by SARS-CoV-2, which will be the focus of the next section and the rest of this chapter.

1.1.4 SARS-CoV-2

At the end of 2019, several patients presented with a pneumonia-like illness caused by an unknown agent in Wuhan, China [39]. The agent was identified as the newly emerged betacoronavirus SARS-CoV-2 (then termed novel coronavirus 2019; nCoV-2019) [39]. As of September 12th 2021, the virus has spread to 193 countries causing 224 million infections and over 4.6 million deaths [40]. It is currently unclear how the virus emerged and spread to humans but there are parallels to the emergence of SARS-CoV-1. At the start of the epidemic, many of the cases were centered around the Huanan market which traded in wild animals including civets and racoon dogs [41]. Serological and sequencing studies also suggest that SARS-CoV-2-like viruses can infect pangolins, which are trafficked and sold for consumption (**Figure 1.1)** [42, 43]. The receptor binding domain of some pangolin derived coronaviruses, share a remarkable similarity to SARS-CoV-2 and can bind effectively to human receptors [41, 44]. None of the pangolin coronaviruses, however, have a polybasic furin-like cleavage site in the S protein which is a distinguishing feature of SARS-CoV-2 [43]. At this stage, it cannot be definitively stated that any of these species are the intermediate hosts (**Figure 1.1)**. Genetically, SARS-CoV-2 most closely resembles a bat coronavirus RatG13, with an approximate 96% average genetic similarity [45, 46]. Coronaviruses are also prone to recombination, meaning that small regions of the viral genome can have independent origins and this can complicate the evolutionary picture [45]. When examined in terms of the virus genome, SARS-CoV-2 is more similar to several other bat coronaviruses (RmYN02, RpYN06, and PrC3) than RatG13 [41, 47]. The reservoir species for SARS-CoV-2 has not been definitively identified, though bats are a reasonable suspect (**Figure 1.1)**. Indeed, SARS-CoV-2-like viruses with similar receptor binding domain residues that can infect human cells have

been recently documented [48]. The evolutionary history of SARS-CoV-2 may be further convoluted by the involvement and genomic contributions from different virus species and further research is needed on the subject [48]. The symptoms of SARS-CoV-2 are reminiscent of the other severe hCoVs. A detailed discussion of the clinical and virological characteristics of SARS-CoV-2 infection is presented in a later section.

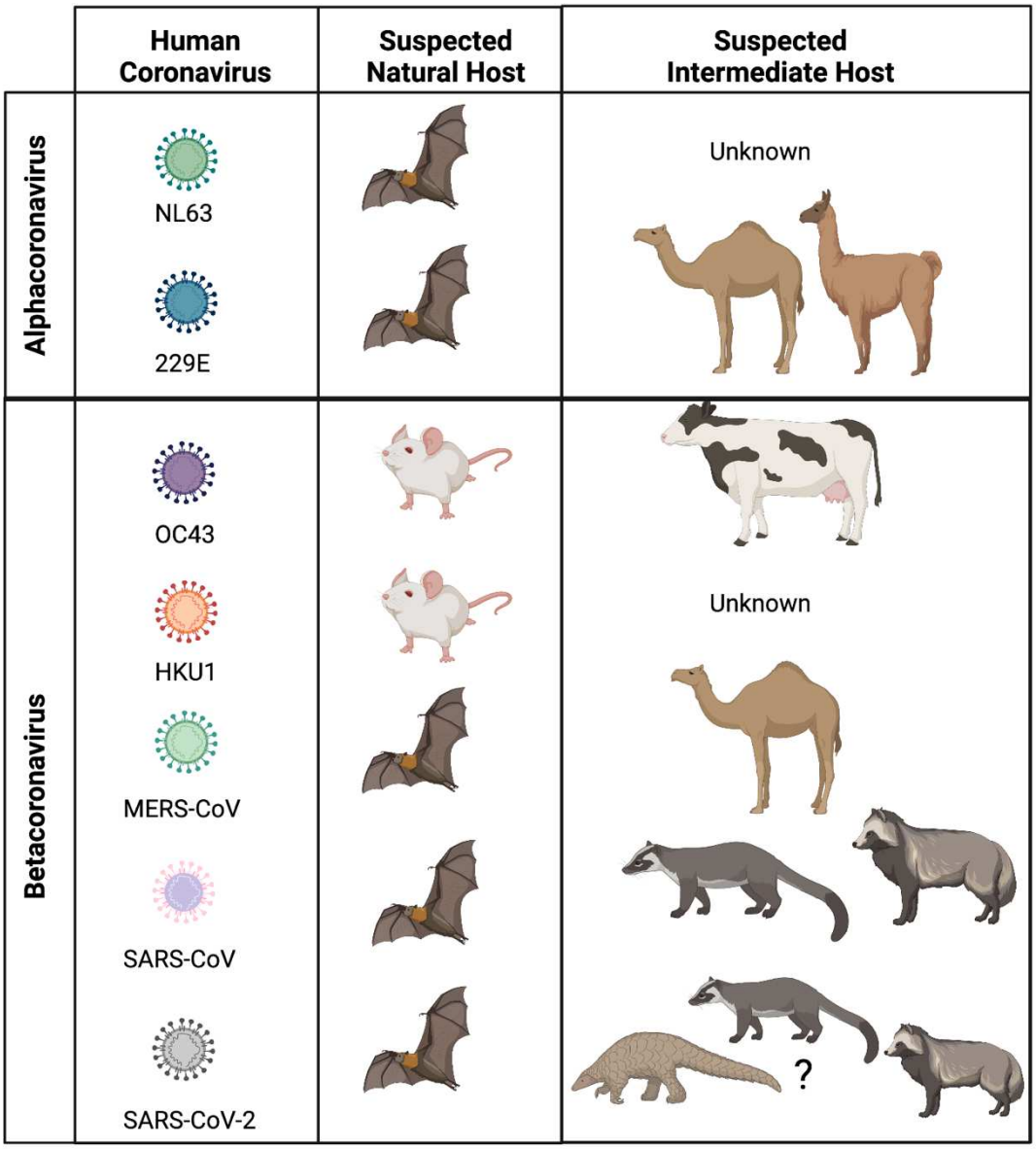

Figure 1.1: Suspected natural and intermediated hosts for each of the human coronaviruses. Created with Biorender.com (Lab subscription, BG231Z43LT)

1.1.4.1 SARS-COV-2 Variants of Concern

Since the emergence of the ancestral Wuhan strain, several novel SARS-CoV-2 variants harbouring a variety of mutations throughout their viral genome have arisen and spread around the world. One of the earliest described variants was the D614G European variant, in which the substitution in the S protein increased the virus' infectivity without altering antibody neutralization [49]. The pandemic then saw the emergence and spread of the Alpha variant (formerly termed B.1.1.7) which first identified in the United Kingdom, the Beta variant (B.1.351) identified in South Africa, the Gamma variant (P.1 & P.2) identified in Brazil, and more recently the Delta variant (B.1.617) identified in India [50-55]. These "variants of concern" (VOC) are characterized by their increased transmissibility and greater potential to evade the neutralizing antibody response; however, their impact on disease severity is debated (**Table 1)** [56-61].

Due to the mosaic and sometimes conflicting nature of the epidemiological and serological data on the VOC, it is difficult to provide an exact comparison. The Alpha variant is 43% to 90% more transmissible than the ancestral Wuhan strain [59]. There also seems to some degree of antibody escape when compared to the Wuhan strain, but antibodies from convalescent sera similarly neutralized both the Alpha and the D614G variant [56, 62]. The Beta variant may also have a slight transmission advantage over the ancestral strain; however, its defining characteristic is its ability to evade antibody neutralization [63]. Relative to D614G and Alpha, neutralization titers from convalescent and vaccinated sera was significantly less effective against the Beta variant [56]. The Beta variant also seems to affect disease progression. Compared to Alpha, infection with the Beta seems to increase the odds of progressing to severe disease, critical disease and death by 1.24-fold,

1.49-fold, and 1.57-fold, respectively [64]. A study in Brazil also found that the P.1 Gamma was twice as transmissible than previously circulating "non-P.1" variants [65]. It also is more resistant to antibody neutralization than the D614G variant [66]. The Delta variant is currently the main VOC and rapidly displaced the aforementioned variants in many countries. The Delta variant is twice as transmissible as the ancestral Wuhan strain and 40% to 60% (possibly 100%) more transmissible than the Alpha variant [67-69]. In addition, the Delta variant has some resistance to neutralizing antibodies from sera isolated from both convalescent individuals and those who received only one vaccine dose [51]. Furthermore, disease severity and risk of hospitalization was also higher with the Delta variant infection, relative to the Alpha variant [70, 71]. The mutations in the S protein of VOC are of particular interest as it can affect both the antigenicity and infectivity of the virus. Indeed, the S protein of the different variants house a variety of mutations that may confer different advantages. The functional characteristics of the mutations associated with the S proteins of the VOCs will be explored in **Chapter 3** and **Chapter 5**.

Table 1: Qualitative comparison of transmissibility, antibody escape and disease severity (hospitalization risk) of the D614G, Alpha, Beta, Gamma and Delta variants relative to the ancestral Wuhan strain. The number of + signs represents an undefined qualitative difference between variants based on the author's interpretation and synthesis of the data described in the text. The + signs do not correspond to set quantitative values and this table is intended to be interpreted as a visual summary of the general trend.

SARS-CoV-2 Variant	Transmissibility	Antibody Escape	Disease Severity
Ancestral Wuhan	Reference	Reference	Reference
D614G	+	idem	idem
Alpha	+++	+	+
Beta	+	+++	+++
Gamma	++	++	++
Delta	++++	++	+++

Part 2: Clinical and Virological Characteristics of SARS-CoV-2

1.2.1 Transmission

SARS-CoV-2 is mainly transmitted between humans through direct or indirect contact with the secretions or aerosolized respiratory droplets from an infected individual [72]. Once inhaled, the virus infects the respiratory tract epithelium including the oropharynx and the upper respiratory tract [73]. In the first five days of infection an individual can be presymptomatic, with symptom onset usually occurring after a week post-infection and around the time of peak viral load (**Figure 1.2**) [73]. The presence of high titers of SARS-CoV-2 early in the course of infection may help explain the increased transmissibility of the virus relative to MERS-CoV and SAR-CoV-1 [74]. In addition, some SARS-CoV-2 VOC may display a more rapid infection kinetic than the ancestral strain. For example, it is suggested that the viral load upon infection by the Delta variant is 1000 times higher. Studies done on animal models demonstrate that VOC can transmit more efficiently than the earlier strains at a lower dose [75]. Faster infection kinetics in the host and greater infectivity may contribute to the increased transmissibility of the VOC [58].

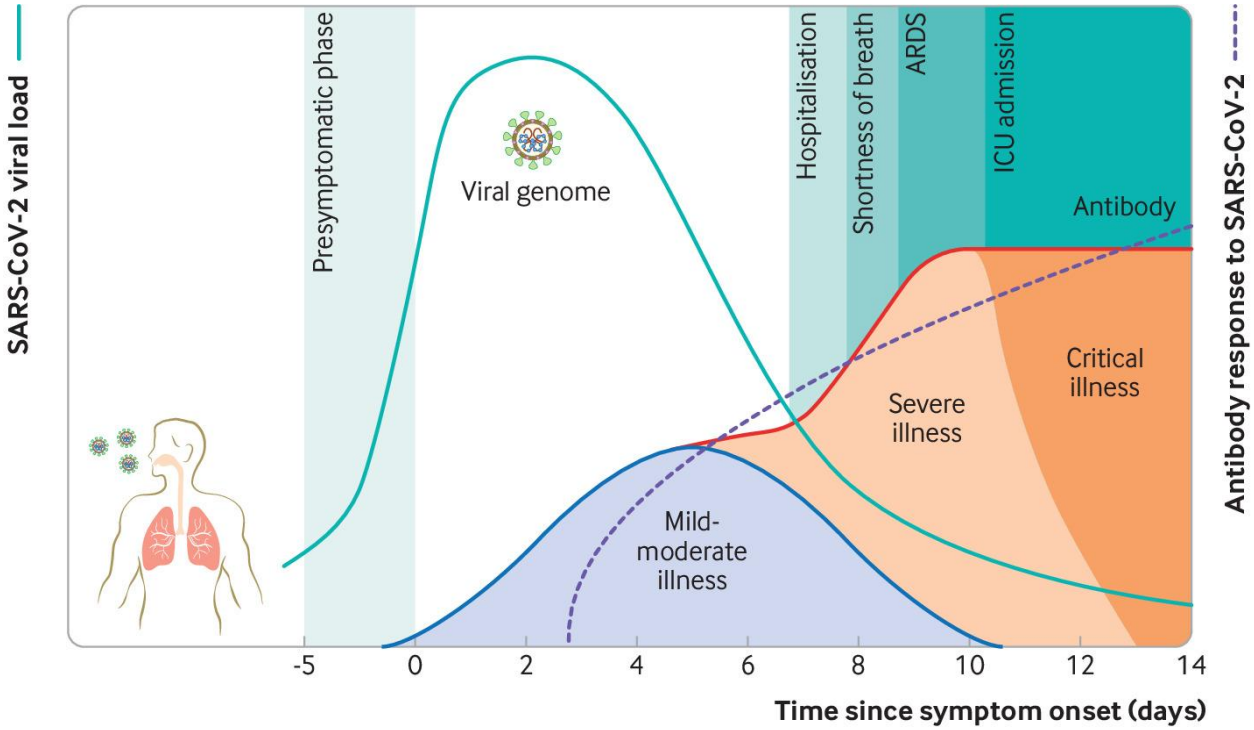

Figure 1.2 SARS-CoV-2 viral load, symptoms and disease progression after initial exposure. Symptoms generally occur 5 days post-infection and viral load peaks after a week. Most infections are asymptomatic or result in mild disease; however, some patients progress to severe and critical illnesses. This generally corresponds with an excessive immune response and increasing antibody titers. Reprinted with permission form BMJ Publishing Group Ltd: The BMJ, Vol 371, Cevik et al., Virology, transmission, and pathogenesis of SARS-CoV-2, Page 3, Copyright (2020) [73]. doi: https://doi.org/10.1136/bmj.m3862. Original data from Cell, Vol 181, Oberfeld et al., 2020 SnapShot: COVID-19 [76]. https://doi.org/10.1016/j.cell.2020.04.013 Permission also secured from Elsevier.

1.2.2 COVID-19: Symptoms and Disease

Coronavirus disease 2019 (COVID-19) is a spectrum disorder and ~80% of cases are either asymptomatic or present with mild or moderate symptoms [77, 78]. The most common symptoms of the disease include fever, muscle pain, coughs and labored breathing [73, 79]. Other reported clinical features include gastrointestinal distress, fatigue, headaches, sore throat, ground glass-like

chest opacity on chest x-rays and lymphopenia [79]. Severe and critical manifestations of the disease can occur in about 20% of cases and are associated with risk factors such as advanced age, preexisting pulmonary and cardiovascular diseases, obesity and the hyperactivation of the immune system [73, 78]. This phase of the disease is associated with decreasing viral loads but a rapidly expanding antibody and inflammatory response (**Figure 1.2**) Severe manifestation of COVID-19 causes acute respiratory distress syndrome (ARDS) with extensive, and occasionally fatal, lung damage (**Figure 1.2**) [80]. The deterioration of lung tissue is characterized by diffuse alveolar damage, micro/macro-vascular thrombosis, and pneumocyte necrosis [80-82]. Many of these lung pathologies are also reminiscent of severe SARS-CoV-1 and MERS-CoV infections [80, 83, 84]. The clinical features of COVID-19, especially the extensive lung thrombosis, are particularly severe in comparison to other causes of acute respiratory syndrome [80, 85]. A combination of hypoxemia, immune-mediated damage, and virus-induced cytopathic effect all contribute to lung epithelial destruction [80, 85, 86]. The overall case-fatality rate for SARS-CoV-2 ranges from 1 to 7% (average 2%) depending on the region but can be as high as 17% in vulnerable populations [87, 88].

1.2.3 Vaccines and Therapeutics

Similar to the other severe hCoVs, treatment for COVID19 disease involves the use of monoclonal antibodies, glucocorticoids, corticosteroid therapy, and broad-spectrum antivirals in combination with supportive therapies including mechanical ventilation and oxygen [79]. However, there are no specific treatment options to date. The SARS-CoV-2 pandemic is remarkable in comparison to the previous hCoV pandemics, due the rapid development and implementation of effective

vaccines. Several different vaccine strategies have been successfully employed and have been critical in controlling the pandemic. **Table 2** summarizes the most widely used vaccine strategies and their efficacy. Inactivated vaccines use the virus particle as the immunogen, after it has been chemically or physically inactivated [89]. Viral vector vaccines deliver genes that encode specific antigens to the host via a non-pathogenic or non-replicating viral (adenovirus) vector. Both the AstraZeneca-University of Oxford and the Gamaleya vaccines use the full length SARS-CoV-2 S protein as the antigen [89].

Similarly, mRNA based vaccines are synthesized *in vitro* and delivered via lipid nanoparticles [89]. They encode viral antigens that are directedly translated into proteins in the host's cytoplasm [89]. The Moderna and Pfizer-BioNtech vaccines both encode the full length S protein with the K986P and V987P mutations that stabilize the protein in a prefusion state [89, 90]. The different vaccines have been shown to drastically reduce disease severity and hospitalizations and are major component in controlling the pandemic. The rise and spread of the SARS-CoV-2 VOC may present a challenge to the currently used vaccine strategies since the variants house several mutations in the S protein. There is some evidence of reduced protection against VOC depending on the vaccine, viral strain and number of vaccine doses received [51, 91]. However, the vaccines are still generally protective against severe forms of disease and they reduce the risk of hospitalization [91].

Table 2: Widely used SARS-CoV-2 vaccines and efficacy data from phase III trials. Adapted from Tregoning et al., 2021; Nature Reviews Immunology [91]

Vaccine/ Manufacturer	Platform	Efficacy	Effect on Disease Severity
Pfizer-BioNTech (BNT162b2)	mRNA	95%	95%-100% effective in preventing severe disease
Moderna (mRNA-1273)	mRNA	94%	100% efficacy against severe disease
AstraZeneca-University of Oxford (AZD1222)	Viral Vector	55%-81% (higher efficacy when doses are 3 months apart)	100% efficacy against hospitalization
Johnson & Johnson (Ad26.COV-S)	Viral Vector	66%	85% efficacy against severe disease
Gamaleya Sputnik V	Viral Vector	92%	No data (June 2021)
Sinovac Biotech	Inactivated Virus	50% to 91% (depending on study)	100% efficacy against severe disease and hospitalization. 51% effective against symptomatic infection.
Sinopharm	Inactivated Virus	78%	79% efficacy against hospitalization

1.2.4 SARS-CoV-2 Virion and RNA

SARS-CoV-2 is an enveloped positive-sense single-stranded RNA (+ssRNA) virus. Based on electron micrographs, the virion can range from 60 to 140nm in diameter (**Figure 1.3**) [39]. The viral envelope is comprised of a lipid bilayer embedded with the envelope (E), membrane (M) and the trimeric S protein, which protrudes from the surface. Enclosed within the virion is the genomic +ssRNA encapsidated by the nucleocapsid (N) structural protein (**Figure 1.3**). A defining feature of coronaviruses is their large genomes which can range from 26-32 kb in length. The viral transcript is also flanked by a 5'-cap structure and a 3' poly (A) tail which form secondary RNA structures necessary for RNA synthesis [92, 93]. Once deposited into the host cell, the first two-

thirds (from the 5' end) of the viral RNA (vRNA) are translated from two open reading frames (ORF), ORF1a and ORF1b [93, 94]. ORF1a is translated into polyprotein (pp)1a and a frameshift upstream of the ORF1a stop codons allows for the continued translation of ORF1b into pp1ab (**Figure 1.3**) [92]. The resulting polyproteins are co- and post- translationally processed into 16 nonstructural proteins (nsp) that make up the viral replication and transcription complex [92, 93]. The structural proteins S, envelope (E), nucleocapsid (N), and membrane (M) as well as several accessory proteins, are expressed from ORFs from the final third of the viral genome from a nested set of sub-genomic mRNAs (sgRNA) in a process referred to as discontinuous transcription [93, 95]. Previous investigations into coronaviruses and recent studies on SARS-CoV-2 have provided insights into the function of the viral proteins (discussed below).

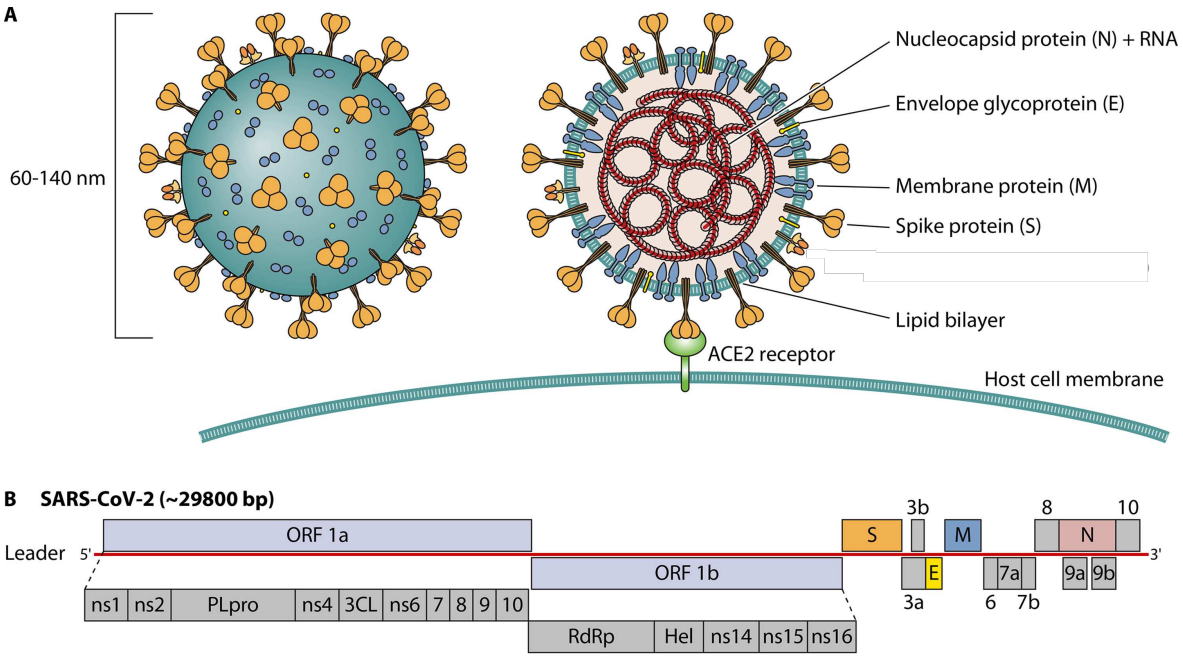

Figure 1.3 (A) SARS-CoV-2 virion morphology with the viral structural proteins **(B)** Viral genome organization with the associated structural, non-structural and accessory proteins. Adapted with permission from The American Society for Microbiology. Clinical Microbiology Reviews, Vol 34, Tali et al., Tools and Techniques for Severe Acute Respiratory Syndrome Coronavirus 2 (SARS-CoV-2)/COVID-19 Detection, Page 4, Copyright (2021) [95].
doi: https://doi.org/10.1128/CMR.00228-20

1.2.5 Coronavirus replication cycle

The current knowledge on the lifecycle of SARS-CoV-2 and function of the viral proteins derives from both recent research as well as previous work conducted on other coronaviruses [93]. The fusion of the viral membrane with the cellular membranes and the deposition and uncoating of viral genomic RNA in the cellular cytoplasm represents the first stage of the viral life cycle [93]. This occurs when the S protein on the surface of the virions interacts with the human angiotensin converting enzyme 2 (ACE2) receptor at the surface of the target cell (**Figure 1.4**). Several auxiliary receptors such as L-SIGN, DC-SIGN, and neuropilin-1 (Nrp1), may facilitate attachment or entry [96-98]. Additionally, a recent investigation identified sialic acid-binding Ig-like lectin 1 as an attachment receptor which can enhance ACE2-mediated infection [98].

The virus can then fuse at the plasma membrane (early entry) or with endosomal membranes (late entry) during uptake. When bound at the plasma membrane, the S protein may be primed by host factors like transmembrane serine protease 2 (TMPRSS2), which enhances SARS-CoV-2 entry [94, 99, 100]. After endocytosis, proteolytic activity by host factors such as cathepsin L/B (CTSL/B) and furin further assists in the priming the S protein [99, 101, 102]. Following fusion and uncoating, the vRNA is translated from ORF1a and ORF1b to produce polyproteins which are then processed into the nonstructural proteins that form viral replication and transcription complexes (**Figure 1.4**). Simultaneously, discontinuous transcription from the viral genome creates sgRNAs from which the viral structural and accessory proteins are expressed (**Figure 1.4**) [93]. The specific roles of the viral proteins both within the viral life and in modulating the cellular environment are described in the following section.

Coronaviruses, like many other described viruses, co-opt intracellular membranes to form viral replication organelles that provide a protective microenvironment for vRNA replication and protein transcription [93, 103]. During the coronavirus assembly process, the E, M, and S proteins are translocated and inserted into the endoplasmic reticulum and are trafficked through the ER-Golgi intermediate compartment (ERGIC) to the Golgi apparatus (**Figure 1.4**). During the course of translocation and viral assembly, the S protein is subjected to processing by furin and other cellular proteases, generating the non-covalently associated S1 and S2 subunits which are primed for fusing with the membrane of naïve cells upon reinfection [104]. The immature virions bud into the ERGIC or Golgi compartments and viral egress occurs through deacidified lysosome-dependent exocytosis [105].

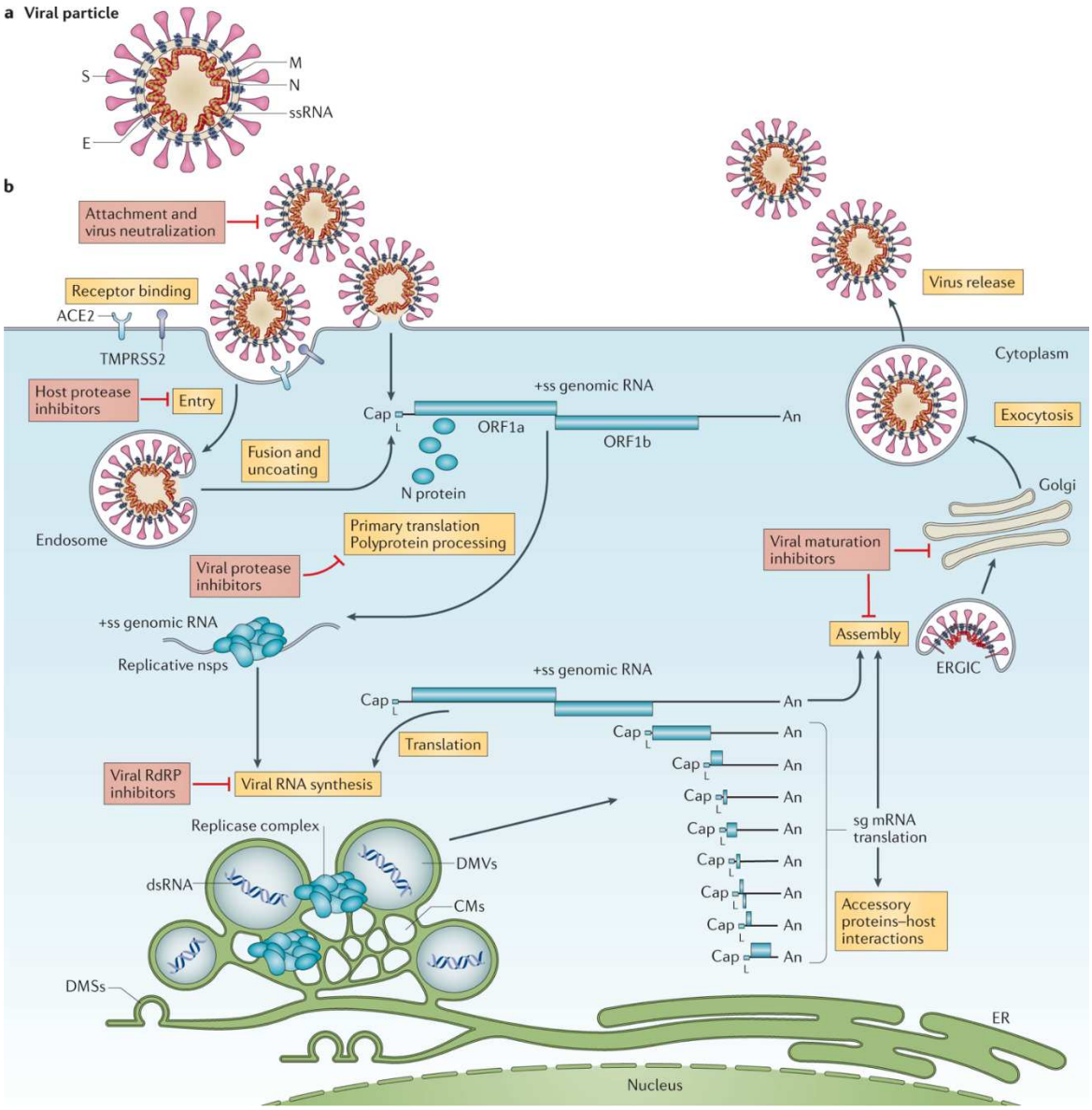

Figure 1.4 Coronavirus replication cycle. The viral S protein interacts with the ACE2 receptor to fuse into the cell at the plasma membrane (early entry) or within endosomes (late entry). The viral genome is deposited into the cytoplasm and is translated from ORF1a and ORF1ab. The resulting polypeptides are post- and co- translationally processed into the non-structural proteins which form the viral replication and transcription complexes, induce remodelling of intracellular membrane and facilitate immune escape. The structural and accessory proteins are produced from a nested set of subgenomic mRNAs encoded in the viral genome. The structural proteins translocate to the ER membranes and transit through the ER-ERGIC-Golgi network and interact with newly synthesize vRNA. Immature virions bud into the intracellular compartments and are maturated as they egress via deacidified lysosome-dependent exocytosis. Reused with permission from Springer Nature. Nature Reviews Microbiology, Vol 19, V'kovski et al., Coronavirus biology and replication: implications for SARS-CoV-2, Page 156, Copyright (2021) [93]. doi: https://doi.org/10.1038/s41579-020-00468-6

1.2.6 Structural Proteins

1.2.6.1 Spike (S) Protein

The S protein facilitates the fusion of the virion with the host cell by interacting with the human ACE2 receptor during the first stage of infection. It is also the driver of SARS-CoV-2 induced syncytia formation through an analogous mechanism; however, this will be explored in a later section. The S protein is a class I fusogen (structurally comprised of α-helices) which facilitates membrane fusion after undergoing structural rearrangements which transition it from a metastable prefusion form to a fusion competent state [106, 107]. It is a glycosylated protein about 1271 amino acids long and is comprised of the S1 and S2 subunits separated by a polybasic cleavage site. Cellular proteases cleave between this S1/S2 site as well as at a S2' site in order to activate the S protein (**Figure 1.5**) [99]. The S1 subunit consists of the N-terminal domain (NTD) and the receptor binding domain (RBD). The function of the NTD is still under investigation, though work on other coronaviruses shows that the NTD may be associated with glycan recognition during initial attachment, receptor recognition and pre-to-post fusion transition of the S protein [108-110]. The C-type lectins DC-SIGN and L-SIGN may act as auxiliary receptors for SARS-CoV-2 by associating with the NTD [96]. SARS-CoV-2 S protein-mediated fusion may also be subject to antibody-dependent enhancement as the binding of antibodies to a specific site on the NTD induces an open RBD state which may enhance fusogenicity [111]. The RBD domain of the S1 interacts with the ACE2 receptor; the presence of which determines cellular tropism (**Figure 1.5**) [46, 49, 112]. The RBDs of the S protein trimer exist in a state of dynamic equilibrium between "up" (open) and "down" (closed) conformations [113, 114]. In the "up" conformation, the RBD can bind to

ACE2 and the binding of one of the RBD monomers to ACE2 is followed by sequential opening up and binding of the remaining two RBD monomers to ACE2 [114].

Since multiple receptors are able to bind to an S protein, considerable mechanical stress is exerted on the S1 [113]. The opening process disrupts contact between ACE2-bound S1 monomers, promoting their dissociation from the complex and revealing the trimeric S2 core, which houses the fusion machinery of the S protein (**Figure 1.5**) [114]. The S2 domain is comprised of the fusion peptide (FP), heptapeptide repeat sequences 1 and 2 (HR1 and HR2), a transmembrane anchor (TA) and a C-terminal domain (CTD). Upon the release of the S1 domain, the unstructured HR1 in the S2 domain becomes helical, and thrusts the FP into the target cell membrane (**Figure 1.5**) [113, 115]. The FP then disrupts the lipid bilayer of the target membrane and anchors it to the fusion machinery (**Figure 1.5**) [116, 117]. On the other end of the S2 domain, the fusion machinery is anchored on either the virion membrane or the S-expressing cell membrane (in the case of syncytia formation), by the TA subdomain (**Figure 1.5**). Upon insertion of the FP into the target membrane, three highly conserved hydrophobic grooves on HR1 are exposed, which allows for interaction with the HR2 subdomain [113]. The HR2 domain contains a rigid helix and a flexible loop [117, 118]. The interaction between HR1 and HR2 forms a six-helix bundle which brings the two anchored membranes into close proximity to one another, overcoming the natural repulsive force that keeps the membranes apart (**Figure 1.5**) [113]. Once the energetic barrier for fusion is reduced, the outer leaflets of the membranes merge in a step referred to as hemi-fusion. This is followed by the formation of a pore which expands to create one continuous membrane, allowing mixing of the viral or cytoplasmic contents (**Figure 1.5**) [113].

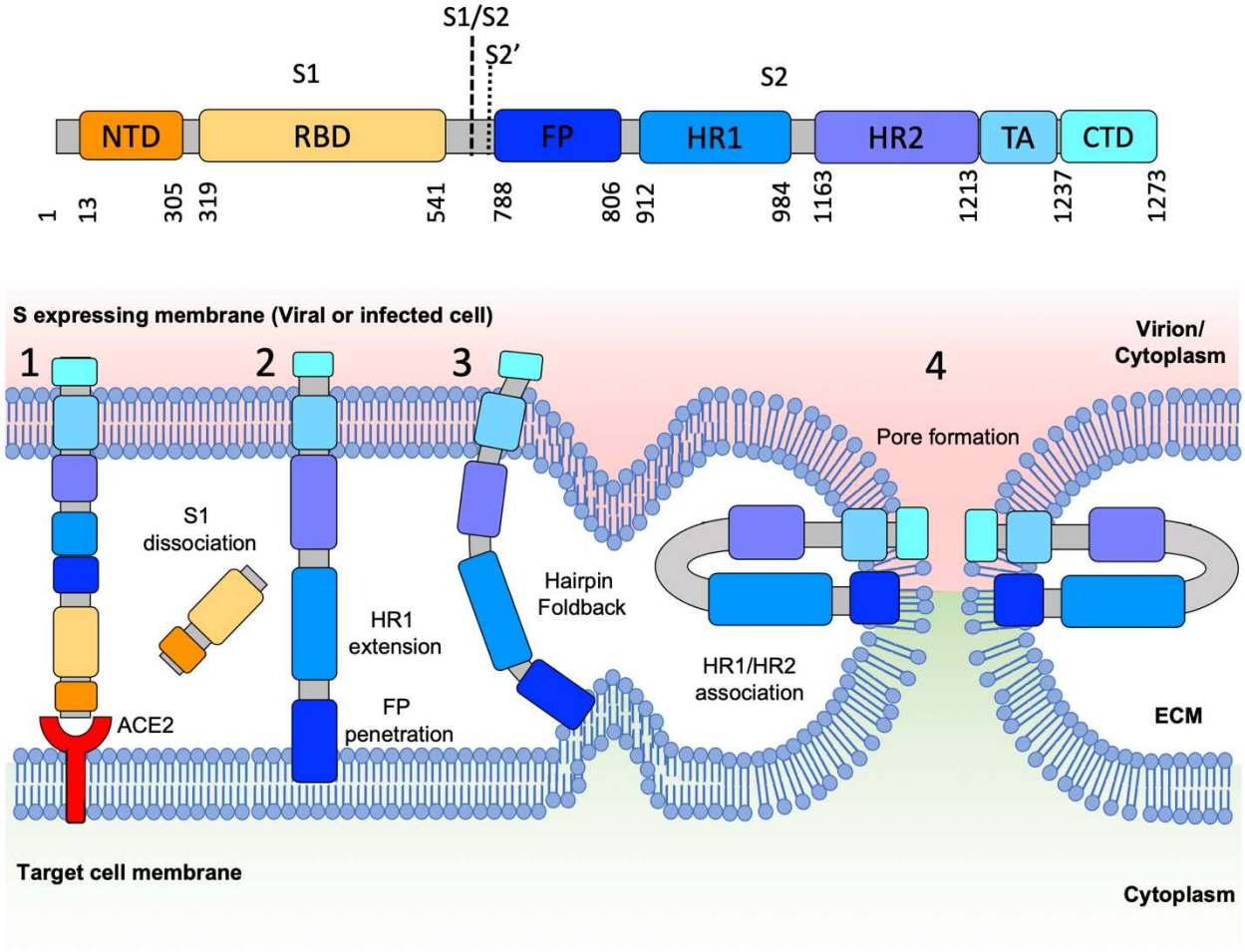

Figure 1.5 Molecular mechanism of Spike (S) protein-mediated virus-cell or cell-cell fusion. **Top:** the functional subdomains of the S protein. N-terminal domain (NTD), receptor binding domain (RBD), fusion peptide (FP), heptapeptide repeat sequences 1 and 2 (HR1 & HR2), transmembrane anchor (TA), C-terminal domain (CTD). **Bottom: 1)** The S protein associates with the ACE2 receptor via its RBD. It is also processed by cellular proteases at the S1/S2 or S2' sites (not shown). **2)** The S1 domain is released which allows for HR1 to extend and thrust the FP into the target cell plasma membrane. The FP anchors the target membrane while the TA anchors the fusion machinery to the viral or infected cell membrane. **3)** Interactions between HR1 and HR2 results in a hairpin-like foldback that overcomes the energetic barrier to fusion and brings the membranes close together. A hemi-fusion step occurs where the outer layers of the fusing membranes merge (not shown). **4)** The association of HR1 and HR2 and the corresponding membrane fusion result in the formation of a pore that will gradually expand. The viral or cytoplasmic contents are then merged. Figure generated by the author and submitted to the Journal of Molecular Biology in an invited review article. Rights retained to use figure in thesis or dissertation. Original source: Elsevier. Journal of Molecular Biology, Rajah et al., 2021 [1].
doi: https://doi.org/10.1016/j.jmb.2021.167280

1.2.6.2 Membrane Protein

M is the most abundant structural protein and is thought to be involved in pathogenesis and in the assembly of viral particles through its interactions with the other structural proteins. During viral assembly, the M protein interacts with the cytoplasmic tail of the S protein and sequesters it on the intracellular membranes [119, 120]. This retention regulates the trafficking and processing of the S protein [119, 120]. Homotypic interactions between M proteins also drives virion formation [121]. Recent investigations suggest that the M protein antagonizes the immune response by suppressing nuclear factor kappa B (NF-Kb), IFN production, and mitochondrial antiviral signaling (MAV) protein activity (**Figure 1.6**) [122-124]. Its immunosuppression function and its abundance would suggest a significant role in viral pathogenesis. M also plays a role in packaging the genomic vRNA through its interaction with the N protein [125].

1.2.6.3 Nucleocapsid protein

The N protein encapsidates newly produced viral genomic RNA forming helical viral ribonucleoprotein (vRNP) complexes [126]. The interaction of neighboring vRNPs allows for the compaction and efficient packaging of the large viral genome into the virion [126]. It has been suggested that the N protein may support virion budding by exerting a "pushing' force from within during assembly [119]. It may also have a role in suppressing the granule-dependent antiviral response as it has been shown to recruit stress granule protein G3BP1 [125]. The immunosuppression role of the N protein is also highlighted by its ability antagonize retinoic acid-inducible gene I (RIG-I) and inhibit IFN induction [127].

1.2.6.4 Envelope Protein

E protein is an integral membrane protein which impacts trafficking, sequestration, and processing of the S protein and is mainly associated with virion assembly [119, 121]. Studies done on other coronaviruses demonstrate that the lack of E protein negatively affects viral maturation and significantly reduces viral titers [121]. Interactions between E and M are required for the formation of viral particles [119]. In contrast to the "pushing" force applied by the N protein, it has been postulated that E and M contribute to viral budding by forming symmetric lattices and creating an optimal curvature which generates a "pulling" force [119].

The E protein also assists in the retention of S on intracellular membranes by modulating the cells secretory pathway [119]. Both E and M, have also been shown to affect the maturation of the N glycans on the S protein independent of their sequestration function [119]. SARS-CoV-2 E proteins can associate with one another and form homopentameric cation channels [128]. In a SARS-COV-1 animal model, mutations that compromised the channel activity of the E protein significantly reduced pathogenesis; however, compensatory mutations that restored channel activity, arose upon passaging [129]. This suggests that the homotypic interaction of coronavirus E proteins has an important viral function and is significant for pathogenesis. Indeed, the transport of calcium through the ion channel form by SARS-CoV-1 E protein stimulates the inflammasome and worsens disease [130]. Furthermore, the SARS-CoV-2 E proteins, recruits PALS1 (a human tight junction protein) to the site of viral maturation and assembly on the ERGIC [131]. This may

compromise the epithelial junctions resulting in increased viral dissemination and immune cell infiltration [131].

1.2.6.5 The interplay between the structural proteins

Taken together, the M, N and E structural proteins of SARS-CoV-2 play intertwined roles in the assembly of the virion and in suppressing the host immune response. The N protein interacts with the newly synthesized vRNA and oligomerizes in order to compact the genome. The M and E localize on intracellular membranes. Interactions between N and M allow for the viral genome to be packaged into virions at the site of assembly. Extrapolating from what is known about the budding process from other enveloped viruses, the N protein exerts a pushing force to create a membranous bud while E and M create a membrane curvature and a pulling force. M and E also play a role in the sequestration and processing of the S protein, keeping the fusogen at sites of virus assembly. The incorporation of the S protein is necessary to ensure the viral progeny are infectious [119]. The final product will be the budding of an immature virion from the ERGIC or Golgi membrane which contains the N protein encapsidated viral genome within and the S, M and E proteins on the virion surface. The viral progeny will continue to mature as they egress. The structural proteins are multifunctional and in addition to their role in viral assembly they also modulate the immune response and increase pathogenesis.

1.2.7 Non-structural protein

The sixteen nonstructural proteins are derived from the co- and post- translational processing of pp1a (nsp1 to nsp11) and pp1ab (nsp1-10, nsp1-16). These proteins are responsible for vRNA replication, mRNA synthesis, processing of pp1a and pp1ab and modulating the host immune response [95]. The two large polyproteins are cleaved by the cystine proteases nsp3 (papain-like protease, PLpro) and nsp5 (chymotrypsin-like protease, 3CLpro) [93]. The majority of the processing is done by nsp5, as such it is also referred to as the main protease (Mpro) [93]. Nsp3 has also been shown to attenuate the type 1 IFN response by cleaving ISG15 [132]. Nsp1 is proteolytically processed and released rapidly from the viral polyproteins and functions as a global "host shutoff factor" [133]. It binds to human ribosomal complexes and interferes with mRNA binding, thus preventing the translation of host proteins [133]. The ultimate effect is the cultivation of a cellular environment that favours the translation of the viral mRNA over the host's mRNA [133].

Nsp3, nsp4, and nsp6 are thought to modify intracellular membranes into environments that support the viral replication and transcription complex (vRTC) [134]. During the course of coronavirus infection, highly dynamic viral replication organelles including double membrane vesicles (DMV), convoluted membranes and double membrane spherules are derived from the endoplasmic reticulum [134, 135]. Intermediate double-stranded vRNA localizes in DMVs and newly synthesized vRNA can be detected in these structures during SARS-CoV and MERS-CoV infection [93, 135, 136]. This suggests that vRNA is synthesized in these replication organelles; however, this has not been conclusively proven [93]. The nsp3 protein of several coronavirus

including SARS-CoV-2, has been shown to form molecular pores on the DMV, which may allow for newly synthesized vRNA to translocate to the translation and encapsidation sites [93, 137]. Furthermore, nsp3 possesses nucleotide triphosphate hydrolase (NTPase) and RNA helicase (Hel) activities that facilitate vRNA replication by presumably unwinding the intermediate double stranded vRNA [138].

Nsp12 is the viral RNA-dependent RNA-polymerase (RdRp) that is responsible for replicating the viral genome and transcribing the sgRNAs [93, 139]. Nsp7 and nsp8 are co-factors for nsp12 that stabilize and support its processing ability. Nsp8 prevents premature disassociation of the RdRp from the vRNA and may also function as a primase and an adenylyltransferase [93, 139]. Nsp14 is an N7-methyltransferase and also functions a 3'-5' exonuclease that proofreads the newly synthesized vRNA [93, 140]. Nsp16 possesses 2'-O-methyltransferase activity and nsp10 is a cofactor for nsp14 and nsp16 [93, 141]. Nsp9 has a modest affinity for RNA-binding and is necessary for efficient viral replication [142] Nsp11 is an intrinsically disordered protein and its function remains to be elucidated [143]. Nsp15 has an endoribonuclease function and mediates evasion from host dsRNA sensors [144, 145].

1.2.8 Accessory proteins

In addition to the previously mentioned structural proteins, the sgRNA transcribed from coronavirus genomes also encodes accessory proteins. The exact number of accessory proteins encoded by SARS-CoV-2 is debated and the existence and function of many of the postulated proteins have yet to be experimentally verified [93]. To complicate matters further, there is little

homology between the accessory proteins of different coronaviruses which makes functional comparisons difficult. There are at least 5 (potentially 6) accessory proteins described for SARS-CoV-2 including ORF3a, ORF6, ORF7a, ORF7b, ORF8, and ORF3b and they mainly function as modulators of the host immune response [93]. The presence of ORF3b and ORF6 antagonizes the activation of IRF3 (interferon regulatory transcription factor 3) and expression from ISRE (interferon-stimulated response element) (**Figure 1.6**) [146-148]. ORF6 also inhibits the nuclear translation of STAT1; which is required to induce the transcription of genes that mount the immune response (**Figure 1.6**) [149] [146]. ORF7a inhibits IFNα signaling by blocking the phosphorylation of STAT2 while ORF7b affects antiviral signaling by interfering MAVS-induced IFNβ production [150, 151]. It has been suggest that in ORF8 expressing cells, major histocompatibility complex I (MHC-I) molecules are targeted for lysosomal degradation which prevents infected cells from being targeted by the immune system [152].

1.2.8 Immune response to SARS-CoV-2 infection

SARS-CoV-2 infection of the respiratory and gastrointestinal tract activates the host immune response. The lung epithelial deterioration seen in severe COVID-19 disease is elicited by a combination of both virus-induced cytopathic effects and immune mediated damage. The antiviral immune response is classically subdivided into adaptive and innate immunity.

1.2.8.1 Adaptive Immune Response

The adaptive immune response is characterized by the activation of B cells, $CD4^+$ T cells and $CD8^+$ T cells. B cells produce specific antibodies in response to viral infection or vaccination [153]. Neutralizing antibodies produced by the B cells can bind to cell-free virus and prevent viral entry and infection. The neutralizing antiviral antibody response to SARS-CoV-2 appears within the first two weeks after symptom onset. The majority of neutralizing antibodies target the RBD of the S protein (>90%) and some target the NTD [153, 154]. $CD4^+$ T cells control viral infections by differentiating into T helper cells (Th1) and T follicular helper cells (Tfh). Th1 cells produce cytokines including IFNγ and also play a role activating and recruiting innate immune cells [153]. Tfh cells assist B cells in the production and affinity maturation of neutralizing antibodies [153]. Furthermore, $CD4^+$ T cells also differentiate into CD4-CTL cells that have direct cytotoxic activity again infected cells. There is a higher proportion of CD4-CTL cells in patients hospitalized with COVID-19 relative to non-hospitalized patients; however, the contribution of CD4-CTL cell to the protective or pathogenic immune response to SARS-CoV-2 remains to be understood [155]. Additionally, CD4 T cells assist in the differentiation and proliferation of CD8 T cells [153]. CD8+ T cells can control viral infection by killing infected cells and the presence of these cells during SARS-CoV-2 infection is associated with more favorable disease outcomes [153]. The adaptive immune response is dependent on the selection, maturation and expansion of specific naïve cells and as such is generally slower to react to infection than the innate immune response [153].

1.2.8.2 Innate Immune Response

In contrast to the adaptive immune response, the innate immune response is triggered within a few hours post-infection. It rapidly antagonizes viral replication and spread while also activating components of the adaptive immune system. Infection of respiratory epithelial cells can lead to monocyte, macrophage and dendritic innate immune cell activation. These innate immune cells recognize pathogen-associated molecular patterns (PAMP) through specific pattern-recognition receptors (**Figure 1.6**) [156]. During the course of the coronavirus infection, viral genetic material is detected by endosomal sensors (Toll-like receptors; TLRs) and by cytosolic sensors (RIG-I and MDA5). This will lead to the activation of transcription factors NF-kB, IRF3 and IRF7 which translocate to the nucleus [156]. NF-kB stimulates the production of proinflammatory cytokines whereas IRF3 and IRF7 mediated the induction of type 1 (IFNα/β) and type 3 (IFNλ) interferons [156]. Secreted IFNs will bind to type 1 IFN receptors (IFNARS) and type 3 IFN receptors (IFNLR) on neighbouring cells which subsequently set off signaling pathways that involves the phosphorylation of STAT1 and STAT2 by janus activated kinases (JAK) (**Figure 1.6**). STAT1 and STAT2 will form a complex with IRF9 and translocate to nucleus and promote the expression of a wide array of interferon-stimulated genes (ISGs) to impede viral replication (**Figure 1.6**) [156, 157]. Several ISGs localize or translocate through the plasma membrane and serve to impede S protein-mediated viral infection as well as syncytia formation (discussed in part 3). It was recently shown that a prenylated membrane-associated isoform of the ISG OAS1 can efficiently detect SARS-CoV-2 is protective against severe COVID-19 disease [158]. As described in previous sections, several of the innate immune signaling pathways are actively antagonized by viral proteins.

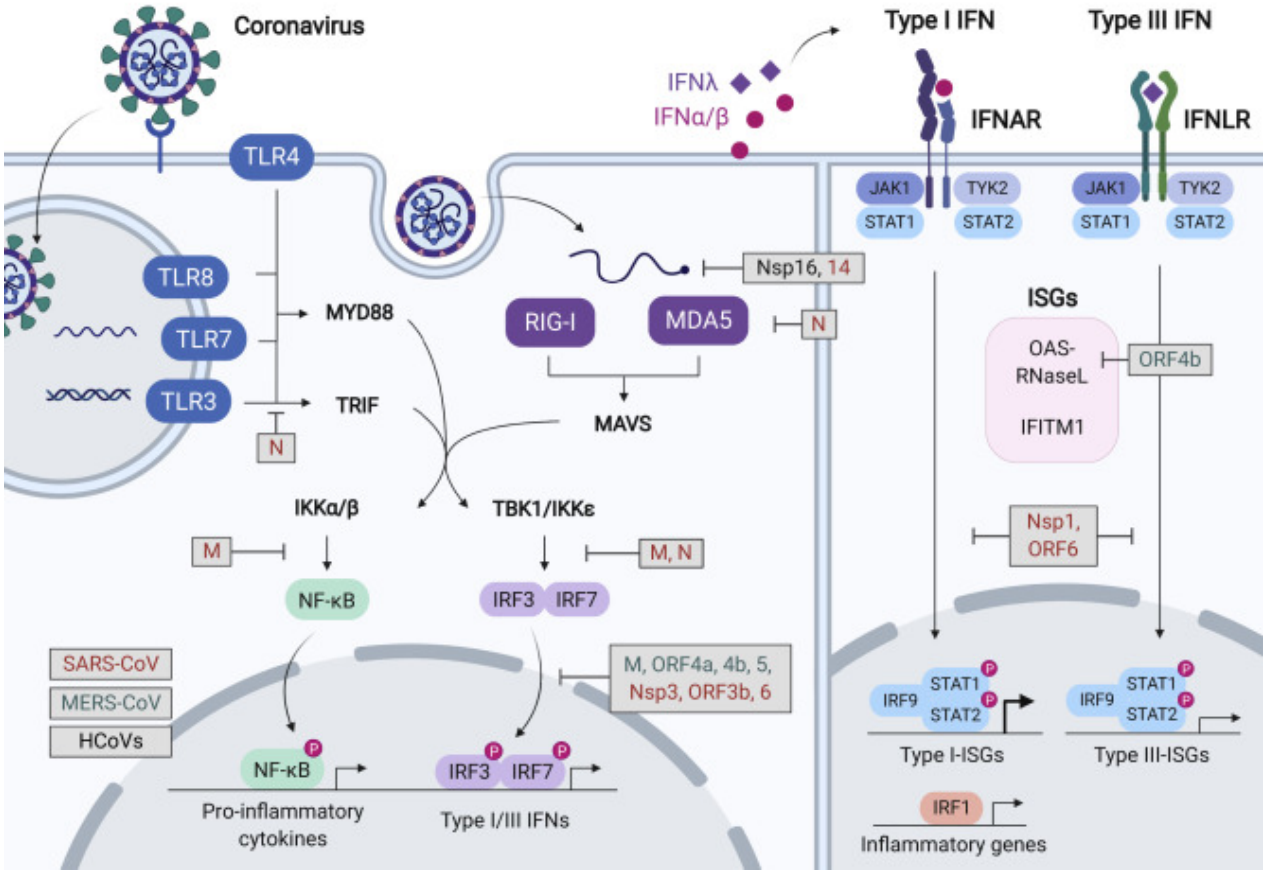

Figure 1.6 The innate immune response to coronavirus infection. Pathogen recognition receptors (TLRs, RIG-I, and MDA5) recognize viral components leading to the transcription of NF-kB, IRF3 and 7, which will subsequently translocate to the nucleus and stimulate cytokine and IFNI/III production. Secreted IFNI/III will be recognized by IFNAR and IFNLR receptors which will set of a signaling pathway that will result in the phosphorylation of the STAT proteins. STAT1 and 2 will complex with IRF9 and translocate to the nucleus to trigger the expression of interferon stimulated genes. Reused with permission from Elsevier. Cell Host & Microbe, Vol 27, Park et al., Page 871, Copyright (2020) [156].doi: https://doi.org/10.1016/j.chom.2020.05.008

Part 3: Syncytia Formation and SARS-CoV-2 S protein-mediated Fusion

1.3.1 Physiological vs Pathological Syncytia formation

Syncytia are large multinucleated cells produced by two or more cells fusing. During syncytia formation, the plasma membranes of different cells merge into a single lipid bilayer and their cytoplasmic contents merge [159, 160]. Many important physiological processes are dependent on cells undergoing syncytialization, including the formation of muscle fibers and the placental barrier as well as bone osteoclast differentiation [160, 161]. The fusion process is facilitated by a class of specialized proteins known as fusogens (in some cases, multiple fusion factors), which help overcome the natural repulsive forces and energetic barriers that act to keep cellular plasma membranes apart [106]. Mechanistically, cell-cell fusion is analogous to virus-cell fusion. Indeed, the membrane of enveloped viruses must fuse with cellular membranes in order for viral contents to be delivered into the cytoplasm, beginning the viral replication cycle. The parallels between the mechanics of physiological cell-cell fusion and virus-cell fusion during infection is appropriately exemplified by the formation of the placenta. The vital placental barrier is formed by a layer of fused cytotrophoblasts called the syncytiotrophoblast [159, 160, 162]. Syncytins, the fusogens that facilitate cytotrophoblast fusion, are derived from the fusogens of endogenous retroviruses (ERV); the genes of which were assimilated into mammalian genomes 10-85 million years ago [162].

Beyond this particular evolutionary association between viruses and cell-cell fusion exists a more immediate causal relationship, in which syncytia are induced as a consequence of viral infection.

In these cases, the viral fusogen may also function to fuse adjacent cells. Syncytia formed in this manner could potentially facilitate viral replication, dissemination, immune evasion as well as cause cytopathic effects and wider tissue damage [163]. The significant differences between physiological and pathological syncytia is that cell-cell fusion under physiological conditions is tightly regulated. For example, during physiological syncytiogenesis, such as in placental trophoblast formation, the cell cycle is arrested at the G0 phase [164]. The expression of the Syncytin-2 (SYN2) fusogen is also restricted to the G0 phase, which allows for strict regulation of the physiological cell-cell fusion process [164]. The transient expression of SYN2 in cells in any other phase (S,G2,M) of the cycle results in the formation of unstable and functionally compromised syncytia [164]. Furthermore, physiological fusion processes like placental formation is controlled through polarized expression of the receptor and fusogen [162]. SYN2 expression is limited to a few cytotrophoblasts, whereas its receptor (major facilitator superfamily domain-containing protein 2) is expressed on syncytiotrophoblasts [162]. In stark contrast, unregulated pathogen-induced syncytia formation, in cells which normally do not fuse, is likely to be pathological.

The most direct example of a syncytiogenic viruses are the non-enveloped reoviruses (e.g. avian orthoreovirus, pteropine orthoreovirus, baboon orthoreovirus, Broome virus, reptilian orthoreovirus and group A aquareovirus) that encode the fusion-associated small transmembrane (FAST) proteins [165]. These fusogens are uniquely specialized cell-cell fusion proteins and they increase pathogenicity and viral dissemination [165, 166]. The existence of such viruses that specifically induce syncytia formation to increase their fitness may suggest that syncytia formation may be beneficial to other viruses. In contrast to the non-enveloped reoviruses, the fusion

machinery of enveloped viruses primarily function to fuse the membrane of viral particles with plasma or endosomal membranes. In particular instances, they may induce infected cells to fuse with adjacent cells. Viruses from a broad range of families including Herpesviridae (varicella-zoster virus, herpes simplex virus 1/2, human cytomegalovirus), Paramyxoviridae (Sendai, Nipah, Hendra, measles virus, respiratory syncytial virus), Retroviridae (human immunodeficiency virus 1, human T-lymphotropic virus) have all been shown to form syncytia *in vivo* and/or *in vitro* [163]. Other virus including some member of the rhabdovirus family can induce syncytia in particular circumstances. For example, the fusion glycoprotein G of the Vesicular stomatitis virus induces cell fusion at an acidic pH [167]. This is a useful feature which is exploited in studies examining the potential of syncytia induction in oncolytic virotherapy [167]. In many cases the syncytia formed by these viruses have a direct and indirect consequences on their pathobiology and on their viral fitness, particularly for dissemination. In the case of HIV-1 infection, the newly synthesized envelope fusogen in an infected cell is trafficked to the plasma membrane where it can interact with receptors on neighboring cells to form syncytia that can further interact with naïve T cells and disseminate virus [168]. Syncytia found in skin lesions is a hallmark of herpes virus infection [163]. The virus uses cell-cell fusion as a mechanism to spread from the mucosal epithelium at the initial site of infection to sensory neuronal cells where it can establish a latent infection [163]. Syncytial cells have also been observed upon infection with some members of the Coronaviridae family including MERS-CoV, the currently pandemic SARS-CoV-2 and to a lesser degree SARS-CoV [163]. The potential consequences of SARS-CoV-2 mediated syncytia formation is discussed in **Chapter 5**.

1.3.2 Syncytia formation: A histopathological feature of coronavirus infection

Most of the described histopathology in SARS-CoV-2 infection is likely related to the immune response; however, virus-induced cytopathic effects may also directly damage the lung tissue while also triggering further immune activation. A peculiar feature noticed in a few clinical reports was the presence of multinucleated pneumocytes. Work by Bussani and colleagues, reported the presence of infected (positive for viral RNA) syncytial pneumocytes in 36/41 patients who died of COVID-19 (**Figure 1.7**) [80, 85]. This observation is supported by several COVID-19 autopsy reports from patients and non-human primate models which also describe the presence of syncytia in infected lung tissue; however, the syncytia present in the macaque model were not positive for N protein staining [169-173]. It should be noted that these clinical observations are from patients presenting the most severe manifestation of COVID-19 disease. It is currently unclear if syncytia formation is also a feature of milder or asymptomatic infections *in vivo*. Autopsy reports conducted on patients who were infected with SARS-CoV-1 and MERS-CoV have also reported the presence of giant multinucleated syncytial cells in the lungs, some of which are of epithelial origin [83, 84, 174-177].

Several of the "common cold" coronaviruses including HKU1, NL63 and 229E form syncytia in cell culture models [178-180]. To our knowledge, there are no documented patient cases of syncytia induced by these widely circulating coronaviruses. This is unsurprising as they are very rarely lethal, so autopsy reports are lacking. More *in vivo* evidence is required to assess the syncytiogenicity of the "common-cold" coronaviruses. It is currently unclear if or how SARS-CoV-2-mediated syncytia formation contributes to pathology; however, it may compound the

detrimental effects of virus-induced cytopathicity and generalized immune-mediated damage and contribute to the deterioration of lung tissue seen in critical cases. Syncytia may also contribute to viral dissemination and immune evasion by protecting the virus from immune cells and from neutralizing antibodies. The current evidence regarding consequences of SARS-CoV-2 mediated syncytia formation is explored in **Chapter 5** (Discussion).

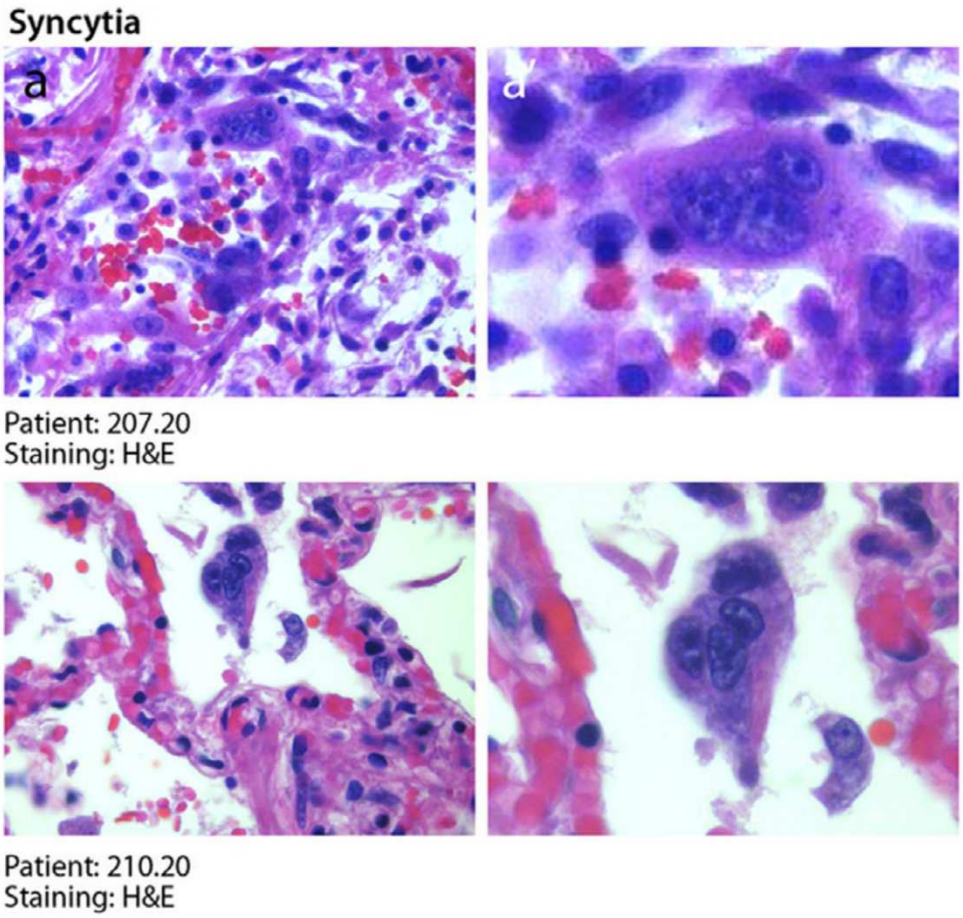

Figure 1.7 Cellular syncytia in the lungs of COVID19 patients. Original image from Figure 4C of Bussani et al., 2020, Persistence of viral RNA, pneumocyte syncytia and thrombosis are hallmarks of advanced COVID-19 pathology (2020) [80], EBioMedicine Vol 61. Reused under creative commons license. https://doi.org/10.1016/j.ebiom.2020.103104.

1.3.3 The Role of the S protein in Syncytia Formation

There have been many investigations into the highly antigenic SARS-CoV-2 Spike (S) protein, which is the viral fusogen. Recent characterizations have provided detailed insights into the properties and domains of the S fusogen and its interaction with receptors. There have also been significant advances in the molecular understanding of the relationship between the SARS-CoV-2 S protein-mediated fusogenicity and the innate immune response. Despite the majority of the genesis and processing of the S protein, as well as viral budding, occurring at intracellular membranes, we and others found that the S protein is present on the surface of infected cells [173, 181]. The interaction of the S protein on the infected cell surface with the ACE2 receptor on neighboring cells is the cause of syncytia formation. This process is further augmented by the presence of the TMPRSS2 protease [181]. The mechanism in which SARS-CoV-2 infected cells form syncytia is explored in **Chapter 2**. The exact role that auxiliary receptors may play in cell-cell fusion remains to be elucidated; however, Daly and colleagues note that knocking out Nrp1 in cells expressing ACE2 is detrimental to syncytia formation [182]. It has been suggested that Nrp1 facilitates earlier separation of the S2 domain, which contains the fusion machinery, by stabilizing the S1 domain [183]. However, prior to any receptor interaction, syncytia formation requires the S protein to be translocated to the plasma membrane. Therein lies the first question regarding the mechanism of SARS-CoV-2 S protein-mediated syncytia formation. If throughout the viral life cycle, the S protein is associated with the intracellular membrane and the virus itself does not bud from the cell surface, how then is the S protein able to localize at the surface?

1.3.3.1 The mechanism of S translocation to the plasma membrane

Many factors act in conjunction to keep the S protein sequestered on the intracellular membrane. In many coronaviruses, the M protein contains a Golgi localization signal and also associates with the S protein, effectively retaining it on intracellular membranes (**Figure 1.8**) [119]. Furthermore, the S protein contains within its cytoplasmic tail a binding site for the cytoplasmic coat protein (COPI), which allows for retrograde transport from the Golgi to the ER and further exposure to M protein-mediated sequestration [119]. The E protein may also induce S retention by slowing down the cell's secretory pathway. The co-expression of M and E with the S protein reduces syncytia formation in cell culture models [119]. A recent investigation by Cattin-Ortolá and colleagues provides relevant mechanistic observation on how the S protein could escape its confines and localize on the cell surface [120]. They suggest that the COPI binding motif of the SARS-CoV-2 S protein tail might be sub-optimal. The presence of a histidine rather than a lysine at residue 1271 as well as threonine at residue 1273 in the S protein contributes to sub-optimal COPI binding and reduced intracellular accumulation (**Figure 1.8**) [120]. Furthermore, the COPI binding site is in close proximity to the COPII (responsible for anterograde transport of protein from ER to Golgi) binding site and replacing the histidine with lysine at residue 1271 also reduced interaction with COPII [120]. This suggests that the S protein might be more prone to exit from the ER (**Figure 1.8**). The co-expression of M and E proteins reduced S surface expression but did not negate it [120]. These lower affinity binding motifs in the S protein cytoplasmic tail allow for the S protein to leak to the cell surface and promote syncytia formation.

1.3.3.2 S protein mediated activation of TMEM16 and phosphatidylserine exposure

A study by Braga and colleagues further provides valuable insights into the mechanism of SARS-CoV-2 induced cell-cell fusion [85]. They screened for inhibitors of S protein-mediated syncytia formation and found that the most effective inhibitors shared the common characteristic of regulating intracellular calcium (Ca^{2+}) levels [85]. They noticed intracellular Ca^{2+} oscillations in individual S-expressing cells and in syncytial cells and they suggest that expression of the S protein amplifies spontaneous Ca^{2+} transients (**Figure 1.8**) [85]. To better understand the relationship between Ca^{2+} fluctuations and syncytia formation, they focused on one of their strongest hits, the anthelminthic drug niclosamide which inhibits the Ca^{2+} activated TMEM16 family of chloride channels and scramblases [85]. The expression of the ubiquitous TMEM16F was increased upon S protein expression [85]. TMEM16F is a non-specific ion channel and a scramblase that translocates phospholipids bidirectionally between the plasma membrane leaflets (**Figure 1.8**). The translocation of specific phospholipids from internal to outer leaflets can serve as a fusion signal [184]. In resting cells, the phosphatidylserine (PS) phospholipid is found on the leaflet facing the cytoplasm. Its translocation to the exofacial leaflet serves as a signal for a variety of cellular processes, including cell-cell fusion [184]. The exposure of PS is associated with a variety of physiological and pathological cell-cell fusion events including skeletal muscle and myoblast formation and repair, macrophage fusion, placental trophoblast fusion, sperm and egg cell fusion during gamete formation, and cancer cell fusion [184]. It is also a marker of cell death through apoptosis. The presence of PS on the viral envelope is important for the entry of viruses including HIV and Ebola and some viruses like alphaherpesvirus induce PS exposure on the host membrane to facilitate infection [184-188]. The translocation of PS may influence the fusogenicity of the

lipid membrane as well as assist in the recruitment and modification of fusion protein (the diverse functions of PS are thoroughly reviewed in [184]). Syncytia formed via S protein-mediated fusion also expose PS on their plasma membrane [85]. The activation of TMEM16F by S protein and the corresponding translocation of PS may represent an important mechanism in which SARS-CoV-2 induces syncytia. It is likely that there may be other mechanisms that facilitate syncytia formation that future studies may elucidate. TMEM16F plays a role in lipid scrambling in platelets during blood coagulation and its activation by S may contribute to the extensive thrombosis in severe cases of COVID-19 [85]. The downregulation or overexpression of TMEM16F results in a corresponding decrease or increase in syncytia formation [85]. Braga et al. also note that the downregulation of TMEM16F does not affect MERS-CoV S protein-mediated syncytia formation [85]. Comparative investigations on this disparity between SARS-CoV-2 S and MERS-CoV S protein in relation to TMEM16F may further elucidate the mechanism of syncytia formation.

1.3.3.3 Summary of the mechanism of S protein-mediated syncytia formation

In brief, the SARS-COV-2 S protein, which is normally sequestered on intracellular membranes, possesses suboptimal COPI binding sites that allow for leakage and translocation to the cell surface. Once at the surface, the S protein interacts with ACE2 and host factors on adjacent cells to induce syncytia. In parallel, the expression of the S protein also affects intracellular Ca^{2+} fluctuations and results in the increased expression of the TMEM16F ion channel and scramblase. TMEM16F translocates PS from the cytofacial leaflet of the plasma membrane to the exofacial leaflet, which promotes the membrane's fusogenic properties (**Figure 1.8**). Since the S protein plays a significant role in fusing together membranes during virus-cell fusion and in syncytia

formation, a more in-depth molecular characterization of its interactions with host factors is warranted. This is the subject of the following section.

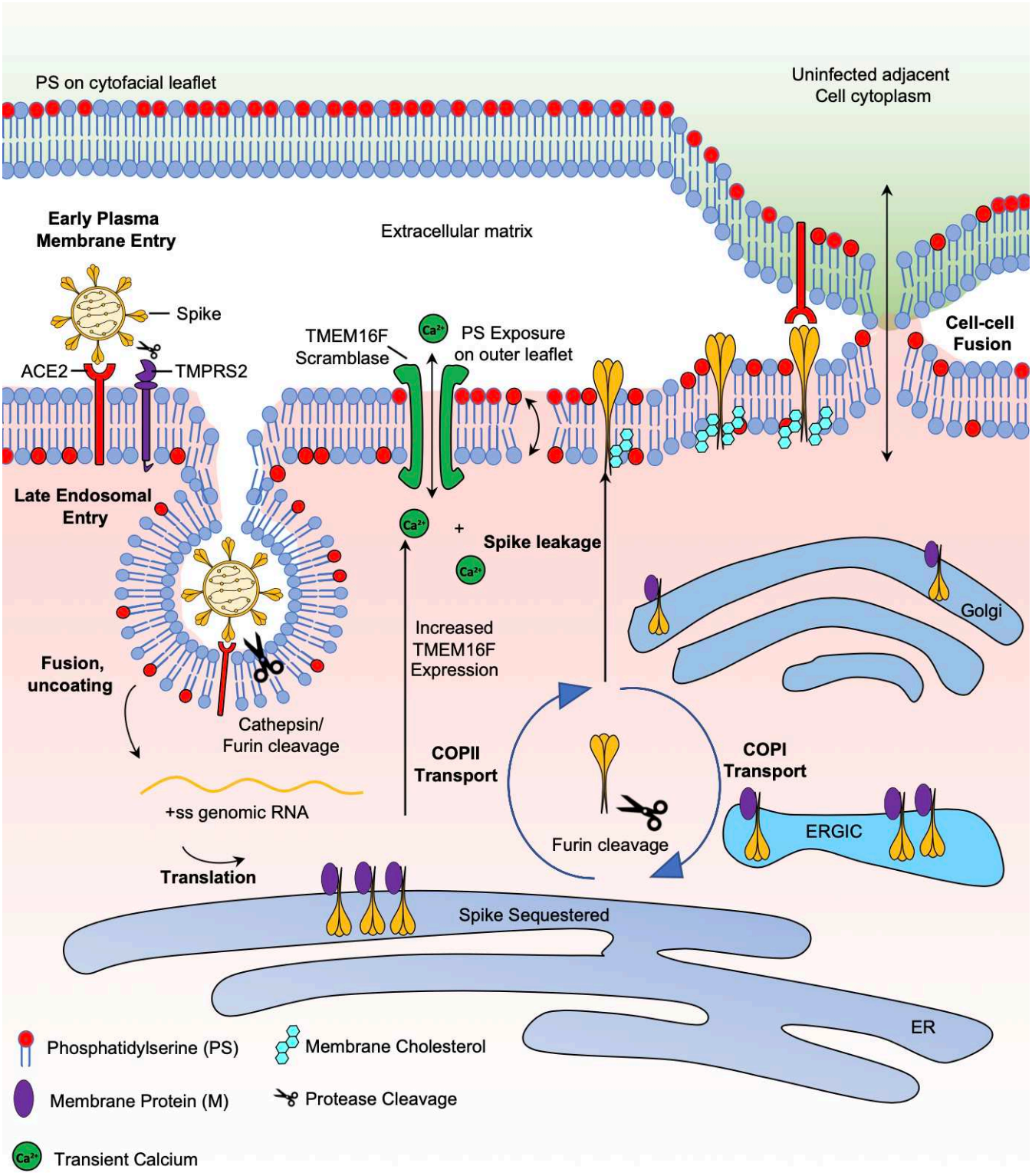

Figure legend on next page

Figure 1.8 Schematic representation of the diverse activities of the SARS-CoV-2 spike (S) protein during infection and syncytia formation. Viral infection begins when the S protein on the surface of the virion interacts with the ACE2 receptor. During early entry, the S protein is processed by the TMPRSS2 protease and fusion occurs on the plasma membrane (PM). The S protein can also fuse with endosomal membranes during late entry, upon being primed by capthespins and furin. The positive-sense single stranded (+ss) viral genomic RNA is deposited in the cytoplasm and translated. Viral RNA replication and transcription occur on intracellular membranes. Upon being transcribed, the S protein is translocated and inserted into the endoplasmic reticulum (ER) and is generally sequestered within intracellular membranes by the membrane structural protein (M). The expression of the S protein leads to intracellular calcium fluctuations and the increased expression of the TMEM16F scramblase. TMEM16F exposes the phosphatidylserine (PS) from the cytofacial leaflet of the PM to the exofacial leaflet. The transcribed S protein is processed by furin and transported throughout the ER-Golgi network. During COPI (retrograde) and COPII (anterograde) transport, leakage of the S protein can occur from vesicles (not shown in simplified schematic). The S protein is then translocated to the PM, where it associates with cholesterols, and induces syncytia formation by interacting with receptors on neighbouring uninfected cells. The sequestered S protein is in packaged into virions that bud into the Golgi or ER-Golgi intermediate compartment (ERGIC), and virions exit the cell via deacidified lysosome-dependent exocytosis (not shown). The ER, ERGIC, and Golgi membranes are bilayers which are represented as single lines in this schematic. Figure generated by the author and submitted to the Journal of Molecular Biology in an invited review article [1]. Rights retained to use figure in thesis or dissertation. Original source: Elsevier. Journal of Molecular Biology, Rajah et al., 2021.
doi: https://doi.org/10.1016/j.jmb.2021.167280

1.3.4 Modulation of S-mediated fusion by membrane-altering host factors

Restriction and enhancement factors play a complex role in regulating viral infection. Several key host factors are membrane-bound and operate at the entry and fusion step of the viral life cycle. This section will examine the role of key membrane-bound restriction and enhancement factors on S protein-mediated fusion and syncytia formation.

1.3.4.1 IFITMs

One such group of host factors are the family of ISGs called the interferon-induced transmembrane (IFITM) proteins. Functional IFITMs can be further categorized into three clades and despite the

nomenclature only members of clade 1, – IFITM1, 2 and 3 as well as the mouse specific IFITM6 and 7 – are truly IFN induced, ubiquitously expressed and possess bona fide innate immune activity [189]. IFITMs restrict a broad spectrum of enveloped viruses including influenza, HIV-1, Ebola, Marburg, dengue, Zika, West Nile, Japanese encephalitis, Rift Valley Fever as well as members of the coronavirus family [190-192].

IFITM1 localizes on the plasma membrane, while IFITM2 and 3 both transit through the plasma membrane and then localize within the endo-lysosomal compartments. IFITMs prevent viruses from crossing the cellular membrane and accessing the cytoplasm, possibly by altering the rigidity and the curvature or the composition of the membrane [190, 192-194]. This serves to increase the energetic barrier for fusion, hindering virus-cell fusion at hemi fusion or pore formation stage [195, 196]. In the case of coronaviruses, IFITMs block the entry of MERS-CoV, SARS-CoV-1, NL63 and 229E [197-199]. However, the interaction between IFITMs and coronavirus S protein-mediated fusion is complex. Work by Zhao and colleagues demonstrated that OC43 uses IFITM2 and 3 as entry factors to facilitate infection [200]. Furthermore, they also identified mutations within the IFITM1 and 3 that can convert them from inhibitors of MERS-CoV and SARS-CoV-1 S mediated entry, into enhancers [199]. The contradictory effects of IFITMs and their mutations on different coronaviruses may be factors of how and where they interact with the different cellular receptors [199].

There have been several reports examining the role of IFITMs on SARS-CoV-2 S mediated fusion. Work by Shi and colleagues show that IFITM1, 2 and 3 are restriction factors of SARS-CoV-2 infection, with IFITM1 being particularly potent [192]. Another study using pseudotyped lentiviral

vectors expressing SARS-CoV-2 S protein found that IFITM2 was the most potent inhibitor of entry and that the polybasic S1/S2 cleavage site makes S protein particularly sensitive to IFITM2 [201]. Shi et al. also suggest that restriction by IFITM3 is independent of its palmitoylation, a post-translation modification thought to affect hydrophobicity and location of IFITM3 to membrane compartments [192, 202]. Since the palmitoylation site is necessary for the antiviral activity of IFITM3 against influenza A virus, 229E and NL63, this may suggest that the restriction of SARS-CoV-2 infection at the endosome may occur in a different manner [192, 199, 202]. Shi et al. confirm that the amphipathic helix domain within the hydrophobic region of IFITM3, is necessary for restricting S mediated fusion. The amphipathic helix is believed to insert into membrane bilayers and mechanically induce a curvature and rearrange lipids in a manner that antagonizes fusion [195, 203-205]. One investigation suggests that endogenous IFITMs in human lung cells may on the contrary, facilitate SARS-CoV-2 infection [206]. The authors proposed that IFITMs interact with the S protein and that reduction of endogenous IFITMs drastically impedes viral replication [206]. They also found that IFN- β enhanced SARS-CoV-2 infection in small airway epithelial cells [206]. The discrepant observations might be a result of the different IFITM expression systems or cell culture models. Further investigations examining the relationship between IFITMs and SARS-CoV-2 are warranted.

SARS-CoV-2 mediated syncytia formation is effectively restricted by IFITMs, with IFITM1 displaying the most potent activity. We reported that restriction of syncytia formation by IFITMs is subject to reversion by TMPRSS2 (**Chapter 2**) [181]. TMPRSS2 drastically augmented S protein-mediated syncytia formation, whether IFITMs were present or absent [181]. This protease also increases infection by SARS-CoV-2 and reverts the inhibitory effect of IFITMs on viral

infection [192]. Studies on other coronaviruses have also found that TMPRSS2 thwarts the antiviral effects of IFITMs [207, 208]. Of note, we also observed that syncytia induced by the S proteins of D614G, Alpha, and Beta variants are effectively restricted by IFITMs (**Chapter 3**) [209].

1.3.4.2 LY6E

Other membrane-bound restriction factors impact S-protein mediated syncytia formation. The IFN inducible Lymphocyte antigen 6 complex locus E (LY6E) is a glycosylphosphatidylinositol (GPI)-anchored protein that associates with membrane lipid rafts [210, 211]. LY6E is a pro-viral factor that promotes the uptake of Yellow Fever virus, the uncoating of influenza A, and HIV-1 infection of high CD4-expressing cells [211-213]. It is also a receptor for endogenous retroviruses. However, LY6E is an inhibitor of OC43, 229E, SARS-CoV-1, SARS-CoV-2, and MERS-CoV infection and associated syncytia formation [214, 215]. The precise mechanism by which LY6E inhibits membrane fusion is not clear [214]. It does not affect S protein maturation or expression of surface receptors [214]. The GPI-anchor associates LY6E to lipid rafts is crucial to its activity. Lipid rafts are cholesterol and glycosphingophospholid rich regions in the plasma membrane that compartmentalize important processes including ligand receptor engagements. The mechanism by which LY6E exerts its restriction is likely different than that of IFITMs. The antifungal drug amphotericin B (AmphoB), which binds cholesterol in the plasma membrane and increases it fluidity, can rescue restriction by IFITMs but not LY6E[215]. Understanding the precise method by which LY6E mediates fusion remains a major question.

1.3.4.3 CH25H

Recently, the ISG Cholesterol 25-hydroxylase (CH25H) has been described as an inhibitor of SARS-CoV-2 membrane fusion [216, 217]. CH25H is induced by SARS-CoV-2 infection and converts cholesterol into 25-hydrocholersterol (25CH) [216]. 25CH inhibits viral-cell fusion by depleting fusion accessible plasma membrane cholesterol through the activation of acyl-CoA: cholesterol acyltransferase (ACAT) localized on the ER membrane [216]. CH25H expression also significantly reduces SARS-CoV-2 S protein-mediated syncytia formation [217]. These observations further emphasize the significance of cholesterol access to S protein-mediated fusion.

In summary, a few important ISGs act to antagonize SARS-CoV-2 S mediated cell-cell fusion by altering the target membranes. IFITMs likely restrict syncytia formation by altering the biomechanical properties of the plasma membrane, whereas LY6E does so through an unknown mechanism. CH25H facilitates the depletion of membrane cholesterol and the compositional change is also unfavorable to cell-cell fusion. Molecular mechanisms by which ISGs inhibit virus-cell and cell-cell fusion remain a pertinent field in understanding SARS-CoV-2 induced pathology.

Research Objectives

Syncytia formation can have an impact on viral pathology by facilitating cell-to-cell dissemination, inducing cytopathic and inflammatory responses and by shielding replicating virus from neutralizing antibodies and immune cells. The coronavirus S protein is a viral fusogen that mediates viral entry by interacting with the cellular receptors. This interaction allows for the merging of the viral membrane with the host cell's plasma membrane and the subsequent deposition of viral contents into the cytoplasm. Interestingly, several reports identified the presence infected multinucleated syncytial cells in the lungs of patients with severe COVID-19 disease. Here, we endeavored to characterize the mechanism of SARS-CoV-2 induced syncytia formation. We hypothesized that SARS-CoV-2 induced cell-cell fusion would be analogous to viral entry and would require the interaction of the S protein with host receptors and can be differentially modulated by various host factors.

Our first objective (**Chapter 2**) was to characterize how SARS-CoV-2 infected cells form syncytia by examining the interplay between the SARS-CoV-2 S protein, human ACE2 receptor and the human TMPRSS2 protease. We also studied the impact of IFITMs, a group of membrane-altering restrictions factors, on virus induced syncytia formation.

As the pandemic progressed, SARS-CoV-2 variants with several mutations within the antigenic S protein emerged and spread around the world. Our second objective (**Chapter 3)** was to characterize the fusogenicity of the S proteins of the Alpha, Beta and Delta variants relative to the early European D614G strain and the ancestral Wuhan strain. We then used a mutagenic approach

to characterize the contribution of each of the individual mutations associated with the Alpha and Beta variants in terms of their fusogenicity, capacity for antibody escape and ACE2 binding potential.

Finally, we employed our syncytia formation reporter system to provide a preliminary characterization of the S protein of the neglected hCoV-HKU1 common cold coronavirus (**Chapter 4**). We further identify some modulatory host factors that affect HKU1 S-mediated fusion, which paves the way for further investigations and comparative studies.

Chapter 2: Syncytia Formation by SARS-CoV-2 Infected Cells

Preface to Chapter 2:

The article presented in this chapter was published in The EMBO Journal in 2020 and is reproduced here with permission from EMBO (see permissions).

Buchrieser J*, Dufloo J*, Hubert M*, Monel B*, Planas D*, **Rajah MM* (Co-first author),** Planchais C, Porrot F, Guivel-Benhassine F, Van der Werf S, Casartelli N, Mouquet H, Bruel T & Schwartz O "Syncytia formation by SARS-CoV-2-infected cells" (2020) **The EMBO Journal**, 39(23):e106267. https://doi.org/10.15252/embj.2020106267.

*co-first authors

This project was the result of a group effort by our team at the start of the pandemic. Amidst the first national lockdown and laboratory closures at the Institut Pasteur everyone switched projects and came together to work on this article. I present this article with full acknowledgment of the work conducted by my co-authors Julian Buchrieser, Jeremy Dufloo, Mathieu Hubert, Blandine Monel, Delphine Planas and all of our other colleagues and collaborators. My contributions included the production of SARS-CoV-2 constructs, fusion experiments as well as revisions and manuscript rewrites upon peer-review. My specific experimental contributions include work on IFITMs and fusion (Figure 3A-C; Figure EV6 A-C) as well as the infection and transfection experiments using natural ACE2 expressing cell (Figure EV5). These experiments were done with and under the supervision of Julian Buchrieser. My pre-pandemic work on Zika virus is presented in the supplemental chapter.

Synopsis

Research Objective:

To understand the mechanism of SARS-CoV-2 mediated cell-cell fusion and characterize the role of the TMPRSS2 and IFITMs on syncytia formation.

Highlights:

- The interaction of S protein on the plasma membrane of an infected cell with the ACE2 receptor on neighbouring cells results in syncytia formation
- TMPRSS2 augments syncytia formation while IFITMs (particularly IFITM1) hampers it
- IFITM mediated restriction is subverted by the presence of TMPRSS2

Graphical Abstract 1 Syncytia formation by SARS-CoV-2-infected cells

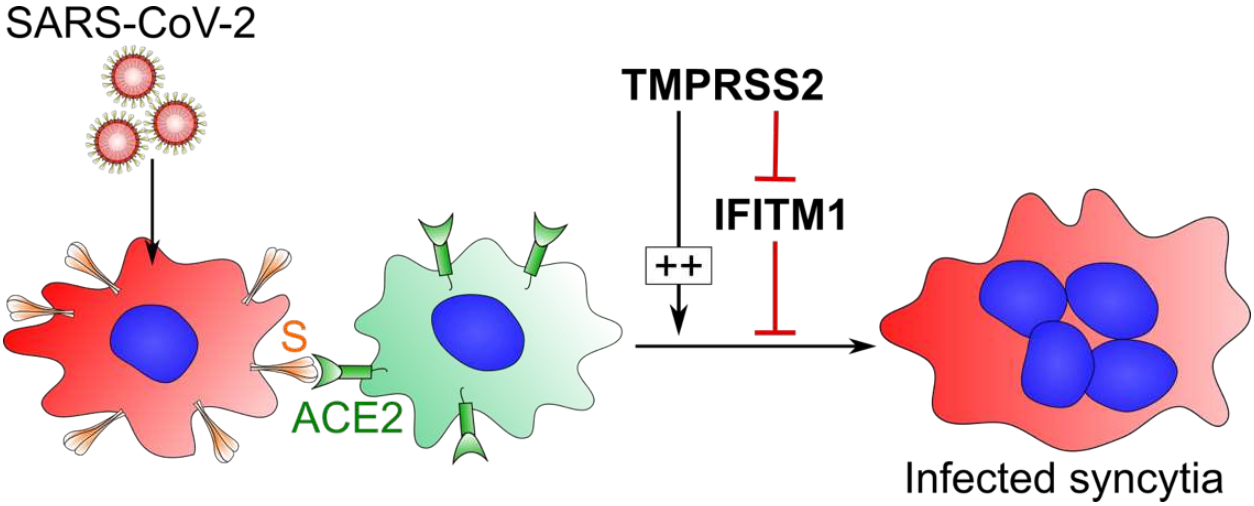

Article

SOURCE DATA | TRANSPARENT PROCESS

THE EMBO JOURNAL

Syncytia formation by SARS-CoV-2-infected cells

Julian Buchrieser[1,2,†], Jérémy Dufloo[1,2,3,†], Mathieu Hubert[1,2,†], Blandine Monel[1,2,†], Delphine Planas[1,2,4,†], Maaran Michael Rajah[1,2,3,†], Cyril Planchais[5], Françoise Porrot[1,2], Florence Guivel-Benhassine[1,2], Sylvie Van der Werf[6,7], Nicoletta Casartelli[1,2], Hugo Mouquet[5], Timothée Bruel[1,2] & Olivier Schwartz[1,2,4,*]

Abstract

Severe cases of COVID-19 are associated with extensive lung damage and the presence of infected multinucleated syncytial pneumocytes. The viral and cellular mechanisms regulating the formation of these syncytia are not well understood. Here, we show that SARS-CoV-2-infected cells express the Spike protein (S) at their surface and fuse with ACE2-positive neighboring cells. Expression of S without any other viral proteins triggers syncytia formation. Interferon-induced transmembrane proteins (IFITMs), a family of restriction factors that block the entry of many viruses, inhibit S-mediated fusion, with IFITM1 being more active than IFITM2 and IFITM3. On the contrary, the TMPRSS2 serine protease, which is known to enhance infectivity of cell-free virions, processes both S and ACE2 and increases syncytia formation by accelerating the fusion process. TMPRSS2 thwarts the antiviral effect of IFITMs. Our results show that SARS-CoV-2 pathological effects are modulated by cellular proteins that either inhibit or facilitate syncytia formation.

Keywords fusion; interferon; SARS-CoV-2; syncytia
Subject Category Immunology
DOI 10.15252/embj.2020106267 | Received 17 July 2020 | Revised 6 October 2020 | Accepted 8 October 2020 | Published online 4 November 2020
The EMBO Journal (2020) 39: e106267

Introduction

COVID-19 consists of a spectrum of syndromes from a mild, flu-like illness to severe pneumonia. Disease severity is linked to lung epithelial destruction, resulting from both immune-mediated damages and viral cytopathic effects. SARS-CoV-2 infection of respiratory epithelial cells likely activates monocytes, macrophages, and dendritic cells, resulting in secretion of proinflammatory cytokines (Huang *et al*, 2020; Ong *et al.*, 2020; Zhou *et al*, 2020). Excessive systemic cytokine production may lead to thrombosis, hypotension, acute respiratory distress syndrome (ARDS), and fatal multi-organ failure. The innate type-I and type-III interferon (IFN) response, which normally controls viral replication is also reduced in severe cases (Blanco-Melo *et al*, 2020; preprint: Hadjadj *et al*, 2020; Park & Iwasaki, 2020). However, prolonged IFN-production aggravates disease by impairing lung epithelial regeneration (Broggi *et al*, 2020; Major *et al*, 2020). In the lung, SARS-CoV-2 infects ciliated cells in the airway, alveolar type 2 pneumocytes, and epithelial progenitors among others (Bost *et al*, 2020; Hou *et al*, 2020; Subbarao & Mahanty, 2020). SARS-CoV-2 and other coronaviruses are cytopathic (Freundt *et al*, 2010; preprint: Gorshkov *et al*, 2020; Ogando *et al*, 2020; Ren *et al*, 2020; Tang *et al*, 2020). The death of infected cells is also a trigger of immune activation.

SARS-CoV-2 entry into cell is initiated by interactions between the spike glycoprotein (S) and its receptor, angiotensin-converting enzyme 2 (ACE2), followed by S cleavage and priming by the cellular protease TMPRSS2 or other surface and endosomal proteases (Letko *et al*, 2020; Matsuyama *et al*, 2020; Hoffmann *et al*, 2020b). The structure of S in complex with ACE2 has been elucidated (Lan *et al*, 2020; Walls *et al*, 2020; Wang *et al*, 2020). S consists of three S1-S2 dimers, displaying conformational changes upon virus entry leading to fusion. Besides fusion mediated by virions, S proteins present at the plasma membrane can trigger receptor-dependent syncytia formation. These syncytia have been observed in cell cultures and in tissues from individuals infected with SARS-CoV-1, MERS-CoV, or SARS-CoV-2 (Franks *et al*, 2003; Matsuyama *et al*, 2010; Chan *et al*, 2013; Qian *et al*, 2013; preprint: Giacca *et al*, 2020; Hoffmann *et al*, 2020a; Tian *et al*, 2020; Xu *et al*, 2020), but they were not precisely characterized. It has been proposed that they may originate from direct infection of target cells or from the indirect immune-mediated fusion of myeloid cells. Fused pneumocytes expressing SARS-CoV-2 RNA and S proteins were observed in

1 Virus and Immunity Unit, Department of Virology, Institut Pasteur, Paris, France
2 CNRS-UMR3569, Paris, France
3 Bio Sorbonne Paris Cité (BioSPC), Université de Paris, Paris, France
4 Vaccine Research Institute, Créteil, France
5 Laboratory of Humoral Immunology, Department of Immunology, Institut Pasteur, INSERM U1222, Paris, France
6 Molecular Genetics of RNA Viruses, Department of Virology, Institut Pasteur, CNRS UMR 3569, Université de Paris, Paris, France
7 National Reference Center for Respiratory Viruses, Institut Pasteur, Paris, France
*Corresponding author. Tel: +33 145688353; E-mail: olivier.schwartz@pasteur.fr
†These authors contributed equally to this work as first co-authors

© 2020 The Authors

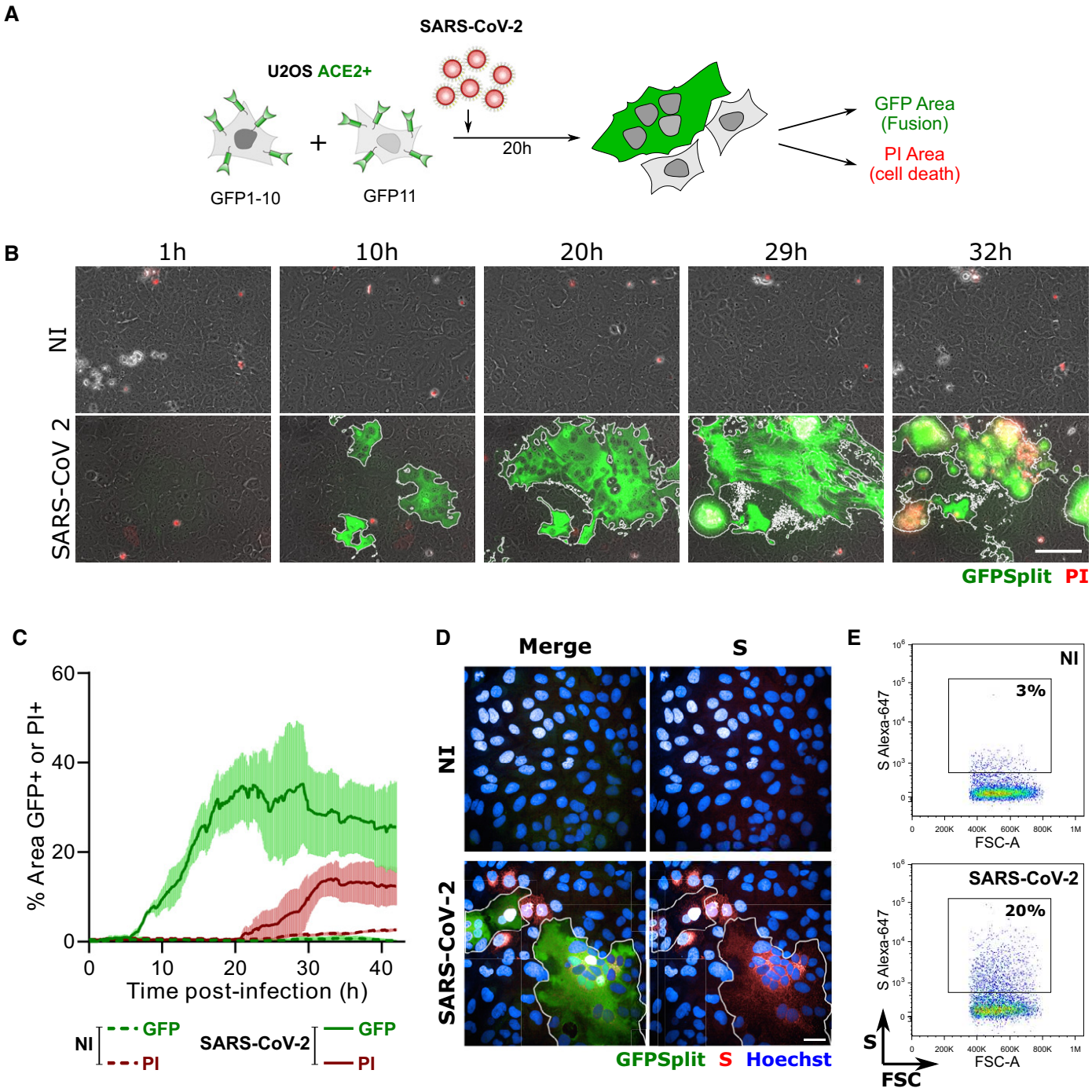

Figure 1. SARS-CoV-2 induced syncytia formation.

A GFP-Split U2OS-ACE2 were co-cultured at a 1:1 ratio and infected with SARS-CoV-2. Syncytia formation and cell death was monitored by video microscopy or at endpoint using confocal microscopy and high-content imaging.

B Still images of GFP (syncytia) and propidium iodide (PI) (cell death) at different time points. Scale bar: 100 μm.

C Quantification of U2OS-ACE2 fusion and death by time-lapse microscopy. Results are mean ± SD from three fields per condition.

D S staining of infected U2OS-ACE2 cells analyzed by immunofluorescence. The Hoechst dye stains the nuclei. Scale bar: 40 μm.

E Surface S staining of infected U2OS-ACE2 cells analyzed by flow cytometry. Results are representative of at least three independent experiments.

post-mortem lung tissues of 20 out of 41 COVID-19-infected patients, indicating that productive infection leads to syncytia formation, at least in critical cases (preprint: Giacca *et al*, 2020).

SARS-CoV-2 replication is in part controlled by the innate host response, through mechanisms that are currently being unveiled. Interferon-stimulated genes (ISGs) inhibit discrete steps of the viral

© 2020 The Authors

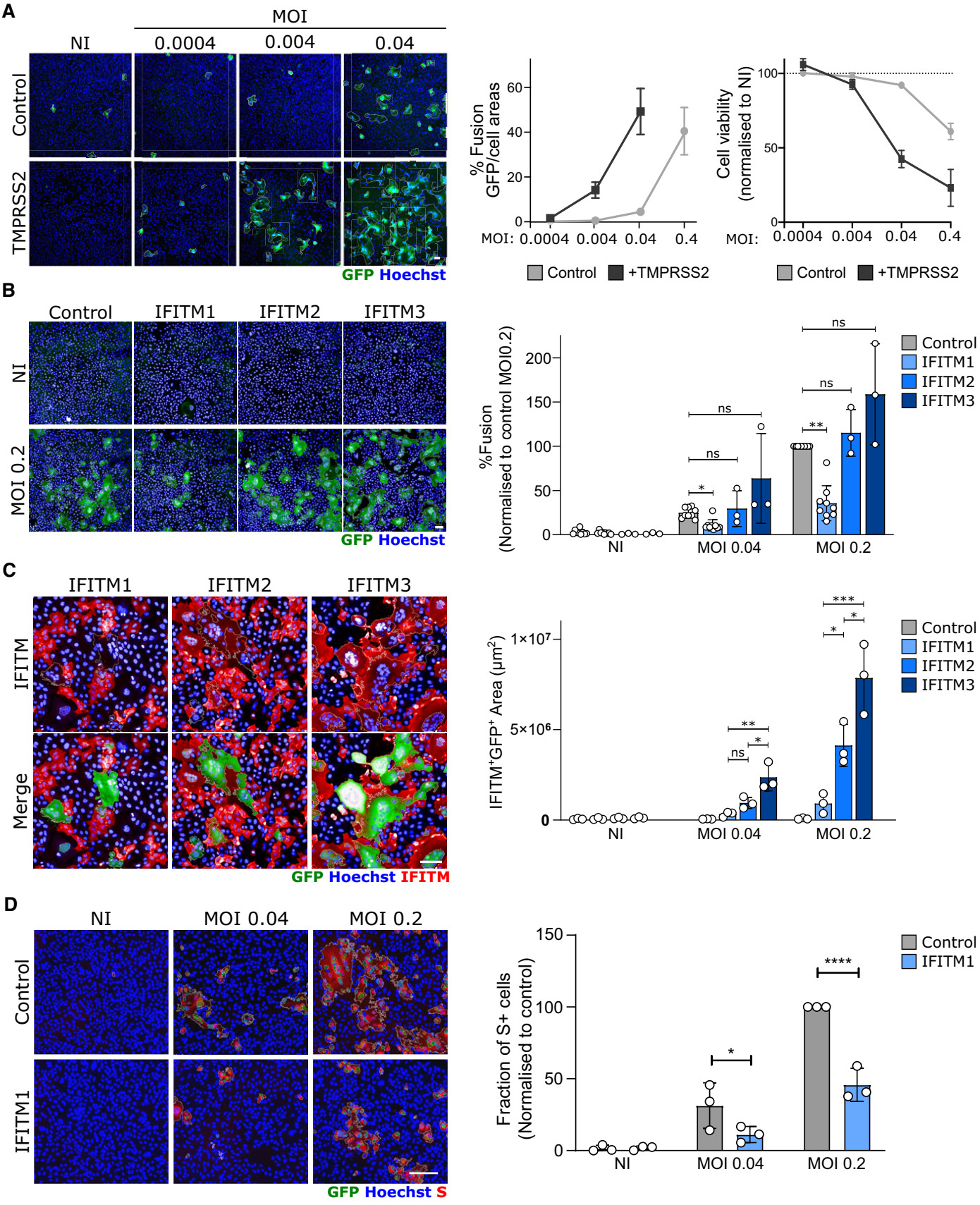

Figure 2.

© 2020 The Authors

Figure 2. Impact of TMPRSS2 and IFITMs on syncytia formation by U2OS-ACE2-infected cells.

Cells were infected at the indicated multiplicity of infection (MOI) and analyzed after 20 h. Image quantification method is described in Fig EV2.

A TMPRSS2 increases fusion and cell mortality. Right panel: Areas of GFP^+ cells and nuclei count normalized to NI.

B IFITM1, but not IFITM2 and 3, inhibits SARS-CoV-2-induced syncytia formation. Right panels: Area of GFP^+ cells

C The fusion of $IFITM1^+$ cells with U2OS-ACE2 syncytia is drastically reduced. Right panel: Area of $IFITM^+$ GFP^+ cells

D IFITM1 decreases the number of infected cells. Right panel: Fraction of cells positive for S, normalized to control cells (transduced with pQCXIP-empty vector).

Data information: Left panels: one representative experiment is shown. Scale bars: 100 μm. Right panels: Data are mean ± SD of 3–9 independent experiments. Statistical analysis: B–C: One-way ANOVA, D: Two-way ANOVA. ns: non-significant, *P < 0. 05, **P < 0.01, ***P < 0.001, ***P < 0.0001.

life cycle. At the entry level, the interferon (IFN)-Induced Transmembrane proteins (IFITM1, IFITM2, or IFITM3) block many viruses by inhibiting virus–cell fusion at hemifusion or pore formation stages (Shi *et al*, 2017). IFITMs act by modifying the rigidity and/or curvature of the membranes in which they reside (Abdel Motal *et al*, 1993; Compton Alex *et al*, 2014; Shi *et al*, 2017; Zani & Yount, 2018). Due to different sorting motifs, IFITM1 is mostly found at the plasma membrane, whereas IFITM2/3 accumulates in the endo-lysosomal compartment after transiting through the surface. IFITMs inhibit SARS-CoV, 229E, and MERS-CoV entry, but promote infection by HCoV-OC43, a coronavirus that causes the common cold (Huang *et al*, 2011; Bertram *et al*, 2013; Warren *et al*, 2014; Wrensch *et al*, 2014; Zhao *et al*, 2014; Zhao *et al*, 2018). IFITMs, as well as other ISGs, including LY6E and Cholesterol 25-hydrolase (CH25H), impair SARS-CoV-2 replication by blocking the fusion of virions (Pfaender *et al*, 2020; preprint: Zang *et al*, 2020; Zhao *et al*, 2020). Most of the experiments regarding these ISGs have been performed with single-cycle viral pseudotypes. Little is known about the impact of IFITMs on SARS-CoV-2-induced syncytia formation.

Here, we characterized the mechanisms of SARS-CoV-2-induced cell–cell fusion and examined how syncytia formation is impacted by IFITMs and TMPRSS2.

Results

Syncytia formation by SARS-CoV-2-infected cells

We first examined whether SARS-CoV-2-infected cells may form syncytia. To this aim, we derived U2OS cells stably expressing ACE2. We selected this cell line because its flat shape facilitates imaging. We generated U2OS-ACE2 cells carrying a GFP–Split complementation system (Buchrieser *et al*, 2019), in which two cells separately produce half of the reporter protein, producing GFP only upon fusion (Fig 1A). These U2OS-ACE2-derived cells, that we termed "S-Fuse" cells, were exposed to various doses of SARS-CoV-2. Video-microscopy analysis showed that syncytia appeared rapidly, starting at 6 h post-infection and grew in size, as bystander cells are incorporated in fused cells (Fig 1B and C and Movie EV1). Most of the syncytia end up dying, as assessed by the acquisition of propidium iodide (PI) (Fig 1B and C and Movie EV1). The extent of fusion was then quantified by measuring the GFP^+ area with a high-content imager. The total area of syncytia within each well correlated with the viral inoculum, indicating that the assay provides a quantitative assessment of viral infection (Fig 2A). S was expressed by the syncytia, but also by single infected cells that have not yet fused, as assessed by immunofluorescence (Fig 1D). Flow cytometry on unpermeabilized infected cells further showed that S was present at the surface (Fig 1E).

Impact of IFITMs and TMPRSS2 on syncytia formation

We then asked whether TMPRSS2 and IFITM1, IFITM2, and IFITM3 impact syncytia formation. We generated S-Fuse cells stably producing each of the four proteins. Their expression was verified by flow cytometry or Western blotting (Fig EV1). We then compared their sensitivity to SARS-CoV-2 infection. The presence of TMPRSS2 increased the appearance of fused cells by 5- to 10-fold (Fig 2A). On the contrary, IFITM1 significantly inhibited syncytia formation (Fig 2B and Movie EV1). Therefore, TMPRSS2 and IFITM1 exert opposite effects on syncytia formation. IFITM2 and 3 were poorly active (Fig 2B), probably because they mostly accumulate within the endosomal compartment, which limits their ability to alter fusion events occurring at the plasma membrane. Since only 40% of each cell population expressed high levels of IFITM, as assessed by flow cytometry (Fig EV1) and immunofluorescence (Fig 2C), we asked whether $IFITM^+$ cells were present in the syncytia. A co-staining with anti-IFITM antibodies indicated that syncytia did not incorporate $IFITM1^+$ cells present in the culture, whereas this was not the case for IFITM2 and 3 (Figs 2C and EV3). Moreover, the inhibitory effect of IFITM1 on syncytia was associated a decreased number of S^+ cells (Fig 2D).

We next assessed whether other cell types form syncytia upon SARS-CoV-2 infection. To this aim, we used 293T cells transiently transfected with ACE2 and also generated stable A549-ACE2 cells. The two cell lines readily formed syncytia upon infection (Fig EV4A and B). In order to rule out the possibility that syncytia formation is solely dependent on ACE2 over-expression, we investigated the naturally permissible Vero cells with the GFP-split system. We did not detect fused infected Vero cells (Fig EV5A); thus, we used as donors U20S-ACE2-infected cells that we co-cultivated with uninfected Vero cells. Numerous heterocellular syncytia were formed in a short period of time (8 h) (Fig EV5D). The ability of Vero cells to fuse was again confirmed when donor 293T cells were transfected with S and co-cultivated with Vero E6 acceptor cells (Fig EV5C). Additionally, Vero cells are also capable of forming syncytia upon transfection of only the S protein (Fig EV5B). Of note, Caco2 cells did not fuse upon SARS-CoV-2 infection (Fig EV4C). Taken together, our data strongly suggest that the ability to form syncytia upon SARS-CoV-2 infection is dependent on cell type as well as on the surface levels of S and ACE2. Fusion is detected in Vero cells with endogenous levels of ACE2.

Syncytia formation by S-expressing cells

We further characterized the mechanisms of fusion and its regulation by IFITMs and TMPRSS2. We asked whether S alone was

 © 2020 The Authors

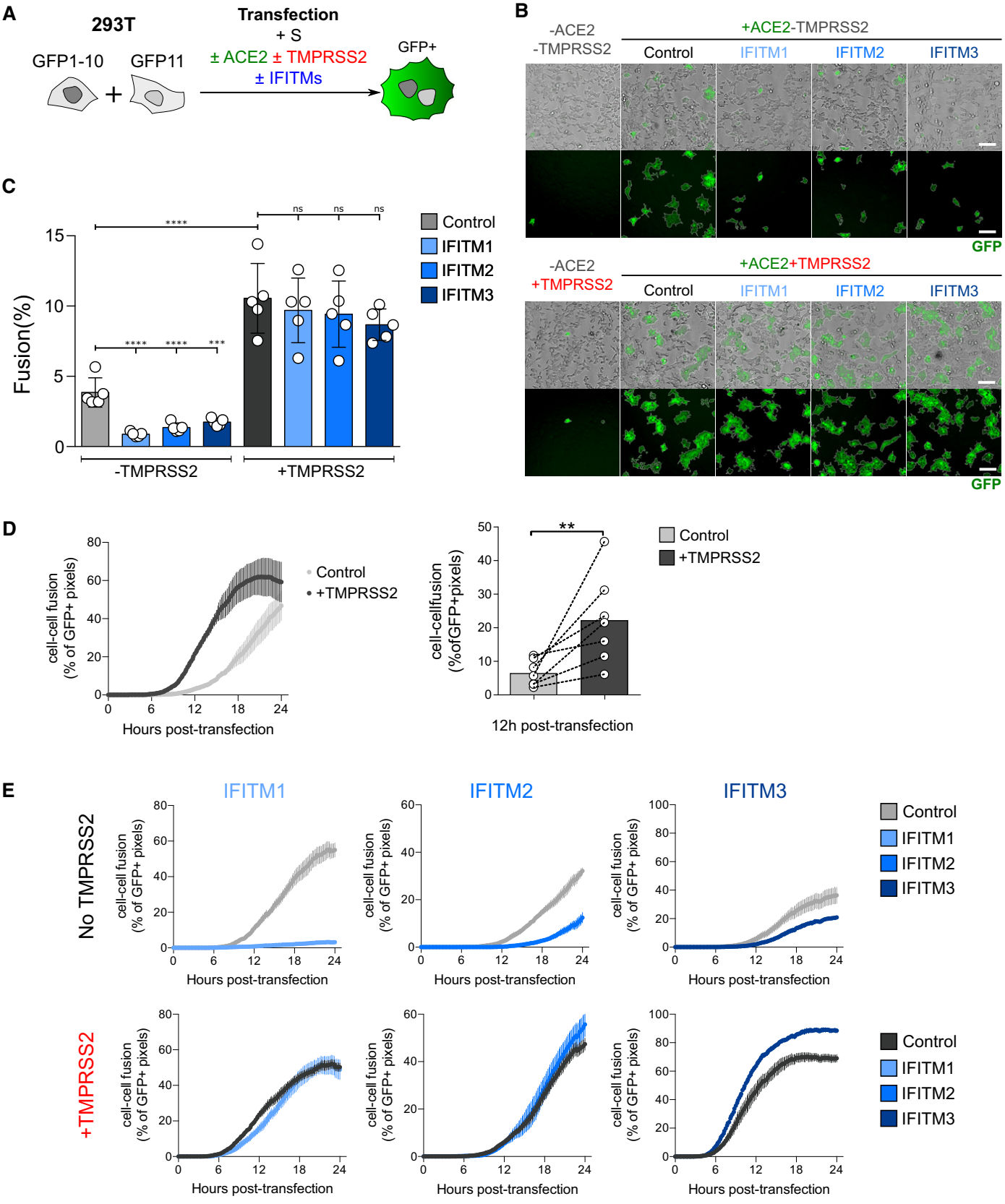

Figure 3.

© 2020 The Authors

Figure 3. Impact of TMPRSS2 and IFITMs on the kinetics of fusion by S-expressing 293T cells.

A 293T-GFP1-10 and -GFP11 cells (1:1 ratio) were co-transfected with S, ACE2, TMPRSS2, IFITM, or control plasmids. Cell fusion was quantified by measuring the GFP^+ area by high-content imaging after 18 h. (B and C) or analyzed over time by video microscopy (D and E).

B Representative images of cell–cell fusion. Scale bar: 100 μm.

C Quantification of GFP^+ areas. Results are mean ± SD from five independent experiments.

D TMPRSS2 accelerates fusion. Cells were monitored by video microscopy, and the GFP area was quantified over time. Left panel: one representative experiment. Results are mean ± SD from three fields per condition. Right panel: Mean ± SD from seven independent experiments (at 12 h post-transfection).

E Impact of TMPRSS2 and IFITMs on the kinetics of fusion by S-expressing 293T cells. One representative out of three independent experiment is shown.

Data information: Statistical analysis: B, C: One-way ANOVA, ns: non-significant, ***$P < 0.001$, ****$P < 0.0001$. D: Wilcoxon matched-pairs signed-rank test, **$P < 0.01$.

sufficient to trigger fusion by transfecting an expression plasmid in 293-T cells harboring the GFP-Split system (Fig 3A). Many large and multinucleated GFP^+ cells were detected, when ACE2 was co-expressed (Fig 3B). S-mediated cell fusion was significantly decreased when cells were co-transfected with flag-tagged IFITM1, 2, or 3 plasmids, compared with a control plasmid (Fig 3B and C). IFITM1 was slightly more inhibitory than IFITM2 and 3 in this system. The transient expression of TMPRSS2 enhanced fusion by 2.5-fold. Interestingly, when the serine protease was present, the inhibitory effect of IFITMs was no longer visible (Fig 3B and C). The anti-fusogenic effect of IFITM1 varied with the amount of transfected IFITM1 plasmid, but TMPRSS2 counteracted IFITM1 at all doses (Fig EV6A–C). We next measured the kinetics of S-mediated cell fusion by live video-microscopy, monitoring in real-time the GFP^+ area. TMPRSS2 accelerated the appearance of GFP^+ cells, indicating that it increases the speed of cell–cell fusion (Movie EV2 and Fig 3D). At 12 h post-transfection, the syncytia area was already fourfold larger than in the control condition (Fig 3D). A similar kinetic analysis indicated that IFITM1 strongly inhibited fusion, whereas IFITM2 and IFITM3 were less efficient (Fig 3E). In the presence of TMPRSS2, the rapid fusion kinetics were similar with or without IFITMs (Fig 3E).

We next studied whether IFITMs and TMPRSS2 impact cell–cell fusion by acting on S-expressing cells ("donor cells"), on ACE2-expressing cells ("acceptor cells") or on both. To this end, we used a co-culture system of 293T-GFP1-10 donor cells with 293T-GFP11 acceptor cells. IFITMs and TMPRSS2 were transfected into either donor or acceptor cells (Fig 4A). In the absence of TMPRSS2, IFITMs were poorly efficient when present in donor cells, but inhibited fusion in acceptor cells. As already observed, IFITM1 was more active than IFITM2 and IFITM3. When TMPRSS2 was present in donor cells, IFITMs lost the weak effect they displayed when they were also in donor cells but retained their ability to inhibit fusion when expressed in acceptor cells (Fig 4A). Finally, when TMPRSS2 was expressed in acceptor cells, inhibition of fusion by IFITM was abolished regardless of their side of expression (Fig 4A). Therefore, IFITMs and TMPRSS2 modulate the efficiency of fusion when present in the same cell as ACE2, rather than in the S-expressing cell.

Impact of TMPRSS2 on S, IFITMs, and ACE2 levels

Our observation that TMPRSS2 counteracts the inhibitory effect of IFITMs prompted us to examine whether it degrades these antiviral proteins. Flow cytometry and Western blot showed that this is not the case, since similar levels of IFITM1, IFITM2, or IFITM3 were detected in the presence or absence of the serine protease (Figs 4B and EV6D). TMPRSS2 decreased S surface levels measured by flow cytometry with antibodies targeting the S1 and S2 domains (Fig 4D), as well as its processing, visualized by the disappearance of a 90 kDa product by Western blot (Fig 4C). In the absence of S, TMPRSS2 also triggered ACE2 processing, a phenomenon which was not inhibited by IFITM1 (Fig 4C). ACE2 cleavage by TMPRSS2 and other cellular proteases was previously reported and proposed to generate a receptor enhancing viral uptake (Haga *et al*, 2008; Shulla *et al*, 2011; Heurich *et al*, 2014). Altogether, our results indicate that TMPRSS2 processes both ACE2 and S, but does not degrade IFITMs.

Discussion

We report here that some SARS-CoV-2-infected cells form large syncytia in culture. This phenomenon occurs in U2OS-ACE2, 293T-ACE2, and A549-ACE2 cells. Naturally permissive Vero cells do not detectably fuse upon infection, but they form syncytia when they encounter infected cells or cells expressing only the Spike protein. Endogenous levels of ACE2 are thus sufficient to trigger cell fusion. Syncytia formation is thus a cell type-dependent process and likely relies on parameters such as the amount of cellular or viral proteins involved in fusion, or intrinsic biophysical properties of the membranes. S is expressed at the surface of infected cells and is sufficient to generate fusion with neighboring cells. IFITMs inhibit syncytia formation, with IFITM1 being the most efficient. IFITM2 and IFITM3 did not inhibit fusion of infected U2OS-ACE2 cells but were partly active in 293-T cells expressing only S. This may be due to the intracellular location of each IFITM, or the high levels of IFITMs generated by transient transfection. Future experiments with IFITM mutants lacking sorting signals or motifs involved in palmitoylation and other post-translational modifications will help understanding how these proteins impact SARS-CoV-2 fusion. Furthermore, recent reports have suggested that IFITMs may either enhance or restrict SARS-CoV-2 infection, depending on the experimental system and the cell type (preprint: Bozzo *et al*, 2020; preprint: Shi *et al*, 2020). Future investigations into the role endogenous IFITMs and TMPRSS2 conducted with primary cells treated or not with type-I IFN will provide a more thorough translational understanding of viral-induced syncytia formation.

We further show that TMPRSS2 accelerates SARS-CoV-2-mediated cell–cell fusion. TMPRSS2, through its serine protease activity, is known to cleave both S and ACE2. TMPRSS2 enhances infectivity and fusogenic activity of different coronaviruses,

 © 2020 The Authors

including HCoV-229E, MERS, and SARS-CoV-1 (Matsuyama *et al*, 2010; Glowacka *et al*, 2011; Shulla *et al*, 2011; Bertram *et al*, 2013; Shirato *et al*, 2013; Reinke *et al*, 2017; Kleine-Weber *et al*, 2018). With SARS-CoV-2, a first cleavage of S by furin at the S1/S2 site is required for subsequent cleavage by TMPRSS2 at S2' site (Hoffmann *et al*, 2020a). ACE2 cleavage by TMPRSS2 at a polybasic site generates a soluble fragment of the receptor (Haga *et al*, 2008; Shulla *et al*, 2011; Heurich *et al*, 2014). It has been proposed that this dual action on S and ACE2 facilitates virion uptake by target cells, through mechanisms that are not fully understood. The enhancement of syncytia formation described here with SARS-CoV-2 suggests that TMPRSS2

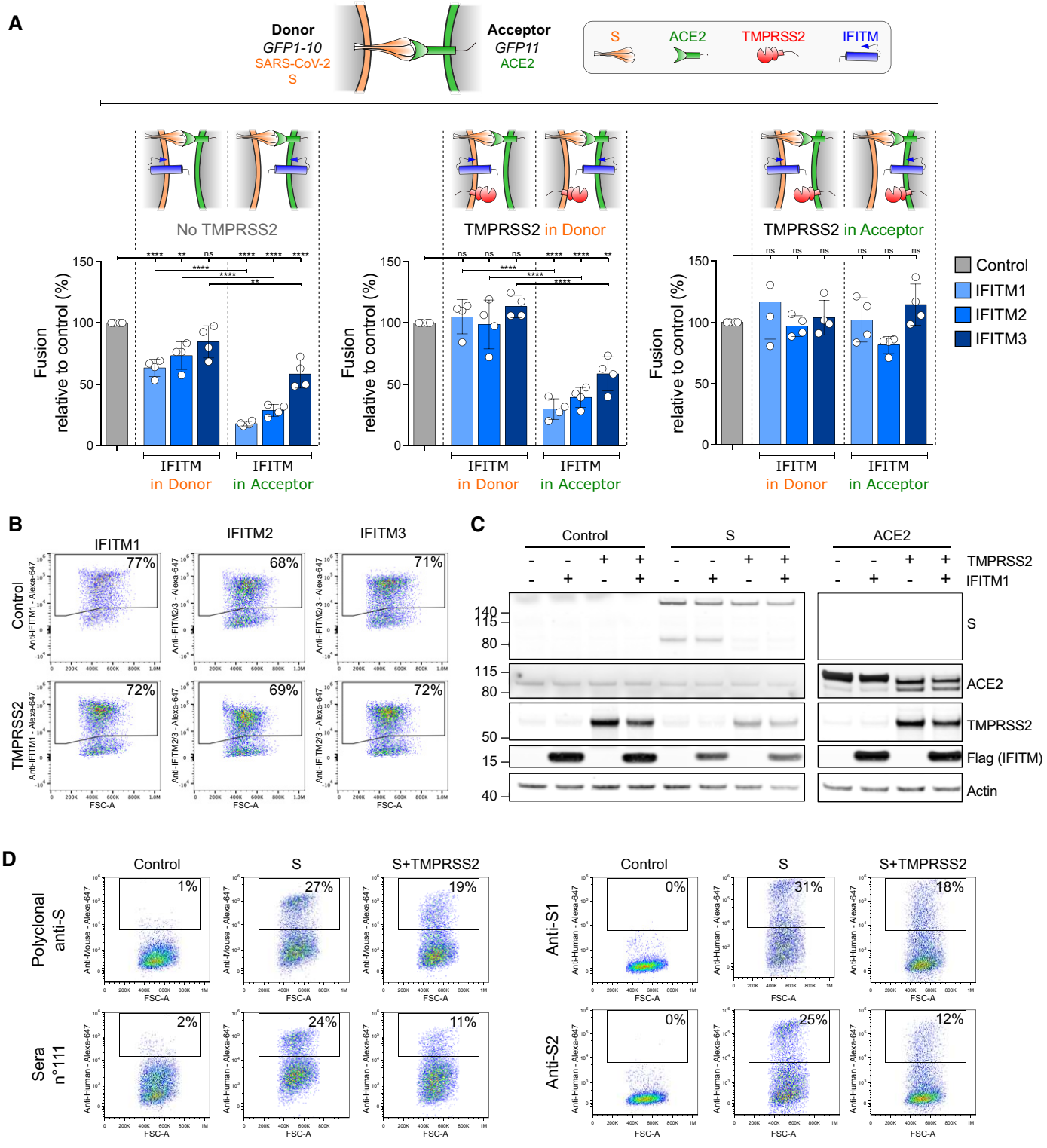

Figure 4.

© 2020 The Authors

Figure 4. Effect of TMPRSS2 and IFITM on S- or ACE2-expressing cells.

A S-expressing cells (Donor cells) and ACE2-expressing cells (Acceptor cells) were co-transfected with TMPRSS2, IFITM, or control plasmids. Cell fusion was quantified by measuring the GFP^+ area after 18 h. The indicated combinations were tested. The impact of IFITMs was measured in absence of TMPRSS2 (left panel), in the presence of TMPRSS2 in donor (middle panel) or acceptor cells (right panel). Data are mean ± SD of four independent experiments. Statistical analysis: One-way ANOVA, ns: non-significant, ***$P < 0.01$, ****$P < 0.0001$.

B–D Impact of TMPRSS2 on IFITMs, ACE2, and S levels. B. TMPRSS2 does not decrease IFITM amounts measured by flow cytometry. 293T cells were transfected with the indicated IFITM plasmids, with or without TMPRSS2, and analyzed 18 h later. C. Impact of TMPRSS2 on S and ACE2, measured by Western blot. 293T cells were transfected with or without IFITM1, TMPRSS2, S, or ACE2 plasmids, and analyzed 18 h later. D. TMPRSS2 decreases S surface levels, measured by flow cytometry. 293T cells were transfected with S plasmid, with or without TMPRSS2, and analyzed 18 h later. Murine polyclonal anti-S antibodies, one serum from a convalescent COVID-19-infected patient (sera n°111), and two monoclonal antibodies (anti-S1 and anti-S2) were tested. Data are representative of three independent experiments.

Source data are available online for this figure.

facilitates a step different from virion uptake. It will be worth determining which structural changes are triggered by TMPRS22 on the viral protein and its receptor, and how these changes may affect the relative affinities of the two proteins and the dynamics of the fusion process.

That TMPRSS2 counteracts the inhibitory activity of IFITMs on SARS-CoV-2-mediated syncytia formation raises interesting questions. This observation is not unprecedented, as two other coronaviruses, HCoV-229E and bat SARS-like WIV1, employ proteolytic pathways to evade IFITM restriction (Bertram *et al*, 2013; Zheng *et al*, 2020). IFITM proteins modify the rigidity or the lipid content of cellular membranes to prevent fusion. How this biophysical constraint is overcome by TMPRSS2 will require further investigations. For instance, it will be worth assessing the motility of ACE2 and S in membranes, before and during syncytia formation, and the impact of IFITM and TMPRSS2 on these processes. Determining the role of other proteins known to inhibit virion fusion, such as Ly6E and CH25H, and other proteases such as furin will provide a global overview of the mechanisms of cell–cell fusion.

An analysis of 41 post-mortem samples from individuals who died of COVID-19 demonstrated extensive alveolar damage and lung vasculature thrombosis (preprint: Giacca *et al*, 2020). In situ hybridization showed the presence of large multinucleated pneumocytes expressing viral RNA and proteins in half of the patients (preprint: Giacca *et al*, 2020). Syncytia may thus be considered as a frequent feature of severe COVID-19. It will be worth determining whether the syncytia are also generated in mild cases and whether severe or critical cases are linked to polymorphisms in IFITMs, as already reported for Flu (Shi *et al*, 2017; Zani & Yount, 2018) and in other IFN-related genes. Our results pave the way for the future assessment of the role played by syncytia in viral persistence and dissemination, the destruction of alveolar architecture, and immune or inflammatory responses.

Materials and Methods

Plasmids

pQCXIP-Empty control plasmid and pQCXIP-IFITM1-N-FLAG, pQCXIP-IFITM2-N-FLAG, and pQCXIP-IFITM3-N-FLAG plasmids were described (Buchrieser *et al*, 2019). The IFITM plasmids used throughout this study, either in transfections or in the generation of stably expressing cell lines, all contain a FLAG tag on the N terminus. pQCXIP-BSR-GFP11 and pQCXIP-GFP1-10 were from Yutaka Hata (Kodaka *et al*, 2015; Addgene plasmid #68716; http://n2t.net/addgene:68716; RRID:Addgene_68716 and Addgene plasmid #68715; http://n2t.net/addgene:68715; RRID:Addgene_68715). pcDNA3.1-hACE2 was from Hyeryun Choe (Li *et al*, 2003) (Addgene plasmid # 1786; http://n2t.net/addgene:1786; RRID:Addgene_1786). pCSDest-TMPRSS2 was from RogerReeves (Edie *et al*, 2018) (Addgene plasmid # 53887; http://n2t.net/addgene:53887; RRID:Addgene_53887). pLenti6-H2B-mCherry was from Torsten Wittmann (Pemble *et al*, 2017) (Addgene plasmid # 89766; http://n2t.net/addgene:89766; RRID:Addgene_89766). pLenti6-attB-hACE2-BSD was generated by cloning hACE2 from pcDNA3.1-hACE2 into the pLenti6-H2B-mCherry. Briefly, hACE2 was PCR amplified adding SpeI, XhoI, and attB sites using forward primer (5'- TCC CTC ACT AGT ACA AGT TTG TAC AAA AAA GCA GGC TGC CAC CAT GTC AAG CTC TTC CTG GCT C -3') and reverse primer (5'- AAA AAA CTC GAG ACC ACT TTG TAC AAG AAA GCT GGG TTT AAG CGG GCG CCA CCT -3') and cloned into pLenti6-H2B-mCherry using XhoI and SpeI sites. phCMV-SARS-CoV2-S was previously described (Grzelak *et al*, 2020). pLV-EF1α-TMPRSS2-IRES-Hygro was generated by gateway cloning of pCSDest-TMPRSS2 into pLV-EF1α-IRES-Hygro-DEST.

Cells

293T cells, platinum-E retroviral packaging cell line, A549, Caco2, and U2OS cells, and derivatives were cultured in DMEM with 10% Fetal Calf Serum (FCS) and 1% Penicillin/Streptomycin (PS). Vero cells were maintained in DMEM with 5% FCS and 1% PS. Cell lines transduced with pQCXIP pLenti6 or pLV-IRES-Hygro-derived vectors were grown with 1 μg/ml puromycin, 10 μg/ml blasticidin, or 100 μg/ml hygromycin B, respectively (InvivoGen). All cells were either purchased form ATCC or gifts from members of the Institut Pasteur.

Lentiviral and Retroviral vectors

For lentiviral production, 293T cells were co-transfected with pLenti6 or pLV-derived vectors, packaging plasmid R8-2, and VSV-G plasmid as previously described (Buchrieser *et al*, 2019). For murine retroviral vector production, the platinum-E (Cell Biolabs) retroviral packaging cell line was transfected with pQCXIP-derived plasmids. Vector containing supernatants were harvested at 36, 48, and 72 h and ultracentrifuged 1 h at 4°C at 22,000 *g*.

Generation of stable cell lines

For lentiviral or retroviral transduction, 2×10^4 cells were resuspended in 150 μl of medium containing 5–25 μl of ultracentrifuged

 © 2020 The Authors

lentiviral or retroviral vectors. Cells were agitated 30 s every 5 min for 2 h 30 min at 37°C in a Thermomixer. For cell lines co-expressing IFITMs and other proteins, vectors expressing the other proteins were transduced before IFITM vectors to avoid restriction of vector transduction by IFITMs. All cell lines were routinely tested for mycoplasma and found negative.

GFP-Split fusion assay

For fusion assays with S-expressing cells, 293T-GFP1-10 and 293T-GFP11 cells (6×10^4 cells/well cells mixed at a 1:1 ratio) in 96 well plates (μClear, #655090) were transfected in suspension using Lipofectamine 2000 (Thermo) with 100 ng of DNA. 10 ng of phCMV-SARS-CoV2-S, 25 ng of pCDNA3.1-hACE2, 25 ng of pCSDest-TMPRSS2, and 40 ng of pQCXIP-Empty or pQCXIP-IFITM-N-FLAG were used and adjusted to 100 ng DNA with pQCXIP-Empty. 18 h post-transfection, 21 images, covering 90% of the well surface, were acquired per well on an Opera Phenix High-Content Screening System (PerkinElmer) and the cell confluence area and GFP area was quantified on Harmony High-Content Imaging and Analysis Software. For "donor/acceptor" experiments, 3×10^4 293T GFP1-10 and GFP11 expressing cells were separately transfected with 50 ng of DNA in suspension at 37°C shaking 900 rpm for 20 min using Lipofectamine 2000 (Thermo). For donor cells, 293T-GFP1-10 cells were transfected with 10 ng of phCMV-SARS-CoV2-S, ±10 ng pCSDest-TMPRSS2, and ±20 ng pQCXIP-IFITM-N-FLAG and adjusted to 50 ng with pQCXIP-Empty. For acceptor cells, 293T-GFP11 cells were transfected with 10 ng of pCDNA3.1-hACE2, ±10 ng pCSDest-TMPRSS2, and ±20 ng pQCXIP-IFITM-N-FLAG and adjusted to 50 ng with pQCXIP-Empty. After transfection, cells were washed and resuspended in DMEM 10% FBS, mixed at a 1:1 ratio in different combinations, plated at 6×10^4 cells per well in a 96-well plate and imaged 18 h post-transfection. For live imaging, 2.5×10^5 GFP1-10 and GFP11-expressing 293T cells, mixed at a 1:1 ratio, were transfected in suspension at 37°C, with a shaking at 900 rpm for 20 min using Lipofectamine 2000 (Thermo) and 100 ng of DNA (10 ng of phCMV-SARS-CoV2-S, 20 ng of pCDNA3.1-hACE2, 20 ng of pCSDest-TMPRSS2, and 40 ng pQCXIP-IFITM-N-FLAG, adjusted to 100 ng with pQCXIP-Empty). Cells were washed and seeded into a μ-Dish 35 mm Quad dish (ibidi—#80416) with 2.5×10^5 cells per quadrant. Transmission and fluorescence images were taken at 37°C every 10 min up to 24 h using a Nikon BioStation IMQ, with three fields for each condition. The GFP area was quantified on ImageJ.

Antibodies

Mouse monoclonal antibodies (mAb): IFITM1 (#60074-1-Ig, Proteintech) 1:250 for FACS, and IF; IFITM2/3 (#66081-1-Ig, Proteintech) 1:250 for FACS, and IF; ACE2 (AC18F) (#AG-20A-0032-C100—adipogen). Rabbit polyclonal antibodies: FLAG-Tag DYKDDDDK (D6W5B) (#14793, Cell Signaling) 1:800 for FACS. TMPRSS2 (#HPA035787—Atlasantibodies) 1:500. ZO-1 (#40-2200—Thermo Fisher) 1:100. Goat polyclonal antibodies: ACE2 (AF933—R&D). SARS_Ssd3 702, SARS_Ssd3 –369, SARS_Ssd3 293, and Ascite Sso14 200705 were kindly gifted by Nicolas Escriou. SARS_Ssd3 702 antibody was used at 0.5 μg/ml for FACS and IF. Human Mab: Anti-SARS-CoV2 monoclonal antibodies 48 and 71 recognize two domains of the S1 protein (Planchais *et al*, manuscript in preparation). Secondary antibodies coupled with Alexa Fluor 488 or 647 (Invitrogen) were used at 1:500 for FACS and IF.

Flow cytometry

For intracellular staining, cells were fixed in 4% PFA for 15 to 30 min at RT and staining was performed in PBS, 1% BSA, 0.05% sodium azide, and 0.05% Saponin. Cells were incubated with primary antibodies and then with secondary antibodies for 30 min at RT. Surface staining was performed before fixation, in PBS 1% BSA. Cells were incubated with primary antibodies and then with secondary antibodies for 30 min at RT. Cells were fixed for 15 min in 4% PFA. Cells were acquired on an Attune NxT Flow Cytometer (Thermo Fisher) and data analyzed with FlowJo software.

U2OS viral-mediated cell–cell fusion, video microscopy, and immunofluorescence

U2OS-ACE2 GFP1-10 or GFP11 stably expressing TMPRSS2, IFITM1, 2, 3, or control cells were mixed (1:1 ratio) and plated at 8×10^3 cells per well in a 96-well plate (μClear, #655090), 24 h before infection. Cells were then infected with different MOI of SARS-CoV-2 in 150 μl of media. 18 h post-infection, media was removed, and cells were fixed in 4% PFA for 30 min at room temperature, washed, and resuspended in PBS. For fusion and viability quantification, cells were stained for 10 min with Hoechst 33342 (1:5,000) before being imaged. For S and IFITM analysis, cells were washed twice PBS and stained with primary antibody for 45 min in PBS, 1% BSA, 0.05% sodium azide, and 0.05% Saponin in the wells. Cells were washed twice with PBS, 0.05% Saponin and stained with secondary antibody for 30 min at RT in PBS, 1% BSA, 0.05% sodium azide, 0.05% Saponin, and Hoechst 33342 (1:10,000) and washed with PBS. Cells were acquired on an Opera Phenix High Content Screening System (PerkinElmer) and analyzed on Harmony High-Content Imaging and Analysis Software. For live imaging, U2OS-ACE2 GFP1-10 and GFP11 were mixed at a 1:1 ratio and plated at 4×10^4 cells per quadrant in a μ-Dish 35 mm Quad dish (ibidi—#80416). Cells were infected the next day with SARS-CoV-2 (MOI 0.2) in media containing propidium iodide. Transmission and fluorescence images were taken at 37°C every 10 min, up to 48 h, using a Nikon BioStation IMQ, with three fields for each condition.

Western blot

Cells were lysed in TXNE buffer (1% Triton X-100, 50 mM Tris–HCl (pH 7.4), 150 mM NaCl, 5 mM EDTA, protease inhibitors) for 30 min on ice. Equal amounts (20–50 μg) of cell lysates were analyzed by Western blot. The following antibodies were diluted in WB-buffer (PBS, 1% BSA, 0.05% Tween, 0.01% Na Azide): goat anti-human ACE2 (R&D cat#AF933, 1:2,000), mouse anti-human ACE2 (Adipogen AC18F cat #AG-20A0032-C100, 1:1,000), rabbit anti-human TMPRSS2 (Atlas antibodies cat# HPA035787, 1:1,000), mouse anti-Flag tag (Sigma cat# F1804, 1:1,000), rabbit anti-human actin (Sigma cat#A2066, 1:2,000), and mouse ascite anti-SARS S, (1:1,000; Siu *et al*, 2008). Specie-specific secondary DyLight-coupled antibodies were used (diluted 1:10,000 in WB-buffer) and proteins revealed using a Licor Imager. Images were quantified and processed using Image Studio Lite software.

© 2020 The Authors

Virus

The strain BetaCoV/France/IDF0372/2020 was supplied by the National Reference Centre for Respiratory Viruses hosted by Institut Pasteur (Paris, France) and headed by Pr. S. van der Werf. The human sample from which the strain was isolated has been provided by Dr. X. Lescure and Pr. Y. Yazdanpanah from the Bichat Hospital, Paris, France. The viral strain was supplied through the European Virus Archive goes Global (Evag) platform, a project that has received funding from the European Union's Horizon 2020 research and innovation program under grant agreement no. 653316. Titration of viral stocks was performed on Vero E6, with a limiting dilution technique allowing a calculation of DCP50.

Statistical analysis

Flow cytometry data were analyzed with FlowJo v10 software (TriStar). Calculations were performed using Excel 365 (Microsoft). Figures were drawn on Prism 8 (GraphPad Software). Statistical analysis was conducted using GraphPad Prism 8. Statistical significance between different groups was calculated using the tests indicated in each figure legend.

Data availability

This study includes no data deposited in external repositories.

Expanded View for this article is available online.

Acknowledgements
We thank members of the Virus and Immunity Unit for discussions and help, Mauro Giacca for discussion and sharing unpublished results, Nathalie Aulner and the UtechS Photonic BioImaging (UPBI) core facility (Institut Pasteur), a member of the France BioImaging network, for image acquisition and analysis, and Nicolas Escriou for the kind gift of anti-SARS-CoV-2 antibodies. OS laboratory is funded by Institut Pasteur, ANRS, the Vaccine Research Institute (ANR-10-LABX-77), Labex IBEID (ANR-10-LABX-62-IBEID), "TIMTAMDEN" ANR-14-CE14-0029, "CHIKV-Viro-Immuno" ANR-14-CE14-0015-01 and the Gilead HIV cure program, ANR/FRM Flash Covid PROTEO-SARS-CoV-2 and IDISCOVR. Work in UPBI is funded by grant ANR-10-INSB-04-01 and Région Ile-de-France program DIM1-Health. HM laboratory is funded by the Institut Pasteur, the Milieu Intérieur Program (ANR-10-LABX-69-01), the INSERM, REACTing, and EU (RECOVER) grants. SVDW laboratory is funded by Institut Pasteur, CNRS, Université de Paris, Santé publique France, Labex IBEID (ANR-10-LABX-62-IBEID), REACTing, and EU (RECOVER) grant. M.M.R is supported by the Pasteur-Paris University (PPU) International Doctoral Program. The funders of this study had no role in study design, data collection, analysis and interpretation, or writing of the article.

Author contributions
Experimental strategy design, experiments: JB, JD, MH, BM, DP, MMR, FP, FGB, NC, TB, OS; Vital materials, expert advice: HM, CP, NE, SVDW; Manuscript writing: JB, OS; Manuscript editing: MMR; Manuscript reviewing, approval: All authors.

Conflict of interest
The authors declare that they have no conflict of interest.

References

Abdel Motal UM, Zhou X, Joki A, Siddiqi AR, Srinivasa BR, Stenvall K, Dahmen J, Jondal M (1993) Major Histocompatibility Complex class I-binding peptides are recycled to the cell surface after internalization. *Eur J Immunol* 23: 3224 – 3229

Bertram S, Dijkman R, Habjan M, Heurich A, Gierer S, Glowacka I, Welsch K, Winkler M, Schneider H, Hofmann-Winkler H *et al* (2013) TMPRSS2 activates the human coronavirus 229E for cathepsin-independent host cell entry and is expressed in viral target cells in the respiratory epithelium. *J Virol* 87: 6150 – 6160

Blanco-Melo D, Nilsson-Payant BE, Liu WC, Uhl S, Hoagland D, Moller R, Jordan TX, Oishi K, Panis M, Sachs D *et al* (2020) Imbalanced host response to SARS-CoV-2 drives development of COVID-19. *Cell* 181: 1036 – 1045.e9

Bost P, Giladi A, Liu Y, Bendjelal Y, Xu G, David E, Blecher-Gonen R, Cohen M, Medaglia C, Li H *et al* (2020) Host-viral infection maps reveal signatures of severe COVID-19 patients. *Cell* 181: 1475 – 1488 e12

Bozzo C, Nchioua R, Volcic M, Wettstein L, Weil T, Krüger J, Heller S, Conzelmann C, Müller J, Gross R*et al* (2020) IFITM proteins promote SARS-CoV-2 infection of human lung cells. *bioRxiv* https://doi.org/10.1101/2020.08.18.255935 [PREPRINT]

Broggi A, Ghosh S, Sposito B, Spreafico R, Balzarini F, Lo Cascio A, Clementi N, De Santis M, Mancini N, Granucci F *et al* (2020) Type III interferons disrupt the lung epithelial barrier upon viral recognition. *Science* 369: 706 – 712

Buchrieser J, Degrelle SA, Couderc T, Nevers Q, Disson O, Manet C, Donahue DA, Porrot F, Hillion KH, Perthame E *et al* (2019) IFITM proteins inhibit placental syncytiotrophoblast formation and promote fetal demise. *Science* 365: 176 – 180

Chan JF, Chan KH, Choi GK, To KK, Tse H, Cai JP, Yeung ML, Cheng VC, Chen H, Che XY *et al* (2013) Differential cell line susceptibility to the emerging novel human betacoronavirus 2c EMC/2012: implications for disease pathogenesis and clinical manifestation. *J Infect Dis* 207: 1743 – 1752

Compton Alex A, Bruel T, Porrot F, Mallet A, Sachse M, Euvrard M, Liang C, Casartelli N, Schwartz O (2014) IFITM proteins incorporated into HIV-1 virions impair viral fusion and spread. *Cell Host Microbe* 16: 736 – 747

Edie S, Zaghloul NA, Leitch CC, Klinedinst DK, Lebron J, Thole JF, McCallion AS, Katsanis N, Reeves RH (2018) Survey of human chromosome 21 gene expression effects on early development in *Danio rerio*. *G3 (Bethesda)* 8: 2215 – 2223

Franks TJ, Chong PY, Chui P, Galvin JR, Lourens RM, Reid AH, Selbs E, McEvoy CPL, Hayden CDL, Fukuoka J *et al* (2003) Lung pathology of severe acute respiratory syndrome (SARS): a study of 8 autopsy cases from Singapore. *Hum Pathol* 34: 743 – 748

Freundt EC, Yu L, Goldsmith CS, Welsh S, Cheng A, Yount B, Liu W, Frieman MB, Buchholz UJ, Screaton GR *et al* (2010) The open reading frame 3a protein of severe acute respiratory syndrome-associated coronavirus promotes membrane rearrangement and cell death. *J Virol* 84: 1097 – 1109

Giacca M, Bussani R, Schneider E, Zentilin L, Collesi C, Ali H, Braga L, Secco I, Volpe MC, Colliva A*et al*(2020) Persistence of viral RNA, widespread thrombosis and abnormal cellular syncytia are hallmarks of COVID-19 lung pathology. *medRxiv* https://doi.org/10.1101/2020.06.22.20136358 [PREPRINT]

Glowacka I, Bertram S, Müller MA, Allen P, Soilleux E, Pfefferle S, Steffen I, Tsegaye TS, He Y, Gnirss K *et al* (2011) Evidence that TMPRSS2 activates the severe acute respiratory syndrome coronavirus spike protein for

 © 2020 The Authors

membrane fusion and reduces viral control by the humoral immune response. *J Virol* 85: 4122 – 4134

Gorshkov K, Chen CZ, Bostwick R, Rasmussen L, Xu M, Pradhan M, Tran BN, Zhu W, Shamim K, Huang W*et al*(2020) The SARS-CoV-2 cytopathic effect is blocked with autophagy modulators. *bioRxiv* https://doi.org/10.1101/2020.05.16.091520 [PREPRINT]

Grzelak L, Temmam S, Planchais C, Demeret C, Tondeur L, Huon C, Guivel-Benhassine F, Staropoli I, Chazal M, Dufloo J *et al* (2020) A comparison of four serological assays for detecting anti-SARS-CoV-2 antibodies in human serum samples from different populations. *Sci Transl Med* 12: eabc3103

Hadjadj J, Yatim N, Barnabei L, Corneau A, Boussier J, Pere H, Charbit B, Bondet V, Chenevier-Gobeaux C, Breillat P*et al* (2020) Impaired type I interferon activity and exacerbated inflammatory responses in severe Covid-19 patients. *medRxiv* https://doi.org/10.1101/2020.04.19.20068015 [PREPRINT]

Haga S, Yamamoto N, Nakai-Murakami C, Osawa Y, Tokunaga K, Sata T, Yamamoto N, Sasazuki T, Ishizaka Y (2008) Modulation of TNF-α-converting enzyme by the spike protein of SARS-CoV and ACE2 induces TNF-α production and facilitates viral entry. *Proc Natl Acad Sci USA* 105: 7809

Heurich A, Hofmann-Winkler H, Gierer S, Liepold T, Jahn O, Pöhlmann S (2014) TMPRSS2 and ADAM17 cleave ACE2 differentially and only proteolysis by TMPRSS2 augments entry driven by the severe acute respiratory syndrome coronavirus spike protein. *J Virol* 88: 1293 – 1307

Hoffmann M, Kleine-Weber H, Pöhlmann S (2020a) A multibasic cleavage site in the spike protein of SARS-CoV-2 is essential for infection of human lung cells. *Mol Cell* 78: 779 – 784.e5

Hoffmann M, Kleine-Weber H, Schroeder S, Kruger N, Herrler T, Erichsen S, Schiergens TS, Herrler G, Wu NH, Nitsche A *et al* (2020b) SARS-CoV-2 cell entry depends on ACE2 and TMPRSS2 and is blocked by a clinically proven protease inhibitor. *Cell* 181: 271 – 280 e8

Hou YJ, Okuda K, Edwards CE, Martinez DR, Asakura T, Dinnon 3rd KH, Kato T, Lee RE, Yount BL, Mascenik TM *et al* (2020) SARS-CoV-2 reverse genetics reveals a variable infection gradient in the respiratory tract. *Cell* 182: 429 – 446.e14

Huang C, Wang Y, Li X, Ren L, Zhao J, Hu Y, Zhang L, Fan G, Xu J, Gu X *et al* (2020) Clinical features of patients infected with 2019 novel coronavirus in Wuhan, China. *Lancet* 395: 497 – 506

Huang IC, Bailey CC, Weyer JL, Radoshitzky SR, Becker MM, Chiang JJ, Brass AL, Ahmed AA, Chi X, Dong L *et al* (2011) Distinct patterns of IFITM-mediated restriction of filoviruses, SARS coronavirus, and influenza A virus. *PLoS Pathog* 7: e1001258

Kleine-Weber H, Elzayat MT, Hoffmann M, Pohlmann S (2018) Functional analysis of potential cleavage sites in the MERS-coronavirus spike protein. *Sci Rep* 8: 16597

Kodaka M, Yang Z, Nakagawa K, Maruyama J, Xu X, Sarkar A, Ichimura A, Nasu Y, Ozawa T, Iwasa H *et al* (2015) A new cell-based assay to evaluate myogenesis in mouse myoblast C2C12 cells. *Exp Cell Res* 336: 171 – 181

Lan J, Ge J, Yu J, Shan S, Zhou H, Fan S, Zhang Q, Shi X, Wang Q, Zhang L *et al* (2020) Structure of the SARS-CoV-2 spike receptor-binding domain bound to the ACE2 receptor. *Nature* 581: 215 – 220

Letko M, Marzi A, Munster V (2020) Functional assessment of cell entry and receptor usage for SARS-CoV-2 and other lineage B betacoronaviruses. *Nat Microbiol* 5: 562 – 569

Li W, Moore MJ, Vasilieva N, Sui J, Wong SK, Berne MA, Somasundaran M, Sullivan JL, Luzuriaga K, Greenough TC *et al* (2003) Angiotensin-converting enzyme 2 is a functional receptor for the SARS coronavirus. *Nature* 426: 450 – 454

Major J, Crotta S, Llorian M, McCabe TM, Gad HH, Priestnall SL, Hartmann R, Wack A (2020) Type I and III interferons disrupt lung epithelial repair during recovery from viral infection. *Science* 369: 712 – 717

Matsuyama S, Nagata N, Shirato K, Kawase M, Takeda M, Taguchi F (2010) Efficient activation of the severe acute respiratory syndrome coronavirus spike protein by the transmembrane protease TMPRSS2. *J Virol* 84: 12658 – 12664

Matsuyama S, Nao N, Shirato K, Kawase M, Saito S, Takayama I, Nagata N, Sekizuka T, Katoh H, Kato F *et al* (2020) Enhanced isolation of SARS-CoV-2 by TMPRSS2-expressing cells. *Proc Natl Acad Sci USA* 117: 7001 – 7003

Ogando NS, Dalebout TJ, Zevenhoven-Dobbe JC, Limpens RWAL, van der Meer Y, Caly L, Druce J, de Vries JJC, Kikkert M, Bárcena M *et al* (2020) SARS-coronavirus-2 replication in Vero E6 cells: replication kinetics, rapid adaptation and cytopathology. *J Gen Virol* 101: 925 – 940

Ong EZ, Chan YFZ, Leong WY, Lee NMY, Kalimuddin S, Haja Mohideen SM, Chan KS, Tan AT, Bertoletti A, Ooi EE *et al* (2020) A dynamic immune response shapes COVID-19 progression. *Cell Host Microbe* 27: 879 – 882 e2

Park A, Iwasaki A (2020) Type I and Type III interferons – induction, signaling, evasion, and application to combat COVID-19. *Cell Host Microbe* 27: 870 – 878

Pemble H, Kumar P, van Haren J, Wittmann T (2017) GSK3-mediated CLASP2 phosphorylation modulates kinetochore dynamics. *J Cell Sci* 130: 1404 – 1412

Pfaender S, Mar KB, Michailidis E, Kratzel A, Boys IN, V'Kovski P, Fan W, Kelly JN, Hirt D, Ebert N *et al* (2020) LY6E impairs coronavirus fusion and confers immune control of viral disease. *Nat Microbiol* 5: 1330 – 1339

Qian Z, Dominguez SR, Holmes KV (2013) Role of the spike glycoprotein of human Middle East respiratory syndrome coronavirus (MERS-CoV) in virus entry and syncytia formation. *PLoS One* 8: e76469

Reinke LM, Spiegel M, Plegge T, Hartleib A, Nehlmeier I, Gierer S, Hoffmann M, Hofmann-Winkler H, Winkler M, Pöhlmann S (2017) Different residues in the SARS-CoV spike protein determine cleavage and activation by the host cell protease TMPRSS2. *PLoS One* 12: e0179177

Ren Y, Shu T, Wu D, Mu J, Wang C, Huang M, Han Y, Zhang X-Y, Zhou W, Qiu Y *et al* (2020) The ORF3a protein of SARS-CoV-2 induces apoptosis in cells. *Cell Mol Immunol* 17: 881 – 883

Shi G, Kenney AD, Kudryashova E, Zhang L, Hall-Stoodley L, Robinson RT, Kudryashov DS, Compton AA, Yount JS (2020) Opposing activities of IFITM proteins in SARS-CoV-2 infection. *bioRxiv* https://doi.org/10.1101/2020.08.11.246678 [PREPRINT]

Shi G, Schwartz O, Compton AA (2017) More than meets the I: the diverse antiviral and cellular functions of interferon-induced transmembrane proteins. *Retrovirology* 14: 53

Shirato K, Kawase M, Matsuyama S (2013) Middle east respiratory syndrome coronavirus infection mediated by the transmembrane serine protease TMPRSS2. *J Virol* 87: 12552 – 12561

Shulla A, Heald-Sargent T, Subramanya G, Zhao J, Perlman S, Gallagher T (2011) A transmembrane serine protease is linked to the severe acute respiratory syndrome coronavirus receptor and activates virus entry. *J Virol* 85: 873 – 882

Siu YL, Teoh KT, Lo J, Chan CM, Kien F, Escriou N, Tsao SW, Nicholls JM, Altmeyer R, Peiris JSM *et al* (2008) The M, E, and N structural proteins of the severe acute respiratory syndrome coronavirus are required for efficient assembly, trafficking, and release of virus-like particles. *J Virol* 82: 11318 – 11330

Subbarao K, Mahanty S (2020) Respiratory virus infections: understanding COVID-19. *Immunity* 52: 905 – 909

© 2020 The Authors

Tang D, Comish P, Kang R (2020) The hallmarks of COVID-19 disease. *PLoS Pathog* 16: e1008536

Tian S, Hu W, Niu L, Liu H, Xu H, Xiao SY (2020) Pulmonary pathology of early-phase 2019 novel coronavirus (COVID-19) pneumonia in two patients with lung cancer. *J Thorac Oncol* 15: 700 – 704

Walls AC, Park YJ, Tortorici MA, Wall A, McGuire AT, Veesler D (2020) Structure, function, and antigenicity of the SARS-CoV-2 spike glycoprotein. *Cell* 181: 281 – 292.e6

Wang Q, Zhang Y, Wu L, Niu S, Song C, Zhang Z, Lu G, Qiao C, Hu Y, Yuen K-Y *et al* (2020) Structural and functional basis of SARS-CoV-2 entry by using human ACE2. *Cell* 181: 894 – 904.e9

Warren CJ, Griffin LM, Little AS, Huang IC, Farzan M, Pyeon D (2014) The antiviral restriction factors IFITM1, 2 and 3 do not inhibit infection of human papillomavirus, cytomegalovirus and adenovirus. *PLoS One* 9: e96579

Wrensch F, Winkler M, Pohlmann S (2014) IFITM proteins inhibit entry driven by the MERS-coronavirus spike protein: evidence for cholesterol-independent mechanisms. *Viruses* 6: 3683 – 3698

Xu Z, Shi L, Wang Y, Zhang J, Huang L, Zhang C, Liu S, Zhao P, Liu H, Zhu L *et al* (2020) Pathological findings of COVID-19 associated with acute respiratory distress syndrome. *Lancet Respir Med* 8: 420 – 422

Zang R, Case JB, Gomez Castro MF, Liu Z, Zeng Q, Zhao H, Son J, Rothlauf PW, Hou G, Bose S, Wang X, Vahey MD, Kirchhausen T, Fremont DH, Diamond MS, Whelan SPJ, Ding S (2020) Cholesterol 25-hydroxylase suppresses SARS-CoV-2 replication by blocking membrane fusion. *bioRxiv* https://doi.org/10.1101/2020.06.08.141077 [PREPRINT]

Zani A, Yount JS (2018) Antiviral protection by IFITM3 in vivo. *Curr Clin Microbiol Rep* 5: 229 – 237

Zhao X, Guo F, Liu F, Cuconati A, Chang J, Block TM, Guo JT (2014) Interferon induction of IFITM proteins promotes infection by human coronavirus OC43. *Proc Natl Acad Sci USA* 111: 6756 – 6761

Zhao X, Sehgal M, Hou Z, Cheng J, Shu S, Wu S, Guo F, Le Marchand SJ, Lin H, Chang J *et al* (2018) Identification of residues controlling restriction versus enhancing activities of IFITM proteins on entry of human coronaviruses. *J Virol* 92: e01535-17

Zhao X, Zheng S, Chen D, Zheng M, Li X, Li G, Lin H, Chang J, Zeng H, Guo JT (2020) LY6E restricts entry of human coronaviruses, including currently pandemic SARS-CoV-2. *J Virol* 94: e00562-20

Zheng M, Zhao X, Zheng S, Chen D, Du P, Li X, Jiang D, Guo J-T, Zeng H, Lin H (2020) Bat SARS-Like WIV1 coronavirus uses the ACE2 of multiple animal species as receptor and evades IFITM3 restriction via TMPRSS2 activation of membrane fusion. *Emerg Microbes Infect* 9: 1567 – 1579

Zhou Z, Ren L, Zhang L, Zhong J, Xiao Y, Jia Z, Guo L, Yang J, Wang C, Jiang S *et al* (2020) Heightened Innate Immune Responses in the Respiratory Tract of COVID-19 Patients. *Cell Host Microbe* 27: 883 – 890 e2

 © 2020 The Authors

Expanded View Figures

Figure EV1. ACE2 and IFITM expression in U2OS-ACE2 cell derivatives.

A ACE2 expression assessed by Western blot in U2OS-ACE2 GFP-split cells expressing or not IFITM1. Cell lysates were analyzed by for ACE2 and actin as a loading control.

B–E Analysis of ACE2 and IFITMs levels by flow cytometry. (B) Gating strategy. Cells were gated by size and granularity. Positive and negative gates were then set on control U2OS cells lacking the protein of interest. (C) ACE2 levels on parental U2OS (control) and various IFITM derivatives. (D) IFITM1 levels on parental U2OS (control) and U2OS-ACE2 IFITM1 cells. (E) IFITM2 and IFITM3 levels on parental U2OS (control) and U2OS-ACE2 IFITM2 and U2OS-ACE2 IFITM3 cells.

© 2020 The Authors

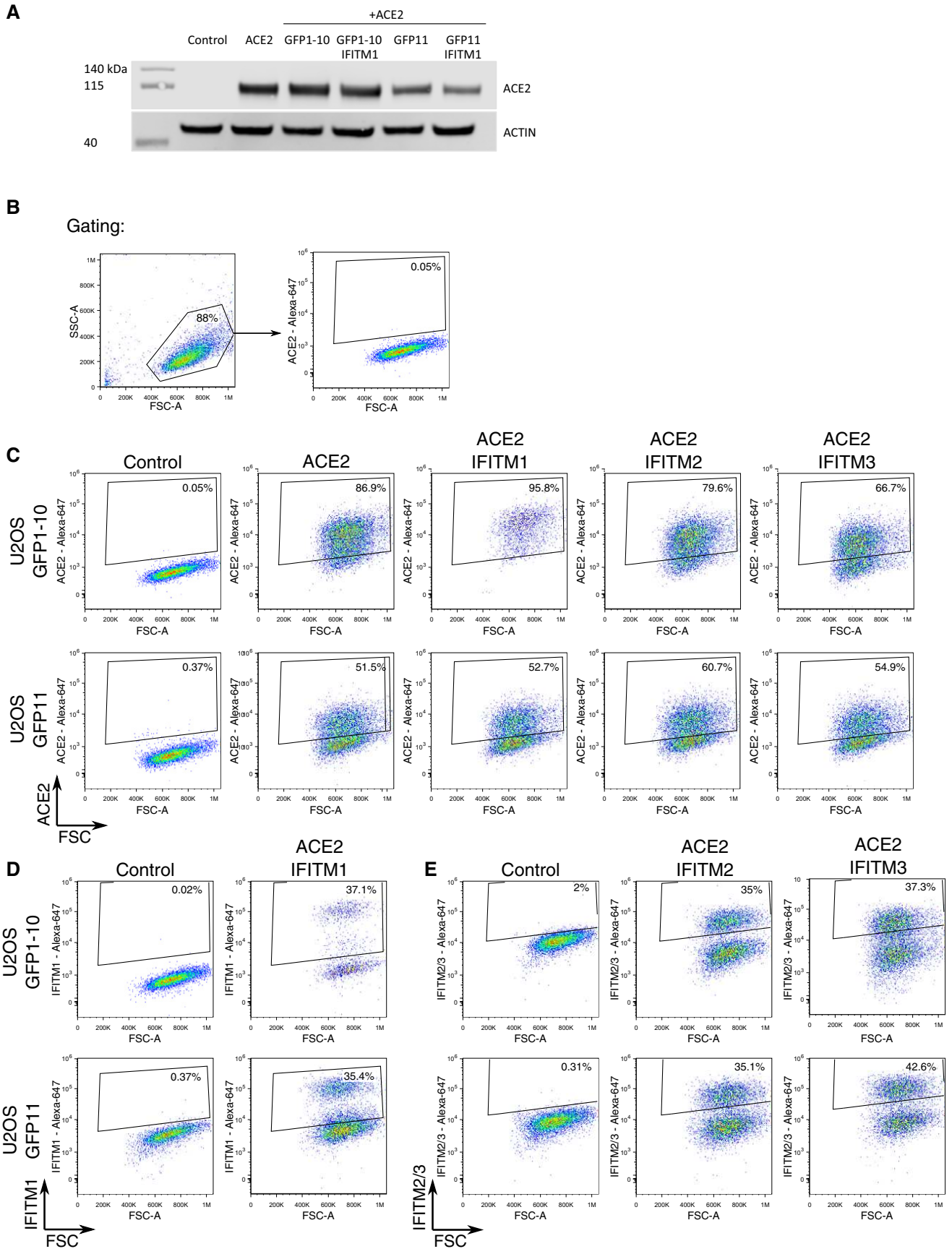

Figure EV1.

© 2020 The Authors

Figure EV2. Image quantification methodology.

A Quantification of fusion and viability. To measure the extent of cell–cell fusion, the GFP area was automatically delimited, measured, and then divided by the total cell area. For cell viability, nuclei were automatically counted, and the total number of nuclei per well was normalized to that of non-infected control cells.

B Quantification of syncytia expressing IFITMs. For IFITM-GFP overlap quantification, the $IFITM^+$ area was first selected on the 647 nm channel (image 2) and the GFP-positive area was quantified within the $IFITM^+$ area (image 3). Image 4 shows the overlap area in gray for simpler visualization.

C Quantification of infected cells expressing the S protein. The cells were stained with anti-S antibodies, and the nuclei were detected with Hoechst. The S^+ area was delimited (each selected object is pseudo-colored). Nuclei present within the S^+ area were scored and divided by the total number of nuclei, to calculate the number of infected cells per well.

Data information: Scale bars: 100 μm. The same field was used in this example for A and C, Hoechst images are therefore identical in A and C.

© 2020 The Authors

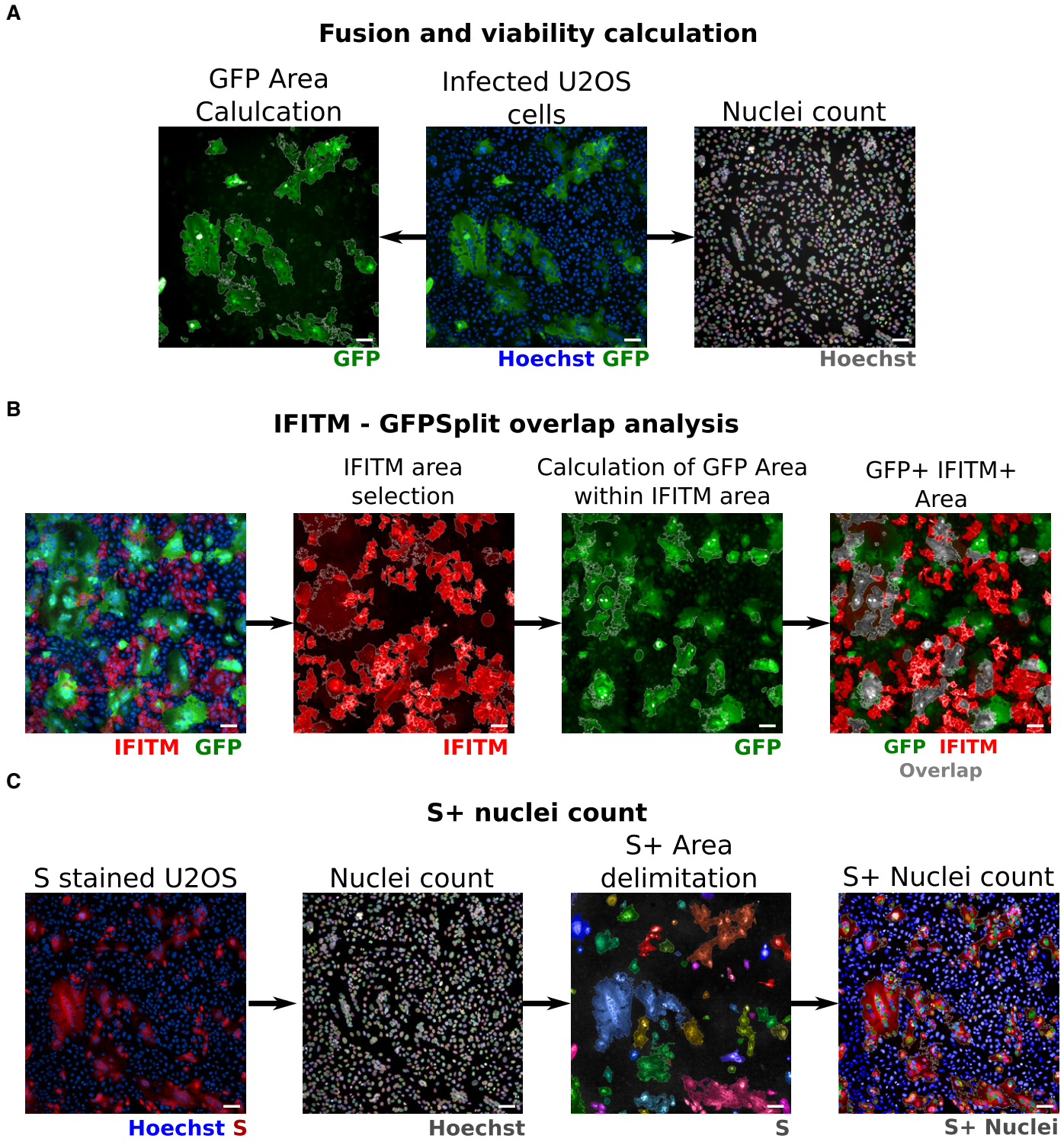

Figure EV2.

 © 2020 The Authors

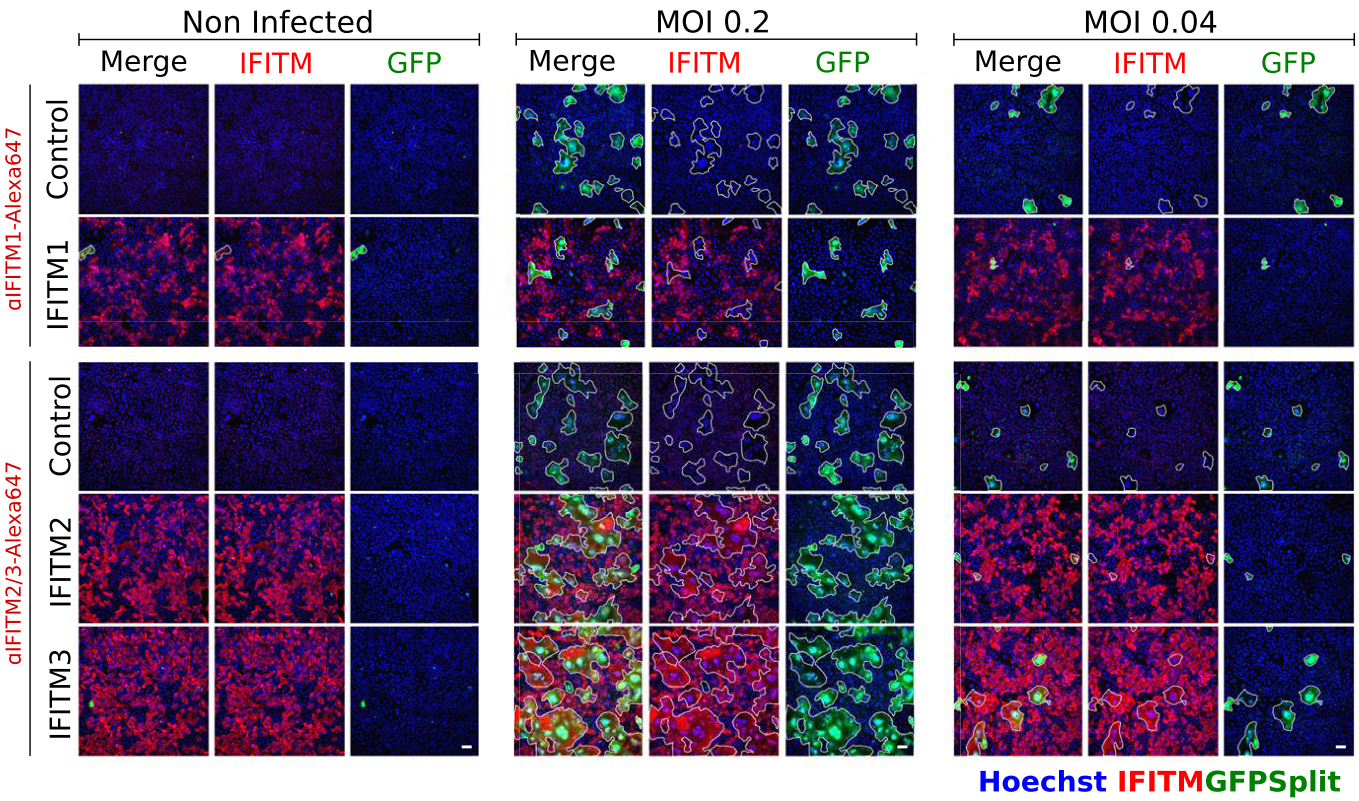

Figure EV3. Expression of IFITM1, IFITM2, and IFITM3 in SARS-CoV-2-infected syncytia.
SARS-CoV-2-induced syncytia in U2OS cells are IFITM1 dim or negative, but IFITM2/3 positive. Left: Non-infected U2OS-ACE2 cells. Middle and right: Cells infected with SARS-CoV-2 at the indicated MOI. The GFP area is delimited in white. With IFITM1, the fused GFP area does not overlap with the red IFITM1 area. For IFITM2 and IFITM3, an overlap with the GFP is visible. Scale bars: 100 μm. Quantifications are presented Fig 2C.

© 2020 The Authors

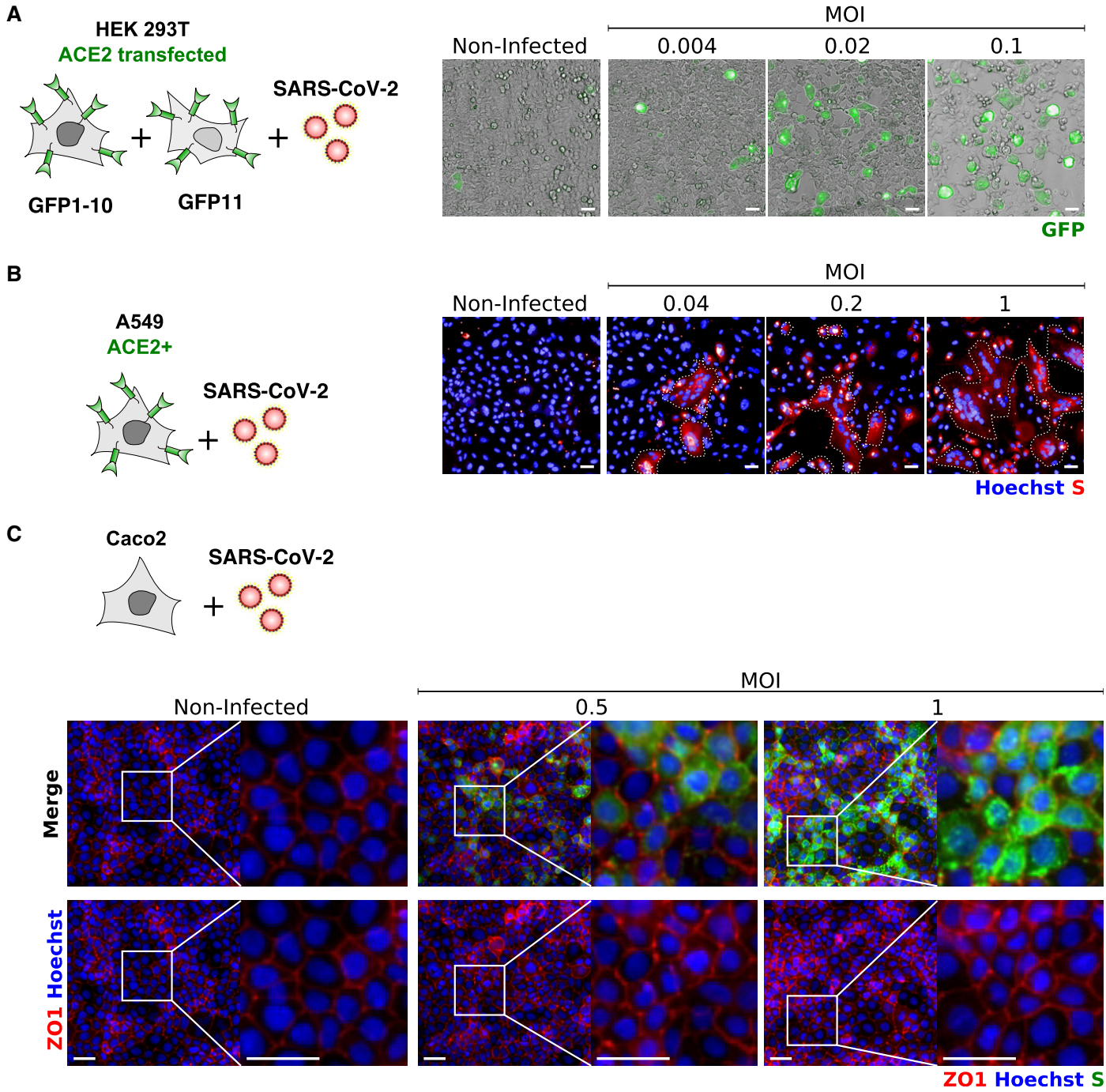

Figure EV4. Characterization of SARS-CoV-2-induced syncytia in different cell lines.

A 293T-GFP1-10 and -GFP11 (1:1 ratio) were transfected with ACE2 and infected with SARS-CoV-2 at the indicated MOIs. Cell fusion was visualized by the GFP^+ area 18 h post-infection. One representative image per condition is shown, and GFP area is delimited in white.

B A549-ACE2 cells were infected with SARS-CoV-2 at the indicated MOIs for 24 h and stained with anti-S antibodies and Hoechst. One representative image per condition is shown, and syncytia are manually delimited in white.

C Caco2 cells were infected with SARS-CoV-2 at the indicated MOIs for 24 h and stained for ZO1 tight junction marker, Hoechst and S. No clear syncytia formation was observed at any of the MOIs tested.

Data information: Scale bar: 50 μm. Data are representative of three independent experiments.

© 2020 The Authors

Figure EV5. Characterization of syncytia formation in Vero cells.

A Vero-GFP1-10 and -GFP11 (1:1 ratio) were infected with SARS-CoV-2 for 24 h and stained with anti-S antibodies and Hoechst. Cell fusion was visualized by the GFP^+ area. No syncytia were observed in infected Vero cells.

B Vero-GFP1-10 and -GFP11 (1:1 ratio) were transfected with S expression plasmid and cell fusion was visualized by the GFP^+ area at 18 h post-transfection. S expression induced extensive syncytia formation.

C S-expressing 293T GFP11 (Donor cells) were co-cultured overnight with Vero GFP1-10 (Acceptor cells). Cell fusion was quantified by measuring the GFP^+ area. S-expressing 293Ts readily fuse with Vero cells.

D SARS-CoV-2-infected U2OS $ACE2^+$ GFP1-10 (Donor cells) were co-cultured for 8 h with Vero GFP11 (Acceptor cells). Cell fusion was quantified by measuring the GFP^+ area. Infected U2OS fuse with Vero cells.

Data information: Scale bar: 50 μm. Representative images of three independent experiments.

© 2020 The Authors

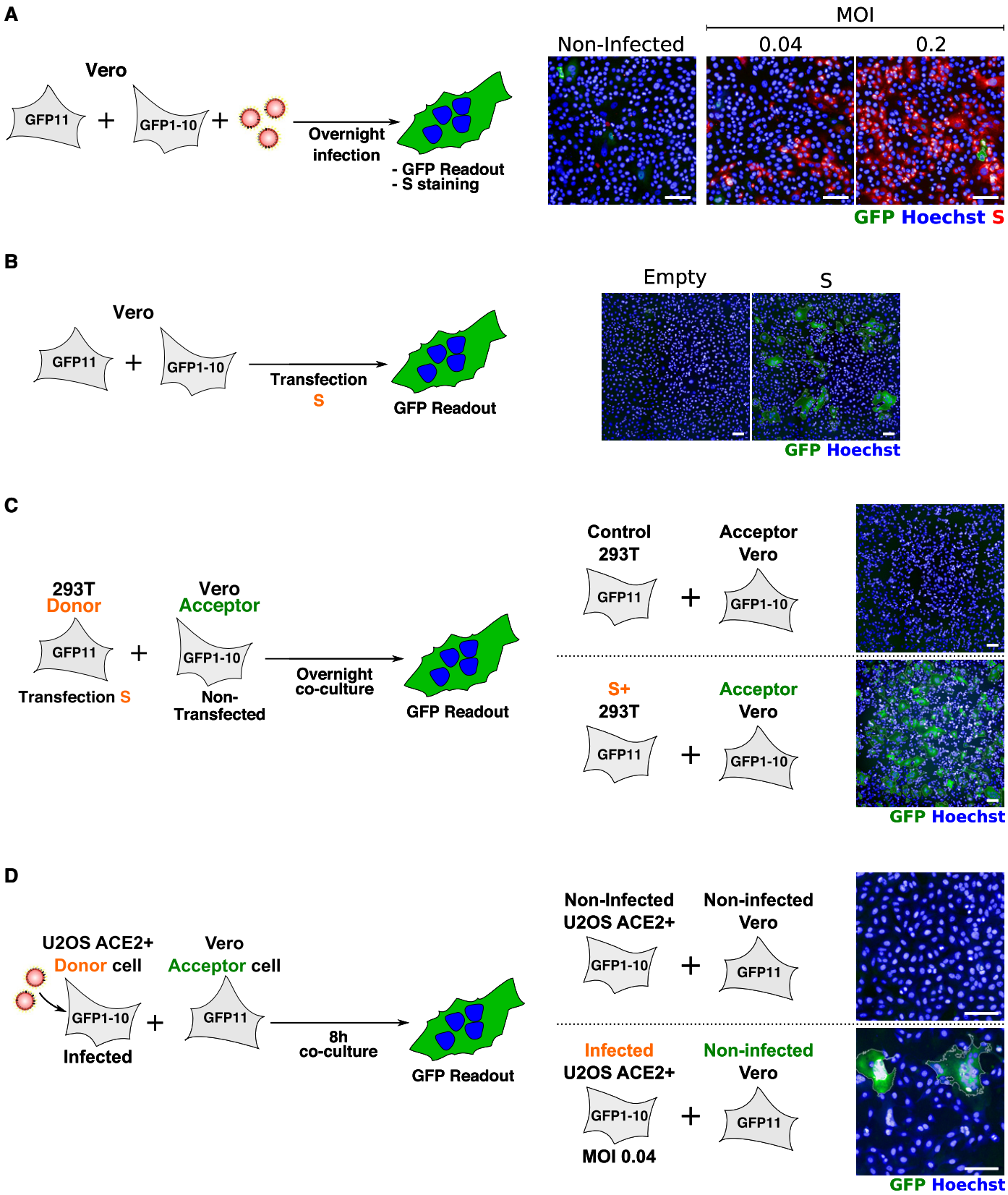

Figure EV5.

© 2020 The Authors

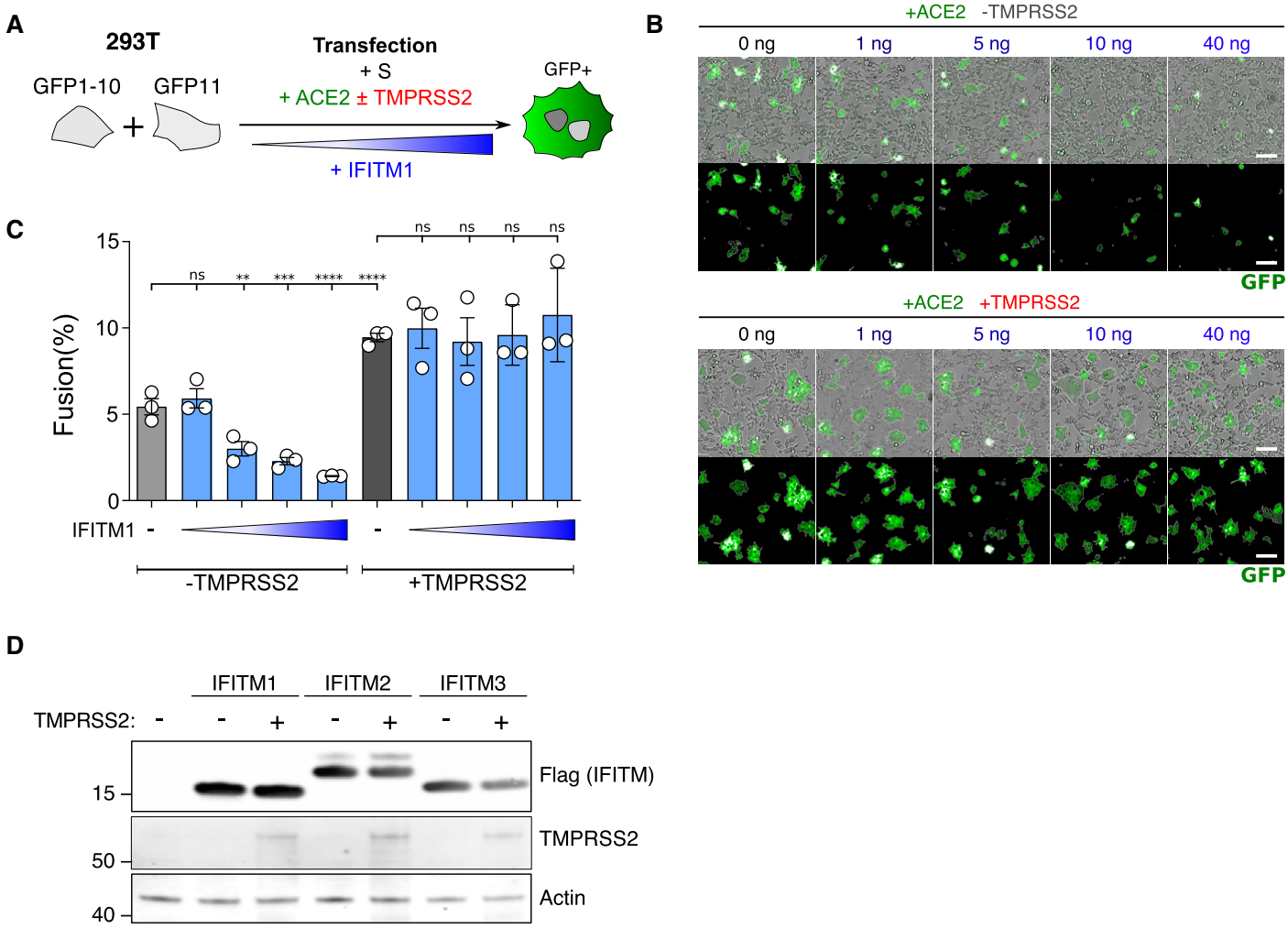

Figure EV6. Dose-response analysis of IFITM1 activity and impact of TMPRSS2 on IFITM1, 2, and 3 levels measured by Western blot.

A 293T-GFP1-10 and -GFP11 (1:1 ratio) were co-transfected with S, ACE2, TMPRSS2, and increasing amounts of IFITM1 plasmids. Cell fusion was quantified by measuring the GFP^+ area by high-content imaging at 18 h post-transfection

B Representative images of cell–cell fusion, with the indicated amounts of transfected plasmids. Scale bar: 100 μm.

C Quantification of GFP^+ area. Results are mean ± SD from three independent experiments. Statistical analysis: One-way ANOVA, ns: non-significant, $^{**}P < 0.01$, $^{***}P < 0.001$, $^{****}P < 0.0001$.

D 293T cells were co-transfected with TMPRSS2 and IFITM1, IFITM2, IFITM3, or control plasmids, and analyzed 18 h post-transfection by Western blot. TMPRSS2 does not cleave or reduce the levels of IFITMs.

© 2020 The Authors

Chapter 3: SARS-CoV-2 Alpha, Beta & Delta variants display enhanced spike-mediated syncytia formation

Preface to Chapter 3:

This chapter presents an article which was published at The EMBO Journal (2021) [218]. It is reproduced here with permission from EMBO (see permissions).

Rajah MM, Hubert M, Bishop E, Saunders N, Robinot R, Grzelak L, Planas D, Dufloo J, Gellenoncourt S, Bongers A, Zivaljic M, Planchais C, Guivel-Benhassine F, Porrot F, Mouquet H, Chakrabarti LA , Buchrieser J, Schwartz O. "SARS-CoV-2 Alpha, Beta and Delta variants display enhanced Spike-mediated Syncytia Formation" (2021) **The EMBO Journal** 0:e108944. https://doi.org/10.15252/embj.2021108944

The majority of the experiments as well as the data processing, figure generation and manuscript writing were done by the author. This work was supervised by Dr. Julian Buchrieser and Pr. Olivier Schwartz. The experiments for Figure 1 were done in collaboration with Mathieu Hubert and Rémy Robinot and the experiments for Figure 5 were done with Ludivine Grzelak. Two master's students Elodie Bishop and Nell Saunders were both supervised and trained by Julian Buchrieser and me and they contributed replicates to the fusion experiments.

Synopsis

Research Objective:

To characterize the fusogenicity of the S proteins of the Alpha, Beta, and Delta variants relative to the early European D614G strain and the ancestral Wuhan strain.

Highlights:

- The S proteins of the Alpha, Beta and Delta variants induce more syncytia than the D614G and Wuhan strains
- The ACE2 affinity of the full variant S proteins correlates to their fusogenicity
- Variant-associated mutations P681H, D1118H, and D215G increase cell-cell fusion, while the antibody escape mutations E484K, K417N and Δ242-244 hampers it.

Graphical Abstract 2 Fusogenicity of SARS-CoV-2 variants and associated S mutations

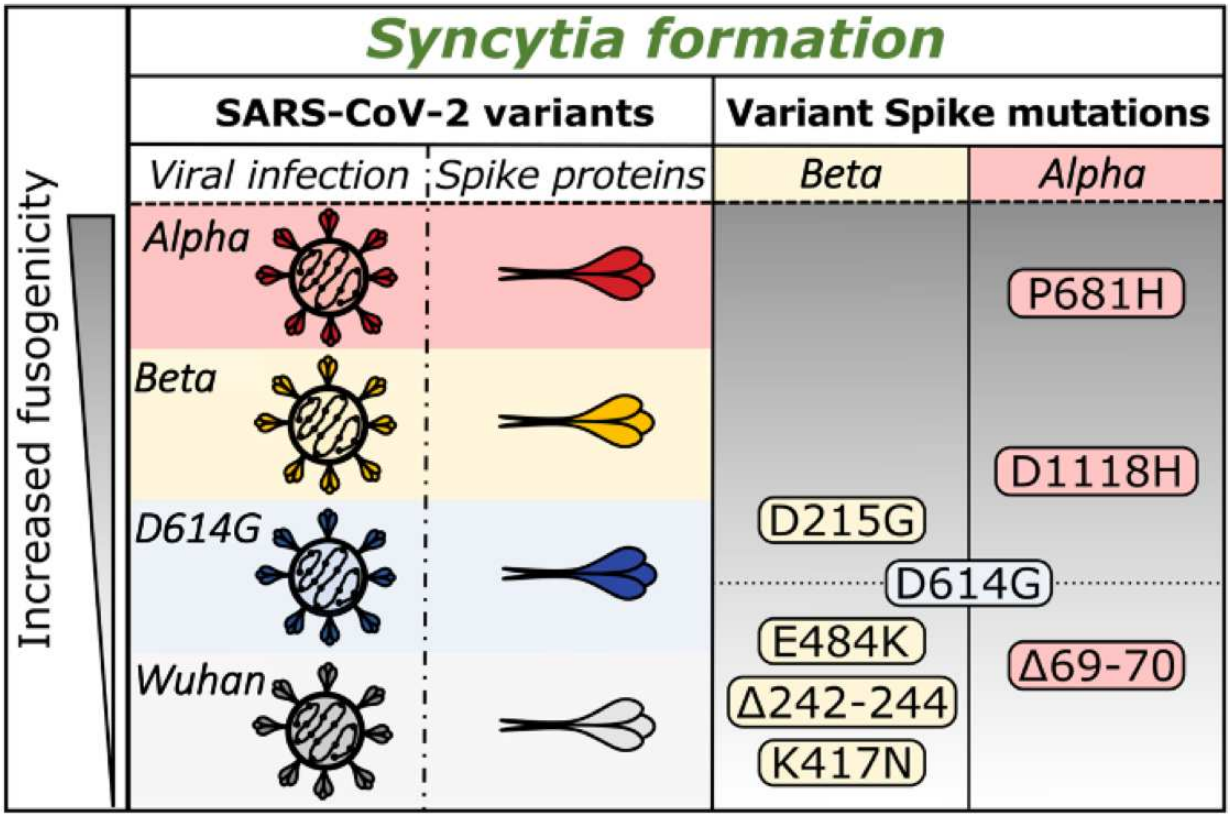

Article

TRANSPARENT PROCESS

THE EMBO JOURNAL

SARS-CoV-2 Alpha, Beta, and Delta variants display enhanced Spike-mediated syncytia formation

Maaran Michael Rajah[1,2], Mathieu Hubert[1,3,†], Elodie Bishop[1,4,†], Nell Saunders[1,†], Remy Robinot[1], Ludivine Grzelak[1,2], Delphine Planas[1,3], Jérémy Dufloo[1,2], Stacy Gellenoncourt[1,2], Alice Bongers[1,2], Marija Zivaljic[5,6], Cyril Planchais[7], Florence Guivel-Benhassine[1], Françoise Porrot[1], Hugo Mouquet[7], Lisa A Chakrabarti[1], Julian Buchrieser[1,*,‡] & Olivier Schwartz[1,2,**,‡]

Abstract

Severe COVID-19 is characterized by lung abnormalities, including the presence of syncytial pneumocytes. Syncytia form when SARS-CoV-2 spike protein expressed on the surface of infected cells interacts with the ACE2 receptor on neighboring cells. The syncytia forming potential of spike variant proteins remain poorly characterized. Here, we first assessed Alpha (B.1.1.7) and Beta (B.1.351) spread and fusion in cell cultures, compared with the ancestral D614G strain. Alpha and Beta replicated similarly to D614G strain in Vero, Caco-2, Calu-3, and primary airway cells. However, Alpha and Beta formed larger and more numerous syncytia. Variant spike proteins displayed higher ACE2 affinity compared with D614G. Alpha, Beta, and D614G fusion was similarly inhibited by interferon-induced transmembrane proteins (IFITMs). Individual mutations present in Alpha and Beta spikes modified fusogenicity, binding to ACE2 or recognition by monoclonal antibodies. We further show that Delta spike also triggers faster fusion relative to D614G. Thus, SARS-CoV-2 emerging variants display enhanced syncytia formation.

Keywords coronavirus; fusion; SARS-CoV-2; spike; syncytia

Subject Categories Immunology; Microbiology, Virology & Host Pathogen Interaction

DOI 10.15252/embj.2021108944 | Received 10 June 2021 | Revised 27 September 2021 | Accepted 28 September 2021

The EMBO Journal (2021) e108944

Introduction

SARS-CoV-2 was initially discovered during an outbreak in Wuhan, China, before it became pandemic (Huang *et al*, 2020a). Since its emergence, the ancestral Wuhan strain has been supplanted by variants harboring a variety of mutations. Several of these mutations occur in the highly antigenic Spike (S) protein which endowed many of the variants with the ability to evade part of the neutralizing antibody response (Weisblum *et al*, 2020; Planas *et al*, 2021a; Liu *et al*, 2021b; Rees-Spear *et al*, 2021; Starr *et al*, 2021). Individual amino acid changes in the S protein also affect viral fitness. One of the earliest identified variants contained the D614G mutation in S protein, which increased infectivity without significantly altering antibody neutralization (Yurkovetskiy *et al*, 2020). Several other variants have since emerged and have become globally dominant, including Alpha (B.1.1.7) first identified in the United Kingdom, Beta (B.1.351) identified in South Africa, Gamma (P.1 & P.2) identified in Brazil, and Delta (B.1.617.2) identified in India (preprint: Tegally *et al*, 2020; Buss *et al*, 2021; Frampton *et al*, 2021; Planas *et al*, 2021b; Sabino *et al*, 2021; preprint: Yadav *et al*, 2021). Some variants are more transmissible but their impact on disease severity is debated (Korber *et al*, 2020; Davies *et al*, 2021; Meng *et al*, 2021).

Clinically, SARS-CoV-2 infections range from asymptomatic or febrile respiratory disorders to severe lung injury characterized by vascular thrombosis and alveolar damage (Bussani *et al*, 2020). The deterioration of respiratory tissue is likely a result of both virus-induced cytopathicity and indirect immune-mediated damage (Buchrieser *et al*, 2020; Zhang *et al*, 2020; Zhou *et al*, 2020; Zhu *et al*, 2020). A peculiar dysmorphic cellular feature is the presence of large infected multinucleated syncytia, predominately comprised of pneumocytes (Bussani *et al*, 2020; Braga *et al*, 2021; Sanders

1 Virus & Immunity Unit, Department of Virology, Institut Pasteur, CNRS UMR 3569, Paris, France
2 Université de Paris, Sorbonne Paris Cité, Paris, France
3 Vaccine Research Institute, Creteil, France
4 Sorbonne Université, Paris, France
5 Integrative Neurobiology of Cholinergic Systems, Department of Neuroscience, Institut Pasteur, CNRS UMR 3571, Paris, France
6 Sorbonne Université, ED3C "Brain, Cognition, Behavior", Paris, France
7 Laboratory of Humoral Immunology, Department of Immunology, Institut Pasteur, INSERM U1222, Paris, France
*Corresponding author. Tel: +33 1 45 68 85 76; E-mail: julian.buchrieser@pasteur.fr
**Corresponding author. Tel: +33 1 45 68 83 53; E-mail: olivier.schwartz@pasteur.fr
†These authors contributed equally to this work as second authors
‡These authors contributed equally to this work as last authors

© 2021 The Authors

et al, 2021). Other coronaviruses including SARS-CoV-1, MERS-CoV, and HKU1 also induce syncytia formation in patient tissues and cell culture systems (Franks *et al*, 2003; Chan *et al*, 2013; Dominguez *et al*, 2013; Qian *et al*, 2013). Syncytial cells may compound SARS-CoV-2-induced cytopathicity, play a role in viral persistence and dissemination, and could be a pathological substrate for respiratory tissue damage (Buchrieser *et al*, 2020; Braga *et al*, 2021; Sanders *et al*, 2021). Release of syncytial cells may contribute to the overall infectious dose (preprint: Beucher *et al*, 2021). Heterocellular syncytia containing lymphocytes have also been documented in the lungs of infected patients (Zhang *et al*, 2021).

The SARS-CoV-2 S protein is a viral fusogen. The interaction of trimeric S with the ACE2 receptor and its subsequent cleavage and priming by surface and endosomal proteases results in virus-cell fusion (Hoffmann *et al*, 2020). Merging of viral and cellular membranes allows for viral contents to be deposited into the cell to begin the viral life cycle. Within the cell, newly synthesized S protein, envelope, and membrane proteins are inserted into the endoplasmic reticulum (ER) and trafficked and processed through the ER-Golgi network (Nal *et al*, 2005; Duan *et al*, 2020; Cattin-Ortolá *et al*, 2021). Virion are formed by budding into ER-Golgi membranes and are then transported to the surface in order to be released from the cell (Klein *et al*, 2020). While the majority of the S protein is sequestered within the ER, motifs within its cytoplasmic tail allow for leakage from the Golgi apparatus and localization at the plasma membrane (Cattin-Ortolá *et al*, 2021). The S protein at the surface of an infected cell interacts with receptors on adjacent cells, fusing the plasma membranes together and merging the cytoplasmic contents. We and others had previously shown that the S protein interacting with the ACE2 receptor induces cell–cell fusion (Buchrieser *et al*, 2020; Braga *et al*, 2021; Lin *et al*, 2021; Sanders *et al*, 2021; Zhang *et al*, 2021). The TMPRSS2 protease further augments cell–cell fusion (Buchrieser *et al*, 2020; Barrett *et al*, 2021; Hornich *et al*, 2021).

The S protein is comprised of S1 and S2 subunits. The S1 subunit includes the N-terminal domain (NTD) and the receptor-binding domain (RBD). The function of the NTD has yet to be fully elucidated but it may be associated with glycan binding, receptor recognition, and pre-fusion-to-post-fusion conformational changes. The NTD is also targeted by neutralizing antibodies (Krempl *et al*, 1997; Zhou *et al*, 2019; Chi *et al*, 2020). The RBD interacts with the ACE2 receptor and is the main target for neutralizing antibodies (Huang *et al*, 2020b). The S2 domain consists of the fusion peptide (FP), heptapeptide repeat sequences 1 and 2 (HR1 and HR2), the transmembrane anchor, and the C-terminal domain. The FP inserts into the target membrane by disrupting the lipid bilayer and anchors the target membrane to the fusion machinery (Huang *et al*, 2020b). This exposes regions of HR1 that interact with HR2, forming a flexible loop that brings the membranes together to facilitate fusion (Huang *et al*, 2020b). The versatility of the S protein suggests that any mutations that may have arisen are of particular concern as they can affect fusogenicity, antibody recognition, affinity to ACE2, proteolytic processing, and incorporation into virions. There is a general paucity of information regarding how the mutations associated with variant S proteins contribute to cell–cell fusion.

S-mediated cell–cell fusion is sensitive to innate immunity components. The interferon response to SARS-CoV-2 is one of the key factors down-modulating viral entry and replication, and deficiencies in the interferon response are associated with severe or critical COVID-19 (Arunachalam *et al*, 2020; Bastard *et al*, 2020, 2021; Hadjadj *et al*, 2020; van der Made *et al*, 2020). SARS-CoV-2-induced syncytia formation by the Wuhan strain is restricted by innate immunity, in part through the action of interferon-induced transmembrane proteins (IFITMs) (Buchrieser *et al*, 2020). IFITM1, 2, and 3 are restriction factors which display antiviral activity against a variety of enveloped viruses including SARS-CoV-2, likely by increasing membrane rigidity and hindering virus–cell fusion (Shi *et al*, 2021). Their effectiveness at restricting cell–cell fusion induced by the novel variants has yet to be assessed.

Here, we compared the replication and syncytia forming potential of D614G, Alpha, and Beta viruses in human cell lines and primary airway cells. We further characterized the fusogenicity of the Alpha and Beta variant S proteins and the individual contribution of each of the component mutations in syncytia formation, ACE2 binding, and evasion from a panel of antibodies. Finally, we examined the syncytia forming potential and ACE2 binding capacity of the Delta variant spike.

Results

Comparative replication kinetics of SARS-CoV-2 variants

We compared the replication kinetics of SARS-CoV-2 variants in relevant cell cultures. We first infected Caco-2, Calu-3, and Vero cells with Alpha, Beta, and D614G variants and generated multi-step growth curves (Fig 1). Cells were infected at an equivalent, non-saturating MOI, initially titrated in Vero cells (Appendix Fig S1A). Viral replication was assessed at 24, 48, and 72 h by flow cytometry upon staining with the pan-SARS-CoV-2 anti-S mAb102 human monoclonal antibody (Planas *et al*, 2021a) and then gating for S+ cells (Appendix Fig S1B). Globally, the variants replicated similarly (Fig 1). This similar replication was observed at different MOIs (Appendix Fig S1A). There were subtle differences at 24 h post-infection, depending on the cell line and the variant. For instance, Beta replicated slightly more than D614G in Caco-2 cells whereas Alpha replicated slight less than D614G in Vero cells (Fig 1A and C). Viral release at each time point was also assessed by extracting RNA from the supernatant and performing RT-qPCR for the gene encoding the N protein. Viral release was again roughly similar with the different variants, especially at early time points. Alpha produced moderately more virus than D614G in all cell lines at later time points (Fig 1A–C). Beta produced more virus than D614G in Caco-2 but less in Calu-3 cells at later time points (Fig 1A and B).

We then used the MucilAirB^{TM} model, which consists of primary human airway epithelial cells (HAEC) grown over a porous membrane and differentiated at the air–liquid interface for over 4 weeks. This relevant model is susceptible to SARS-CoV-2 infection (Pizzorno *et al*, 2020; Robinot *et al*, 2021; Touret *et al*, 2021). The cells were infected with each variant at a similar low viral inoculum (10^4 TCID50). Viral RNA and infectious virus release were monitored over 96 h by RT-qPCR and TCID50. Alpha and Beta variants produced slightly more extracellular viral RNA than D614G at later time points but not significantly higher levels of infectious particles (Fig 1D).

 © 2021 The Authors

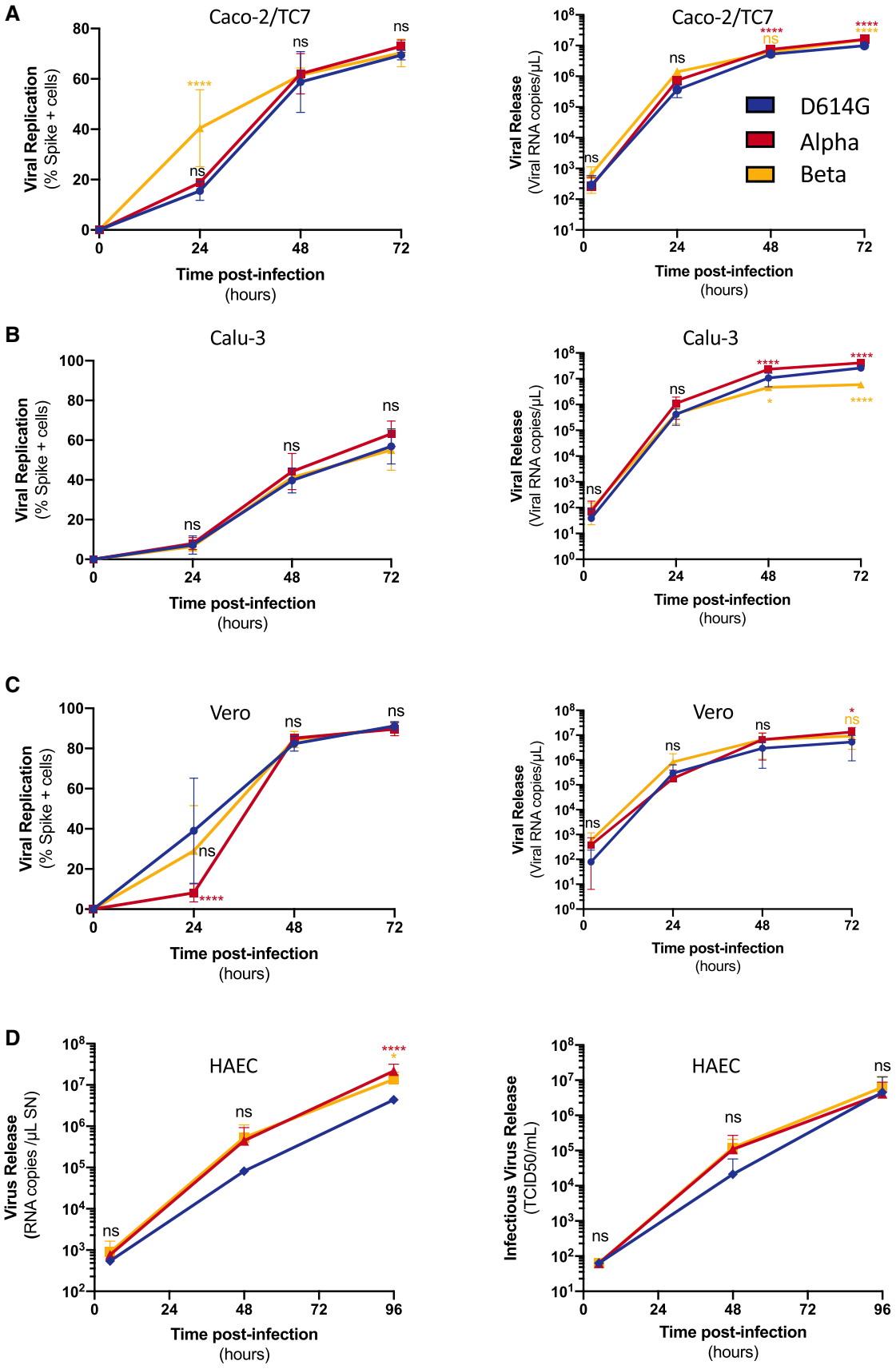

Figure 1.

© 2021 The Authors

Figure 1. Replication kinetics of D614G, Alpha, and Beta variants in cell culture.

A–D Cells were infected at the indicated MOI. Viral replication (left) and release (right) were assessed by flow cytometry and RT-qPCR. (A) Caco2/TC7 cells (MOI 0.01), (B) Calu-3 cells (MOI 0.001), (C) Vero cells (MOI 0.01), (D) primary human airway epithelial cells (HAEC) virus release (Right) and infectious virus release (Left) (MOI 0.01). Data are mean ± SD of at least three independent experiments. Statistical analysis: mixed-effect analysis or two-way ANOVA compared with D614G reference, ns: non-significant, *$P < 0.05$, ****$P < 0.0001$.

Taken together our data show that Alpha and Beta variants replicate similarly to the ancestral D614G strain in a panel of human cell lines and in primary cells, with some slight differences.

Syncytia formation in cells infected with SARS-CoV-2 variants

We next assessed the potential of SARS-CoV-2 variants to induce syncytia. In order to visualize cell–cell fusion, we employed our previously described S-Fuse assay, using U2OS-ACE2 GFP-split cells (Buchrieser *et al*, 2020). In the GFP-split complementation system, two cell lines containing half of the reporter protein are co-cultured, producing a GFP signal only upon fusion (Fig 2A). Upon infection of S-Fuse cells, we noticed that the Alpha and Beta variants formed larger and more numerous infected syncytia than either D614G or the ancestral Wuhan strain (Fig EV1A). We then characterized quantitatively the differences in fusogenicity by calculating the total syncytia (GFP) area and then normalizing it to nuclei number (Hoechst) (Fig EV1B). Relative to D614G, Alpha and Beta variants produced significantly more syncytia, approximately 4.5-fold and threefold respectively, after 20 h of infection with the same MOI (Fig 2B and Appendix Fig S2A). In order to characterize syncytia formation in a cell line expressing endogenous ACE2, we generated Vero cells carrying the GFP-split system. After 48 h of infection with the same MOI, we again found that Alpha and Beta variants produced significantly more syncytia than D614G (Fig 2C and Appendix Fig S2B) despite similar infection levels (Fig 1C). Of note, D614G produced similar levels of syncytia as the Wuhan strain in both Vero and S-Fuse cells (Fig 2 and Appendix Fig S2).

Therefore, Alpha and Beta variants appear more fusogenic than D614G in S-Fuse and Vero cells.

Syncytia formation in cells expressing variant S proteins

Since syncytia formation is a consequence of the S protein expressed on the surface of an infected cell interacting with ACE2 receptors on neighboring cell, we sought to compare the fusogenic potential of the individual variant S proteins. We introduced the D614G mutation into the Wuhan protein and designed plasmids to express Alpha and Beta S proteins. We transfected the respective plasmids into Vero GFP-split cells and quantified syncytia formation 18 h later (Fig 3A). Alpha and Beta S proteins were twofold and 1.7-fold more fusogenic than D614G S, respectively (Fig 3B). The Wuhan S was slightly less fusogenic that the D614G S (Fig 3B). We then verified that the variation in S-mediated fusion was not due to differential cell surface levels. Due to extensive fusion in transfected Vero cells, we were unable to compare S protein surface expression (Fig 3B and Movie EV1), as the S protein-positive syncytia were damaged and lost during the flow cytometry procedure. As such, we transfected 293T cells, which lack ACE2 and thus will not fuse with one another upon S expression, with the different variant plasmids in order to assess S protein surface levels by flow cytometry. The variants S proteins were equally expressed after transfection (Fig EV2A–C). In order to unify the surface expression control with our fusion results, we performed an acceptor/donor experiment. 293T GFP1-10 (donor) cells were transfected with each of the variant S plasmids. The transfected donor cells (equal number for each transfection condition) were then co-cultured with Vero GFP11 (acceptor) cells (Fig EV2E). Some of the transfected 293T donor cells were set aside and stained for S protein to show equal surface expression between the variants (Fig EV2E). In the acceptor/donor co-culture, we found that the 293T donor cells expressing the novel variant S proteins formed more syncytia with the Vero acceptor cells than either the D614G or Wuhan (Fig EV2E). The results of the acceptor/donor co-culture experiment matched our fusion results in Vero cells.

We then measured the kinetics of syncytia formation induced by the different S proteins in Vero GFP-Split cells. We conducted a comparative videomicroscopy analysis where cell–cell fusion could be visualized as soon as 6 h post-transfection. The fusion kinetics of Alpha S protein was more rapid than any of the other variants (Fig 3C and Movie EV1). Beta also induced significantly faster fusion than D614G, whereas the Wuhan S was the slowest of all the compared proteins (Fig 3C and Movie EV1).

Altogether, our data indicate that the S proteins of Alpha and Beta variants form more syncytia than the D614G or Wuhan strains.

Restriction of S-mediated syncytia formation by IFN-β1 and IFITMs

As the variants did not show any major difference in replication under basal conditions, we next investigated whether they were differently sensitive to the interferon response. To this aim, we pretreated Vero cells or U2OS-ACE2 (S-Fuse) cells with increasing doses of IFN-β1 and infected them with the different variants. IFN-β1 was equally effective at reducing viral replication of D614G, Alpha, and Beta variants in Vero cells (Fig EV3A). Preincubation of S-Fuse cells with IFN-β1 also abrogated infection and syncytia formation to the same extent for the different variants (Fig EV3B). Therefore, IFN-β1 similarly inhibited viral replication and reduced syncytia formation by D614G, Alpha, and Beta variants.

IFITMs are interferon-stimulated transmembrane proteins that restrict early stages of the viral life cycle by inhibiting virus-cell fusion, likely by modifying the rigidity or curvature of membranes (Compton *et al*, 2014; Shi *et al*, 2017; Zani & Yount, 2018). IFITM1 localizes at the plasma membrane while IFITM2 and 3 transit through surface and localize in endo-lysosomal compartments (Buchrieser *et al*, 2020). We previously reported that IFITMs restrict Wuhan S-mediated cell–cell fusion and that their activity was counteracted by the TMPRSS2 protease (Buchrieser *et al*, 2020). As infection with Alpha and Beta induce more syncytia, we further investigated if this resulted in an increased resistance to IFITM

© 2021 The Authors

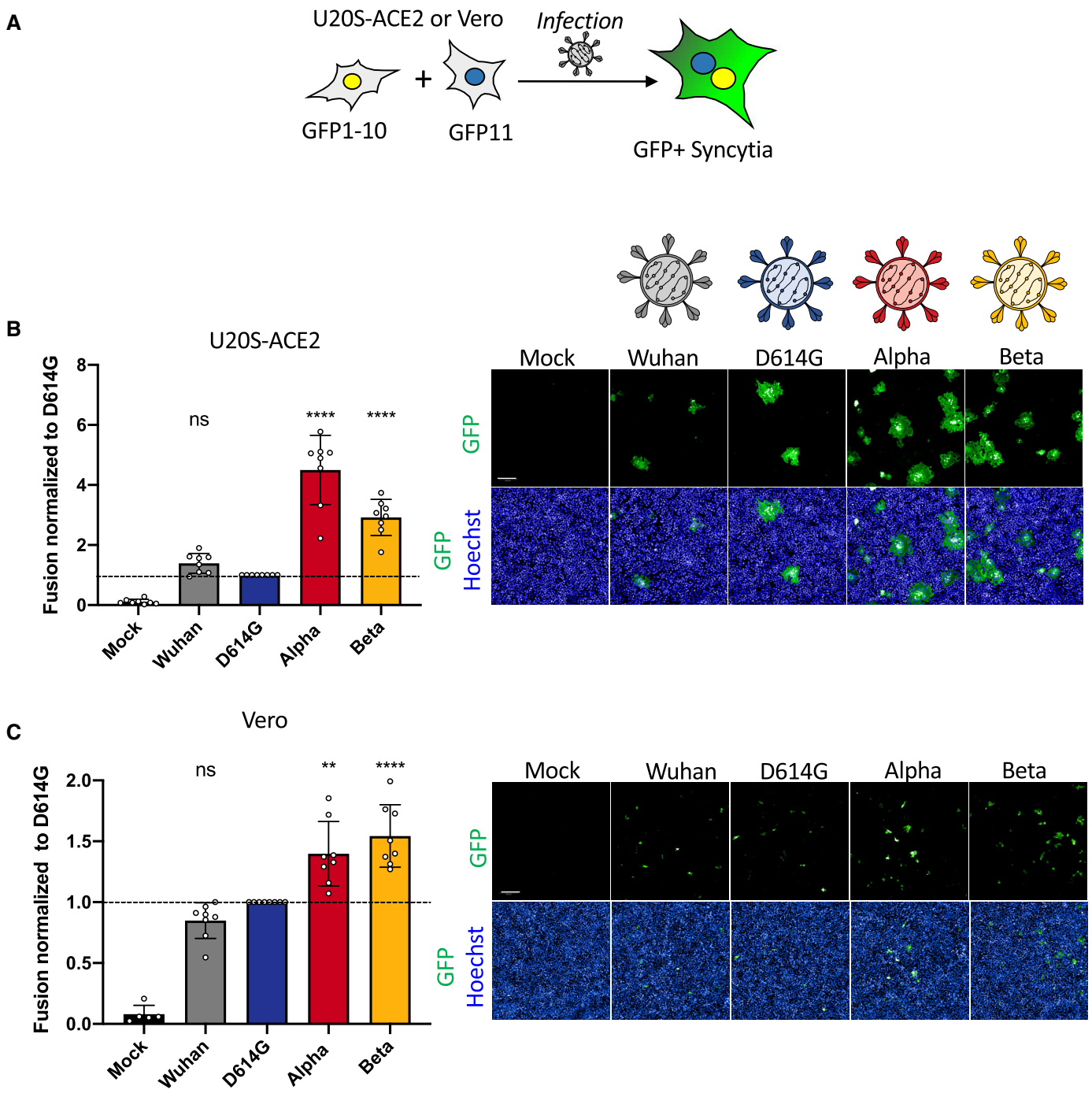

Figure 2. SARS-CoV-2 variant infection increases formation of syncytia in U2OS-ACE2 and Vero GFP-split cells.

A U2OS-ACE2 or Vero cells expressing either GFP 1–10 or GFP 11 (1:1 ratio) were infected 24 h after plating and imaged 20 h (U2OS-ACE2) or 48 h (Vero) post-infection.

B Left Panel: Fusion was quantified by GFP area/ number of nuclei and normalized to D614G for U2OS-ACE2 20 h post-infection at MOI 0.001. Right Panel: Representative images of U2OS-ACE2 20 h post-infection, GFP-Split (green), and Hoechst (blue). Top and bottom are the same images with and without Hoechst channel.

C Left Panel: Quantified fusion of Vero cells infected at MOI 0.01. Right Panel: Representative images of Vero cells 48 h post-infection, GFP-Split (green), and Hoechst (blue).

Data information: Scale bars: 200 μm. Data are mean ± SD of eight independent experiments. Statistical analysis: one-way ANOVA compared with D614G reference, ns: non-significant, $^{**}P < 0.01$, $^{****}P < 0.0001$.

© 2021 The Authors

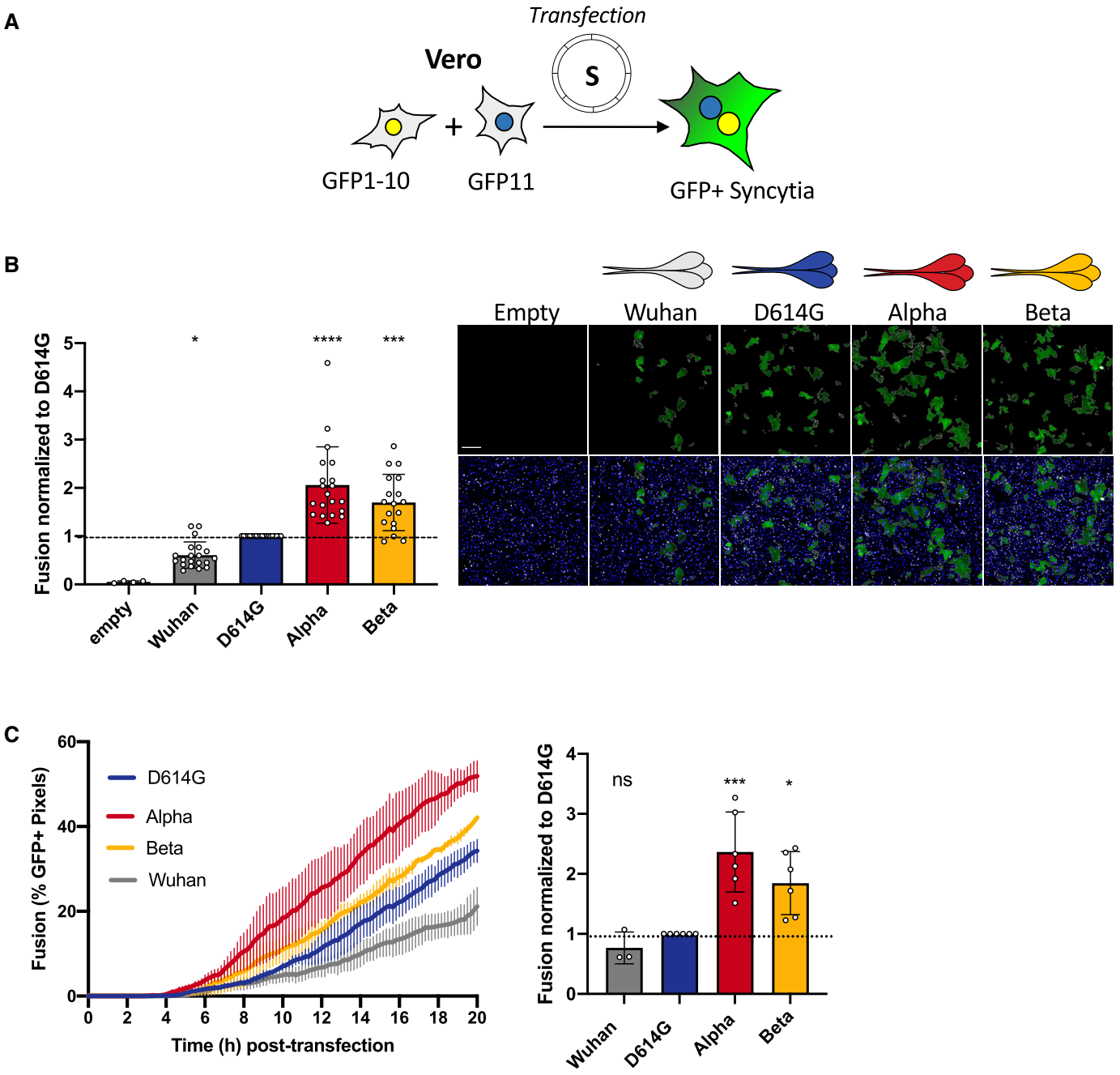

Figure 3. Alpha and Beta SARS-CoV-2 S proteins induce more robust syncytia formation than D614G.

A Vero GFP-split cells were transfected with variant S proteins and imaged 18 h post-transfection.

B Left Panel: Fusion was quantified by GFP area/number of nuclei and normalized to D614G for each of the transfected variant S proteins. Right Panel: Representative images of Vero GFP-split cells 18 h post-transfection, GFP (green), and Hoechst (blue). Top and bottom are the same images with and without Hoechst channel. Scale bars: 200 μm.

C Left Panel: Quantification of variant S protein-mediated fusion in Vero GFP-split cells by video microscopy. Results are mean ± SD from three fields per condition from one representative experiment. Right Panel: Fusion quantification of at least three independent video microscopy experiments, 20 h post-transfection, normalized to D614G.

Data information: Data are mean ± SD of at least three independent experiments. Statistical analysis: one-way ANOVA compared with D614G reference, ns: non-significant, *$P < 0.05$, ***$P < 0.001$, ****$P < 0.0001$.

restriction. We thus characterized the impact of IFITMs on syncytia formed upon expression of D614G, Alpha, and Beta S proteins in 293T cells. The variants were all effectively restricted by IFITMs (Fig EV3C–G). The three IFITMs were expressed at similar levels in our system (not shown). The presence of TMPRSS2 increased fusion of all S proteins and reverted the restriction by IFITMs

© 2021 The Authors

(Fig EV3C–G). Taken together, our data show that Alpha and Beta variants induce more syncytia, but their S proteins remain similarly sensitive to IFITMs.

Contribution of individual variant-associated mutations on S protein-mediated fusogenicity

We next sought to determine the contribution of each variant-associated mutation to cell–cell fusion. Both Alpha and Beta S proteins contain the N501Y mutation in the RBD and the D614G mutation in the S1/S2 cleavage site (Fig 4A). Alpha S contains the Δ69/70 and ΔY144 deletions in the N-terminal domain (NTD), P681H and T716I mutations in the S1/S2 cleavage site, the S982A mutation in the heptad repeat 1 (HR1) site and the D1118H mutation in between HR1 and HR2. The Beta S is comprised of the L18F, D80A, D215G, and Δ242-244 mutations in the NTD, K417N and E484K mutations in the receptor-binding domain (RBD), and A701V in the S1/S2 cleavage site. We introduced individual mutations into the D614G background. Following reports of the emergence of the E484K mutation within the Alpha variant (Collier *et al*, 2021), we also generated a mutant Alpha S protein with the E484K mutation. We observed by flow cytometry that the mutant S proteins were similarly expressed at the cell surface (Fig EV2A–D). We expressed each mutant S into Vero GFP split cells and measured their potential to induce cell–cell fusion in comparison to the D614G S protein.

Of the mutations that are associated with Alpha, we found that the Δ69/70 deletion in the NTD decreased cell–cell fusion whereas P681H and D1118H substitutions both increase fusion (Figs 4A and EV4E). P681H displayed the greatest fusogenicity of all investigated mutations, being almost 2.5-fold higher than D614G S (Figs 4A and EV4E). As previously mentioned, the introduction of the D614G mutation in the S1/S2 border of the Wuhan S protein also relatively increased fusion, stressing the importance of this cleavage site in fusogenicity (Fig 3B).

Among the mutations associated with Beta, the Δ242-244 deletion, as well as the K417N and E484K mutations in the RBD significantly decreased syncytia formation (Figs 4A and EV4F). Only the D251G mutation in the NTD modestly increased syncytia formation relative to D614G (Figs 4A and EV4F). The introduction of the E484K RBD mutation into the Alpha S protein significantly decreased its potential to form syncytia, despite not changing cell surface expression, further supporting the mutation's restrictive effect on cell–cell fusion (Figs 4B and EV2B). Taken together, our data suggest that variant S proteins are comprised of mutations that play contrasting roles in cell–cell fusion. P681H, D1118H, and D215G substitutions facilitate fusion, whereas mutations Δ69/70, Δ242-244, K417N, and E484K antagonize cell–cell fusion.

Binding of S proteins bearing individual variant-associated mutations to ACE2

We next explored the impact of variant-associated mutations on S binding to the ACE2 receptor. To this aim, we transiently expressed each mutant protein in 293T cells. Cells were then stained with a serial dilution of soluble biotinylated ACE2, revealed with fluorescent streptavidin, and then analyzed by flow cytometry (Fig 5A). Titration binding curves were generated, and EC50 (the amount of ACE2 needed for 50% binding) was calculated. The S protein of Alpha had the highest affinity to ACE2, confirming previous results by us and others (Planas *et al*, 2021; Ramanathan *et al*, 2021). Alpha was sequentially followed by Beta, D614G, and Wuhan S (Figs 5B and EV5A). As expected, mutations within the RBD had the most significant impact on ACE2 binding. N501Y found in both Alpha and Beta drastically increased ACE2 binding, in line with previous reports indicating that this mutation enhances affinity of the viral protein to its receptor (Ali *et al*, 2021; Luan *et al*, 2021; Tian *et al*, 2021). The K417N substitution present in the Beta S decreased ACE2 binding (Figs 5B and EV5C). The E484K mutant had a slightly, but not significantly, higher binding to ACE2 (Fig EV5C). This was corroborated by the observation that addition of the E484K mutation to Alpha S protein also slightly increased ACE2 binding (Figs 5B and EV5A). Mutation in the S1/S2 cleavage site, HR1/HR2 sites, or NTD did not have any significant impact on ACE2 binding (Figs 5B and EV5B–E). It is worth noting that the NTD Δ242-244 mutant displayed a marginally lower binding to ACE2 (Figs 5B and EV5B). Therefore, the N501Y mutation is the most significant contributor to increased ACE2 binding of the variants, though it does not affect cell–cell fusion on its own. The K417N, Δ242-244, and E484K mutations restrict fusogenicity but differently affect ACE2 binding, with the former two decreasing affinity and the latter slightly increasing.

Therefore, ACE2 binding and fusogenicity are two functions of the S protein that can be partially deconvoluted through individual mutations.

Antibody binding to S proteins bearing individual variant-associated mutations

We had previously found that certain neutralizing antibodies differentially affect SARS-CoV-2 D614G, Alpha, and Beta variants (Planas *et al*, 2021a). For instance, neutralizing monoclonal antibody 48 (mAb48) restricts D614G virus but not Alpha or Beta variants (Planas *et al*, 2021a). We sought to determine which mutations in variant S proteins contributed to the lack of recognition by the neutralizing antibodies. To this aim, we assessed by flow cytometry the binding of a panel of four human monoclonal antibodies (mAbs) to the different S mutants. As a control we used mAb10, a pan-coronavirus antibody that targets an unknown but conserved epitope within the S2 region (Planchais, manuscript in preparation). mAb10 equally recognized all variants and associated individual mutations (Fig 5C). mAb48 and mAb98 target the RBD and mAb71 the NTD (Planas *et al*, 2021b) (Planchais, manuscript in preparation). mAb48 did not recognize the Beta variant and more specifically did not bind to the K417N mutant (Fig 5C). The mAb71 recognized neither Alpha nor Beta variants and did not bind to their respective NTD ΔY144 and Δ242-244 mutations. The K417N and Δ242-244 mutations were also responsible for decreasing S-mediated fusion, suggesting a tradeoff between antibody escape and fusion (Fig 5C). mAb98 did not recognize the Beta variant. However, none of the associated mutations were specifically responsible for the lack of binding (Fig 5C), suggesting a combined effect on the structure of the S protein that may affect antibody escape.

Therefore, several of the mutations found in the variants S proteins are advantageous in terms of antibody escape, despite slightly reducing the ability of the proteins to fuse.

© 2021 The Authors

S protein-mediated syncytia formation by the Delta variant

With the emergence and rapid spread of the Delta variant, we sought to characterize its potential to form syncytia. We recently showed that the Delta variant induces large syncytia in S-Fuse cells (Planas *et al*, 2021b). We thus compared the fusogenicity of the Delta S protein to that of D614G and Alpha. We transiently expressed the three S proteins in Vero GFP-split cells. The Delta S protein triggered more cell–cell fusion than the D614G variant but was similar to the Alpha S protein (Fig 6A). The fusion kinetic of the Delta S was also similar to Alpha but more rapid than D614G (Fig 6B). We confirmed that the variant S proteins were equally expressed on the surface by transfecting them into non-fusogenic 293T cells and performing flow cytometry upon staining with the pan-SARS-CoV-2 mAb129 (Fig EV2D). We next examined the ACE2 binding potential of Delta S protein using our aforementioned

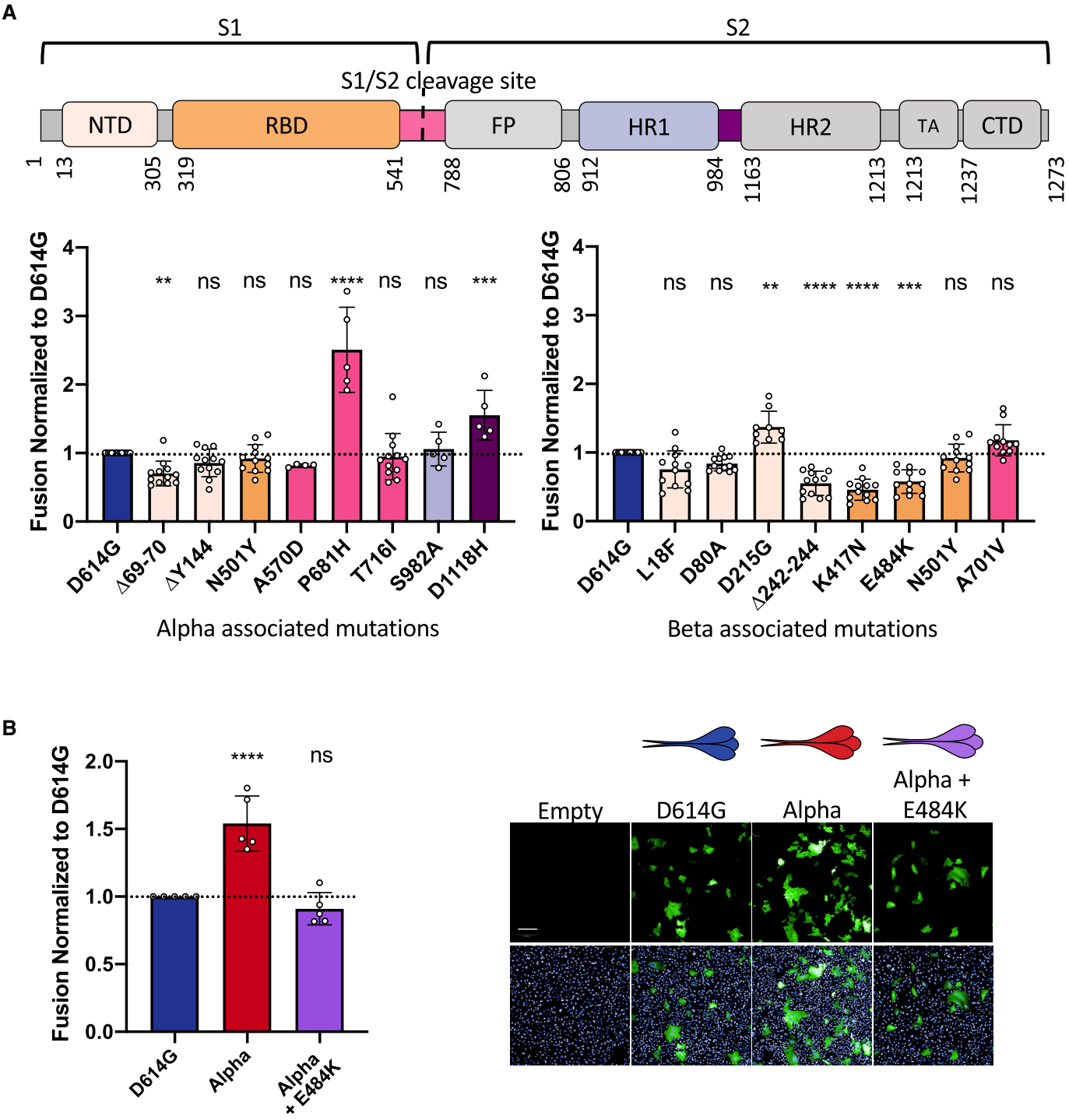

Figure 4.

© 2021 The Authors

Figure 4. Mutations associated with Alpha and Beta S proteins differentially affect cell–cell fusion.

A Top Panel: Schematic representation of the S protein color-coded for the functional regions: N-terminal domain (NTD), receptor-binding domain (RBD), fusion peptide (FP), heptad repeat 1,2 (HR1, HR2), transmembrane anchor (TA), C-terminal domain (CTD). Bottom left Panel: Vero GFP-split cells were transfected with S plasmids containing each of the individual mutations associated with Alpha variant in the D614G background. The amount of fusion was quantified at 20 h and normalized to D614G reference plasmid. Bottom right Panel: Quantified fusion for each of the individual S protein mutations associated with the Beta variant. Color code of each mutation corresponds to S protein functional regions represented in the schematic on the Top Panel. Data set for N501Y and D614G reference mutations are duplicated between bottom left and bottom right panels for presentation as these mutations are common to both variants.

B Left Panel: Quantified fusion of the Alpha + E484K variant S protein normalized to D614G S. Right Panel: Representative images of fusion at 20 h. Scale bar: 200 μm. Top and bottom are the same images with and without Hoechst channel.

Data information: Data are mean ± SD of at least four independent experiments. Top and bottom are the same images with and without Hoechst channel. Statistical analysis: statistics for both left and right panels of A were conducted together. One-way ANOVA compared with D614G reference, ns: non-significant, $^{**}P < 0.01$, $^{***}P < 0.001$, $^{****}P < 0.0001$.

soluble biotinylated ACE2. The Delta S protein has a higher binding capacity to ACE2 than the D614G S protein, but the binding was lower than the Alpha S protein (Fig 6C).

S protein-mediated syncytia formation and TMPRSS2

We then asked whether the TMPRSS2 protease, which cleaves S and facilitates viral fusion, may act differently on the variant S proteins. To this aim, we generated a Caco2 GFP-split cell line and then expressed the different S proteins to examine fusogenicity. Human Caco2 cells express endogenous levels of TMPRSS2 and ACE2. In line with our results in Vero cells which lack endogenous TMPRSS2 (Fig 3B), we found that the Alpha, Beta, and Delta variants fused more than the D614G, and the Wuhan S protein fused the least (Fig 6D). Thus, the differences in variant fusogenicity can also be visualized in the presence of TMPRSS2. In order to see whether TMPRSS2 differentially processes the variants S proteins, we expressed each of them without or with TMPRSS2 in 293T cells in the absence ACE2. We examined the processing of the different S by western blot and the expression levels of S1 and S2 by flow cytometry. While all S proteins are processed, the cleavage profile induced by TMPRSS2 and the expression levels between the different variant S proteins were similar (Appendix Fig S3).

Discussion

The replication and cytopathic effects of SARS-CoV-2 variants are under intense scrutiny, with contrasting results in the literature (Hou *et al*, 2020; Frampton *et al*, 2021; Leung *et al*, 2021; preprint: Liu *et al*, 2021a; Touret *et al*, 2021). For instance, there was no major difference in the replication kinetics of Alpha and D614G strains in some reports (preprint: Thorne *et al*, 2021; Touret *et al*, 2021), whereas others suggested that Alpha may outcompete D614G in a co-infection assay (Touret *et al*, 2021). Some studies proposed that the N501Y mutation may provide a replication advantage, whereas others suggested that N501Y is deleterious (Hou *et al*, 2020; Frampton *et al*, 2021; Leung *et al*, 2021; preprint: Liu *et al*, 2021a). These discrepant results may be due to the use of different experimental systems, viral strains, multiplicities of infection, and cell types.

Here, we show that Alpha and Beta variants replicate to the same extent as the early D614G strain in different human cell lines and primary airway cells. Moreover, Alpha and Beta induced more cell–cell fusion than D614G. Increased fusion was observed in U2OS-ACE2 cells and in naturally permissive Vero cells. In agreement with infection data, transfection of Alpha and Beta S proteins in the absence of any other viral factors, produced significantly more syncytia than D614G, which in turn, fused more than the Wuhan S. Comparative video microscopy analysis revealed that Alpha S fused the most rapidly, followed by Beta, D614G, and finally Wuhan. Thus, Alpha and Beta variants display enhanced S-mediated syncytia formation. One limitation of our study resides in the fact that were unable to look at surface expression of the variant S proteins in Vero and Caco2 without losing the large S protein-positive syncytia. We thus used the non-fusogenic 293T cells to control for surface expression. We further show that S-expressing 293T cells fuse with Vero cells in donor/acceptor experiments. The experiments confirmed the enhanced fusogenicity of the variants in cells with similar levels of S protein at their surface.

We further show that Alpha and Beta remain sensitive to restriction by IFN-β1. The fusion mediated by their respective S proteins is inhibited by IFITMs. This extends previous results by us and others demonstrating that ancestral Wuhan S is effectively inhibited by this family of restriction factors (Buchrieser *et al*, 2020; Shi *et al*, 2021). It has been recently reported in a pre-print that Alpha may lead to lower levels of IFN-β1 production by infected Calu-3 cells and may be less sensitive to IFN-β pre-treatment, when compared to first wave viral isolates (preprint: Thorne *et al*, 2021). We did not detect here differences of IFN-β1 sensitivity between the variants in Vero and U2OS-ACE2 cells. Again, these discrepant results may reflect inherent differences between Calu-3, Vero, and U2OS-ACE2 cells, or the use of different viral isolates.

We then characterized the contribution of the individual mutations present in Alpha and Beta S proteins to their respective fusogenicity. The highly fusogenic Alpha S consists of more mutations that robustly increase fusion (P681H and D1118H) than mutations that decrease fusion (Δ69/70). In contrast, the Beta variant is comprised of several restrictive mutations (Δ242-244, K417N, and E484K) and only one mutation that modestly increased fusion (D215G). The strongest increase in fusion was elicited by the P681H mutation at the S1/S2 border. This mutation likely facilitates proteolytic cleavage of S and thus promotes S mediate cell–cell fusion. Indeed, the analogous P681R mutation present in B.1.617.2 and B.1.617.3 variants increases S1/S2 cleavage and facilitates syncytia formation (Jiang *et al*, 2020; preprint: Ferreira *et al*, 2021). Of note, another report with indirect assessment of variant S fusogenicity

© 2021 The Authors

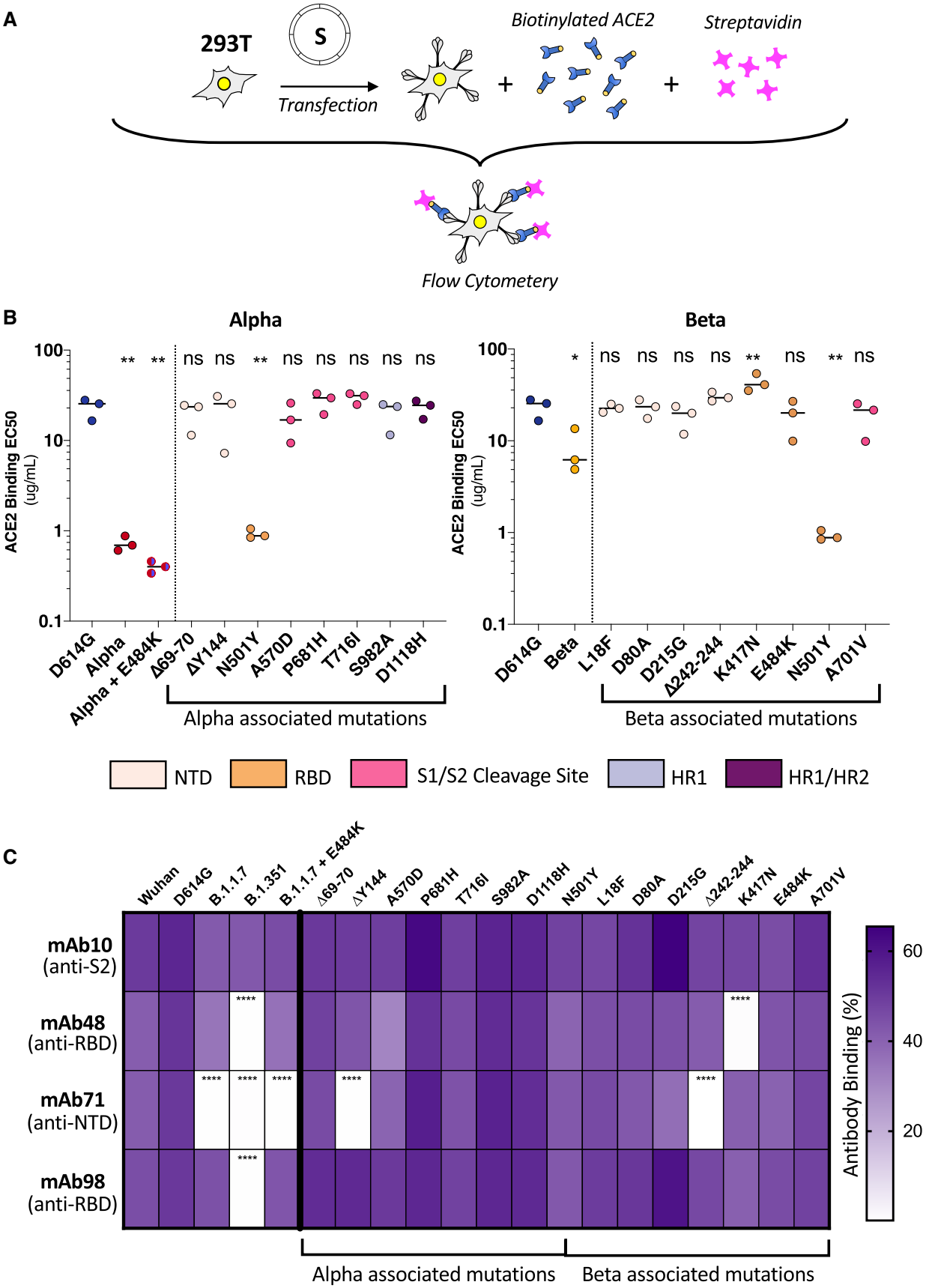

Figure 5.

© 2021 The Authors

Figure 5. ACE2 and monoclonal antibody binding to S proteins with Alpha and Beta associated mutations.

A 293T cells were transfected S proteins with each variant-associated mutation for 24 h and stained with biotinylated ACE2 and fluorescent streptavidin before analysis by flow cytometry.

B Left Panel: EC50 values (concentration of ACE2 needed for 50% binding) for Alpha and associated mutations. Color code corresponds to location on S protein functional domains and lower EC50 values signify higher affinity to ACE2 binding. Right Panel: EC50 values for Beta and associated mutations. Data set for N501Y and D614G reference mutations are duplicated between left and right panels as mutations are common to both variants.

C S protein transfected 293T cells were stained with human monoclonal antibodies targeting the S2 (mAb10), RBD (mAb48 and mAb98), and the NTD (mAb71). Cells were analyzed by flow cytometry. The percentage of positive cells is indicated.

Data information: Data are mean of at least three independent experiments. Statistical analysis: one-way ANOVA compared with D614G reference, ns: non-significant, $*P < 0.05$, $**P < 0.01$, $****P < 0.0001$.

suggested a mild decrease or no difference in cell–cell fusion of Alpha and Beta relative to Wuhan S (Hoffmann *et al*, 2021). These previous experiments were performed in 293T cells at a late time points (24 h post-transfection), which may preclude detection of the accelerated fusion triggered by the variants.

We show that the binding of variant S to soluble ACE2 paralleled their fusogenicity. Alpha bound the most efficiently to ACE2, followed by Beta, D614G, and finally Wuhan. However, the ACE2 affinity of S proteins carrying individual mutations did not exactly correlate to fusogenicity. For instance, the N501Y and D614G mutations drastically increased ACE2 affinity, but only D614G enhanced fusogenicity. The K417N substitution, and to a lesser degree Δ242–244, had a lower affinity to ACE2 and also restricted cell–cell fusion. The E484K mutation significantly restricts fusion, but mildly increases ACE2 affinity. This suggests that on the level of individual S mutations, the relationship between ACE2 affinity and increased fusogenicity is not always linear. Variant mutations may also confer advantages in an ACE2-independent manner. Indeed, recent work has suggested that the E484 mutation may facilitate viral entry into H522 lung cells, requiring surface heparan sulfates rather than ACE2 (Puray-Chavez *et al*, 2021). It would be of future interest to examine the syncytia formation potential of the variant mutations in other cell types.

We selected a panel of 4 mAbs that displayed different profiles of binding to Alpha, Beta, D614G, and Wuhan S proteins. The mAb10 targeting the S2 domain recognized all variants and was used as a positive control. Wuhan and D614G were recognized by the three other antibodies, targeting either the NTD or RBD. Alpha lost recognition by the anti-NTD mAb71, whereas Beta was neither recognized by mab71 nor by the two anti-RBD antibodies mAb48 and mAb 98. Upon examining the potential of S proteins carrying individual mutations to bind to human monoclonal antibodies, we found that the ones that restrict (Δ242–244, K417N) or have no effect on fusogenicity (ΔY144) are also not recognized by some mAbs. This suggests that variant S proteins have undergone evolutionary trade-off in some circumstances, selecting for mutations that provide antibody escape at the detriment of fusogenicity. In accordance with our findings, deep sequence binding analysis and in vitro evolution studies suggest the N501Y mutation increases affinity to ACE2 without disturbing antibody neutralization (preprint: Liu *et al*, 2021a; Starr *et al*, 2021; Zahradník *et al*, 2021). The E484K and K417N RBD mutations in the Beta variant may also increase ACE2 affinity, particularly when in conjunction with N501Y (preprint: Nelson *et al*, 2021; Zahradník *et al*, 2021). However, the resulting conformational change of the S protein RBD may also decrease sensitivity to neutralizing antibodies (preprint: Nelson *et al*, 2021). Future work assessing the structural and conformational changes in the S protein elicited by a combination of individual mutations or deletions may further help elucidate the increased fusogenicity and antibody escape potential of the variants.

While we had previously shown that the interaction between the S protein on the plasma membrane with the ACE2 receptor on neighboring cells is sufficient to induce syncytia formation, there is compelling evidence of the importance of the TMPRSS2 protease in S activation (Buchrieser *et al*, 2020; Dittmar *et al*, 2021; Koch *et al*, 2021; Ou *et al*, 2021). We found that the S protein of the novel variants induced more syncytia formation than the D614G and Wuhan S proteins in human Caco2 cells which express endogenous ACE2 and TMPRSS2. However, we did not detect any major differences in the processing of the variant S proteins by TMPRSS2. It will be worth further characterizing how the fusogenicity of variant-associated mutations is influenced by other cellular proteases like furin.

The presence of infected syncytial pneumocytes was documented in the lungs of patients with severe COVID-19 (Bussani *et al*, 2020; Tian *et al*, 2020; Xu *et al*, 2020). Syncytia formation may contribute to SARS-CoV-2 replication and spread, immune evasion, and tissue damage. A report using reconstituted bronchial epithelia found that viral infection results in the formation and release of infected syncytia that contribute to the infectious dose (preprint: Beucher *et al*, 2021). The neutralizing antibody response to SARS-CoV-2 infection has divergent effect on cell–cell fusion, with some antibodies restricting S-mediated fusion, while other increase syncytia formation (Asarnow *et al*, 2021). Cell-to-cell spread of virus may be less sensitive to neutralization by monoclonal antibodies and convalescent plasma than cell-free virus (preprint: Jackson *et al*, 2021). It is thus possible that infected syncytial cells facilitate viral spread. Within this context, it is necessary to better understand the fusogenic potential of the SARS-CoV-2 variants that have arisen and will continue to emerge.

We have characterized here the replication, fusogenicity, ACE2 binding, and antibody recognition of Alpha and Beta variants and the role of their S-associated mutations. Despite the insights we provide into the S-mediated fusogenicity of the variants, we did not address the conformational changes that the mutations individually or in combination may elicit. We further show that Alpha, Beta, and Delta S proteins more efficiently bind to ACE2 and are more fusogenic than D614G. The virological and immunological features of the Delta variant which explain its higher transmissibility rate compared to the Alpha and other variants at the population level remains an outstanding question.

© 2021 The Authors

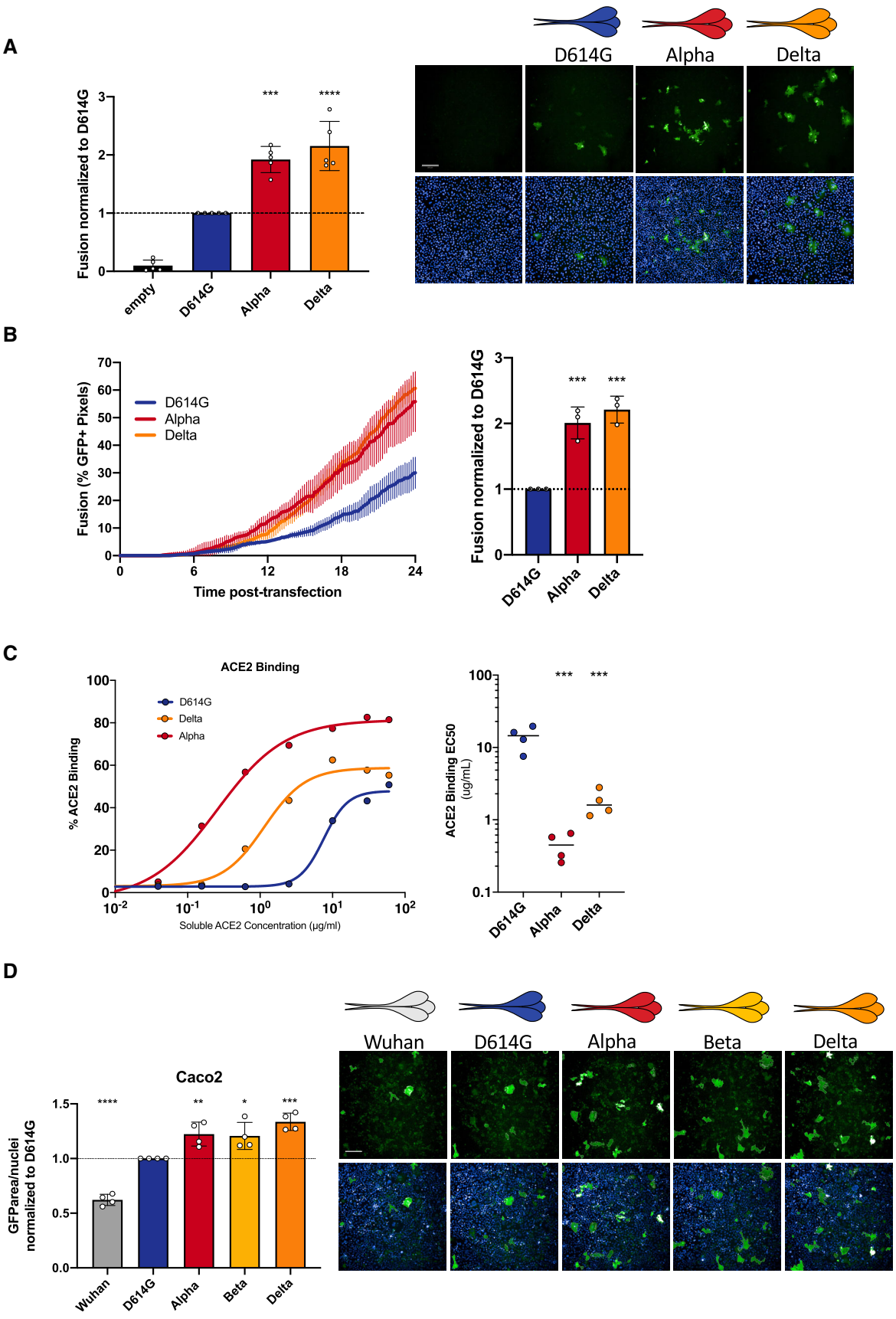

Figure 6.

© 2021 The Authors

Figure 6. Delta SARS-CoV-2 S protein induces more syncytia formation and binds more to ACE2 than D614G.

A Vero GFP-split cells were transfected with variant S proteins and imaged 18 h post-transfection. Left Panel: Fusion was quantified by GFP area/number of nuclei and normalized to D614G for each of the transfected variant S proteins. Right Panel: Representative images of Vero GFP-split cells 18 h post-transfection, GFP (green), and Hoechst (blue). Top and bottom are the same images with and without Hoechst channel. Scale bars: 200 μm.

B Left Panel: Quantification of Delta S protein-mediated fusion in Vero GFP-split cells by video microscopy. Results are mean ± SD from three fields per condition from one representative experiment. Right Panel: Fusion quantification of three independent video microscopy experiments, 20 h post-transfection, normalized to D614G.

C 293T cells were transfected S proteins with each variant-associated mutation for 24 h and stained with biotinylated ACE2 and fluorescent streptavidin before analysis by flow cytometry. Left Panel: Representative ACE2 binding dilution curves for the Delta variant in relation to Alpha and D614G. Right Panel: EC50 values (concentration of ACE2 needed for 50% binding) for Alpha for the Delta variant.

D Caco2 GFP-split cells were transfected with variant S proteins and imaged 18 h post-transfection. Left Panel: Fusion was quantified by GFP area/ number of nuclei and normalized to D614G for each of the transfected variant S proteins. Right Panel: Representative images of Caco2 GFP-split cells 18 h post-transfection, GFP (green), and Hoechst (blue). Top and bottom are the same images with and without Hoechst channel. Scale bars: 200 μm.

Data information: Data are mean ± SD of at least three independent experiments. Statistical analysis: one-way ANOVA compared with D614G reference, $*P < 0.05$, $**P < 0.01$, $***P < 0.001$, $****P < 0.0001$.

Materials and Methods

Plasmids

A codon-optimized version of the reference Wuhan SARS-CoV-2 Spike (GenBank: QHD43416.1) was ordered as a synthetic gene (GeneArt, Thermo Fisher Scientific) and was cloned into a phCMV backbone (GeneBank: AJ318514), by replacing the VSV-G gene. The mutations for Alpha and Beta (Fig 4A) were added in silico to the codon-optimized Wuhan strain and ordered as synthetic genes (GeneArt, Thermo Fisher Scientific) and cloned into the same backbone (Planas *et al*, 2021a). The D614G S plasmid was generated by introducing the mutation into the Wuhan reference strain via Q5 site-directed mutagenesis (NEB). Other individual mutations were subsequently introduced into the D614G S by the same process. Plasmids were sequenced prior to use. The primers used for sequencing and the site-directed mutagenesis are listed in the tables (Tables EV1 and EV2). pQCXIP-Empty control plasmid, pQCXIP-IFITM1-N-FLAG, pQCXIP-IFITM2-N-FLAG, pQCXIP-IFITM3-N-FLAG were previously described (Buchrieser *et al*, 2019). pQCXIP-BSR-GFP11 and pQCXIP-GFP1-10 were from Yutaka Hata ((Kodaka *et al*, 2015); Addgene plasmid #68716; http://n2t.net/addgene:68716; RRID: Addgene_68716 and Addgene plasmid #68715; http://n2t.net/addgene:68715; RRID: Addgene_68715). pcDNA3.1-hACE2 was from Hyeryun Choe ((Li *et al*, 2003); Addgene plasmid # 1786; http://n2t.net/addgene:1786; RRID: Addgene_1786). pCSDest-TMPRSS2 was from Roger Reeves ((Edie *et al*, 2018); Addgene plasmid # 53887; http://n2t.net/addgene:53887; RRID: Addgene_53887).

Cells

Vero E6, HEK293T, U2OS, Caco2/TC7, Calu3 were cultured in DMEM with 10% fetal bovine serum (FBS) and 1% penicillin/streptomycin (PS). Vero and 293T GFP-split cells transduced cells with pQCXIP were cultured with 4 μg/ml and 1 μg/ml of puromycin (InvivoGen), respectively. U2OS GFP-split cells transduced with pLenti6 were cultured in 1 μg/ml puromycin and 10 μg/ml blasticidin (InvivoGen). The MucilAir^{TM} primary human bronchial epithelial model was previously described (Robinot *et al*, 2021). All cells lines were either purchased from ATCC or were kind donations from members of the Institut Pasteur and were routinely screened for mycoplasma.

Viruses

Experiments with SARS-CoV-2 isolates were performed in a BSL-3 laboratory, following safety and security protocols approved by the risk prevention service of Institut Pasteur. The Wuhan SARS-CoV-2 strain (BetaCoV/France/IDF0372/2020) and the D614G strain (hCoV-19/France/GE1973/2020) were supplied by Dr. S. van der Werf of the National Reference Centre for Respiratory Viruses (Institut Pasteur, Paris, France). The D614G viral strain was sourced through the European Virus Archive goes Global (EVAg) platform, which is funded by the European Union's Horizon 2020 research and innovation program under grant agreement 653316. The Alpha strain was isolated in Tours, France, from an individual who returned from the United Kingdom. The Beta strain (CNRT 202100078) originated from an individual in Creteil, France. Informed consent was provided by the individuals for use of their biological materials. The viruses were isolated from nasal swabs on Vero cells and further amplified one or two passages on Vero cells. The viruses were sequenced directly from the nasal squabs and again upon passaging. Titration of viral stocks was performed by 50% tissue culture infectious dose (TCID50).

Viral release

For quantification of extracellular viral RNA, supernatants were diluted and heat-inactivated for 20 min at 80°C. qRT-PCR was performed from 1 μl of template RNA in a final volume of 5 μl per reaction in 384-well plates using the Luna Universal Probe One-Step RT-qPCR Kit (New England Biolabs) with SARS-CoV-2 N-specific primers (Table EV1) on a QuantStudio 6 Flex thermocycler (Applied Biosystems). Standard curve was performed in parallel using purified SARS-CoV-2 viral RNA. Infectious virus release was assessed by harvesting supernatant at each time point and preforming a TCID50 assay using Vero cells.

GFP-split fusion assay

For cell–cell fusion assays, Vero, U2OS-ACE2, or 293T cell lines stably expressing GFP1-10 and GFP11 were co-cultured at a 1:1 ratio (3×10^4, 2×10^4, and 7×10^4 cells/well total, respectively) and were transfected in suspension with a total of 100 ng of DNA with Lipofectamine 2000 (Thermo) in a 96-well plate (uClear, #655090). 10 ng of phCMV-SARS-CoV2-S and/or 25 ng of pCDNA3.1-hACE2,

© 2021 The Authors

25 ng of pCSDest-TMPRSS2, and 40 ng of pQCXIP-IFITM were used and adjusted to 100 ng DNA with pQCXIP-Empty (control plasmid). At 20 h post-transfection, images covering 80–90% of the well surface, were acquired per well on an Opera Phenix High-Content Screening System (PerkinElmer). The GFP area and the number of nuclei were quantified on Harmony High-Content Imaging and Analysis Software (Fig EV1B). For infection, cells were plated at the aforementioned concentrations and infected the next day with a range of MOIs and fixed at 20 h (U2OS-ACE) or 48 h (Vero) post-infection with 4% paraformaldehyde for 30 min. For video microscopy experiments, Vero GFP-split cells (mixed 1:1) were transfected in suspension with 50 ng of phCMV-SARS-CoV2-S and 450 ng of pQCXIP-Empty for 30 min at 37°C. Cells were washed twice and then seeded at a confluency of 2×10^5 cells per quadrant in a u-Dish 35-mm Quad dish (Ibidi #80416). Cells were allowed to settle, and fluorescence images were taken at 37°C every 10 min up to 24 h using a Nikon BioStation IMQ, with three fields for each condition. Fusion defined as percent of GFP pixels was calculated with ImageJ.

Flow cytometry

For ACE2 binding, 293T cells transfected with S proteins for 24 h were stained with soluble biotinylated ACE2 diluted in MACS buffer at indicated concentrations (from 60 to 0.01 μg/ml) for 30 min at 4°C. The cells were then washed twice with PBS and then incubated with Alexa Fluor 647-conjugated streptavidin (Thermo Fisher Scientific, 1:400) for 30 min at 4°C. Finally, the cells were washed twice with PBS and then fixed with 4% paraformaldehyde. The results were acquired using an Attune Nxt Flow Cytometer (Life Technologies). Transfection efficiency was assessed by staining with pan-SARS-CoV-2 human mAb129. Antibody binding to S proteins was assessed by an analogous protocol where transfected 293T cells were first stained with either human mAb10 (pan-coronavirus anti-S2), mAb102 and mAb129 (pan-SARS-CoV-2), mAb48 and mAb98 (SARS-CoV-2 anti-RBD), and mAb71 (SARS-CoV-2 anti-NTD) at 1 μg/ml. The antibodies were derived from convalescent individuals by the Mouquet laboratory at the Institut Pasteur. mAb10 was generated during the early stages of the epidemic from a patient infected with the Wuhan strain and thus has a higher affinity for the Wuhan S protein (Planas *et al*, 2021a). For viral replication, infected cells were fixed at each time with 4% paraformaldehyde for 30 min. The cells were stained in the same manner described above with anti-spike mAb102 and secondary Alexa Fluor 647 (1:500) in MACS buffer containing 0.05% saponin. The gating strategy to determine S protein-positive cells is represented in the supplement (Appendix Fig S1B).

Western Blot

Cells were lysed in TXNE buffer (1% Triton X-100, 50 mM Tris–HCl (pH 7.4), 150 mM NaCl, 5 mM EDTA, protease inhibitors) for 30 min on ice. Equal amounts (20–50 μg) of cell lysates were analyzed by Western blot. The following antibodies were diluted in WB buffer (PBS, 1% BSA, 0.05% Tween, 0.01% Na Azide): rabbit anti-human TMPRSS2 (Atlas antibodies cat# HPA035787, 1:1,000), rabbit anti-human actin (Sigma cat#A2066, 1:2,000), and human anti-S serum derived from a convalescent individual (1:1,000). Species-specific secondary DyLight-coupled antibodies were used (diluted 1:10,000 in WB buffer) and proteins were revealed using a Licor Imager. Images were processed using Image Studio Lite software.

Statistical analysis

Flow cytometry data were analyzed with FlowJo v10 software (Tristar). Calculations were all performed with Microsoft Excel 365. GraphPad Prism 9 was used to generate figures and for statistical analysis. Statistical significance between different conditions was calculated using the tests indicated in the corresponding figure legends.

Data availability

This study includes no data deposited in external repositories.

Expanded View for this article is available online.

Acknowledgements
We thank members of the Virus and Immunity Unit for helpful discussions, Dr. Nicoletta Casartelli for her critical reading of the manuscript, and Nathalie Aulner and the UtechS Photonic BioImaging (UPBI) core facility (Institut Pasteur), a member of the France BioImaging network, for image acquisition and analysis support. Work in OS lab is funded by Institut Pasteur, Urgence COVID-19 Fundraising Campaign of Institut Pasteur, ANRS, the Vaccine Research Institute (ANR-10-LABX-77), Fondation Pour la Recherche Médicale (FRM), Labex IBEID (ANR-10-LABX62-IBEID), ANR/FRM Flash Covid PROTEO-SARS-CoV-2, ANR CoronaMito AAP RA-COVID-19 V14, and IDISCOVR. Work in UPBI is funded by grant ANR-10-INSB-04-01 and Région Ile-de-France program DIM1-Health. MMR and MZ are supported by the Pasteur-Paris University (PPU) International Doctoral Program. MMR is also supported by Institut Pasteur Department of Virology "Bourse de Soudure" fellowship. DP is supported by the Vaccine Research Institute. LG is supported by the French Ministry of Higher Education, Research and Innovation. EB is supported by the Medecine-Sciences ENS-PSL Program. HM laboratory is funded by the Institut Pasteur, the Milieu Intérieur Program (ANR-10-LABX-69- 01), the INSERM, REACTing, EU (RECOVER), and Fondation de France (#00106077) grants. The funders of this study had no role in study design, data collection, analysis, interpretation, or the writing of the article.

Author contributions
MMR, JB, MH, LG, RR, LAC, OS made experimental strategy and design. MMR, JB, MH, EB, RR, NS, LG, FG-B, FP, RR, JD, SG, AB, DP, MZ contributed to experimentation. CP and HM contributed to vital materials and expert advice. MMR processed the data and generated the figures. MMR, JB, OS wrote and edited the manuscript. JB and OS supervised the study. All authors reviewed and approved the manuscript.

Conflict of interest
CP, HM, and OS have a pending patent application for some of the anti-SARS-CoV-2 mAbs described in the present study (PCT/FR2021/070522).

References

Ali F, Kasry A, Amin M (2021) The new SARS-CoV-2 strain shows a stronger binding affinity to ACE2 due to N501Y mutant. *Med Drug Discov* 10: 100086

© 2021 The Authors

Arunachalam PS, Wimmers F, Mok CKP, Perera RAPM, Scott M, Hagan T, Sigal N, Feng Y, Bristow L, Tak-Yin Tsang O *et al* (2020) Systems biological assessment of immunity to mild versus severe COVID-19 infection in humans. *Science* 369: 1210 – 1220

Asarnow D, Wang B, Lee W-H, Hu Y, Huang C-W, Faust B, Ng PML, Ngoh EZX, Bohn M, Bulkley D *et al* (2021) Structural insight into SARS-CoV-2 neutralizing antibodies and modulation of syncytia. *Cell* 184: 3192 – 3204.e16

Barrett CT, Neal HE, Edmonds K, Moncman CL, Thompson R, Branttie JM, Boggs KB, Wu CY, Leung DW, Dutch RE (2021) Effect of clinical isolate or cleavage site mutations in the SARS-CoV-2 spike protein on protein stability, cleavage, and cell-cell fusion. *J Biol Chem* 297: 100902

Bastard P, Orlova E, Sozaeva L, Levy R, James A, Schmitt MM, Ochoa S, Kareva M, Rodina Y, Gervais A *et al* (2021) Preexisting autoantibodies to type I IFNs underlie critical COVID-19 pneumonia in patients with APS-1. *J Exp Med* 218: e20210554

Bastard P, Rosen LB, Zhang Q, Michailidis E, Hoffmann HH, Zhang Y, Dorgham K, Philippot Q, Rosain J, Beziat V *et al* (2020) Autoantibodies against type I IFNs in patients with life-threatening COVID-19. *Science* 370: eabd4585

Beucher G, Blondot M-L, Celle A, Pied N, Recordon-Pinson P, Esteves P, Faure M, Métifiot M, Lacomme S & Dacheaux D et al (2021) SARS-CoV-2 transmission via apical syncytia release from primary bronchial epithelia and infectivity restriction in children epithelia. bioRxiv 2021.2005.2028.446159 [PREPRINT]

Braga L, Ali H, Secco I, Chiavacci E, Neves G, Goldhill D, Penn R, Jimenez-Guardeño JM, Ortega-Prieto AM, Bussani R *et al* (2021) Drugs that inhibit TMEM16 proteins block SARS-CoV-2 spike-induced syncytia. *Nature* 594: 88 – 93

Buchrieser J, Degrelle SA, Couderc T, Nevers Q, Disson O, Manet C, Donahue DA, Porrot F, Hillion KH, Perthame E *et al* (2019) IFITM proteins inhibit placental syncytiotrophoblast formation and promote fetal demise. *Science* 365: 176 – 180

Buchrieser J, Dufloo J, Hubert M, Monel B, Planas D, Rajah MM, Planchais C, Porrot F, Guivel-Benhassine F, Van der Werf S *et al* (2020) Syncytia formation by SARS-CoV-2-infected cells. *EMBO J* 39: e106267

Buss LF, Prete CA, Abrahim CMM, Mendrone A, Salomon T, de Almeida-Neto C, França RFO, Belotti MC, Carvalho MPSS, Costa AG *et al* (2021) Three-quarters attack rate of SARS-CoV-2 in the Brazilian Amazon during a largely unmitigated epidemic. *Science* 371: 288 – 292

Bussani R, Schneider E, Zentilin L, Collesi C, Ali H, Braga L, Volpe MC, Colliva A, Zanconati F, Berlot G *et al* (2020) Persistence of viral RNA, pneumocyte syncytia and thrombosis are hallmarks of advanced COVID-19 pathology. *EBioMedicine* 61: 103104

Cattin-Ortolá J, Welch L, Maslen SL, Skehel JM, Papa G, James LC, Munro S, Cattin-Ortolá J, Welch LG, Maslen SL *et al* (2021) Sequences in the cytoplasmic tail of SARS-CoV-2 Spike facilitate expression at the cell surface and syncytia formation. *Nat Commun* 12: 5333

Chan J-W, Chan K-H, Choi G-Y, To K-W, Tse H, Cai J-P, Yeung ML, Cheng V-C, Chen H, Che X-Y *et al* (2013) Differential cell line susceptibility to the emerging novel human betacoronavirus 2c EMC/2012: implications for disease pathogenesis and clinical manifestation. *J Infect Dis* 207: 1743 – 1752

Chi X, Yan R, Zhang J, Zhang G, Zhang Y, Hao M, Zhang Z, Fan P, Dong Y, Yang Y *et al* (2020) A neutralizing human antibody binds to the N-terminal domain of the Spike protein of SARS-CoV-2. *Science* 369: 650 – 655

Collier DA, De Marco A, Ferreira IATM, Meng BO, Datir RP, Walls AC, Kemp SA, Bassi J, Pinto D, Silacci-Fregni C *et al* (2021) Sensitivity of SARS-CoV-2 B.1.1.7 to mRNA vaccine-elicited antibodies. *Nature* 593: 136 – 141

Compton AA, Bruel T, Porrot F, Mallet A, Sachse M, Euvrard M, Liang C, Casartelli N, Schwartz O (2014) IFITM proteins incorporated into HIV-1 virions impair viral fusion and spread. *Cell Host Microbe* 16: 736 – 747

Davies NG, Abbott S, Barnard RC, Jarvis CI, Kucharski AJ, Munday JD, Pearson CAB, Russell TW, Tully DC, Washburne AD *et al* (2021) Estimated transmissibility and impact of SARS-CoV-2 lineage B.1.1.7 in England. *Science* 372: eabg3055

Dittmar M, Lee JS, Whig K, Segrist E, Li M, Kamalia B, Castellana L, Ayyanathan K, Cardenas-Diaz FL, Morrisey EE *et al* (2021) Drug repurposing screens reveal cell-type-specific entry pathways and FDA-approved drugs active against SARS-Cov-2. *Cell Rep* 35: 108959

Dominguez SR, Travanty EA, Qian Z, Mason RJ (2013) Human coronavirus HKU1 infection of primary human type II alveolar epithelial cells: cytopathic effects and innate immune response. *PLoS One* 8: e70129

Duan L, Zheng Q, Zhang H, Niu Y, Lou Y, Wang H (2020) The SARS-CoV-2 spike glycoprotein biosynthesis, structure, function, and antigenicity: implications for the design of spike-based vaccine immunogens. *Front Immunol* 11: 576622

Edie S, Zaghloul NA, Leitch CC, Klinedinst DK, Lebron J, Thole JF, McCallion AS, Katsanis N, Reeves RH (2018) Survey of human chromosome 21 gene expression effects on early development in Danio Rerio. *G3* 8: 2215 – 2223

Ferreira I, Datir R, Papa G, Kemp S, Meng B, Rakshit P, Singh S, Pandey R, Ponnusamy K, Radhakrishnan VS *et al* (2021) SARS-CoV-2 B.1.617 emergence and sensitivity to vaccine-elicited antibodies. *bioRxiv* https://doi.org/10.1101/2021.05.08.443253 [PREPRINT]

Frampton D, Rampling T, Cross A, Bailey H, Heaney J, Byott M, Scott R, Sconza R, Price J, Margaritis M *et al* (2021) Genomic characteristics and clinical effect of the emergent SARS-CoV-2 B.1.1.7 lineage in London, UK: a whole-genome sequencing and hospital-based cohort study. *Lancet Infect Dis* 21: 1246 – 1256

Franks TJ, Chong PY, Chui P, Galvin JR, Lourens RM, Reid AH, Selbs E, Mcevoy CPL, Hayden CDL, Fukuoka J *et al* (2003) Lung pathology of severe acute respiratory syndrome (SARS): a study of 8 autopsy cases from Singapore. *Hum Pathol* 34: 743 – 748

Hadjadj J, Yatim N, Barnabei L, Corneau A, Boussier J, Smith N, Pere H, Charbit B, Bondet V, Chenevier-Gobeaux C *et al* (2020) Impaired type I interferon activity and inflammatory responses in severe COVID-19 patients. *Science* 369: 718 – 724

Hoffmann M, Arora P, Gross R, Seidel A, Hornich BF, Hahn AS, Kruger N, Graichen L, Hofmann-Winkler H, Kempf A *et al* (2021) SARS-CoV-2 variants B.1.351 and P.1 escape from neutralizing antibodies. *Cell* 184: 2384 – 2393 e2312

Hoffmann M, Kleine-Weber H, Schroeder S, Krüger N, Herrler T, Erichsen S, Schiergens TS, Herrler G, Wu N-H, Nitsche A *et al* (2020) SARS-CoV-2 cell entry depends on ACE2 and TMPRSS2 and is blocked by a clinically proven protease inhibitor. *Cell* 181: 271 – 280.e8

Hornich BF, Grosskopf AK, Schlagowski S, Tenbusch M, Kleine-Weber H, Neipel F, Stahl-Hennig C, Hahn AS (2021) SARS-CoV-2 and SARS-CoV spike-mediated cell-cell fusion differ in their requirements for receptor expression and proteolytic activation. *J Virol* 95: e00002-21

Hou YJ, Chiba S, Halfmann P, Ehre C, Kuroda M, Dinnon KH, Leist SR, Schäfer A, Nakajima N, Takahashi K *et al* (2020) SARS-CoV-2 D614G variant exhibits efficient replication ex vivo and transmission *in vivo*. *Science* 370: 1464 – 1468

Huang C, Wang Y, Li X, Ren L, Zhao J, Hu YI, Zhang LI, Fan G, Xu J, Gu X *et al* (2020a) Clinical features of patients infected with 2019 novel coronavirus in Wuhan, China. *Lancet* 395: 497 – 506

© 2021 The Authors

Huang Y, Yang C, Xu XF, Xu W, Liu SW (2020b) Structural and functional properties of SARS-CoV-2 spike protein: potential antivirus drug development for COVID-19. *Acta Pharmacol Sin* 41: 1141 – 1149

Jackson L, Rodel H, Hwa S-H, Cele S, Ganga Y, Tegally H, Bernstein M, Giandhari J, Gosnell BI, Khan K *et al* (2021) SARS-CoV-2 cell-to-cell spread occurs rapidly and is insensitive to antibody neutralization. *bioRxiv* https://doi.org/10.1101/2021.06.01.446516 [PREPRINT]

Jiang X, Zhang Z, Wang C, Ren H, Gao L, Peng H, Niu Z, Ren H, Huang H, Sun Q (2020) Bimodular effects of D614G mutation on the spike glycoprotein of SARS-CoV-2 enhance protein processing, membrane fusion, and viral infectivity. *Signal Transduct Target Ther* 5: 268

Klein S, Cortese M, Winter SL, Wachsmuth-Melm M, Neufeldt CJ, Cerikan B, Stanifer ML, Boulant S, Bartenschlager R, Chlanda P (2020) SARS-CoV-2 structure and replication characterized by in situ cryo-electron tomography. *Nat Commun* 11: 5885

Koch J, Uckeley ZM, Doldan P, Stanifer M, Boulant S, Lozach PY (2021) TMPRSS2 expression dictates the entry route used by SARS-CoV-2 to infect host cells. *EMBO J* 40: e107821

Kodaka M, Yang Z, Nakagawa K, Maruyama J, Xu X, Sarkar A, Ichimura A, Nasu Y, Ozawa T, Iwasa H *et al* (2015) A new cell-based assay to evaluate myogenesis in mouse myoblast C2C12 cells. *Exp Cell Res* 336: 171 – 181

Korber B, Fischer WM, Gnanakaran S, Yoon H, Theiler J, Abfalterer W, Hengartner N, Giorgi EE, Bhattacharya T, Foley B *et al* (2020) Tracking changes in SARS-CoV-2 spike: evidence that D614G increases infectivity of the COVID-19 virus. *Cell* 182: 812 – 827.e19

Krempl C, Schultze B, Laude H, Herrler G (1997) Point mutations in the S protein connect the sialic acid binding activity with the enteropathogenicity of transmissible gastroenteritis coronavirus. *J Virol* 71: 3285 – 3287

Leung K, Shum MH, Leung GM, Lam TT, Wu JT (2021) Early transmissibility assessment of the N501Y mutant strains of SARS-CoV-2 in the United Kingdom, October to November 2020. *Euro Surveill* 26

Li W, Moore MJ, Vasilieva N, Sui J, Wong SK, Berne MA, Somasundaran M, Sullivan JL, Luzuriaga K, Greenough TC *et al* (2003) Angiotensin-converting enzyme 2 is a functional receptor for the SARS coronavirus. *Nature* 426: 450 – 454

Lin L, Li Q, Wang Y, Shi Y (2021) Syncytia formation during SARS-CoV-2 lung infection: a disastrous unity to eliminate lymphocytes. *Cell Death Differ* 28: 2019 – 2021

Liu Y, Liu J, Plante KS, Plante JA, Xie X, Zhang X, Ku Z, An Z, Scharton D, Schindewolf C *et al* (2021a) The N501Y spike substitution enhances SARS-CoV-2 transmission. *bioRxiv* https://doi.org/10.1101/2021.03.08.434499 [PREPRINT]

Liu Z, VanBlargan LA, Bloyet L-M, Rothlauf PW, Chen RE, Stumpf S, Zhao H, Errico JM, Theel ES, Liebeskind MJ *et al* (2021b) Identification of SARS-CoV-2 spike mutations that attenuate monoclonal and serum antibody neutralization. *Cell Host Microbe* 29: 477 – 488.e4

Luan B, Wang H, Huynh T (2021) Enhanced binding of the N501Y-mutated SARS-CoV-2 spike protein to the human ACE2 receptor: insights from molecular dynamics simulations. *FEBS Lett* 595: 1454 – 1461

Meng B, Kemp SA, Papa G, Datir R, Ferreira IA, Marelli S, Harvey WT, Lytras S, Mohamed A, Gallo G *et al* (2021) Recurrent emergence of SARS-CoV-2 spike deletion H69/V70 and its role in the Alpha variant B.1.1.7. *Cell Rep* 35: 109292

Nal B, Chan C, Kien F, Siu L, Tse J, Chu K, Kam J, Staropoli I, Crescenzo-Chaigne B, Escriou N *et al* (2005) Differential maturation and subcellular localization of severe acute respiratory syndrome coronavirus surface proteins S, M and E. *J Gen Virol* 86: 1423 – 1434

Nelson G, Buzko O, Spilman P, Niazi K, Rabizadeh S, Soon-Shiong P (2021) Molecular dynamic simulation reveals E484K mutation enhances spike RBD-ACE2 affinity and the combination of E484K, K417N and N501Y mutations (501Y.V2 variant) induces conformational change greater than N501Y mutant alone, potentially resulting in an escape mutant. *bioRxiv* https://doi.org/10.1101/2021.01.13.426558 [PREPRINT]

Ou T, Mou H, Zhang L, Ojha A, Choe H, Farzan M (2021) Hydroxychloroquine-mediated inhibition of SARS-CoV-2 entry is attenuated by TMPRSS2. *PLoS Pathog* 17: e1009212

Pizzorno A, Padey B, Julien T, Trouillet-Assant S, Traversier A, Errazuriz-Cerda E, Fouret J, Dubois J, Gaymard A, Lescure F-X *et al* (2020) Characterization and treatment of SARS-CoV-2 in nasal and bronchial human airway epithelia. *Cell Rep Med* 1: 100059

Planas D, Bruel T, Grzelak L, Guivel-Benhassine F, Staropoli I, Porrot F, Planchais C, Buchrieser J, Rajah MM, Bishop E *et al* (2021a) Sensitivity of infectious SARS-CoV-2 B.1.1.7 and B.1.351 variants to neutralizing antibodies. *Nat Med* 27: 917 – 924

Planas D, Veyer D, Baidaliuk A, Staropoli I, Guivel-Benhassine F, Rajah MM, Planchais C, Porrot F, Robillard N, Puech J *et al* (2021b) Reduced sensitivity of SARS-CoV-2 variant Delta to antibody neutralization. *Nature* 596: 276 – 280

Puray-Chavez M, LaPak KM, Schrank TP, Elliott JL, Bhatt DP, Agajanian MJ, Jasuja R, Lawson DQ, Davis K, Rothlauf PW *et al* (2021) Systematic analysis of SARS-CoV-2 infection of an ACE2-negative human airway cell. *Cell Rep* 36: 109364

Qian Z, Dominguez SR, Holmes KV (2013) Role of the spike glycoprotein of human Middle East respiratory syndrome coronavirus (MERS-CoV) in virus entry and syncytia formation. *PLoS One* 8: e76469

Ramanathan M, Ferguson ID, Miao W, Khavari PA (2021) SARS-CoV-2 B.1.1.7 and B.1.351 spike variants bind human ACE2 with increased affinity. *Lancet Infect Dis* 21: 1070

Rees-Spear C, Muir L, Griffith SA, Heaney J, Aldon Y, Snitselaar JL, Thomas P, Graham C, Seow J, Lee N *et al* (2021) The effect of spike mutations on SARS-CoV-2 neutralization. *Cell Rep* 34: 108890

Robinot R, Hubert M, de Melo GD, Lazarini F, Bruel T, Smith N, Levallois S, Larrous F, Fernandes J, Gellenoncourt S *et al* (2021) SARS-CoV-2 infection induces the dedifferentiation of multiciliated cells and impairs mucociliary clearance. *Nat Commun* 12: 4354

Sabino EC, Buss LF, Carvalho MPS, Prete CA, Crispim MAE, Fraiji NA, Pereira RHM, Parag KV, da Silva Peixoto P, Kraemer MUG *et al* (2021) Resurgence of COVID-19 in Manaus, Brazil, despite high seroprevalence. *Lancet* 397: 452 – 455

Sanders DW, Jumper CC, Ackerman PJ, Bracha D, Donlic A, Kim H, Kenney D, Castello-Serrano I, Suzuki S, Tamura T *et al* (2021) SARS-CoV-2 requires cholesterol for viral entry and pathological syncytia formation. *Elife* 10: e65962

Shi G, Kenney AD, Kudryashova E, Zani A, Zhang L, Lai KK, Hall-Stoodley L, Robinson RT, Kudryashov DS, Compton AA *et al* (2021) Opposing activities of IFITM proteins in SARS-CoV-2 infection. *EMBO J* 40: e106501

Shi G, Schwartz O, Compton AA (2017) More than meets the I: the diverse antiviral and cellular functions of interferon-induced transmembrane proteins. *Retrovirology* 14: 53

Starr TN, Greaney AJ, Addetia A, Hannon WW, Choudhary MC, Dingens AS, Li JZ, Bloom JD (2021) Prospective mapping of viral mutations that escape antibodies used to treat COVID-19. *Science* 371: 850 – 854

Tegally H, Wilkinson E, Giovanetti M, Iranzadeh A, Fonseca V, Giandhari J, Doolabh D, Pillay S, San EJ, Msomi N *et al* (2020) Emergence and rapid spread of a new severe acute respiratory syndrome-related coronavirus 2

 © 2021 The Authors

(SARS-CoV-2) lineage with multiple spike mutations in South Africa. *medRxiv* https://doi.org/10.1101/2020.12.21.20248640 [PREPRINT]

Thorne LG, Bouhaddou M, Reuschl A-K, Zuliani-Alvarez L, Polacco B, Pelin A, Batra J, Whelan MVX, Ummadi M, Rojc A *et al* (2021) Evolution of enhanced innate immune evasion by the SARS-CoV-2 B.1.1.7 UK variant. *bioRxiv* https://doi.org/10.1101/2021.06.06.446826 [PREPRINT]

Tian F, Tong B, Sun L, Shi S, Zheng B, Wang Z, Dong X, Zheng P (2021) N501Y mutation of spike protein in SARS-CoV-2 strengthens its binding to receptor ACE2. *eLife* 10: e69091

Tian S, Hu W, Niu L, Liu H, Xu H, Xiao SY (2020) Pulmonary pathology of early-phase 2019 novel Coronavirus (COVID-19) pneumonia in two patients with lung cancer. *J Thorac Oncol* 15: 700 – 704

Touret F, Luciani L, Baronti C, Cochin M, Driouich J-S, Gilles M, Thirion L, Nougairède A, de Lamballerie X (2021) Replicative fitness of a SARS-CoV-2 20I/501Y.V1 variant from lineage B.1.1.7 in human reconstituted bronchial epithelium. *mBio* 12: e00850-21

van der Made CI, Simons A, Schuurs-Hoeijmakers J, van den Heuvel G, Mantere T, Kersten S, van Deuren RC, Steehouwer M, van Reijmersdal SV, Jaeger M *et al* (2020) Presence of genetic variants among young men with severe COVID-19. *JAMA* 324: 663 – 673

Weisblum Y, Schmidt F, Zhang F, DaSilva J, Poston D, Lorenzi JCC, Muecksch F, Rutkowska M, Hoffmann HH *et al* (2020) Escape from neutralizing antibodies by SARS-CoV-2 spike protein variants. *eLife* 9: e61312

Xu Z, Shi L, Wang Y, Zhang J, Huang L, Zhang C, Liu S, Zhao P, Liu H, Zhu LI *et al* (2020) Pathological findings of COVID-19 associated with acute respiratory distress syndrome. *Lancet Respir Med* 8: 420 – 422

Yadav PD, Sapkal GN, Abraham P, Ella R, Deshpande G, Patil DY, Nyayanit DA, Gupta N, Sahay RR, Shete AM *et al* (2021) Neutralization of variant under investigation B.1.617 with sera of BBV152 vaccinees. *bioRxiv* https://doi.org/10.1101/2021.04.23.441101 [PREPRINT]

Yurkovetskiy L, Wang X, Pascal KE, Tomkins-Tinch C, Nyalile TP, Wang Y, Baum A, Diehl WE, Dauphin A, Carbone C *et al* (2020) Structural and functional analysis of the D614G SARS-CoV-2 spike protein variant. *Cell* 183: 739 – 751 e738

Zahradník J, Marciano S, Shemesh M, Zoler E, Chiaravalli J, Meyer B, Rudich Y, Dym O, Elad N, Schreiber G *et al* (2021) SARS-CoV-2 variant prediction and antiviral drug design are enabled by RBD in vitro evolution. *Nat Microbiol* 6: 1188 – 1198

Zani A, Yount JS (2018) Antiviral protection by IFITM3 *in vivo*. *Curr Clin Microbiol Rep* 5: 229 – 237

Zhang X, Tan Y, Ling Y, Lu G, Liu F, Yi Z, Jia X, Wu M, Shi B, Xu S *et al* (2020) Viral and host factors related to the clinical outcome of COVID-19. *Nature* 583: 437 – 440

Zhang Z, Zheng Y, Niu Z, Zhang BO, Wang C, Yao X, Peng H, Franca DN, Wang Y, Zhu Y *et al* (2021) SARS-CoV-2 spike protein dictates syncytium-mediated lymphocyte elimination. *Cell Death Differ* 28: 2765 – 2777

Zhou H, Chen Y, Zhang S, Niu P, Qin K, Jia W, Huang B, Zhang S, Lan J, Zhang L *et al* (2019) Structural definition of a neutralization epitope on the N-terminal domain of MERS-CoV spike glycoprotein. *Nat Commun* 10: 3068

Zhou Z, Ren L, Zhang LI, Zhong J, Xiao Y, Jia Z, Guo LI, Yang J, Wang C, Jiang S *et al* (2020) Heightened innate immune responses in the respiratory tract of COVID-19 patients. *Cell Host Microbe* 27: 883 – 890.e2

Zhu NA, Wang W, Liu Z, Liang C, Wang W, Ye F, Huang B, Zhao LI, Wang H, Zhou W *et al* (2020) Morphogenesis and cytopathic effect of SARS-CoV-2 infection in human airway epithelial cells. *Nat Commun* 11: 3910

© 2021 The Authors

Expanded View Figures

Figure EV1. Qualitative and quantitative assessment of syncytia formation.

A U2OS-ACE2 GFP-split cells were infected at MOI 0.01 with the Wuhan, D614G, Alpha, and Beta strains for 20 h. Cells were stained for S protein with the human pan-SARS-CoV-2 102 mAb and Alex647 fluorescent secondary antibody. Representative confocal images of the variant induced syncytia formation: GFP-Split (green), Spike (red), and Hoechst (blue). Scale bars: 50 μm.

B Quantification method for syncytia formation using the Opera Phenix high content imager and harmony software: Total syncytia area (GFP area) is normalized for cell number upon quantifying the number of nuclei (Hoechst).

© 2021 The Authors

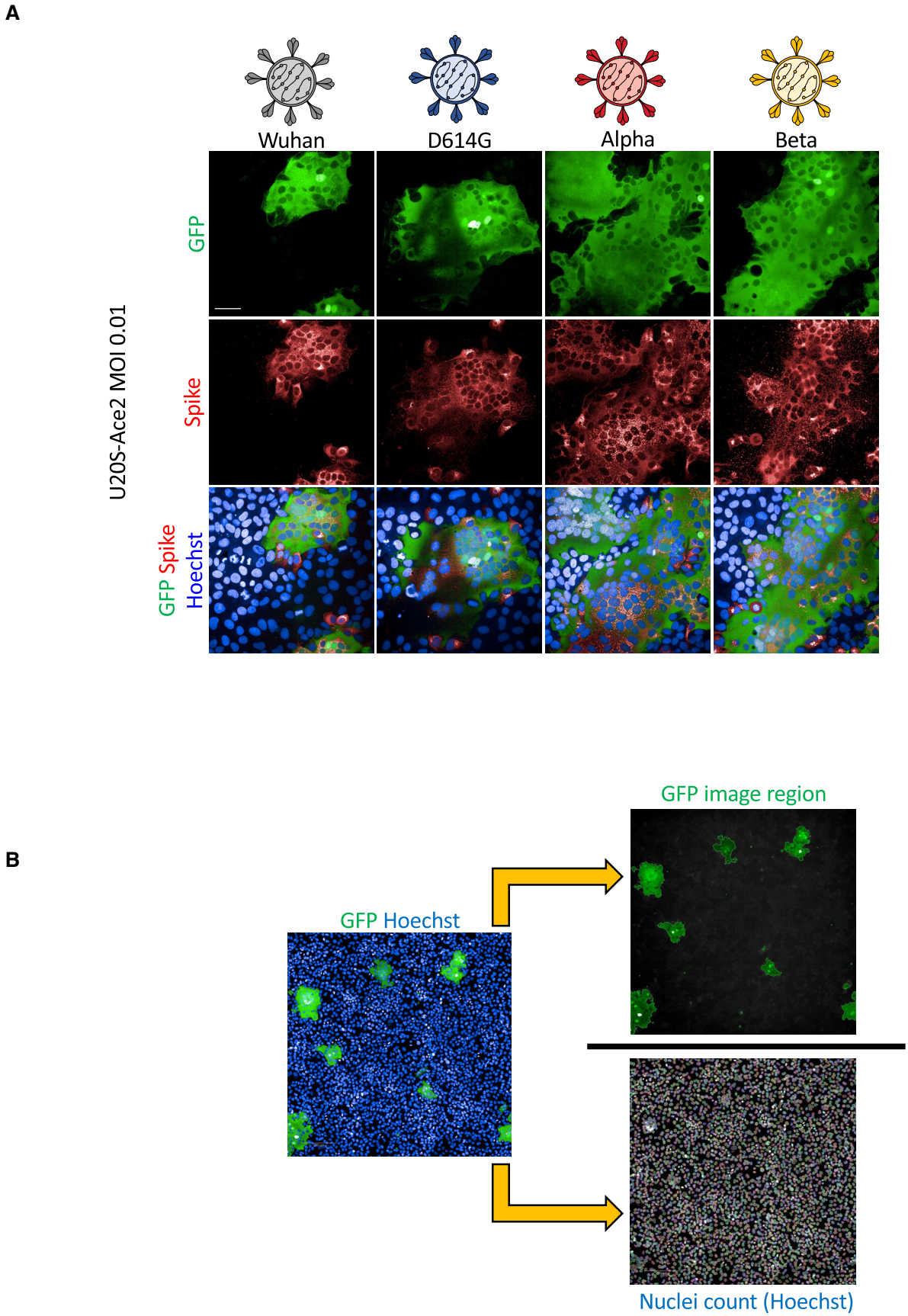

Figure EV1.

© 2021 The Authors

Figure EV2. SARS-CoV-2 variant S proteins are expressed equally at the cell surface.

293T cells were transfected with variant S proteins for 20 h and stained with human pan-coronavirus mAb10 without permeabilization. 293T cells were chosen because they lack ACE2 and do not fuse upon S transfection; this makes them suitable for single-cell flow cytometry.

A Left Panel: Quantification of percent of cells expressing each S protein at the surface. Right Panel: Representative FACs plots.
B Quantification of median florescent intensity (MFI) of variant S protein at the cell surface and representative histograms of MFI of the Wuhan, D614G, Alpha, Beta, and Alpha + E484K variants S protein using mAb10.
C Quantification of median florescent intensity (MFI) of variant S protein at the cell surface and representative histograms of MFI of the Wuhan, D614G, Alpha, Beta, and Alpha + E484K variants S protein using mAb129.
D Quantification of median florescent intensity (MFI) of variant S protein at the cell surface and representative histograms of MFI of the Delta variant compared with the Alpha and D614G using mAb129.
E Controlled acceptor/donor experiment 293T GFP1-10 donor cells transfected with S protein and verified to have equal S protein expression on the surface (top), were then added to Vero GFP11 acceptor cells (bottom) to assess fusion.

Data information: Flow cytometry data are mean ± SD of at least three independent experiments. Statistical analysis: one-way ANOVA compared with D614G reference, ns: non-significant, $*P < 0.05$, $****P < 0.0001$.

© 2021 The Authors

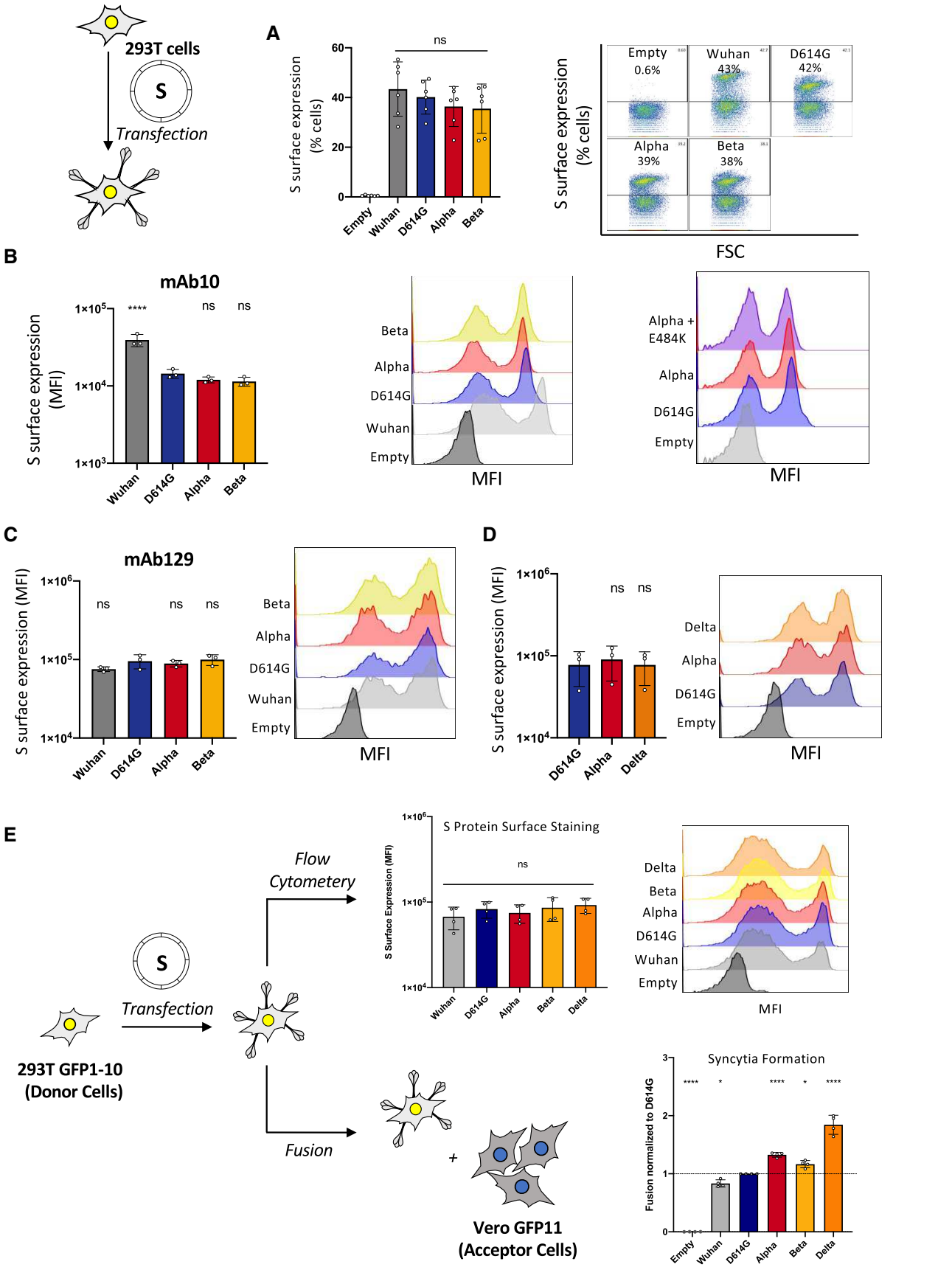

Figure EV2.

© 2021 The Authors

Figure EV3. Impact of IFN-β1 and IFITMs on SARS-CoV-2 variant replication and S protein-mediated cell–cell fusion.

A Vero cells were pre-treated for 2 h with a serial dilution of IFN-β1 prior to infection with the SARS-CoV-2 variants. Infected cells were maintained in media containing IFN-β1 and analyzed by flow cytometry 48 h post-infection to determine relative infection change.

B U2OS-ACE2 GFP-split cells were pre-treated for 2 h with a serial dilution of IFN-β1 prior to infection with the SARS-CoV-2 variants. Infected cells were maintained in media containing IFN-β1 and relative inhibition of syncytia formation 20 h post-infection was determined via GFP signal.

C–G A co-culture of 293T GFP-Split cells were transfected with combination of S, control, ACE2, TMPRSS2, and IFITM plasmids and then imaged 18 h post-transfection. Effect of IFITMs and TMPRSS2 on the cell–cell fusion induced by different S proteins, (D) Wuhan, (E) D614G, (F) Alpha, and (G) Beta.

Data information: Data are mean ± SD of at least three independent experiments. Statistical analysis: one-way ANOVA compared with D614G reference or control plasmid transfection, ns: non-significant, *$P < 0.05$, **$P < 0.01$, ***$P < 0.001$, ****$P < 0.0001$.

© 2021 The Authors

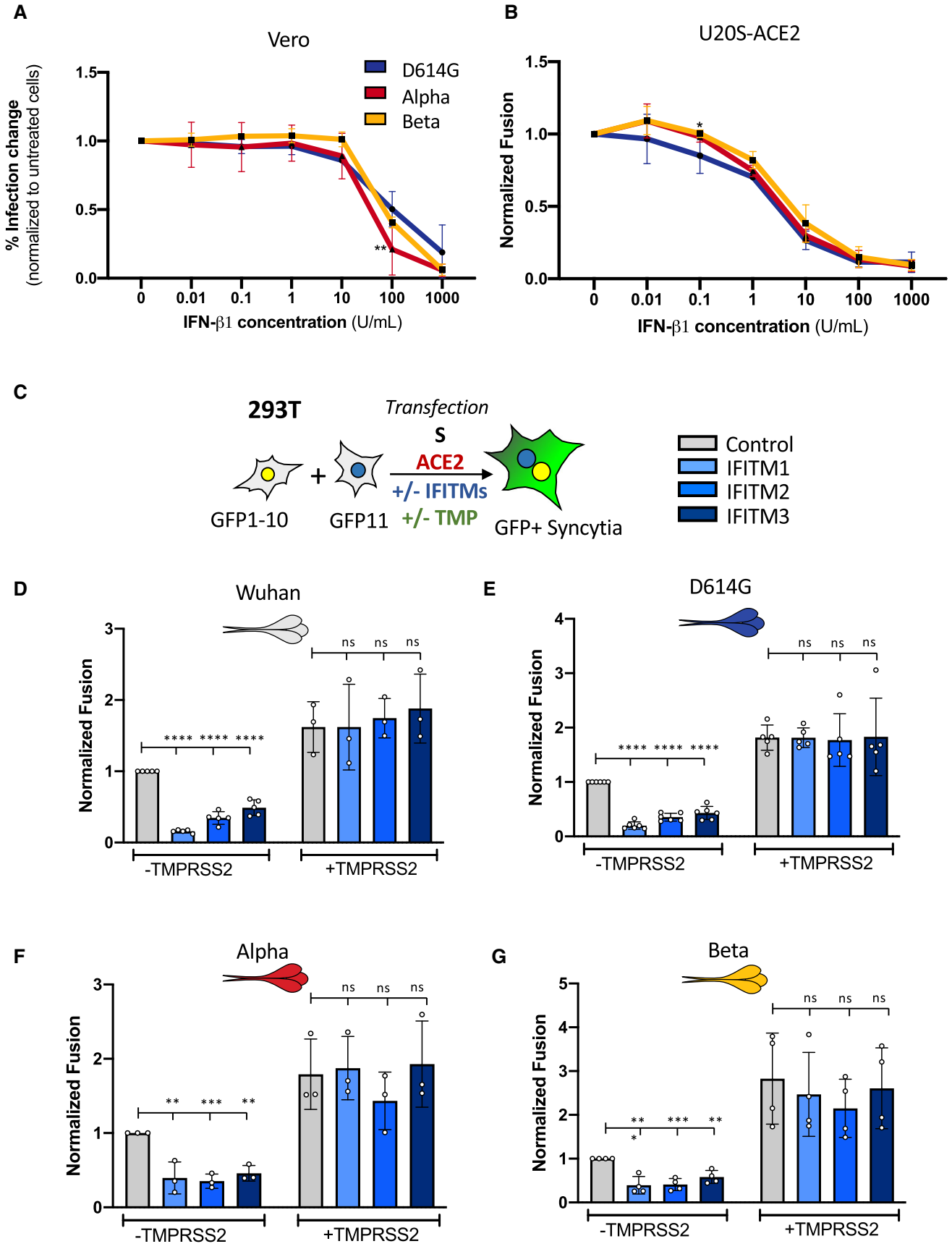

Figure EV3.

© 2021 The Authors

Figure EV4. SARS-CoV-2 variant S protein-associated mutations are expressed equally at the cell surface.

293T cells were transfected with S proteins with each of the variant-associated mutations for 18 h and stained with human pan-coronavirus mAb10 without permeabilization.

A Representative FAC plots of percent of cells expressing each mutant S protein at the surface.
B Quantification of percent of cells expressing each S protein at the surface.
C Quantification of median florescent intensity (MFI) of the mutant S protein at the cell surface.
D Representative histograms of MFI of each mutant S protein.
E Representative images of Vero GFP-split cells 20 h after transfection with each Alpha variant-associated mutant S protein, GFP-Split (Green). Scale bars: 200 μm.
F Representative images of Vero GFP-split cells 20 h after transfection with each Beta variant-associated mutant S protein. Scale bars: 200 μm.

Data information: Data are mean ± SD of at least three independent experiments. Statistical analysis: one-way ANOVA compared with D614G reference, ns: non-significant.

© 2021 The Authors

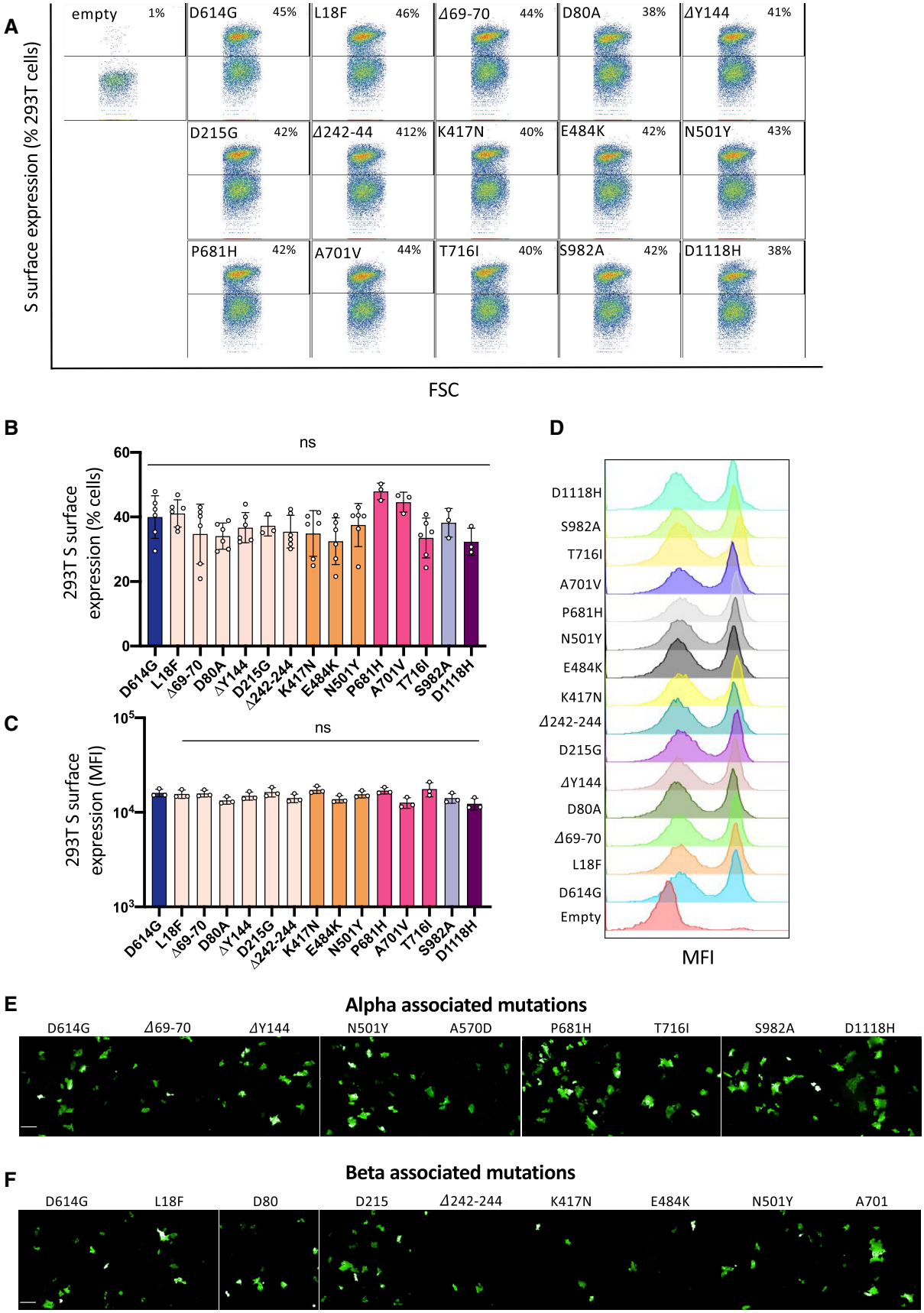

Figure EV4.

© 2021 The Authors

Figure EV5. ACE2 binding curves to SARS-CoV-2 variant S proteins and associated mutations.

293T cells were transfected with variant or mutant S proteins for 24 h and stained with a serial dilution of soluble biotinylated ACE2 and revealed by fluorescent streptavidin before analysis by flow cytometry.

A ACE2 binding dilution curves of each variant S protein.

B–E ACE2 binding dilution curves of each variant-associated mutation located in (B) S protein n-terminal domain (NTD), (C) receptor-binding domain (RBD), (D) S1/S2 cleavage site, and (E) heptad repeat 1–2 site (HR1-HR2).

Data information: Data are mean ± SD of three independent experiments.

© 2021 The Authors

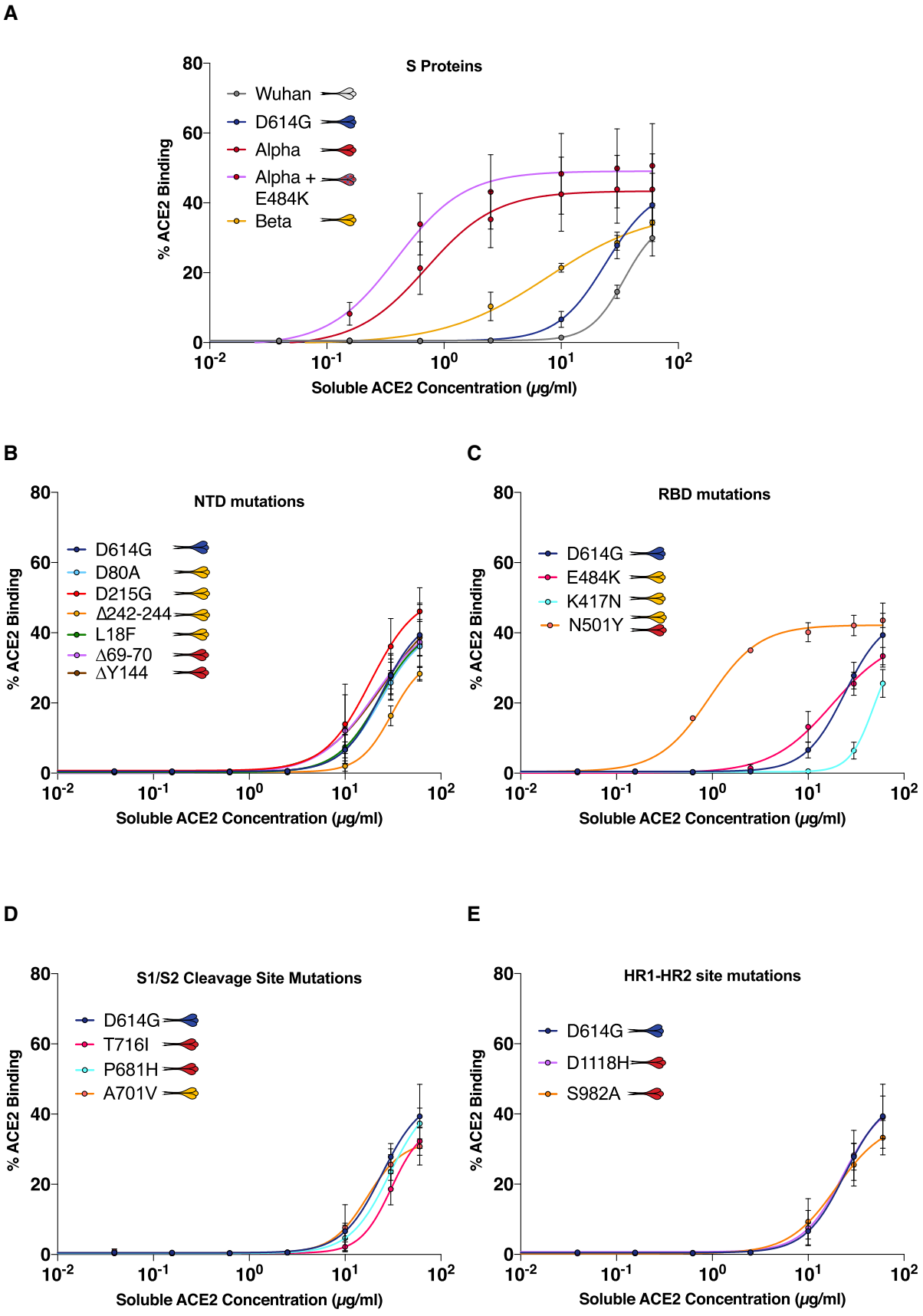

Figure EV5.

© 2021 The Authors

EV Table 1 : Sequecing and qRT-PCR primers

Primer name	Sequence (5'-3')
Sequencing Primers	
phCMV For	CTCTTTCCTACAGCTCCTGG
phCMV Rev	TAGCCAGAAGTCAGATGCTC
phCMV Int1 For	AGCGAGTTCCGCGTGTACAG
phCMV Int2 For	CGCAAGCGCATTAGCAACTG
phCMV Int3 For	GCGTGCTGACCGAGAGTAAC
phCMV Int4 For	GCAACCTGCTGCTGCAGTAC
phCMV Int5 For	GTGGTCAACCAGAACGCTCAG
phCMV Int6 For	AGAACCACACAAGCCCCGAC
qRT-PCR Primers	**SARS-CoV-2 N protein specific**
For	TAATCAGAC15AAGGAACTGATTA
Rev	CGAAGGTGTGACTTCCATG

EV Table 2 : Site directed mutagenesis primers

Mutant	Site Directed Mutagenesis Primers (5'-3')
D614G	For : CTGTACCAGGgcGTGAATTGCACAGAGGTG Rev : AACGGCCACCTGGTTGCT
L18F	For : GTGCGTGAACttcACCACACGAAC Rev TGACTGGACACCAGTGGC
Δ69-70	For : TCCGGCACCAATGGCACC Rev : GATGGCGTGGAACCAGGTC
D80A	For : AAGCGCTTCGcTAATCCCGTGC Rev : GGTGCCATTGGTGCCGGA
Y144	For : TACCACAAGAACAACAAGAGCTGG Rev : GACGCCCAGGAAGGGGTC
D215G	For : CTCGTGCGCGgcCTGCCACAGG Rev : GTTGATTGGGGTGTGCTTG
Δ242-244	For : CACCGCAGTTACTTGACAC Rev : CAGTGTCTGAAAGCGGGT
K417N	For : AGACCGGCAAcATCGCCGACTAC Rev : GGCCTGGGGCAATCTGTC
E484K	For : CAACGGCGTGaAAGGCTTCAACTG Rev : CATGGGGTGCTTCCGGCC
N501Y	For : TCAGCCCACAtATGGCGTGGG Rev : AATCCGTAGGACTGCAGTG
A570D	For : CGCGACATTGaCGATACAACC Rev : GCCAAACTGCTGGAATGG
P681H	For : ACCAATAGTCacCGACGAGCCC Rev : CTGGGTCTGATAGGAGGC
A701V	For : AGCCTGGGCGtgGAGAATAGCG Rev : CATGGTATAGGCAATGATG
T716I	For : GCTATCCCCAtCAACTTCACC Rev : AATGCTGTTGTTGGAGTAG
S982A	For : CGATATCCTGgcCCGCCTGGATAAG Rev : TTCAGCACGCTACTGATG
D1118H	For : CATCACCACCcACAACACCTTC Rev : ATCTGGGGCTCGTAGAAG

Appendix Table of Contents:

Appendix Figure S1: Assessment of viral replication by flow cytometry in cell lines
Appendix Figure S2: Syncytia formation by SARS-CoV-2 variants
Appendix Figure S3: Variant S protein processing by TMPRSS2

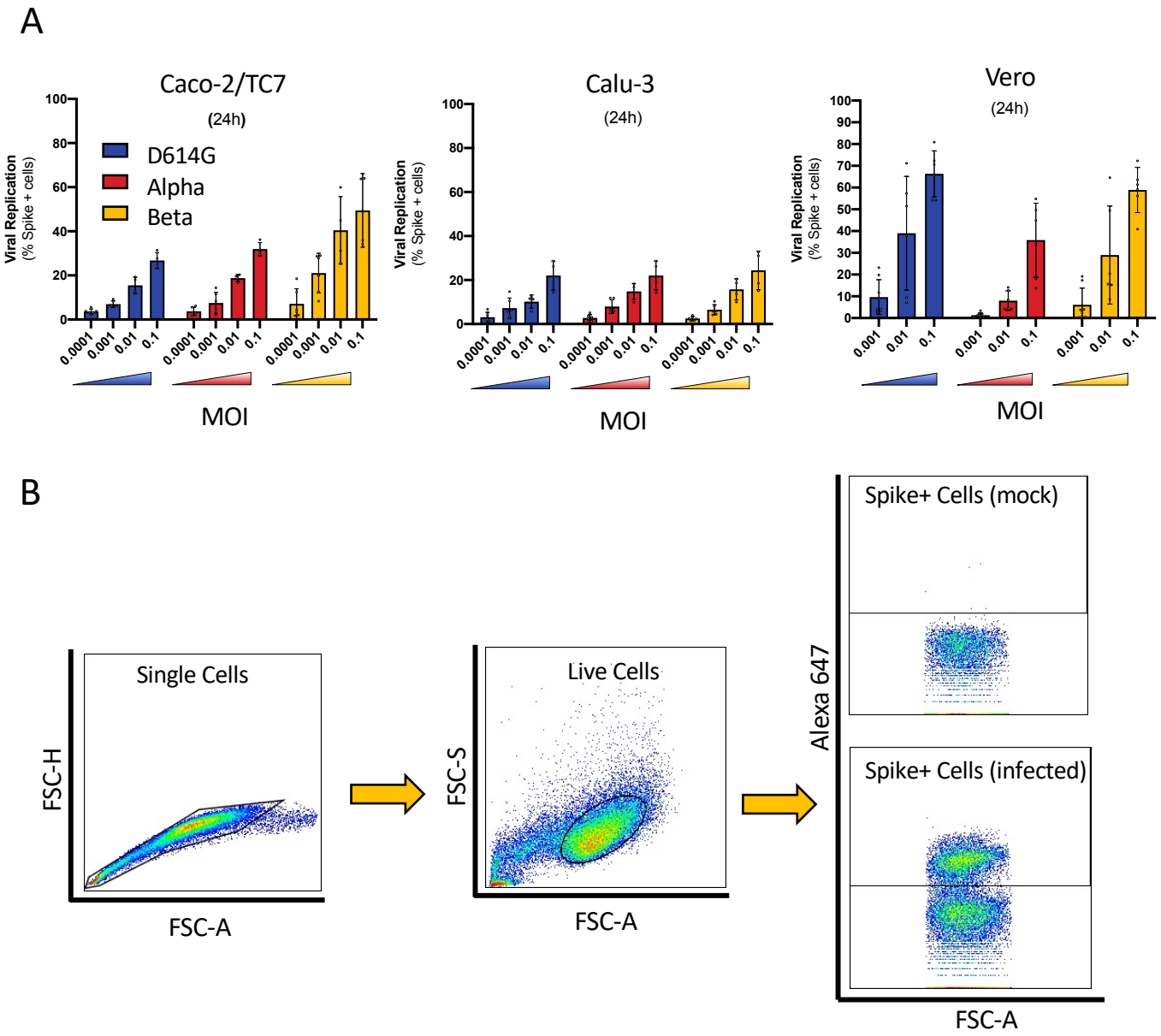

Appendix Figure S1 . Assessment of viral replication by flow cytometry in cell lines

(A) Caco-2/TC7 (left), Calu-3 (middle), and Vero cells (right) were infected at the indicated MOIs with SARS-CoV-2 variants for 24h. The number of S protein positive cells was determined by flow cytometry upon staining with human pan-SARS-CoV-2 mAb102. Only MOIs that were not saturating were used to generate replication curves for each cell line studied.

(B) Representative image of gating strategy used for flow cytometry to determine S protein positive cells.

Data information: Data are mean ± SD of at least 3 biological replicates

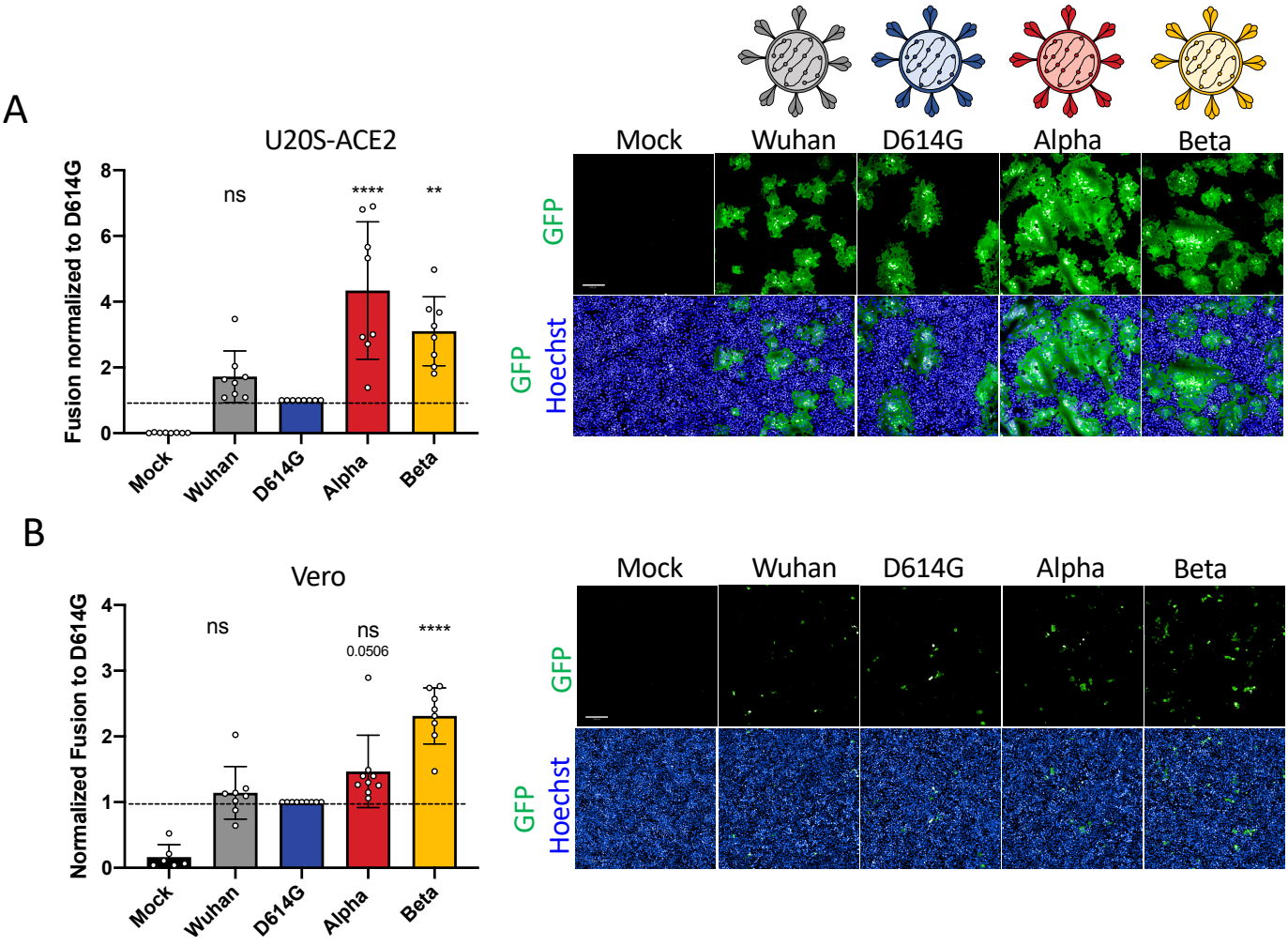

Appendix Figure S2. Syncytia formation by SARS-CoV-2 variants

(A) Left Panel: Fusion normalized to D614G for U2OS-ACE2 20h post infection at MOI 0.01. **Right Panel:** Representative images of U2OS-ACE2 20h post infection, GFP (Green) and Hoechst (Blue). Top and bottom are the same images with and without Hoechst channel.

(B) Left Panel: Quantified fusion of Vero cells infected at MOI 0.1. **Right Panel:** Representative images of Vero cells 48h post infection.

Data information: Scale bars: 200 µm. Data are mean ± SD of at least 3 independent experiments. Statistical analysis: One-way ANOVA compared to D614G reference, ns: non-significant, **P < 0.01, ****P < 0.0001.

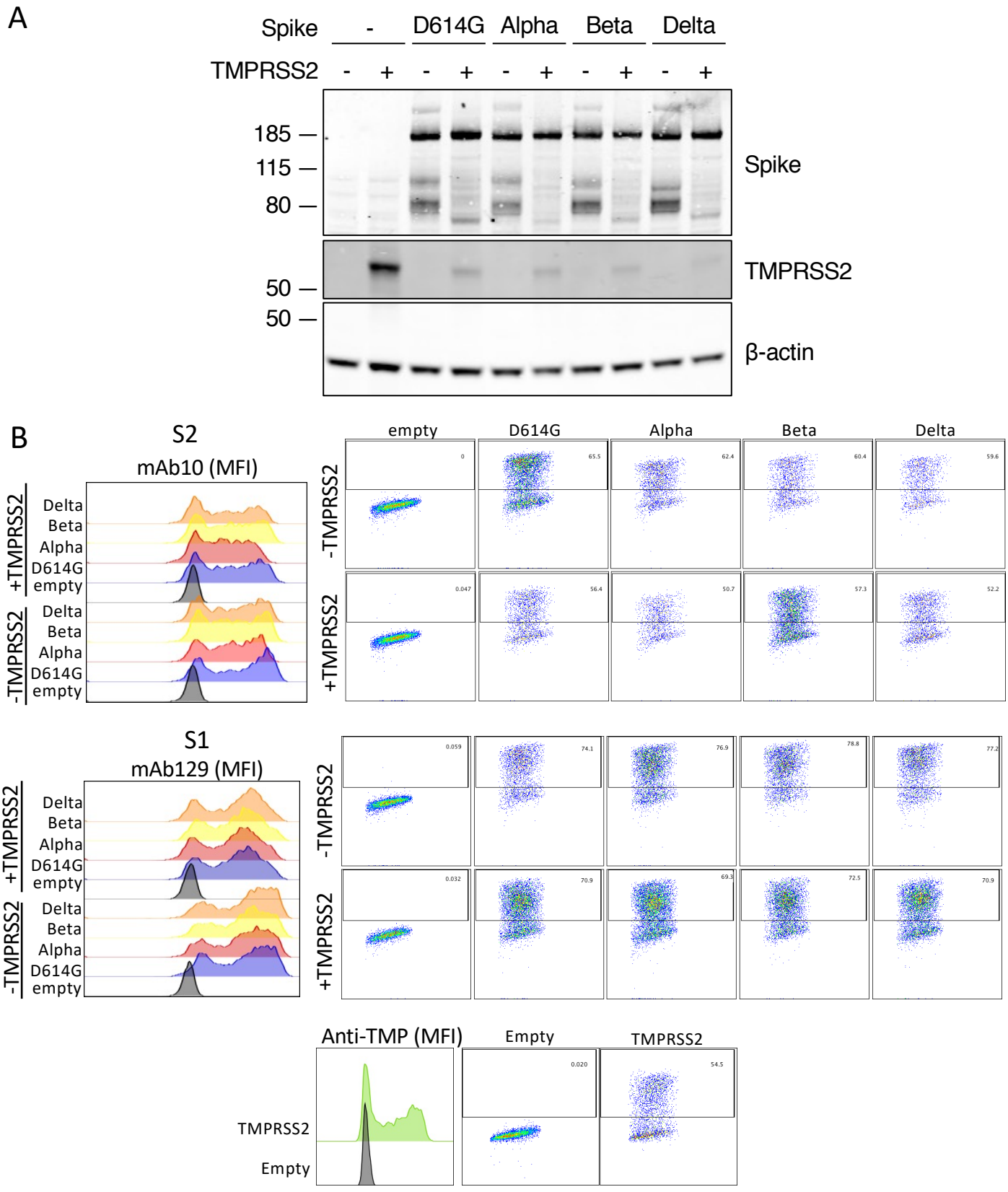

Appendix Figure S3. Variant S protein processing by TMPRSS2

(A) Comparison of the impact of TMPRSS2 on variant S protein processing measured by western blot. Plasmids encoding for S protein were co-transfected with or without plasmids expressing TMPRSS2 in 293T cells for 24h.

(B) Representative histograms of median florescent intensity (MFI) and FACs plots of 293T cells co-transfected with S protein with and without TMPRSS2 and stained with anti-S1 and anti-S2 .

Data information: Representative image of 2 experiments.

Chapter 4: Preliminary characterizations of hCoV-HKU1 S mediated syncytia formation & modulation by host factors

---

Preface to Chapter 4:

This chapter presents preliminary results on the subject of human coronavirus HKU1 and S-mediated fusion. Work on this project is ongoing and more experiments and controls are necessary to validate the conclusions. I present this data with the belief that even a small investigation into a neglected virus like HKU1, has scientific value. This study was supervised by Pr. Olivier Schwartz and Dr. Julian Buchrieser.

4.1 Abstract

Here we developed a novel cell-cell fusion assay for HKU1 S protein and used it to functionally characterize the fusogenicity and restriction of the HKU1 S. We find that the TMPRSS2 protease is necessary for HKU S-mediated fusion and must be present on the target cell membrane. Both the cleavage site and the protease activity of TMPRSS2 is necessary for fusion. We further show that human IFITM1 and LY6E are potent restriction factors of HKU1 S-mediated fusion; however, mouse IFITM1 enhances fusion.

4.2 Introduction: Human coronavirus HKU1

The pandemic potential of human coronaviruses (hCoVs) was progressively realized with the sequential emergence and spread of SARS-CoV-1 (2002), MERS-CoV (2012) and more recently SARS-CoV-2 (2019 and ongoing). Much scientific attention has been rightfully focused on these three highly pathogenic hCoVs since they are responsible for placing a significant burden on the global economic and public health infrastructure. Also, within the hCoVs are the often overlooked "common-cold" or "seasonal" coronaviruses 229E, NL63, OC43 and HKU1. These viruses are endemic to humans and infection in healthy individuals generally results in mild pathogenicity characterized by "cold-like" symptoms [6]. However, disease can occasionally progress to respiratory distress, asthma exacerbations and chronic bronchitis among vulnerable patients including the elderly, children and the immunocompromised [6]. They are also globally distributed and display seasonality, with infections peaking between December and May [12].

Among the hCoVs, HKU1 remains particularly enigmatic and poorly characterized in the scientific literature. It was first isolated in 2004 in Hong Kong from an elderly patient suffering from pneumonia [11]. The circumstances of the emergence of HKU1 is not known and the intermediate host has not been identified but it is likely that rodents were the ancestral reservoir [17]. Indeed, HKU1 and OC43 both belong to lineage A of *betacoronavirus* genus and are closely related to the rodent coronaviruses, mouse hepatitis virus (MHV) and rat coronavirus (rCoV) [17].

Unlike the other hCoVs, a bona fide host receptor for HKU1 has yet to be identified. Viral trophism and the entry step of the infection cycle is determined by the binding of the coronavirus Spike (S) protein to a host receptor. The coronavirus S protein comprises of an S1 domain that is responsible for initial attachment and receptor binding as well as a conserved S2 domain, which contains the machinery that fuses the viral membrane with the host's cellular membrane; allowing for viral contents to be deposited into the cell. SARS-CoV-1, NL63, and SARS-CoV-2 primarily use angiotensin converting enzyme 2 (ACE2) as the entry receptor and MERS-CoV S protein binds to dipeptidyl peptidase (DPP4). OC43, the closest hCoV relative to HKU1, uses a glycan-based receptor carrying 9-O acetylated sialic acid (9-O-Ac-Sia) for viral entry [219]. The receptor binding site (RBS) on the S protein of OC43 is conserved and functional in HKU1; however, HKU1 has a significantly lower affinity to 9-O-Ac-Sia and the architecture of the RBS on its S proteins makes its less accessible to the receptor [219]. In contrast to OC43, o-acetylated sialic acids are not sufficient for HKU1 infection and instead behave as receptor recognition or initial attachment factors [220].

The cell surface TMPRSS2 protease has also been shown to be important for the entry of HKU1 and drug treatments that inhibit TMPRSS2 drastically reduce viral entry [221]. Importantly, clinical isolates of HKU1 (as well as 229E and OC43) are more reliant on TMPRSS2 for viral entry, which suggests that wild type virus preferential fuses at the plasma membrane or in early endosomes [173, 221]. This is in contrast to cell-culture adapted hCoVs that seem to prefer fusion at late endosomes and some progressively lose their ability to infect and replicate with increased passaging [221]. This highlights another issue that hampers scientific research into the virology of HKU1; the virus is notoriously difficult to culture and passage [222]. HKU1 has only been shown to replicate in the human airway epithelial cell culture (HAE) model, primary human bronchial-tracheal epithelial cell (HTBEC) culture model and primary human alveolar type II cells; however, it is unclear if passaging alters the biology of the virus [180, 221, 223]. Nonetheless, with the current lack of autopsy reports (HKU1 infection is rarely lethal and patients are prone to secondary infections) and animal models, primary cell cultures are the most convincing model to reproduce viral infection and pathogenesis in the human airway epithelium [222].

Interestingly, it has been reported that HKU1 infection of primary human alveolar type II cells results in the formation of large fused multinucleated syncytia [180]. Patient autopsy reports and studies with animal models have described the presence of syncytia in the lung tissue upon infection with the highly pathogenic coronavirus including SARS-COV-2, MERS-CoV and SARS-CoV-1 [80, 85, 169, 170] [83, 84, 171-177]. Among the other common cold hCoVs, both 229E and NL63 have been shown to form syncytia in cell culture [178, 179]. It is currently not known if syncytia formation also occurs during asymptomatic or mild infections; however, it is now a well-documented pathological feature of severe coronavirus disease. Recent work done on

SARS-CoV-2, suggest that syncytia may contribute to cytopathicity and the inflammatory response, cell-to-cell viral dissemination and evasion from neutralizing antibodies and immune cell elimination [173, 224].

From a practical standpoint, syncytia formation can be used a proxy to study viral fusion since there are mechanistic parallels between S-mediated virus-cell and cell-cell fusion. We and others have shown SARS-CoV-2 S-mediated syncytia formation can be used to functionally characterize fusion via interaction with viral receptors, host proteases like TMPRSS2 and membrane-localized interferon-stimulated genes (ISGS) [173, 181, 209]. IFITMs are a family of ISGs of particular interest since they antagonize the entry of several enveloped viruses by altering the curvature and biophysical properties of the plasma membrane [181, 190, 192].

In this preliminary communication, we add to the sparse literature on the virology of HKU1 by developing a HKU1 syncytia formation model which we used to functionally characterize the fusogenicity of the HKU1 S protein and its interactions with TMPRSS2, IFITMs, and LY6E (Lymphocyte antigen 6 complex locus E). We find that a fully active TMPRSS2 is required for HKU1 S-mediated fusion and that human IFITM1 is a potent inhibitor of fusion. In contrast, mouse IFITM1 behaves as fusion enhancement factor.

4.3 Results

4.3.1 TMPRSS2 must be present on the target membrane for HKU1-S mediated fusion

To quantitatively assess the fusogenicity of the HKU S protein we used our previously described 293T GFP complementation split system [181]. Briefly, 293T cells expressing GFP10 are co-cultured with an equal number of cells expressing GFP11 and a GFP signal will be produced upon cell-cell fusion (**Figure 1A**). The degree of fusion can be quantified based on the GFP signal relative to the total cell area or nuclei number. We confirm that 293T cells can be efficiently transfected and that the HKU1 S protein is expressed at the cell surface, using a pan-coronavirus monoclonal antibody (mAb10) that targets the S2 domain (**Figure S1A**). We found that HKU1 S can only induce cell-cell fusion in the presence of TMPRSS2 (TMP) (**Figure 1B**). The expression of the ACE2 receptor, which is necessary for SARS-CoV-2 S-mediated fusion, had no effect on HKU1 S-mediated fusion (data not shown). Increasing the amount of TMP expression does not correspond with increased fusion nor does TMP expression affect the viability of the cells (**Figure 1B, S1B-C, S1D**). We then asked if syncytia formation requires TMP to be present on the same membrane that is expressing the HKU1 S or on the target membrane. To this aim, we performed an acceptor/donor experiment where TMP is either transfected together with S on the donor GFP10 cells or transfected on the acceptor GFP11 cells before co-culture (**Figure 1C**). We found that TMP must be on the acceptor cell membrane that opposes the membrane expressing HKU1 S protein in order to induce efficient syncytia formation. Transfection of only S protein without TMP did not induce fusion (**Figure 1C**).

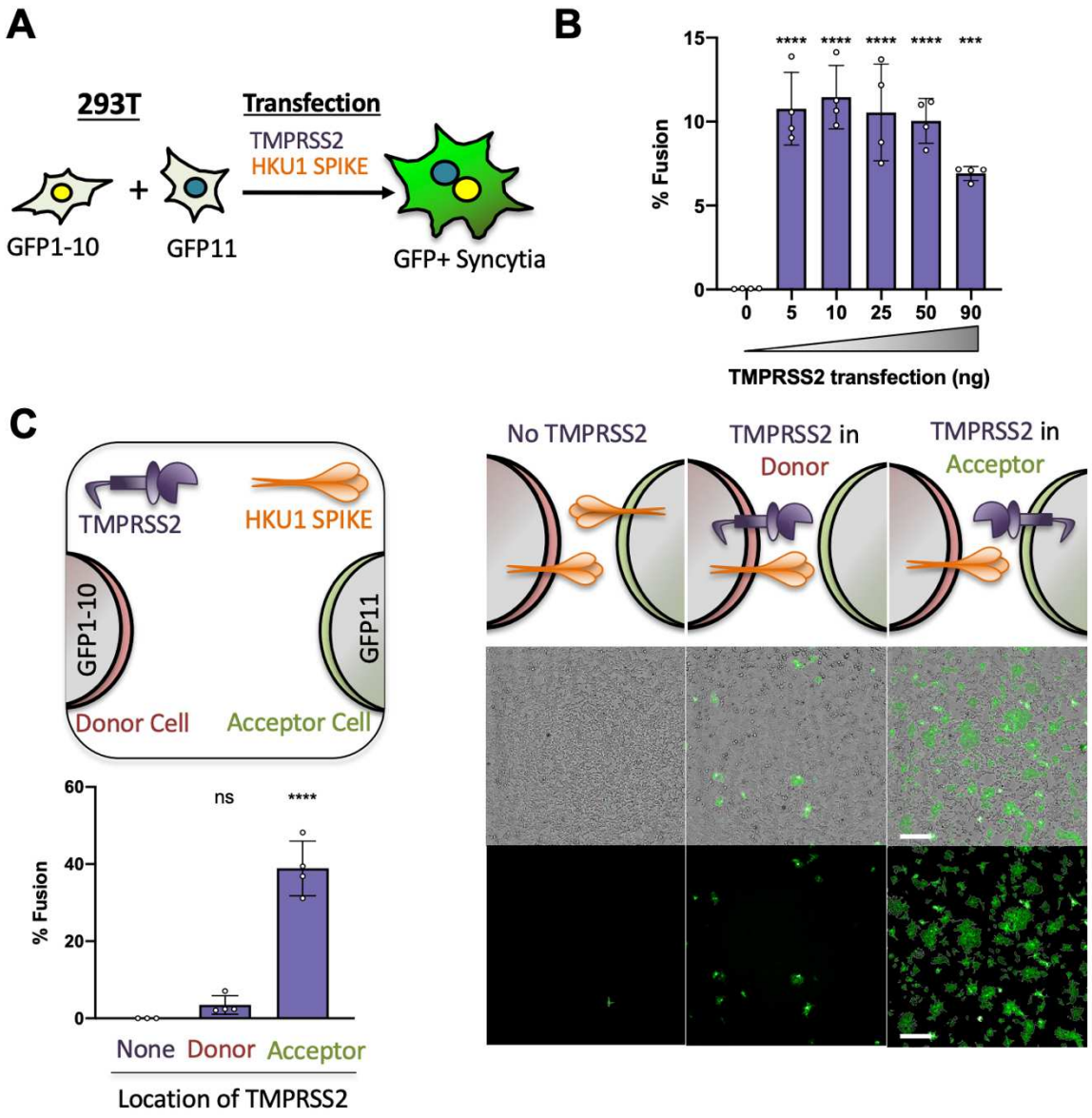

Figure 1 TMP must be present on the target membrane for HKU1 S-mediated syncytia formation. **(A)** 293T GFP-split cells were transfected with HKU1 S protein and TMPRSS2 and imaged 18h post-transfection. (B) Quantification of fusion at different quantities of TMP. **(C)** TMPRSS2 and HKU1 S acceptor/donor experiment **Left panel**: experiment schematic and quantification. **Right Panel**: Representative images of 293T GFP-split cells 18h post-transfection, GFP (Green). Top and bottom are the same images with and without Bright Field. Scale bars: 200 µm. Data are mean ± SD of at least 3 independent experiments. Statistical analysis: One-way ANOVA, ns: non-significant, *P < 0. 05, **P < 0.01, ***P < 0.001, ****P < 0.0001.

4.3.2 TMPRSS2 must be fully functional for HKU S-mediated fusion

We then sought to characterize the importance of the enzymatic activity of TMP on HKU1 S-mediated fusion by generating TMP mutants. The TMP polypeptide is 492 amino acids in length and contains a transmembrane domain, scavenger receptor cystine-rich domain, LDL receptor class A and a serine peptidase (**Figure 2A**) [225]. The catalytic activity of TMP can be disrupted by a serine-to-alanine substitution at amino acid position 441 (S441A) in the serine peptidase [226]. Additionally, TMP also possess autocatalytic activity that allows for self-cleavage and protease secretion [227]. An arginine-to-glutamine substitution at amino acid position 255 (R225Q) prevent autocleavage by disrupting the recognition motif [226]. We generated both TMP mutations and confirmed that their expression did not affect the viability of the cells; however, the expression levels of the mutations were slightly lower than the wild type TMP (**Figure S1D)**. We adjusted for this by normalizing for expression levels and characterized their contribution to HKU1 S-mediated fusion (**Figure 2B and S1B, C)**. We found that peptidase activity and autocleavage site are needed for S-mediated fusion. (**Figure 2C**). This was true even when the mutant TMPs were expressed at greater levels than the WT TMP (data not shown). There was no fusion when HKU1 S protein was co-expressed with the protease inactive TMP-S441A and when co-expressed with autocleavage mutant (TMP-R225Q) it induced negligible (less than 10% of the WT) fusion **(Figure 2B**). We then preformed video microscopy experiments where we normalized for expression and examined the fusion kinetics of the mutants relative to the WT. Again, we found the kinetics of fusion for the mutants was drastically reduced **(Figure 2D and S1B, C)**. In summary, a fully functional TMP with both the autocleavage site and functional peptidase is required for HKU1 S mediated fusion. Future experiments will investigate if HKU1 S is cleaved by TMP.

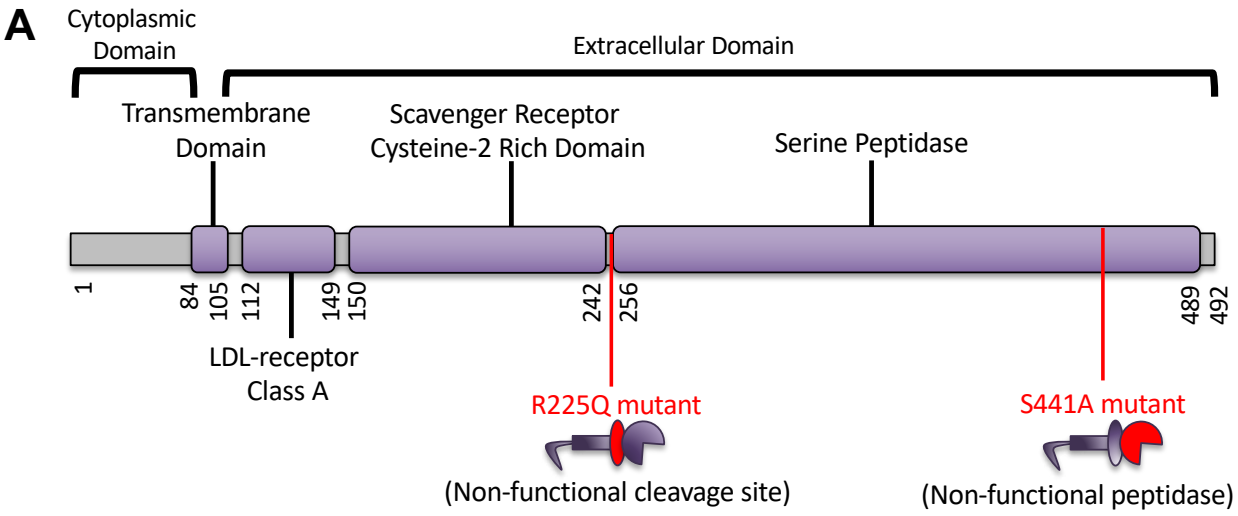

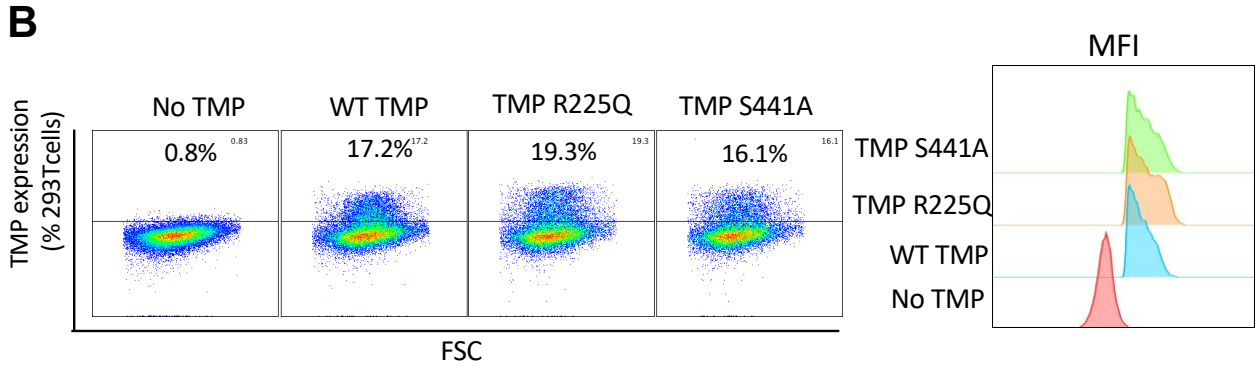

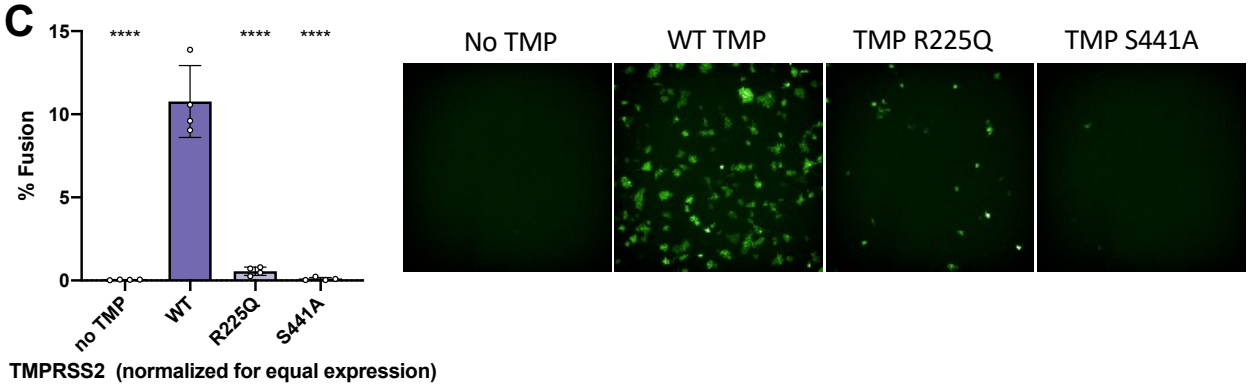

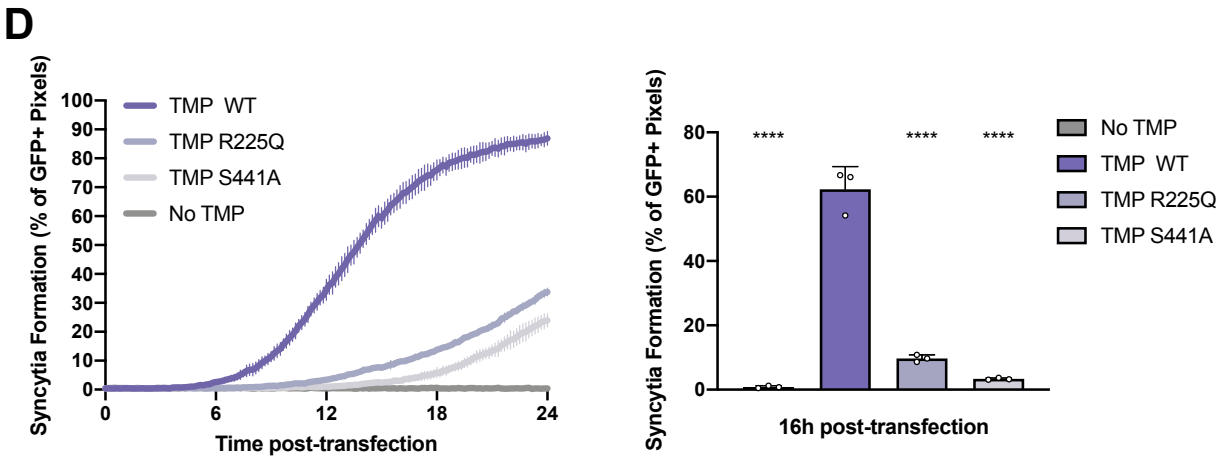

Figure legend on next page

Figure 2 Fully functional TMPRSS2 is require for HKU1 S-mediated fusion **(A)** Schematic of the TMPRSS2 protein with functional domain and mutation sites. **(B)** TMPRSS2 WT, R225Q, and S441A are expressed equally at chosen concentration. **Left:** FACS plots **Right**: MFI. **(C) Left**: Quantification of HKU1 S-mediated fusion in the presence of WT and mutant TMP. **Right:** Representative images of 293T GFP-split cells 18h post-transfection with TMP and TMP mutants. **(D) Left Panel**: Quantification of variant S protein mediated fusion kinetics in 293T-GFP split cells by video microscopy. Results are mean ± SD from three fields per condition from one representative experiment. **Right Panel**: Fusion quantification of at least 3 independent video microscopy experiments, 16h post transfection. Scale bars: 200 μm. Data are mean ± SD of at least 3 independent experiments.

4.3.3 The modulation of HKU1-S mediated fusion by membrane ISGs

We and other had previously reported that the SARS-CoV-2 S-mediated fusion is restricted by human IFITMs, particularly IFITM1 [181, 192]. IFITM1 localizes on the plasma membrane, while IFITM2 and 3 transit through the plasma membrane before localizing on the endosomes. To characterize the role of IFITMs on HKU1 S-mediated fusion, we co-transfected hIFITM1, 2 and 3 in addition to S and TMP into our 293T GFP-split system (**Figure 3A**). hIFITM2 and 3 had no noticeable effect on HKU1 S-mediated syncytia formation (**Figure 3B**). As was the case for SARS-CoV-2 S-mediated fusion, hIFITM1 was a potent restriction factor of the HKU1 S fusogenicity. Following reports that the membrane-bound ISG LY6E is also an effective restriction factor of SARS-CoV-2, SARS-CoV, MERS-CoV, OC43 and 229E [215], we checked to see if it also restricts HKU1. Indeed, we found that LY6E is also a strong inhibitor of HKU1 S-mediated fusion (**Figure 3B**). Since rodents are thought to be the ancestral source of HKU1, we wondered if mouse IFITM1 would behave similarly to hIFITM1. To our surprise, we found that mIFITM1 drastically augments HKU1 S-mediated fusion (**Figure 3B**). We preformed video microscopy to assess the kinetics of fusion in the presence of the different host factors. In line with our previous results, hIFITM2 and hIFITM3 did not have an effect on fusion while hIFITM1 and hLY6E both

drastically restricted the fusion kinetic of HKU1 S protein (**Figure 3C-F**). In contrast, HKU1 S mediated fusion in the presence of mIFITM1 occurred more rapidly and reached a plateau faster (**Figure 3G**). In the future, we will need to confirm that the expression of HKU1 S or TMP does not differentially affect IFITM expression. This remains a major caveat to these preliminary results. Additionally, the effect of IFITMs on HKU1, could be further supported through the use of pseudotyped virus expressing the HKU1 S protein.

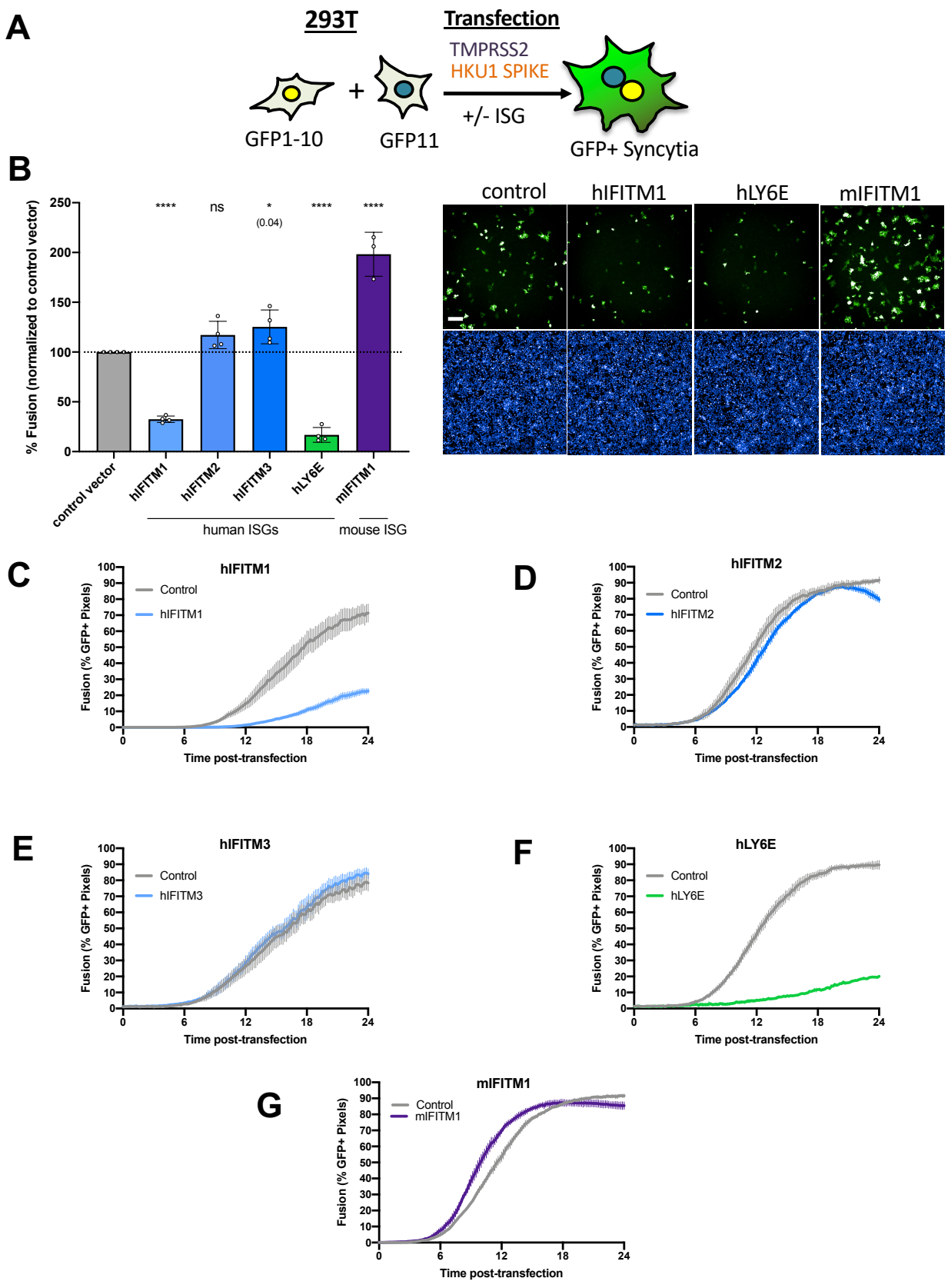

Figure legend on next page

Figure 3 Modulation of HKU1 S mediated fusion by membrane host factors **(A)** 293T GFP-split cells were transfected with HKU1 S protein and TMPRSS2 with or without ISGs (hIFITMs, hLY6E, mIFITM1) and imaged 18h post-transfection. **(B) Left:** Quantification of the effect of ISGs on fusion. Normalized to transfection control. **Right:** Representative images of 293T GFP-split cells 18h post-transfection with select ISGs, GFP (Green) and Hoechst (Blue). Top and bottom are the same images with and without Hoechst channel. Scale bars: 200 μm. Data are mean ± SD of at least 3 independent experiments. **(C-G)** Fusion kinetics of HKU1 S-mediated fusion in the presence of TMP and ISGs analysed by video microscopy **(C)** hIFITM1 **(D)** hIFITM2 **(E)** hIFITM3 **(F)** LY6E **(G)** mIIFTM1. Representative graphs of at least 2 experiments.

4.4 Discussion

Despite being endemic to humans, research into HKU1 has been neglected due to its mild pathogenicity and the lack of accessible experiment systems. Additionally, HKU1 infection of primary human alveolar type II cells results in the formation of syncytia [11]. With this in mind, we endeavored to functionally characterize the fusogenicity of the HKU1 S protein in our GFP-split syncytia formation system. We find that TMPRSS2 must be present on the target membrane and its enzymatic activity must be intact for HKU-S mediated cell-cell fusion to occur. This is in line with a previous report that demonstrates that clinical isolates HKU1 require surface TMP for viral entry. TMP is also present in the human airway and in the handful of human epithelial culture models that are susceptible to HKU1 infection. The function of TMP on HKU1 S is not currently known. The S protein of HKU1 possesses a furin-like cleavage site between the S1 and S2 domains and a cleavage site at the S2' [9]. It has been recently reported that HKU1 S1/S2 can be cleaved by the kallikrein 13 (KLK13) protease and it has been postulated that TMP may cleave at the S2' site, like it does for SARS-CoV and SARS-CoV-2 S proteins [35-37]. However, an investigation by Siu and colleagues found that the HKU1 S protein was not cleaved by TMP in 293T cells [38]. How TMP modulates HKU1 S fusion remains an outstanding question and future work on the cleavage of HKU1 S by TMP and KLK13 will provide a more thorough understanding into its

mechanism of fusion. As the receptor for HKU1 has yet to be identified, there is also a possibility that TMP acts upon an unknown receptor or attachment factor which warrants further exploration.

As is the case for SARS-CoV-2, we found that the human antiviral restriction factors IFITM1 and LY6E strongly inhibit HKU S-mediated syncytia formation [27, 39]. Interesting, we found that mouse IFITM1 strongly augments fusion. Rodents were the original reservoir species for HKU1, and this difference might suggest that in its initial host, HKU1 has evolved a way of exploiting subtle differences in IFITM genes to counteract their restriction and enhance its fusion. Work done on OC43 (also of rodent origin) found that mouse IFITM1, and to a lesser degree, human IFITMs increase viral fusion [40]. An understanding of how fusion modulators from the different hosts affect viral fusogenicity will provide insights into viral emergence and pathogenesis. Future characterizations, with infectious HKU1 virus or pseudotyped virus is necessary to validate these observations. Chimeric models that swap out the functional domains of human and mouse IFITM1 may also help elucidate the mechanism of action.

In our previous work, we found that hIFITMs strongly inhibit ACE2-dependent SARS-CoV-2 S-mediated syncytia formation. However, the addition of TMP reverted the inhibitory activity of IFITMs. This contrasts with our current observation that hIFITM1 is capable of restricting HKU1 S-mediated fusion even in the presence of TMP. Interestingly, TMP reverted the effect of IFITMs when present in the same cells as ACE2, suggesting a potential role of ACE2 cleavage by TMP in the context of SARS-CoV-2 [181]. By examining and comparing the interplay of TMP, ACE2 and IFITM1 with either the SARS-COV-2 S or HKU1 S protein, we may be able to dissect the modulatory effects of TMP and IFITM1 on fusion.

This work provides a preliminary characterization of the fusogenicity of the HKU1 S protein; however, thorough mechanistic studies and more control experiments are required to contextualize its relevance. Our syncytia formation system can also be employed as a useful proxy to study S-mediated viral entry and the role character membrane-bound host factors.

4.5 Material and Methods

Plasmids

A codon optimized version of the human coronavirus HKU1 Spike [11] (Sequence ID: YP 173238.1) was ordered as a synthetic gene (GeneArt, Thermo Fisher Scientific) and was cloned into a phCMV backbone (GeneBank: AJ318514), by replacing the VSV-G gene. pQCXIP-Empty control plasmid, pQCXIP-IFITM1-N-FLAG, pQCXIP-IFITM2-N-FLAG, pQCXIP-IFITM3-N-FLAG were previously described [181, 228]. LY6E and mIFITM1 were also cloned into the pQCXIP backbone. pQCXIP-BSR-GFP11 and pQCXIP-GFP1-10 were from Yutaka Hata [229]; Addgene plasmid #68716; http://n2t.net/addgene:68716; RRID: Addgene_68716 and Addgene plasmid #68715; http://n2t.net/addgene:68715; RRID: Addgene_68715). pCSDest-TMPRSS2 was from Roger Reeves [230]; Addgene plasmid # 53887; http://n2t.net/addgene:53887; RRID: Addgene_53887). TMPRSS2 mutants R225Q and S441A were generated via Q5 Site-directed mutagenesis (NEB) [226]. The primers used to generate the TMPRSS2 mutants are as follows: R225Q (For: CCGCCAGAGCcaGATCGTGGGC, Rev: CTTGAGTTCAAGTTGACCCC) and S441A (For: CCAGGGTGACgcgGGAGGGCCTC, Rev: CAAGAATCGACGTTCCCC) [226].

Cells

HEK293T cells were cultured in DMEM with 10% Fetal Bovine Serum (FBS) and 1% Penicillin/Streptomycin (PS). All cells lines were either purchased from ATCC or were kind donations from members of the Institut Pasteur and were routinely screened for mycoplasma.

GFP-Split Fusion assay

For cell-cell fusion assays, 293T cell lines stably expressing GFP1-10 and GFP11 were co-cultured at a 1:1 ratio ($7x10^4$ cells/well total) and were transfected in suspension with a total of 100ng of DNA with Lipofectamine 2000 (Thermo) in a 96 well plate (uClear, #655090) [181]. 10 ng of phCMV-HKU1-S and/or 5ng (unless otherwise stated) of pCSDest-TMPRSS2, and 40 ng of pQCXIP-IFITM were used and adjusted to 100 ng DNA with pQCXIP-Empty (control plasmid). At 16-18 h post-transfection images covering 80-90% of the well surface, were acquired per well on an Opera Phenix High-Content Screening System (PerkinElmer). The GFP area, total cell area and/or the number of nuclei was quantified on Harmony High-Content Imaging and Analysis. For video microscopy experiments, 293T GFP split cells (mixed 1:1) were transfected in suspension with 50ng of phCMV-HKU1-S, 25ng of TMP, and 100ng of pQCXIP-ISGs and normalized to 500ng with pQCXIP-Empty for 30mins at 37°C. Cells were washed twice and then seeded at a confluency of $2x10^5$ cells per quadrant in a u-Dish 35mm Quad dish (ibidi-#80416). Cells were allowed to settle, and fluorescence images were taken at 37°C every 10min up to 24h using a Nikon BioStation IMQ, with three fields for each condition. Fusion defined as percent of GFP pixels was calculated with ImageJ.

Flow cytometry

The expression of the HKU1 S protein was assessed via transfection into 293T cells for 24h followed by staining with human mAb10 (pan-coronavirus anti-S2) at 1 μg/mL and secondary staining with Alexa Fluor 647 (1:500) in MACs buffer. TMPRRS2 (and mutant) expression was assessed in a similar manner using rabbit anti-human TMPRSS2 (Atlas antibodies cat# HPA035787, 1:1,000) and Alexa Fluor 488 (1:500) as the secondary antibody.

Statistical analysis

Flow cytometry data was analyzed with FlowJo v10 software (Tristar). Calculations were all performed with Microsoft Excel 365. GraphPad Prism 9 was used to generate figures and for statistical analysis. Statistical significance between different conditions was calculated using the tests indicated in the corresponding figure legends.

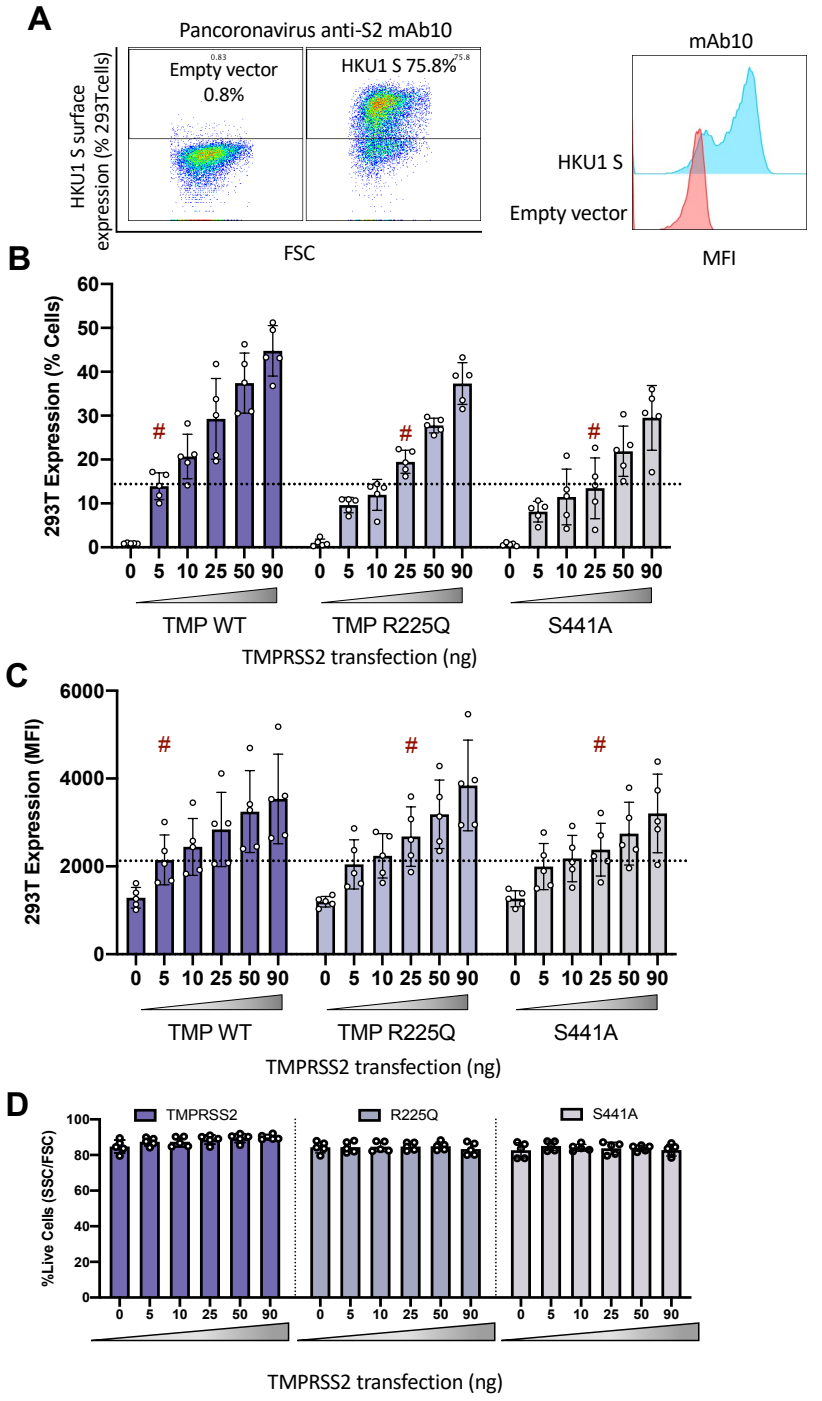

Supplemental Figure 1 (A) FACs plot and MFI showing HKU1 S protein is expressed at 293T cell surface. **(B)** Quantified percent expression level of WT TMP, TMP-R225Q and TMP-S441A in 293T cells 18h post-transfection. **(C)** Quantified MFI of WT TMP, TMP-R225Q and TMP-S441A in 293T cells after 18h post-transfection. **(D)** Percent of live cells upon transfection with TMP and mutant TMPs. Data are mean ± SD of at least 3 independent experiments. # denotes concentration used for equal expression in main figures.

Chapter 5: Discussion & Perspectives

Preface to Chapter 5:

This chapter serves as a general discussion on the subject of SARS-CoV-2 and syncytia formation. It was written by Maaran Michael Rajah, with editorial support from Pr. Olivier Schwartz and Dr. Julian Buchrieser. Sections of this discussion chapter were adapted and submitted as an invited review article to the Journal of Molecular Biology [1]. Permission has been granted by the publisher to include the article in this thesis (see appendix).

Rajah MM, Bernier A, Buchrieser J, Schwartz S. The mechanism and consequences of SARS-CoV-2 spike-mediated fusion and syncytia formation, Journal of Molecular Biology (2021), doi: https://doi.org/10.1016/j.jmb.2021.167280**.**

5.1 General Discussion & Perspectives

Histopathological reports during the early stages of the pandemic, identified the presence of infected multinucleated syncytial cells in COVID-19 patient lung tissues [80]. The mechanism by which SARS-CoV-2 induces syncytia and the degree to which it affects pathology is not fully understood. Our investigation found that SARS-CoV-2 infected cells express the S protein on the cell surface, which can then interact with ACE2 receptors on neighboring cells to induce cell-cell fusion [181]. Syncytia formation is augmented by the presence of the TMPRSS2 protease and restricted by the ISGs, IFITM1, 2 and 3 [181]. Interestingly, TMPRSS2 reverts the IFITM mediated restriction [181]. The mechanism by which TMPRSS2 subverts the biophysical constraints imposed by IFITMs remains an outstanding question. Proteolytic processing by TMPRSS2 has also been shown to undermine IFITM-mediated restriction of S mediated cell entry for other coronaviruses including hCoV-229E and the bat SARS-like WIV1 [207, 208]. The SARS-CoV-2 S protein is first cleaved at the S1/S2 site by furin and subsequently by TMPRSS2 at the S2' site [94, 99]. It is possible that the processing of the S protein elicits conformational or structural changes allows for more efficient fusion that overrides IFITM restriction. However, in our acceptor/donor experiments, we found that TMPRSS2 and IFITMs modulate fusion when expressed on the same cell as the ACE2 receptor, rather than on the cells expressing the S protein. Furthermore, we found that TMPRSS2 processes S protein and ACE2 but does not degrade IFITMs. Indeed, TMPRSS2 is known to cleave ACE2 and generate soluble receptor fragments. Therefore, it is plausible that the proteolytic activity TMPRSS2 exerts on ACE2 may alter the interaction between ACE2 and the S protein in a way that circumvents IFITM restriction. Examining the motility and interaction dynamics of these interactors on the plasma membrane during syncytia formation, may bring us closer to understanding the precise mechanism by which

syncytia formation is facilitated or restricted. Future experiments with non-cleavable ACE2 mutants and florescent proteins will provide a deeper understanding of this phenomenon.

Additionally, we present preliminary results that suggest TMPRSS2 is necessary for HKU1 S-mediated syncytia formation and that mouse and human IFITM1 either augment or restrict fusion, respectively. TMPRSS2 does not seem to revert the restriction of HKU1 S-mediated fusion by human IFITM1, as it does for SARS-CoV-2 S-mediated fusion. As the ACE2 receptor is not involved in HKU1 S-mediated fusion, this observation supports to the hypothesis that TMPRSS2 interacting with ACE2 somehow hampers IFITM restriction of SARS-CoV-2 S-mediated fusion. While we still need to validate these observations with additional experiments and controls, future comparative studies that characterize the different roles of TMPRSS2 on SARS-CoV-2 and HKU1 S-mediated fusion may help elucidate their mechanism of action.

As the virus continued to evolve during the course of the pandemic, we set out to functionally characterized the fusogenicity of the SARS-CoV-2 variants of concern. We found that while the Alpha and Beta variants replicated similarly to the early European D614G variant and the ancestral Wuhan strain. We did not characterize the replication of the Delta variant; however, other groups have suggested that it replicates more efficiently than the Alpha variant [231, 232]. We found that Alpha, Beta, and Delta variants induced more syncytia than both the D614G and Wuhan strains. The fusogenicity of the SARS-CoV-2 variants correlated with the affinity of the respective S proteins to the ACE2 receptor. The individual mutations associated with the variant S proteins differentially affected fusogenicity and antibody evasion potential. The VOCs are associated with increased transmission and worsened disease outcomes. It is currently unknown if the lung

pathology induced by the VOCs also includes the formation of more syncytial pneumocytes. It would be of interest, to retrospectively compare autopsy reports in order to analyze the size and frequency of syncytia in the lungs of patients who were infected with the different variants. Furthermore, the greater fusogenicity of the variants may have implications on their transmissibility and general lung pathology. The development of primary cell culture systems as well as animal models will be necessary to better evaluate the contribution of syncytia to pathology. Our study of the VOC S proteins also provides a functional characterization of the evolution of the SARS-CoV-2 S protein throughout the progression of the pandemic.

This thesis is presented in a manuscript format, as such each of the aforementioned chapters concludes with a subject specific discussion. Here, I endeavor to provide a global discussion regarding the fusogenicity of the SARS-CoV-2 S protein and the potential consequences of S-mediated syncytia formation. The first section contextualizes our findings on the fusogenicity of the VOC S proteins and their associated mutations in the context of the continuously expanding literature. This is followed by a general discussion on the impact and potential consequence of syncytia formation on SARS-CoV-2 infection and pathology. In each section I highlight areas of interests for future investigations. Finally, I provide a short description on how our S-mediated syncytia formation system could be applied to characterize S fusogenicity, viral entry, and antibody neutralization.

5.2 Variants of Concern S proteins and Fusogenicity

Figure 5.1 Spike protein mutations associated with Alpha, Beta, Delta and Gamma SARS-CoV-2

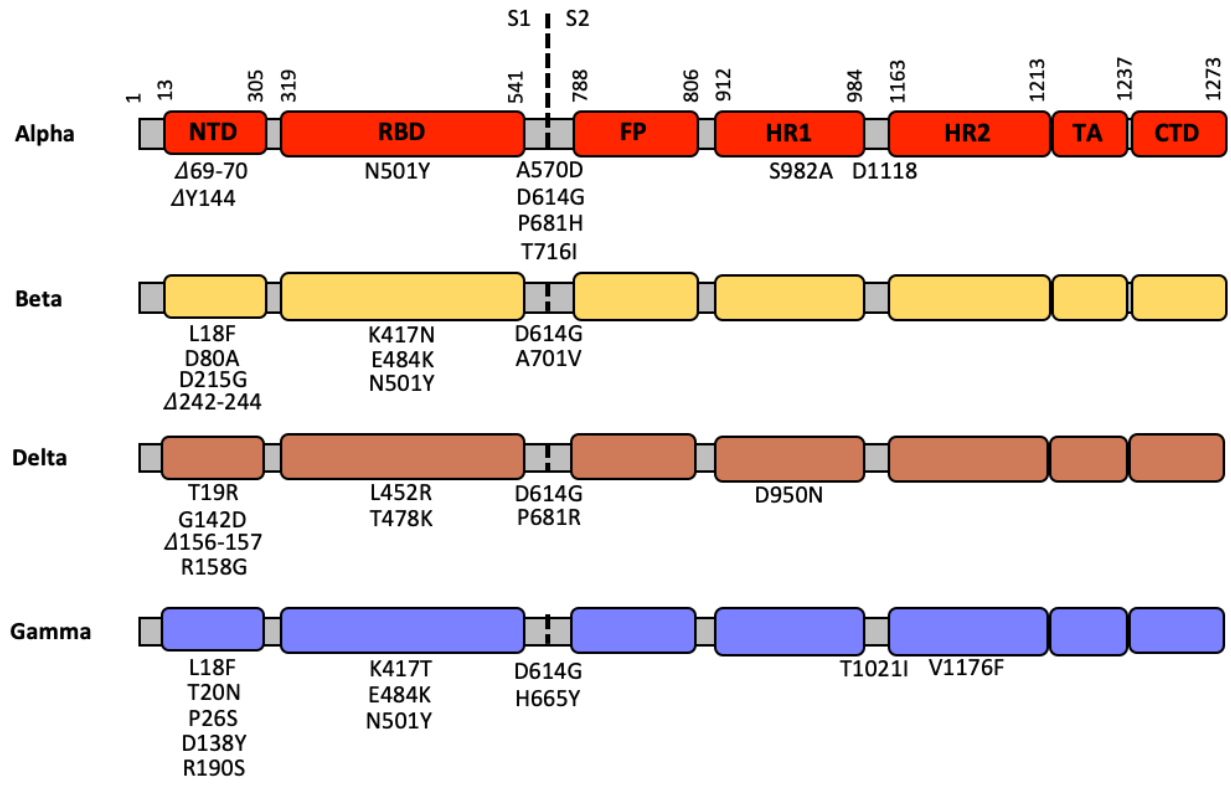

variants. N-terminal domain (NTD), receptor binding domain (RBD), fusion peptide (FP), heptapeptide repeat sequences 1 and 2 (HR1 & HR2), transmembrane anchor (TA), C-terminal domain (CTD). Figure generated by the author and submitted to the Journal of Molecular Biology in an invited review article [1]. Rights retained to use figure in thesis or dissertation. Original source: Elsevier. Journal of Molecular Biology, Rajah et al., 2021.
doi: https://doi.org/10.1016/j.jmb.2021.167280

Since the start of the pandemic, the ancestral Wuhan strain has been replaced by variants containing several mutations throughout their genome. Variants Alpha (B.1.1.7) originating from the United Kingdom; Beta (B.1.351) from South Africa; Gamma (P1 and P2) from Brazil; and more recently Delta (B.1.617.2) from India are of concern both regionally and globally. While the variant-associated mutations are found throughout the viral genome, many mutations are

associated with the S protein (**Figure 5.1**). In addition to be the viral fusogen, the S protein is highly antigenic and therefore the target for neutralizing antibodies. As such, many of the mutations found in the variants' S proteins have arisen in the context of antibody escape. The impact of the variants, with all of their accumulated mutations, on pathology is not clear, but some variants are more transmissible [59, 60]. Several recent studies including ours, had sought to characterize and compare the S proteins of the variants in terms of their fusogenicity.

One of the earlier variants identified was the European variant, which contained the D614G mutation proximal to the S1/S2 cleavage site. This mutation shifts the conformation of the S protein to a state that is more competent for ACE2 binding, while not significantly altering antibody neutralization [49, 233]. The D614G replicates more efficiently in primary cell culture models [233]. Furthermore, greater levels of viral genetic material has been found in the upper respiratory tract of infected individuals which may be more associated with transmission rather than disease severity [60]. In terms of fusogenicity, pseudovirus assays have shown that the D614G substitution increases the efficiency of cellular entry [60, 234]. The D614G mutant produces more syncytia than the ancestral Wuhan strain in cell culture models [209, 235]. We and others have shown that relative to D614G, the Alpha, Beta, and Delta variants are more syncytiogenic in cell culture [209, 232, 236]. The Alpha and Delta S proteins induce the most cell-cell fusion and they do so more rapidly than the other variants [209, 232]. The Beta variant S is also more fusogenic than D614G [209]. In the most general sense, the degree of syncytia formation seems to correlate with the affinity of the variant S proteins to ACE2 [51, 209]. A contradictory study found no difference (Alpha) or a slight reduction (Beta and Gamma) in variant S mediated cell-cell fusion; however, work by the same group found the Delta variant to be more syncytiogenic [237, 238].

This discrepancy may be explained by variations in the experimental systems and the time-points in which syncytia formation was assessed. Highly fusogenic cells and late time-points may risk missing differences in fusogenicity. The D614G mutation alone elicited significant changes in the S protein that impacted its structure, receptor affinity and fusogenicity. As such, it is worth examining the changes elicited by other individual variant-associated mutations.

The S1 domain is part of the spike that is most exposed to neutralizing antibodies on the virion. As such, it is under persistent evolutionary pressure and prone to mutations. Some of the more recent variants (Alpha, Beta, Gamma) also share the N501Y mutation within the RBD. This mutation increases the affinity of S protein to ACE2 and viral transmission but does not affect antibody neutralization [209, 239-243]. The hydrophobic pocket formed by the Y41 and K353 regions of ACE2, interacts more efficiently with the Y501 mutant than with the wild type S [244]. Despite its higher affinity to ACE2, the N501Y mutation alone did not increase syncytia formation in cell culture [209]. E484K, another significant mutation within the RBD, present in Beta and Gamma variants, also later emerged in a subset of the Alpha lineage [245]. The RBD of Beta variant also includes the K417N (K417T in Gamma). The E484K and K417N mutations are associated with antibody escape, though they may alter ACE2 binding when in conjunction with N501Y [243, 245-247]. E484K may increase affinity to ACE2, whereas K417N seems to decrease it [240, 248]. Individually, both mutations reduced syncytia formation [209]. The E484 mutation has been suggested to allow for infection of H522 human lung cells independently of ACE2 [249]. This alternate entry pathway may rely on surface heparan sulfates and clathrin-mediated endocytosis [249].

Within the NTD domain of the variant S proteins are several mutations that are generally associated with antigenicity [247]. As previously mentioned, the NTD is also involved in receptor binding and structural changes, and some of the variant associated mutations within the domain have been shown to impact S protein-mediated fusogenicity. The Δ69/70 mutation that is associated with the Alpha variant increases infectivity through greater incorporation of cleaved S protein into virions [61]. Furthermore, Δ69/70 may compensate for the reduced infectivity brought about the antibody escape mutation in the RBD of the variants [61]. Interestingly, restoring the Δ69/70 mutation abrogates the relative increase in syncytia formation elicited by the Alpha S protein relative to the D614G S protein [61]. However, the deletion on its own within the D614G S protein is detrimental to syncytia formation [209]. The comparatively greater syncytia formation induced by the Alpha variant S protein may thus be a result of the Δ69/70 mutation working in conjunction with other mutations. The deletion of 242-244 in the NTD of the Beta variant also restricts syncytia formation on its own [209]. It remains to be seen how it functions within the context of partner mutations. Interestingly, the D215G mutation of the Beta variant facilitates syncytia formation [209]. The mechanism of its action is unknown, and future investigations examining it within the context of L-SIGN, DC-Sign and neuropilin-1 binding and overall S structural changes would be of interest [96]. Such investigation could broaden the scope of target cells that may be able to form syncytia.

Of particular interest are the P681H and P681R mutations found in the S1/S2 cleavage site of Alpha and Delta variants, respectively. The P681 site is positioned in a surface-exposed loop of the S protein and is accessible to proteases. A recent investigation in the Alpha variant with the P681H mutation showed that there is a greater exposure of the furin cleavage site which naturally

increases affinity to furin [250]. The presence of more cleaved Spike in the virion or at the cell surface can increase fusogenicity. Indeed, we showed that the P681H mutation drastically increased syncytia formation [209]. It has also been suggested that O-glycosylation modulates furin cleavage of the S protein, and the presence of the P681 region facilitates the activity of glycosylation enzyme GALNT1 [251]. How the variant-associated mutations affect glycosylation and subsequent furin cleavage would be of future interest. Work by Saito and colleagues suggest that the P681R mutation of Delta variants increases S protein cleavage and subsequent viral fusion [236]. The P681R mutation was also responsible for larger syncytia forming in experiments conducted with artificial virus reversed engineered to contain the mutation [236]. Infection with virus housing the P681R resulted in higher pathogenicity in a hamster model: animals infected with the mutant virus experienced greater weight loss and reduced pulmonary function than with the D614G virus [236].

The A570D and S982A mutations, also within proximity of the cleavage site of the Alpha variant, did not significantly affect syncytia formation individually; however, structural studies suggest that they may reduce contact between individual chains of the trimeric spike [209, 252]. In conjunction with other mutations like P681H, they may augment cleavage of the S protein [252]. The D1118H mutation in the S2 of the Alpha variant, between the HR1 and HR2 domain potently increases syncytia formation [209]. Characterization of this mutation in the literature is scarce. From its location, it would not be unreasonable to speculate that it may impact the fusion machinery and HR1/HR2 association. Further investigations examining the effects of D1118H on the structure and function of the S protein, and the overall infectivity of the S protein would be of interest. A more thorough understanding of the variants and their respective mutation, especially

in *in vivo* models, would be of great value in understanding the transmission and pathology of the novel variants.

5.3 Potential consequences of syncytia formation in SARS-CoV-2 pathogenesis

SARS-CoV-2 mediated syncytia formation has been proposed to be a potential contributor to overall pathology. While syncytia have been observed in the lung tissue of patients with fatal COVID19 disease, its relative significance and its general contribution to the viral infection remains unknown. Furthermore, it is unclear if syncytia formation is a feature of asymptomatic or mild SARS-CoV-2 infections or if occurs *in vivo* upon infection with the common cold coronaviruses like HKU1. Recent literature suggests that SAR-CoV-2 induced syncytia may represent a form of cytopathic effect, trigger an inflammatory or immune response and support viral dissemination and persistence. This section examines and summarizes the potential impact of S-mediated syncytia formation on pathology and highlights avenues for further investigation.

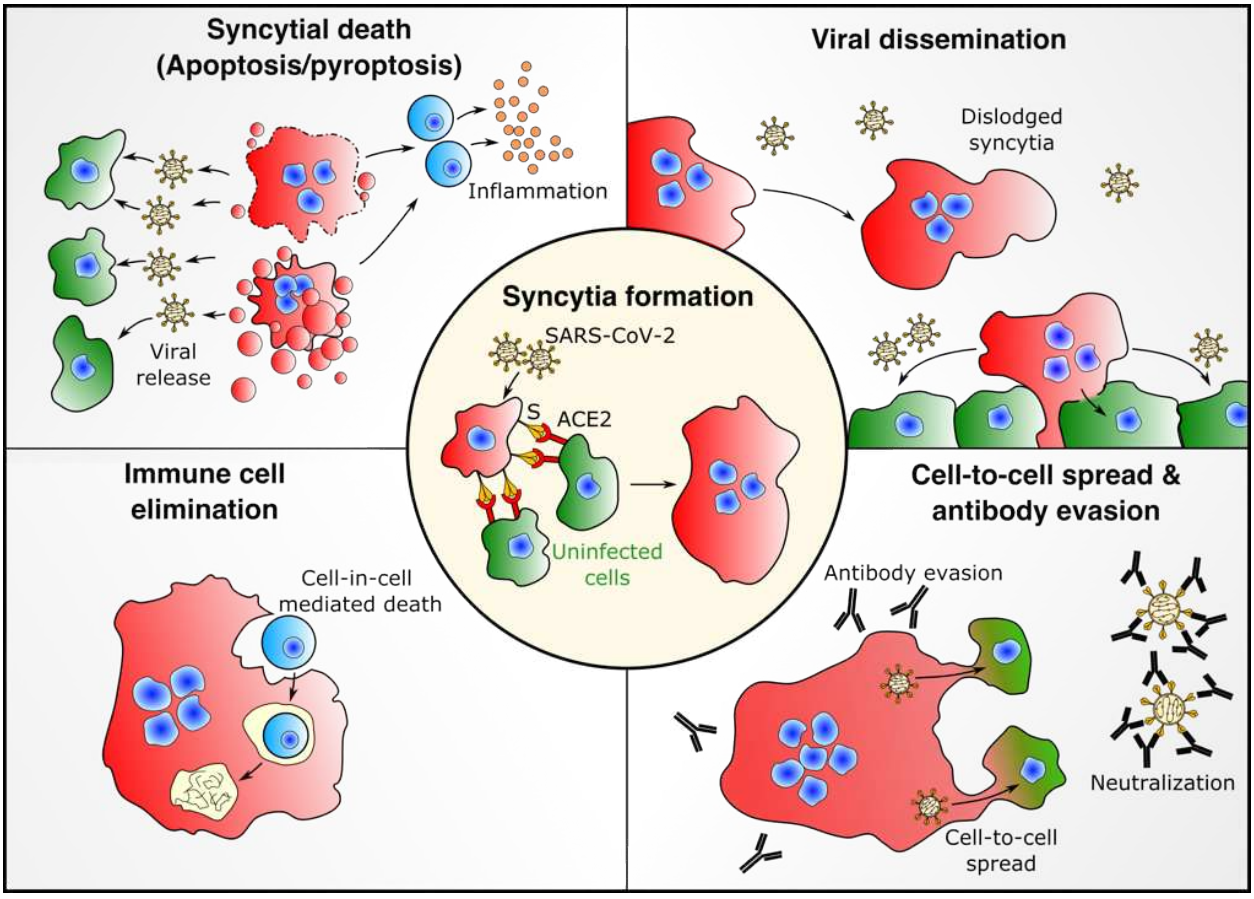

Figure 5.2 The potential consequences of syncytia formation on SARS-CoV-2 pathology. Center: Cells infected with SARS-CoV-2 express the spike protein at the surface and form large multinucleated syncytia. Top left: The process of syncytial death via apoptosis or pyroptosis can release virus to infect neighbouring cells and/or trigger an inflammatory response. Top right: Infected syncytia can lift off to contribute to viral dissemination and the overall infectious dose. Bottom left: Syncytial cells can target lymphocytes for cell-in-cell mediated death. Bottom right: Syncytia can facilitate cell-to-cell spread of the virus and shield the virus from neutralizing antibodies. Figure generated by the author and Julian Buchrieser and submitted to the Journal of Molecular Biology in an invited review article [1]. Rights retained to use figure in thesis or dissertation. Original source: Elsevier. Journal of Molecular Biology, Rajah et al., 2021. doi: https://doi.org/10.1016/j.jmb.2021.167280

5.3.1 Cytopathic effects

Unnaturally occurring syncytia are susceptible to rapid cytopathicity. This phenomenon of "syncytial apoptosis" has been well documented in HIV-1 infection *in vitro*, *in vivo* and in infected patient tissues [253]. Upon cell-cell fusion, the HIV-1 envelope protein triggers a pro-apoptotic

signaling pathway that triggers karyogamy (nuclear fusion) and DNA damage [253]. SARS-CoV-2 S protein-mediated syncytia also collapse and die during the later stages of the process. Of particular interest is the observation that the nuclei within S protein-mediated syncytium cluster together which could potentially be the first step of nuclear fusion and decay [181, 254]. Future investigations characterizing the cell death pathways triggered within SARS-CoV-2 induced syncytium, and the roles of other viral proteins would be of interest. There is also a possibility that the death of infected cells may release virions into the surrounding environment, spreading the infection (**Figure 5.2**). Syncytial pneumocytes in COVID-19 patient tissues are scarce and the degree to which cytopathic effects contribute to pathology is unclear. There is also a paucity of information regarding presence, clearance or turnover of syncytia during early infection. There is also possibility that if syncytia are prone to premature death, they may be detrimental to viral replication. The relationship between syncytial death and viral replication remains to be explored more thoroughly.

5.3.2 Immunological and inflammatory consequences

The formation of syncytia may also have immunological consequences. Zhang and colleagues found the presence of lymphocytes contained within syncytia as a cell-in-cell structure among COVID-19 patient lung tissue [173]. Using cell culture models, they demonstrated that syncytia formed through S protein-mediated fusion can internalize various T and B cell lines, monocytes and peripheral blood mononuclear cells (**Figure 5.2**) [173]. The internalized cells readily underwent shriveling, deterioration of the plasma membrane and death [173]. This study provides a possible mechanism by which syncytia may contribute to lymphopenia among patients with COVID-19 [173]. This phenomenon was described in one article and more investigations to

support these observations as well mechanistic studies examining how syncytia contribute to cell-in-cell mediated death would be of interest to the field. There is also an outstanding question whether S-mediated syncytia trigger elements of the innate immunity. Cell-cell fusion events induced by other pathogens have been documented to induce interferon expression. Syncytia induced by measles virus amplifies IFN- β production *in vitro* [255]. Similarly, cell-cell fusion induced by the bacterial pathogen *Burkholderia pseudomallei* elicits type I IFN expression through the DNA sensing cGAS-STING pathway [256]. This reportedly occurs independently of bacterial ligands [256]. How S protein-mediated pathological syncytia formation is related to immune activation or recognition should be explored further.

Recent work suggests that S protein-mediated syncytia formation results in the activation of Caspase-9, followed downstream by the activation of Caspase-3/7, and later by gasdermin E (GSDME)-mediated pyroptosis (**Figure 5.2**) [224] . This inflammatory form of cell death may have significant implication in triggering the immune response and warrants further investigation. The adaptive immune response also has profound implications for SAR-CoV-2 mediated cell-cell fusion. Antiviral antibodies may have contradictory roles in cell fusion [257]. Some neutralizing antibodies restrict cell-cell fusion by locking the spike in a pre-fusion state, whereas some weakly neutralizing antibodies behave as allosteric effectors that promote S2 unsheathing and increase syncytia formation [257]. The opposing activities of neutralizing antibodies will need to be elucidated further in order to be understood in terms of pathology.

5.3.3 Virological consequences

Finally, syncytia formation can have direct virological consequences rather than just trigger a generalized cytopathic effect or immune response. Syncytia may allow viruses to spread directly from cell-to-cell without having to enter the extracellular environment (**Figure 5.2**). This strategy shields the virus from neutralizing antibodies, physical barriers like the mucociliary blanket, as well as components of the immune system [258]. Many respiratory viruses such as measles, influenza, respiratory syncytia virus, parainfluenza virus, and human metapneumonia virus exploit this mechanism of dissemination [258]. As previously discussed (**Chapter 1**), nonenveloped reoviruses employ evolutionarily conserved fusogens, dedicated to the induction of cell-cell fusion, as a mechanism of cell-to-cell transmission [165, 166]. Recent cell culture studies suggest that SARS-CoV-2 cell-to-cell dissemination is a possible route of spread. Cell-free virus was effectively neutralized by monoclonal antibodies and convalescent plasma; however, cell-to-cell viral spread was either not or less sensitive to neutralization (**Figure 5.2**) [254, 259]. The direct spread of HIV from cell-to-cell has also been demonstrated to be less sensitive to the restrictive effects of antiretrovirals and neutralizing antibodies [260-262]. A more thorough understanding of the significance of SARS-CoV-2 cell-to-cell spread to the pathology and antibody response is warranted. Beyond direct cell-to-cell spread, syncytia may potentially contribute to the overall infectious dose and viral dissemination upon being dislodged [263]. In reconstituted primary bronchial epithelia, multi-ciliated cells and basal cells form syncytia which are then released into the apical lumen (**Figure 5.2**) [263]. Vesicular inclusions containing virus particles were detected within the released syncytia, potentially suggesting continued viral replication [263]. Infected single and syncytial cells that are released may spread infection. Like several of the aforementioned processes, syncytial release is not unique to SARS-CoV-2 [263]. Infection of

epithelial cell cultures from macaque respiratory tissue with measles virus also results in the formation and shedding of infectious syncytia [264].

5.4 Applications of S-mediated Syncytia formation

From a methodological standpoint, syncytia formation in cell culture can also be utilized as an effective, albeit imperfect, surrogate to characterize the early stages of virion entry via S protein fusogenicity. It has the added benefit for being suitable for biosafety level 2 research environments, when the S protein is expressed alone, in the absence of infectious virus. We also developed a rapid, sensitive and semi-automated assay we termed “S-Fuse”, which employed virus-induced syncytia formation as a marker to detect and measure infectious virus in various human samples [181, 265]. The S-Fuse assay is now routinely used in our laboratory to assess the activity of anti-SARS-CoV-2 monoclonal antibodies or other antiviral molecules, and to measure the neutralizing antibody response in sera from vaccinated and convalescent individuals [51, 56]. Quantitative syncytia formation has also been employed in high-throughput drug screens in order to identify inhibitors of S mediated fusion [85, 266]. There are several reporter systems that can be used to quantify syncytia formation and they are compared by Sanders et al [266].

Conclusion

Several histopathological reports have identified the presence of infected multinucleated syncytial cells in COVID-19 patient lung tissues. The mechanism of how cells fuse and the contribution of syncytia formation to SARS-CoV-2 pathology was not fully understood. Here, we found that cells infected with SARS-CoV-2 virus express the S protein on the surface which then interacts with ACE2 receptors on neighboring cells to induce cell-cell fusion. IFITMs a family of ISGs that are thought alter the local biophysical properties of cellular membranes effectively restrict syncytia formation. The TMPRSS2 protease not only augments S-mediated syncytia formation but also reverts restriction by IFITMs. SARS-CoV-2 evolved during the course of the pandemic, with many mutations arising within the highly antigenic S protein. We examined the syncytiogenicity of the novel variants of concerns and functionally characterized the fusogenicity of their respective S proteins. We showed that the S protein of the Alpha, Beta and Delta variants are more fusogenic and also have a higher ACE2 binding affinity than both the early D614G variant and the ancestral Wuhan strain. The individual mutations harbored by the novel variants have a significant impact on S function and syncytia formation, both individually and cumulatively. The impact of syncytia on the pathology of emerging variants remains an outstanding question. We then used our syncytia formation system to provide a preliminary description of the HKU1 S protein.

We suggest that a fully function TMPRSS2 protease is necessary for HKU1 S-mediated fusion and that human and mouse IFITM1 differentially modulate fusion. Overall, this work provides a function characterization of the SARS-CoV-2 S protein and syncytia formation. The tools developed could also be applied to study other coronaviruses, like HKU1. Syncytial cells may facilitate infection by disseminating the virus through cell-to-cell contact or upon cell death. They

can also target immune cells for cell-in-cell mediated death and also protect the virus against neutralizing antibodies. Rapid syncytial collapse may be detrimental to viral replication and could trigger an inflammatory immune response. Understanding S-mediated syncytia formation may provide insights into SARS-CoV-2 induced pathology

References

1. Michael Rajah M, Bernier A, Buchrieser J, Schwartz O. The mechanism and consequences of SARS-CoV-2 spike-mediated fusion and syncytia formation. Journal of Molecular Biology. 2021:167280. doi: https://doi.org/10.1016/j.jmb.2021.167280.
2. Cui J, Li F, Shi ZL. Origin and evolution of pathogenic coronaviruses. Nat Rev Microbiol. 2019;17(3):181-92. Epub 2018/12/12. doi: 10.1038/s41579-018-0118-9. PubMed PMID: 30531947; PubMed Central PMCID: PMCPMC7097006.
3. Woo PC, Lau SK, Lam CS, Lau CC, Tsang AK, Lau JH, et al. Discovery of seven novel Mammalian and avian coronaviruses in the genus deltacoronavirus supports bat coronaviruses as the gene source of alphacoronavirus and betacoronavirus and avian coronaviruses as the gene source of gammacoronavirus and deltacoronavirus. J Virol. 2012;86(7):3995-4008. Epub 2012/01/27. doi: 10.1128/JVI.06540-11. PubMed PMID: 22278237; PubMed Central PMCID: PMCPMC3302495.
4. Wertheim JO, Chu DK, Peiris JS, Kosakovsky Pond SL, Poon LL. A case for the ancient origin of coronaviruses. J Virol. 2013;87(12):7039-45. Epub 2013/04/19. doi: 10.1128/JVI.03273-12. PubMed PMID: 23596293; PubMed Central PMCID: PMCPMC3676139.
5. McIntosh K, editor Coronaviruses: A Comparative Review1974; Berlin, Heidelberg: Springer Berlin Heidelberg.
6. Kahn JS, McIntosh K. History and recent advances in coronavirus discovery. Pediatr Infect Dis J. 2005;24(11 Suppl):S223-7, discussion S6. Epub 2005/12/27. doi: 10.1097/01.inf.0000188166.17324.60. PubMed PMID: 16378050.
7. Hamre D, Procknow JJ. A new virus isolated from the human respiratory tract. Proc Soc Exp Biol Med. 1966;121(1):190-3. Epub 1966/01/01. doi: 10.3181/00379727-121-30734. PubMed PMID: 4285768.
8. McIntosh K, Dees JH, Becker WB, Kapikian AZ, Chanock RM. Recovery in tracheal organ cultures of novel viruses from patients with respiratory disease. Proc Natl Acad Sci U S A. 1967;57(4):933-40. Epub 1967/04/01. doi: 10.1073/pnas.57.4.933. PubMed PMID: 5231356; PubMed Central PMCID: PMCPMC224637.
9. Tyrrell DA, Bynoe ML. Cultivation of viruses from a high proportion of patients with colds. Lancet. 1966;1(7428):76-7. Epub 1966/01/08. doi: 10.1016/s0140-6736(66)92364-6. PubMed PMID: 4158999.
10. van der Hoek L, Pyrc K, Jebbink MF, Vermeulen-Oost W, Berkhout RJ, Wolthers KC, et al. Identification of a new human coronavirus. Nat Med. 2004;10(4):368-73. Epub 2004/03/23. doi: 10.1038/nm1024. PubMed PMID: 15034574; PubMed Central PMCID: PMCPMC7095789.
11. Woo PC, Lau SK, Chu CM, Chan KH, Tsoi HW, Huang Y, et al. Characterization and complete genome sequence of a novel coronavirus, coronavirus HKU1, from patients with pneumonia. J Virol. 2005;79(2):884-95. Epub 2004/12/23. doi: 10.1128/jvi.79.2.884-895.2005. PubMed PMID: 15613317; PubMed Central PMCID: PMCPMC538593.
12. Monto AS. Medical reviews. Coronaviruses. Yale J Biol Med. 1974;47(4):234-51. Epub 1974/12/01. PubMed PMID: 4617423; PubMed Central PMCID: PMCPMC2595130.
13. Huynh J, Li S, Yount B, Smith A, Sturges L, Olsen JC, et al. Evidence supporting a zoonotic origin of human coronavirus strain NL63. J Virol. 2012;86(23):12816-25. Epub

2012/09/21. doi: 10.1128/JVI.00906-12. PubMed PMID: 22993147; PubMed Central PMCID: PMCPMC3497669.
14. Tao Y, Shi M, Chommanard C, Queen K, Zhang J, Markotter W, et al. Surveillance of Bat Coronaviruses in Kenya Identifies Relatives of Human Coronaviruses NL63 and 229E and Their Recombination History. J Virol. 2017;91(5). Epub 2017/01/13. doi: 10.1128/JVI.01953-16. PubMed PMID: 28077633; PubMed Central PMCID: PMCPMC5309958.
15. Pfefferle S, Oppong S, Drexler JF, Gloza-Rausch F, Ipsen A, Seebens A, et al. Distant relatives of severe acute respiratory syndrome coronavirus and close relatives of human coronavirus 229E in bats, Ghana. Emerg Infect Dis. 2009;15(9):1377-84. Epub 2009/10/01. doi: 10.3201/eid1509.090224. PubMed PMID: 19788804; PubMed Central PMCID: PMCPMC2819850.
16. Corman VM, Eckerle I, Memish ZA, Liljander AM, Dijkman R, Jonsdottir H, et al. Link of a ubiquitous human coronavirus to dromedary camels. Proc Natl Acad Sci U S A. 2016;113(35):9864-9. Epub 2016/08/17. doi: 10.1073/pnas.1604472113. PubMed PMID: 27528677; PubMed Central PMCID: PMCPMC5024591.
17. Lau SK, Woo PC, Li KS, Tsang AK, Fan RY, Luk HK, et al. Discovery of a novel coronavirus, China Rattus coronavirus HKU24, from Norway rats supports the murine origin of Betacoronavirus 1 and has implications for the ancestor of Betacoronavirus lineage A. J Virol. 2015;89(6):3076-92. Epub 2015/01/02. doi: 10.1128/JVI.02420-14. PubMed PMID: 25552712; PubMed Central PMCID: PMCPMC4337523.
18. Vijgen L, Keyaerts E, Moes E, Thoelen I, Wollants E, Lemey P, et al. Complete genomic sequence of human coronavirus OC43: molecular clock analysis suggests a relatively recent zoonotic coronavirus transmission event. J Virol. 2005;79(3):1595-604. Epub 2005/01/15. doi: 10.1128/JVI.79.3.1595-1604.2005. PubMed PMID: 15650185; PubMed Central PMCID: PMCPMC544107.
19. Al-Khannaq MN, Ng KT, Oong XY, Pang YK, Takebe Y, Chook JB, et al. Molecular epidemiology and evolutionary histories of human coronavirus OC43 and HKU1 among patients with upper respiratory tract infections in Kuala Lumpur, Malaysia. Virol J. 2016;13:33. Epub 2016/02/27. doi: 10.1186/s12985-016-0488-4. PubMed PMID: 26916286; PubMed Central PMCID: PMCPMC4766700.
20. Dijkman R, Jebbink MF, Gaunt E, Rossen JW, Templeton KE, Kuijpers TW, et al. The dominance of human coronavirus OC43 and NL63 infections in infants. J Clin Virol. 2012;53(2):135-9. Epub 2011/12/23. doi: 10.1016/j.jcv.2011.11.011. PubMed PMID: 22188723; PubMed Central PMCID: PMCPMC7108278.
21. Cherry JD, Krogstad P. SARS: the first pandemic of the 21st century. Pediatr Res. 2004;56(1):1-5. Epub 2004/05/21. doi: 10.1203/01.PDR.0000129184.87042.FC. PubMed PMID: 15152053; PubMed Central PMCID: PMCPMC7086556.
22. Drosten C, Gunther S, Preiser W, van der Werf S, Brodt HR, Becker S, et al. Identification of a novel coronavirus in patients with severe acute respiratory syndrome. N Engl J Med. 2003;348(20):1967-76. Epub 2003/04/12. doi: 10.1056/NEJMoa030747. PubMed PMID: 12690091.
23. Zhong NS, Zheng BJ, Li YM, Poon, Xie ZH, Chan KH, et al. Epidemiology and cause of severe acute respiratory syndrome (SARS) in Guangdong, People's Republic of China, in February, 2003. Lancet. 2003;362(9393):1353-8. Epub 2003/10/31. doi: 10.1016/s0140-6736(03)14630-2. PubMed PMID: 14585636; PubMed Central PMCID: PMCPMC7112415.

24. Guan Y, Zheng BJ, He YQ, Liu XL, Zhuang ZX, Cheung CL, et al. Isolation and characterization of viruses related to the SARS coronavirus from animals in southern China. Science. 2003;302(5643):276-8. Epub 2003/09/06. doi: 10.1126/science.1087139. PubMed PMID: 12958366.
25. Stadler K, Masignani V, Eickmann M, Becker S, Abrignani S, Klenk HD, et al. SARS--beginning to understand a new virus. Nat Rev Microbiol. 2003;1(3):209-18. Epub 2004/03/24. doi: 10.1038/nrmicro775. PubMed PMID: 15035025; PubMed Central PMCID: PMCPMC7097337.
26. Centers for Disease C, Prevention. Prevalence of IgG antibody to SARS-associated coronavirus in animal traders--Guangdong Province, China, 2003. MMWR Morb Mortal Wkly Rep. 2003;52(41):986-7. Epub 2003/10/17. PubMed PMID: 14561956.
27. Li W, Shi Z, Yu M, Ren W, Smith C, Epstein JH, et al. Bats are natural reservoirs of SARS-like coronaviruses. Science. 2005;310(5748):676-9. Epub 2005/10/01. doi: 10.1126/science.1118391. PubMed PMID: 16195424.
28. Peiris JS, Lai ST, Poon LL, Guan Y, Yam LY, Lim W, et al. Coronavirus as a possible cause of severe acute respiratory syndrome. Lancet. 2003;361(9366):1319-25. Epub 2003/04/25. doi: 10.1016/s0140-6736(03)13077-2. PubMed PMID: 12711465; PubMed Central PMCID: PMCPMC7112372.
29. Donnelly CA, Ghani AC, Leung GM, Hedley AJ, Fraser C, Riley S, et al. Epidemiological determinants of spread of causal agent of severe acute respiratory syndrome in Hong Kong. Lancet. 2003;361(9371):1761-6. Epub 2003/06/05. doi: 10.1016/S0140-6736(03)13410-1. PubMed PMID: 12781533; PubMed Central PMCID: PMCPMC7112380.
30. Hon KL, Leung CW, Cheng WT, Chan PK, Chu WC, Kwan YW, et al. Clinical presentations and outcome of severe acute respiratory syndrome in children. Lancet. 2003;361(9370):1701-3. Epub 2003/05/28. doi: 10.1016/s0140-6736(03)13364-8. PubMed PMID: 12767737; PubMed Central PMCID: PMCPMC7112484.
31. Zaki AM, van Boheemen S, Bestebroer TM, Osterhaus AD, Fouchier RA. Isolation of a novel coronavirus from a man with pneumonia in Saudi Arabia. N Engl J Med. 2012;367(19):1814-20. Epub 2012/10/19. doi: 10.1056/NEJMoa1211721. PubMed PMID: 23075143.
32. Bleibtreu A, Bertine M, Bertin C, Houhou-Fidouh N, Visseaux B. Focus on Middle East respiratory syndrome coronavirus (MERS-CoV). Med Mal Infect. 2020;50(3):243-51. Epub 2019/11/16. doi: 10.1016/j.medmal.2019.10.004. PubMed PMID: 31727466; PubMed Central PMCID: PMCPMC7125975.
33. Lau SK, Li KS, Tsang AK, Lam CS, Ahmed S, Chen H, et al. Genetic characterization of Betacoronavirus lineage C viruses in bats reveals marked sequence divergence in the spike protein of pipistrellus bat coronavirus HKU5 in Japanese pipistrelle: implications for the origin of the novel Middle East respiratory syndrome coronavirus. J Virol. 2013;87(15):8638-50. Epub 2013/05/31. doi: 10.1128/JVI.01055-13. PubMed PMID: 23720729; PubMed Central PMCID: PMCPMC3719811.
34. Memish ZA, Mishra N, Olival KJ, Fagbo SF, Kapoor V, Epstein JH, et al. Middle East respiratory syndrome coronavirus in bats, Saudi Arabia. Emerg Infect Dis. 2013;19(11):1819-23. Epub 2013/11/12. doi: 10.3201/eid1911.131172. PubMed PMID: 24206838; PubMed Central PMCID: PMCPMC3837665.
35. Ithete NL, Stoffberg S, Corman VM, Cottontail VM, Richards LR, Schoeman MC, et al. Close relative of human Middle East respiratory syndrome coronavirus in bat, South Africa.

Emerg Infect Dis. 2013;19(10):1697-9. Epub 2013/09/21. doi: 10.3201/eid1910.130946. PubMed PMID: 24050621; PubMed Central PMCID: PMCPMC3810765.
36. Alagaili AN, Briese T, Mishra N, Kapoor V, Sameroff SC, Burbelo PD, et al. Middle East respiratory syndrome coronavirus infection in dromedary camels in Saudi Arabia. mBio. 2014;5(2):e00884-14. Epub 2014/02/27. doi: 10.1128/mBio.00884-14. PubMed PMID: 24570370; PubMed Central PMCID: PMCPMC3940034.
37. Hemida MG, Perera RA, Wang P, Alhammadi MA, Siu LY, Li M, et al. Middle East Respiratory Syndrome (MERS) coronavirus seroprevalence in domestic livestock in Saudi Arabia, 2010 to 2013. Euro Surveill. 2013;18(50):20659. Epub 2013/12/18. doi: 10.2807/1560-7917.es2013.18.50.20659. PubMed PMID: 24342517.
38. de Wit E, van Doremalen N, Falzarano D, Munster VJ. SARS and MERS: recent insights into emerging coronaviruses. Nat Rev Microbiol. 2016;14(8):523-34. Epub 2016/06/28. doi: 10.1038/nrmicro.2016.81. PubMed PMID: 27344959; PubMed Central PMCID: PMCPMC7097822.
39. Zhu N, Zhang D, Wang W, Li X, Yang B, Song J, et al. A Novel Coronavirus from Patients with Pneumonia in China, 2019. N Engl J Med. 2020;382(8):727-33. Epub 2020/01/25. doi: 10.1056/NEJMoa2001017. PubMed PMID: 31978945; PubMed Central PMCID: PMCPMC7092803.
40. Organization WH. COVID-19 Weekly Epidemiological Update. WHO.int: WHO, 2021.
41. Holmes EC, Goldstein SA, Rasmussen AL, Robertson DL, Crits-Christoph A, Wertheim JO, et al. The origins of SARS-CoV-2: A critical review. Cell. 2021. Epub 2021/09/05. doi: 10.1016/j.cell.2021.08.017. PubMed PMID: 34480864; PubMed Central PMCID: PMCPMC8373617.
42. Wacharapluesadee S, Tan CW, Maneeorn P, Duengkae P, Zhu F, Joyjinda Y, et al. Evidence for SARS-CoV-2 related coronaviruses circulating in bats and pangolins in Southeast Asia. Nat Commun. 2021;12(1):972. Epub 2021/02/11. doi: 10.1038/s41467-021-21240-1. PubMed PMID: 33563978; PubMed Central PMCID: PMCPMC7873279.
43. Lam TT, Jia N, Zhang YW, Shum MH, Jiang JF, Zhu HC, et al. Identifying SARS-CoV-2-related coronaviruses in Malayan pangolins. Nature. 2020;583(7815):282-5. Epub 2020/03/29. doi: 10.1038/s41586-020-2169-0. PubMed PMID: 32218527.
44. Andersen KG, Rambaut A, Lipkin WI, Holmes EC, Garry RF. The proximal origin of SARS-CoV-2. Nat Med. 2020;26(4):450-2. Epub 2020/04/15. doi: 10.1038/s41591-020-0820-9. PubMed PMID: 32284615; PubMed Central PMCID: PMCPMC7095063.
45. Boni MF, Lemey P, Jiang X, Lam TT, Perry BW, Castoe TA, et al. Evolutionary origins of the SARS-CoV-2 sarbecovirus lineage responsible for the COVID-19 pandemic. Nat Microbiol. 2020;5(11):1408-17. Epub 2020/07/30. doi: 10.1038/s41564-020-0771-4. PubMed PMID: 32724171.
46. Zhou P, Yang XL, Wang XG, Hu B, Zhang L, Zhang W, et al. A pneumonia outbreak associated with a new coronavirus of probable bat origin. Nature. 2020;579(7798):270-3. Epub 2020/02/06. doi: 10.1038/s41586-020-2012-7. PubMed PMID: 32015507; PubMed Central PMCID: PMCPMC7095418.
47. Zhou H, Ji J, Chen X, Bi Y, Li J, Wang Q, et al. Identification of novel bat coronaviruses sheds light on the evolutionary origins of SARS-CoV-2 and related viruses. Cell. 2021;184(17):4380-91 e14. Epub 2021/06/21. doi: 10.1016/j.cell.2021.06.008. PubMed PMID: 34147139; PubMed Central PMCID: PMCPMC8188299.

48. Temmam S, Vongphayloth K, Salazar EB, Munier S, Bonomi, Max, Régnault B, Douangboubpha B, et al. Coronaviruses with a SARS-CoV-2-like receptor-binding domain allowing ACE2-mediated entry into human cells isolated from bats of Indochinese peninsula. Nature Portfolio Journal Research Square. 2021. doi: 10.21203/rs.3.rs-871965/v1.
49. Yurkovetskiy L, Wang X, Pascal KE, Tomkins-Tinch C, Nyalile TP, Wang Y, et al. Structural and Functional Analysis of the D614G SARS-CoV-2 Spike Protein Variant. Cell. 2020;183(3):739-51 e8. Epub 2020/09/30. doi: 10.1016/j.cell.2020.09.032. PubMed PMID: 32991842; PubMed Central PMCID: PMCPMC7492024.
50. Buss LF, Prete CA, Jr., Abrahim CMM, Mendrone A, Jr., Salomon T, de Almeida-Neto C, et al. Three-quarters attack rate of SARS-CoV-2 in the Brazilian Amazon during a largely unmitigated epidemic. Science. 2021;371(6526):288-92. Epub 2020/12/10. doi: 10.1126/science.abe9728. PubMed PMID: 33293339; PubMed Central PMCID: PMCPMC7857406.
51. Planas D, Veyer D, Baidaliuk A, Staropoli I, Guivel-Benhassine F, Rajah MM, et al. Reduced sensitivity of SARS-CoV-2 variant Delta to antibody neutralization. Nature. 2021. Epub 2021/07/09. doi: 10.1038/s41586-021-03777-9. PubMed PMID: 34237773.
52. Yadav PD, Sapkal GN, Abraham P, Ella R, Deshpande G, Patil DY, et al. Neutralization of variant under investigation B.1.617 with sera of BBV152 vaccinees. bioRxiv. 2021:2021.04.23.441101. doi: 10.1101/2021.04.23.441101.
53. Tegally H, Wilkinson E, Giovanetti M, Iranzadeh A, Fonseca V, Giandhari J, et al. Emergence and rapid spread of a new severe acute respiratory syndrome-related coronavirus 2 (SARS-CoV-2) lineage with multiple spike mutations in South Africa. medRxiv. 2020:2020.12.21.20248640. doi: 10.1101/2020.12.21.20248640.
54. Sabino EC, Buss LF, Carvalho MPS, Prete CA, Jr., Crispim MAE, Fraiji NA, et al. Resurgence of COVID-19 in Manaus, Brazil, despite high seroprevalence. Lancet. 2021;397(10273):452-5. Epub 2021/01/31. doi: 10.1016/S0140-6736(21)00183-5. PubMed PMID: 33515491; PubMed Central PMCID: PMCPMC7906746.
55. Frampton D, Rampling T, Cross A, Bailey H, Heaney J, Byott M, et al. Genomic characteristics and clinical effect of the emergent SARS-CoV-2 B.1.1.7 lineage in London, UK: a whole-genome sequencing and hospital-based cohort study. Lancet Infect Dis. 2021;21(9):1246-56. Epub 2021/04/16. doi: 10.1016/S1473-3099(21)00170-5. PubMed PMID: 33857406; PubMed Central PMCID: PMCPMC8041359 manufacture of UCL-Ventura continuous positive airway pressure device for patients with COVID-19 from the UK Department of Health and Social Care, during the conduct of the study; grants and advisory board fees paid to institution research fund from NewB; grants from DSTL; advisory board and speaking fees paid into institutional research fund from Amormed, Biotest, General ElectricBaxter, Baxter, Roche, Bayer, and Shionogi; and grants from Critical Pressure and Apollo Therapeutics, outside the submitted work. All other authors declare no competing interests.
56. Planas D, Bruel T, Grzelak L, Guivel-Benhassine F, Staropoli I, Porrot F, et al. Sensitivity of infectious SARS-CoV-2 B.1.1.7 and B.1.351 variants to neutralizing antibodies. Nat Med. 2021;27(5):917-24. Epub 2021/03/28. doi: 10.1038/s41591-021-01318-5. PubMed PMID: 33772244.
57. Galloway SE, Paul P, MacCannell DR, Johansson MA, Brooks JT, MacNeil A, et al. Emergence of SARS-CoV-2 B.1.1.7 Lineage - United States, December 29, 2020-January 12, 2021. MMWR Morb Mortal Wkly Rep. 2021;70(3):95-9. Epub 2021/01/22. doi:

10.15585/mmwr.mm7003e2. PubMed PMID: 33476315; PubMed Central PMCID: PMCPMC7821772 Journal Editors form for disclosure of potential conflicts of interest. No potential conflicts of interest were disclosed.
58. Li B, Deng A, Li K, Hu Y, Li Z, Xiong Q, et al. Viral infection and transmission in a large, well-traced outbreak caused by the SARS-CoV-2 Delta variant. medRxiv. 2021:2021.07.07.21260122. doi: 10.1101/2021.07.07.21260122.
59. Davies NG, Abbott S, Barnard RC, Jarvis CI, Kucharski AJ, Munday JD, et al. Estimated transmissibility and impact of SARS-CoV-2 lineage B.1.1.7 in England. Science. 2021;372(6538). Epub 2021/03/05. doi: 10.1126/science.abg3055. PubMed PMID: 33658326; PubMed Central PMCID: PMCPMC8128288.
60. Korber B, Fischer WM, Gnanakaran S, Yoon H, Theiler J, Abfalterer W, et al. Tracking Changes in SARS-CoV-2 Spike: Evidence that D614G Increases Infectivity of the COVID-19 Virus. Cell. 2020;182(4):812-27 e19. Epub 2020/07/23. doi: 10.1016/j.cell.2020.06.043. PubMed PMID: 32697968; PubMed Central PMCID: PMCPMC7332439.
61. Meng B, Kemp SA, Papa G, Datir R, Ferreira I, Marelli S, et al. Recurrent emergence of SARS-CoV-2 spike deletion H69/V70 and its role in the Alpha variant B.1.1.7. Cell Rep. 2021;35(13):109292. Epub 2021/06/25. doi: 10.1016/j.celrep.2021.109292. PubMed PMID: 34166617; PubMed Central PMCID: PMCPMC8185188.
62. Supasa P, Zhou D, Dejnirattisai W, Liu C, Mentzer AJ, Ginn HM, et al. Reduced neutralization of SARS-CoV-2 B.1.1.7 variant by convalescent and vaccine sera. Cell. 2021;184(8):2201-11 e7. Epub 2021/03/22. doi: 10.1016/j.cell.2021.02.033. PubMed PMID: 33743891; PubMed Central PMCID: PMCPMC7891044.
63. Wang L, Didelot X, Bi Y, Gao GF. Comparative evaluation of the transmissibility of SARS-CoV-2 variants of concern. medRxiv. 2021:2021.06.25.21259565. doi: 10.1101/2021.06.25.21259565.
64. Abu-Raddad LJ, Chemaitelly H, Ayoub HH, Yassine HM, Benslimane FM, Al Khatib HA, et al. Severity, criticality, and fatality of the SARS-CoV-2 Beta variant. medRxiv. 2021:2021.08.02.21261465. doi: 10.1101/2021.08.02.21261465.
65. Faria NR, Mellan TA, Whittaker C, Claro IM, Candido DDS, Mishra S, et al. Genomics and epidemiology of the P.1 SARS-CoV-2 lineage in Manaus, Brazil. Science. 2021;372(6544):815-21. Epub 2021/04/16. doi: 10.1126/science.abh2644. PubMed PMID: 33853970; PubMed Central PMCID: PMCPMC8139423.
66. Fernandez J, Bruneau N, Fasce R, Martin HS, Balanda M, Bustos P, et al. Neutralization of alpha, gamma, and D614G SARS-CoV-2 variants by CoronaVac vaccine-induced antibodies. J Med Virol. 2021. Epub 2021/08/31. doi: 10.1002/jmv.27310. PubMed PMID: 34460119.
67. Bolze A, Cirulli ET, Luo S, White S, Wyman D, Rossi AD, et al. SARS-CoV-2 variant Delta rapidly displaced variant Alpha in the United States and led to higher viral loads. medRxiv. 2021:2021.06.20.21259195. doi: 10.1101/2021.06.20.21259195.
68. Campbell F, Archer B, Laurenson-Schafer H, Jinnai Y, Konings F, Batra N, et al. Increased transmissibility and global spread of SARS-CoV-2 variants of concern as at June 2021. Euro Surveill. 2021;26(24). Epub 2021/06/19. doi: 10.2807/1560-7917.ES.2021.26.24.2100509. PubMed PMID: 34142653; PubMed Central PMCID: PMCPMC8212592.
69. Scientific Pandemic Influenza Group on Modelling Os-gS-M-O. SPI-M-O: Consensus statement on COVID-19, 30 June 2021. GOV.UK: 2021.
70. Twohig KA, Nyberg T, Zaidi A, Thelwall S, Sinnathamby MA, Aliabadi S, et al. Hospital admission and emergency care attendance risk for SARS-CoV-2 delta (B.1.617.2)

compared with alpha (B.1.1.7) variants of concern: a cohort study. Lancet Infect Dis. 2021. Epub 2021/08/31. doi: 10.1016/S1473-3099(21)00475-8. PubMed PMID: 34461056; PubMed Central PMCID: PMCPMC8397301 funding from GlaxoSmithKline for a research project related to seasonal influenza and antiviral treatment; this project preceded and had no relation to COVID-19, and GD had no role in and received no funding from the project. All other authors declare no competing interests.
71. Bager P, Wohlfahrt J, Rasmussen M, Albertsen M, Krause TG. Hospitalisation associated with SARS-CoV-2 delta variant in Denmark. Lancet Infect Dis. 2021. Epub 2021/09/07. doi: 10.1016/S1473-3099(21)00580-6. PubMed PMID: 34487704; PubMed Central PMCID: PMCPMC8415919 are located in the Danish national COVID-19 surveillance system database at Statens Serum Institut, and the data are becoming or are already available for research upon request and with permission from the Danish Data Protection Agency and Danish Health Authority (https://sundhedsdatastyrelsen.dk/da/forskerservice).
72. Organization WH. Transmission of SARS-CoV-2: implications for infection prevention precautions. 2020.
73. Cevik M, Kuppalli K, Kindrachuk J, Peiris M. Virology, transmission, and pathogenesis of SARS-CoV-2. BMJ. 2020;371:m3862. Epub 2020/10/25. doi: 10.1136/bmj.m3862. PubMed PMID: 33097561.
74. Cevik M, Tate M, Lloyd O, Maraolo AE, Schafers J, Ho A. SARS-CoV-2, SARS-CoV, and MERS-CoV viral load dynamics, duration of viral shedding, and infectiousness: a systematic review and meta-analysis. Lancet Microbe. 2021;2(1):e13-e22. Epub 2021/02/02. doi: 10.1016/S2666-5247(20)30172-5. PubMed PMID: 33521734; PubMed Central PMCID: PMCPMC7837230.
75. Mok BW-Y, Liu H, Deng S, Liu J, Zhang AJ, Lau S-Y, et al. Low dose inocula of SARS-CoV-2 Alpha variant transmits more efficiently than earlier variants in hamsters. Communications Biology. 2021;4(1):1102. doi: 10.1038/s42003-021-02640-x.
76. Oberfeld B, Achanta A, Carpenter K, Chen P, Gilette NM, Langat P, et al. SnapShot: COVID-19. Cell. 2020;181(4):954-.e1. doi: https://doi.org/10.1016/j.cell.2020.04.013.
77. Wu Z, McGoogan JM. Characteristics of and Important Lessons From the Coronavirus Disease 2019 (COVID-19) Outbreak in China: Summary of a Report of 72314 Cases From the Chinese Center for Disease Control and Prevention. JAMA. 2020;323(13):1239-42. Epub 2020/02/25. doi: 10.1001/jama.2020.2648. PubMed PMID: 32091533.
78. Chua RL, Lukassen S, Trump S, Hennig BP, Wendisch D, Pott F, et al. COVID-19 severity correlates with airway epithelium-immune cell interactions identified by single-cell analysis. Nat Biotechnol. 2020;38(8):970-9. Epub 2020/06/28. doi: 10.1038/s41587-020-0602-4. PubMed PMID: 32591762.
79. Seyed Hosseini E, Riahi Kashani N, Nikzad H, Azadbakht J, Hassani Bafrani H, Haddad Kashani H. The novel coronavirus Disease-2019 (COVID-19): Mechanism of action, detection and recent therapeutic strategies. Virology. 2020;551:1-9. Epub 2020/10/04. doi: 10.1016/j.virol.2020.08.011. PubMed PMID: 33010669; PubMed Central PMCID: PMCPMC7513802.
80. Bussani R, Schneider E, Zentilin L, Collesi C, Ali H, Braga L, et al. Persistence of viral RNA, pneumocyte syncytia and thrombosis are hallmarks of advanced COVID-19 pathology. EBioMedicine. 2020;61:103104. Epub 2020/11/08. doi: 10.1016/j.ebiom.2020.103104. PubMed PMID: 33158808; PubMed Central PMCID: PMCPMC7677597.

81. Menter T, Haslbauer JD, Nienhold R, Savic S, Hopfer H, Deigendesch N, et al. Postmortem examination of COVID-19 patients reveals diffuse alveolar damage with severe capillary congestion and variegated findings in lungs and other organs suggesting vascular dysfunction. Histopathology. 2020;77(2):198-209. Epub 2020/05/05. doi: 10.1111/his.14134. PubMed PMID: 32364264; PubMed Central PMCID: PMCPMC7496150.
82. Carsana L, Sonzogni A, Nasr A, Rossi RS, Pellegrinelli A, Zerbi P, et al. Pulmonary post-mortem findings in a series of COVID-19 cases from northern Italy: a two-centre descriptive study. Lancet Infect Dis. 2020;20(10):1135-40. Epub 2020/06/12. doi: 10.1016/S1473-3099(20)30434-5. PubMed PMID: 32526193; PubMed Central PMCID: PMCPMC7279758.
83. Franks TJ, Chong PY, Chui P, Galvin JR, Lourens RM, Reid AH, et al. Lung pathology of severe acute respiratory syndrome (SARS): a study of 8 autopsy cases from Singapore. Hum Pathol. 2003;34(8):743-8. Epub 2003/09/25. doi: 10.1016/s0046-8177(03)00367-8. PubMed PMID: 14506633; PubMed Central PMCID: PMCPMC7119137.
84. Alsaad KO, Hajeer AH, Al Balwi M, Al Moaiqel M, Al Oudah N, Al Ajlan A, et al. Histopathology of Middle East respiratory syndrome coronovirus (MERS-CoV) infection - clinicopathological and ultrastructural study. Histopathology. 2018;72(3):516-24. Epub 2017/09/01. doi: 10.1111/his.13379. PubMed PMID: 28858401; PubMed Central PMCID: PMCPMC7165512.
85. Braga L, Ali H, Secco I, Chiavacci E, Neves G, Goldhill D, et al. Drugs that inhibit TMEM16 proteins block SARS-CoV-2 spike-induced syncytia. Nature. 2021;594(7861):88-93. Epub 2021/04/08. doi: 10.1038/s41586-021-03491-6. PubMed PMID: 33827113; PubMed Central PMCID: PMCPMC7611055.
86. Guzik TJ, Mohiddin SA, Dimarco A, Patel V, Savvatis K, Marelli-Berg FM, et al. COVID-19 and the cardiovascular system: implications for risk assessment, diagnosis, and treatment options. Cardiovasc Res. 2020;116(10):1666-87. Epub 2020/05/01. doi: 10.1093/cvr/cvaa106. PubMed PMID: 32352535; PubMed Central PMCID: PMCPMC7197627.
87. Medicine JHU. MORTALITY ANALYSES: Johns Hopkins Univeristy; 2021 [updated September 20, 2021; cited 2021 September 20]. Available from: https://coronavirus.jhu.edu/data/mortality.
88. Feng W, Zong W, Wang F, Ju S. Severe acute respiratory syndrome coronavirus 2 (SARS-CoV-2): a review. Mol Cancer. 2020;19(1):100. Epub 2020/06/04. doi: 10.1186/s12943-020-01218-1. PubMed PMID: 32487159; PubMed Central PMCID: PMCPMC7264920.
89. Dai L, Gao GF. Viral targets for vaccines against COVID-19. Nat Rev Immunol. 2021;21(2):73-82. Epub 2020/12/20. doi: 10.1038/s41577-020-00480-0. PubMed PMID: 33340022; PubMed Central PMCID: PMCPMC7747004.
90. Berger I, Schaffitzel C. The SARS-CoV-2 spike protein: balancing stability and infectivity. Cell Res. 2020;30(12):1059-60. Epub 2020/11/04. doi: 10.1038/s41422-020-00430-4. PubMed PMID: 33139926; PubMed Central PMCID: PMCPMC7604330.
91. Tregoning JS, Flight KE, Higham SL, Wang Z, Pierce BF. Progress of the COVID-19 vaccine effort: viruses, vaccines and variants versus efficacy, effectiveness and escape. Nat Rev Immunol. 2021. Epub 2021/08/11. doi: 10.1038/s41577-021-00592-1. PubMed PMID: 34373623; PubMed Central PMCID: PMCPMC8351583.
92. Kim D, Lee JY, Yang JS, Kim JW, Kim VN, Chang H. The Architecture of SARS-CoV-2 Transcriptome. Cell. 2020;181(4):914-21 e10. Epub 2020/04/25. doi:

10.1016/j.cell.2020.04.011. PubMed PMID: 32330414; PubMed Central PMCID: PMCPMC7179501.
93. V'Kovski P, Kratzel A, Steiner S, Stalder H, Thiel V. Coronavirus biology and replication: implications for SARS-CoV-2. Nat Rev Microbiol. 2021;19(3):155-70. Epub 2020/10/30. doi: 10.1038/s41579-020-00468-6. PubMed PMID: 33116300; PubMed Central PMCID: PMCPMC7592455.
94. Hoffmann M, Kleine-Weber H, Schroeder S, Kruger N, Herrler T, Erichsen S, et al. SARS-CoV-2 Cell Entry Depends on ACE2 and TMPRSS2 and Is Blocked by a Clinically Proven Protease Inhibitor. Cell. 2020;181(2):271-80 e8. Epub 2020/03/07. doi: 10.1016/j.cell.2020.02.052. PubMed PMID: 32142651; PubMed Central PMCID: PMCPMC7102627.
95. Safiabadi Tali SH, LeBlanc JJ, Sadiq Z, Oyewunmi OD, Camargo C, Nikpour B, et al. Tools and Techniques for Severe Acute Respiratory Syndrome Coronavirus 2 (SARS-CoV-2)/COVID-19 Detection. Clin Microbiol Rev. 2021;34(3). Epub 2021/05/14. doi: 10.1128/CMR.00228-20. PubMed PMID: 33980687; PubMed Central PMCID: PMCPMC8142517.
96. Soh WT, Liu Y, Nakayama EE, Ono C, Torii S, Nakagami H, et al. The N-terminal domain of spike glycoprotein mediates SARS-CoV-2 infection by associating with L-SIGN and DC-SIGN. bioRxiv. 2020:2020.11.05.369264. doi: 10.1101/2020.11.05.369264.
97. Cantuti-Castelvetri L, Ojha R, Pedro LD, Djannatian M, Franz J, Kuivanen S, et al. Neuropilin-1 facilitates SARS-CoV-2 cell entry and infectivity. Science. 2020;370(6518):856-60. Epub 2020/10/22. doi: 10.1126/science.abd2985. PubMed PMID: 33082293; PubMed Central PMCID: PMCPMC7857391.
98. Lempp FA, Soriaga L, Montiel-Ruiz M, Benigni F, Noack J, Park Y-J, et al. Lectins enhance SARS-CoV-2 infection and influence neutralizing antibodies. Nature. 2021. doi: 10.1038/s41586-021-03925-1.
99. Hoffmann M, Kleine-Weber H, Pohlmann S. A Multibasic Cleavage Site in the Spike Protein of SARS-CoV-2 Is Essential for Infection of Human Lung Cells. Mol Cell. 2020;78(4):779-84 e5. Epub 2020/05/05. doi: 10.1016/j.molcel.2020.04.022. PubMed PMID: 32362314; PubMed Central PMCID: PMCPMC7194065.
100. Peacock TP, Goldhill DH, Zhou J, Baillon L, Frise R, Swann OC, et al. The furin cleavage site in the SARS-CoV-2 spike protein is required for transmission in ferrets. Nat Microbiol. 2021;6(7):899-909. Epub 2021/04/29. doi: 10.1038/s41564-021-00908-w. PubMed PMID: 33907312.
101. Jaimes JA, Millet JK, Whittaker GR. Proteolytic Cleavage of the SARS-CoV-2 Spike Protein and the Role of the Novel S1/S2 Site. iScience. 2020;23(6):101212. Epub 2020/06/09. doi: 10.1016/j.isci.2020.101212. PubMed PMID: 32512386; PubMed Central PMCID: PMCPMC7255728.
102. Zhao MM, Yang WL, Yang FY, Zhang L, Huang WJ, Hou W, et al. Cathepsin L plays a key role in SARS-CoV-2 infection in humans and humanized mice and is a promising target for new drug development. Signal Transduct Target Ther. 2021;6(1):134. Epub 2021/03/29. doi: 10.1038/s41392-021-00558-8. PubMed PMID: 33774649; PubMed Central PMCID: PMCPMC7997800.
103. Rajah MM, Monel B, Schwartz O. The entanglement between flaviviruses and ER-shaping proteins. PLoS Pathog. 2020;16(4):e1008389. Epub 2020/04/17. doi:

10.1371/journal.ppat.1008389. PubMed PMID: 32298390; PubMed Central PMCID: PMCPMC7161947.
104. Tortorici MA, Veesler D. Structural insights into coronavirus entry. Adv Virus Res. 2019;105:93-116. Epub 2019/09/17. doi: 10.1016/bs.aivir.2019.08.002. PubMed PMID: 31522710; PubMed Central PMCID: PMCPMC7112261.
105. Ghosh S, Dellibovi-Ragheb TA, Kerviel A, Pak E, Qiu Q, Fisher M, et al. beta-Coronaviruses Use Lysosomes for Egress Instead of the Biosynthetic Secretory Pathway. Cell. 2020;183(6):1520-35 e14. Epub 2020/11/07. doi: 10.1016/j.cell.2020.10.039. PubMed PMID: 33157038; PubMed Central PMCID: PMCPMC7590812.
106. Segev N, Avinoam O, Podbilewicz B. Fusogens. Curr Biol. 2018;28(8):R378-R80. Epub 2018/04/25. doi: 10.1016/j.cub.2018.01.024. PubMed PMID: 29689218.
107. Wrapp D, Wang N, Corbett KS, Goldsmith JA, Hsieh CL, Abiona O, et al. Cryo-EM structure of the 2019-nCoV spike in the prefusion conformation. Science. 2020;367(6483):1260-3. Epub 2020/02/23. doi: 10.1126/science.abb2507. PubMed PMID: 32075877; PubMed Central PMCID: PMCPMC7164637.
108. Chi X, Yan R, Zhang J, Zhang G, Zhang Y, Hao M, et al. A neutralizing human antibody binds to the N-terminal domain of the Spike protein of SARS-CoV-2. Science. 2020;369(6504):650-5. Epub 2020/06/24. doi: 10.1126/science.abc6952. PubMed PMID: 32571838; PubMed Central PMCID: PMCPMC7319273.
109. Krempl C, Schultze B, Laude H, Herrler G. Point mutations in the S protein connect the sialic acid binding activity with the enteropathogenicity of transmissible gastroenteritis coronavirus. J Virol. 1997;71(4):3285-7. Epub 1997/04/01. doi: 10.1128/JVI.71.4.3285-3287.1997. PubMed PMID: 9060696; PubMed Central PMCID: PMCPMC191465.
110. Zhou H, Chen Y, Zhang S, Niu P, Qin K, Jia W, et al. Structural definition of a neutralization epitope on the N-terminal domain of MERS-CoV spike glycoprotein. Nat Commun. 2019;10(1):3068. Epub 2019/07/13. doi: 10.1038/s41467-019-10897-4. PubMed PMID: 31296843; PubMed Central PMCID: PMCPMC6624210.
111. Liu Y, Soh WT, Kishikawa JI, Hirose M, Nakayama EE, Li S, et al. An infectivity-enhancing site on the SARS-CoV-2 spike protein targeted by antibodies. Cell. 2021;184(13):3452-66 e18. Epub 2021/06/18. doi: 10.1016/j.cell.2021.05.032. PubMed PMID: 34139176; PubMed Central PMCID: PMCPMC8142859.
112. Lan J, Ge J, Yu J, Shan S, Zhou H, Fan S, et al. Structure of the SARS-CoV-2 spike receptor-binding domain bound to the ACE2 receptor. Nature. 2020;581(7807):215-20. Epub 2020/04/01. doi: 10.1038/s41586-020-2180-5. PubMed PMID: 32225176.
113. Rey F. Structure-function relations of the SARS-CoV-2 spike protein and impact of mutations in the variants of concern. C R Biol. 2021;344(1):77-110. Epub 2021/07/03. doi: 10.5802/crbiol.53. PubMed PMID: 34213849.
114. Benton DJ, Wrobel AG, Xu P, Roustan C, Martin SR, Rosenthal PB, et al. Receptor binding and priming of the spike protein of SARS-CoV-2 for membrane fusion. Nature. 2020;588(7837):327-30. Epub 2020/09/18. doi: 10.1038/s41586-020-2772-0. PubMed PMID: 32942285; PubMed Central PMCID: PMCPMC7116727.
115. Su R, Zeng J, O'Shaughnessy B. Host cell membrane capture by the SARS CoV-2 spike protein fusion intermediate. bioRxiv. 2021:2021.04.09.439051. doi: 10.1101/2021.04.09.439051.
116. Millet JK, Whittaker GR. Physiological and molecular triggers for SARS-CoV membrane fusion and entry into host cells. Virology. 2018;517:3-8. Epub 2017/12/26. doi:

10.1016/j.virol.2017.12.015. PubMed PMID: 29275820; PubMed Central PMCID: PMCPMC7112017.
117. Huang Y, Yang C, Xu XF, Xu W, Liu SW. Structural and functional properties of SARS-CoV-2 spike protein: potential antivirus drug development for COVID-19. Acta Pharmacol Sin. 2020;41(9):1141-9. Epub 2020/08/05. doi: 10.1038/s41401-020-0485-4. PubMed PMID: 32747721; PubMed Central PMCID: PMCPMC7396720.
118. Xia S, Yan L, Xu W, Agrawal AS, Algaissi A, Tseng CK, et al. A pan-coronavirus fusion inhibitor targeting the HR1 domain of human coronavirus spike. Sci Adv. 2019;5(4):eaav4580. Epub 2019/04/17. doi: 10.1126/sciadv.aav4580. PubMed PMID: 30989115; PubMed Central PMCID: PMCPMC6457931.
119. Boson B, Legros V, Zhou B, Siret E, Mathieu C, Cosset FL, et al. The SARS-CoV-2 envelope and membrane proteins modulate maturation and retention of the spike protein, allowing assembly of virus-like particles. J Biol Chem. 2021;296:100111. Epub 2020/11/25. doi: 10.1074/jbc.RA120.016175. PubMed PMID: 33229438; PubMed Central PMCID: PMCPMC7833635.
120. Cattin-Ortola J, Welch LG, Maslen SL, Papa G, James LC, Munro S. Sequences in the cytoplasmic tail of SARS-CoV-2 Spike facilitate expression at the cell surface and syncytia formation. Nat Commun. 2021;12(1):5333. Epub 2021/09/11. doi: 10.1038/s41467-021-25589-1. PubMed PMID: 34504087.
121. Schoeman D, Fielding BC. Coronavirus envelope protein: current knowledge. Virol J. 2019;16(1):69. Epub 2019/05/28. doi: 10.1186/s12985-019-1182-0. PubMed PMID: 31133031; PubMed Central PMCID: PMCPMC6537279.
122. Fu YZ, Wang SY, Zheng ZQ, Yi H, Li WW, Xu ZS, et al. SARS-CoV-2 membrane glycoprotein M antagonizes the MAVS-mediated innate antiviral response. Cell Mol Immunol. 2021;18(3):613-20. Epub 2020/10/29. doi: 10.1038/s41423-020-00571-x. PubMed PMID: 33110251; PubMed Central PMCID: PMCPMC7588591.
123. Fang X, Gao J, Zheng H, Li B, Kong L, Zhang Y, et al. The membrane protein of SARS-CoV suppresses NF-kappaB activation. J Med Virol. 2007;79(10):1431-9. Epub 2007/08/21. doi: 10.1002/jmv.20953. PubMed PMID: 17705188; PubMed Central PMCID: PMCPMC7166727.
124. Sui L, Zhao Y, Wang W, Wu P, Wang Z, Yu Y, et al. SARS-CoV-2 Membrane Protein Inhibits Type I Interferon Production Through Ubiquitin-Mediated Degradation of TBK1. Front Immunol. 2021;12:662989. Epub 2021/06/05. doi: 10.3389/fimmu.2021.662989. PubMed PMID: 34084167; PubMed Central PMCID: PMCPMC8168463.
125. Lu S, Ye Q, Singh D, Cao Y, Diedrich JK, Yates JR, 3rd, et al. The SARS-CoV-2 nucleocapsid phosphoprotein forms mutually exclusive condensates with RNA and the membrane-associated M protein. Nat Commun. 2021;12(1):502. Epub 2021/01/23. doi: 10.1038/s41467-020-20768-y. PubMed PMID: 33479198; PubMed Central PMCID: PMCPMC7820290.
126. Klein S, Cortese M, Winter SL, Wachsmuth-Melm M, Neufeldt CJ, Cerikan B, et al. SARS-CoV-2 structure and replication characterized by in situ cryo-electron tomography. Nat Commun. 2020;11(1):5885. Epub 2020/11/20. doi: 10.1038/s41467-020-19619-7. PubMed PMID: 33208793; PubMed Central PMCID: PMCPMC7676268.
127. Oh SJ, Shin OS. SARS-CoV-2 Nucleocapsid Protein Targets RIG-I-Like Receptor Pathways to Inhibit the Induction of Interferon Response. Cells. 2021;10(3). Epub 2021/04/04. doi: 10.3390/cells10030530. PubMed PMID: 33801464; PubMed Central PMCID: PMCPMC7999926.

128. Mandala VS, McKay MJ, Shcherbakov AA, Dregni AJ, Kolocouris A, Hong M. Structure and drug binding of the SARS-CoV-2 envelope protein transmembrane domain in lipid bilayers. Nat Struct Mol Biol. 2020;27(12):1202-8. Epub 2020/11/13. doi: 10.1038/s41594-020-00536-8. PubMed PMID: 33177698; PubMed Central PMCID: PMCPMC7718435.
129. Nieto-Torres JL, DeDiego ML, Verdia-Baguena C, Jimenez-Guardeno JM, Regla-Nava JA, Fernandez-Delgado R, et al. Severe acute respiratory syndrome coronavirus envelope protein ion channel activity promotes virus fitness and pathogenesis. PLoS Pathog. 2014;10(5):e1004077. Epub 2014/05/03. doi: 10.1371/journal.ppat.1004077. PubMed PMID: 24788150; PubMed Central PMCID: PMCPMC4006877.
130. Nieto-Torres JL, Verdia-Baguena C, Jimenez-Guardeno JM, Regla-Nava JA, Castano-Rodriguez C, Fernandez-Delgado R, et al. Severe acute respiratory syndrome coronavirus E protein transports calcium ions and activates the NLRP3 inflammasome. Virology. 2015;485:330-9. Epub 2015/09/04. doi: 10.1016/j.virol.2015.08.010. PubMed PMID: 26331680; PubMed Central PMCID: PMCPMC4619128.
131. Chai J, Cai Y, Pang C, Wang L, McSweeney S, Shanklin J, et al. Structural basis for SARS-CoV-2 envelope protein recognition of human cell junction protein PALS1. Nat Commun. 2021;12(1):3433. Epub 2021/06/10. doi: 10.1038/s41467-021-23533-x. PubMed PMID: 34103506; PubMed Central PMCID: PMCPMC8187709.
132. Shin D, Mukherjee R, Grewe D, Bojkova D, Baek K, Bhattacharya A, et al. Papain-like protease regulates SARS-CoV-2 viral spread and innate immunity. Nature. 2020;587(7835):657-62. Epub 2020/07/30. doi: 10.1038/s41586-020-2601-5. PubMed PMID: 32726803; PubMed Central PMCID: PMCPMC7116779.
133. Schubert K, Karousis ED, Jomaa A, Scaiola A, Echeverria B, Gurzeler LA, et al. SARS-CoV-2 Nsp1 binds the ribosomal mRNA channel to inhibit translation. Nat Struct Mol Biol. 2020;27(10):959-66. Epub 2020/09/11. doi: 10.1038/s41594-020-0511-8. PubMed PMID: 32908316.
134. Angelini MM, Akhlaghpour M, Neuman BW, Buchmeier MJ. Severe acute respiratory syndrome coronavirus nonstructural proteins 3, 4, and 6 induce double-membrane vesicles. mBio. 2013;4(4). Epub 2013/08/15. doi: 10.1128/mBio.00524-13. PubMed PMID: 23943763; PubMed Central PMCID: PMCPMC3747587.
135. Snijder EJ, Limpens R, de Wilde AH, de Jong AWM, Zevenhoven-Dobbe JC, Maier HJ, et al. A unifying structural and functional model of the coronavirus replication organelle: Tracking down RNA synthesis. PLoS Biol. 2020;18(6):e3000715. Epub 2020/06/09. doi: 10.1371/journal.pbio.3000715. PubMed PMID: 32511245; PubMed Central PMCID: PMCPMC7302735.
136. Knoops K, Kikkert M, Worm SH, Zevenhoven-Dobbe JC, van der Meer Y, Koster AJ, et al. SARS-coronavirus replication is supported by a reticulovesicular network of modified endoplasmic reticulum. PLoS Biol. 2008;6(9):e226. Epub 2008/09/19. doi: 10.1371/journal.pbio.0060226. PubMed PMID: 18798692; PubMed Central PMCID: PMCPMC2535663.
137. Wolff G, Limpens R, Zevenhoven-Dobbe JC, Laugks U, Zheng S, de Jong AWM, et al. A molecular pore spans the double membrane of the coronavirus replication organelle. Science. 2020;369(6509):1395-8. Epub 2020/08/09. doi: 10.1126/science.abd3629. PubMed PMID: 32763915; PubMed Central PMCID: PMCPMC7665310.
138. Shu T, Huang M, Wu D, Ren Y, Zhang X, Han Y, et al. SARS-Coronavirus-2 Nsp13 Possesses NTPase and RNA Helicase Activities That Can Be Inhibited by Bismuth Salts. Virol

Sin. 2020;35(3):321-9. Epub 2020/06/06. doi: 10.1007/s12250-020-00242-1. PubMed PMID: 32500504; PubMed Central PMCID: PMCPMC7271831.
139. Hillen HS, Kokic G, Farnung L, Dienemann C, Tegunov D, Cramer P. Structure of replicating SARS-CoV-2 polymerase. Nature. 2020;584(7819):154-6. Epub 2020/05/22. doi: 10.1038/s41586-020-2368-8. PubMed PMID: 32438371.
140. Eckerle LD, Lu X, Sperry SM, Choi L, Denison MR. High fidelity of murine hepatitis virus replication is decreased in nsp14 exoribonuclease mutants. J Virol. 2007;81(22):12135-44. Epub 2007/09/07. doi: 10.1128/JVI.01296-07. PubMed PMID: 17804504; PubMed Central PMCID: PMCPMC2169014.
141. Chen Y, Su C, Ke M, Jin X, Xu L, Zhang Z, et al. Biochemical and structural insights into the mechanisms of SARS coronavirus RNA ribose 2'-O-methylation by nsp16/nsp10 protein complex. PLoS Pathog. 2011;7(10):e1002294. Epub 2011/10/25. doi: 10.1371/journal.ppat.1002294. PubMed PMID: 22022266; PubMed Central PMCID: PMCPMC3192843.
142. Littler DR, Gully BS, Colson RN, Rossjohn J. Crystal Structure of the SARS-CoV-2 Non-structural Protein 9, Nsp9. iScience. 2020;23(7):101258. Epub 2020/06/28. doi: 10.1016/j.isci.2020.101258. PubMed PMID: 32592996; PubMed Central PMCID: PMCPMC7282741.
143. Gadhave K, Kumar P, Kumar A, Bhardwaj T, Garg N, Giri R. Conformational dynamics of 13 amino acids long NSP11 of SARS-CoV-2 under membrane mimetics and different solvent conditions. Microb Pathog. 2021;158:105041. Epub 2021/06/14. doi: 10.1016/j.micpath.2021.105041. PubMed PMID: 34119626; PubMed Central PMCID: PMCPMC8191288.
144. Pillon MC, Frazier MN, Dillard LB, Williams JG, Kocaman S, Krahn JM, et al. Cryo-EM structures of the SARS-CoV-2 endoribonuclease Nsp15 reveal insight into nuclease specificity and dynamics. Nat Commun. 2021;12(1):636. Epub 2021/01/29. doi: 10.1038/s41467-020-20608-z. PubMed PMID: 33504779; PubMed Central PMCID: PMCPMC7840905.
145. Deng X, Hackbart M, Mettelman RC, O'Brien A, Mielech AM, Yi G, et al. Coronavirus nonstructural protein 15 mediates evasion of dsRNA sensors and limits apoptosis in macrophages. Proc Natl Acad Sci U S A. 2017;114(21):E4251-E60. Epub 2017/05/10. doi: 10.1073/pnas.1618310114. PubMed PMID: 28484023; PubMed Central PMCID: PMCPMC5448190.
146. Kopecky-Bromberg SA, Martinez-Sobrido L, Frieman M, Baric RA, Palese P. Severe acute respiratory syndrome coronavirus open reading frame (ORF) 3b, ORF 6, and nucleocapsid proteins function as interferon antagonists. J Virol. 2007;81(2):548-57. Epub 2006/11/17. doi: 10.1128/JVI.01782-06. PubMed PMID: 17108024; PubMed Central PMCID: PMCPMC1797484.
147. Konno Y, Kimura I, Uriu K, Fukushi M, Irie T, Koyanagi Y, et al. SARS-CoV-2 ORF3b Is a Potent Interferon Antagonist Whose Activity Is Increased by a Naturally Occurring Elongation Variant. Cell Rep. 2020;32(12):108185. Epub 2020/09/18. doi: 10.1016/j.celrep.2020.108185. PubMed PMID: 32941788; PubMed Central PMCID: PMCPMC7473339.
148. Xia H, Cao Z, Xie X, Zhang X, Chen JY, Wang H, et al. Evasion of Type I Interferon by SARS-CoV-2. Cell Rep. 2020;33(1):108234. Epub 2020/09/28. doi: 10.1016/j.celrep.2020.108234. PubMed PMID: 32979938; PubMed Central PMCID: PMCPMC7501843.

149. Yuen CK, Lam JY, Wong WM, Mak LF, Wang X, Chu H, et al. SARS-CoV-2 nsp13, nsp14, nsp15 and orf6 function as potent interferon antagonists. Emerg Microbes Infect. 2020;9(1):1418-28. Epub 2020/06/13. doi: 10.1080/22221751.2020.1780953. PubMed PMID: 32529952; PubMed Central PMCID: PMCPMC7473193.
150. Cao Z, Xia H, Rajsbaum R, Xia X, Wang H, Shi PY. Ubiquitination of SARS-CoV-2 ORF7a promotes antagonism of interferon response. Cell Mol Immunol. 2021;18(3):746-8. Epub 2021/01/22. doi: 10.1038/s41423-020-00603-6. PubMed PMID: 33473190; PubMed Central PMCID: PMCPMC7815971.
151. Shemesh M, Aktepe TE, Deerain JM, McAuley JL, Audsley MD, David CT, et al. SARS-CoV-2 suppresses IFNbeta production mediated by NSP1, 5, 6, 15, ORF6 and ORF7b but does not suppress the effects of added interferon. PLoS Pathog. 2021;17(8):e1009800. Epub 2021/08/27. doi: 10.1371/journal.ppat.1009800. PubMed PMID: 34437657; PubMed Central PMCID: PMCPMC8389490.
152. Zhang Y, Zhang J, Chen Y, Luo B, Yuan Y, Huang F, et al. The ORF8 Protein of SARS-CoV-2 Mediates Immune Evasion through Potently Downregulating MHC-I. bioRxiv. 2020:2020.05.24.111823. doi: 10.1101/2020.05.24.111823.
153. Sette A, Crotty S. Adaptive immunity to SARS-CoV-2 and COVID-19. Cell. 2021;184(4):861-80. Epub 2021/01/27. doi: 10.1016/j.cell.2021.01.007. PubMed PMID: 33497610; PubMed Central PMCID: PMCPMC7803150 Epitogenesis, Gilead, and Avalia. S.C. is a consultant for Avalia. LJI has filed for patent protection for various aspects of T cell epitope and vaccine design work.
154. Dispinseri S, Secchi M, Pirillo MF, Tolazzi M, Borghi M, Brigatti C, et al. Neutralizing antibody responses to SARS-CoV-2 in symptomatic COVID-19 is persistent and critical for survival. Nat Commun. 2021;12(1):2670. Epub 2021/05/13. doi: 10.1038/s41467-021-22958-8. PubMed PMID: 33976165; PubMed Central PMCID: PMCPMC8113594.
155. Meckiff BJ, Ramirez-Suastegui C, Fajardo V, Chee SJ, Kusnadi A, Simon H, et al. Imbalance of Regulatory and Cytotoxic SARS-CoV-2-Reactive CD4(+) T Cells in COVID-19. Cell. 2020;183(5):1340-53 e16. Epub 2020/10/24. doi: 10.1016/j.cell.2020.10.001. PubMed PMID: 33096020; PubMed Central PMCID: PMCPMC7534589.
156. Park A, Iwasaki A. Type I and Type III Interferons - Induction, Signaling, Evasion, and Application to Combat COVID-19. Cell Host Microbe. 2020;27(6):870-8. Epub 2020/05/29. doi: 10.1016/j.chom.2020.05.008. PubMed PMID: 32464097; PubMed Central PMCID: PMCPMC7255347.
157. Hosseini A, Hashemi V, Shomali N, Asghari F, Gharibi T, Akbari M, et al. Innate and adaptive immune responses against coronavirus. Biomed Pharmacother. 2020;132:110859. Epub 2020/10/30. doi: 10.1016/j.biopha.2020.110859. PubMed PMID: 33120236; PubMed Central PMCID: PMCPMC7580677.
158. Wickenhagen A, Sugrue E, Lytras S, Kuchi S, Noerenberg M, Turnbull ML, et al. A prenylated dsRNA sensor protects against severe COVID-19. Science. 0(0):eabj3624. doi: doi:10.1126/science.abj3624.
159. Buchrieser J, Schwartz O. Pregnancy complications and Interferon-induced transmembrane proteins (IFITM): balancing antiviral immunity and placental development. C R Biol. 2021;344(2):145-56. Epub 2021/07/03. doi: 10.5802/crbiol.54. PubMed PMID: 34213852.
160. Hernandez JM, Podbilewicz B. The hallmarks of cell-cell fusion. Development. 2017;144(24):4481-95. Epub 2017/12/20. doi: 10.1242/dev.155523. PubMed PMID: 29254991.

161. Brukman NG, Uygur B, Podbilewicz B, Chernomordik LV. How cells fuse. J Cell Biol. 2019;218(5):1436-51. Epub 2019/04/03. doi: 10.1083/jcb.201901017. PubMed PMID: 30936162; PubMed Central PMCID: PMCPMC6504885.
162. Lavialle C, Cornelis G, Dupressoir A, Esnault C, Heidmann O, Vernochet C, et al. Paleovirology of 'syncytins', retroviral env genes exapted for a role in placentation. Philos Trans R Soc Lond B Biol Sci. 2013;368(1626):20120507. Epub 2013/08/14. doi: 10.1098/rstb.2012.0507. PubMed PMID: 23938756; PubMed Central PMCID: PMCPMC3758191.
163. Leroy H, Han M, Woottum M, Bracq L, Bouchet J, Xie M, et al. Virus-Mediated Cell-Cell Fusion. Int J Mol Sci. 2020;21(24). Epub 2020/12/23. doi: 10.3390/ijms21249644. PubMed PMID: 33348900; PubMed Central PMCID: PMCPMC7767094.
164. Lu X, Wang R, Zhu C, Wang H, Lin HY, Gu Y, et al. Fine-Tuned and Cell-Cycle-Restricted Expression of Fusogenic Protein Syncytin-2 Maintains Functional Placental Syncytia. Cell Rep. 2017;21(5):1150-9. Epub 2017/11/02. doi: 10.1016/j.celrep.2017.10.019. PubMed PMID: 29091755.
165. Ciechonska M, Duncan R. Reovirus FAST proteins: virus-encoded cellular fusogens. Trends Microbiol. 2014;22(12):715-24. Epub 2014/09/24. doi: 10.1016/j.tim.2014.08.005. PubMed PMID: 25245455.
166. Kanai Y, Kawagishi T, Sakai Y, Nouda R, Shimojima M, Saijo M, et al. Cell-cell fusion induced by reovirus FAST proteins enhances replication and pathogenicity of non-enveloped dsRNA viruses. PLoS Pathog. 2019;15(4):e1007675. Epub 2019/04/26. doi: 10.1371/journal.ppat.1007675. PubMed PMID: 31022290; PubMed Central PMCID: PMCPMC6504114.
167. Burton C, Bartee E. Syncytia Formation in Oncolytic Virotherapy. Mol Ther Oncolytics. 2019;15:131-9. Epub 2020/01/01. doi: 10.1016/j.omto.2019.09.006. PubMed PMID: 31890866; PubMed Central PMCID: PMCPMC6931088.
168. Compton AA, Schwartz O. They Might Be Giants: Does Syncytium Formation Sink or Spread HIV Infection? PLoS Pathog. 2017;13(2):e1006099. Epub 2017/02/06. doi: 10.1371/journal.ppat.1006099. PubMed PMID: 28152024; PubMed Central PMCID: PMCPMC5289631.
169. Bryce C, Grimes Z, Pujadas E, Ahuja S, Beasley MB, Albrecht R, et al. Pathophysiology of SARS-CoV-2: the Mount Sinai COVID-19 autopsy experience. Mod Pathol. 2021;34(8):1456-67. Epub 2021/04/03. doi: 10.1038/s41379-021-00793-y. PubMed PMID: 33795830; PubMed Central PMCID: PMCPMC8015313.
170. Luo WR, Yu H, Gou JZ, Li XX, Sun Y, Li JX, et al. Histopathologic Findings in the Explant Lungs of a Patient With COVID-19 Treated With Bilateral Orthotopic Lung Transplant. Transplantation. 2020;104(11):e329-e31. Epub 2020/10/31. doi: 10.1097/TP.0000000000003412. PubMed PMID: 33122591.
171. Rockx B, Kuiken T, Herfst S, Bestebroer T, Lamers MM, Oude Munnink BB, et al. Comparative pathogenesis of COVID-19, MERS, and SARS in a nonhuman primate model. Science. 2020;368(6494):1012-5. Epub 2020/04/19. doi: 10.1126/science.abb7314. PubMed PMID: 32303590; PubMed Central PMCID: PMCPMC7164679.
172. Tian S, Hu W, Niu L, Liu H, Xu H, Xiao SY. Pulmonary Pathology of Early-Phase 2019 Novel Coronavirus (COVID-19) Pneumonia in Two Patients With Lung Cancer. J Thorac Oncol. 2020;15(5):700-4. Epub 2020/03/03. doi: 10.1016/j.jtho.2020.02.010. PubMed PMID: 32114094; PubMed Central PMCID: PMCPMC7128866.

173. Zhang Z, Zheng Y, Niu Z, Zhang B, Wang C, Yao X, et al. SARS-CoV-2 spike protein dictates syncytium-mediated lymphocyte elimination. Cell Death Differ. 2021. Epub 2021/04/22. doi: 10.1038/s41418-021-00782-3. PubMed PMID: 33879858; PubMed Central PMCID: PMCPMC8056997.
174. Nicholls JM, Poon LL, Lee KC, Ng WF, Lai ST, Leung CY, et al. Lung pathology of fatal severe acute respiratory syndrome. Lancet. 2003;361(9371):1773-8. Epub 2003/06/05. doi: 10.1016/s0140-6736(03)13413-7. PubMed PMID: 12781536; PubMed Central PMCID: PMCPMC7112492.
175. Lee N, Hui D, Wu A, Chan P, Cameron P, Joynt GM, et al. A major outbreak of severe acute respiratory syndrome in Hong Kong. N Engl J Med. 2003;348(20):1986-94. Epub 2003/04/16. doi: 10.1056/NEJMoa030685. PubMed PMID: 12682352.
176. Ksiazek TG, Erdman D, Goldsmith CS, Zaki SR, Peret T, Emery S, et al. A novel coronavirus associated with severe acute respiratory syndrome. N Engl J Med. 2003;348(20):1953-66. Epub 2003/04/12. doi: 10.1056/NEJMoa030781. PubMed PMID: 12690092.
177. Ng DL, Al Hosani F, Keating MK, Gerber SI, Jones TL, Metcalfe MG, et al. Clinicopathologic, Immunohistochemical, and Ultrastructural Findings of a Fatal Case of Middle East Respiratory Syndrome Coronavirus Infection in the United Arab Emirates, April 2014. Am J Pathol. 2016;186(3):652-8. Epub 2016/02/10. doi: 10.1016/j.ajpath.2015.10.024. PubMed PMID: 26857507; PubMed Central PMCID: PMCPMC7093852.
178. Orenstein JM, Banach B, Baker SC. Morphogenesis of Coronavirus HCoV-NL63 in Cell Culture: A Transmission Electron Microscopic Study. Open Infect Dis J. 2008;2:52-8. Epub 2008/01/01. doi: 10.2174/1874279300802010052. PubMed PMID: 19844604; PubMed Central PMCID: PMCPMC2763395.
179. Parry R, Macnaughton MR. Syncytium production by human coronavirus 229E group viruses. FEMS Microbiology Letters. 1983;20:23 - 6.
180. Dominguez SR, Travanty EA, Qian Z, Mason RJ. Human coronavirus HKU1 infection of primary human type II alveolar epithelial cells: cytopathic effects and innate immune response. PLoS One. 2013;8(7):e70129. Epub 2013/07/31. doi: 10.1371/journal.pone.0070129. PubMed PMID: 23894604; PubMed Central PMCID: PMCPMC3722178.
181. Buchrieser J, Dufloo J, Hubert M, Monel B, Planas D, Rajah MM, et al. Syncytia formation by SARS-CoV-2-infected cells. EMBO J. 2020;39(23):e106267. Epub 2020/10/15. doi: 10.15252/embj.2020106267. PubMed PMID: 33051876; PubMed Central PMCID: PMCPMC7646020.
182. Daly JL, Simonetti B, Klein K, Chen KE, Williamson MK, Anton-Plagaro C, et al. Neuropilin-1 is a host factor for SARS-CoV-2 infection. Science. 2020;370(6518):861-5. Epub 2020/10/22. doi: 10.1126/science.abd3072. PubMed PMID: 33082294.
183. Li ZL, Buck M. Neuropilin-1 assists SARS-CoV-2 infection by stimulating the separation of Spike protein S1 and S2. Biophys J. 2021;120(14):2828-37. Epub 2021/06/05. doi: 10.1016/j.bpj.2021.05.026. PubMed PMID: 34087218; PubMed Central PMCID: PMCPMC8169233.
184. Whitlock JM, Chernomordik LV. Flagging fusion: Phosphatidylserine signaling in cell-cell fusion. J Biol Chem. 2021;296:100411. Epub 2021/02/14. doi: 10.1016/j.jbc.2021.100411. PubMed PMID: 33581114; PubMed Central PMCID: PMCPMC8005811.
185. Chua BA, Ngo JA, Situ K, Morizono K. Roles of phosphatidylserine exposed on the viral envelope and cell membrane in HIV-1 replication. Cell Commun Signal. 2019;17(1):132. Epub

2019/10/23. doi: 10.1186/s12964-019-0452-1. PubMed PMID: 31638994; PubMed Central PMCID: PMCPMC6805584.
186. Nanbo A, Maruyama J, Imai M, Ujie M, Fujioka Y, Nishide S, et al. Ebola virus requires a host scramblase for externalization of phosphatidylserine on the surface of viral particles. PLoS Pathog. 2018;14(1):e1006848. Epub 2018/01/18. doi: 10.1371/journal.ppat.1006848. PubMed PMID: 29338048; PubMed Central PMCID: PMCPMC5786336.
187. Azab W, Gramatica A, Herrmann A, Osterrieder N. Binding of alphaherpesvirus glycoprotein H to surface alpha4beta1-integrins activates calcium-signaling pathways and induces phosphatidylserine exposure on the plasma membrane. mBio. 2015;6(5):e01552-15. Epub 2015/10/23. doi: 10.1128/mBio.01552-15. PubMed PMID: 26489864; PubMed Central PMCID: PMCPMC4620472.
188. Morizono K, Chen IS. Role of phosphatidylserine receptors in enveloped virus infection. J Virol. 2014;88(8):4275-90. Epub 2014/01/31. doi: 10.1128/JVI.03287-13. PubMed PMID: 24478428; PubMed Central PMCID: PMCPMC3993771.
189. Zhang Z, Liu J, Li M, Yang H, Zhang C. Evolutionary dynamics of the interferon-induced transmembrane gene family in vertebrates. PLoS One. 2012;7(11):e49265. Epub 2012/11/21. doi: 10.1371/journal.pone.0049265. PubMed PMID: 23166625; PubMed Central PMCID: PMCPMC3499546.
190. Bailey CC, Zhong G, Huang IC, Farzan M. IFITM-Family Proteins: The Cell's First Line of Antiviral Defense. Annu Rev Virol. 2014;1:261-83. Epub 2015/01/20. doi: 10.1146/annurev-virology-031413-085537. PubMed PMID: 25599080; PubMed Central PMCID: PMCPMC4295558.
191. Savidis G, Perreira JM, Portmann JM, Meraner P, Guo Z, Green S, et al. The IFITMs Inhibit Zika Virus Replication. Cell Rep. 2016;15(11):2323-30. Epub 2016/06/09. doi: 10.1016/j.celrep.2016.05.074. PubMed PMID: 27268505.
192. Shi G, Kenney AD, Kudryashova E, Zani A, Zhang L, Lai KK, et al. Opposing activities of IFITM proteins in SARS-CoV-2 infection. EMBO J. 2021;40(3):e106501. Epub 2020/12/04. doi: 10.15252/embj.2020106501. PubMed PMID: 33270927; PubMed Central PMCID: PMCPMC7744865.
193. Amini-Bavil-Olyaee S, Choi YJ, Lee JH, Shi M, Huang IC, Farzan M, et al. The antiviral effector IFITM3 disrupts intracellular cholesterol homeostasis to block viral entry. Cell Host Microbe. 2013;13(4):452-64. Epub 2013/04/23. doi: 10.1016/j.chom.2013.03.006. PubMed PMID: 23601107; PubMed Central PMCID: PMCPMC3646482.
194. Zani A, Yount JS. Antiviral Protection by IFITM3 In Vivo. Curr Clin Microbiol Rep. 2018;5(4):229-37. Epub 2019/01/22. doi: 10.1007/s40588-018-0103-0. PubMed PMID: 30662816; PubMed Central PMCID: PMCPMC6334760.
195. Shi G, Schwartz O, Compton AA. More than meets the I: the diverse antiviral and cellular functions of interferon-induced transmembrane proteins. Retrovirology. 2017;14(1):53. Epub 2017/11/23. doi: 10.1186/s12977-017-0377-y. PubMed PMID: 29162141; PubMed Central PMCID: PMCPMC5697417.
196. Desai TM, Marin M, Chin CR, Savidis G, Brass AL, Melikyan GB. IFITM3 restricts influenza A virus entry by blocking the formation of fusion pores following virus-endosome hemifusion. PLoS Pathog. 2014;10(4):e1004048. Epub 2014/04/05. doi: 10.1371/journal.ppat.1004048. PubMed PMID: 24699674; PubMed Central PMCID: PMCPMC3974867.

197. Huang IC, Bailey CC, Weyer JL, Radoshitzky SR, Becker MM, Chiang JJ, et al. Distinct patterns of IFITM-mediated restriction of filoviruses, SARS coronavirus, and influenza A virus. PLoS Pathog. 2011;7(1):e1001258. Epub 2011/01/22. doi: 10.1371/journal.ppat.1001258. PubMed PMID: 21253575; PubMed Central PMCID: PMCPMC3017121.
198. Wrensch F, Winkler M, Pohlmann S. IFITM proteins inhibit entry driven by the MERS-coronavirus spike protein: evidence for cholesterol-independent mechanisms. Viruses. 2014;6(9):3683-98. Epub 2014/09/27. doi: 10.3390/v6093683. PubMed PMID: 25256397; PubMed Central PMCID: PMCPMC4189045.
199. Zhao X, Sehgal M, Hou Z, Cheng J, Shu S, Wu S, et al. Identification of Residues Controlling Restriction versus Enhancing Activities of IFITM Proteins on Entry of Human Coronaviruses. J Virol. 2018;92(6). Epub 2017/12/22. doi: 10.1128/JVI.01535-17. PubMed PMID: 29263263; PubMed Central PMCID: PMCPMC5827390.
200. Zhao X, Guo F, Liu F, Cuconati A, Chang J, Block TM, et al. Interferon induction of IFITM proteins promotes infection by human coronavirus OC43. Proc Natl Acad Sci U S A. 2014;111(18):6756-61. Epub 2014/04/23. doi: 10.1073/pnas.1320856111. PubMed PMID: 24753610; PubMed Central PMCID: PMCPMC4020042.
201. Winstone H, Lista MJ, Reid AC, Bouton C, Pickering S, Galao RP, et al. The Polybasic Cleavage Site in SARS-CoV-2 Spike Modulates Viral Sensitivity to Type I Interferon and IFITM2. J Virol. 2021;95(9). Epub 2021/02/11. doi: 10.1128/JVI.02422-20. PubMed PMID: 33563656; PubMed Central PMCID: PMCPMC8104117.
202. Benfield CT, MacKenzie F, Ritzefeld M, Mazzon M, Weston S, Tate EW, et al. Bat IFITM3 restriction depends on S-palmitoylation and a polymorphic site within the CD225 domain. Life Sci Alliance. 2020;3(1). Epub 2019/12/13. doi: 10.26508/lsa.201900542. PubMed PMID: 31826928; PubMed Central PMCID: PMCPMC6907390.
203. Chesarino NM, Compton AA, McMichael TM, Kenney AD, Zhang L, Soewarna V, et al. IFITM3 requires an amphipathic helix for antiviral activity. EMBO Rep. 2017;18(10):1740-51. Epub 2017/08/25. doi: 10.15252/embr.201744100. PubMed PMID: 28835547; PubMed Central PMCID: PMCPMC5623871.
204. Rahman K, Coomer CA, Majdoul S, Ding SY, Padilla-Parra S, Compton AA. Homology-guided identification of a conserved motif linking the antiviral functions of IFITM3 to its oligomeric state. Elife. 2020;9. Epub 2020/10/29. doi: 10.7554/eLife.58537. PubMed PMID: 33112230; PubMed Central PMCID: PMCPMC7665892.
205. Guo X, Steinkuhler J, Marin M, Li X, Lu W, Dimova R, et al. Interferon-Induced Transmembrane Protein 3 Blocks Fusion of Diverse Enveloped Viruses by Altering Mechanical Properties of Cell Membranes. ACS Nano. 2021;15(5):8155-70. Epub 2021/03/04. doi: 10.1021/acsnano.0c10567. PubMed PMID: 33656312; PubMed Central PMCID: PMCPMC8159881.
206. Prelli Bozzo C, Nchioua R, Volcic M, Koepke L, Kruger J, Schutz D, et al. IFITM proteins promote SARS-CoV-2 infection and are targets for virus inhibition in vitro. Nat Commun. 2021;12(1):4584. Epub 2021/07/30. doi: 10.1038/s41467-021-24817-y. PubMed PMID: 34321474; PubMed Central PMCID: PMCPMC8319209.
207. Bertram S, Dijkman R, Habjan M, Heurich A, Gierer S, Glowacka I, et al. TMPRSS2 activates the human coronavirus 229E for cathepsin-independent host cell entry and is expressed in viral target cells in the respiratory epithelium. J Virol. 2013;87(11):6150-60. Epub 2013/03/29. doi: 10.1128/JVI.03372-12. PubMed PMID: 23536651; PubMed Central PMCID: PMCPMC3648130.

208. Zheng M, Zhao X, Zheng S, Chen D, Du P, Li X, et al. Bat SARS-Like WIV1 coronavirus uses the ACE2 of multiple animal species as receptor and evades IFITM3 restriction via TMPRSS2 activation of membrane fusion. Emerg Microbes Infect. 2020;9(1):1567-79. Epub 2020/07/01. doi: 10.1080/22221751.2020.1787797. PubMed PMID: 32602823; PubMed Central PMCID: PMCPMC7473123.
209. Rajah MM, Hubert M, Bishop E, Saunders N, Robinot R, Grzelak L, et al. SARS-CoV-2 Alpha, Beta and Delta variants display enhanced Spike-mediated Syncytia Formation. bioRxiv. 2021:2021.06.11.448011. doi: 10.1101/2021.06.11.448011.
210. Yu J, Murthy V, Liu SL. Relating GPI-Anchored Ly6 Proteins uPAR and CD59 to Viral Infection. Viruses. 2019;11(11). Epub 2019/11/20. doi: 10.3390/v11111060. PubMed PMID: 31739586; PubMed Central PMCID: PMCPMC6893729.
211. Yu J, Liang C, Liu SL. CD4-Dependent Modulation of HIV-1 Entry by LY6E. J Virol. 2019;93(7). Epub 2019/01/25. doi: 10.1128/JVI.01866-18. PubMed PMID: 30674630; PubMed Central PMCID: PMCPMC6430548.
212. Mar KB, Rinkenberger NR, Boys IN, Eitson JL, McDougal MB, Richardson RB, et al. LY6E mediates an evolutionarily conserved enhancement of virus infection by targeting a late entry step. Nat Commun. 2018;9(1):3603. Epub 2018/09/08. doi: 10.1038/s41467-018-06000-y. PubMed PMID: 30190477; PubMed Central PMCID: PMCPMC6127192.
213. Yu J, Liu SL. Emerging Role of LY6E in Virus-Host Interactions. Viruses. 2019;11(11). Epub 2019/11/07. doi: 10.3390/v11111020. PubMed PMID: 31684192; PubMed Central PMCID: PMCPMC6893646.
214. Pfaender S, Mar KB, Michailidis E, Kratzel A, Boys IN, V'Kovski P, et al. LY6E impairs coronavirus fusion and confers immune control of viral disease. Nat Microbiol. 2020;5(11):1330-9. Epub 2020/07/25. doi: 10.1038/s41564-020-0769-y. PubMed PMID: 32704094; PubMed Central PMCID: PMCPMC7916999.
215. Zhao X, Zheng S, Chen D, Zheng M, Li X, Li G, et al. LY6E Restricts Entry of Human Coronaviruses, Including Currently Pandemic SARS-CoV-2. J Virol. 2020;94(18). Epub 2020/07/10. doi: 10.1128/JVI.00562-20. PubMed PMID: 32641482; PubMed Central PMCID: PMCPMC7459569.
216. Wang S, Li W, Hui H, Tiwari SK, Zhang Q, Croker BA, et al. Cholesterol 25-Hydroxylase inhibits SARS-CoV-2 and other coronaviruses by depleting membrane cholesterol. EMBO J. 2020;39(21):e106057. Epub 2020/09/19. doi: 10.15252/embj.2020106057. PubMed PMID: 32944968; PubMed Central PMCID: PMCPMC7537045.
217. Zang R, Case JB, Yutuc E, Ma X, Shen S, Gomez Castro MF, et al. Cholesterol 25-hydroxylase suppresses SARS-CoV-2 replication by blocking membrane fusion. Proc Natl Acad Sci U S A. 2020;117(50):32105-13. Epub 2020/11/27. doi: 10.1073/pnas.2012197117. PubMed PMID: 33239446; PubMed Central PMCID: PMCPMC7749331.
218. Michael Rajah M, Hubert M, Bishop E, Saunders N, Robinot R, Grzelak L, et al. SARS-CoV-2 Alpha, Beta and Delta variants display enhanced Spike-mediated Syncytia Formation. The EMBO Journal. n/a(n/a):e108944. doi: https://doi.org/10.15252/embj.2021108944.
219. Hulswit RJG, Lang Y, Bakkers MJG, Li W, Li Z, Schouten A, et al. Human coronaviruses OC43 and HKU1 bind to 9-O-acetylated sialic acids via a conserved receptor-binding site in spike protein domain A. Proc Natl Acad Sci U S A. 2019;116(7):2681-90. Epub 2019/01/27. doi: 10.1073/pnas.1809667116. PubMed PMID: 30679277; PubMed Central PMCID: PMCPMC6377473.

220. Huang X, Dong W, Milewska A, Golda A, Qi Y, Zhu QK, et al. Human Coronavirus HKU1 Spike Protein Uses O-Acetylated Sialic Acid as an Attachment Receptor Determinant and Employs Hemagglutinin-Esterase Protein as a Receptor-Destroying Enzyme. J Virol. 2015;89(14):7202-13. Epub 2015/05/01. doi: 10.1128/JVI.00854-15. PubMed PMID: 25926653; PubMed Central PMCID: PMCPMC4473545.
221. Shirato K, Kawase M, Matsuyama S. Wild-type human coronaviruses prefer cell-surface TMPRSS2 to endosomal cathepsins for cell entry. Virology. 2018;517:9-15. Epub 2017/12/09. doi: 10.1016/j.virol.2017.11.012. PubMed PMID: 29217279; PubMed Central PMCID: PMCPMC7112029.
222. Pyrc K, Berkhout B, van der Hoek L. The novel human coronaviruses NL63 and HKU1. J Virol. 2007;81(7):3051-7. Epub 2006/11/03. doi: 10.1128/JVI.01466-06. PubMed PMID: 17079323; PubMed Central PMCID: PMCPMC1866027.
223. Pyrc K, Sims AC, Dijkman R, Jebbink M, Long C, Deming D, et al. Culturing the unculturable: human coronavirus HKU1 infects, replicates, and produces progeny virions in human ciliated airway epithelial cell cultures. J Virol. 2010;84(21):11255-63. Epub 2010/08/20. doi: 10.1128/JVI.00947-10. PubMed PMID: 20719951; PubMed Central PMCID: PMCPMC2953148.
224. Ma H, Zhu Z, Lin H, Wang S, Zhang P, Li Y, et al. Pyroptosis of syncytia formed by fusion of SARS-CoV-2 spike and ACE2-expressing cells. Cell Discov. 2021;7(1):73. Epub 2021/08/26. doi: 10.1038/s41421-021-00310-0. PubMed PMID: 34429403; PubMed Central PMCID: PMCPMC8384103.
225. Paoloni-Giacobino A, Chen H, Peitsch MC, Rossier C, Antonarakis SE. Cloning of the TMPRSS2 gene, which encodes a novel serine protease with transmembrane, LDLRA, and SRCR domains and maps to 21q22.3. Genomics. 1997;44(3):309-20. Epub 1997/11/05. doi: 10.1006/geno.1997.4845. PubMed PMID: 9325052.
226. Shirogane Y, Takeda M, Iwasaki M, Ishiguro N, Takeuchi H, Nakatsu Y, et al. Efficient multiplication of human metapneumovirus in Vero cells expressing the transmembrane serine protease TMPRSS2. J Virol. 2008;82(17):8942-6. Epub 2008/06/20. doi: 10.1128/jvi.00676-08. PubMed PMID: 18562527; PubMed Central PMCID: PMCPMC2519639.
227. Afar DE, Vivanco I, Hubert RS, Kuo J, Chen E, Saffran DC, et al. Catalytic cleavage of the androgen-regulated TMPRSS2 protease results in its secretion by prostate and prostate cancer epithelia. Cancer Res. 2001;61(4):1686-92. Epub 2001/03/14. PubMed PMID: 11245484.
228. Buchrieser J, Degrelle SA, Couderc T, Nevers Q, Disson O, Manet C, et al. IFITM proteins inhibit placental syncytiotrophoblast formation and promote fetal demise. Science. 2019;365(6449):176-80. Epub 2019/07/13. doi: 10.1126/science.aaw7733. PubMed PMID: 31296770.
229. Kodaka M, Yang Z, Nakagawa K, Maruyama J, Xu X, Sarkar A, et al. A new cell-based assay to evaluate myogenesis in mouse myoblast C2C12 cells. Exp Cell Res. 2015;336(2):171-81. Epub 2015/06/28. doi: 10.1016/j.yexcr.2015.06.015. PubMed PMID: 26116467.
230. Edie S, Zaghloul NA, Leitch CC, Klinedinst DK, Lebron J, Thole JF, et al. Survey of Human Chromosome 21 Gene Expression Effects on Early Development in Danio rerio. G3 (Bethesda). 2018;8(7):2215-23. Epub 2018/05/16. doi: 10.1534/g3.118.200144. PubMed PMID: 29760202; PubMed Central PMCID: PMCPMC6027891.
231. Liu Y, Liu J, Johnson BA, Xia H, Ku Z, Schindewolf C, et al. Delta spike P681R mutation enhances SARS-CoV-2 fitness over Alpha variant. bioRxiv. 2021:2021.08.12.456173. doi: 10.1101/2021.08.12.456173.

232. Mlcochova P, Kemp S, Dhar MS, Papa G, Meng B, Ferreira I, et al. SARS-CoV-2 B.1.617.2 Delta variant replication and immune evasion. Nature. 2021. Epub 2021/09/07. doi: 10.1038/s41586-021-03944-y. PubMed PMID: 34488225.
233. Zhou B, Thao TTN, Hoffmann D, Taddeo A, Ebert N, Labroussaa F, et al. SARS-CoV-2 spike D614G change enhances replication and transmission. Nature. 2021;592(7852):122-7. Epub 2021/02/27. doi: 10.1038/s41586-021-03361-1. PubMed PMID: 33636719.
234. Ozono S, Zhang Y, Ode H, Sano K, Tan TS, Imai K, et al. SARS-CoV-2 D614G spike mutation increases entry efficiency with enhanced ACE2-binding affinity. Nat Commun. 2021;12(1):848. Epub 2021/02/10. doi: 10.1038/s41467-021-21118-2. PubMed PMID: 33558493; PubMed Central PMCID: PMCPMC7870668.
235. Jiang X, Zhang Z, Wang C, Ren H, Gao L, Peng H, et al. Bimodular effects of D614G mutation on the spike glycoprotein of SARS-CoV-2 enhance protein processing, membrane fusion, and viral infectivity. Signal Transduct Target Ther. 2020;5(1):268. Epub 2020/11/19. doi: 10.1038/s41392-020-00392-4. PubMed PMID: 33203835; PubMed Central PMCID: PMCPMC7670837.
236. Saito A, Irie T, Suzuki R, Maemura T, Nasser H, Uriu K, et al. SARS-CoV-2 spike P681R mutation, a hallmark of the Delta variant, enhances viral fusogenicity and pathogenicity. bioRxiv. 2021:2021.06.17.448820. doi: 10.1101/2021.06.17.448820.
237. Hoffmann M, Arora P, Gross R, Seidel A, Hornich BF, Hahn AS, et al. SARS-CoV-2 variants B.1.351 and P.1 escape from neutralizing antibodies. Cell. 2021;184(9):2384-93 e12. Epub 2021/04/02. doi: 10.1016/j.cell.2021.03.036. PubMed PMID: 33794143; PubMed Central PMCID: PMCPMC7980144.
238. Arora P, Kempf A, Nehlmeier I, Sidarovich A, Krüger N, Graichen L, et al. Increased lung cell entry of B.1.617.2 and evasion of antibodies induced by infection and BNT162b2 vaccination. bioRxiv. 2021:2021.06.23.449568. doi: 10.1101/2021.06.23.449568.
239. Starr TN, Greaney AJ, Addetia A, Hannon WW, Choudhary MC, Dingens AS, et al. Prospective mapping of viral mutations that escape antibodies used to treat COVID-19. Science. 2021;371(6531):850-4. Epub 2021/01/27. doi: 10.1126/science.abf9302. PubMed PMID: 33495308; PubMed Central PMCID: PMCPMC7963219.
240. Starr TN, Greaney AJ, Hilton SK, Ellis D, Crawford KHD, Dingens AS, et al. Deep Mutational Scanning of SARS-CoV-2 Receptor Binding Domain Reveals Constraints on Folding and ACE2 Binding. Cell. 2020;182(5):1295-310 e20. Epub 2020/08/26. doi: 10.1016/j.cell.2020.08.012. PubMed PMID: 32841599; PubMed Central PMCID: PMCPMC7418704.
241. Liu Y, Liu J, Plante KS, Plante JA, Xie X, Zhang X, et al. The N501Y spike substitution enhances SARS-CoV-2 transmission. bioRxiv. 2021:2021.03.08.434499. doi: 10.1101/2021.03.08.434499.
242. Ali F, Kasry A, Amin M. The new SARS-CoV-2 strain shows a stronger binding affinity to ACE2 due to N501Y mutant. Med Drug Discov. 2021;10:100086. Epub 2021/03/09. doi: 10.1016/j.medidd.2021.100086. PubMed PMID: 33681755; PubMed Central PMCID: PMCPMC7923861.
243. Zahradnik J, Marciano S, Shemesh M, Zoler E, Harari D, Chiaravalli J, et al. SARS-CoV-2 variant prediction and antiviral drug design are enabled by RBD in vitro evolution. Nat Microbiol. 2021;6(9):1188-98. Epub 2021/08/18. doi: 10.1038/s41564-021-00954-4. PubMed PMID: 34400835.

244. Luan B, Wang H, Huynh T. Enhanced binding of the N501Y-mutated SARS-CoV-2 spike protein to the human ACE2 receptor: insights from molecular dynamics simulations. FEBS Lett. 2021;595(10):1454-61. Epub 2021/03/18. doi: 10.1002/1873-3468.14076. PubMed PMID: 33728680; PubMed Central PMCID: PMCPMC8250610.
245. Collier DA, De Marco A, Ferreira I, Meng B, Datir RP, Walls AC, et al. Sensitivity of SARS-CoV-2 B.1.1.7 to mRNA vaccine-elicited antibodies. Nature. 2021;593(7857):136-41. Epub 2021/03/12. doi: 10.1038/s41586-021-03412-7. PubMed PMID: 33706364.
246. Jangra S, Ye C, Rathnasinghe R, Stadlbauer D, Personalized Virology Initiative study g, Krammer F, et al. SARS-CoV-2 spike E484K mutation reduces antibody neutralisation. Lancet Microbe. 2021;2(7):e283-e4. Epub 2021/04/14. doi: 10.1016/S2666-5247(21)00068-9. PubMed PMID: 33846703; PubMed Central PMCID: PMCPMC8026167 members and their affiliations, declarations of interests, and acknowledgments are listed in the appendix. This research was partly funded by the Center for Research for Influenza Pathogenesis, a Center of Excellence for Influenza Research and Surveillance supported by the National Institute of Allergy and Infectious Diseases (contract number HHSN272201400008C), by the National Cancer Institute grant U54CA260560, by the JPB Foundation and the Open Philanthropy Project (research grant 2020-215611 [5384], and by anonymous donors to AG-S. Work on SARS-CoV-2 in the Krammer and Simon laboratories was funded by the Collaborative Influenza Vaccine Innovation Centers' contract number 75N93019C00051. Research in the Martinez-Sobrido laboratory was partly funded by the New York Influenza Center of Excellence, a member of the National Institute of Allergy and Infectious Diseases, and was also partially funded by the National Institutes of Health, the Department of Health and Human Services, and the Centers of Excellence for Influenza Research and Surveillance (contract number HHSN272201400005C, New York Influenza Center of Excellence). Funding sources had no role in the study design, in the collection, analysis, and interpretation of the data, in the writing of the Correspondence, and in the decision to submit the Correspondence for publication. The Garcia-Sastre laboratory has received research support from Pfizer, Senhwa Biosciences, and 7Hills Pharma. AG-S has consulting agreements for 7Hills Pharma, Avimex, and Esperovax involving cash, and Vivaldi Biosciences, Contrafect, Accurius, and Vaxalto involving stock. The Icahn School of Medicine at Mount Sinai has filed patent applications relating to SARS-CoV-2 serological assays and Newcastle disease virus-based SARS-CoV-2 vaccines which list FK as co-inventor. DS and VS are also listed on the serological assay patent application as co-inventors. FK has consulted for Merck and Pfizer (before 2020), and is currently consulting for Seqirus and Avimex. The Krammer laboratory is also collaborating with Pfizer on animal models of SARS-CoV-2. All other authors declare no competing interests.
247. Harvey WT, Carabelli AM, Jackson B, Gupta RK, Thomson EC, Harrison EM, et al. SARS-CoV-2 variants, spike mutations and immune escape. Nat Rev Microbiol. 2021;19(7):409-24. Epub 2021/06/03. doi: 10.1038/s41579-021-00573-0. PubMed PMID: 34075212; PubMed Central PMCID: PMCPMC8167834.
248. Wang WB, Liang Y, Jin YQ, Zhang J, Su JG, Li QM. E484K mutation in SARS-CoV-2 RBD enhances binding affinity with hACE2 but reduces interactions with neutralizing antibodies and nanobodies: Binding free energy calculation studies. bioRxiv. 2021:2021.02.17.431566. doi: 10.1101/2021.02.17.431566.
249. Puray-Chavez M, LaPak KM, Schrank TP, Elliott JL, Bhatt DP, Agajanian MJ, et al. Systematic analysis of SARS-CoV-2 infection of an ACE2-negative human airway cell. Cell

Rep. 2021;36(2):109364. Epub 2021/07/03. doi: 10.1016/j.celrep.2021.109364. PubMed PMID: 34214467; PubMed Central PMCID: PMCPMC8220945.
250. Mohammad A, Abubaker J, Al-Mulla F. Structural modelling of SARS-CoV-2 alpha variant (B.1.1.7) suggests enhanced furin binding and infectivity. Virus Res. 2021;303:198522. Epub 2021/07/28. doi: 10.1016/j.virusres.2021.198522. PubMed PMID: 34314772; PubMed Central PMCID: PMCPMC8310422.
251. Zhang L, Mann M, Syed Z, Reynolds HM, Tian E, Samara NL, et al. Furin cleavage of the SARS-CoV-2 spike is modulated by O-glycosylation. bioRxiv. 2021:2021.02.05.429982. doi: 10.1101/2021.02.05.429982.
252. Ostrov DA. Structural Consequences of Variation in SARS-CoV-2 B.1.1.7. J Cell Immunol. 2021;3(2):103-8. Epub 2021/05/11. doi: 10.33696/immunology.3.085. PubMed PMID: 33969357; PubMed Central PMCID: PMCPMC8104447.
253. Nardacci R, Perfettini JL, Grieco L, Thieffry D, Kroemer G, Piacentini M. Syncytial apoptosis signaling network induced by the HIV-1 envelope glycoprotein complex: an overview. Cell Death Dis. 2015;6:e1846. Epub 2015/08/08. doi: 10.1038/cddis.2015.204. PubMed PMID: 26247731; PubMed Central PMCID: PMCPMC4558497.
254. Jackson L, Rodel H, Hwa S-H, Cele S, Ganga Y, Tegally H, et al. SARS-CoV-2 cell-to-cell spread occurs rapidly and is insensitive to antibody neutralization. bioRxiv. 2021:2021.06.01.446516. doi: 10.1101/2021.06.01.446516.
255. Herschke F, Plumet S, Duhen T, Azocar O, Druelle J, Laine D, et al. Cell-cell fusion induced by measles virus amplifies the type I interferon response. J Virol. 2007;81(23):12859-71. Epub 2007/09/28. doi: 10.1128/JVI.00078-07. PubMed PMID: 17898060; PubMed Central PMCID: PMCPMC2169089.
256. Ku JWK, Chen Y, Lim BJW, Gasser S, Crasta KC, Gan YH. Bacterial-induced cell fusion is a danger signal triggering cGAS-STING pathway via micronuclei formation. Proc Natl Acad Sci U S A. 2020;117(27):15923-34. Epub 2020/06/24. doi: 10.1073/pnas.2006908117. PubMed PMID: 32571920; PubMed Central PMCID: PMCPMC7355030.
257. Asarnow D, Wang B, Lee WH, Hu Y, Huang CW, Faust B, et al. Structural insight into SARS-CoV-2 neutralizing antibodies and modulation of syncytia. Cell. 2021;184(12):3192-204 e16. Epub 2021/05/12. doi: 10.1016/j.cell.2021.04.033. PubMed PMID: 33974910; PubMed Central PMCID: PMCPMC8064868.
258. Cifuentes-Munoz N, Dutch RE, Cattaneo R. Direct cell-to-cell transmission of respiratory viruses: The fast lanes. PLoS Pathog. 2018;14(6):e1007015. Epub 2018/06/29. doi: 10.1371/journal.ppat.1007015. PubMed PMID: 29953542; PubMed Central PMCID: PMCPMC6023113.
259. Zeng C, Evans JP, King T, Zheng Y-M, Oltz EM, Whelan SPJ, et al. SARS-CoV-2 Spreads through Cell-to-Cell Transmission. bioRxiv. 2021:2021.06.01.446579. doi: 10.1101/2021.06.01.446579.
260. Abela IA, Berlinger L, Schanz M, Reynell L, Gunthard HF, Rusert P, et al. Cell-cell transmission enables HIV-1 to evade inhibition by potent CD4bs directed antibodies. PLoS Pathog. 2012;8(4):e1002634. Epub 2012/04/13. doi: 10.1371/journal.ppat.1002634. PubMed PMID: 22496655; PubMed Central PMCID: PMCPMC3320602.
261. Sigal A, Kim JT, Balazs AB, Dekel E, Mayo A, Milo R, et al. Cell-to-cell spread of HIV permits ongoing replication despite antiretroviral therapy. Nature. 2011;477(7362):95-8. Epub 2011/08/19. doi: 10.1038/nature10347. PubMed PMID: 21849975.

262. Schiffner T, Sattentau QJ, Duncan CJ. Cell-to-cell spread of HIV-1 and evasion of neutralizing antibodies. Vaccine. 2013;31(49):5789-97. Epub 2013/10/22. doi: 10.1016/j.vaccine.2013.10.020. PubMed PMID: 24140477.
263. Beucher G, Blondot M-L, Celle A, Pied N, Recordon-Pinson P, Esteves P, et al. SARS-CoV-2 transmission via apical syncytia release from primary bronchial epithelia and infectivity restriction in children epithelia. bioRxiv. 2021:2021.05.28.446159. doi: 10.1101/2021.05.28.446159.
264. Lin WW, Tsay AJ, Lalime EN, Pekosz A, Griffin DE. Primary differentiated respiratory epithelial cells respond to apical measles virus infection by shedding multinucleated giant cells. Proc Natl Acad Sci U S A. 2021;118(11). Epub 2021/04/11. doi: 10.1073/pnas.2013264118. PubMed PMID: 33836570; PubMed Central PMCID: PMCPMC7980467.
265. Monel B, Planas D, Grzelak L, Smith N, Robillard N, Staropoli I, et al. Release of infectious virus and cytokines in nasopharyngeal swabs from individuals infected with non-B.1.1.7 or B.1.1.7 SARS-CoV-2 variants. medRxiv. 2021:2021.05.20.21257393. doi: 10.1101/2021.05.20.21257393.
266. Sanders DW, Jumper CC, Ackerman PJ, Bracha D, Donlic A, Kim H, et al. SARS-CoV-2 requires cholesterol for viral entry and pathological syncytia formation. Elife. 2021;10. Epub 2021/04/24. doi: 10.7554/eLife.65962. PubMed PMID: 33890572; PubMed Central PMCID: PMCPMC8104966.
267. Monel B, Rajah MM, Hafirassou ML, Sid Ahmed S, Burlaud-Gaillard J, Zhu PP, et al. Atlastin Endoplasmic Reticulum-Shaping Proteins Facilitate Zika Virus Replication. J Virol. 2019;93(23). Epub 2019/09/20. doi: 10.1128/JVI.01047-19. PubMed PMID: 31534046; PubMed Central PMCID: PMCPMC6854498.
268. Rajah MM, Pardy RD, Condotta SA, Richer MJ, Sagan SM. Zika Virus: Emergence, Phylogenetics, Challenges, and Opportunities. ACS Infect Dis. 2016;2(11):763-72. Epub 2016/10/06. doi: 10.1021/acsinfecdis.6b00161. PubMed PMID: 27704772.
269. Musso D, Ko AI, Baud D. Zika Virus Infection - After the Pandemic. N Engl J Med. 2019;381(15):1444-57. Epub 2019/10/10. doi: 10.1056/NEJMra1808246. PubMed PMID: 31597021.
270. Barnard TR, Abram QH, Lin QF, Wang AB, Sagan SM. Molecular Determinants of Flavivirus Virion Assembly. Trends Biochem Sci. 2021;46(5):378-90. Epub 2021/01/12. doi: 10.1016/j.tibs.2020.12.007. PubMed PMID: 33423940.
271. Mohd Ropidi MI, Khazali AS, Nor Rashid N, Yusof R. Endoplasmic reticulum: a focal point of Zika virus infection. J Biomed Sci. 2020;27(1):27. Epub 2020/01/22. doi: 10.1186/s12929-020-0618-6. PubMed PMID: 31959174; PubMed Central PMCID: PMCPMC6971992.
272. Long RKM, Moriarty KP, Cardoen B, Gao G, Vogl AW, Jean F, et al. Super resolution microscopy and deep learning identify Zika virus reorganization of the endoplasmic reticulum. Sci Rep. 2020;10(1):20937. Epub 2020/12/03. doi: 10.1038/s41598-020-77170-3. PubMed PMID: 33262363; PubMed Central PMCID: PMCPMC7708840.
273. Grzelak L, Temmam S, Planchais C, Demeret C, Tondeur L, Huon C, et al. A comparison of four serological assays for detecting anti-SARS-CoV-2 antibodies in human serum samples from different populations. Sci Transl Med. 2020;12(559). Epub 2020/08/21. doi: 10.1126/scitranslmed.abc3103. PubMed PMID: 32817357; PubMed Central PMCID: PMCPMC7665313.

Appendices

Appendix 1

Supplemental chapter: The role of ER-Shaping proteins on Zika Virus replication

Appendix 2

Permission for reprinting copyrighted materials and title pages of articles

Appendix 3

Other articles & Press releases

Supplemental Chapter: The role of ER-Shaping proteins on Zika Virus replication

This supplemental chapter presents my work prior to the pandemic that was done with and under the supervision of Dr. Blandine Monel. I present here, two published articles that explore the role of ER-shaping protein on Zika virus replication.

The first of which, is a short review titled "**The entanglement between flaviviruses and ER-shaping proteins**" [103] published in PLOS pathogens which describes the role of each of the ER-Shaping proteins and how they impact the virology of *Flaviviruses*. This will serve as an in-depth introduction as well as a discussion of the subject. This article was researched and written by me, under the supervision and editorial guidance of Dr. Blandine Monel and Pr. Olivier Schwartz. The article is reprinted under the creative commons license.

Rajah MM, Monel B, Schwartz O "The entanglement between flaviviruses and ER-shaping proteins". (2020) **PLOS Pathogens**, 16(4): e1008389. *(Review Article)*
https://doi.org/10.1371/journal.ppat.1008389

The second is a research article titled "**Atlastin Endoplasmic Reticulum-Shaping Proteins Facilitate Zika Virus Replication**" [267] published in the Journal of Virology and describes interaction between the atlastin ER-shaping protein and ZIKV. This projected was started and led by my supervisor Dr. Blandine Monel. I was offered a co-first authorship for taking the project to its completion during her pregnancy and maternity leave. I present this work with full acknowledgement of Dr. Monel's generosity and her role in my training and development.
The article is reprinted with permission from the American Society for Microbiology (see permissions).

Monel B*, **Rajah MM** (**Co-first author**)*, Hafirassou ML, Sid-Ahmed S, Burlaud-Gaillard J, Zhu PP, Nevers Q, Buchrieser J, Porrot F, Meunier C, Amraoui S, Chazal M, Salles A, Jouvenet N, Roingeard P, Blackstone C, Amara A, Schwartz O "The Atlastin ER-shaping proteins facilitate Zika virus replication". (2019) **Journal of Virology**, 93(23): e01047-19. doi: 10.1128/JVI.01047-19

S1 Short Introduction: Zika Virus

S1.1 ZIKV Epidemiology, Transmission and Clinical Features

Zika Virus (ZIKV) is a member of the *Flavivirus* genus, which includes other significant pathogens like Dengue virus (DENV) and West Nile virus (WNV). It is an arbovirus that is primarily transmitted to humans by *Aedes* mosquitoes; however, it can also be transmitted sexually and from mother-to-child (vertical transmission) [268].

It was initially isolated from the Zika forest of Uganda in the late 1940s and for the latter half of the 1900s it circulated in equatorial Africa and Southeast Asia in relative obscurity, causing only sporadic infections [268, 269]. The virus expanded beyond its endemic regions and caused large scale epidemics on Yap Island in the Federated States of Micronesia in 2007 and then in French Polynesia in 2013 [268]. By 2015, ZIKV had become pandemic and spread to 87 countries (mainly in the Americas and the Caribbean) and caused more than 500,000 human infections [269]. Most infections are asymptomatic. When symptoms are present, the illness is generally mild and self-limiting and characterized by fever, fatigue, rashes and joint and muscle pains [268, 269]. The progressive ZIKV epidemics correlated with reports of more severe neurological symptoms. An increase in Guillain-Barré syndrome, a demyelinating disease characterized by peripheral nerve damage and paralysis, was reported during the French Polynesian epidemic [269]. During the 2015 pandemic more than 3,700 cases of congenital birth defects were reported including fetal microcephaly [269]. The pandemic has since subsided; however, the experience of the pandemic has left scientific and public health institutions better prepared to deal with the potential re-emergence of ZIKV or other related viruses [269]. There are currently no approved therapeutics for ZIKV, and a couple of candidate vaccines are undergoing clinical trials [269].

S1.2 Viral Replication and Proteins

ZIKV is a single-stranded positive-sense RNA virus with a single open reading frame flanked by highly structured 3' and 5' untranslated regions. The viral genome encodes for three structural protein (capsid, pre-membrane and envelope) and seven non-structural protein (NS1, NS2A, NS2B, NS3, NS4A, NS4B, NS5). The envelope protein mediates viral entry via receptor mediated endocytosis, where acidification of the endosome results in the fusion of the viral and the endosomal membranes and the release of the viral genome into the cellular cytoplasm [270]. The vRNA is translated into a single polyprotein that is co- and post- translationally processed by viral and host factors. The NS3 protein functions as a protease, helicase and nucleotide triphosphates and is important for polyprotein processing, vRNA replication and synthesis. The NS1, NS2A and NS2B proteins facilitate immune evasion, the formation of the viral replication complex and also mediate viral assembly [268, 270]. NS2B also functions as a co-factor for NS3. ZIKV hijacks the intracellular membranes as well as several host factors to form endoplasmic reticulum (ER)-derived replication structures. Several of viral protein, including NS2A, NS2B, NS4A and NS4B may be implicated in this process [271, 272]. The NS5 protein is an RNA-dependent RNA polymerase which synthesizes vRNA and the capsid protein bind to the vRNA and forms the nucleocapsid that that is packaged into the virion [268, 270]. Immature viral particles bud into the ER and are maturated by pH changes and by the action of the host protease furin, before exiting the cell via the secretory pathway [270]

S1.3 Research question

ZIKV replication occurs on the ER membrane where viral protein generates ER-derived replication structures that provide a protective microenvironment for viral replication. Several host proteins are hijacked for this purpose including a family of proteins known as “ER-Shaping proteins”. This protein family includes atlastins, receptor expression-enhancing proteins (REEPs), and reticulons and they collectively function to maintain the shape, structure and integrity of the ER. Understanding how ZIKV interacts with ER-Shaping proteins and the impact on viral replication will provide a better understanding into the biology of the virus. The following article summarizes the role of ER Shaping proteins on *Flavivirus* replication. This is then followed by a research article on the role of the atlastin protein on ZIKV replication.

PLOS PATHOGENS

PEARLS

The entanglement between flaviviruses and ER-shaping proteins

Maaran Michael Rajah[1,2], **Blandine Monel**[1☯*], **Olivier Schwartz**[1,3☯*]

1 Institut Pasteur, Virus and Immunity Unit, CNRS-UMR3569, Paris France, **2** Ecole Doctorale Bio Sorbonne Paris Cité (BioSPC) -Université de Paris, Paris, France, **3** Vaccine Research Institute, Creteil, France

☯ These authors contributed equally to this work.
* blandine.monel@pasteur.fr (BM); olivier.schwartz@pasteur.fr (OS)

Check for updates

OPEN ACCESS

Citation: Rajah MM, Monel B, Schwartz O (2020) The entanglement between flaviviruses and ER-shaping proteins. PLoS Pathog 16(4): e1008389. https://doi.org/10.1371/journal.ppat.1008389

Editor: Matthew J. Evans, Mount Sinai School of Medicine, UNITED STATES

Published: April 16, 2020

Copyright: © 2020 Rajah et al. This is an open access article distributed under the terms of the Creative Commons Attribution License, which permits unrestricted use, distribution, and reproduction in any medium, provided the original author and source are credited.

Funding: M.M.R is supported by the Pasteur-Paris University (PPU) International Doctoral Program. Work in the O.S. lab is funded by Institut Pasteur, ANRS, Sidaction, the Vaccine Research Institute (ANR-10-LABX-77), Labex IBEID (ANR-10-LABX-62-IBEID), TIMTAMDEN ANR-14-CE14-0029, CHIKV-Viro-Immuno ANR-14-CE14-0015-01, and the Gilead HIV cure program. B.M. is supported by the Pasteur-Roux/Pasteur-Cantarini fellowship from Institut Pasteur (Paris). The funders had no role in study design, data collection and analysis, decision to publish, or preparation of the manuscript.

Competing interests: The authors have declared that no competing interests exist.

Love at first site: The endoplasmic reticulum and Flavivirus replication

The endoplasmic reticulum (ER) is a continuous intracellular membrane system that composes the nuclear envelope and radiates out to the peripheries of the cell, transitioning from ribosome-studded, flat cisternal sheets to highly curved reticulated tubules. It has been implicated in a diverse array of cellular functions, including production, trafficking, and degradation of proteins; synthesis and distribution of lipids and steroids; calcium sequestration and release; cell signaling and innate immunity; carbohydrate metabolism; and detoxification of harmful substances [1]. Such a ubiquitous and functionally versatile organelle is parasitized by viruses in order to facilitate their life cycle. Rotavirus, vaccinia virus (VV), hepatitis C virus (HCV), as well as members of the Flavivirus genus—dengue virus (DENV), West Nile virus (WNV), yellow fever virus (YFV), and Zika virus (ZIKV)—are all intimately associated with the ER [2]. The flaviviruses replicate on the ER membranes and form immature viral particles that bud into the ER lumen. These particles are then trafficked through the ER–Golgi network and undergo a maturation process brought about by pH alteration and cleavage by the host-protease Furin. This viral takeover of the ER requires the co-opting of cellular proteins as well as the active remodeling of the ER membrane to create a cellular environment more conducive to replication [3]. Several ER proteins have been identified as host factors in flavivirus replication [4], but a class of resident proteins that shape and maintain the dynamic ER architecture are of particular interest. These "ER-shaping" proteins could potentially serve as host factors that support viral replication or restriction factors that protect the ER. Interactome and CRISPR screens have produced somewhat discordant results, but the less stringent screens suggest that ER-shaping proteins may be targets of viral proteins [5] [6] [7]. This Pearl review will explore the virus-induced ER-membrane rearrangement and the relationship between ER-shaping proteins and the flavivirus life cycle.

Virulent and manipulative passions: Virus-induced manipulation to the ER structure

Virus-induced morphological changes to the ER membrane are brought about by active restructuring facilitated by interactions between viral proteins and host factors. The functional benefits of membrane alterations include the spatial compartmentalization of the viral-replication machinery—increasing the accessibility and concentration of necessary host factors—protection from the innate immune response, and the possibility of increased viral spread [3] [8]. The characteristics of the replication-supporting ER-membrane structures differ between viruses. HCV forms a "membranous web" and double-membrane vesicles, and VV

manipulates the ER into wrapping around the cytosolic site of viral-DNA replication [9] [10]. Flaviviruses form invaginations in the ER referred to as vesicle packets (VPs), which are clusters of vesicle membranes housing the viral-replication machinery [3] [11] [12] [13] [14]. Immature flavivirus virions form paracrystalline arrays within the ER lumen [11]. In some cell types, flaviviruses also form convoluted membranes (CMs), which are potential sites for the translation and processing of viral proteins [3] [11] [12]. Interestingly, ZIKV infection in certain cell types produces large ER-derived vacuoles, which are followed by an implosive cell death (Fig 1A) [8]. Several Flavivirus proteins and host factors (i.e., reticulophagy factor FAM134B [15]) have been implicated in the ER-modification process. Of recent interest are ER-shaping proteins, that can be operationally subdivided into proteins that help form the structure and curvature of the ER and fusogens that maintain the reticulated ER network.

Curvy and sturdy: ER curvature-stabilizing proteins and virus interactions

The class of ER-shaping proteins labeled as curvature-stabilizing proteins are subdivided into two families, the receptor expression-enhancing protein (REEP)/DP1/yop1p and the reticulons [1]. The REEPs are a family of six proteins that interact with microtubules through an extended C-terminal cytoplasmic domain. By facilitating the association of the ER membrane to cytoskeletal dynamics, they provide the mechanics necessary to extend ER tubules, as well as to form the positive curvature of the ER membrane [16] [1]. Mutations in the REEP1 proteins are associated with hereditary spastic paraplegias (HSP), a family of inherited neurological disorders characterized by spastic weakness in the extremities, which is partly reminiscent of symptoms induced by neurotropic flaviviruses [1] [16]. The effect of the REEP family on flavivirus replication has not been thoroughly explored, with one investigation reporting that the depletion of REEP1 does not affect DENV replication [17].

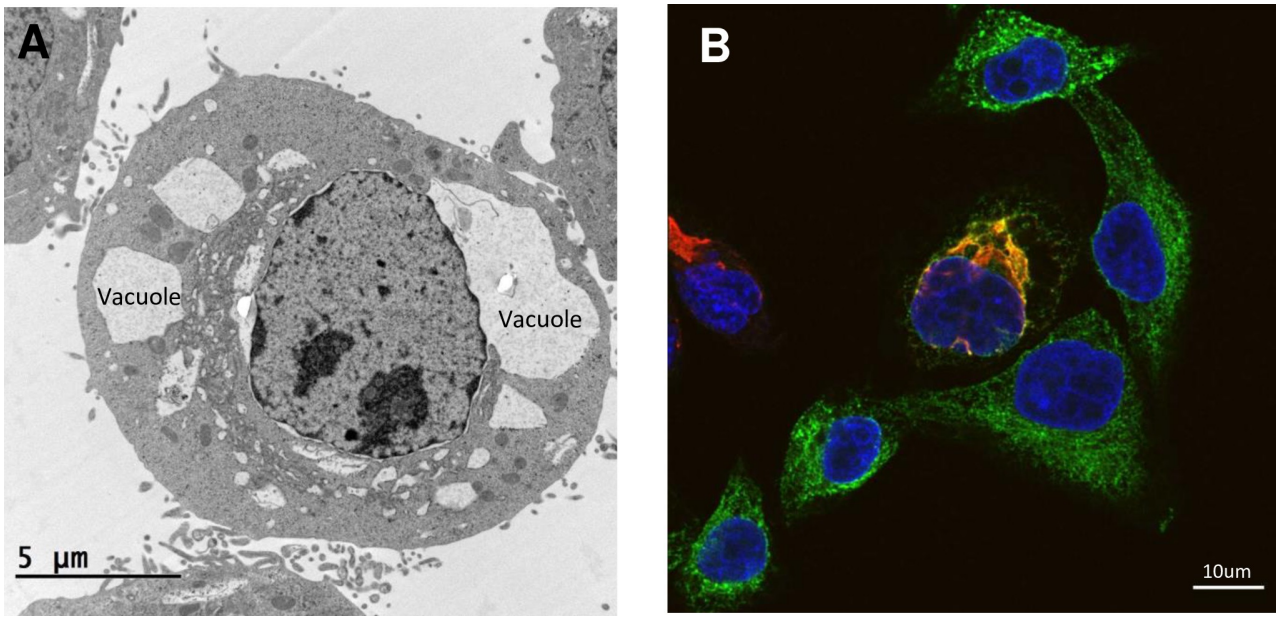

Fig 1. Microscopy images of ZIKV-infected HeLa Cells 24 hours after infection. (A) Electron micrograph of ER-derived vacuoles in a ZIKV-infected cell. (B) Confocal microscopy image showing the colocalization (yellow/orange) of ER-shaping protein ATL3 (green) with the ZIKV protein NS3 (red). ATL3, Atlastin-3; ER, endoplasmic reticulum; NS3, nonstructural protein 3; ZIKV, Zika virus.

https://doi.org/10.1371/journal.ppat.1008389.g001

The reticulon family consists of four (Reticulon 1 [RTN1] to RTN4) membrane-bound proteins that contain hydrophobic domains occupying the outer leaflet of the ER membrane. The resultant hydrophobic wedging, and possibly the scaffolding and protein–protein crowding formed by reticulon oligomers, contributes to the curvature of the ER membrane [1]. Several studies have identified reticulons as host factors in viral replication; Enterovirus 71 protein 2C and brome mosaic virus protein 1a both interact with RTNs to facilitate replication [18] [19]. Contrarily, RTN3 acts as a restriction factor in HCV replication by preventing nonstructural protein 4A (NS4A) self-interaction [20].

DENV, WNV, and ZIKV recruit RTN3.1A to the viral-replication site [21]. RTN3.1A depletion reduces viral titers and decreases viral RNA and protein levels [21]. The RTN3.1A colocalizes with the NS4A proteins of DENV, ZIKV, and WNV, but it only directly interacts with WNV NS4A via its N-terminal transmembrane domain (Fig 2A) [21]. The expression of WNV and DENV NS4A alone is sufficient to induce ER rearrangements [22] [23]. Depletion of RTN3.1A differentially alters the formation of the ER-derived replication organelles between flaviviruses. In ZIKV-infected and WNV-infected cells, there is a noticeable decrease in the amount of vesicle membranes present per VP (Fig 2C) [21]. While amount of vesicle membranes per VP was not altered in DENV-infected cells, their morphology became more elongated (Fig 2C), and there was an increase in immature viral particles upon RTN3.1A depletion (Fig 2C) [21]. Overall, while RTN3.1A may differently influence the life cycle of specific flaviviruses, it interacts with viral proteins and induces morphological changes to the ER in order to promote replication.

Together at-last-in each other's embrace: Virus interaction with the atlastin fusogens

The atlastins (ATLs) are a family of three membrane-bound, dynamin-related guanosine triphosphate (GTP)ases that mediate the construction of the reticulated ER network. The hydrolysis of GTP dissociates *cis*-membrane dimers and supports the tethering and dimerization with ATLs situated on a different ER membrane [24]. The homotypic fusion of ER membranes results in the formation of three-way junctions, shaping the smooth ER into an intricate and dynamic web of tubules. The depletion of ATL reduces the density of the ER network [25], and mutations in ATLs are also associated with HSP. In addition to their role as an ER-shaping protein, ATLs also influence protein targeting to the inner nuclear membrane and the biogenesis of nuclear pore complexes, regulate lipid droplet size, and facilitate selective autophagy [26] [27] [28]. Thus, ATLs could potentially be expedient host factors for several pathogens. A previous study implicated ATL3 in remodeling the ER to promote the formation of vacuoles that facilitate the intracellular replication of *Legionella pneumophila* [29].

Two recent investigations examined the relationship between the three ATLs and different flaviviruses and found varying effects based on the virus [17] [30]. Silencing ATL2 resulted in a significant reduction of DENV, WNV, and ZIKV titers and viral RNA [17]. ATL2 depletion affected formation of ER-derived DENV-replication organelles, distorting the size and shape of the vesicles and condensing them into a small perinuclear region (Fig 2D) [17]. The depletion of ATL3 reduced the titers of ZIKV and DENV (but not WNV) and had no effect on viral-RNA levels [17] [30]. ATL3 depletion did not change the morphology of the DENV-induced vesicles but resulted in an increased accumulation of intracellular viral particles in the ER lumen (Fig 2D) [17]. The GTPase function of ATLs is important for DENV and ZIKV replication [30] [17].

The different ATL proteins exhibit variation in their interaction with flavivirus proteins. ATL3 relocates to the ZIKV-replication site and directly interacts with nonstructural protein 3

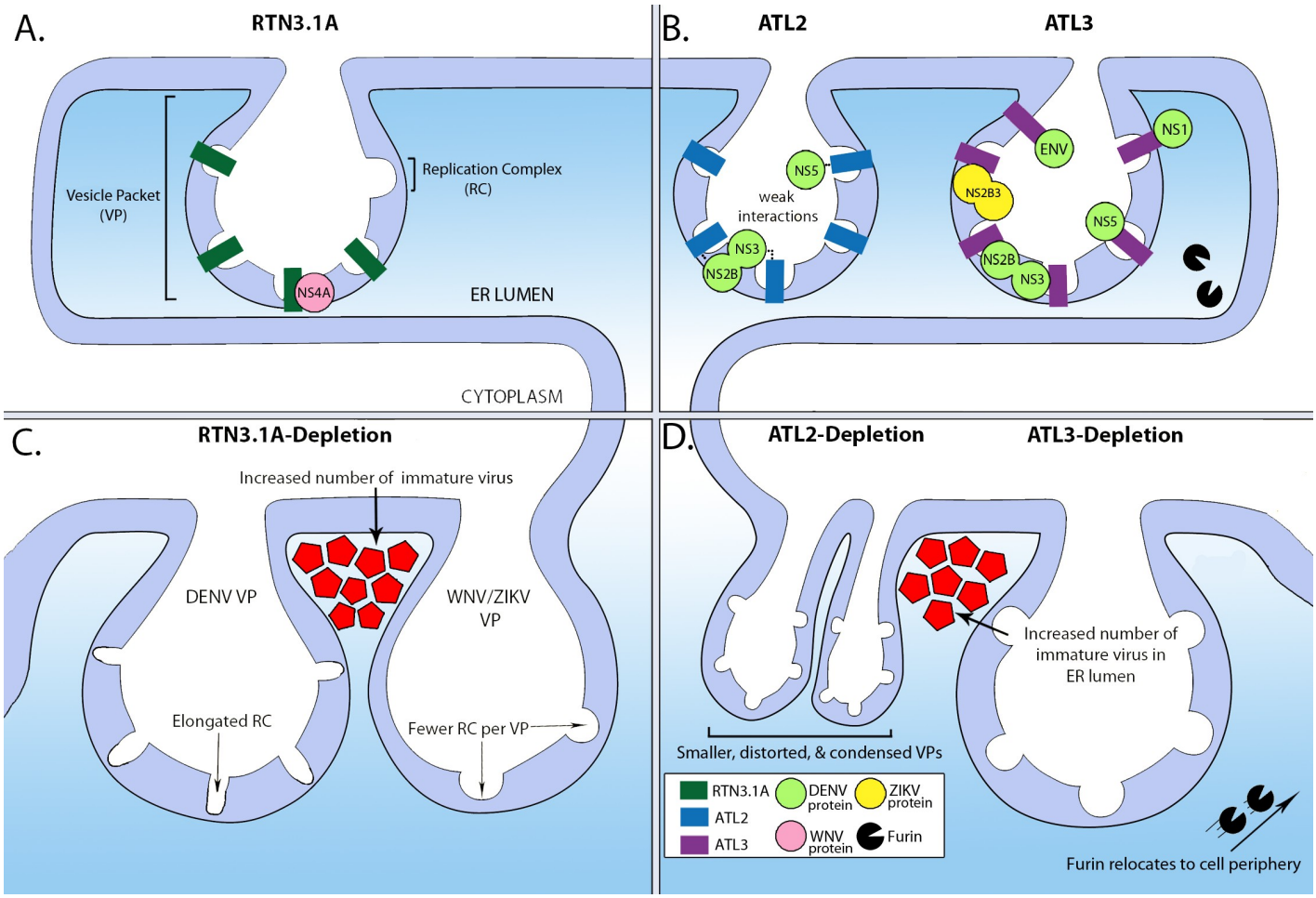

Fig 2. The relationship between ER-shaping proteins and flaviviruses during infection. A simplified schematic showing the interaction between different flavivirus proteins and ER-shaping proteins: (A) RTN3.1A and (B) ATL2 (left) and ATL3 (right). (C) Depleting RTN3.1 results in elongated RCs in DENV-infected cells and fewer RCs per VP in WNV-infected and ZIKV-infected cells. (D) Depleting ATL2 (left) results in VPs that are smaller, distorted, and condensed but does not change the overall number of VPs, whereas ATL3 depletion results in the host-protease Furin relocating from the perinuclear region to the cell periphery and accumulation of immature virus particles in the ER lumen. Immature virus particles are represented smaller than they would be in relation to VPs. ATL2, Atlastin-2; ATL3, Atlastin-3; DENV, dengue virus; ENV, envelope; ER, endoplasmic reticulum; NS1, nonstructural protein 1; RC, replication complex; RTN3.1A, Reticulon 3.1A; VP, vesicle packet; WNV, West Nile virus; ZIKV, Zika virus.

https://doi.org/10.1371/journal.ppat.1008389.g002

(NS3; Fig 1B) and NS2B3, that belong to the viral-replication complex (Fig 2B) [30]. Both ATL2 and ATL3 interact with DENV NS3, NS5, and NS2B proteins, though interactions with ATL2 are relatively weak (Fig 2B) [17]. DENV NS1 protein and the envelope and capsid proteins also interact with ATL3 (Fig 2B) [17]. ATL3 is recruited to DENV-replication organelles and is enriched in the membrane-surrounding virions, but it is not necessarily associated with the site of viral-RNA replication [17]. In DENV-infected cells, ATL3 interacts with ADP-ribosylation factor 4 (ARF4), a protein that is associated with trafficking of proteins and vesicle processing [17]. Depletion of AFR4 and the related ARF5 protein impairs DENV assembly and release. The depletion of ATL3 results in the relocalization of Furin from the perinuclear region to the cell periphery (Fig 2D), suggesting that ATL3 may play a role in providing immature viral particles access to Furin (Fig 2D) in addition to a potential direct role on assembly and trafficking of viral particles [17]. Overall, these studies show that ATL3 is associated with

the cytoplasmic transport of vesicles and is intimately involved with flavivirus assembly and maturation [17].

Happily, ever after: How the future could shape out

ER-shaping proteins impact the life cycle of flaviviruses by interacting with viral proteins, influencing viral assembly and maturation and promoting the formation of ER-derived factories. Future investigations could examine the role of other ER-shaping proteins including Spastin, Lunapark, and other REEP proteins that are involved in the regulation of ER shape through microtubule dynamics, stabilization of three-way ER tubular junctions, and formation and stabilization of the ER curvature, respectively. It will be worth investigating if ER-shaping proteins are involved in ZIKV-induced cytoskeleton modifications [12] and the formation of vacuoles to understand if these proteins are related to ER stress, innate sensing of infection, and viral replication [30] [8] [29]. The interplay between different ER-shaping proteins [31] within the context of viral infection is also of potential interest. Finally, since mutations in several of the ER-shaping proteins are associated with inherited neurological complications, it would be interesting to determine if they are implicated in the pathology induced by neurotropic flaviviruses in relevant cell and animal models [32].

Acknowledgments

The authors would like to thank the UtechS Photonic BioImaging (Imagopole), C2RT, Institut Pasteur (supported by the French National Research Agency; France BioImaging; ANR-10–INSB–04; Investments for the Future) for confocal imaging and Philippe Roingeard's team (Université de Tours) for generating the electron microscope image. The authors also thank Beatrice de Cougny for her graphic design assistance and Ludivine Grzelak for her artistic insights.

References

1. Goyal U, Blackstone C. Untangling the web: mechanisms underlying ER network formation. Biochim Biophys Acta. 2013; 1833(11):2492–8. Epub 2013/04/23. https://doi.org/10.1016/j.bbamcr.2013.04.009 PMID: 23602970; PubMed Central PMCID: PMC3729797.
2. Inoue T, Tsai B. How viruses use the endoplasmic reticulum for entry, replication, and assembly. Cold Spring Harb Perspect Biol. 2013; 5(1):a013250. Epub 2013/01/04. https://doi.org/10.1101/cshperspect.a013250 PMID: 23284050; PubMed Central PMCID: PMC3579393.
3. Chatel-Chaix L, Bartenschlager R. Dengue virus- and hepatitis C virus-induced replication and assembly compartments: the enemy inside—caught in the web. J Virol. 2014; 88(11):5907–11. Epub 2014/03/14. https://doi.org/10.1128/JVI.03404-13 PMID: 24623440; PubMed Central PMCID: PMC4093888.
4. Rothan HA, Kumar M. Role of Endoplasmic Reticulum-Associated Proteins in Flavivirus Replication and Assembly Complexes. Pathogens. 2019; 8(3). Epub 2019/09/25. https://doi.org/10.3390/pathogens8030148 PMID: 31547236; PubMed Central PMCID: PMC6789530.
5. Zhang R, Miner JJ, Gorman MJ, Rausch K, Ramage H, White JP, et al. A CRISPR screen defines a signal peptide processing pathway required by flaviviruses. Nature. 2016; 535(7610):164–8. Epub 2016/07/08. https://doi.org/10.1038/nature18625 PMID: 27383988; PubMed Central PMCID: PMC4945490.
6. Marceau CD, Puschnik AS, Majzoub K, Ooi YS, Brewer SM, Fuchs G, et al. Genetic dissection of Flaviviridae host factors through genome-scale CRISPR screens. Nature. 2016; 535(7610):159–63. Epub 2016/07/08. https://doi.org/10.1038/nature18631 PMID: 27383987; PubMed Central PMCID: PMC4964798.
7. Coyaud E, Ranadheera C, Cheng D, Goncalves J, Dyakov BJA, Laurent EMN, et al. Global Interactomics Uncovers Extensive Organellar Targeting by Zika Virus. Mol Cell Proteomics. 2018; 17(11):2242–55. Epub 2018/07/25. https://doi.org/10.1074/mcp.TIR118.000800 PMID: 30037810; PubMed Central PMCID: PMC6210227.
8. Monel B, Compton AA, Bruel T, Amraoui S, Burlaud-Gaillard J, Roy N, et al. Zika virus induces massive cytoplasmic vacuolization and paraptosis-like death in infected cells. EMBO J. 2017; 36(12):1653–68. https://doi.org/10.15252/embj.201695597 PMID: 28473450; PubMed Central PMCID: PMC5470047.

9. Romero-Brey I, Merz A, Chiramel A, Lee JY, Chlanda P, Haselman U, et al. Three-dimensional architecture and biogenesis of membrane structures associated with hepatitis C virus replication. PLoS Pathog. 2012; 8(12):e1003056. Epub 2012/12/14. https://doi.org/10.1371/journal.ppat.1003056 PMID: 23236278; PubMed Central PMCID: PMC3516559.
10. Tolonen N, Doglio L, Schleich S, Krijnse Locker J. Vaccinia virus DNA replication occurs in endoplasmic reticulum-enclosed cytoplasmic mini-nuclei. Mol Biol Cell. 2001; 12(7):2031–46. Epub 2001/07/14. https://doi.org/10.1091/mbc.12.7.2031 PMID: 11452001; PubMed Central PMCID: PMC55651.
11. Welsch S, Miller S, Romero-Brey I, Merz A, Bleck CK, Walther P, et al. Composition and three-dimensional architecture of the dengue virus replication and assembly sites. Cell Host Microbe. 2009; 5 (4):365–75. https://doi.org/10.1016/j.chom.2009.03.007 PMID: 19380115.
12. Cortese M, Goellner S, Acosta EG, Neufeldt CJ, Oleksiuk O, Lampe M, et al. Ultrastructural Characterization of Zika Virus Replication Factories. Cell Rep. 2017; 18(9):2113–23. Epub 2017/03/02. https://doi.org/10.1016/j.celrep.2017.02.014 PMID: 28249158; PubMed Central PMCID: PMC5340982.
13. Miorin L, Romero-Brey I, Maiuri P, Hoppe S, Krijnse-Locker J, Bartenschlager R, et al. Three-dimensional architecture of tick-borne encephalitis virus replication sites and trafficking of the replicated RNA. J Virol. 2013; 87(11):6469–81. Epub 2013/04/05. https://doi.org/10.1128/JVI.03456-12 PMID: 23552408; PubMed Central PMCID: PMC3648123.
14. Gillespie LK, Hoenen A, Morgan G, Mackenzie JM. The endoplasmic reticulum provides the membrane platform for biogenesis of the flavivirus replication complex. J Virol. 2010; 84(20):10438–47. Epub 2010/08/06. https://doi.org/10.1128/JVI.00986-10 PMID: 20686019; PubMed Central PMCID: PMC2950591.
15. Lennemann NJ, Coyne CB. Dengue and Zika viruses subvert reticulophagy by NS2B3-mediated cleavage of FAM134B. Autophagy. 2017; 13(2):322–32. Epub 2017/01/20. https://doi.org/10.1080/15548627.2016.1265192 PMID: 28102736; PubMed Central PMCID: PMC5324851.
16. Park SH, Zhu PP, Parker RL, Blackstone C. Hereditary spastic paraplegia proteins REEP1, spastin, and atlastin-1 coordinate microtubule interactions with the tubular ER network. J Clin Invest. 2010; 120 (4):1097–110. https://doi.org/10.1172/JCI40979 PMID: 20200447; PubMed Central PMCID: PMC2846052.
17. Neufeldt CJ, Cortese M, Scaturro P, Cerikan B, Wideman JG, Tabata K, et al. ER-shaping atlastin proteins act as central hubs to promote flavivirus replication and virion assembly. Nat Microbiol. 2019. Epub 2019/10/23. https://doi.org/10.1038/s41564-019-0586-3 PMID: 31636417.
18. Tang WF, Yang SY, Wu BW, Jheng JR, Chen YL, Shih CH, et al. Reticulon 3 binds the 2C protein of enterovirus 71 and is required for viral replication. J Biol Chem. 2007; 282(8):5888–98. Epub 2006/12/22. https://doi.org/10.1074/jbc.M611145200 PMID: 17182608.
19. Diaz A, Wang X, Ahlquist P. Membrane-shaping host reticulon proteins play crucial roles in viral RNA replication compartment formation and function. Proc Natl Acad Sci U S A. 2010; 107(37):16291–6. Epub 2010/09/02. https://doi.org/10.1073/pnas.1011105107 PMID: 20805477; PubMed Central PMCID: PMC2941330.
20. Wu MJ, Ke PY, Hsu JT, Yeh CT, Horng JT. Reticulon 3 interacts with NS4B of the hepatitis C virus and negatively regulates viral replication by disrupting NS4B self-interaction. Cell Microbiol. 2014; 16 (11):1603–18. Epub 2014/06/06. https://doi.org/10.1111/cmi.12318 PMID: 24898729.
21. Aktepe TE, Liebscher S, Prier JE, Simmons CP, Mackenzie JM. The Host Protein Reticulon 3.1A Is Utilized by Flaviviruses to Facilitate Membrane Remodelling. Cell Rep. 2017; 21(6):1639–54. Epub 2017/11/09. https://doi.org/10.1016/j.celrep.2017.10.055 PMID: 29117567.
22. Roosendaal J, Westaway EG, Khromykh A, Mackenzie JM. Regulated cleavages at the West Nile virus NS4A-2K-NS4B junctions play a major role in rearranging cytoplasmic membranes and Golgi trafficking of the NS4A protein. J Virol. 2006; 80(9):4623–32. Epub 2006/04/14. https://doi.org/10.1128/JVI.80.9.4623-4632.2006 PMID: 16611922; PubMed Central PMCID: PMC1472005.
23. Miller S, Sparacio S, Bartenschlager R. Subcellular localization and membrane topology of the Dengue virus type 2 Non-structural protein 4B. J Biol Chem. 2006; 281(13):8854–63. Epub 2006/01/27. https://doi.org/10.1074/jbc.M512697200 PMID: 16436383.
24. Liu TY, Bian X, Romano FB, Shemesh T, Rapoport TA, Hu J. Cis and trans interactions between atlastin molecules during membrane fusion. Proc Natl Acad Sci U S A. 2015; 112(15):E1851–60. Epub 2015/04/01. https://doi.org/10.1073/pnas.1504368112 PMID: 25825753; PubMed Central PMCID: PMC4403200.
25. Zhao G, Zhu PP, Renvoise B, Maldonado-Baez L, Park SH, Blackstone C. Mammalian knock out cells reveal prominent roles for atlastin GTPases in ER network morphology. Exp Cell Res. 2016; 349(1):32–44. Epub 2016/09/28. https://doi.org/10.1016/j.yexcr.2016.09.015 PMID: 27669642.

26. Liang JR, Lingeman E, Ahmed S, Corn JE. Atlastins remodel the endoplasmic reticulum for selective autophagy. J Cell Biol. 2018; 217(10):3354–67. Epub 2018/08/26. https://doi.org/10.1083/jcb.201804185 PMID: 30143524; PubMed Central PMCID: PMC6168278.

27. Klemm RW, Norton JP, Cole RA, Li CS, Park SH, Crane MM, et al. A conserved role for atlastin GTPases in regulating lipid droplet size. Cell Rep. 2013; 3(5):1465–75. Epub 2013/05/21. https://doi.org/10.1016/j.celrep.2013.04.015 PMID: 23684613; PubMed Central PMCID: PMC3742324.

28. Pawar S, Ungricht R, Tiefenboeck P, Leroux JC, Kutay U. Efficient protein targeting to the inner nuclear membrane requires Atlastin-dependent maintenance of ER topology. Elife. 2017; 6. Epub 2017/08/23. https://doi.org/10.7554/eLife.28202 PMID: 28826471; PubMed Central PMCID: PMC5587084.

29. Steiner B, Swart AL, Welin A, Weber S, Personnic N, Kaech A, et al. ER remodeling by the large GTPase atlastin promotes vacuolar growth of Legionella pneumophila. EMBO Rep. 2017; 18 (10):1817–36. https://doi.org/10.15252/embr.201743903 PMID: 28835546; PubMed Central PMCID: PMC5623866.

30. Monel B, Rajah MM, Hafirassou ML, Sid-Ahmed S, Burlaud-Gaillard J, Zhu PP, et al. The Atlastin ER-shaping proteins facilitate Zika virus replication. J Virol. 2019. Epub 2019/09/20. https://doi.org/10.1128/JVI.01047-19

31. Espadas J, Pendin D, Bocanegra R, Escalada A, Misticoni G, Trevisan T, et al. Dynamic constriction and fission of endoplasmic reticulum membranes by reticulon. Nat Commun. 2019; 10(1):5327. Epub 2019/11/24. https://doi.org/10.1038/s41467-019-13327-7 PMID: 31757972; PubMed Central PMCID: PMC6876568.

32. Zhao J, Hedera P. Hereditary spastic paraplegia-causing mutations in atlastin-1 interfere with BMPRII trafficking. Mol Cell Neurosci. 2013; 52:87–96. https://doi.org/10.1016/j.mcn.2012.10.005 PMID: 23079343; PubMed Central PMCID: PMC3587122.

AMERICAN SOCIETY FOR MICROBIOLOGY | Journal of Virology®

VIRUS-CELL INTERACTIONS

Atlastin Endoplasmic Reticulum-Shaping Proteins Facilitate Zika Virus Replication

Blandine Monel,[a] Maaran Michael Rajah,[a,b] Mohamed Lamine Hafirassou,[c] Samy Sid Ahmed,[a] Julien Burlaud-Gaillard,[d] Peng-Peng Zhu,[e] Quentin Nevers,[a] Julian Buchrieser,[a] Françoise Porrot,[a] Cécile Meunier,[a] Sonia Amraoui,[a] Maxime Chazal,[f] Audrey Salles,[g] Nolwenn Jouvenet,[f] Philippe Roingeard,[d] Craig Blackstone,[e] Ali Amara,[c] Olivier Schwartz[a]

[a]Institut Pasteur, Virus and Immunity Unit, CNRS-UMR3569, Paris, France
[b]Ecole Doctorale Bio Sorbonne Paris Cité (BioSPC)–Université Paris Diderot, Paris, France
[c]Equipe Biologie Cellulaire des Infections Virales, INSERM U944 CNRS 7212, Centre de Recherche Saint-Louis, Paris, France
[d]INSERM U1259–Plateforme IBiSA de Microscopie Electronique, Université et CHU de Tours, Tours, France
[e]Cell Biology Section, Neurogenetics Branch, National Institutes of Health, Bethesda, Maryland, USA
[f]Institut Pasteur, Viral Genomics and Vaccination Unit, Paris, France
[g]Institut Pasteur, UtechS Photonic BioImaging PBI (Imagopole), Centre de Recherche et de Resources Technologiques C2RT, Paris, France

ABSTRACT The endoplasmic reticulum (ER) is the site for Zika virus (ZIKV) replication and is central to the cytopathic effects observed in infected cells. ZIKV induces the formation of ER-derived large cytoplasmic vacuoles followed by "implosive" cell death. Little is known about the nature of the ER factors that regulate flavivirus replication. Atlastins (ATL1, -2, and -3) are dynamin-related GTPases that control the structure and the dynamics of the ER membrane. We show here that ZIKV replication is significantly decreased in the absence of ATL proteins. The appearance of infected cells is delayed, the levels of intracellular viral proteins and released virus are reduced, and the cytopathic effects are strongly impaired. We further show that ATL3 is recruited to viral replication sites and interacts with the nonstructural viral proteins NS2A and NS2B3. Thus, proteins that shape and maintain the ER tubular network ensure efficient ZIKV replication.

IMPORTANCE Zika virus (ZIKV) is an emerging virus associated with Guillain-Barré syndrome, and fetal microcephaly as well as other neurological complications. There is no vaccine or specific antiviral treatment against ZIKV. We found that endoplasmic reticulum (ER)-shaping atlastin proteins (ATL1, -2, and -3), which induce ER membrane fusion, facilitate ZIKV replication. We show that ATL3 is recruited to the viral replication site and colocalize with the viral proteins NS2A and NS2B3. The results provide insights into host factors used by ZIKV to enhance its replication.

KEYWORDS atlastin, Zika, endoplasmic reticulum

Flaviviruses are transmitted to vertebrate hosts by mosquitoes or ticks. Dengue virus (DENV), Yellow fever virus (YFV), West Nile virus (WNV), and Zika virus (ZIKV) are highly pathogenic to humans and constitute major international health problems. The recent ZIKV epidemics, associated with neurological disorders such as Guillain-Barré syndrome and microcephaly, provoked a public health emergency in 2016 (1, 2). An intensive research effort led to important progress regarding ZIKV epidemiology, diagnosis, and potential therapeutic and prophylactic strategies (3–5). The mechanisms involved in ZIKV replication, host responses, and pathogenesis have also been extensively studied (6, 7). However, the role of cellular proteins, in particular those present in the endoplasmic reticulum (ER), where viral production occurs, remains only partly characterized.

The ZIKV genome consists of a single-stranded positive-sense RNA encoding a

Citation Monel B, Rajah MM, Hafirassou ML, Sid Ahmed S, Burlaud-Gaillard J, Zhu P-P, Nevers Q, Buchrieser J, Porrot F, Meunier C, Amraoui S, Chazal M, Salles A, Jouvenet N, Roingeard P, Blackstone C, Amara A, Schwartz O. 2019. Atlastin endoplasmic reticulum-shaping proteins facilitate Zika virus replication. J Virol 93:e01047-19. https://doi.org/10.1128/JVI.01047-19.

Editor Mark T. Heise, University of North Carolina at Chapel Hill

Copyright © 2019 American Society for Microbiology. All Rights Reserved.

Address correspondence to Blandine Monel, blandine.monel@pasteur.fr, or Olivier Schwartz, olivier.schwartz@pasteur.fr.

B.M. and M.M.R. contributed equally to this article.

Received 21 June 2019
Accepted 8 September 2019
Accepted manuscript posted online 18 September 2019
Published 13 November 2019

Downloaded from https://journals.asm.org/journal/jvi on 05 October 2021 by 157.99.64.254.

polyprotein precursor that gives rise to seven nonstructural (NS) and three structural proteins (capsid C, premembrane prM, and envelope E). Cellular receptors for the virus include AXL and Tim-1 (8, 9). After endocytosis, pH-dependent fusion of viral and endosomal membranes, uncoating, and release of the viral material into the cytoplasm, the subsequent steps of the viral life cycle, including RNA replication, synthesis of viral proteins, and particle assembly, take place in the ER (10–15). The viral genome serves as mRNA for protein synthesis (16, 17). The viral polyprotein is processed by cellular and viral (NS3/NS2B, also termed NS2B3) proteases. NS proteins form a replication complex (RC) with cellular factors that induces membrane rearrangements and formation of novel organelles (14, 18, 19). NS2A and NS4A/B proteins contain helices that reside in the plane of the ER-luminal membrane leaflets, thereby increasing their surface. The membrane curvature is further induced by oligomerization of NS4A, which interacts with NS4B and NS1. There, the viral positive-strand RNA is copied into a negative-strand intermediate that serves as a template for RNA replication performed by NS5 polymerase and NS3 helicase (14, 20).

Remodeling of the ER and accumulation of viral proteins trigger a stress pathway and activate the unfolded protein response (UPR) (21–23). Uncontrolled UPR response leads to cell death and instigate inflammation. We recently showed that ZIKV induces massive ER-derived vacuolization and UPR, followed by paraptosis, a nonapoptotic form of cell death (23). Therefore, in addition to serving as the site for virus replication and production, the ER is central to the death of infected cells.

The ER is a complex architecture of membranes comprising the nuclear envelope, peripheral sheets, and an interconnected network of tubules. The structure and dynamic nature of the ER allow it to be involved in many processes, including protein production and degradation, cell signaling, and the synthesis and distribution of lipids. Several proteins that shape the ER have been identified. Proteins of the reticulon (RTN) and receptor expression enhancing protein (REEP) families generate curves in membranes and act to maintain the tubules (24–26). Atlastin proteins (ATLs) mediate the tethering and fusion of tubules to one other to form three-way junctions (27, 28), which are stabilized by the Lunapark protein (26). ATLs are large dynamin-related GTPases that dimerize in *cis* and *trans* to allow fusion of adjacent ER membranes. Humans have three ATLs (ATL1, ATL2, and ATL3), with redundant activities and various levels of expression in different cell types (29). Several other proteins help the ER to maintain contact with the plasma membrane, other compartments, and the cytoskeleton (25). Mutations in ATL1 and ATL3 or other ER-shaping proteins are associated with neurological diseases, such as hereditary sensory neuropathy and spastic paraplegia, and are characterized by axon and dendrite growth deficits (30–36).

Reticulon 3.1A (RTN3.1A) is used by flaviviruses to facilitate ER membrane remodeling (37), but the role of other ER-shaping proteins is uncharacterized. Here, we report that ATL proteins enhance ZIKV replication and cytopathic effects. We further characterize the underlying viral and cellular mechanisms and report that ATL3 is recruited to viral replication sites and interacts with NS2A and NS2B3.

RESULTS

Silencing of the ATL proteins impairs ZIKV replication and vacuole formation. We first sought to determine whether ATLs impact ZIKV spread. HeLa cells express ATL2 and ATL3 and background levels of ATL1 (29). We silenced ATL1, -2, and -3 (ATL1/2/3) by using small interfering RNA (siRNA) in these cells. As a positive control, we silenced dolichyl-diphosphooligosaccharide protein glycosyltransferase (DDOST), an ER enzyme required for ZIKV replication (38–41). Silencing reduced by 80 to 90% the levels of ATL1/2/3 or DDOST mRNA, respectively, as measured by quantitative reverse transcription-PCR (RT-qPCR), without affecting cell viability (Fig. 1A and B). HeLa cells were then challenged with an African isolate of ZIKV (HD78788, referred to as HD78) at different multiplicities of infection (MOIs). Viral replication was followed over time by flow cytometry, by measuring the frequency of cells harboring the viral envelope (E) protein, using the pan-flavivirus anti-E antibody 4G2 (Fig. 1C). Silencing of ATL significantly

Downloaded from https://journals.asm.org/journal/jvi on 05 October 2021 by 157.99.64.254.

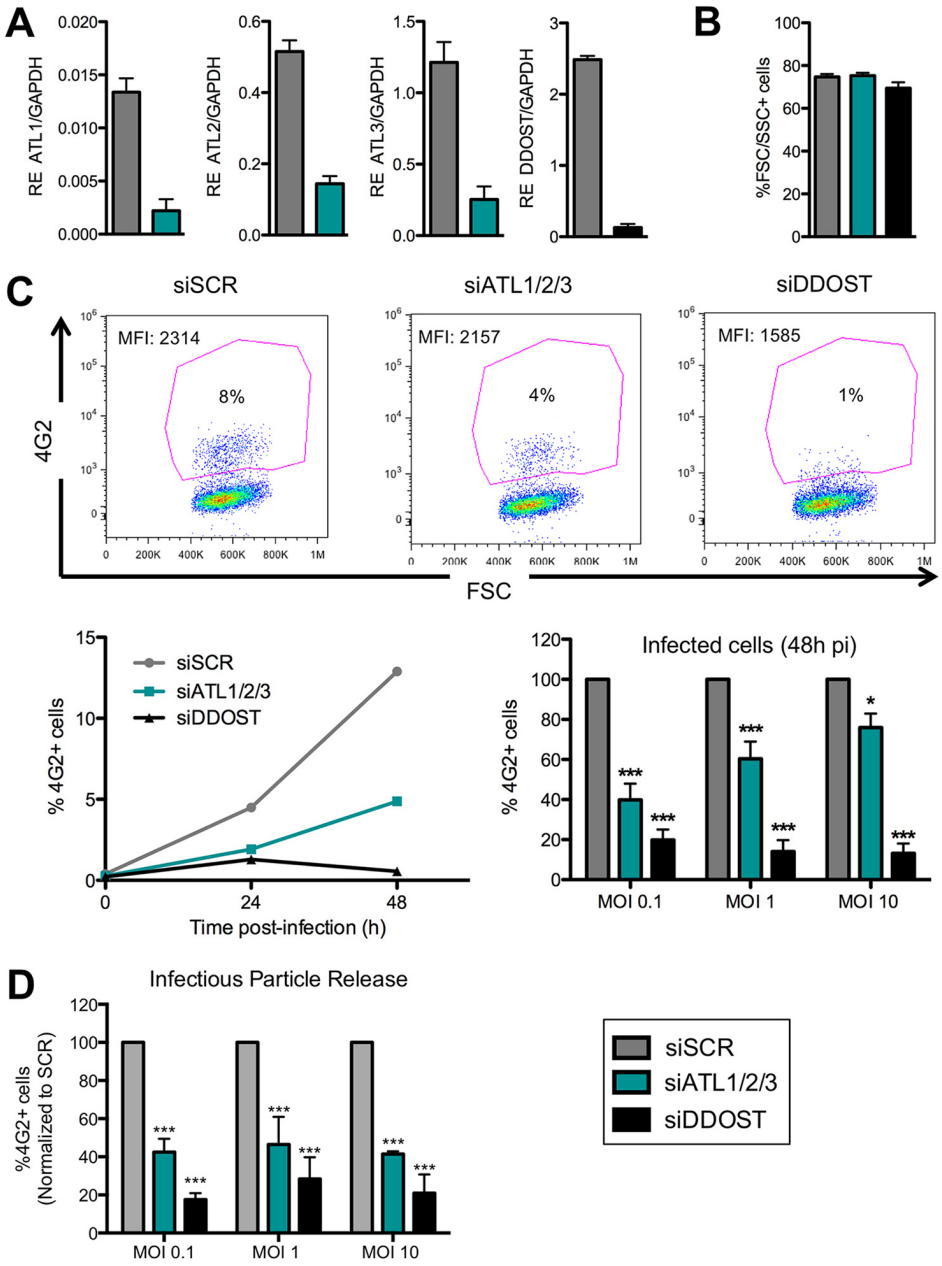

FIG 1 Silencing of ATL impairs ZIKV replication. (A) HeLa cells were transfected with siRNAs targeting a control scrambled RNA (siSCR), dolichyl-diphosphooligosaccharide–protein glycosyltransferase RNA (siDDOST), or targeting ATL1, ATL2, and ATL3 (siATL1/2/3). The efficiency of the silencing was checked by RT-qPCR at 3 days posttransfection. The relative expression of each RNA compared to GAPDH is shown. (B) Cell viability was assessed by flow cytometry after 4 days of siRNA treatment using forward- and side-scatter parameters. (C) Cells were infected with ZIKV HD78 (at the indicated MOI), and the percent E-positive cells was determined by flow cytometry at 48 h p.i. using 4G2 antibody. (Upper panel) Representative experiment (MOI of 1 at 48 h p.i.) showing fluorescence-activated cell sorting (FACS) dot plots. (Left panel) Representative experiment showing kinetics (MOI of 1). (Right panel) Means ± the standard errors of the mean (SEM) of five independent experiments at 48 h p.i. (D) Supernatants from infected cells (at 24 h p.i.) were used to infect fresh HeLa cells. The percent E-positive cells was determined at 24 h p.i. The means ± the SEM of three independent experiments are shown. Statistical significance was determined by using analysis of variance (ANOVA) and Bonferroni posttests. ***, $P < 0.001$; **, $P < 0.01$; *, $P < 0.05$.

decreased viral replication. The effect of ATL silencing was more marked at a low MOI. As expected, ZIKV replication was abrogated in the absence of DDOST. We next assessed the release of infectious virus in the medium. To this aim, supernatants were harvested at 24 h and exposed to fresh cells. The release of infectious

Downloaded from https://journals.asm.org/journal/jvi on 05 October 2021 by 157.99.64.254.

particles was significantly decreased in cells where ATL or DDOST had been silenced (Fig. 1D).

We previously described the appearance of large ER-derived cytoplasmic vacuoles in ZIKV infected cells (23). In ATL-silenced ZIKV-infected HeLa cells, the formation of these vacuoles was strongly decreased at 24 h, as assessed by light microscopy and visual scoring (Fig. 2A and B). The fraction of cells displaying vacuoles remained low, even at a high viral inoculum (MOI of 10) and at a later time point (48 h postinfection [p.i.]), when about 60% of the cells were $4G2^+$. To provide ultrastructural detail, we performed transmission electron microscopy of ZIKV-infected cells at 24 h p.i. (MOI of 10) (Fig. 2C). As expected, large intracellular vacuoles were observed in control infected cells. These vacuoles were much smaller and rarer in the absence of ATL (Fig. 2). In infected cells treated with the control RNAi, we observed membrane alterations and electron-dense structures with enlarged ERs, convoluted membranes, and spherule-like structures (Fig. 3). Virions were observed in these rearranged structures as single or clustered particles within membrane invaginations (Fig. 3). A similar alteration of the ER morphology and the presence of virus particles were observed in ATL-silenced cells. It was difficult to precisely quantify the number of vesicle pockets containing virions with this technique. However, at the high MOI required for transmission electron microscopy experiments, we observed a trend to a decreased number of pockets in the absence of ATL (Fig. 3).

We next examined the role of ATL1/2/3 in primary human adult dermal fibroblasts (HDFa), which represent natural target cells for the virus upon mosquito bite. Silencing of ATL1/2/3 by siRNA resulted in decreased production of viral proteins (Fig. 4A to C). The large intracellular vacuoles were no longer visible in the absence of ATL (Fig. 4D).

ZIKV replication and cytopathic effects in ATL KO cells. To further characterize the role of ATL, we generated an ATL 2/3 double-knockout (dKO) HeLa cell clone, termed 21/1 dKO (and referred to here as dKO) by CRISPR-mediated gene editing (42). We did not target ATL1, which is expressed at background levels in HeLa cells. In dKO cells, DNA sequencing revealed mutations prematurely truncating ATL proteins (42; also, data not shown). Western Blot with an anti-ATL3 antibody confirmed a strong decrease of protein levels in dKO cells, compared to parental (WT) cells (Fig. 5A). We could not assess ATL2 levels, due to the lack of commercially available antibodies. As controls, we stably reexpressed a wild-type (WT) or a GTPase-deficient (ATL3 KA) mutant in dKO cells. We also introduced a wild-type myc-tagged protein (ATL3 myc) to facilitate imaging studies. These proteins were readily detected by Western blotting in reconstituted cells (Fig. 5A). As previously described in another cell line (3T3-derived cells) (42), the shape of the ER was modified in dKO cells (Fig. 5B). Staining of the cells with a red fluorescent ER tracker and analysis by super-resolution microscopy demonstrated a disrupted peripheral ER tubular network. These morphology changes were rescued by WT ATL3 or ATL3-myc, whereas cells expressing the GTPase-defective ATL3KA mutant retained an abnormal ER (Fig. 5B).

We then assessed ZIKV replication in these cells. Viral spread was decreased by more than 2-fold in dKO cells compared to WT cells (Fig. 6A), confirming the results obtained with siRNAs. Viral replication was rescued in dKO reexpressing WT ATL3 and not the KA mutant (Fig. 6A). We also observed a marked decrease of vacuole formation in dKO-infected cells (Fig. 6B). Again, reexpression of WT, but not that of ATL3 KA mutant, restored a rapid appearance of vacuoles. At a later time point (72 h p.i.), the fraction of dying cells was augmented in the presence of functional ATL3 proteins (Fig. 6C). As observed with siRNAs, the release of infectious particles was also significantly decreased in dKO cells and rescued with ATL3, as assessed by a flow-cytometry based assay. These results were also supported by a traditional plaque assay (data not shown). In addition to the African ZIKV strain HD78, replication of three Asian-lineage strain (FG16, PF13, and NC14) ZIKV isolates was also impaired in the absence of ATL (Fig. 6D).

Downloaded from https://journals.asm.org/journal/jvi on 05 October 2021 by 157.99.64.254.

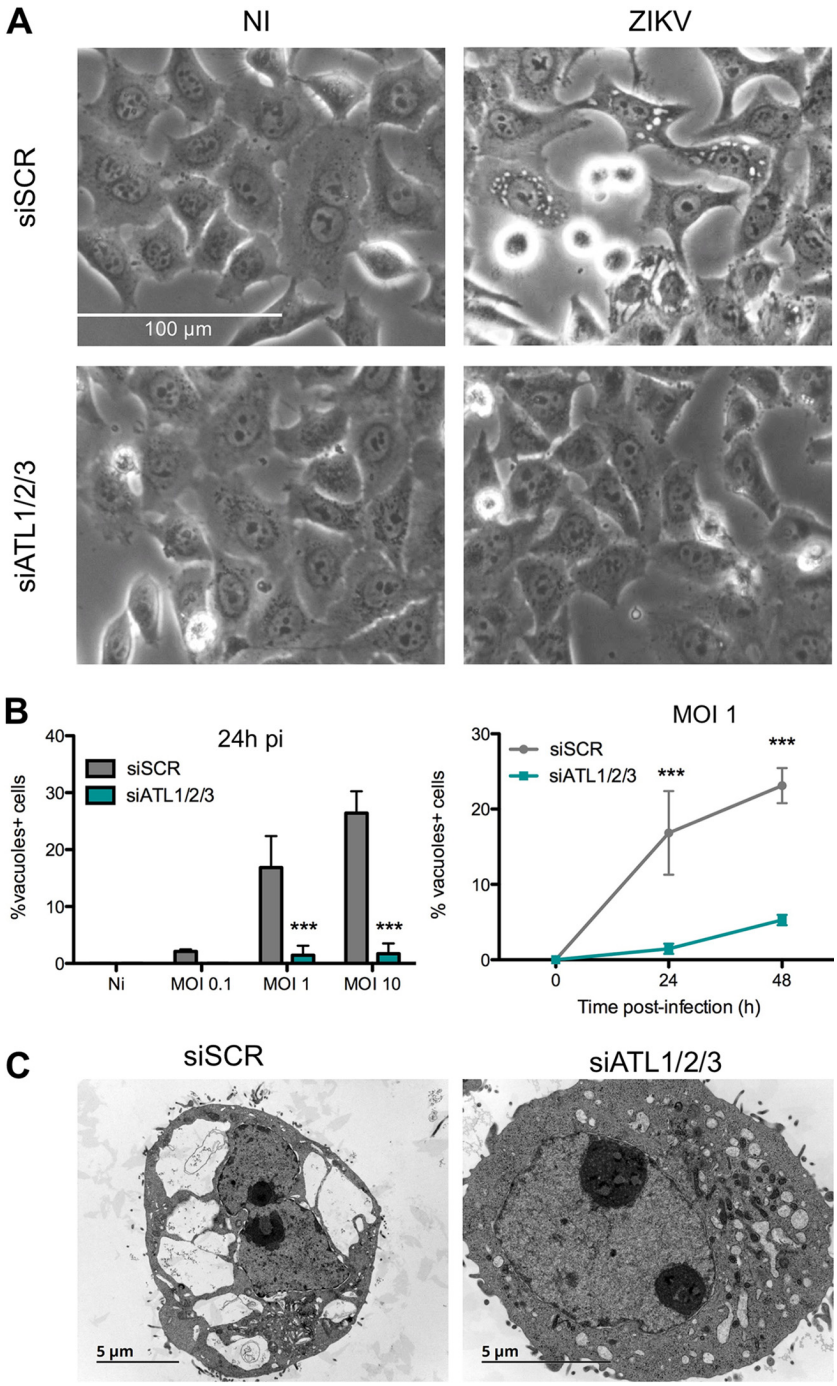

FIG 2 Silencing of ATL impairs ZIKV-induced vacuoles. (A) HeLa siSCR or siATL1/2/3 cells infected or not with ZIKV (MOI of 10) were observed by light microscopy at 24 h p.i. to visualize virus-induced vacuoles. (B) Cells infected with ZIKV were observed by light microscopy at 24 h p.i., and the percentage of vacuole-positive cells was calculated. (C) HeLa siSCR or siATL1/2/3 cells infected or not with ZIKV (MOI of 10) were observed by transmission electron microscopy at 24 h p.i. to visualize virus-induced vacuoles. (Left) Percent vacuoles and cells quantified at 24 h p.i. at the indicated MOI. (Right) Percent vacuoles and cells at the indicated times (MOI of 1). The means ± the SEM of three independent experiments are shown. Statistical significance was determined by using ANOVA and Bonferroni posttests. ***, $P < 0.001$.

To rule out a clone-dependent effect on ZIKV replication, we used another HeLa dKO clone. In the absence of infection, the viability and growth kinetics of the two dKO clones were similar to the parental HeLa cells. ZIKV replication was impaired in both clones (not shown).

Downloaded from https://journals.asm.org/journal/jvi on 05 October 2021 by 157.99.64.254.

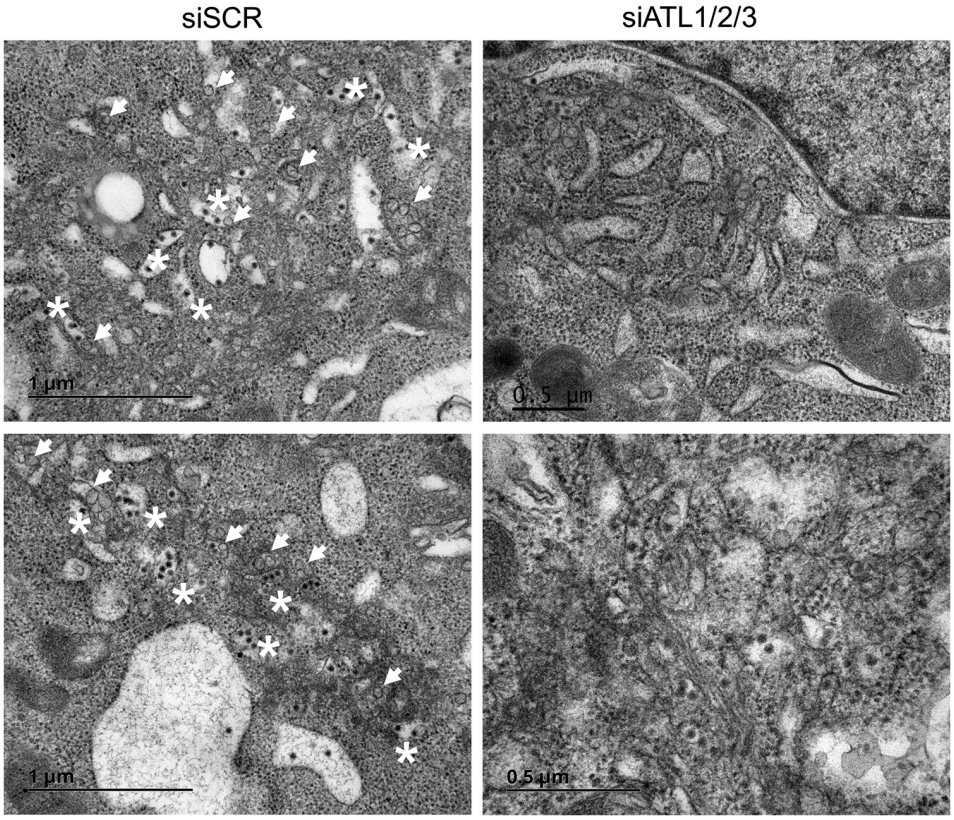

FIG 3 Ultrastructural analysis of ZIKV-infected HeLa cells. HeLa siSCR or siATL1/2/3 cells infected with ZIKV (MOI of 10) were observed by electron microscopy at 24 h p.i. Two representative pictures are shown for each condition. White arrows, examples of ZIKV-induced spherules (vRNA replication); white asterisks, examples of viral particles.

Altogether, our results obtained in either silenced or knocked out cells indicate that ATL proteins facilitate the replication of ZIKV strains of different origins and enhance the formation of ER-derived vacuoles in infected cells.

ER modifications in ZIKV-infected WT and dKO cells. ZIKV infection induces a profound modification of the topography of ER that can be visualized by immunofluorescence or transmission electron microscopy. To study the impact of ATL on these changes, we generated WT or dKO cells stably expressing a fluorescent Sec61β-mEmmerald protein (Fig. 7). Sec61 is the main protein translocation complex of the ER membrane. As expected, in the absence of infection, in HeLa WT cells, Sec6β was mainly detected in a perinuclear region, associated with a dispersed staining throughout the cytoplasm. A similar global pattern was observed in dKO cells. Analysis by super-resolution confirmed the presence of an abnormal tubular ER (not shown).

We visualized cells using time-lapse fluorescence microscopy after incubation with virus, with images acquired every 5 min for up to 24 h. Representative examples are shown in Fig. 7A (see also Videos S1 and S2 in the supplemental material). In both WT and dKO cells, ZIKV modified the aspect of the ER, with a condensation and intensification the Sec61β signal that was visible at 12 to 16 h p.i. In WT cells, this contraction of the ER was followed by formation of cytoplasmic vacuoles and cell death (Fig. 7A; see Videos S1 and S2). The vacuoles were surrounded by Sec61β, supporting our finding that they originate from the ER (23). In dKO cells, the changes in ER topology were much less associated with vacuolization (Fig. 7), confirming our results obtained by optic and electron microscopy (Fig. 2). We then examined viral production sites and ATL localization by confocal microscopy. As expected, in both WT and dKO cells, the viral protein E accumulated in the ER, in a region enriched for Sec61β (Fig. 7B). In noninfected cells, ATL3, visualized with an anti-myc antibody, appeared as a dispersed signal

Downloaded from https://journals.asm.org/journal/jvi on 05 October 2021 by 157.99.64.254.

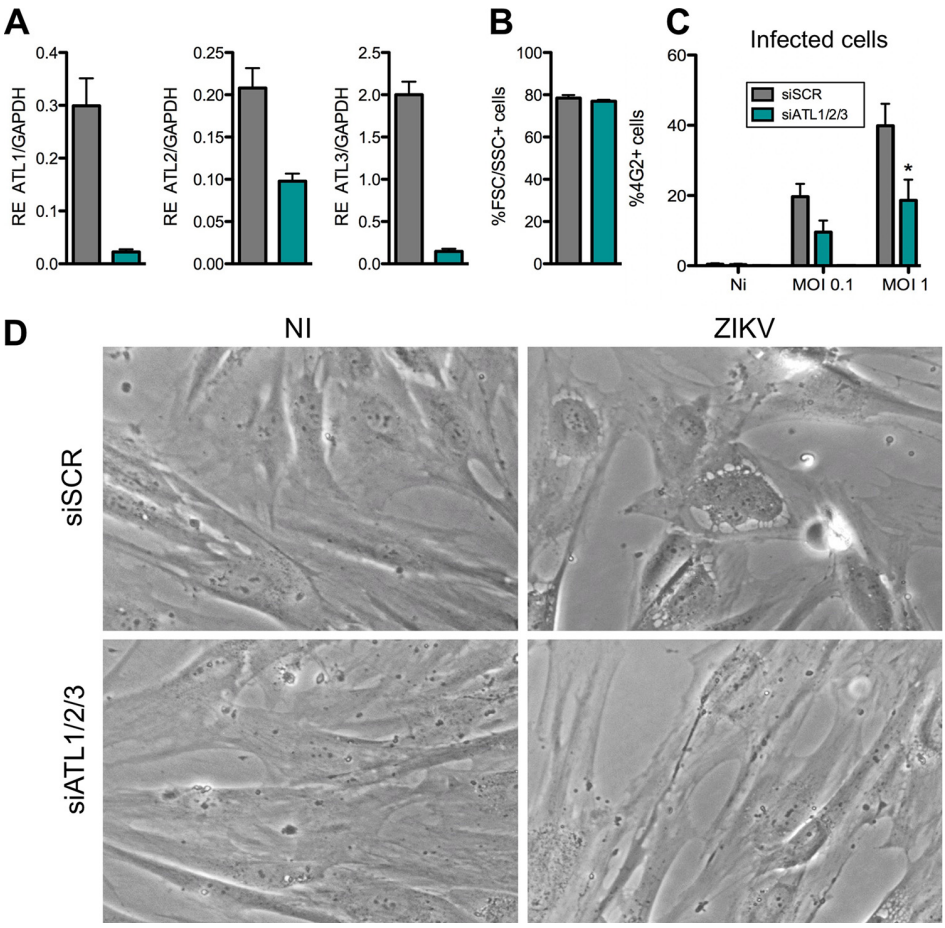

FIG 4 Silencing of ATL impairs ZIKV replication in primary adult human dermal fibroblast (HDFa) cells. (A) HDFa cells were transfected with siRNAs targeting a control scrambled RNA (siSCR) or targeting ATL1, ATL2, and ATL3 (siATL1/2/3). The efficiency of the silencing was checked by RT-qPCR at 3 days posttransfection. The relative expression of each RNA compared to GAPDH is shown. (B) Cell viability was assessed by flow cytometry after 4 days of siRNA treatment using forward- and side-scatter parameters. (C) Cells were infected with ZIKV HD78 (at the indicated MOI), and the percent E-positive cells was determined by flow cytometry at 48 h p.i. using 4G2 antibody. (Left) Representative experiment (MOI of 1). (Right) Means ± the SEM of three independent experiments at 48 h p.i. The statistical significance was determined by using ANOVA and Bonferroni posttests. *, $P < 0.05$. (D) Cells infected or not with ZIKV (MOI of 1) were observed by light microscopy at 24 h p.i. to visualize virus-induced vacuoles.

throughout the cytoplasm, with dots that likely correspond to three-way ER junctions (26) (Fig. 8). ZIKV induced a profound modification of ATL3 repartition, corresponding to ER morphological changes (Fig. 8).

Therefore, ATL3 is present at viral replication or viral production sites. In infected cells, ATLs are not required for global ER rearrangements triggered by the virus but enhance the formation of vacuoles and cytopathic effects.

ATLs enhance viral production after ZIKV entry and interact with NS proteins. We next studied how ATL positively impacts ZIKV spread. We first measured viral binding and entry in HeLa WT and dKO cells. The cells were exposed to ZIKV for 1 h at 4°C at two MOIs. The viral input was then removed, and half of the cells were harvested to quantify bound particles. The other half was kept at 37°C for two additional hours to allow endocytosis and fusion, and extracellular bound particles were removed with a trypsin treatment. Trypsin eliminated >90% of bound viral RNA (not shown). Viral RNA was quantified by RT-qPCR (Fig. 9A and B). The signal was proportional to the MOI, indicating that nonsaturating conditions were used. We did not observe any difference in viral binding and entry between the two cell types. To further study the impact of

Downloaded from https://journals.asm.org/journal/jvi on 05 October 2021 by 157.99.64.254.

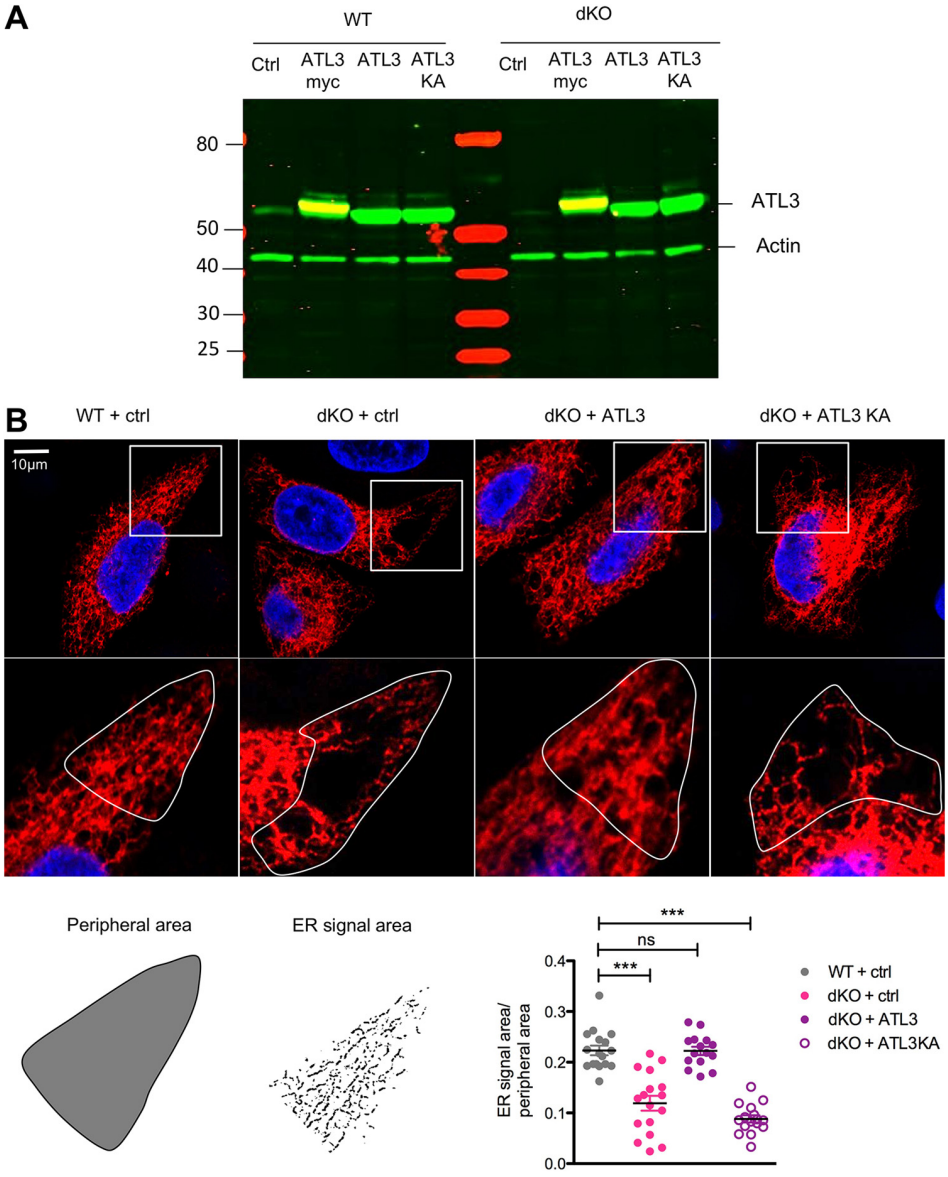

FIG 5 Characterization of ATL KO HeLa cells. (A) HeLa cells were knocked out for ATL2 and ATL3 genes (dKO) using CRISPR. HeLa WT or dKO cells were then transduced to express exogenous ATL3-myc, ATL3 WT, or ATL3 mutated in the GTPase activity domain (ATL3KA). ATL3 expression was assessed by Western blotting. Actin was used as a loading control. (B) HeLa WT or dKO cells transduced with control (ctrl), ATL3 WT, or ATL3KA vectors and expressing an ER-tracker dsRed2 were examined by confocal microscopy to observe the structure of the peripheral ER tubular network. Three-way junctions were quantified as previously described (42). At least three cells per condition per experiment from three independent experiments were analyzed and plotted. Statistical significance was determined by using a one-way ANOVA test and a Dunnett posttest. ***, $P < 0.001$.

ATLs on viral RNA amplification, we transfected WT and dKO cells with RNA produced from a ZIKV infectious clone expressing a reporter luciferase (43). The ZIKV RNA triggered a luciferase signal that increased over time in WT cells and remained low in dKO cells (Fig. 9C). Similar results were obtained when cells were treated with NH_4Cl, an inhibitor of vesicular acidification that prevents secondary cycles of viral replication (Fig. 9C). Therefore, ATLs do not improve the early steps of the viral life cycle but facilitate viral RNA production and/or accumulation after viral entry.

We hypothesized that ATL may interact with NS proteins, as previously suggested in an interactome study (44). To test this hypothesis, we performed a coimmunoprecipitation of ATL3-myc and individual NS-HA proteins upon transfection in 293T cells. This

Downloaded from https://journals.asm.org/journal/jvi on 05 October 2021 by 157.99.64.254.

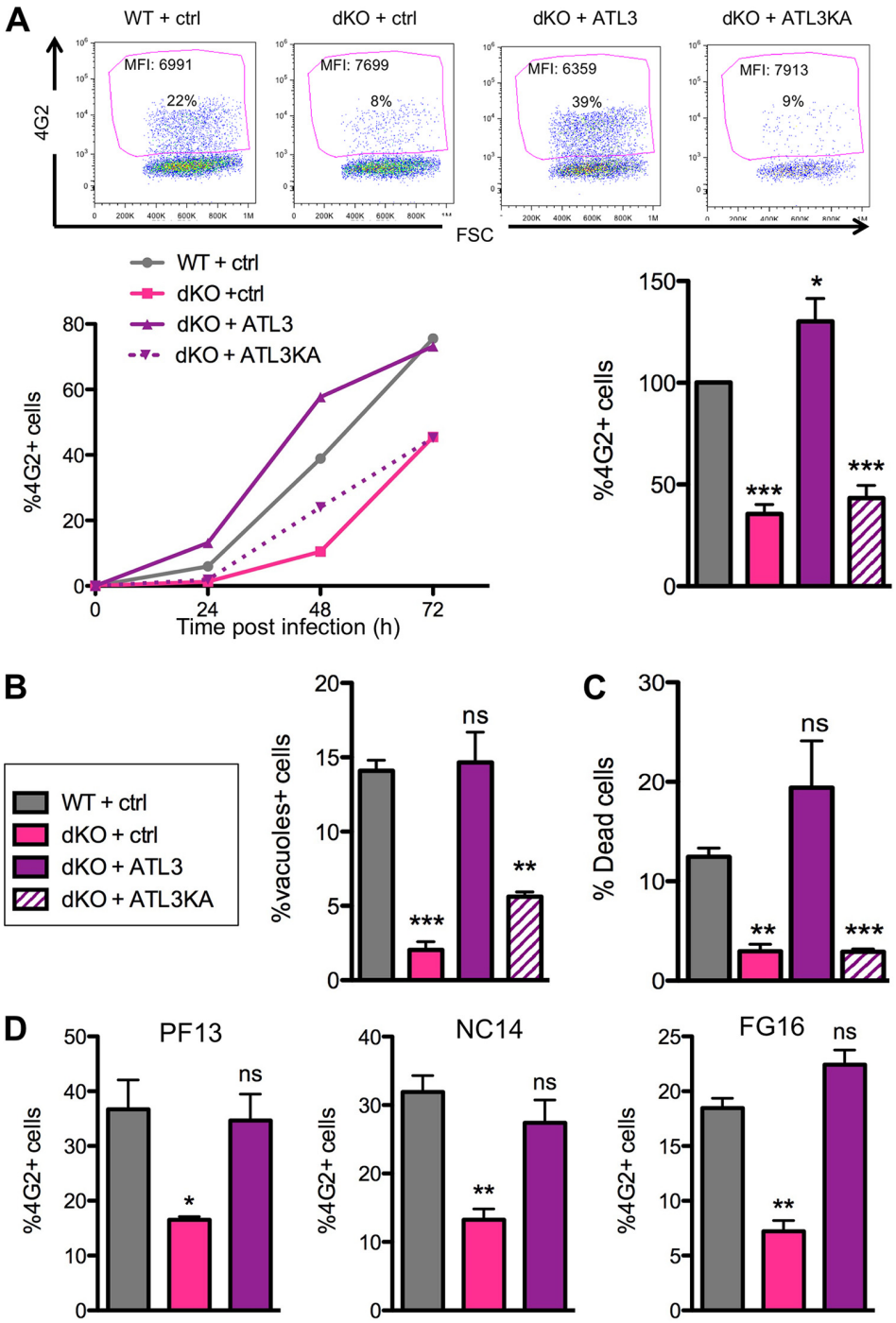

FIG 6 Knockout of ATL impairs ZIKV replication. (A) HeLa WT or dKO cells, transduced with control (ctrl), ATL3 WT, or ATL3KA vectors were infected with ZIKV (MOI of 0.1). The percentage of E^+ cells was monitored over time by flow cytometry using 4G2 antibody. (Upper panels) Representative FACS dot plots. (Lower left panel) A representative experiment. (Lower right panel) Means ± the SEM of five independent experiments at 48 h p.i. (B) Percent vacuoles and cells quantified at 24 h p.i. (MOI of 1). The means ± the SEM of three independent experiments are shown. (C) The percent dead cells were quantified at 72 h p.i. (MOI of 0.1) by Live/Dead staining and flow cytometry. The means ± the SEM of three independent experiments are shown. (D) HeLa WT or dKO cells transduced with control (ctrl) or ATL3 WT vectors were infected with ZIKV PF13, NC14, or ZIKV FG16 (MOI of 0.01), and the percent E^+ cells was determined by flow cytometry at 48 h p.i. The means ± the SEM of three independent experiments are shown. Statistical significance was determined by using a *t* test in comparison to the WT+Ctrl condition. ***, $P < 0.001$; **, $P < 0.01$; *, $P < 0.05$.

Downloaded from https://journals.asm.org/journal/jvi on 05 October 2021 by 157.99.64.254.

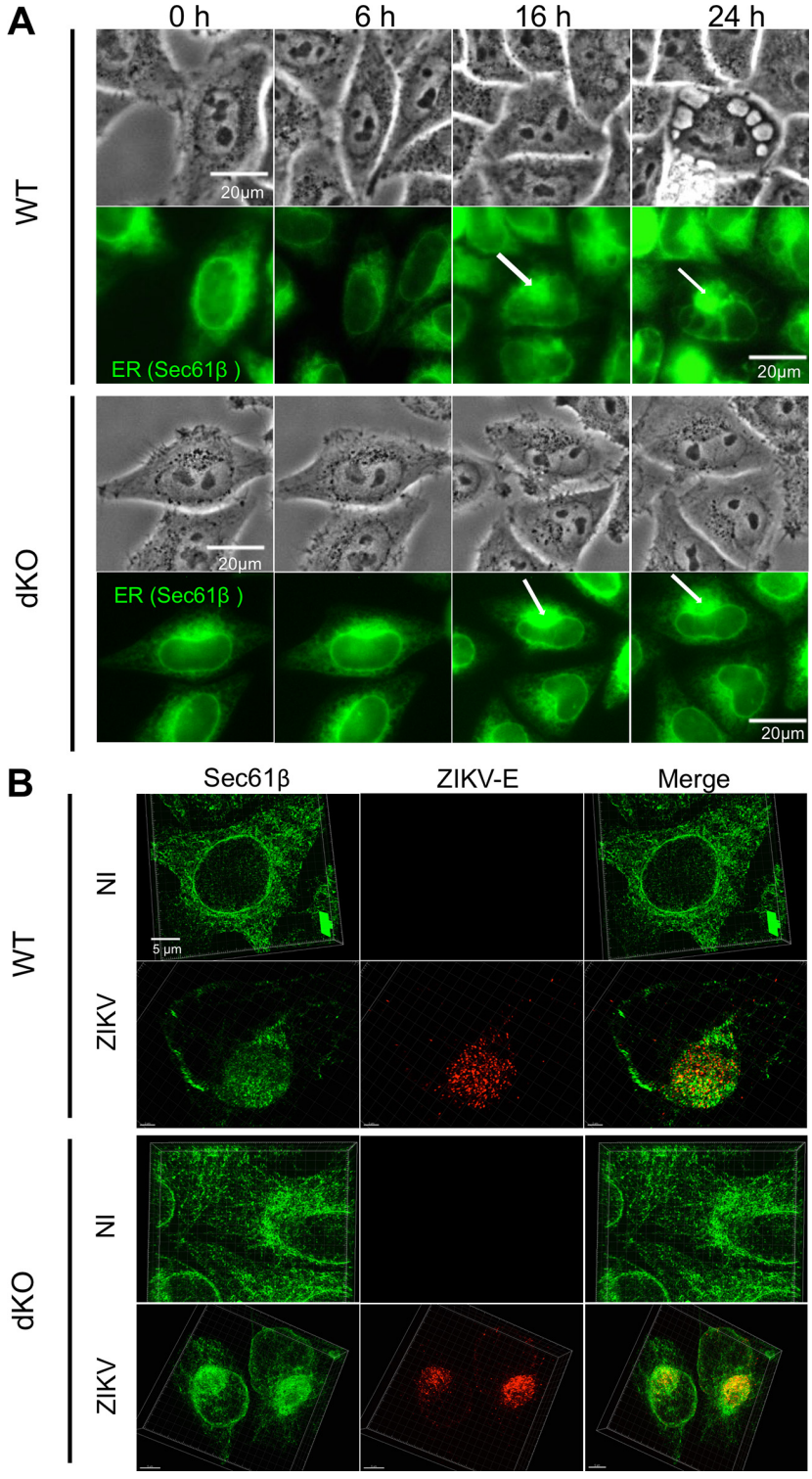

FIG 7 Impact of ATL on ZIKV-induced ER relocation. HeLa WT or dKO cells expressing a fluorescent Sec61β-mEmmerald ER protein (green) were infected with ZIKV (MOI of 1). (A) The ER structure was observed by time-lapse microscopy for 24 h. Still images extracted from Video S1 in the supplemental material are shown for transmitted light and Sec61β at the specified time points. White arrows indicate ZIKV-induced ER relocation. (B) HeLa WT or HeLa cells expressing Sec61β-mEmmerald (green) were infected or not for 24 h with ZIKV (MOI of 1). Cells were fixed and stained for the viral E protein (red) and observed by super-resolution imaging (SIM). A representative image is shown.

Downloaded from https://journals.asm.org/journal/jvi on 05 October 2021 by 157.99.64.254.

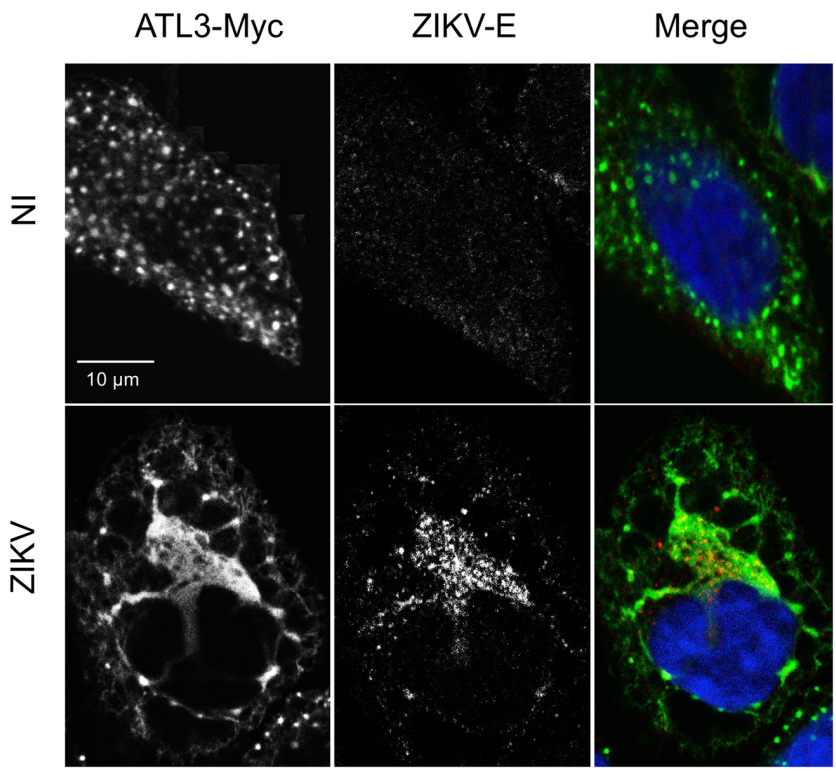

FIG 8 ATL3 is recruited to the viral replication site. HeLa cells expressing ATL3-myc were infected or not with ZIKV (MOI of 1) for 24 h. The cells were then fixed and stained for ATL3-myc (green) and viral E protein (white) and analyzed by confocal microscopy. A representative image is shown.

demonstrated an interaction between ATL3 and the NS2A and NS2B3 proteins, whereas the other NS proteins either did not associate or only poorly associated with ATL3 (Fig. 10A). Hemagglutinin (HA)-tagged NS2B3 and NS1 proteins were then transiently transfected in HeLa cells stably expressing ATL3-myc, and we examined the intracellular localization of the proteins by immunofluorescence. NS1 and NS2B3 displayed a punctuate staining which resembled that of ATL (Fig. 10B). Deconvolution of the images demonstrated a strong colocalization of ALT3 with NS2B3, and, to a much lower extent, with NS1 (Fig. 10B). To analyze NS3 and ATL3 localization in the context of viral infection, we infected HeLa dKO cells stably expressing ATL3-myc with ZIKV (MOI of 1 for 24 h) and stained the cells for NS3 and ATL3. We observed a strong colocalization between the two proteins (Fig. 11).

Altogether, these results indicate that ATL facilitates ZIKV production at the level of viral RNA and protein synthesis. ATL colocalizes and interacts with different NS proteins, mostly NS2A and NS2B3.

DISCUSSION

Flaviviruses such as ZIKV replicate their genomes in remodeled ER membranes (13, 18, 20). These viral factories allow the spatiotemporal control of the viral life cycle, ensures RNA amplification and production of viral proteins, and protects the viral RNA from the cytoplasmic environment and detection by sensors (13, 14). The ER is also central to ZIKV-induced cytopathic effect, which includes massive cellular vacuolization, triggering of an UPR response, and paraptosis-like cell death (21–23).

Genome-scale CRISPR and siRNA screens and proteomic analysis of cellular proteins associated with ZIKV or DENV proteins identified numerous host factors required for viral replication (38–41, 44–46). A large part of these host dependency factors are localized in the ER. For instance, (i) the ER membrane protein complex (EMC), which promotes the maturation of polytopic membrane proteins, (ii) the ER-associated pro-

Downloaded from https://journals.asm.org/journal/jvi on 05 October 2021 by 157.99.64.254.

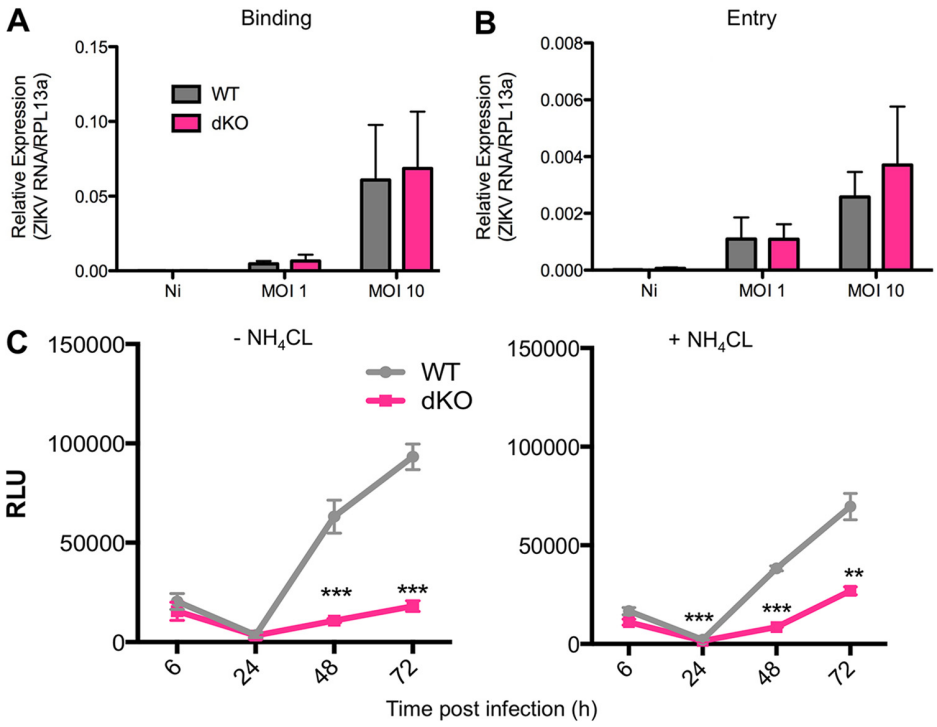

FIG 9 ATLs facilitate ZIKV replication after viral entry. (A) HeLa WT or dKO cells were exposed to ZIKV for 1 h at 4°C to allow viral binding. Viral input was washed out, and bound viral particles were quantified by RT-qPCR. The data are means ± the SEM of three independent experiments. (B) HeLa WT or dKO cells were exposed to ZIKV for 1 h at 4°C, washed out, and treated with trypsin to remove the bound viral particles. The cells were incubated at 37°C for 2 h to allow endocytosis and/or viral fusion. Intracellular viral RNA was quantified by RT-qPCR. Means ± the SEM of three independent experiments are shown. (C) HeLa WT or dKO cells were transfected with RNA from a ZIKV infectious clone expressing luciferase. The results are expressed in relative light units (RLU). The means ± the SEM of at least three independent experiments are shown. Statistical significance was determined using a *t* test, and each group was compared to the WT+ctrl condition. ***, $P < 0.001$; **, $P < 0.01$; *, $P < 0.05$.

tein degradation (ERAD), which targets misfolded proteins of the ER for ubiquitination and degradation by the proteasome, and (iii) the retrotranslocon Sec61, an oligosaccharyl transferase complex (OST) that glycosylates nascent proteins, are all required for ZIKV replication (38–41).

The role of ER-shaping proteins is less characterized. Reticulons (RTNs), atlastins (ATLs), receptor expression enhancing proteins (REEPs), and Lunapark regulate the structure and the dynamics of the ER compartment (25). These proteins were not identified in genomic screens of flavivirus infections. This suggests either that they are not important for viral replication or that the screening procedure may have missed this category of proteins for different reasons. One possible reason could be that their long-term deletion is deleterious to cell growth, independent of any infection. With other approaches than genome-wide screenings, it has been reported that RTN are required for the replication of enterovirus 71 and brome mosaic virus but negatively regulates hepatitis C virus (47–49). The RTN protein family is a large group of membrane-associated proteins involved in vesicle formation and membrane morphogenesis. RTNs control the formation of ER tubules and increase peripheral ER sheets (24, 50). Mutations in RTN2 are associated with hereditary spastic paraplegia disorders similarly to ATL1 (34). RTN3.1A is also required for the efficient replication of WNV, DENV-2, and ZIKV (37). In the absence of RTN3.1A, the number and size of ER membrane structures in flavivirus-infected cells are reduced (37). The impact of RTN3.1A on the viability of infected cells remains unknown.

We report that ATL enhance ZIKV spread by 2- to 3-fold. Reexpression of ATL3 in cells devoid of ATL restores viral replication. The three ATL display extensive homology,

Downloaded from https://journals.asm.org/journal/jvi on 05 October 2021 by 157.99.64.254.

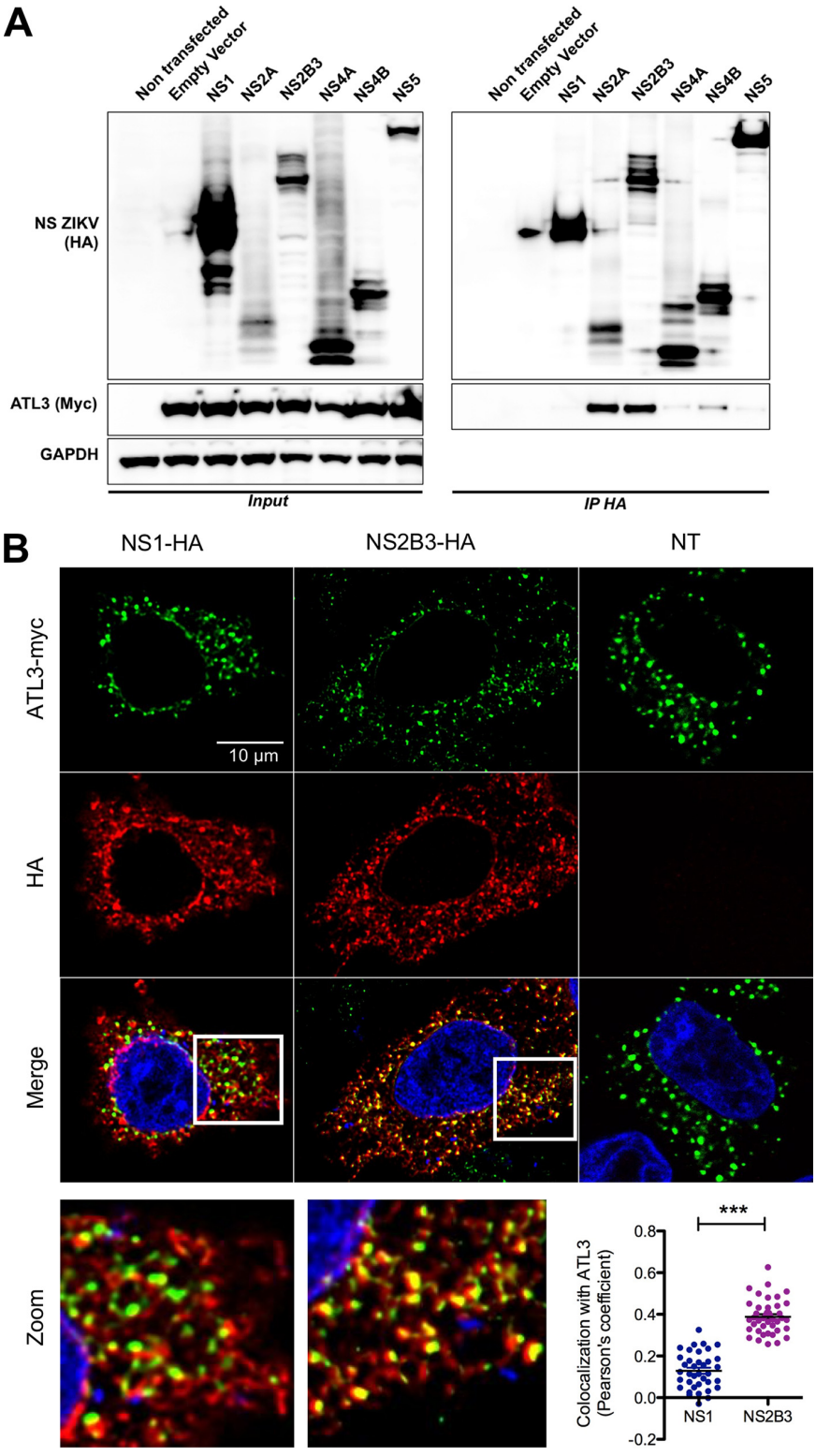

FIG 10 ATL3 colocalizes and interacts with ZIKV NS proteins. (A) HeLa cells expressing ATL3-myc were transfected with plasmids coding for individual NS-HA tagged proteins. NS proteins were eluted with an anti-HA antibody, and elution fractions were stained with an anti-myc antibody to detect coimmunoprecipitated ATL3. A representative blot from three independent experiments is shown. (B) HeLa cells expressing ATL3-myc were transfected with plasmids coding for HA-tagged NS1 or NS2B3 ZIKV proteins. The cells were fixed, stained for ATL3-myc (green) and NS-HA (red), and observed by confocal microscopy.

(Continued on next page)

Downloaded from https://journals.asm.org/journal/jvi on 05 October 2021 by 157.99.64.254.

with ATL1 being prominently expressed in neurons, and ATL2 and ATL3 more broadly in different cell types (51). It will be of interest to determineg whether the three ATL redundantly facilitate ZIKV replication. We further show that ATLs act after viral entry by increasing the levels of viral RNA and proteins. In the absence of ATL, the amounts of infectious virus released in the supernatants are strongly reduced. Our analysis of ZIKV-infected cells by confocal microscopy, video-microscopy, and electron microscopy indicates that intracellular structures associated with viral production are formed both in the presence and in the absence of ATL. We observed a similar condensation of the ER by immunofluorescence, with the appearance of an electron-dense region and vesicle pockets carrying viral particles. Distinct types of flavivirus-induced membrane alterations have been observed by electron tomography and other techniques (13, 18). The alterations include single-membrane invaginations of the ER, which may be associated with RNA synthesis, convoluted double membrane structures containing nonstructural proteins found in the vicinity of ER membranes, and invaginated vesicles (13, 18). Our electron microscopy results suggest that in the absence of ATLs, the number of such structures is decreased. Thus, since our results suggest a role for ATL at the replication step (Fig. 9), and given the endogenous role of ATL in ER membrane fusion/curvature, ZIKV likely overcomes the absence of ATL by replicating in viral factories that are much less efficiently formed than in presence of these proteins. It will be worth determining more precisely, by electron tomography and three-dimensional reconstruction, the characteristics and number of viral factories in cells that are either expressing or are deficient in ATL.

Membrane remodeling and accumulation of viral proteins in the ER trigger a stress pathway and activate the unfolded protein response (UPR) (5, 21, 23, 52). Knockout of ATL genes in mammalian cells alters ER sensitivity to UPR stress independently of any viral infection (42). We show here that in the absence of ATL, the appearance of large ER-derived vacuoles is strongly reduced, even at a high MOI. Moreover, the death of infected cells is attenuated without ATL. These observations strongly suggest that ATLs are key players in ZIKV-induced cytopathic effects, either directly or as a consequence of reduced viral replication. A decrease in the efficiency of cell death may also limit the release of infectious virus and further viral spread. Future work will help to determine whether the UPR response in ZIK-infected cells is impaired in the absence of ATL.

We report a recruitment of ATL3 to viral production sites and an interaction and colocalization of ATL3 with some NS proteins, mostly NS2A and NS2B3. We also show that the GTPase activity of ATL3 is required to enhance ZIKV replication and cytopathic effects. These observations raise interesting questions about the consequences of the interaction between NS proteins and ALT3. It will be worth determining whether this interaction modifies the enzymatic activity of ATL or stabilizes the formation or the function of the viral replication complex. RTN3.1 interacts with NS4A and protects NS4A from proteasomal degradation (37). It is tempting to speculate that the interaction of different NS proteins with various ER-shaping proteins may stabilize the docking of replication complexes and/or modulate the dynamics and structure of the ER to facilitate formation of viral factories. Alternatively, ER-shaping proteins could provide a dynamic environment for the creation of viral replication complexes, without requiring a direct interaction with NS proteins. Future work will help understanding the functional consequences of ATL-NS protein interaction. Furthermore, a recent study shows a role for ATL3 in ER export of cargo proteins into COPII vesicles (53). It would be of interest to determine whether ATL play also a role the transport or release of viral particles.

During flavivirus replication, a double-stranded intermediate RNA is produced and can be sensed in the cytoplasm by RIG-I-like receptors such as MD5 or RIG-I (54–57). It

FIG 10 Legend (Continued)
One field from a representative experiment is shown. Colocalization (Pearson's coefficient) was determined after deconvolution with Imaris software. At least 10 cells per condition (from three independent experiments) were plotted. Statistical significance was determined by using a *t* test ***, $P < 0.001$.

Downloaded from https://journals.asm.org/journal/jvi on 05 October 2021 by 157.99.64.254.

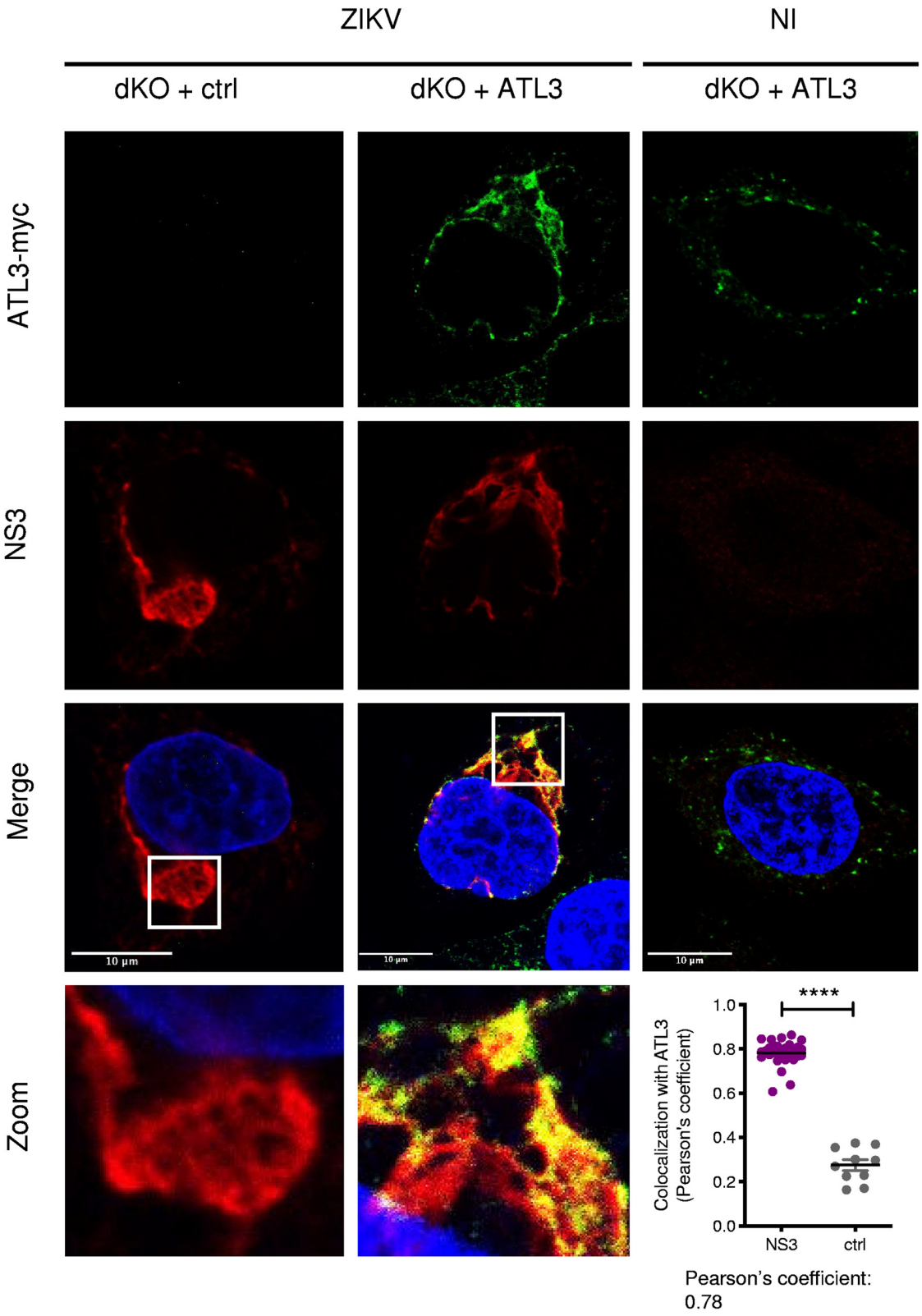

FIG 11 ATL3 colocalizes with NS3 in ZIKV-infected cells. HeLa dKO cells transduced with a control vector (dKO+ctrl) or stably expressing ATL3-myc (dKO+ATL3) were infected with ZIKV (MOI of 1) for 24 h. The cells were then fixed and stained for ATL3-myc (green) and NS3 (red). One field from a representative experiment is shown. Colocalization (Pearson's coefficient) was determined after deconvolution with Imaris software. At least 10 cells were plotted from three independent experiments. Statistical significance was determined using a *t* test. ****, $P < 0.0001$.

Downloaded from https://journals.asm.org/journal/jvi on 05 October 2021 by 157.99.64.254.

may be of interest to analyze how viral sensing and production of type I IFN is modulated by ATL and other ER-shaping proteins.

Hereditary sensory and autonomic neuropathies (HSAN) and spastic paraplegia (HSP) involve genes controlling the architecture of the ER and coding for proteins with RTN-like domain, namely, ARL6IP1, ATL1 and -3, FAM134B, REEP1, RTN2, and SPAST (33, 58). These mutations induce length-dependent axonopathy of projecting neurons. ZIKV infection during pregnancy leads to severe fetal abnormalities, including debilitating neuropathological outcomes and microcephaly (59). In adults, ZIKV infection can also result in peripheral neuropathy and meningoencephalitis (60). In some individuals, ZIKV accesses the central nervous system, where it infects neurons and neural progenitor cells (61). Experiments with cultured human neuroprogenitor stem cells, organoids, brain slices, and mouse inoculation studies demonstrated that ZIKV (i) targets neural progenitor cells of the cortex, neurons, microglial cells, and astrocytes, (ii) reduces cell proliferation and differentiation, and (iii) modulates inflammation and cell death (62–75). In ZIKV-Infected neurons, BP1/RIPK1/RIPK3 induces a transcriptional response that reprograms neuronal metabolism in a manner that further restricts viral replication (76). Future ZIKV infection experiments with cells from healthy individuals or from patients with HSP or HSAN should allow further characterization of the role of ATL and other ER-shaping proteins during ZIKV replication and will help to determine whether the virus may impact axonal growth.

MATERIALS AND METHODS

Cells, lentivectors, and viruses. HeLa cells (ATCC) and primary human adult dermal fibroblasts (HDFa; ATCC) were cultured in Dulbecco modified Eagle minimal essential medium supplemented with 10% fetal bovine serum and 1% penicillin-streptomycin at 37°C with 5% CO_2. HeLa cells stably expressing a fluorescent, calreticulin-based ER marker were established via transfection with pDsRed2-ER Vector (Clontech 632409) and G418 selection. HeLa knockouts for ATL2/ATL3 (dKO cells) were generated using a CRISPR strategy as previously described (42). HeLa cells stably expressing the mEmmerald Sec61β protein were generated by transduction with a lentivector expressing Sec61-mEmmerald. HeLa dKO cells were transduced with lentiviral vectors to stably express ATL3 WT, ATL3-myc, or ATL3KA.

ZIKV strains HD78788, PF13, NC14, and FG16 were previously described (8, 77–80). Virus stocks were produced on C6/36 cells, and titers were determined on Vero cells. Cells were seeded 1 day prior to infection and overlaid with ZIKV at the desired MOI in a final volume of 200 μl. After 2 h at 37°C, the inoculum was removed and replaced with fresh medium.

Plasmids. The Sec61-mEmmerald was amplified using PCR from the pUC_CMV-mEmmerald-Serc61 plasmid (Addgene, catalog no. 90992) and cloned into the pLV-EF1a-IRES-Puro Addgene (catalog no. 85132) using EcoRI to generate the pLV-EF1a-Sec61-mEmmerald-IRES-Puro plasmid. The pLVX-ATL3 is derived frompLVX-IRES-ZsGreen1 (Clontech, catalog no. 632187) and encodes WT AXL3. pLVX-ATL3-myc and pLVX-ATL3KA were generated as follows: restriction sites, Kozak sequence, and myc tag were added to ATL3 or ATL3KA from pGW1-ATL3 or pGW1-ATL3KA by PCR. The myc-ATL3 fragment was then inserted into pLVX-IRES-ZsGreen1.

Flow cytometry analysis. Cells were fixed with 4% paraformaldehyde (PFA) and permeabilized with 1% Triton X-100, followed by 30-min incubations with anti-E protein (4G2, purified from the ATCC hybridoma) and anti-mouse secondary antibodies. A Live/Dead Fixable Aqua dead cell stain kit (Thermo Fisher, catalog no. L34965) was used for cell death analysis. Samples were acquired with an Attune NxT flow cytometer (Becton Dickinson), and data were analyzed using FlowJo software. The gating strategy used to determine 4G2-positive cells is outlined in Fig. S6 in the supplemental material.

RNA measurement by RT-qPCR. Total RNA was extracted from cells using a QIAamp RNeasy extraction kit (Qiagen). RNA (500 ng) was used for cDNA synthesis using SuperScript II reverse transcriptase (Life Technologies) in an Eppendorf EP Mastercycler Gradient S thermocycler. The following primers were used to amplify viral cDNA as described previously (9): forward (AARTACACATACCARAACAAAGT GGT) and reverse (TCCRCTCCCYCTYTGGTCTTG). cDNAs corresponding to cellular transcripts were amplified using the following primers: ATL1, forward (TTG GCT ACT TAG TCC CGA GAG) and reverse (TGT AAC ATG GAT TTG GGA TGT GG); ATL2, forward (AGT AGT GGT ATC TGT GGC AGG) and reverse (CAC CTC GCC ATG TAA AGC CT); ATL3, forward (ACA GCC AGT CAA CTG TGA AAG) and reverse (CCA GAC GAC CGT ATT CTG TGA); DDOST, forward (GAG ACT CAT TCG CTT TTC TTC CG) and reverse (CTC CAA AAT CTT CTA CCG AAG GG); and RLP13, forward (AGG CAT CAA CAT TTC TGG CA) and reverse (CCA TCC GCT TTT TCT TGT CG).

cDNA amplification was performed by qPCR using 500 nM concentrations of each primer, 25 ng of cDNA, and 10 μl of SYBR green. An activation step of 15 min at 95°C was followed by 40 amplification cycles of 95°C for 15 s, 60°C for 20 s, and 72°C for 30 s. The levels of viral RNA or cellular transcripts were normalized to GAPDH (glyceraldehyde-3-phosphate dehydrogenase) or to RLP13.

Transmission electron microscopy. HeLa siSCR or HeLa siATL1/2/3 cells were fixed for 24 h in 4% PFA and 1% glutaraldehyde (Sigma) in 0.1 M phosphate buffer (pH 7.2). Cells were washed in PBS and postfixed with 2% osmium tetroxide (Agar Scientific) for 1 h. The cells were fully dehydrated in a graded

Downloaded from https://journals.asm.org/journal/jvi on 05 October 2021 by 157.99.64.254.

series of ethanol solutions and propylene oxide. The impregnation step was performed with a mixture of (1:1) propylene oxide/Epon resin (Sigma) and left overnight in pure resin. The cells were then embedded in resin blocks, which were allowed to polymerize for 48 h at 60°C. Ultrathin sections (70 nm) of blocks were obtained with a Leica EM UC7 ultramicrotome (Wetzlar). Sections were stained with 5% uranyl acetate (Agar Scientific) and 5% lead citrate (Sigma), and observations were made with a JEOL 1011 transmission electron microscope.

Western blotting. Cells were lysed in 1% radioimmunoprecipitation assay (RIPA) buffer in the presence of protease inhibitor cocktail (Sigma, catalog no. R0278), and 10 to 20 μg of protein lysates was loaded into 12% Bis-Tris SDS-PAGE gels. The following antibodies were used: anti-ATL3 (Atlas Antibodies, catalog no. HPA065702) and mouse anti-cMyc (Fisher Scientific, catalog no. 10416023). DyLight-coupled secondary antibodies (Thermo Fisher) were used for protein detection on a Li-Cor Odyssey imaging system.

Confocal microscopy and structured illumination microscopy. For ER morphology analysis, HeLa WT, dKO, dKO+ATL3, and dKO+ATL3KA cells stably expressing the red ER-tracker were plated on coverslips and fixed with 4% PFA for 10 min at room temperature. The coverslips were then mounted on slides with Fluoromount-G with DAPI (Thermo Fisher Scientific, catalog no. 00-4959-52). The cells were analyzed using confocal microscopy (Leica SP5 HyD inverted), a 63× oil immersion objective, and LAS AF software. The ER-tracker signal was analyzed and normalized to the selected area of the cells after background subtraction using ImageJ software.

Sec61β relocation and viral replication site: HeLa WT or dKO cells stably expressing mEmmerald-Sec61β protein were plated on coverslips in 24-well plates and challenged with ZIKV (MOI of 1) for 24 h. The cells were fixed 30 min at room temperature with 4% PFA, permeabilized with Triton 1% for 10 min blocked with 1% PBS-BSA for 30 min, and stained for viral E protein using 4G2 antibody (1 μg/ml) for 45 and 30 min with an anti-mouse secondary antibody. The coverslips were mounted on slides using Fluoromount-G with DAPI and analyzed using confocal microscopy or super-resolution microscopy (structured illumination microscopy [SIM]; Zeiss LSM 780-Elyra PS.1). A Plan Apo 63×/1.4 oil objective with a 1.518 refractive index oil (Zeiss) and an EMCCD Andor Ixon 887 1K camera were used. Fifteen images per plane per channel (five phases, three angles) were acquired to obtaine SIM images. The SIM images were processed with Zen software and then aligned with Zen using 100-nm TetraSpeck microspheres (Thermo Fisher Scientific) embedded under the same conditions as the sample. The acquired pictures were analyzed using ImageJ software.

For colocalization of ATL3-myc and NS-HA proteins, HeLa dKO or HeLa dKO+ATL3-myc cells were transfected with plasmids coding for individual viral NS-HA proteins with TurboFect (Thermo Fisher Scientific, catalog no. 0531). After 40 h, the cells were fixed 30 min at room temperature with 4% PFA, permeabilized with Triton 1% for 10 min at room temperature, blocked with 1% PBS-BSA for 30 min at room temperature, and stained with rat anti-HA antibody 3F10 (Roche, catalog no. 11867423001) and mouse anti-cMyc (Fisher Scientific, catalog no. 10416023) antibody. For colocalization of ATL3 and NS3 in the context of viral infections, HeLa dKO or dKO+ATL3-myc cells were infected with ZIKV at an MOI of 1 for 24 h and stained with a rabbit anti-NS3 antibody kindly provided by Andres Merits (81). The cells were analyzed using confocal microscopy (Leica SP5 HyD inverted), a 63× oil immersion objective, and LAS AF software. The acquired pictures were deconvoluted using Huygens software, and the colocalization was quantified with Imaris software.

Time-lapse microscopy. HeLa cells stably expressing Sec61β-mEmmerald were plated in Hi-Q4 microdishes (10,000 cells per chamber; Ibidi). The following day, the cells were infected with ZIKV (MOI of 1). Transmission and fluorescence images were taken every 5 min for up to 48 h using a Nikon Biostation IMQ, with three fields captured simultaneously for each condition. The images were analyzed with Fiji software.

ZIKV cell attachment and entry. HeLa cells were plated in 24-well plates (50,000 cells/well) with at least four wells/condition. The cells were challenged with ZIKV (MOI of 1 or 10) for 1 h at 4°C. The viral input was removed, and the cells were washed with PBS to remove the unbound particles. Half of the wells were treated with PBS-EDTA to gently detach the cells. The other half of the wells were kept at 37°C for 2 h to allow viral endocytosis/fusion. The cells were then treated with trypsin for 30 min at 37°C to remove the bound particles. The cells were pelleted for lysis, RNA extraction, and RT-qPCR to quantify the viral RNA.

Reporter viral RNA transfection and replication kinetics. To assess ZIKV RNA amplification, HeLa WT and dKO cells were transfected with a genomic viral RNA expressing *Renilla* luciferase (R-Luc), kindly provided by Pei-Yong Shi (University of Texas Medical Branch) (43). The ZIKV R-Luc reporter viral RNA was generated as previously described (43). A total of 3×10^4 cells were plated on a 48-well plate and transfected with 100 ng of RNA using Lipofectamine MessengerMax (Thermo Fisher). At the indicated time points, cells were lysed with 1× *Renilla* lysis buffer (Promega). The lysates were kept at −20°C until all of the samples were collected. Viral replication was measured with the *Renilla* luciferase assay (E2820; Promega) on a TriStar2 LB942 microplate reader (Berthold Technologies).

Coimmunoprecipitation. 293T cells were plated in 10-cm dishes and transfected with 7.5-μg portions of each indicated plasmid. After 24 h, the cells were washed and collected with a scrapper, and the pellets were lysed for 30 min in cold immunoprecipitation lysis buffer supplemented with Halt protease and phosphatase inhibitor cocktail (Thermo Fisher Scientific) and cleared by centrifugation (15 min at 6,000 × *g*). Supernatants were incubated overnight at 4°C with anti-HA magnetic beads (catalog no. 88837; Thermo Fisher Scientific). Beads were washed three times with BO15 buffer (20 mM Tris-HCl [pH 7.4], 150 mM NaCl, 5 mM $MgCl_2$, 10% glycerol, 0.5 mM EDTA, 0.05% Triton, 0.1% Tween 20). The retained complexes were eluted twice with HA peptide (400 μg/ml; Roche, catalog no. 11666975001)

Downloaded from https://journals.asm.org/journal/jvi on 05 October 2021 by 157.99.64.254.

for 30 min at room temperature. Samples were then subjected to immunoblotting with the following antibodies: mouse anti-GAPDH (SC-47724, 1:5,000; Santa Cruz), rabbit anti-HA (catalog no. 3724, 1:5,000; Cell Signaling Technology), and mouse anti-Myc (catalog no. 2276S, 1:2,000; Cell Signaling Technology). The signals were acquired by using a Fusion Fx camera (VILBERT Lourmat).

SUPPLEMENTAL MATERIAL

Supplemental material for this article may be found at https://doi.org/10.1128/JVI.01047-19.

SUPPLEMENTAL FILE 1, AVI file, 7 MB.

SUPPLEMENTAL FILE 2, AVI file, 6.2 MB.

SUPPLEMENTAL FILE 3, PDF file, 0.03 MB.

ACKNOWLEDGMENTS

We thank members of the Virus and Immunity Unit for discussions and assistance, Pei-Yong Shi (University of Texas Medical Branch) for the kind gift of the infectious ZIKV clone, and Andrès Merits (Institute of Technology, University of Tartu, Tartu, Estonia) for the kind gift of the anti-NS3 antibody. We also thank the World Reference Center for Emerging Viruses and Arboviruses (University of Texas Medical Branch, Galveston, TX) for the ZIKV luciferase clone.

Work in the O.S. lab is funded by Institut Pasteur, ANRS, Sidaction, the Vaccine Research Institute (ANR-10-LABX-77), Labex IBEID (ANR-10-LABX-62-IBEID), TIMTAMDEN ANR-14-CE14-0029, CHIKV-Viro-Immuno ANR-14-CE14-0015-01, and the Gilead HIV cure program. Work in the A.A. lab is funded by ANR (ANR-15-CE15-00029 ZIKAHOST). This study was supported in part by the Intramural Research Program of the NINDS, NIH. UTechS PBI is part of the France–BioImaging infrastructure network (FBI) supported by the French National Research Agency (ANR-10–INSB–04; Investments for the Future) and acknowledges support from ANR/FBI and the Région Ile-de-France (program "Domaine d'Intérêt Majeur-Malinf") for the use of the Zeiss LSM 780 Elyra PS1 microscope. M.M.R. is supported by the Pasteur-Paris University International PhD program.

B.M., N.J., P.R., C.B., A.A., and O.S. designed the experimental strategy. B.M., M.M.R., M.-L.H., S.S.-A., J.B.-G., Q.N., J.B., F.P., C.M., S.A., M.C., and A.S. designed and performed experiments. P.-P.Z. and C.B. provided vital materials and expert advice. B.M. and O.S. wrote the manuscript. All authors agreed on the final version and declare no competing interests.

REFERENCES

1. Weaver SC, Costa F, Garcia-Blanco MA, Ko AI, Ribeiro GS, Saade G, Shi PY, Vasilakis N. 2016. Zika virus: history, emergence, biology, and prospects for control. Antiviral Res 130:69–80. https://doi.org/10.1016/j.antiviral.2016.03.010.
2. Pierson TC, Diamond MS. 2018. The emergence of Zika virus and its new clinical syndromes. Nature 560:573–581. https://doi.org/10.1038/s41586-018-0446-y.
3. Liu ZY, Shi WF, Qin CF. 2019. The evolution of Zika virus from Asia to the Americas. Nat Rev Microbiol 17:131. https://doi.org/10.1038/s41579-018-0134-9.
4. da Silva S, Oliveira Silva Martins D, Jardim A. 2018. A review of the ongoing research on Zika Virus treatment. Viruses 10:255. https://doi.org/10.3390/v10050255.
5. Abbink P, Stephenson KE, Barouch DH. 2018. Zika virus vaccines. Nat Rev Microbiol 16:594–600. https://doi.org/10.1038/s41579-018-0039-7.
6. Lee I, Bos S, Li G, Wang S, Gadea G, Despres P, Zhao RY. 2018. Probing molecular insights into Zika virus(–)host interactions. Viruses 10:233. https://doi.org/10.3390/v10050233.
7. Richner JM, Diamond MS. 2018. Zika virus vaccines: immune response, current status, and future challenges. Curr Opin Immunol 53:130–136. https://doi.org/10.1016/j.coi.2018.04.024.
8. Hamel R, Dejarnac O, Wichit S, Ekchariyawat P, Neyret A, Luplertlop N, Perera-Lecoin M, Surasombatpattana P, Talignani L, Thomas F, Cao-Lormeau V-M, Choumet V, Briant L, Desprès P, Amara A, Yssel H, Missé D. 2015. Biology of Zika virus infection in human skin cells. J Virol 89:8880–8896. https://doi.org/10.1128/JVI.00354-15.
9. Meertens L, Labeau A, Dejarnac O, Cipriani S, Sinigaglia L, Bonnet-Madin L, Le Charpentier T, Hafirassou ML, Zamborlini A, Cao-Lormeau VM, Coulpier M, Misse D, Jouvenet N, Tabibiazar R, Gressens P, Schwartz O, Amara A. 2017. Axl mediates ZIKA virus entry in human glial cells and modulates innate immune responses. Cell Rep 18:324–333. https://doi.org/10.1016/j.celrep.2016.12.045.
10. Pierson TC, Kielian M. 2013. Flaviviruses: braking the entering. Curr Opin Virol 3:3–12. https://doi.org/10.1016/j.coviro.2012.12.001.
11. Gillespie LK, Hoenen A, Morgan G, Mackenzie JM. 2010. The endoplasmic reticulum provides the membrane platform for biogenesis of the flavivirus replication complex. J Virol 84:10438–10447. https://doi.org/10.1128/JVI.00986-10.
12. Neufeldt CJ, Cortese M, Acosta EG, Bartenschlager R. 2018. Rewiring cellular networks by members of the *Flaviviridae* family. Nat Rev Microbiol 16:125–142. https://doi.org/10.1038/nrmicro.2017.170.
13. Blanchard E, Roingeard P. 2015. Virus-induced double-membrane vesicles. Cell Microbiol 17:45–50. https://doi.org/10.1111/cmi.12372.
14. Paul D, Bartenschlager R. 2015. *Flaviviridae* replication organelles: oh, what a tangled web we weave. Annu Rev Virol 2:289–310. https://doi.org/10.1146/annurev-virology-100114-055007.
15. Ravindran MS, Bagchi P, Cunningham CN, Tsai B. 2016. Opportunistic intruders: how viruses orchestrate ER functions to infect cells. Nat Rev Microbiol 14:407–420. https://doi.org/10.1038/nrmicro.2016.60.
16. Saeedi BJ, Geiss BJ. 2013. Regulation of flavivirus RNA synthesis and capping. Wiley Interdiscip Rev RNA 4:723–735. https://doi.org/10.1002/wrna.1191.

Downloaded from https://journals.asm.org/journal/jvi on 05 October 2021 by 157.99.64.254.

17. Klema VJ, Padmanabhan R, Choi KH. 2015. Flaviviral replication complex: coordination between RNA synthesis and 5′-RNA capping. Viruses 7:4640–4656. https://doi.org/10.3390/v7082837.
18. Cortese M, Goellner S, Acosta EG, Neufeldt CJ, Oleksiuk O, Lampe M, Haselmann U, Funaya C, Schieber N, Ronchi P, Schorb M, Pruunsild P, Schwab Y, Chatel-Chaix L, Ruggieri A, Bartenschlager R. 2017. Ultrastructural characterization of Zika virus replication factories. Cell Rep 18:2113–2123. https://doi.org/10.1016/j.celrep.2017.02.014.
19. Rossignol ED, Peters KN, Connor JH, Bullitt E. 2017. Zika virus induced cellular remodeling. Cell Microbiol. https://doi.org/10.1111/cmi.12740.
20. Aktepe TE, Mackenzie JM. 2018. Shaping the flavivirus replication complex: it is curvaceous!. Cell Microbiol 20:e12884. https://doi.org/10.1111/cmi.12884.
21. Blázquez A-B, Escribano-Romero E, Merino-Ramos T, Saiz J-C, Martín-Acebes MA. 2014. Stress responses in flavivirus-infected cells: activation of unfolded protein response and autophagy. Front Microbiol 5:266. https://doi.org/10.3389/fmicb.2014.00266.
22. Tan Z, Zhang W, Sun J, Fu Z, Ke X, Zheng C, Zhang Y, Li P, Liu Y, Hu Q, Wang H, Zheng Z. 2018. ZIKV infection activates the IRE1-XBP1 and ATF6 pathways of unfolded protein response in neural cells. J Neuroinflammation 15:275. https://doi.org/10.1186/s12974-018-1311-5.
23. Monel B, Compton AA, Bruel T, Amraoui S, Burlaud-Gaillard J, Roy N, Guivel-Benhassine F, Porrot F, Génin P, Meertens L, Sinigaglia L, Jouvenet N, Weil R, Casartelli N, Demangel C, Simon-Lorière E, Moris A, Roingeard P, Amara A, Schwartz O. 2017. Zika virus induces massive cytoplasmic vacuolization and paraptosis-like death in infected cells. EMBO J 36:1653–1668. https://doi.org/10.15252/embj.201695597.
24. Voeltz GK, Prinz WA, Shibata Y, Rist JM, Rapoport TA. 2006. A class of membrane proteins shaping the tubular endoplasmic reticulum. Cell 124:573–586. https://doi.org/10.1016/j.cell.2005.11.047.
25. Goyal U, Blackstone C. 2013. Untangling the web: mechanisms underlying ER network formation. Biochim Biophys Acta 1833:2492–2498. https://doi.org/10.1016/j.bbamcr.2013.04.009.
26. Wang S, Tukachinsky H, Romano FB, Rapoport TA. 2016. Cooperation of the ER-shaping proteins atlastin, lunapark, and reticulons to generate a tubular membrane network. Elife 5:e18605. https://doi.org/10.7554/eLife.18605.
27. Hu J, Shibata Y, Zhu PP, Voss C, Rismanchi N, Prinz WA, Rapoport TA, Blackstone C. 2009. A class of dynamin-like GTPases involved in the generation of the tubular ER network. Cell 138:549–561. https://doi.org/10.1016/j.cell.2009.05.025.
28. Orso G, Pendin D, Liu S, Tosetto J, Moss TJ, Faust JE, Micaroni M, Egorova A, Martinuzzi A, McNew JA, Daga A. 2009. Homotypic fusion of ER membranes requires the dynamin-like GTPase atlastin. Nature 460:978–983. https://doi.org/10.1038/nature08280.
29. Rismanchi N, Soderblom C, Stadler J, Zhu PP, Blackstone C. 2008. Atlastin GTPases are required for Golgi apparatus and ER morphogenesis. Hum Mol Genet 17:1591–1604. https://doi.org/10.1093/hmg/ddn046.
30. Blackstone C, O'Kane CJ, Reid E. 2011. Hereditary spastic paraplegias: membrane traffic and the motor pathway. Nat Rev Neurosci 12:31. https://doi.org/10.1038/nrn2946.
31. Evans K, Keller C, Pavur K, Glasgow K, Conn B, Lauring B. 2006. Interaction of two hereditary spastic paraplegia gene products, spastin and atlastin, suggests a common pathway for axonal maintenance. Proc Natl Acad Sci U S A 103:10666–10671. https://doi.org/10.1073/pnas.0510863103.
32. Sanderson CM, Connell JW, Edwards TL, Bright NA, Duley S, Thompson A, Luzio JP, Reid E. 2006. Spastin and atlastin, two proteins mutated in autosomal-dominant hereditary spastic paraplegia, are binding partners. Hum Mol Genet 15:307–318. https://doi.org/10.1093/hmg/ddi447.
33. Park SH, Zhu PP, Parker RL, Blackstone C. 2010. Hereditary spastic paraplegia proteins REEP1, spastin, and atlastin-1 coordinate microtubule interactions with the tubular ER network. J Clin Invest 120:1097–1110. https://doi.org/10.1172/JCI40979.
34. Montenegro G, Rebelo AP, Connell J, Allison R, Babalini C, D'Aloia M, Montieri P, Schüle R, Ishiura H, Price J, Strickland A, Gonzalez MA, Baumbach-Reardon L, Deconinck T, Huang J, Bernardi G, Vance JM, Rogers MT, Tsuji S, De Jonghe P, Pericak-Vance MA, Schöls L, Orlacchio A, Reid E, Züchner S. 2012. Mutations in the ER-shaping protein reticulon 2 cause the axon-degenerative disorder hereditary spastic paraplegia type 12. J Clin Invest 122:538–544. https://doi.org/10.1172/JCI60560.
35. Zhao J, Hedera P. 2013. Hereditary spastic paraplegia-causing mutations in atlastin-1 interfere with BMPRII trafficking. Mol Cell Neurosci 52:87–96. https://doi.org/10.1016/j.mcn.2012.10.005.
36. Willkomm L, Heredia R, Hoffmann K, Wang H, Voit T, Hoffman EP, Cirak S. 2016. Homozygous mutation in atlastin GTPase 1 causes recessive hereditary spastic paraplegia. J Hum Genet 61:571–573. https://doi.org/10.1038/jhg.2016.6.
37. Aktepe TE, Liebscher S, Prier JE, Simmons CP, Mackenzie JM. 2017. The host protein reticulon 3.1A is utilized by flaviviruses to facilitate membrane remodeling. Cell Rep 21:1639–1654. https://doi.org/10.1016/j.celrep.2017.10.055.
38. Savidis G, McDougall WM, Meraner P, Perreira JM, Portmann JM, Trincucci G, John SP, Aker AM, Renzette N, Robbins DR, Guo Z, Green S, Kowalik TF, Brass AL. 2016. Identification of Zika virus and dengue virus dependency factors using functional genomics. Cell Rep 16:232–246. https://doi.org/10.1016/j.celrep.2016.06.028.
39. Marceau CD, Puschnik AS, Majzoub K, Ooi YS, Brewer SM, Fuchs G, Swaminathan K, Mata MA, Elias JE, Sarnow P, Carette JE. 2016. Genetic dissection of *Flaviviridae* host factors through genome-scale CRISPR screens. Nature 535:159–163. https://doi.org/10.1038/nature18631.
40. Hafirassou ML, Meertens L, Umana-Diaz C, Labeau A, Dejarnac O, Bonnet-Madin L, Kummerer BM, Delaugerre C, Roingeard P, Vidalain PO, Amara A. 2017. A global interactome map of the dengue virus NS1 identifies virus restriction and dependency host factors. Cell Rep 21:3900–3913. https://doi.org/10.1016/j.celrep.2017.11.094.
41. Petrova E, Gracias S, Beauclair G, Tangy F, Jouvenet N. 2019. Uncovering flavivirus host dependency factors through a genome-wide gain-of-function screen. Viruses 11:68. https://doi.org/10.3390/v11010068.
42. Zhao G, Zhu PP, Renvoise B, Maldonado-Baez L, Park SH, Blackstone C. 2016. Mammalian knock out cells reveal prominent roles for atlastin GTPases in ER network morphology. Exp Cell Res 349:32–44. https://doi.org/10.1016/j.yexcr.2016.09.015.
43. Shan C, Xie X, Muruato AE, Rossi SL, Roundy CM, Azar SR, Yang Y, Tesh RB, Bourne N, Barrett AD, Vasilakis N, Weaver SC, Shi PY. 2016. An infectious cDNA clone of Zika virus to study viral virulence, mosquito transmission, and antiviral inhibitors. Cell Host Microbe 19:891–900. https://doi.org/10.1016/j.chom.2016.05.004.
44. Coyaud E, Ranadheera C, Cheng D, Goncalves J, Dyakov BJA, Laurent EMN, St-Germain J, Pelletier L, Gingras AC, Brumell JH, Kim PK, Safronetz D, Raught B. 2018. Global interactomics uncovers extensive organellar targeting by Zika virus. Mol Cell Proteomics 17:2242–2255. https://doi.org/10.1074/mcp.TIR118.000800.
45. Scaturro P, Stukalov A, Haas DA, Cortese M, Draganova K, Płaszczyca A, Bartenschlager R, Götz M, Pichlmair A. 2018. An orthogonal proteomic survey uncovers novel Zika virus host factors. Nature 561:253–257. https://doi.org/10.1038/s41586-018-0484-5.
46. Shah PS, Link N, Jang GM, Sharp PP, Zhu T, Swaney DL, Johnson JR, Von Dollen J, Ramage HR, Satkamp L, Newton B, Huttenhain R, Petit MJ, Baum T, Everitt A, Laufman O, Tassetto M, Shales M, Stevenson E, Iglesias GN, Shokat L, Tripathi S, Balasubramaniam V, Webb LG, Aguirre S, Willsey AJ, Garcia-Sastre A, Pollard KS, Cherry S, Gamarnik AV, Marazzi I, Taunton J, Fernandez-Sesma A, Bellen HJ, Andino R, Krogan NJ. 2018. Comparative flavivirus-host protein interaction mapping reveals mechanisms of dengue and Zika virus pathogenesis. Cell 175:1931–1945 e18. https://doi.org/10.1016/j.cell.2018.11.028.
47. Tang WF, Yang SY, Wu BW, Jheng JR, Chen YL, Shih CH, Lin KH, Lai HC, Tang P, Horng JT. 2007. Reticulon 3 binds the 2C protein of enterovirus 71 and is required for viral replication. J Biol Chem 282:5888–5898. https://doi.org/10.1074/jbc.M611145200.
48. Diaz A, Wang X, Ahlquist P. 2010. Membrane-shaping host reticulon proteins play crucial roles in viral RNA replication compartment formation and function. Proc Natl Acad Sci U S A 107:16291–16296. https://doi.org/10.1073/pnas.1011105107.
49. Wu MJ, Ke PY, Hsu JT, Yeh CT, Horng JT. 2014. Reticulon 3 interacts with NS4B of the hepatitis C virus and negatively regulates viral replication by disrupting NS4B self-interaction. Cell Microbiol 16:1603–1618. https://doi.org/10.1111/cmi.12318.
50. Westrate LM, Lee JE, Prinz WA, Voeltz GK. 2015. Form follows function: the importance of endoplasmic reticulum shape. Annu Rev Biochem 84:791–811. https://doi.org/10.1146/annurev-biochem-072711-163501.
51. Zhu PP, Patterson A, Lavoie B, Stadler J, Shoeb M, Patel R, Blackstone C. 2003. Cellular localization, oligomerization, and membrane association of the hereditary spastic paraplegia 3A (SPG3A) protein atlastin. J Biol Chem 278:49063–49071. https://doi.org/10.1074/jbc.M306702200.
52. Gladwyn-Ng I, Cordon-Barris L, Alfano C, Creppe C, Couderc T, Morelli G, Thelen N, America M, Bessieres B, Encha-Razavi F, Bonniere M, Suzuki IK, Flamand M, Vanderhaeghen P, Thiry M, Lecuit M, Nguyen L. 2018. Stress-

Downloaded from https://journals.asm.org/journal/jvi on 05 October 2021 by 157.99.64.254.

induced unfolded protein response contributes to Zika virus-associated microcephaly. Nat Neurosci 21:63–71. https://doi.org/10.1038/s41593-017-0038-4.
53. Niu L, Ma T, Yang F, Yan B, Tang X, Yin H, Wu Q, Huang Y, Yao ZP, Wang J, Guo Y, Hu J. 2019. Atlastin-mediated membrane tethering is critical for cargo mobility and exit from the endoplasmic reticulum. Proc Natl Acad Sci U S A 116:14029–14038. https://doi.org/10.1073/pnas.1908409116.
54. Suthar MS, Aguirre S, Fernandez-Sesma A. 2013. Innate immune sensing of flaviviruses. PLoS Pathog 9:e1003541. https://doi.org/10.1371/journal.ppat.1003541.
55. Green AM, Beatty PR, Hadjilaou A, Harris E. 2014. Innate immunity to dengue virus infection and subversion of antiviral responses. J Mol Biol 426:1148–1160. https://doi.org/10.1016/j.jmb.2013.11.023.
56. Kim J-A, Seong R-K, Son SW, Shin OS. 2018. Insights into ZIKV-mediated innate immune responses in human dermal fibroblasts and epidermal keratinocytes. J Invest Dermatol. https://doi.org/10.1016/j.jid.2018.07.038.
57. Chazal M, Beauclair G, Gracias S, Najburg V, Simon-Lorière E, Tangy F, Komarova AV, Jouvenet N. 2018. RIG-I recognizes the 5′ region of dengue and Zika virus genomes. Cell Rep 24:320–328. https://doi.org/10.1016/j.celrep.2018.06.047.
58. Hubner CA, Kurth I. 2014. Membrane-shaping disorders: a common pathway in axon degeneration. Brain 137:3109–3121. https://doi.org/10.1093/brain/awu287.
59. Coyne CB, Lazear HM. 2016. Zika virus: reigniting the TORCH. Nat Rev Microbiol 14:707–715. https://doi.org/10.1038/nrmicro.2016.125.
60. Hygino da Cruz LC, Jr, Nascimento OJM, Lopes F, da Silva I. 2018. Neuroimaging findings of Zika virus-associated neurologic complications in adults. AJNR 39:1967–1974. https://doi.org/10.3174/ajnr.A5649.
61. Miner JJ, Diamond MS. 2017. Zika virus pathogenesis and tissue tropism. Cell Host Microbe 21:134–142. https://doi.org/10.1016/j.chom.2017.01.004.
62. Dang J, Tiwari SK, Lichinchi G, Qin Y, Patil VS, Eroshkin AM, Rana TM. 2016. Zika virus depletes neural progenitors in human cerebral organoids through activation of the innate immune receptor TLR3. Cell Stem Cell 19:258–265. https://doi.org/10.1016/j.stem.2016.04.014.
63. Garcez PP, Loiola EC, Madeiro da Costa R, Higa LM, Trindade P, Delvecchio R, Nascimento JM, Brindeiro R, Tanuri A, Rehen SK. 2016. Zika virus impairs growth in human neurospheres and brain organoids. Science 352:816–818. https://doi.org/10.1126/science.aaf6116.
64. Retallack H, Di Lullo E, Arias C, Knopp KA, Laurie MT, Sandoval-Espinosa C, Mancia Leon WR, Krencik R, Ullian EM, Spatazza J, Pollen AA, Mandel-Brehm C, Nowakowski TJ, Kriegstein AR, DeRisi JL. 2016. Zika virus cell tropism in the developing human brain and inhibition by azithromycin. Proc Natl Acad Sci U S A 113:14408–14413. https://doi.org/10.1073/pnas.1618029113.
65. Simonin Y, Loustalot F, Desmetz C, Foulongne V, Constant O, Fournier-Wirth C, Leon F, Moles JP, Goubaud A, Lemaitre JM, Maquart M, Leparc-Goffart I, Briant L, Nagot N, Van de Perre P, Salinas S. 2016. Zika virus strains potentially display different infectious profiles in human neural cells. EBioMedicine 12:161–169. https://doi.org/10.1016/j.ebiom.2016.09.020.
66. Souza BS, Sampaio GL, Pereira CS, Campos GS, Sardi SI, Freitas LA, Figueira CP, Paredes BD, Nonaka CK, Azevedo CM, Rocha VP, Bandeira AC, Mendez-Otero R, Dos Santos RR, Soares MB. 2016. Zika virus infection induces mitosis abnormalities and apoptotic cell death of human neural progenitor cells. Sci Rep 6:39775. https://doi.org/10.1038/srep39775.
67. Tang H, Hammack C, Ogden SC, Wen Z, Qian X, Li Y, Yao B, Shin J, Zhang F, Lee EM, Christian KM, Didier RA, Jin P, Song H, Ming GL. 2016. Zika virus infects human cortical neural progenitors and attenuates their growth. Cell Stem Cell 18:587–590. https://doi.org/10.1016/j.stem.2016.02.016.
68. Anfasa F, Siegers JY, van der Kroeg M, Mumtaz N, Stalin Raj V, de Vrij FMS, Widagdo W, Gabriel G, Salinas S, Simonin Y, Reusken C, Kushner SA, Koopmans MPG, Haagmans B, Martina BEE, van Riel D. 2017. Phenotypic differences between Asian and African lineage Zika viruses in human neural progenitor cells. mSphere 2. https://doi.org/10.1128/mSphere.00292-17.
69. Garcez PP, Nascimento JM, de Vasconcelos JM, Madeiro da Costa R, Delvecchio R, Trindade P, Loiola EC, Higa LM, Cassoli JS, Vitória G, Sequeira PC, Sochacki J, Aguiar RS, Fuzii HT, de Filippis AMB, da Silva Gonçalves Vianez Júnior JL, Tanuri A, Martins-de-Souza D, Rehen SK. 2017. Zika virus disrupts molecular fingerprinting of human neurospheres. Sci Rep 7:40780. https://doi.org/10.1038/srep40780.
70. Lin MY, Wang YL, Wu WL, Wolseley V, Tsai MT, Radic V, Thornton ME, Grubbs BH, Chow RH, Huang IC. 2017. Zika virus infects intermediate progenitor cells and post-mitotic committed neurons in human fetal brain tissues. Sci Rep 7:14883. https://doi.org/10.1038/s41598-017-13980-2.
71. Lum FM, Low DK, Fan Y, Tan JJ, Lee B, Chan JK, Renia L, Ginhoux F, Ng LF. 2017. Zika virus infects human fetal brain microglia and induces inflammation. Clin Infect Dis 64:914–920. https://doi.org/10.1093/cid/ciw878.
72. Olmo IG, Carvalho TG, Costa VV, Alves-Silva J, Ferrari CZ, Izidoro-Toledo TC, da Silva JF, Teixeira AL, Souza DG, Marques JT, Teixeira MM, Vieira LB, Ribeiro FM. 2017. Zika virus promotes neuronal cell death in a non-cell autonomous manner by triggering the release of neurotoxic factors. Front Immunol 8:1016. https://doi.org/10.3389/fimmu.2017.01016.
73. Rosenfeld AB, Doobin DJ, Warren AL, Racaniello VR, Vallee RB. 2017. Replication of early and recent Zika virus isolates throughout mouse brain development. Proc Natl Acad Sci U S A 114:12273–12278. https://doi.org/10.1073/pnas.1714624114.
74. He Z, Chen J, Zhu X, An S, Dong X, Yu J, Zhang S, Wu Y, Li G, Zhang Y, Wu J, Li M. 2018. NLRP3 inflammasome activation mediates Zika virus-associated inflammation. J Infect Dis 217:1942–1951. https://doi.org/10.1093/infdis/jiy129.
75. Muffat J, Li Y, Omer A, Durbin A, Bosch I, Bakiasi G, Richards E, Meyer A, Gehrke L, Jaenisch R. 2018. Human induced pluripotent stem cell-derived glial cells and neural progenitors display divergent responses to Zika and dengue infections. Proc Natl Acad Sci U S A 115:7117–7122. https://doi.org/10.1073/pnas.1719266115.
76. Daniels BP, Kofman SB, Smith JR, Norris GT, Snyder AG, Kolb JP, Gao X, Locasale JW, Martinez J, Gale M, Jr, Loo YM, Oberst A. 2019. The nucleotide sensor ZBP1 and kinase RIPK3 induce the enzyme IRG1 to promote an antiviral metabolic state in neurons. Immunity 50:64–76. https://doi.org/10.1016/j.immuni.2018.11.017.
77. Hamel R, Ferraris P, Wichit S, Diop F, Talignani L, Pompon J, Garcia D, Liegeois F, Sall AA, Yssel H, Misse D. 2017. African and Asian Zika virus strains differentially induce early antiviral responses in primary human astrocytes. Infect Genet Evol 49:134–137. https://doi.org/10.1016/j.meegid.2017.01.015.
78. Barba-Spaeth G, Dejnirattisai W, Rouvinski A, Vaney MC, Medits I, Sharma A, Simon-Loriere E, Sakuntabhai A, Cao-Lormeau VM, Haouz A, England P, Stiasny K, Mongkolsapaya J, Heinz FX, Screaton GR, Rey FA. 2016. Structural basis of potent Zika-dengue virus antibody cross-neutralization. Nature 536:48–53. https://doi.org/10.1038/nature18938.
79. Chouin-Carneiro T, Vega-Rua A, Vazeille M, Yebakima A, Girod R, Goindin D, Dupont-Rouzeyrol M, Lourenço-de-Oliveira R, Failloux A-B. 2016. Differential susceptibilities of *Aedes aegypti* and *Aedes albopictus* from the Americas to Zika virus. PLoS Negl Trop Dis 10:e0004543. https://doi.org/10.1371/journal.pntd.0004543.
80. Fritzell C, Raude J, Kazanji M, Flamand C. 2018. Emerging trends of Zika apprehension in an epidemic setting. PLoS Negl Trop Dis 12:e0006167. https://doi.org/10.1371/journal.pntd.0006167.
81. Mutso M, Saul S, Rausalu K, Susova O, Zusinaite E, Mahalingam S, Merits A. 2017. Reverse genetic system, genetically stable reporter viruses and packaged subgenomic replicon based on a Brazilian Zika virus isolate. J Gen Virol 98:2712–2724. https://doi.org/10.1099/jgv.0.000938.

Downloaded from https://journals.asm.org/journal/jvi on 05 October 2021 by 157.99.64.254.

Copyright Permissions

Copyright permissions for the articles and figures presented in this document.

Rajah MM, Bernier A, Buchrieser J, Schwartz S. The mechanism and consequences of SARS-CoV-2 spike-mediated fusion and syncytia formation, Journal of Molecular Biology (2021), doi: https://doi.org/10.1016/j.jmb.2021.167280**.** *(Review Article)*

Introduction (Text), Discussion (Text), Figures 1.5, 1.8, 5.1, 5.1

The mechanism and consequences of SARS-CoV-2 spike-mediated fusion and syncytia formation

Author:
Maaran Michael Rajah,Annie Bernier,Julian Buchrieser,Olivier Schwartz
Publication:
Journal of Molecular Biology
Publisher:
Elsevier
Date:
Available online 1 October 2021
© 2021 Elsevier Ltd. All rights reserved.
Journal Author Rights
Please note that, as the author of this Elsevier article, you retain the right to include it in a thesis or dissertation, provided it is not published commercially. Permission is not required, but please ensure that you reference the journal as the original source. For more information on this and on your other retained rights, please visit: https://www.elsevier.com/about/our-business/policies/copyright#Author-rights

Buchrieser J*, Dufloo J*, Hubert M*, Monel B*, Planas D*, **Rajah MM* (Co-first author),** Planchais C, Porrot F, Guivel-Benhassine F, Van der Werf S, Casartelli N, Mouquet H, Bruel T & Schwartz O "Syncytia formation by SARS-CoV-2-infected cells" (2020) **The EMBO Journal**, 39(23):e106267. https://doi.org/10.15252/embj.2020106267.

Chapter 2 (article)

This Agreement between Institut Pasteur -- Maaran RAJAH ("You") and John Wiley and Sons ("John Wiley and Sons") consists of your license details and the terms and conditions provided by John Wiley and Sons and Copyright Clearance Center.

License Number	5144750952342
License date	Sep 09, 2021
Licensed Content Publisher	John Wiley and Sons
Licensed Content Publication	The EMBO Journal
Licensed Content Title	Syncytia formation by SARS-CoV-2-infected cells
Licensed Content Author	Olivier Schwartz, Timothée Bruel, Hugo Mouquet, et al
Licensed Content Date	Nov 4, 2020
Licensed Content Volume	39
Licensed Content Issue	23
Licensed Content Pages	12
Type of Use	Dissertation/Thesis
Requestor type	Author of this Wiley article
Format	Print and electronic
Portion	Full article
Will you be translating?	No
Title	Functional characterization of the SARS-CoV-2 spike protein and syncytia formation
Institution name	Université de Paris
Expected presentation date	Dec 2021
Requestor Location	Institut Pasteur 28 rue du Dr Roux Paris, 75724 Cedex 15 France Attn: Institut Pasteur
Publisher Tax ID	EU826007151
Total	**0.00 EUR**

Rajah MM, Hubert M, Bishop E, Saunders N, Robinot R, Grzelak L, Planas D, Dufloo J, Gellenoncourt S, Bongers A, Zivaljic M, Planchais C, Guivel-Benhassine F, Porrot F, Mouquet H, Chakrabarti LA , Buchrieser J, Schwartz O. "SARS-CoV-2 Alpha, Beta and Delta variants display enhanced Spike-mediated Syncytia Formation" (2021) **The EMBO Journal** 0:e108944.
https://doi.org/10.15252/embj.2021108944

Chapter 3 (article)

JOHN WILEY AND SONS LICENSE
TERMS AND CONDITIONS

Nov 03, 2021

This Agreement between Institut Pasteur -- Maaran RAJAH ("You") and John Wiley and Sons ("John Wiley and Sons") consists of your license details and the terms and conditions provided by John Wiley and Sons and Copyright Clearance Center.

License Number	5181301161621
License date	Nov 03, 2021
Licensed Content Publisher	John Wiley and Sons
Licensed Content Publication	The EMBO Journal
Licensed Content Title	SARS−CoV−2 Alpha, Beta, and Delta variants display enhanced Spike−mediated syncytia formation
Licensed Content Author	Maaran Michael Rajah, Mathieu Hubert, Elodie Bishop, et al
Licensed Content Date	Oct 25, 2021
Licensed Content Volume	0
Licensed Content Issue	0
Licensed Content Pages	17

Type of use	Dissertation/Thesis
Requestor type	Author of this Wiley article
Format	Print and electronic
Portion	Full article
Will you be translating?	No
Title	Functional characterization of the SARS-CoV-2 spike protein and syncytia formation
Institution name	Université de Paris
Expected presentation date	Dec 2021
Requestor Location	Institut Pasteur 28 rue du Dr Roux Paris, 75724 Cedex 15 France Attn: Institut Pasteur
Publisher Tax ID	EU826007151
Total	0.00 EUR

Terms and Conditions

TERMS AND CONDITIONS

This copyrighted material is owned by or exclusively licensed to John Wiley & Sons, Inc. or one of its group companies (each a"Wiley Company") or handled on behalf of a society with which a Wiley Company has exclusive publishing rights in relation to a particular work (collectively "WILEY"). By clicking "accept" in connection with completing this licensing transaction, you agree that the following terms and conditions apply to this transaction (along with the billing and payment terms and conditions established by the Copyright Clearance Center Inc., ("CCC's Billing and Payment terms and conditions"), at the time that

Supplemental chapter:

1) **Rajah MM**, Monel B, Schwartz O "The entanglement between flaviviruses and ER-shaping proteins". (2020) **PLOS Pathogens**, 16(4): e1008389. *(Review Article)* https://doi.org/10.1371/journal.ppat.1008389

Copyright: © 2020 Rajah et al. This is an open access article distributed under the terms of the Creative Commons Attribution License, which permits unrestricted use, distribution, and reproduction in any medium, provided the original author and source are credited.

2) Monel B*, **Rajah MM** (**Co-first author**)*, Hafirassou ML, Sid-Ahmed S, Burlaud-Gaillard J, Zhu PP, Nevers Q, Buchrieser J, Porrot F, Meunier C, Amraoui S, Chazal M, Salles A, Jouvenet N, Roingeard P, Blackstone C, Amara A, Schwartz O "The Atlastin ER-shaping proteins facilitate Zika virus replication". (2019) **Journal of Virology**, 93(23): e01047-19. doi: 10.1128/JVI.01047-19

(next page)

CCC Marketplace™

Order Number: 1146595
Order Date: 09 Sep 2021

Payment Information

Maaran RAJAH
maaran.rajah@pasteur.fr
Payment method: Invoice

Billing Address:
Maaran RAJAH
Institut Pasteur
28 rue du Dr Roux
Paris, 75724 Cedex 15
France

+33 0612908886
maaran.rajah@pasteur.fr

Customer Location:
Maaran RAJAH
Institut Pasteur
28 rue du Dr Roux
Paris, 75724 Cedex 15
France

Order Details

1. Journal of virology : JVI

Billing Status: Open

Article: Atlastin Endoplasmic Reticulum-Shaping Proteins Facilitate Zika Virus Replication.

Order License ID	1146595-1	**Type of use**	Republish in a thesis/dissertation
Order detail status	Completed	**Publisher**	AMERICAN SOCIETY FOR MICROBIOLOGY
ISSN	1098-5514	**Portion**	Chapter/article

0.00 USD
Republication Permission

LICENSED CONTENT

Publication Title	Journal of virology : JVI	**Rightsholder**	American Society for Microbiology - Journals
Article Title	Atlastin Endoplasmic Reticulum-Shaping Proteins Facilitate Zika Virus Replication.	**Publication Type**	e-Journal
		Issue	23
		Volume	93
Author/Editor	American Society for Microbiology.	**URL**	https://journals.asm.org/journal/jvi
Date	01/01/1971		
Language	English		
Country	United States of America		

REQUEST DETAILS

Portion Type	Chapter/article	**Rights Requested**	Main product
Page range(s)	Full article	**Distribution**	Worldwide

Total number of pages	20	**Translation**	Original language of publication
Format (select all that apply)	Print,Electronic	**Copies for the disabled?**	No
Who will republish the content?	Academic institution	**Minor editing privileges?**	No
Duration of Use	Life of current edition	**Incidental promotional use?**	No
Lifetime Unit Quantity	Up to 499	**Currency**	USD

NEW WORK DETAILS

Title	Functional characterization of the SARS-CoV-2 spike protein and syncytia formation	**Institution name**	Université de Paris
		Expected presentation date	2021-12-31
Instructor name	Olivier Schwartz		

ADDITIONAL DETAILS

The requesting person / organization to appear on the license	Maaran RAJAH / Université de Paris

REUSE CONTENT DETAILS

Title, description or numeric reference of the portion(s)	Atlastin Endoplasmic Reticulum-Shaping Proteins Facilitate Zika Virus Replication.	**Title of the article/chapter the portion is from**	Atlastin Endoplasmic Reticulum-Shaping Proteins Facilitate Zika Virus Replication.
Editor of portion(s)	Mark T. Heise	**Author of portion(s)**	Monel, Blandine; Rajah, Maaran Michael; Schwartz, Olivier
Volume of serial or monograph	93		
Page or page range of portion	1-20	**Issue, if republishing an article from a serial**	23
		Publication date of portion	2019-12-01

American Society for Microbiology - Journals Terms and Conditions

We ask that you review the copyright information associated with the article that you are interested in, as some articles in the ASM Journals are covered by creative commons licenses that would permit free reuse with attribution. Please note that ASM cannot grant permission to reuse figures or images that are credited to publications other than ASM journals. For images credited to non-ASM journal publications, you will need to obtain permission from the journal referenced in the figure or table legend or credit line before making any use of the image(s) or table(s). ASM is unable to grant permission to reuse supplemental material as copyright for the supplemental material remains with the author.

This journal title may publish some Open Access articles, which provide specific user rights for reuse. Please refer to the article copyright line to determine whether the content you wish to use is Open Access. For Open Access content, permission to reuse is granted subject to the terms of the License under which the work was published. Please check the License conditions for the work which you wish to reuse. Full and appropriate attribution must be given. This permission does not cover any third party copyrighted material which may appear in the work requested. Please contact the publisher with any questions.

Total Items: 1 Subtotal: 0.00 USD

Figure 1.2 SARS-CoV-2 viral load, symptoms and disease progression after intial exposure. Symptoms generally occur 5 days post-infection and viral load peaks after a week. Most infections are asymptomatic or result in mild disease; however, some patients progress to severe and critical illnesses. This generally corresponds with an excessive immune response and increasing antibody titers. Reprinted with permission form BMJ Publishing Group Ltd: The BMJ, Vol 371, Cevik et al., Virology, transmission, and pathogenesis of SARS-CoV-2, Page 3, Copyright (2020). doi: https://doi.org/10.1136/bmj.m3862. Original data from Cell, Vol 181, Oberfeld et al., 2020 SnapShot: COVID-19. https://doi.org/10.1016/j.cell.2020.04.013 Permission also secured from Elsevier.

License Number	5154180060722
License date	Sep 22, 2021
Licensed Content Publisher	BMJ Publishing Group Ltd.
Licensed Content Publication	The BMJ
Licensed Content Title	Virology, transmission, and pathogenesis of SARS-CoV-2
Licensed Content Author	Muge Cevik, Krutika Kuppalli, Jason Kindrachuk, Malik Peiris
Licensed Content Date	Oct 23, 2020
Licensed Content Volume	371
Type of Use	Dissertation/Thesis
Requestor Type	Individual Account
Format	Print and electronic
Portion Used	Figure/table/extract
Number of figure/table/extracts	1
Will you be translating?	No
Title	Functional characterization of the SARS-CoV-2 spike protein and syncytia formation
Institution name	Université de Paris
Expected presentation date	Dec 2021
Portions	Figure 2
Circulation	100000
Requestor Location	Institut Pasteur 28 rue du Dr Roux Paris, 75724 Cedex 15 France Attn: Institut Pasteur
Publisher Tax ID	GB674738491
Total	**0.00 EUR**

License Number	5165360790277
License date	Oct 10, 2021
Licensed Content Publisher	Elsevier
Licensed Content Publication	Cell
Licensed Content Title	SnapShot: COVID-19
Licensed Content Author	Blake Oberfeld,Aditya Achanta,Kendall Carpenter,Pamela Chen,Nicole M. Gilette,Pinky Langat,J Schiff,Allen S. Zhou,Amy K. Barczak,Shiv Pillai
Licensed Content Date	May 14, 2020
Licensed Content Volume	181
Licensed Content Issue	4
Licensed Content Pages	2
Type of Use	reuse in a thesis/dissertation
Portion	figures/tables/illustrations
Number of figures/tables/illustrations	1
Format	both print and electronic
Are you the author of this Elsevier article?	No
Will you be translating?	No
Title	Functional characterization of the SARS-CoV-2 spike protein and syncytia formation
Institution name	Université de Paris
Expected presentation date	Dec 2021
Portions	1
Requestor Location	Institut Pasteur 28 rue du Dr Roux Paris, 75724 Cedex 15 France Attn: Institut Pasteur
Publisher Tax ID	GB 494 6272 12
Total	**0.00 EUR**

Figure 1.7 Cellular syncytia in the lungs of COVID19 patients. Original image from Figure 4C of Bussani et al., 2020, Persistence of viral RNA, pneumocyte syncytia and thrombosis are hallmarks of advanced COVID-19 pathology (2020), EBioMedicine Vol 61. Reused under creative commons license. https://doi.org/10.1016/j.ebiom.2020.103104.

Persistence of viral RNA, pneumocyte syncytia and thrombosis are hallmarks of advanced COVID-19 pathology

Author:
Rossana Bussani,Edoardo Schneider,Lorena Zentilin,Chiara Collesi,Hashim Ali,Luca Braga,Maria Concetta Volpe,Andrea Colliva,Fabrizio Zanconati,Giorgio Berlot,Furio Silvestri,Serena Zacchigna,Mauro Giacca
Publication:
EBioMedicine
Publisher:
Elsevier
Date:
November 2020
© 2020 The Authors. Published by Elsevier B.V.

Creative Commons Attribution-NonCommercial-No Derivatives License (CC BY NC ND)

This article is published under the terms of the Creative Commons Attribution-NonCommercial-No Derivatives License (CC BY NC ND).

For non-commercial purposes you may copy and distribute the article, use portions or extracts from the article in other works, and text or data mine the article, provided you do not alter or modify the article without permission from Elsevier. You may also create adaptations of the article for your own personal use only, but not distribute these to others. You must give appropriate credit to the original work, together with a link to the formal publication through the relevant DOI, and a link to the Creative Commons user license above. If changes are permitted, you must indicate if any changes are made but not in any way that suggests the licensor endorses you or your use of the work.

Permission is not required for this non-commercial use. For commercial use please continue to request permission via RightsLink

Figure 1.3 (A) SARS-CoV-2 virion morphology with the viral structural proteins **(B)** Viral genome organization with the associated structural, non-structural and accessory proteins. Adapted with permission from The American Society for Microbiology. Clinical Microbiology Reviews, Vol 34, Tali et al., Page 4, Copyright (2021). doi: https://doi.org/10.1128/CMR.00228-20

CCC Marketplace™

Order Number: 1149442
Order Date: 22 Sep 2021

Payment Information

Maaran RAJAH
maaran.rajah@pasteur.fr
Payment method: Invoice

Billing Address:
Maaran RAJAH
Institut Pasteur
28 rue du Dr Roux
Paris, 75724 Cedex 15
France

+33 0612908886
maaran.rajah@pasteur.fr

Customer Location:
Maaran RAJAH
Institut Pasteur
28 rue du Dr Roux
Paris, 75724 Cedex 15
France

Order Details

1. Clinical microbiology reviews : CMR

Billing Status: Open

Article: Tools and Techniques for Severe Acute Respiratory Syndrome Coronavirus 2 (SARS-CoV-2)/COVID-19 Detection

Order License ID	1149442-1	**Type of use**	Republish in a thesis/dissertation
Order detail status	Completed		
ISSN	1098-6618	**Publisher**	AMERICAN SOCIETY FOR MICROBIOLOGY,
		Portion	Image/photo/illustration

0,00 EUR
Republication Permission

LICENSED CONTENT

Publication Title	Clinical microbiology reviews : CMR	**Rightsholder**	American Society for Microbiology - Journals
Article Title	Tools and Techniques for Severe Acute Respiratory Syndrome Coronavirus 2 (SARS-CoV-2)/COVID-19 Detection	**Publication Type**	e-Journal
		Issue	3
		Volume	34
		URL	https://journals.asm.org/journal/cmr
Author/Editor	American Society for Microbiology.		
Date	01/01/1988		
Language	English		
Country	United States of America		

REQUEST DETAILS

Portion Type	Image/photo/illustration	**Distribution**	Worldwide
Number of images / photos / illustrations	1	**Translation**	Original language of publication
Format (select all that apply)	Print,Electronic	**Copies for the disabled?**	No
Who will republish the content?	Academic institution	**Minor editing privileges?**	Yes
Duration of Use	Life of current edition	**Incidental promotional use?**	No
Lifetime Unit Quantity	Up to 99,999	**Currency**	EUR
Rights Requested	Main product		

NEW WORK DETAILS

Title	Functional characterization of the SARS-CoV-2 spike protein and syncytia formation	**Institution name**	Université de Paris/Institut Pasteur
Instructor name	Olivier Schwartz	**Expected presentation date**	2021-12-10

ADDITIONAL DETAILS

The requesting person / organization to appear on the license	Universite de Paris / Institut Pasteur

REUSE CONTENT DETAILS

Title, description or numeric reference of the portion(s)	Figure 2	**Title of the article/chapter the portion is from**	Tools and Techniques for Severe Acute Respiratory Syndrome Coronavirus 2 (SARS-CoV-2)/COVID-19 Detection
Editor of portion(s)	Safiabadi Tali, Seyed Hamid; LeBlanc, Jason J.; Sadiq, Zubi; Oyewunmi, Oyejide Damilola; Camargo, Carolina; Nikpour, Bahareh; Armanfard, Narges; Sagan, Selena M.; Jahanshahi-Anbuhi, Sana	**Author of portion(s)**	Safiabadi Tali, Seyed Hamid; LeBlanc, Jason J.; Sadiq, Zubi; Oyewunmi, Oyejide Damilola; Camargo, Carolina; Nikpour, Bahareh; Armanfard, Narges; Sagan, Selena M.; Jahanshahi-Anbuhi, Sana
Volume of serial or monograph	34		
Page or page range of portion	Page 4 Figure 2	**Issue, if republishing an article from a serial**	3
		Publication date of portion	2021-06-16

Figure 1.4 Coronavirus replication cycle. The viral S protein interacts with the ACE2 receptor to fuse into the cell at the plasma membrane (early entry) or within endosomes (late entry). The viral genome is deposited into the cytoplasm and is translated from ORF1a and ORF1ab. The resulting polypeptides are post- and co- translationally processed into the non-structural proteins which form the viral replication and transcription complexes, induce remodelling of intracellular membrane and facilitate immune escape. The structural and accessory proteins are produced from a nested set of subgenomic mRNAs encoded in the viral genome. The structural proteins translocate to the ER membranes and transit through the ER-ERGIC-Golgi network and interact with newly synthesize vRNA. Immature virions bud into the intracellular compartments and are maturated as they egress via deacidified lysosome-dependent exocytosis. Reused with permission from Springer Nature. Nature Reviews Microbiology, Vol 19, V'kovski et al., Page 156, Copyright (2021). doi: https://doi.org/10.1038/s41579-020-00468-6

This Agreement between Institut Pasteur -- Maaran RAJAH ("You") and Springer Nature ("Springer Nature") consists of your license details and the terms and conditions provided by Springer Nature and Copyright Clearance Center.

License Number	5153741255690
License date	Sep 21, 2021
Licensed Content Publisher	Springer Nature
Licensed Content Publication	Nature Reviews Microbiology
Licensed Content Title	Coronavirus biology and replication: implications for SARS-CoV-2
Licensed Content Author	Philip V'kovski et al
Licensed Content Date	Oct 28, 2020
Type of Use	Thesis/Dissertation
Requestor type	academic/university or research institute
Format	print and electronic
Portion	figures/tables/illustrations
Number of figures/tables/illustrations	1
High-res required	no
Will you be translating?	no
Circulation/distribution	50000 or greater
Author of this Springer Nature content	no
Title	Functional characterization of the SARS-CoV-2 spike protein and syncytia formation
Institution name	Université de Paris
Expected presentation date	Dec 2021

Portions	Fig. 1: The coronavirus virion and life cycle.
	Institut Pasteur 28 rue du Dr Roux
Requestor Location	
	Paris, 75724 Cedex 15 France Attn: Institut Pasteur
Total	0.00 USD

Figure 1.6 The innate immune response and signaling response to coronavirus infection. Pathogen recognition receptors (TLRs, RIG-I, and MDA5) recognize viral components leading to the transcription of NF-kB, IRF3 and 7, which will subsequently translocate to the nucleus and stimulate cytokine and IFNI/III production. Secreted IFNI/III will be recognized by IFNAR and IFNLR receptors which will set of a signaling pathway that will result in the phosphorylation of the STAT proteins. STAT1 and 2 will complex with IRF9 and translocate to the nucleus to trigger the expression of interferon stimulated genes. Reused with permission from Elsevier. Cell Host & Microbe, Vol 27, Park et al., Page 871, Copyright (2020).
doi: https://doi.org/10.1016/j.chom.2020.05.008

License Number	5165441480771
License date	Oct 10, 2021
Licensed Content Publisher	Elsevier
Licensed Content Publication	Cell Host & Microbe
Licensed Content Title	Type I and Type III Interferons – Induction, Signaling, Evasion, and Application to Combat COVID-19
Licensed Content Author	Annsea Park,Akiko Iwasaki
Licensed Content Date	Jun 10, 2020
Licensed Content Volume	27
Licensed Content Issue	6
Licensed Content Pages	9
Type of Use	reuse in a thesis/dissertation
Portion	figures/tables/illustrations
Number of figures/tables/illustrations	1
Format	both print and electronic
Are you the author of this Elsevier article?	No
Will you be translating?	No
Title	Functional characterization of the SARS-CoV-2 spike protein and syncytia formation
Institution name	Université de Paris
Expected presentation date	Dec 2021
Portions	Figure 1
Requestor Location	Institut Pasteur 28 rue du Dr Roux Paris, 75724 Cedex 15 France Attn: Institut Pasteur
Publisher Tax ID	GB 494 6272 12
Total	**0.00 EUR**

Article Covers:

Grzelak L, Temmam S, Planchais C, Demeret C, Tondeur L, Huon C, Guivel-Benhassine F, Staropoli I, Chazal M, Dufloo J, Planas D, Buchrieser J, **Rajah MM**, et al. "A comparison of four serological assays for detecting anti-SARS-CoV-2 antibodies in human serum samples from different populations" (2020) Science Translational Medicine, 12(559): eabc3103. doi: 10.1126/scitranslmed.abc3103 [273]

Copyright
Copyright © 2020 The Authors, some rights reserved; exclusive licensee American Association for the Advancement of Science. No claim to original U.S. Government Works. Distributed under a Creative Commons Attribution License 4.0 (CC BY).
https://creativecommons.org/licenses/by/4.0/
This is an open-access article distributed under the terms of the Creative Commons Attribution license, which permits unrestricted use, distribution, and reproduction in any medium, provided the original work is properly cited.

Planas D, Veyer D, Baidaliuk A, Staropoli I , Guivel-Benhassine F , **Rajah MM**, et al. "Reduced sensitivity of SARS-CoV-2 variant Delta to antibody neutralization" (2021) Nature**,** 596 (276-280) https://doi.org/10.1038/s41586-021-03777-9 [51]

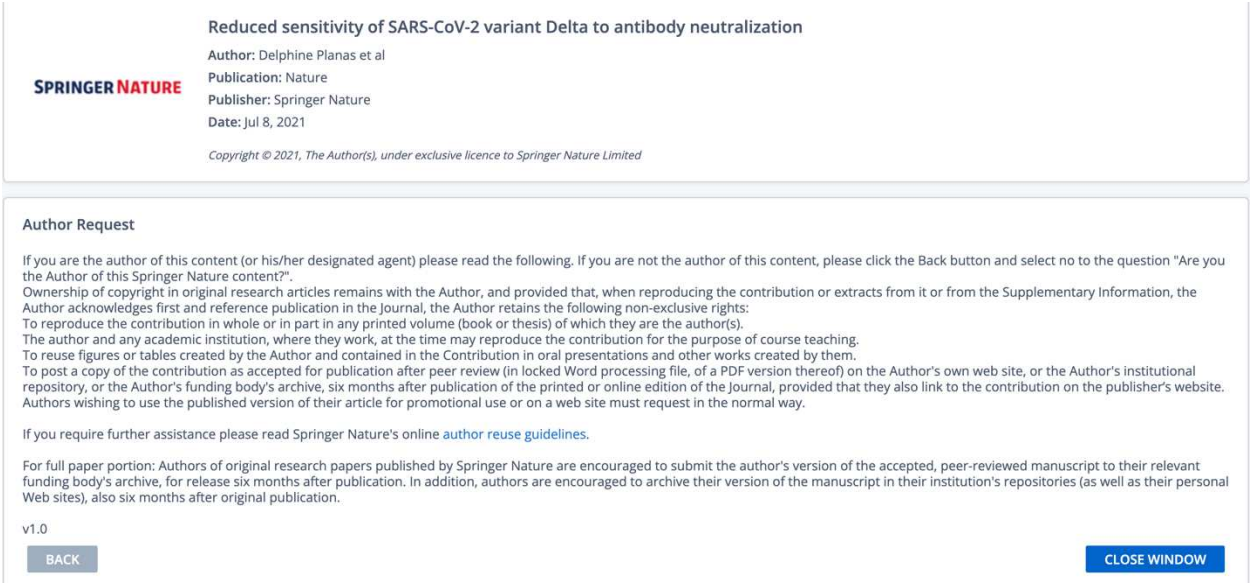

SPRINGER NATURE

Reduced sensitivity of SARS-CoV-2 variant Delta to antibody neutralization

Author: Delphine Planas et al
Publication: Nature
Publisher: Springer Nature
Date: Jul 8, 2021

Copyright © 2021, The Author(s), under exclusive licence to Springer Nature Limited

Author Request

If you are the author of this content (or his/her designated agent) please read the following. If you are not the author of this content, please click the Back button and select no to the question "Are you the Author of this Springer Nature content?".
Ownership of copyright in original research articles remains with the Author, and provided that, when reproducing the contribution or extracts from it or from the Supplementary Information, the Author acknowledges first and reference publication in the Journal, the Author retains the following non-exclusive rights:
To reproduce the contribution in whole or in part in any printed volume (book or thesis) of which they are the author(s).
The author and any academic institution, where they work, at the time may reproduce the contribution for the purpose of course teaching.
To reuse figures or tables created by the Author and contained in the Contribution in oral presentations and other works created by them.
To post a copy of the contribution as accepted for publication after peer review (in locked Word processing file, of a PDF version thereof) on the Author's own web site, or the Author's institutional repository, or the Author's funding body's archive, six months after publication of the printed or online edition of the Journal, provided that they also link to the contribution on the publisher's website.
Authors wishing to use the published version of their article for promotional use or on a web site must request in the normal way.

If you require further assistance please read Springer Nature's online author reuse guidelines.

For full paper portion: Authors of original research papers published by Springer Nature are encouraged to submit the author's version of the accepted, peer-reviewed manuscript to their relevant funding body's archive, for release six months after publication. In addition, authors are encouraged to archive their version of the manuscript in their institution's repositories (as well as their personal Web sites), also six months after original publication.

v1.0

BACK

CLOSE WINDOW

Planas D, Bruel T, Grzelak L, Guivel-Benhassine F, Staropoli I, Porrot F, Planchais C , Buchrieser J, **Rajah MM**, et al. "Sensitivity of infectious SARS-CoV-2 B.1.1.7 and B.1.351 variants to neutralizing antibodies" (2021) Nature Medicine, 27 (917-924) https://doi.org/10.1038/s41591-021-01318-5 [56]

Sensitivity of infectious SARS-CoV-2 B.1.1.7 and B.1.351 variants to neutralizing antibodies

Author: Delphine Planas et al
Publication: Nature Medicine
Publisher: Springer Nature
Date: Mar 26, 2021

Copyright © 2021, The Author(s), under exclusive licence to Springer Nature America, Inc.

Author Request

If you are the author of this content (or his/her designated agent) please read the following. If you are not the author of this content, please click the Back button and select no to the question "Are you the Author of this Springer Nature content?".
Ownership of copyright in original research articles remains with the Author, and provided that, when reproducing the contribution or extracts from it or from the Supplementary Information, the Author acknowledges first and reference publication in the Journal, the Author retains the following non-exclusive rights:
To reproduce the contribution in whole or in part in any printed volume (book or thesis) of which they are the author(s).
The author and any academic institution, where they work, at the time may reproduce the contribution for the purpose of course teaching.
To reuse figures or tables created by the Author and contained in the Contribution in oral presentations and other works created by them.
To post a copy of the contribution as accepted for publication after peer review (in locked Word processing file, of a PDF version thereof) on the Author's own web site, or the Author's institutional repository, or the Author's funding body's archive, six months after publication of the printed or online edition of the Journal, provided that they also link to the contribution on the publisher's website.
Authors wishing to use the published version of their article for promotional use or on a web site must request in the normal way.

If you require further assistance please read Springer Nature's online author reuse guidelines.

For full paper portion: Authors of original research papers published by Springer Nature are encouraged to submit the author's version of the accepted, peer-reviewed manuscript to their relevant funding body's archive, for release six months after publication. In addition, authors are encouraged to archive their version of the manuscript in their institution's repositories (as well as their personal Web sites), also six months after original publication.

v1.0

Other Articles & Press Releases

1) Full review article derived from Chapter 1 & 5 of this thesis

Rajah MM, Bernier A, Buchrieser J, Schwartz S. The mechanism and consequences of SARS-CoV-2 spike-mediated fusion and syncytia formation, Journal of Molecular Biology (2021), doi: https://doi.org/10.1016/j.jmb.2021.167280**.**

1) Title pages of other articles not included in this thesis:

Planas D, Veyer D, Baidaliuk A, Staropoli I , Guivel-Benhassine F , **Rajah MM**, et al. "Reduced sensitivity of SARS-CoV-2 variant Delta to antibody neutralization" (2021) **Nature,** 596 (276-280) https://doi.org/10.1038/s41586-021-03777-9

Planas D, Bruel T, Grzelak L, Guivel-Benhassine F, Staropoli I, Porrot F, Planchais C , Buchrieser J, **Rajah MM**, et al. "Sensitivity of infectious SARS-CoV-2 B.1.1.7 and B.1.351 variants to neutralizing antibodies" (2021) **Nature Medicine,** 27 (917-924) https://doi.org/10.1038/s41591-021-01318-5

Grzelak L, Temmam S, Planchais C, Demeret C, Tondeur L, Huon C, Guivel-Benhassine F, Staropoli I, Chazal M, Dufloo J, Planas D, Buchrieser J, **Rajah MM**, et al. "A comparison of four serological assays for detecting anti-SARS-CoV-2 antibodies in human serum samples from different populations" (2020) **Science Translational Medicine**, 12(559): eabc3103. Doi: 10.1126/scitranslmed.abc3103

2) Press release:

Rajah MM, Hubert M, Bishop E, Saunders N, Robinot R, Grzelak L, Planas D, Dufloo J, Gellenoncourt S, Bongers A, Zivaljic M, Planchais C, Guivel-Benhassine F, Porrot F, Mouquet H, Chakrabarti LA , Buchrieser J, Schwartz O. "SARS-CoV-2 Alpha, Beta and Delta variants display enhanced Spike-mediated Syncytia Formation" (2021) **The EMBO Journal**

Review Article

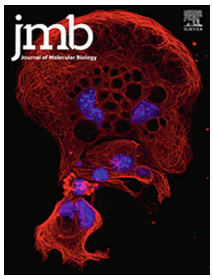

The Mechanism and Consequences of SARS-CoV-2 Spike-Mediated Fusion and Syncytia Formation

Maaran Michael Rajah [1,2], **Annie Bernier** [3], **Julian Buchrieser** [1†] and **Olivier Schwartz** [1,2,4*†]

*1 - **Virus & Immunity Unit,** Department of Virology, Institut Pasteur, CNRS UMR 3569, Paris, France*
*2 - **Université de Paris,** Sorbonne Paris Cité, Paris, France*
*3 - **Institut Curie,** INSERM U932, Paris, France*
*4 - **Vaccine Research Institute,** Creteil, France*

Correspondence to Olivier Schwartz: Virus & Immunity Unit, Department of Virology, Institut Pasteur, CNRS UMR 3569, Paris, France. *olivier.schwartz@pasteur.fr (O. Schwartz), @MaaranRajah (M.M. Rajah), @nini_bernier (A. Bernier), @JBuchrieser (J. Buchrieser), @OlivierSchwartz (O. Schwartz)*
https://doi.org/10.1016/j.jmb.2021.167280
Edited by Alex Compton

Abstract

Syncytia are formed when individual cells fuse. SARS-CoV-2 induces syncytia when the viral spike (S) protein on the surface of an infected cell interacts with receptors on neighboring cells. Syncytia may potentially contribute to pathology by facilitating viral dissemination, cytopathicity, immune evasion, and inflammatory response. SARS-CoV-2 variants of concern possess several mutations within the S protein that enhance receptor interaction, fusogenicity and antibody binding. In this review, we discuss the molecular determinants of S mediated fusion and the antiviral innate immunity components that counteract syncytia formation. Several interferon-stimulated genes, including IFITMs and LY6E act as barriers to S protein-mediated fusion by altering the composition or biophysical properties of the target membrane. We also summarize the effect that the mutations associated with the variants of concern have on S protein fusogenicity. Altogether, this review contextualizes the current understanding of Spike fusogenicity and the role of syncytia during SARS-CoV-2 infection and pathology.

© 2021 Elsevier Ltd. All rights reserved.

Introduction

Since their identification in the 1960s, coronaviruses have proven to be a persistent threat. Previous outbreaks of SARS-CoV (2001) and MERS-CoV (2012) as well as the commonly circulating HKU1, NL63, OC43, and 229E viruses have all collectively placed a significant burden on the global public health infrastructure.[1] The current global outbreak of SARS-CoV-2 has been truly staggering in its impact with over 220 million confirmed cases and 4.6 million deaths (as of September 20, 2021).[2] Since the emergence of the ancestral Wuhan strain, several new variants have arisen and spread across the globe. The scale and impact of the pandemic and subsequent vaccination campaigns have piqued scientific interest in SARS-CoV-2; particularly into the virological and molecular determinants of SARS-CoV-2 pathology. The presence of syncytia in the lung tissues of infected patients represents one such pathological feature under scrutiny.[3] The contribution of syncytia to SARS-CoV-2 virology and pathology is currently unclear; however, this past year has seen an unprecedented flurry of research on the molecular and viral determinant of coronavirus induced syncytia formation as well as its potential impact on viral dissemination, pathology and the immune response.

Please cite tts article as: Maaran Michael Rajah, A. Bernier, J. Buchrieser, et al., The Mechanism and Consequences of SARS-CoV-2 Spike-Mediated Fusion and Syncytia FormationJournal of Molecular Biology, https://doi.org/10.1016/j.jmb.2021.167280

Syncytia are large multinucleated cells produced by two or more cells fusing. During syncytia formation, the plasma membrane of different cells merge into a single lipid bilayer and their cytoplasmic contents merge.[4,5] Many important physiological processes are dependent on cells undergoing syncytialization, including the formation of muscle fibers and the placental barrier as well as bone osteoclast differentiation.[5,6] The fusion process is facilitated by a class of specialized proteins known as fusogens, which help overcome the natural repulsive forces and energetic barriers that act to keep cellular plasma membranes apart.[7] Mechanistically, cell–cell fusion is analogous to virus-cell fusion. Indeed, the membrane of enveloped viruses must fuse with cellular membranes in order for viral contents to be delivered into the cytoplasm, beginning the viral replication cycle. The parallels between the mechanics of physiological cell–cell fusion and virus-cell fusion during infection is appropriately exemplified by the formation of the placenta. The vital placental barrier is formed by a layer of fused cytotrophoblasts called the syncytiotrophoblast.[4,5,8] Syncytins, the fusogens that facilitate cytotrophoblast fusion, are in fact derived from the fusogens of endogenous retroviruses (ERV); the genes of which were assimilated into mammalian genomes 10–85 million years ago.[8]

Beyond this particular evolutionary association between viruses and cell–cell fusion exists a more immediate causal relationship, in which syncytia are induced as a consequence of viral infection. Such syncytia could potentially facilitate viral replication, dissemination, immune evasion as well as cause cytopathic effects and wider tissue damage.[9] The most direct example is the fusion-associated small transmembrane (FAST) proteins encoded by the non-enveloped reovirus.[10] These fusogens are uniquely specialized cell–cell fusion proteins and they increase pathogenicity and viral dissemination.[10,11] In contrast, the fusion machinery of enveloped viruses primarily function to fuse the membrane of viral particles with plasma or endosomal membranes. In particular instances, they may induce infected cells to fuse with adjacent cells. Viruses from a broad range of families including Herpesviridae (varicella-zoster virus, herpes simplex virus 1/2, human cytomegalovirus), Paramyxoviridae (Sendai, Nipah, Hendra, measles virus, respiratory syncytial virus), Retroviridae (human immunodeficiency virus 1, human T-lymphotropic virus) have all been shown to form syncytia *in vivo* and/or *in vitro*. For a broader discussion on how, and potentially why, different viruses induce syncytia formation we refer the reader to the insightful review by Leroy and colleagues.[9] Syncytial cells have also been observed upon infection with some members of the Coronaviridae family including MERS-CoV, the currently pandemic SARS-CoV-2 and to a lesser degree SARS-CoV.[9] There have been many investigations into the highly antigenic SARS-CoV-2 Spike (S) protein, which is the viral fusogen. Recent characterizations have provided detailed insights into the properties and domains of the S fusogen and its interaction with receptors. There have also been significant advances in the molecular understanding of the relationship between the SARS-CoV-2 S protein-mediated fusogenicity and the innate immune response.

In this article, we endeavor to summarize and contextualize the recent literature, including our own work, on the subject of SARS-CoV-2 induced syncytia formation. We summarize the clinical evidence for coronavirus-induced syncytia formation, examine the molecular determinants of S protein-mediated fusion, and discuss the antiviral innate immunity components that restrict cell–cell fusion. We also examine the molecular and virological implications of the S protein mutations carried by the novel variants of concern in terms of fusogenicity. Finally, we discuss possible consequences of virus-induced syncytia formation on viral infection, dissemination, immune response and pathogenicity.

Clinical Evidence for Coronavirus-Induced Syncytia formation

The clinical manifestations of SARS-CoV-2 infection can range from a mild febrile illness to acute respiratory distress to extensive and occasionally fatal lung damage.[3] The deterioration of lung tissue is characterized by diffuse alveolar damage, micro/macro-vascular thrombosis, and pneumocyte necrosis.[3,12,13] Many of these lung pathologies are also reminiscent of SARS-CoV and MERS-CoV infections.[3,14,15] The clinical features of COVID-19, especially the extensive lung thrombosis, are particularly severe in comparison to other causes of acute respiratory syndrome.[3,16] A combination of hypoxemia, immune-mediated damage, and virus-induced cytopathic effect all contribute to lung epithelial destruction.[3,16,17] Amongst these factors, most of the described histopathology is likely related to the immune response. Indeed, infection of respiratory epithelial cells can lead to monocyte, macrophage and dendritic cell activation and the secretion of proinflammatory cytokines. Excessive cytokine production has been documented in the blood of patients presenting the most severe form of disease.[18–21] Virus-induced cytopathic effects may also directly damage the lung tissue while also triggering further immune activation. A peculiar feature noticed in many clinical reports was the presence of multinucleated pneumocytes. One team reported the presence of infected syncytial pneumocytes in 36/41 patients who died of COVID-19.[3,16] This observation is supported by several COVID-19 autopsy reports from patients and non-human primate mod-

els which also describe the prevalence of syncytia in infected lung tissue.[22–26] It should be noted that these clinical observations are from patients presenting the most severe manifestation of COVID-19 disease and it is currently unclear if syncytia formation is also a feature of milder or asymptomatic SARS-CoV-2 infections. Autopsy reports conducted on patients who were infected with SARS-CoV and MERS-CoV have also reported the presence of giant multinucleated syncytial cells in the lungs, some of which are of epithelial origin.[14,15,27–30]

Several of the "common cold" coronaviruses including hCoV-HKU1, hCoV-NL63 and hCoV-229E form syncytia in cell culture models.[31–33] To our knowledge, there are no documented patient case of syncytia induced by these widely circulating coronaviruses. This is unsurprising as they are not known to be lethal, so autopsy reports are scarce. More *in vivo* evidence in animal models is required to assess the syncytiogenicity of the common cold coronaviruses. It is currently unclear if or how SARS-CoV-2-mediated syncytia formation contributes to pathology; however, it may compound the detrimental effects of virus-induced cytopathicity and generalized immune-mediated damage and contribute to the deterioration of lung tissue seen in critical cases. Furthermore, syncytia may also contribute to viral dissemination and immune evasion by protecting the virus from immune cells and from neutralizing antibodies (discussed in later sections).

SARS-CoV-2 Viral Life Cycle and the S Protein

The S protein is important for both virions and cell–cell fusion. As such, its genesis, action, processing, and translocation within the context of the viral life cycle is of importance to understand syncytia formation. The surface of the SARS-CoV-2 virion contains the trimeric S protein, which protrudes from the surface of the virus giving the virion a "crown-like" appearance from which the family nomenclature of "corona" derives. The structure and features of the S protein are described in depth in a later section. The S protein is a class I fusogen (structurally comprised of α-helices) which facilitates membrane fusion after undergoing structural rearrangements which transition it from a metastable prefusion form to a fusion competent state.[7,34] The fusion of the viral membrane with the cellular membranes and the deposition and uncoating of viral genomic RNA into the cellular cytoplasm represents the first stage of the viral life cycle (Figure 1).[35] This occurs when the S protein on the surface of the virions interacts with the human angiotensin converting enzyme 2 (ACE2) receptor at the surface of the target cell. Several auxiliary receptors such as L-SIGN, DC-SIGN, and neuropilin-1 (Nrp1), may facilitate attachment or entry.[36,37] The virus can then fuse at the plasma membrane (early entry) or with endosomal membranes (late entry) during uptake (Figure 1). When bound at the plasma membrane, the S protein may be primed by host factors like transmembrane serine protease 2 (TMPRSS2), which enhances SARS-CoV-2 entry.[38–40] After endocytosis, proteolytic activity by host factors such as cathepsin L/B (CTSL/B) and furin further assists in the priming the S protein (Figure 1).[38,41,42]

Following fusion and uncoating, the first two-thirds (from the 5′ end) of the viral RNA is translated from two open reading frames, ORF1a and ORF1b.[35,39] The resulting polyproteins are co– and post-translationally processed into the non-structural proteins (nsp1-nsp16) that make up the viral replication and transcription complex.[35] Coronaviruses, like many other described viruses, co-opt intracellular membranes to form viral replication organelles that provide a protective microenvironment for the genomic viral RNA replication and protein transcription.[35,43] The structural proteins S, envelope (E), nucleocapsid (N), and membrane (M) as well as several accessory proteins, are transcribed from ORFs from the final third of the viral genome from a nested set of sub-genomic mRNAs.[35] These accessory proteins are thought to play a role in viral pathogenicity and in modulating the host's immune response. During the coronavirus assembly process, the E, M, and S proteins are translocated and inserted into the endoplasmic reticulum and are trafficked through the ER-Golgi intermediate compartment (ERGIC) to the Golgi apparatus (Figure 1). The immature virions then bud into the ERGIC or Golgi compartments. Viral egress occurs through deacidified lysosome-dependent exocytosis.[44] During the course of S protein translocation and viral assembly, the S protein is subjected to processing by furin and other cellular proteases, generating the non-covalently associated S1 and S2 subunits which are primed for fusing with the membrane of naïve cells.[45]

The Role of S Protein in Syncytia Formation

Despite the majority of the genesis and processing of the S protein, as well as viral budding, occurring at intracellular membranes, we and other found that the S protein is present on the surface of infected cells.[26,46] The interaction of the S protein on the infected cell surface with the ACE2 receptor on neighboring cells is the cause of syncytia formation (Figure 1). This process is further augmented by the presence of the TMPRSS2 protease.[46] The exact role that auxiliary receptors may play in cell–cell fusion remains to be elucidated; however, Daly and colleagues note that knocking out Nrp1 in cells expressing ACE2 is detrimental to syncytia formation.[47] It has been suggested that Nrp1 facilitates earlier separation of

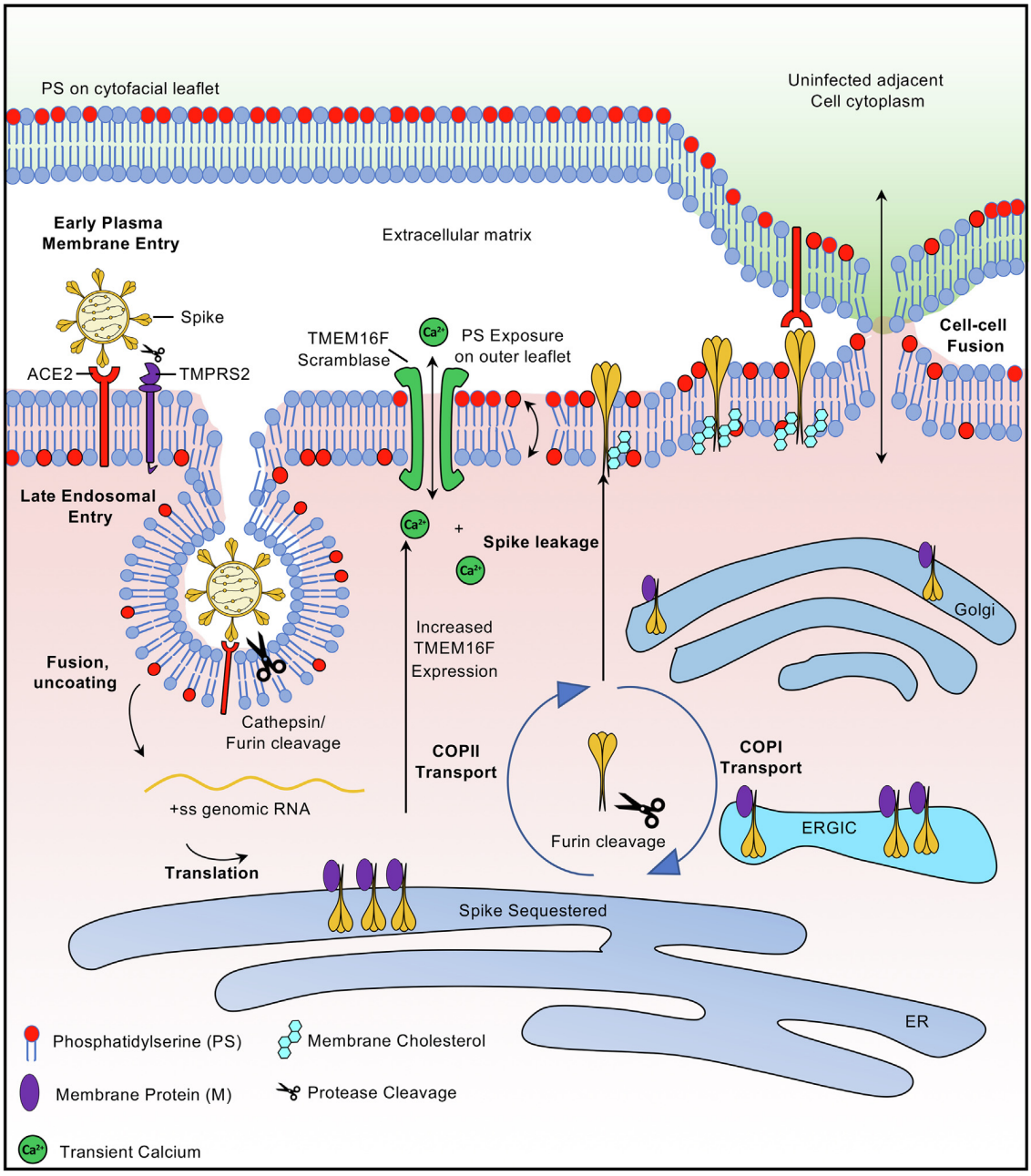

Figure 1. Schematic representation of the diverse activities of the SARS-CoV-2 spike (S) protein during infection and syncytia formation. Viral infection begins when the S protein on the surface of the virion interacts with the ACE2 receptor. During early entry, the S protein is processed by the TMPRSS2 protease and fusion occurs on the plasma membrane (PM). The S protein can also fuse with endosomal membranes during late entry, upon being primed by cathepsins and furin. The positive-sense single stranded (+ss) viral genomic RNA is deposited in the cytoplasm and translated. Viral RNA replication and transcription occur on membranes. Upon being transcribed, the S protein is translocated and inserted into the endoplasmic reticulum (ER) and is generally sequestered within intracellular membranes by the membrane structural protein (M). The expression of the S protein leads to intracellular calcium fluctuations and the increased expression of the TMEM16F scramblase. TMEM16F exposes the phosphatidylserine (PS) from the cytofacial leaflet of the PM to the exofacial leaflet. The transcribed S protein is processed by furin and transported throughout the ER-Golgi network. During COPI (retrograde) and COPII (anterograde) transport, leakage of the S protein can occur from vesicles (not shown in simplified schematic). The S protein is then translocated to the PM, where it associates with cholesterols, and induces syncytia formation by interacting with receptors on neighbouring uninfected cells. The sequestered S protein is in packaged into virions that bud into the Golgi or ER-Golgi intermediate compartment (ERGIC), and virions exit the cell via deacidified lysosome-dependent exocytosis (not shown). The ER, ERGIC, and Golgi membranes are bilayers which are represented as single lines in this schematic.

the S2 domain, which contains the fusion machinery, by stabilizing the S1 domain.[48] However, prior to any receptor interaction, syncytia formation requires the S protein to be translocated to the plasma membrane.

Therein lies the first question regarding the mechanism of SARS-CoV-2 S protein-mediated syncytia formation. If throughout the viral life cycle, the S protein is associated with the intracellular membrane and the virus itself does not bud from the cell surface (Figure 1), how then is the S protein able to localize there? Many factors act in conjunction to keep the S protein sequestered on the intracellular membranes. In many coronaviruses, the M protein contains a Golgi localization signal and also associates with the S protein, effectively retaining it on intracellular membranes (Figure 1).[49] Furthermore, the S protein contains within its cytoplasmic tail a binding site for the cytoplasmic coat protein (COPI), which allows for retrograde transport from the Golgi to the ER and further exposure to M protein-mediated sequestration (Figure 1).[49] The E protein may also induce S retention by slowing down the cell's secretory pathway. The co-expression of M and E with the S protein reduces syncytia formation in cell culture models.[49] A recent investigation by Cattin-Ortolá and colleagues provides relevant mechanistic observation on how the S protein could escape its confines and localize on the cell surface.[50] They suggest that the COPI binding motif of the SARS-CoV-2 S protein tail might be sub-optimal. The presence of a histidine rather than a lysine at residue 1271 as well as threonine at residue 1273 in the S protein contributes to sub-optimal COPI binding and reduced intracellular accumulation.[50] Furthermore, the COPI binding site is in close proximity to the COPII (responsible for anterograde transport of proteins from ER to Golgi) binding site and replacing the histidine with lysine at residue 1271 also reduced interaction with COPII.[50] This suggests that the S protein maybe more prone to exit from the ER (Figure 1). The co-expression of M and E proteins reduced S surface expression but did not negate it.[50] These lower affinity binding motifs in the S protein cytoplasmic tail allow for the S protein to leak to the cell surface and promote syncytia formation (Figure 1).

A study by Braga and colleagues further provides valuable insights into the mechanism of SARS-CoV-2 induced cell–cell fusion.[16] They screened for inhibitors of S protein-mediated syncytia formation and found that the most effective inhibitors shared the common characteristic of regulating intracellular calcium (Ca^{2+}) levels.[16] They noticed intracellular Ca^{2+} oscillations in individual S-expressing cells and in syncytial cells and they suggest that expression of the S protein amplifies spontaneous Ca^{2+} transients (Figure 1).[16] To better understand the relationship between Ca^{2+} fluctuations and syncytia formation, they focused on one of their strongest hits, the anthelminthic drug niclosamide which inhibits the Ca^{2+} activated TMEM16 family of chloride channels and scramblases.[16] The expression of the ubiquitous TMEM16F was increased upon S protein expression (Figure 1).[16] The downregulation or overexpression of TMEM16F results in a corresponding decrease or increase in syncytia formation.[16] TMEM16F is a non-specific ion channel and a scramblase that translocates phospholipids bidirectionally between the plasma membrane leaflets. The translocation of specific phospholipids from internal to outer leaflets can serve as a fusion signal (Figure 1).[51] In resting cells, the phosphatidylserine (PS) phospholipid is found on the leaflet facing the cytoplasm. Its translocation to the exofacial leaflet serves as a signal for a variety of cellular processes, including cell–cell fusion (Figure 1).[51] The exposure of PS is associated with a variety of physiological and pathological cell–cell fusion events including skeletal muscle and myoblast formation and repair, macrophage fusion, placental trophoblast fusion, sperm and egg cell fusion during gamete formation, and cancer cell fusion.[51] It is also a marker of cell death through apoptosis. The presence of PS on the viral envelope is important for the entry of viruses including HIV and Ebola and some viruses like alphaherpesvirus induce PS exposure on the host membrane to facilitate infection.[51–55] The translocation of PS may influence the fusogenicity of the lipid membrane as well as assist in the recruitment and modification of fusion protein (the diverse functions of PS is thoroughly reviewed in [51]). Syncytium formed via S protein-mediated fusion also expose PS on their plasma membrane.[16] The activation of TMEM16F by S and the corresponding translocation of PS may represent one of the mechanisms by which SARS-CoV-2 induces syncytia. TMEM16F also plays a role in lipid scrambling in platelets during blood coagulation and its activation by S may contribute to the extensive thrombosis in severe cases of COVID-19.[16] Additional studies will be needed to fully understand the contribution of PS exposition and other functions of TMEM16F to SARS-CoV-2 infection and syncytia formation.[16,51] Braga *et al*. also note that the downregulation of TMEM16F does not affect MERS-CoV S protein-mediated syncytia formation.[16] Comparative investigations on this disparity between SARS-CoV-2 S and MERS-CoV S protein in relation to TMEM16F may further elucidate the mechanism of syncytia formation.

In brief, the SARS-COV-2 S protein, which is normally sequestered on intracellular membranes, possesses suboptimal COPI binding sites that allow for leakage and translocation to the cell surface (Figure 1). Once at the surface, the S protein interacts with ACE2 and host factors on adjacent cells to induce syncytia. In parallel, the expression of the S protein also affects intracellular Ca^{2+} fluctuations and results in the increased expression of the TMEM16F ion

channel and scramblase. TMEM16F translocates PS from the cytofacial leaflet of the plasma membrane to the exofacial leaflet, which promotes the membrane's fusogenic properties (Figure 1). Since the S protein plays a significant role in fusing together membrane during virus-cell fusion and in syncytia formation, a more in-depth molecular characterization of its interactions with host factors and with itself is warranted, which is the subject of the following section.

Molecular Mechanism of S Protein-Mediated Fusion

The S protein is about 1271 amino acids long and is comprised of the S1 and S2 subunits separated by a polybasic cleavage site. Cellular proteases cleave between this S1/S2 site as well as at a S2′ site in order to activate the S protein.[38] Hoffman and colleagues reported that optimization of the S1/S2 cleavage site facilitates cell–cell but not virus-cell fusion, further suggesting a prominent role in SARS-CoV-2 mediated syncytia formation.[38] The removal of the S1/S2 furin cleavage site reduces cell–cell fusion but does not prevent viral entry.[56] Other studies suggest that removal of the furin cleavage site substantially reduces, but does not prevent, the production of infection particles and cell–cell fusion.[57] Viral replication was attenuated, but not abolished, in human respiratory cell lines and hamster and mouse models upon infection with SARS-CoV-2 lacking the furin cleavage site.[58] These studies highlight the significance of the S1/S2 furin cleavage site in SARS-CoV-2 infection particularly in case of syncytia formation. Indeed, natural occurring mutations in these sites augment syncytia formation and this is detailed in a later section.

The S1 subunit consists of the N-terminal domain (NTD) and the receptor binding domain (RBD). The function of the NTD is still under investigation, though work on other coronaviruses shows that the NTD may be associated with glycan recognition during initial attachment, receptor recognition and pre-to-post fusion transition of the S protein.[59–61] The C-type lectins DC-SIGN and L-SIGN may act as auxiliary receptors for SARS-CoV-2 by associating with the NTD.[36] SARS-CoV-2 S protein-mediated fusion may also be subject to antibody-dependent enhancement as the binding of antibodies to a specific site on the NTD induces an open RBD state which may enhance fusogenicity.[62]

The RBD domain of the S1 interacts with the ACE2 receptor; the presence of which determines cellular tropism (Figure 2).[63–65] The RBDs of the S protein trimer exist in a state of dynamic equilibrium between "up" (open) and "down" (closed) conformations.[66,67] In the "up" conformation, the RBD can bind to ACE2 and the binding of one of the RBDs monomers to ACE2 is followed by sequential opening up and binding of the remaining two RBD monomers to ACE2.[67] As multiple receptors could bind to the S protein, considerable mechanical stress is exerted on the S1.[66] The opening process disrupts contact between ACE2-bound S1 monomers, promoting their dissociation from the complex and revealing the trimeric S2 core, which houses the fusion machinery of the S protein (Figure 2).[67] The S2 domain is comprised of the fusion peptide (FP), heptapeptide repeat sequences 1 and 2 (HR1 and HR2), a transmembrane anchor (TA) and a C-terminal domain (CTD). Upon the release of the S1 domain, the unstructured HR1 in the S2 domain becomes helical, and thrusts the FP into the target cell membrane (Figure 2).[66,68] The FP then disrupts the lipid bilayer of the target membrane and anchors it to the fusion machinery (Figure 2).[69,70] On the other end of the S2 domain, the fusion machinery is anchored on either the virion membrane or the S-expressing cell membrane (in the case of syncytia formation), by the TA subdomain (Figure 2). Upon insertion of the FP into the target membrane, three highly conserved hydrophobic grooves on HR1 are exposed, which allows for interaction with the HR2 subdomain.[66] The HR2 domain contains a rigid helix and a flexible loop.[70,71] The interaction between HR1 and HR2 forms a six-helix bundle which brings the two anchored membranes into close proximity to one another, overcoming the natural repulsive force that keeps the membranes apart (Figure 2).[66] Once the energetic barrier for fusion is reduced, the outer leaflets of the membranes merge in a step referred to as hemi-fusion. This is followed by the formation of a pore which expands to create one continuous membrane, allowing mixing of the viral or cytoplasmic contents (Figure 2).[66] The CTD is associated with COPI/II binding and intracellular transport.[50] Furthermore, work by Sanders *et al*. found that the cystine-rich membrane proximal cytoplasmic region of the S protein CTD is necessary for syncytia formation, and that it associates with membrane cholesterol in a raft-independent manner (Figure 1).[72]

The subdomains of the S protein play important roles in receptor recognition and binding, translocation, and fusogenicity. The S protein is also highly antigenic and has been subject to evolutionary pressure throughout the pandemic, leading to the rise of several variants of concern (VOC). These variants' S proteins contain several mutations that alter its propensity to carry out its aforementioned functions. The following section will examine how the mutations within VOC S proteins influence syncytia formation.

Variants of Concern S Proteins and Fusogenicity

Since the start of the pandemic, the ancestral Wuhan strain has been replaced by variants

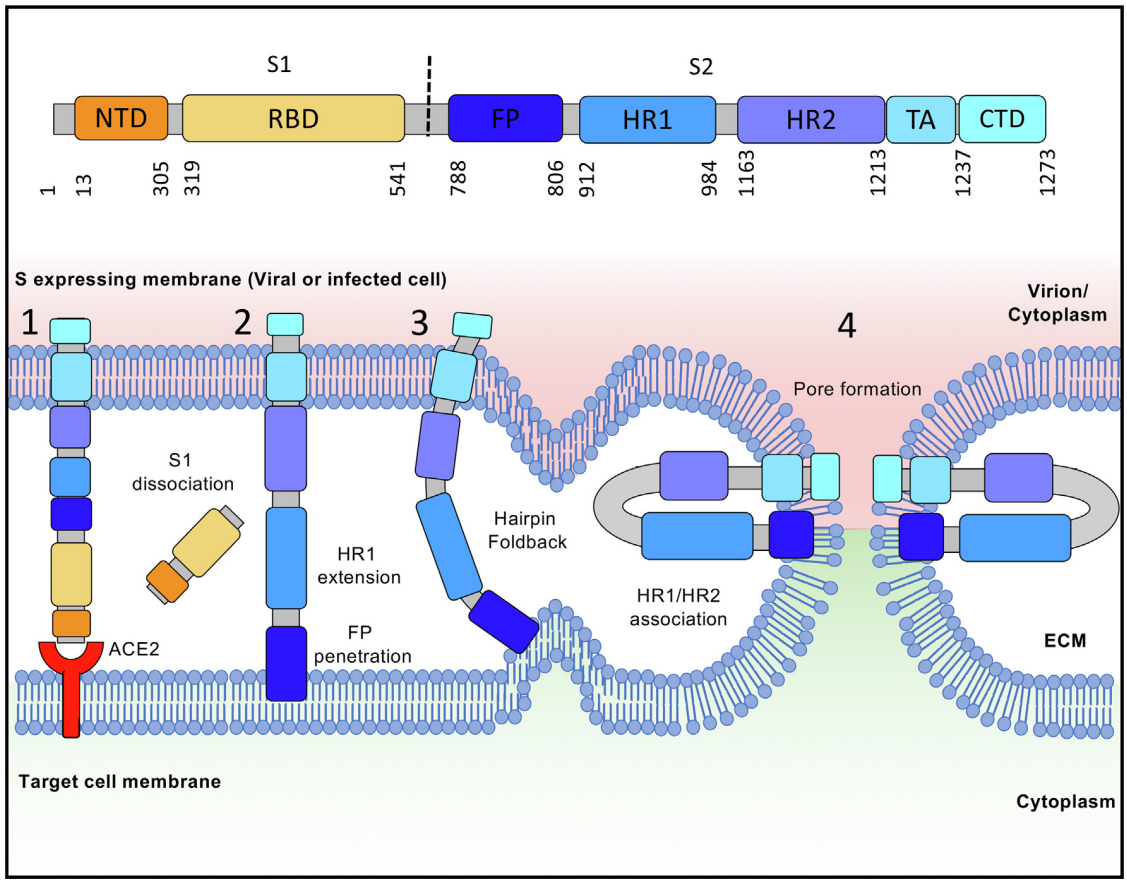

Figure 2. Molecular mechanism of Spike (S) protein-mediated virus-cell or cell–cell fusion. Top: the functional subdomains of the S protein. N-terminal domain (NTD), receptor binding domain (RBD), fusion peptide (FP), heptapeptide repeat sequences 1 and 2 (HR1 & HR2), transmembrane anchor (TA), C-terminal domain (CTD). Bottom: 1) The S protein associates with the ACE2 receptor via its RBD. It is also processed by cellular proteases at the S1/S2 or S2′ sites (not shown). 2) The S1 domain is released which allows for HR1 to extend and thrust the FP into the target cell plasma membrane. The FP anchors the target membrane while the TA anchors the fusion machinery to the viral or infected cell membrane. 3) Interactions between HR1 and HR2 results in a hairpin-like foldback that overcomes the energetic barrier to fusion and brings the membranes close together. A hemi-fusion step occurs where the outer layers of the fusing membranes merge (not shown). 4) The association of HR1 and HR2 and the corresponding membrane fusion result in the formation of a pore that will gradually expand. The viral or cytoplasmic contents are then merged.

containing several mutations throughout their genome. Variants Alpha (B.1.1.7) originating from the United Kingdom; Beta (B.1.351) from South Africa; Gamma (P1 and P2) from Brazil; and more recently Delta (B.1.617.2) from India are of concern both regionally and globally. While the variant-associated mutations are found throughout the viral genome, many mutations are associated with the S protein (Figure 3). In addition to being the viral fusogen, the S protein is highly antigenic and therefore the target for neutralizing antibodies. As such, many of the mutations found in the variants' S proteins have arisen in the context of antibody escape. The impact of the variants, with all of their accumulated mutations, on pathology is not clear, but some variants are more transmissible.[73,74] Several recent studies have sought to characterize and compare the S proteins of the variants in terms of their fusogenicity.

One of the earlier variants identified was the European variant, which contained the D614G mutation proximal to the S1/S2 cleavage site. This mutation shifts the conformation of the S protein to a state that is more competent for ACE2 binding, while not significantly altering antibody neutralization.[65,75] The D614G variant replicates more efficiently in primary cell culture models.[75] Furthermore, greater levels of viral genetic material has been found in the upper respiratory tract of infected individuals which may be more associated with transmission rather than disease severity.[73] In terms of fusogenicity, pseudovirus assays have shown that the D614G substitution increases the efficiency of cellular entry.[73,76] The D614G mutant

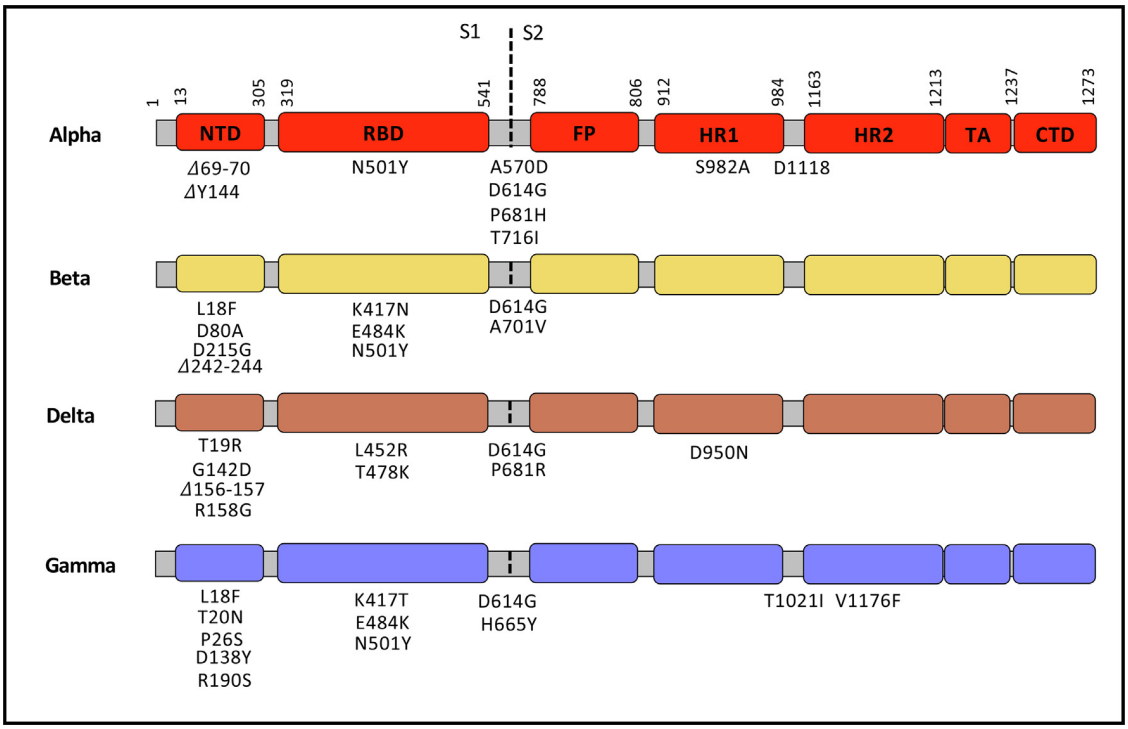

Figure 3. Spike protein mutations associated with Alpha, Beta, Delta and Gamma SARS-CoV-2 variants. N-terminal domain (NTD), receptor binding domain (RBD), fusion peptide (FP), heptapeptide repeat sequences 1 and 2 (HR1 & HR2), transmembrane anchor (TA), C-terminal domain (CTD).

produces more syncytia than the ancestral Wuhan strain in cell culture models.[77,78] We and others have shown that relative to D614G, the Alpha, Beta, and Delta variants are more syncytiogenic in cell culture.[77,79,80] The Alpha and Delta S proteins induce the most cell–cell fusion and they do so more rapidly than the other variants.[77,79] The Beta variant S is also more fusogenic than D614G.[77] In the most general sense, the degree of syncytia formation seems to correlate with the affinity of the variant S proteins to ACE2.[77,81] A contradictory study found no difference (Alpha) or a slight reduction (Beta and Gamma) in variant S mediated cell–cell fusion; however, work by the same group found the Delta variant to be more syncytiogenic.[82,83] This discrepancy may be explained by variations in the experimental systems and the time-points in which syncytia formation was assessed. Highly fusogenic cells and late time-points may risk missing differences in fusogenicity. The D614G mutation alone elicited significant changes in the S protein that impacted its structure, receptor affinity and fusogenicity. As such, it is worth examining the changes elicited by other individual variant-associated mutations.

The S1 domain is part of the spike that is most exposed to neutralizing antibodies on the virion. As such, it is under persistent evolutionary pressure and prone to mutations. Some of the more recent variants (Alpha, Beta, Gamma) also share the N501Y mutation within the RBD. This mutation increases the affinity of S protein to ACE2 and viral transmission but does not affect antibody neutralization.[77,84–88] The hydrophobic pocket formed by the Y41 and K353 regions of ACE2, interacts more efficiently with the Y501 mutant than with the wild type S.[89] Despite its higher affinity to ACE2, the N501Y mutation alone did not increase syncytia formation in cell culture.[77] E484K, another significant mutation within the RBD, present in Beta and Gamma variants, also later emerged in a subset of the Alpha lineage.[90] The RBD of Beta variant also includes the K417N (K417T in Gamma). The E484K and K417N mutations are associated with antibody escape, though they may alter ACE2 binding when in conjunction with N501Y.[88,90–92] E484K may increase affinity to ACE2, whereas K417N seems to decrease it.[85,93] Individually, both mutations reduced syncytia formation.[77] The E484K mutation has been suggested to allow for infection of H522 human lung cells independently of ACE2.[94] This alternate entry pathway may rely on surface heparan sulfates and clathrin-mediated endocytosis.[94]

Within the NTD domain of the variant S proteins are several mutations that are generally associated with antigenicity.[92] As previously mentioned, the NTD is also involved in receptor binding and structural changes, and some of the variant associated mutations within the domain have been

shown to impact S protein-mediated fusogenicity. The Δ69/70 mutation that is associated with the Alpha variant increases infectivity through greater incorporation of cleaved S protein into virions.[95] Furthermore, Δ69/70 may compensate for the reduced infectivity brought about the antibody escape mutation in the RBD of the variants.[95] Interestingly, restoring the Δ69/70 mutation abrogates the relative increase in syncytia formation elicited by the Alpha S protein relative to the D614G S protein.[95] However, the deletion on its own within the D614G S protein is detrimental to syncytia formation.[77] The comparatively greater syncytia formation induced by the Alpha variant S protein may thus be a result of the Δ69/70 mutation working in conjunction with other mutations. The deletion of 242–244 in the NTD of the Beta variant also restricts syncytia formation on its own.[77] It remains to be seen how it functions within the context of partner mutations. Interestingly, the D215G mutation of the Beta variant facilitates syncytia formation.[77] The mechanism of its action is unknown, and future investigations examining it within the context of L-SIGN, DC-Sign and neuropilin-1 binding and overall S structural changes would be of interest.[36] Such investigation could broaden the scope of target cells that may be able to form syncytia.

Of particular interest are the P681H and P681R mutations found in the S1/S2 cleavage site of Alpha and Delta variants, respectively. The P681 site is positioned in a surface-exposed loop of the S protein and is accessible to proteases. A recent investigation in the Alpha variant with the P681H mutation showed that there is a greater exposure of the furin cleavage site which naturally increases affinity to furin.[96] The presence of more cleaved Spike in the virion or at the cell surface can increase fusogenicity. Indeed, we showed that the P681H mutation drastically increased syncytia formation.[77] It has also been suggested that O-glycosylation modulates furin cleavage of the S protein, and the presence of the P681 region facilitates the activity of glycosylation enzyme GALNT1.[97] How the variant-associated mutations affect glycosylation and subsequent furin cleavage would be of future interest. Work by Saito and colleagues suggest that the P681R mutation of Delta variants increases S protein cleavage and subsequent viral fusion.[80] The P681R mutation was also responsible for larger syncytia forming in experiments conducted with artificial virus reversed engineered to contain the mutation.[80] Infection with virus housing the P681R resulted in higher pathogenicity in a hamster model: animals infected with the mutant virus experienced greater weight loss and reduced pulmonary function than with the D614G virus.[80]

The A570D and S982A mutations, also within proximity of the cleavage site of the Alpha variant, did not significantly affect syncytia formation individually; however, structural studies suggest that they may reduce contact between individual chains of the trimeric spike.[77,98] In conjunction with other mutations like P681H, they may augment cleavage of the S protein.[98] The D1118H mutation in the S2 of the Alpha variant, between the HR1 and HR2 domain potently increases syncytia formation.[77] Characterization of this mutation in the literature is scarce. From its location, it would not be unreasonable to speculate that it may impact the fusion machinery and HR1/HR2 association. Further investigations examining the effects of D1118H on the structure and function of the S protein, and the overall infectivity of the S protein would be of interest. A more thorough understanding of the variants and their respective mutation, especially in *in vivo* models, would be of great value in understanding the transmission and pathology of the novel variants.

Modulation of S-Mediated Fusion by Host Factors

Restriction and enhancement factors play a complex role in regulating viral infection. Several of these are membrane-bound and operate at the entry and fusion step of the viral life cycle. This section will examine the role of key membrane-bound restriction and enhancement factors on S protein-mediated fusion and syncytia formation. Upon infection, cytosolic sensors detect viral genetic material and trigger the expression of type I, II and III interferons (IFN), which subsequently set off signaling pathways that promote the expression of a wide array of interferon-stimulated genes (ISGs) to impede viral replication. One such family of ISGs are the interferon-induced transmembrane (IFITM) proteins. Functional IFITMs can be further categorized into three clades and despite the nomenclature only members of clade 1, – IFITM1, 2 and 3 as well as the mouse specific IFITM6 and 7 – are truly IFN induced, ubiquitously expressed and possess bona fide innate immune activity.[99] IFITMs restrict a broad spectrum of enveloped viruses including influenza, HIV-1, Ebola, Marburg, dengue, Zika, West Nile, Japanese encephalitis, Rift Valley Fever as well as members of the coronavirus family.[100–102]

IFITM1 localizes on the plasma membrane, while IFITM2 and 3 both transit through the plasma membrane and then localize within the endo-lysosomal compartments. IFITMs prevent viruses from crossing the cellular membrane and accessing the cytoplasm, possibly by altering the rigidity and the curvature or the composition of the membrane.[100,102–104] This serves to increase the energetic barrier for fusion, hindering virus-cell fusion at hemi fusion or pore formation stage.[105,106] In the case of coronaviruses, IFITMs block the entry of MERS-CoV, SARS-CoV, hCoV-NL63 and hCoV-229E.[107–109] However, the interaction between IFITMs and coronavirus S protein-mediated fusion

is complex. Work by Zhao and colleagues demonstrated that the hCoV-OC43 uses IFITM2 and 3 as entry factors to facilitate infection.[110] Furthermore, they also identified mutations within the IFITM1 and 3 that can convert them from inhibitors of MERS-CoV and SARS-CoV S mediated entry, into enhancers.[109] The contradictory effects of IFITMs and their mutations on different coronaviruses may be a result of how and where they interact with the different cellular receptors.[109]

There have been several reports examining the role of IFITMs on SARS-CoV-2 S mediated fusion. Work by Shi and colleagues show that IFITM1, 2 and 3 are restriction factors of SARS-CoV-2 infection, with IFITM1 being particularly potent.[102] Another study using pseudotyped lentiviral vectors expressing SARS-CoV-2 S protein found that IFITM2 was the most potent inhibitor of entry and that removal of the polybasic S1/S2 cleavage site makes S protein particularly sensitive to IFITM2.[111] Shi *et al*. also suggest that restriction by IFITM3 is independent of its palmitoylation, a post-translation modification thought to affect hydrophobicity and location of IFITM3 to membrane compartments.[102,112] Since the palmitoylation site is necessary for the antiviral activity of IFITM3 against IAV, hCoV-229E and hCoV-NL63, this may suggest that the restriction of SARS-CoV-2 infection at the endosome may occur in a different manner.[102,109,112] Shi *et al*. confirm that the amphipathic helix domain within the hydrophobic region of IFITM3, is necessary for restricting S mediated fusion. The amphipathic helix is believed to insert into membrane bilayers and mechanically induce a curvature and rearrange lipids in a manner that antagonizes fusion.[105,113–115] One investigation suggests that endogenous IFITMs in human lung cells may on the contrary, facilitate SARS-CoV-2 infection.[116] The authors proposed that IFITMs interact with the S protein and that reduction of endogenous IFITMs drastically impedes viral replication.[116] They also found that IFN- β enhanced SARS-CoV-2 infection in small airway epithelial cells.[116] The discrepant observations might be a result of the different IFITM expression systems or cell culture models. Further investigations examining the relationship between IFITMs and SARS-CoV-2 are warranted.

SARS-CoV-2 mediated syncytia formation is effectively restricted by IFITMs, with IFITM1 displaying the most potent activity. We reported that restriction of syncytia formation by IFITMs is subject to reversion by TMPRSS2.[46] TMPRSS2 drastically augmented S protein-mediated syncytia formation, whether IFITMs were present or absent.[46] This protease also increases infection by SARS-CoV-2 and reverts the inhibitory effect of IFITMs on viral infection.[102] Studies on other coronaviruses have also found that TMPRSS2 thwarts the antiviral effects of IFITMs.[117,118] It would be of future interest to characterize the relationship between TMPRSS2, ACE2, and IFITMs to better understand how TMPRSS2 subverts the potential biophysical constraints imposed by IFITMs. Understanding the mobility and interaction dynamics of these three interactors during infection or syncytia formation may be informative of the precise mechanism in which syncytia formation is restricted. Of note, we also observed that syncytia induced by the S proteins of D614G, Alpha, and Beta variants are effectively restricted by IFITMs.[77]

Other membrane-bound restriction factors impact S-protein mediated syncytia formation. The IFN inducible Lymphocyte antigen 6 complex locus E (LY6E) is a glycosylphosphatidylinositol (GPI)-anchored protein that associates with membrane lipid rafts.[119,120] LY6E is a pro-viral factor that promotes the uptake of Yellow Fever virus, the uncoating of influenza A, and HIV-1 infection of high CD4-expressing cell.[120–122] It is also a receptor for syncytin-A, a mouse endogenous retroviral envelope.[123] However, LY6E is an inhibitor of hCoV-OC43, hCoV-229E, SARS-CoV, SARS-CoV-2, and MERS-CoV infection and associated syncytia.[124,125] The precise mechanism by which LY6E inhibits membrane fusion is not clear.[124] It does not affect S protein maturation or expression of surface receptors.[124] The GPI-anchor which associates LY6E to lipid rafts is crucial to its activity. Lipid rafts are cholesterol and glycosphingophospolipid rich regions in the plasma membrane that compartmentalize important processes including ligand receptor engagements. The mechanism by which LY6E exerts its restriction is likely different than that of IFITMs. The antifungal drug amphotericin B (AmphoB), which binds cholesterol in the plasma membrane and increases it fluidity, can rescue restriction by IFITMs but not LY6E. Understanding the precise mechanism by which LY6E restricts fusion would be of interest.

Recently, the ISG Cholesterol 25-hydroxylase (CH25H) has been described as an inhibitor of SARS-CoV-2 membrane fusion.[126,127] CH25H is induced by SARS-CoV-2 infection and converts cholesterol into 25-hydrocholersterol (25CH).[126] 25CH inhibits viral-cell fusion by depleting fusion accessible plasma membrane cholesterol through the activation of acyl-CoA: cholesterol acyltransferase (ACAT) localized on the ER membrane.[126] CH25H expression also significantly reduces SARS-CoV-2 S protein-mediated syncytia formation.[127] These observations further emphasize the significance of cholesterol access to S protein-mediated fusion.

In summary, a few important ISGs act to antagonize SARS-CoV-2 S mediated cell–cell fusion by altering the target membranes. IFITMs likely restrict syncytia formation by altering the biomechanical properties of the plasma membrane, whereas LY6E does so through an unknown mechanism. CH25H facilitates the depletion of membrane cholesterol and the

compositional change is also unfavorable to cell–cell fusion. Molecular mechanisms by which ISGs inhibit virus-cell and cell–cell fusion remain a pertinent field in understanding SARS-CoV-2 induced pathology.

The Potential Roles of Syncytia Formation in SARS-CoV-2 Infection

SARS-CoV-2 mediated syncytia formation has been proposed to be a potential contributor to overall pathology. However, its relative significance and its general contribution to the viral infection remains unknown. Formation of abnormal multinucleated pneumocytes represents a form of cytopathic effect. There are significant differences between physiological and pathological syncytia. During physiological syncytiogenesis, such as in placental trophoblast formation, the cell cycle is arrested at the G0 phase.[128] The expression of the Syncytin-2 (SYN2) fusogen is also restricted to the G0 phase, which allows for strict regulation of the physiological cell–cell fusion process.[128] The transient expression of SYN2 in cells in any other phase (S,G2,M) of the cycle results in the formation of unstable and functionally compromised syncytia.[128] Furthermore, physiological fusion processes like placental formation is controlled through polarized expression of the receptor and fusogen.[8] SYN2 expression is limited to a few cytotrophoblasts, whereas its receptor (major facilitator superfamily domain-containing protein 2) is expressed on syncytiotrophoblasts.[8] In stark contrast, unregulated pathogen-induced syncytia formation, in cells which normally do not fuse, is likely to be pathological.

Unnaturally occurring syncytia cells are susceptible to rapid cytopathicity. This phenomenon of "syncytial apoptosis" has been well documented in HIV-1 infections *in vitro, in vivo* and in infected patient tissues.[129] Upon cell–cell fusion, the HIV-1 envelope protein triggers a pro-apoptotic signaling pathway that triggers karyogamy (nuclear fusion) and DNA damage.[129] SARS-CoV-2 S protein-mediated syncytia also collapse and die during the later stages of the process, and of particular interest is the observation that the nuclei within S protein-mediated syncytium cluster together (Figure 4 top left).[46,130] Future investigations characterizing the cell death pathways triggered within SARS-CoV-2 induced syncytium, and

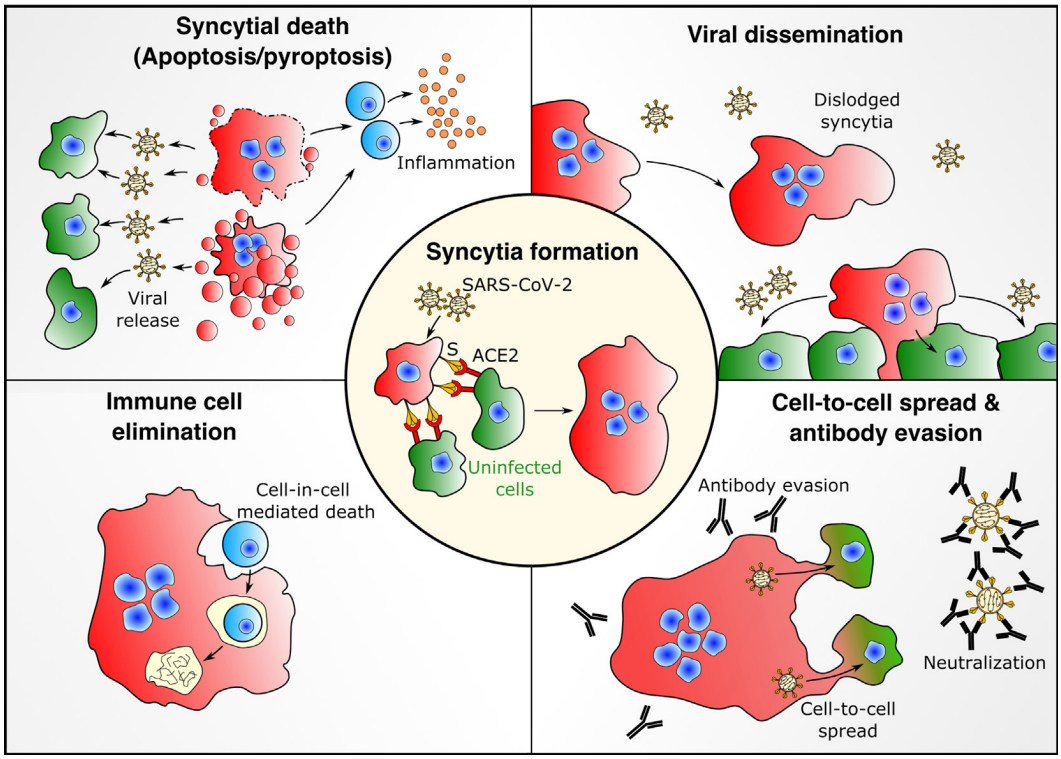

Figure 4. The potential consequences of syncytia formation on SARS-CoV-2 pathology. Center: Cells infected with SARS-CoV-2 express the spike protein at the surface and form large multinucleated syncytia. Top left: The process of syncytial death via apoptosis or pyroptosis can release virus to infect neighbouring cells and/or trigger an inflammatory response. Top right: Infected syncytia can lift off to contribute to viral dissemination and the overall infectious dose. Bottom left: Syncytial cells can target lymphocytes for cell-in-cell mediated death. Bottom right: Syncytia can facilitate cell-to-cell spread of the virus and shield the virus from neutralizing antibodies.

the roles of other viral proteins would be of interest. There is also a possibility that the death of infected cells may release virions into the surrounding environment, spreading the infection (Figure 4 top left). Syncytial pneumocytes in COVID-19 patient tissues are scarce and the degree to which cytopathic effects contribute to pathology is unclear. There is also a paucity of information regarding presence, clearance or turnover of syncytia during early infection. There is also possibility that if syncytia are prone to premature death, they may be detrimental to viral replication. The relationship between syncytial death and viral replication remains to be explored more thoroughly.

The formation of syncytia may also have immunological consequences. Zhang and colleagues found the presence of lymphocytes contained within syncytia as a cell-in-cell structure among COVID-19 patient lung tissue.[26] Using cell culture models, they demonstrated that syncytia formed through S protein-mediated fusion can internalize various T and B cell lines, monocytes and peripheral blood mononuclear cells (Figure 4 bottom left).[26] The internalized cells readily underwent shriveling, deterioration of the plasma membrane and death (Figure 4 bottom left).[26] These studies provide a possible mechanism by which syncytia may contribute to lymphopenia among patients with COVID-19.[26] There is also an outstanding question whether S-mediated syncytia trigger elements of the innate immunity. Cell-cell fusion events induced by other pathogens have been documented to induce interferon expression. Syncytia induced by measles virus amplifies IFN- β production *in vitro*.[131] Similarly, cell–cell fusion induced by the bacterial pathogen *Burkholderia pseudomallei* elicits type I IFN expression through the DNA sensing cGAS-STING pathway.[132] This reportedly occurs independently of bacterial ligands.[132] How S protein-mediated pathological syncytia formation is related to immune activation or recognition remains an outstanding question.

Recent work suggests that S protein-mediated syncytia formation results in the activation of Caspase-9, followed downstream by the activation of Caspase-3/7, and later by gasdermin E (GSDME)-mediated pyroptosis.[133] This inflammatory form of cell death may have significant implication in triggering the immune response and warrants further investigation (Figure 4 top left). The adaptive immune response also has profound implications for SARS-CoV-2 mediated cell–cell fusion. Antiviral antibodies may have contradictory roles in cell fusion.[134] Some neutralizing antibodies restrict cell–cell fusion by locking the spike in a pre-fusion state, whereas some weakly neutralizing antibodies behave as allosteric effectors that promote S2 unsheathing and increase syncytia formation.[134] The opposing activities of neutralizing antibodies will need to be elucidated further in order to be understood in terms of pathology.

Finally, syncytia formation can have direct virological consequences rather than just trigger a generalized cytopathic effect or immune response. Syncytia may allow viruses to spread directly from cell-to-cell without having to enter the extracellular environment. This strategy shields the virus from neutralizing antibodies, physical barriers like the mucociliary blanket, as well as components of the immune system (Figure 4 bottom right).[135] Many respiratory viruses such as measles, influenza, respiratory syncytia virus, parainfluenza virus, and human metapneumonia virus exploit this mechanism of dissemination.[135] As already discussed above, nonenveloped reoviruses employ evolutionarily conserved fusogens, dedicated to the induction of cell–cell fusion, as a mechanism of cell-to-cell transmission.[10,11] Recent cell culture studies suggest that SARS-CoV-2 cell-to-cell dissemination is a possible route of spread (Figure 4 bottom right). Cell-free virus was effectively neutralized by monoclonal antibodies and convalescent plasma; however, cell-to-cell viral spread was either not or less sensitive to neutralization (Figure 4 bottom right).[130,136] The direct spread of HIV from cell-to-cell has also been demonstrated to be less sensitive to the restrictive effects of antiretrovirals and neutralizing antibodies.[137,139] A more thorough understanding of the significance of SARS-CoV-2 cell-to-cell spread to the pathology and antibody response is warranted. Beyond direct cell-to-cell spread, syncytia can contribute to the overall infectious dose and viral dissemination upon being dislodged (Figure 4 top right). In reconstituted primary bronchial epithelia, multi-ciliated cells and basal cells form syncytia which are then released into the apical lumen.[140] Vesicular inclusions containing virus particles were detected within the released syncytia, potentially suggesting continued viral replication.[140] Infected single and syncytial cells that are released may thus spread infection (Figure 4 top right). Like several of the aforementioned processes, syncytial release is not unique to SARS-CoV-2.[140] Infection of epithelial cell cultures from macaque respiratory tissue with measles virus also results in the formation and shedding of infectious syncytia.[141]

From a methodological standpoint, syncytia formation in cell culture can also be utilized as an effective, albeit imperfect, surrogate to characterize the early stages of virion entry via S protein fusogenicity. It has the added benefit for being suitable for biosafety level 2 research environments, when the S protein is expressed alone, in the absence of infectious virus. We also developed a rapid, sensitive and semi-automated assay we termed “S-Fuse”, which employed virus-induced syncytia formation as a marker to detect and measure infectious virus in various human samples.[46,142] The S-Fuse assay is now routinely used in our laboratory to assess the activity of anti-SARS-CoV-2 monoclonal antibodies or other

antiviral molecules, and to measure the neutralizing antibody response in sera from vaccinated and convalescent individuals.[81,143] Quantitative syncytia formation has also been employed in high-throughput drug screens in order to identify inhibitors of S mediated fusion.[16,72] There are several reporter systems that can be used to quantify syncytia formation and they are compared by Sanders *et al.*[72]

Conclusion and Perspectives

Several histopathological reports have identified the presence of infected multinucleated syncytial cells in COVID-19 patient lung tissues. The degree to which syncytia affect pathology is not fully understood. Recent studies have provided valuable insights into the role of syncytia in SARS-CoV-2 infection as well as into mechanism of their formation. Syncytia might facilitate infection by disseminating the virus through cell-to-cell contacts or upon cell death, targeting immune cells, and protecting the virus against neutralizing antibodies. On the contrary, rapid syncytial collapse may be detrimental to viral replication and could trigger an inflammatory immune response. In either case, SARS-CoV-2 syncytia most likely contribute to viral pathogenicity.

Syncytia formation is sensitive to the antiviral innate immune response. Some ISGs modify the membrane in ways that are unfavorable to fusion. SARS-CoV-2 is a rapidly evolving virus, with many mutations within the S protein. The individual mutations harbored by Alpha, Beta, Gamma, and Delta variants have significant impact on S function and syncytia formation, both individually and cumulatively. The impact of syncytia in the pathology of emerging variants remains an outstanding question.

CRediT authorship contribution statement

Maaran Michael Rajah: Conceptualization, Investigation, Writing – original draft, Writing – review & editing, Visualization. **Annie Bernier:** Writing –review & editing. **Julian Buchrieser:** Writing –review & editing, Conceptualization, Supervision. **Olivier Schwartz:** Writing –review & editing, Conceptualization, Supervision, Funding acquisition.

Acknowledgments

We thank Dr. Nicoletta Casartelli for her critical reading of the manuscript. Work in OS lab is funded by Institut Pasteur, Urgence COVID-19 Fundraising Campaign of Institut Pasteur, ANRS, the Vaccine Research Institute (ANR-10-LABX-77), Fondation Pour la Recherche Médicale (FRM), Labex IBEID (ANR-10-LABX62-IBEID), ANR/FRM Flash Covid PROTEO-SARS-CoV-2 and IDISCOVR. MMR is supported by the Pasteur-Paris University (PPU) International Doctoral Program and the Institut Pasteur Department of Virology "Bourse de Soudure" fellowship. The funders of this study had no role in the research or writing of this article.

Declaration of Competing Interest

The authors declare that they have no known competing financial interests or personal relationships that could have appeared to influence the work reported in this paper.

Received 19 August 2021;
Accepted 27 September 2021;
Available online xxxx

Keywords:
SARS-CoV-2;
syncytia;
cell-cell fusion;
coronavirus;
spike

† Last co-authors.

References

1. Kahn, J.S., McIntosh, K., (2005). History and recent advances in coronavirus discovery. *Pediatr. Infect. Dis. J.* **24**, S223–S227. discussion S6.
2. Organization, W.H., (2021). COVID-19 Weekly Epidemiological Update Weekly epidemiological update on COVID-19. WHO, WHO.
3. Bussani, R., Schneider, E., Zentilin, L., Collesi, C., Ali, H., Braga, L., et al., (2020). Persistence of viral RNA, pneumocyte syncytia and thrombosis are hallmarks of advanced COVID-19 pathology. *EBioMedicine.* **61**, 103104
4. Buchrieser, J., Schwartz, O., (2021). Pregnancy complications and Interferon-induced transmembrane proteins (IFITM): balancing antiviral immunity and placental development. *C R Biol.* **344**, 145–156.
5. Hernandez, J.M., Podbilewicz, B., (2017). The hallmarks of cell-cell fusion. *Development* **144**, 4481–4495.
6. Brukman, N.G., Uygur, B., Podbilewicz, B., Chernomordik, L.V., (2019). How cells fuse. *J. Cell Biol.* **218**, 1436–1451.
7. Segev, N., Avinoam, O., Podbilewicz, B., (2018). Fusogens. *Curr Biol.* **28**, R378–R380.
8. Lavialle, C., Cornelis, G., Dupressoir, A., Esnault, C., Heidmann, O., Vernochet, C., et al., (2013). Paleovirology of 'syncytins', retroviral env genes exapted for a role in placentation. *Philos. Trans. R. Soc. London B Biol. Sci.* **368**, 20120507.
9. Leroy, H., Han, M., Woottum, M., Bracq, L., Bouchet, J., Xie, M., et al., (2020). Virus-mediated cell-cell fusion. *Int. J. Mol. Sci.* **21**

10. Ciechonska, M., Duncan, R., (2014). Reovirus FAST proteins: virus-encoded cellular fusogens. *Trends Microbiol.* **22**, 715–724.
11. Kanai, Y., Kawagishi, T., Sakai, Y., Nouda, R., Shimojima, M., Saijo, M., et al., (2019). Cell-cell fusion induced by reovirus FAST proteins enhances replication and pathogenicity of non-enveloped dsRNA viruses. *PLoS Pathog.* **15**, e1007675
12. Menter, T., Haslbauer, J.D., Nienhold, R., Savic, S., Hopfer, H., Deigendesch, N., et al., (2020). Postmortem examination of COVID-19 patients reveals diffuse alveolar damage with severe capillary congestion and variegated findings in lungs and other organs suggesting vascular dysfunction. *Histopathology* **77**, 198–209.
13. Carsana, L., Sonzogni, A., Nasr, A., Rossi, R.S., Pellegrinelli, A., Zerbi, P., et al., (2020). Pulmonary post-mortem findings in a series of COVID-19 cases from northern Italy: a two-centre descriptive study. *Lancet Infect Dis.* **20**, 1135–1140.
14. Franks, T.J., Chong, P.Y., Chui, P., Galvin, J.R., Lourens, R.M., Reid, A.H., et al., (2003). Lung pathology of severe acute respiratory syndrome (SARS): a study of 8 autopsy cases from Singapore. *Hum. Pathol.* **34**, 743–748.
15. Alsaad, K.O., Hajeer, A.H., Al Balwi, M., Al Moaiqel, M., Al Oudah, N., Al Ajlan, A., et al., (2018). Histopathology of Middle East respiratory syndrome coronovirus (MERS-CoV) infection - clinicopathological and ultrastructural study. *Histopathology* **72**, 516–524.
16. Braga, L., Ali, H., Secco, I., Chiavacci, E., Neves, G., Goldhill, D., et al., (2021). Drugs that inhibit TMEM16 proteins block SARS-CoV-2 spike-induced syncytia. *Nature* **594**, 88–93.
17. Guzik, T.J., Mohiddin, S.A., Dimarco, A., Patel, V., Savvatis, K., Marelli-Berg, F.M., et al., (2020). COVID-19 and the cardiovascular system: implications for risk assessment, diagnosis, and treatment options. *Cardiovasc. Res.* **116**, 1666–1687.
18. Zhou, Z., Ren, L., Zhang, L., Zhong, J., Xiao, Y., Jia, Z., et al., (2020). Heightened innate immune responses in the respiratory tract of COVID-19 patients. *Cell Host Microbe* **27** 883–90 e2.
19. Ong, E.Z., Chan, Y.F.Z., Leong, W.Y., Lee, N.M.Y., Kalimuddin, S., Haja Mohideen, S.M., et al., (2020). A dynamic immune response shapes COVID-19 progression. *Cell Host Microbe* **27** 879–82 e2.
20. Huang, C., Wang, Y., Li, X., Ren, L., Zhao, J., Hu, Y., et al., (2020). Clinical features of patients infected with 2019 novel coronavirus in Wuhan, China. *Lancet* **395**, 497–506.
21. Mehta, P., McAuley, D.F., Brown, M., Sanchez, E., Tattersall, R.S., Manson, J.J., et al., (2020). COVID-19: consider cytokine storm syndromes and immunosuppression. *Lancet* **395**, 1033–1034.
22. Bryce, C., Grimes, Z., Pujadas, E., Ahuja, S., Beasley, M. B., Albrecht, R., et al., (2021). Pathophysiology of SARS-CoV-2: the Mount Sinai COVID-19 autopsy experience. *Mod. Pathol.* **34**, 1456–1467.
23. Luo, W.R., Yu, H., Gou, J.Z., Li, X.X., Sun, Y., Li, J.X., et al., (2020). Histopathologic findings in the explant lungs of a patient with COVID-19 treated with bilateral orthotopic lung transplant. *Transplantation* **104**, e329–e331.
24. Rockx, B., Kuiken, T., Herfst, S., Bestebroer, T., Lamers, M.M., Oude Munnink, B.B., et al., (2020). Comparative pathogenesis of COVID-19, MERS, and SARS in a nonhuman primate model. *Science* **368**, 1012–1015.
25. Tian, S., Hu, W., Niu, L., Liu, H., Xu, H., Xiao, S.Y., (2020). Pulmonary pathology of early-phase 2019 novel coronavirus (COVID-19) pneumonia in two patients with lung cancer. *J. Thorac. Oncol.* **15**, 700–704.
26. Zhang, Z., Zheng, Y., Niu, Z., Zhang, B., Wang, C., Yao, X., et al., (2021). SARS-CoV-2 spike protein dictates syncytium-mediated lymphocyte elimination. *Cell Death Differ.*
27. Nicholls, J.M., Poon, L.L., Lee, K.C., Ng, W.F., Lai, S.T., Leung, C.Y., et al., (2003). Lung pathology of fatal severe acute respiratory syndrome. *Lancet* **361**, 1773–1778.
28. Lee, N., Hui, D., Wu, A., Chan, P., Cameron, P., Joynt, G. M., et al., (2003). A major outbreak of severe acute respiratory syndrome in Hong Kong. *N. Engl. J. Med.* **348**, 1986–1994.
29. Ksiazek, T.G., Erdman, D., Goldsmith, C.S., Zaki, S.R., Peret, T., Emery, S., et al., (2003). A novel coronavirus associated with severe acute respiratory syndrome. *N. Engl. J. Med.* **348**, 1953–1966.
30. Ng, D.L., Al Hosani, F., Keating, M.K., Gerber, S.I., Jones, T.L., Metcalfe, M.G., et al., (2016). Clinicopathologic, immunohistochemical, and ultrastructural findings of a fatal case of Middle East respiratory syndrome coronavirus infection in the United Arab Emirates, April 2014. *Am. J. Pathol.* **186**, 652–658.
31. Orenstein, J.M., Banach, B., Baker, S.C., (2008). Morphogenesis of coronavirus HCoV-NL63 in cell culture: a transmission electron microscopic study. *Open Infect Dis J.* **2**, 52–58.
32. Parry, R., Macnaughton, M.R., (1983). Syncytium production by human coronavirus 229E group viruses. *FEMS Microbiol. Letters* **20**, 23–26.
33. Dominguez, S.R., Travanty, E.A., Qian, Z., Mason, R.J., (2013). Human coronavirus HKU1 infection of primary human type II alveolar epithelial cells: cytopathic effects and innate immune response. *PLoS One* **8**, e70129
34. Wrapp, D., Wang, N., Corbett, K.S., Goldsmith, J.A., Hsieh, C.L., Abiona, O., et al., (2020). Cryo-EM structure of the 2019-nCoV spike in the prefusion conformation. *Science* **367**, 1260–1263.
35. V'Kovski, P., Kratzel, A., Steiner, S., Stalder, H., Thiel, V., (2021). Coronavirus biology and replication: implications for SARS-CoV-2. *Nature Rev. Microbiol.* **19**, 155–170.
36. Soh, W.T., Liu, Y., Nakayama, E.E., Ono, C., Torii, S., Nakagami, H., et al., (2020). The N-terminal domain of spike glycoprotein mediates SARS-CoV-2 infection by associating with L-SIGN and DC-SIGN. *biorxiv.* 2020.11.05.369264.
37. Cantuti-Castelvetri, L., Ojha, R., Pedro, L.D., Djannatian, M., Franz, J., Kuivanen, S., et al., (2020). Neuropilin-1 facilitates SARS-CoV-2 cell entry and infectivity. *Science* **370**, 856–860.
38. Hoffmann, M., Kleine-Weber, H., Pohlmann, S., (2020). A multibasic cleavage site in the spike protein of SARS-CoV-2 is essential for infection of human lung cells. *Mol Cell.* **78** 779–84 e5.
39. Hoffmann, M., Kleine-Weber, H., Schroeder, S., Kruger, N., Herrler, T., Erichsen, S., et al., (2020). SARS-CoV-2 cell entry depends on ACE2 and TMPRSS2 and is blocked by a clinically proven protease inhibitor. *Cell* **181**, (271–80) e8

40. Peacock, T.P., Goldhill, D.H., Zhou, J., Baillon, L., Frise, R., Swann, O.C., et al., (2021). The furin cleavage site in the SARS-CoV-2 spike protein is required for transmission in ferrets. *Nature Microbiol.* **6**, 899–909.
41. Jaimes, J.A., Millet, J.K., Whittaker, G.R., (2020). Proteolytic Cleavage of the SARS-CoV-2 Spike Protein and the Role of the Novel S1/S2 Site. *iScience* **23**, 101212
42. Zhao, M.M., Yang, W.L., Yang, F.Y., Zhang, L., Huang, W.J., Hou, W., et al., (2021). Cathepsin L plays a key role in SARS-CoV-2 infection in humans and humanized mice and is a promising target for new drug development. *Signal Transduct. Target Ther.* **6**, 134.
43. Rajah, M.M., Monel, B., Schwartz, O., (2020). The entanglement between flaviviruses and ER-shaping proteins. *PLoS Pathog.* **16**, e1008389
44. Ghosh, S., Dellibovi-Ragheb, T.A., Kerviel, A., Pak, E., Qiu, Q., Fisher, M., et al., (2020). beta-coronaviruses use lysosomes for egress instead of the biosynthetic secretory pathway. *Cell.* **183** 1520–35 e14.
45. Tortorici, M.A., Veesler, D., (2019). Structural insights into coronavirus entry. *Adv Virus Res.* **105**, 93–116.
46. Buchrieser, J., Dufloo, J., Hubert, M., Monel, B., Planas, D., Rajah, M.M., et al., (2020). Syncytia formation by SARS-CoV-2-infected cells. *EMBO J.* **39**, e106267
47. Daly, J.L., Simonetti, B., Klein, K., Chen, K.E., Williamson, M.K., Anton-Plagaro, C., et al., (2020). Neuropilin-1 is a host factor for SARS-CoV-2 infection. *Science.* **370**, 861–865.
48. Li, Z.L., Buck, M., (2021). Neuropilin-1 assists SARS-CoV-2 infection by stimulating the separation of Spike protein S1 and S2. *Biophys J.* **120**, 2828–2837.
49. Boson, B., Legros, V., Zhou, B., Siret, E., Mathieu, C., Cosset, F.L., et al., (2021). The SARS-CoV-2 envelope and membrane proteins modulate maturation and retention of the spike protein, allowing assembly of virus-like particles. *J. Biol. Chem.* **296**, 100111
50. Cattin-Ortola, J., Welch, L.G., Maslen, S.L., Papa, G., James, L.C., Munro, S., (2021). Sequences in the cytoplasmic tail of SARS-CoV-2 Spike facilitate expression at the cell surface and syncytia formation. *Nature Commun.* **12**, 5333.
51. Whitlock, J.M., Chernomordik, L.V., (2021). Flagging fusion: Phosphatidylserine signaling in cell-cell fusion. *J. Biol. Chem.* **296**, 100411
52. Chua, B.A., Ngo, J.A., Situ, K., Morizono, K., (2019). Roles of phosphatidylserine exposed on the viral envelope and cell membrane in HIV-1 replication. *Cell Commun. Signal.* **17**, 132.
53. Nanbo, A., Maruyama, J., Imai, M., Ujie, M., Fujioka, Y., Nishide, S., et al., (2018). Ebola virus requires a host scramblase for externalization of phosphatidylserine on the surface of viral particles. *PLoS Pathog.* **14**, e1006848
54. Azab, W., Gramatica, A., Herrmann, A., Osterrieder, N., (2015). Binding of alphaherpesvirus glycoprotein H to surface alpha4beta1-integrins activates calcium-signaling pathways and induces phosphatidylserine exposure on the plasma membrane. *mBio* **6**, e01552–e1615.
55. Morizono, K., Chen, I.S., (2014). Role of phosphatidylserine receptors in enveloped virus infection. *J. Virol.* **88**, 4275–4290.
56. Nguyen, H.T., Zhang, S., Wang, Q., Anang, S., Wang, J., Ding, H., et al., (2020). Spike glycoprotein and host cell determinants of SARS-CoV-2 entry and cytopathic effects. *J. Virol.*.
57. Papa, G., Mallery, D.L., Albecka, A., Welch, L.G., Cattin-Ortola, J., Luptak, J., et al., (2021). Furin cleavage of SARS-CoV-2 Spike promotes but is not essential for infection and cell-cell fusion. *PLoS Pathog.* **17**, e1009246
58. Johnson, B.A., Xie, X., Bailey, A.L., Kalveram, B., Lokugamage, K.G., Muruato, A., et al., (2021). Loss of furin cleavage site attenuates SARS-CoV-2 pathogenesis. *Nature* **591**, 293–299.
59. Chi, X., Yan, R., Zhang, J., Zhang, G., Zhang, Y., Hao, M., et al., (2020). A neutralizing human antibody binds to the N-terminal domain of the Spike protein of SARS-CoV-2. *Science* **369**, 650–655.
60. Krempl, C., Schultze, B., Laude, H., Herrler, G., (1997). Point mutations in the S protein connect the sialic acid binding activity with the enteropathogenicity of transmissible gastroenteritis coronavirus. *J. Virol.* **71**, 3285–3287.
61. Zhou, H., Chen, Y., Zhang, S., Niu, P., Qin, K., Jia, W., et al., (2019). Structural definition of a neutralization epitope on the N-terminal domain of MERS-CoV spike glycoprotein. *Nature Commun.* **10**, 3068.
62. Liu, Y., Soh, W.T., Kishikawa, J.I., Hirose, M., Nakayama, E.E., Li, S., et al., (2021). An infectivity-enhancing site on the SARS-CoV-2 spike protein targeted by antibodies. *Cell.* **184** 3452–66 e18.
63. Zhou, P., Yang, X.L., Wang, X.G., Hu, B., Zhang, L., Zhang, W., et al., (2020). A pneumonia outbreak associated with a new coronavirus of probable bat origin. *Nature* **579**, 270–273.
64. Lan, J., Ge, J., Yu, J., Shan, S., Zhou, H., Fan, S., et al., (2020). Structure of the SARS-CoV-2 spike receptor-binding domain bound to the ACE2 receptor. *Nature* **581**, 215–220.
65. Yurkovetskiy, L., Wang, X., Pascal, K.E., Tomkins-Tinch, C., Nyalile, T.P., Wang, Y., et al., (2020). Structural and functional analysis of the D614G SARS-CoV-2 spike protein variant. *Cell* **183** 739–51 e8.
66. Rey, F., (2021). Structure-function relations of the SARS-CoV-2 spike protein and impact of mutations in the variants of concern. *C. R. Biol.* **344**, 77–110.
67. Benton, D.J., Wrobel, A.G., Xu, P., Roustan, C., Martin, S. R., Rosenthal, P.B., et al., (2020). Receptor binding and priming of the spike protein of SARS-CoV-2 for membrane fusion. *Nature* **588**, 327–330.
68. Su, R., Zeng, J., O'Shaughnessy, B., (2021). Host cell membrane capture by the SARS CoV-2 spike protein fusion intermediate. *bioRxiv.*. 2021.04.09.439051.
69. Millet, J.K., Whittaker, G.R., (2018). Physiological and molecular triggers for SARS-CoV membrane fusion and entry into host cells. *Virology* **517**, 3–8.
70. Huang, Y., Yang, C., Xu, X.F., Xu, W., Liu, S.W., (2020). Structural and functional properties of SARS-CoV-2 spike protein: potential antivirus drug development for COVID-19. *Acta Pharmacol. Sin.* **41**, 1141–1149.
71. Xia, S., Yan, L., Xu, W., Agrawal, A.S., Algaissi, A., Tseng, C.K., et al., (2019). A pan-coronavirus fusion inhibitor targeting the HR1 domain of human coronavirus spike. *Sci. Adv.*. eaav4580.
72. Sanders, D.W., Jumper, C.C., Ackerman, P.J., Bracha, D., Donlic, A., Kim, H., et al., (2021). SARS-CoV-2 requires cholesterol for viral entry and pathological syncytia formation. *Elife* **10**
73. Korber, B., Fischer, W.M., Gnanakaran, S., Yoon, H., Theiler, J., Abfalterer, W., et al., (2020). Tracking changes

in SARS-CoV-2 spike: evidence that D614G increases infectivity of the COVID-19 virus. *Cell* **182**, (812–27) e19
74. Davies, N.G., Abbott, S., Barnard, R.C., Jarvis, C.I., Kucharski, A.J., Munday, J.D., et al., (2021). Estimated transmissibility and impact of SARS-CoV-2 lineage B.1.1.7 in England. *Science* **372**
75. Zhou, B., Thao, T.T.N., Hoffmann, D., Taddeo, A., Ebert, N., Labroussaa, F., et al., (2021). SARS-CoV-2 spike D614G change enhances replication and transmission. *Nature* **592**, 122–127.
76. Ozono, S., Zhang, Y., Ode, H., Sano, K., Tan, T.S., Imai, K., et al., (2021). SARS-CoV-2 D614G spike mutation increases entry efficiency with enhanced ACE2-binding affinity. *Nature Commun.* **12**, 848.
[77]. Rajah, M.M., Hubert, M., Bishop, E., Saunders, N., Robinot, R., Grzelak, L., et al., (2021). SARS-CoV-2 Alpha, Beta and Delta variants display enhanced Spike-mediated Syncytia Formation. *EMBO J* e108944.
78. Jiang, X., Zhang, Z., Wang, C., Ren, H., Gao, L., Peng, H., et al., (2020). Bimodular effects of D614G mutation on the spike glycoprotein of SARS-CoV-2 enhance protein processing, membrane fusion, and viral infectivity. *Signal Transduct. Target Ther.* **5**, 268.
79. Mlcochova, P., Kemp, S., Dhar, M.S., Papa, G., Meng, B., Ferreira, I., et al., (2021). SARS-CoV-2 B.1.617.2 Delta variant replication and immune evasion. *Nature*.
80. Saito, A., Irie, T., Suzuki, R., Maemura, T., Nasser, H., Uriu, K., et al., (2021). SARS-CoV-2 spike P681R mutation, a hallmark of the Delta variant, enhances viral fusogenicity and pathogenicity. *bioRxiv*. 2021.06.17.448820.
81. Planas, D., Veyer, D., Baidaliuk, A., Staropoli, I., Guivel-Benhassine, F., Rajah, M.M., et al., (2021). Reduced sensitivity of SARS-CoV-2 variant Delta to antibody neutralization. *Nature*.
82. Hoffmann, M., Arora, P., Gross, R., Seidel, A., Hornich, B. F., Hahn, A.S., et al., (2021). SARS-CoV-2 variants B.1.351 and P.1 escape from neutralizing antibodies. *Cell* **184** 2384–93 e12.
83. Arora, P., Kempf, A., Nehlmeier, I., Sidarovich, A., Krüger, N., Graichen, L., et al., (2021). Increased lung cell entry of B.1.617.2 and evasion of antibodies induced by infection and BNT162b2 vaccination. *bioRxiv*. 2021.06.23.449568.
84. Starr, T.N., Greaney, A.J., Addetia, A., Hannon, W.W., Choudhary, M.C., Dingens, A.S., et al., (2021). Prospective mapping of viral mutations that escape antibodies used to treat COVID-19. *Science* **371**, 850–854.
85. Starr, T.N., Greaney, A.J., Hilton, S.K., Ellis, D., Crawford, K.H.D., Dingens, A.S., et al., (2020). Deep mutational scanning of SARS-CoV-2 receptor binding domain reveals constraints on folding and ACE2 binding. *Cell* **182** 1295–310 e20.
86. Liu, Y., Liu, J., Plante, K.S., Plante, J.A., Xie, X., Zhang, X., et al., (2021). The N501Y spike substitution enhances SARS-CoV-2 transmission. *bioRxiv*. 2021.03.08.434499.
87. Ali, F., Kasry, A., Amin, M., (2021). The new SARS-CoV-2 strain shows a stronger binding affinity to ACE2 due to N501Y mutant. *Med. Drug Discov.* **10**, 100086
88. Zahradnik, J., Marciano, S., Shemesh, M., Zoler, E., Harari, D., Chiaravalli, J., et al., (2021). SARS-CoV-2 variant prediction and antiviral drug design are enabled by RBD in vitro evolution. *Nature Microbiol.* **6**, 1188–1198.
89. Luan, B., Wang, H., Huynh, T., (2021). Enhanced binding of the N501Y-mutated SARS-CoV-2 spike protein to the human ACE2 receptor: insights from molecular dynamics simulations. *FEBS Letters* **595**, 1454–1461.
90. Collier, D.A., De Marco, A., Ferreira, I., Meng, B., Datir, R. P., Walls, A.C., et al., (2021). Sensitivity of SARS-CoV-2 B.1.1.7 to mRNA vaccine-elicited antibodies. *Nature* **593**, 136–141.
91. Jangra, S., Ye, C., Rathnasinghe, R., Stadlbauer, D., Personalized Virology Initiative study g, Krammer, F., et al., (2021). SARS-CoV-2 spike E484K mutation reduces antibody neutralisation. *Lancet Microbe* **2** e283-e4.
92. Harvey, W.T., Carabelli, A.M., Jackson, B., Gupta, R.K., Thomson, E.C., Harrison, E.M., et al., (2021). SARS-CoV-2 variants, spike mutations and immune escape. *Nature Rev. Microbiol.* **19**, 409–424.
93. Wang, W.B., Liang, Y., Jin, Y.Q., Zhang, J., Su, J.G., Li, Q.M., (2021). E484K mutation in SARS-CoV-2 RBD enhances binding affinity with hACE2 but reduces interactions with neutralizing antibodies and nanobodies: binding free energy calculation studies. *bioRxiv*. 2021.02.17.431566.
94. Puray-Chavez, M., LaPak, K.M., Schrank, T.P., Elliott, J. L., Bhatt, D.P., Agajanian, M.J., et al., (2021). Systematic analysis of SARS-CoV-2 infection of an ACE2-negative human airway cell. *Cell Rep.* **36**, 109364
95. Meng, B., Kemp, S.A., Papa, G., Datir, R., Ferreira, I., Marelli, S., et al., (2021). Recurrent emergence of SARS-CoV-2 spike deletion H69/V70 and its role in the Alpha variant. *Cell Rep.* **35**, 109292
96. Mohammad, A., Abubaker, J., Al-Mulla, F., (2021). Structural modelling of SARS-CoV-2 alpha variant (B.1.1.7) suggests enhanced furin binding and infectivity. *Virus Res.* **303**
97. Zhang, L., Mann, M., Syed, Z., Reynolds, H.M., Tian, E., Samara, N.L., et al., (2021). Furin cleavage of the SARS-CoV-2 spike is modulated by O-glycosylation. *bioRxiv*. 2021.02.05.429982.
98. Ostrov, D.A., (2021). Structural consequences of variation in SARS-CoV-2 B.1.1.7. *J. Cell Immunol.* **3**, 103–108.
99. Zhang, Z., Liu, J., Li, M., Yang, H., Zhang, C., (2012). Evolutionary dynamics of the interferon-induced transmembrane gene family in vertebrates. *PLoS One* **7**, e49265
100. Bailey, C.C., Zhong, G., Huang, I.C., Farzan, M., (2014). IFITM-family proteins: the cell's first line of antiviral defense. *Annu. Rev. Virol.* **1**, 261–283.
101. Savidis, G., Perreira, J.M., Portmann, J.M., Meraner, P., Guo, Z., Green, S., et al., (2016). The IFITMs inhibit zika virus replication. *Cell Rep.* **15**, 2323–2330.
102. Shi, G., Kenney, A.D., Kudryashova, E., Zani, A., Zhang, L., Lai, K.K., et al., (2021). Opposing activities of IFITM proteins in SARS-CoV-2 infection. *EMBO J.* **40**, e106501
103. Amini-Bavil-Olyaee, S., Choi, Y.J., Lee, J.H., Shi, M., Huang, I.C., Farzan, M., et al., (2013). The antiviral effector IFITM3 disrupts intracellular cholesterol homeostasis to block viral entry. *Cell Host Microbe* **13**, 452–464.
104. Zani, A., Yount, J.S., (2018). Antiviral protection by IFITM3 in vivo. *Curr. Clin. Microbiol. Rep.* **5**, 229–237.
105. Shi, G., Schwartz, O., Compton, A.A., (2017). More than meets the I: the diverse antiviral and cellular functions of

interferon-induced transmembrane proteins. *Retrovirology* **14**, 53.
106. Desai, T.M., Marin, M., Chin, C.R., Savidis, G., Brass, A. L., Melikyan, G.B., (2014). IFITM3 restricts influenza A virus entry by blocking the formation of fusion pores following virus-endosome hemifusion. *PLoS Pathog.* **10**, e1004048
107. Huang, I.C., Bailey, C.C., Weyer, J.L., Radoshitzky, S.R., Becker, M.M., Chiang, J.J., et al., (2011). Distinct patterns of IFITM-mediated restriction of filoviruses, SARS coronavirus, and influenza A virus. *PLoS Pathog.* **7**, e1001258
108. Wrensch, F., Winkler, M., Pohlmann, S., (2014). IFITM proteins inhibit entry driven by the MERS-coronavirus spike protein: evidence for cholesterol-independent mechanisms. *Viruses* **6**, 3683–3698.
109. Zhao, X., Sehgal, M., Hou, Z., Cheng, J., Shu, S., Wu, S., et al., (2018). Identification of residues controlling restriction versus enhancing activities of IFITM proteins on entry of human coronaviruses. *J. Virol.* **92**
110. Zhao, X., Guo, F., Liu, F., Cuconati, A., Chang, J., Block, T.M., et al., (2014). Interferon induction of IFITM proteins promotes infection by human coronavirus OC43. *Proc. Natl. Acad. Sci. USA* **111**, 6756–6761.
111. Winstone, H., Lista, M.J., Reid, A.C., Bouton, C., Pickering, S., Galao, R.P., et al., (2021). The polybasic cleavage site in SARS-CoV-2 spike modulates viral sensitivity to type I interferon and IFITM2. *J. Virol.* **95**
112. Benfield, C.T., MacKenzie, F., Ritzefeld, M., Mazzon, M., Weston, S., Tate, E.W., et al., (2020). Bat IFITM3 restriction depends on S-palmitoylation and a polymorphic site within the CD225 domain. *Life Sci. Alliance* **3**
113. Chesarino, N.M., Compton, A.A., McMichael, T.M., Kenney, A.D., Zhang, L., Soewarna, V., et al., (2017). IFITM3 requires an amphipathic helix for antiviral activity. *EMBO Rep.* **18**, 1740–1751.
114. Rahman, K., Coomer, C.A., Majdoul, S., Ding, S.Y., Padilla-Parra, S., Compton, A.A., (2020). Homology-guided identification of a conserved motif linking the antiviral functions of IFITM3 to its oligomeric state. *Elife* **9**
115. Guo, X., Steinkuhler, J., Marin, M., Li, X., Lu, W., Dimova, R., et al., (2021). Interferon-induced transmembrane protein 3 blocks fusion of diverse enveloped viruses by altering mechanical properties of cell membranes. *ACS Nano* **15**, 8155–8170.
116. Prelli Bozzo, C., Nchioua, R., Volcic, M., Koepke, L., Kruger, J., Schutz, D., et al., (2021). IFITM proteins promote SARS-CoV-2 infection and are targets for virus inhibition in vitro. *Nature Commun.* **12**, 4584.
117. Bertram, S., Dijkman, R., Habjan, M., Heurich, A., Gierer, S., Glowacka, I., et al., (2013). TMPRSS2 activates the human coronavirus 229E for cathepsin-independent host cell entry and is expressed in viral target cells in the respiratory epithelium. *J. Virol.* **87**, 6150–6160.
118. Zheng, M., Zhao, X., Zheng, S., Chen, D., Du, P., Li, X., et al., (2020). Bat SARS-Like WIV1 coronavirus uses the ACE2 of multiple animal species as receptor and evades IFITM3 restriction via TMPRSS2 activation of membrane fusion. *Emerg. Microbes Infect.* **9**, 1567–1579.
119. Yu, J., Murthy, V., Liu, S.L., (2019). Relating GPI-Anchored Ly6 Proteins uPAR and CD59 to Viral Infection. *Viruses* **11**
120. Yu, J., Liang, C., Liu, S.L., (2019). CD4-Dependent Modulation of HIV-1 Entry by LY6E. *J. Virol.* **93**
121. Mar, K.B., Rinkenberger, N.R., Boys, I.N., Eitson, J.L., McDougal, M.B., Richardson, R.B., et al., (2018). LY6E mediates an evolutionarily conserved enhancement of virus infection by targeting a late entry step. *Nature Commun.* **9**, 3603.
122. Yu, J., Liu, S.L., (2019). Emerging Role of LY6E in Virus-Host Interactions. *Viruses* **11**
123. Bacquin, A., Bireau, C., Tanguy, M., Romanet, C., Vernochet, C., Dupressoir, A., et al., (2017). A cell fusion-based screening method identifies glycosylphosphatidylinositol-anchored protein ly6e as the receptor for mouse endogenous retroviral envelope syncytin-A. *J. Virol.* **91**
124. Pfaender, S., Mar, K.B., Michailidis, E., Kratzel, A., Boys, I.N., V'Kovski, P., et al., (2020). LY6E impairs coronavirus fusion and confers immune control of viral disease. *Nature Microbiol.* **5**, 1330–1339.
125. Zhao, X., Zheng, S., Chen, D., Zheng, M., Li, X., Li, G., et al., (2020). LY6E restricts entry of human coronaviruses, including currently pandemic SARS-CoV-2. *J. Virol.* **94**
126. Wang, S., Li, W., Hui, H., Tiwari, S.K., Zhang, Q., Croker, B.A., et al., (2020). Cholesterol 25-Hydroxylase inhibits SARS-CoV-2 and other coronaviruses by depleting membrane cholesterol. *EMBO J.* **39**, e106057
127. Zang, R., Case, J.B., Yutuc, E., Ma, X., Shen, S., Gomez Castro, M.F., et al., (2020). Cholesterol 25-hydroxylase suppresses SARS-CoV-2 replication by blocking membrane fusion. *Proc. Natl. Acad. Sci. USA* **117**, 32105–32113.
128. Lu, X., Wang, R., Zhu, C., Wang, H., Lin, H.Y., Gu, Y., et al., (2017). Fine-tuned and cell-cycle-restricted expression of fusogenic protein syncytin-2 maintains functional placental syncytia. *Cell. Rep.* **21**, 1150–1159.
129. Nardacci, R., Perfettini, J.L., Grieco, L., Thieffry, D., Kroemer, G., Piacentini, M., (2015). Syncytial apoptosis signaling network induced by the HIV-1 envelope glycoprotein complex: an overview. *Cell Death Dis.* **6**, e1846
130. Jackson, L., Rodel, H., Hwa, S.-H., Cele, S., Ganga, Y., Tegally, H., et al., (2021). SARS-CoV-2 cell-to-cell spread occurs rapidly and is insensitive to antibody neutralization. *bioRxiv.* 2021.06.01.446516.
131. Herschke, F., Plumet, S., Duhen, T., Azocar, O., Druelle, J., Laine, D., et al., (2007). Cell-cell fusion induced by measles virus amplifies the type I interferon response. *J. Virol.* **81**, 12859–12871.
132. Ku, J.W.K., Chen, Y., Lim, B.J.W., Gasser, S., Crasta, K. C., Gan, Y.H., (2020). Bacterial-induced cell fusion is a danger signal triggering cGAS-STING pathway via micronuclei formation. *Proc. Natl. Acad. Sci. USA* **117**, 15923–15934.
133. Ma, H., Zhu, Z., Lin, H., Wang, S., Zhang, P., Li, Y., et al., (2021). Pyroptosis of syncytia formed by fusion of SARS-CoV-2 spike and ACE2-expressing cells. *Cell Discov.* **7**, 73.
134. Asarnow, D., Wang, B., Lee, W.H., Hu, Y., Huang, C.W., Faust, B., et al., (2021). Structural insight into SARS-CoV-2 neutralizing antibodies and modulation of syncytia. *Cell* **184** 3192–204 e16.

135. Cifuentes-Munoz, N., Dutch, R.E., Cattaneo, R., (2018). Direct cell-to-cell transmission of respiratory viruses: The fast lanes. *PLoS Pathog.* **14**, e1007015
136. Zeng, C., Evans, J.P., King, T., Zheng, Y.-M., Oltz, E.M., Whelan, S.P.J., et al., (2021). SARS-CoV-2 spreads through cell-to-cell transmission. *bioRxiv*. 2021.06.01.446579.
137. Abela, I.A., Berlinger, L., Schanz, M., Reynell, L., Gunthard, H.F., Rusert, P., et al., (2012). Cell-cell transmission enables HIV-1 to evade inhibition by potent CD4bs directed antibodies. *PLoS Pathog.* **8**, e1002634
138. Sigal, A., Kim, J.T., Balazs, A.B., Dekel, E., Mayo, A., Milo, R., et al., (2011). Cell-to-cell spread of HIV permits ongoing replication despite antiretroviral therapy. *Nature* **477**, 95–98.
139. Schiffner, T., Sattentau, Q.J., Duncan, C.J., (2013). Cell-to-cell spread of HIV-1 and evasion of neutralizing antibodies. *Vaccine* **31**, 5789–5797.
140. Beucher, G., Blondot, M.-L., Celle, A., Pied, N., Recordon-Pinson, P., Esteves, P., et al., (2021). SARS-CoV-2 transmission via apical syncytia release from primary bronchial epithelia and infectivity restriction in children epithelia. *bioRxiv*. 2021.05.28.446159..
141. Lin, W.W., Tsay, A.J., Lalime, E.N., Pekosz, A., Griffin, D. E., (2021). Primary differentiated respiratory epithelial cells respond to apical measles virus infection by shedding multinucleated giant cells. *Proc. Natl. Acad. Sci. USA* **118**
142. Monel, B., Planas, D., Grzelak, L., Smith, N., Robillard, N., Staropoli, I., et al., (2021). Release of infectious virus and cytokines in nasopharyngeal swabs from individuals infected with non-B.1.1.7 or B.1.1.7 SARS-CoV-2 variants. *medRxiv*. 2021.05.20.21257393.
143. Planas, D., Bruel, T., Grzelak, L., Guivel-Benhassine, F., Staropoli, I., Porrot, F., et al., (2021). Sensitivity of infectious SARS-CoV-2 B.1.1.7 and B.1.351 variants to neutralizing antibodies. *Nature Med.* **27**, 917–924.

Article

Reduced sensitivity of SARS-CoV-2 variant Delta to antibody neutralization

https://doi.org/10.1038/s41586-021-03777-9

Received: 26 May 2021

Accepted: 29 June 2021

Published online: 8 July 2021

Check for updates

Delphine Planas[1,2], David Veyer[3,4], Artem Baidaliuk[5], Isabelle Staropoli[1], Florence Guivel-Benhassine[1], Maaran Michael Rajah[1,6], Cyril Planchais[7], Françoise Porrot[1], Nicolas Robillard[4], Julien Puech[4], Matthieu Prot[5], Floriane Gallais[8,9], Pierre Gantner[8,9], Aurélie Velay[8,9], Julien Le Guen[10], Najiby Kassis-Chikhani[11], Dhiaeddine Edriss[4], Laurent Belec[4], Aymeric Seve[12], Laura Courtellemont[12], Hélène Péré[3], Laurent Hocqueloux[12], Samira Fafi-Kremer[8,9], Thierry Prazuck[12], Hugo Mouquet[7], Timothée Bruel[1,2,14] ✉, Etienne Simon-Lorière[5,14], Felix A. Rey[13,14] & Olivier Schwartz[1,2,14] ✉

The SARS-CoV-2 B.1.617 lineage was identified in October 2020 in India[1–5]. Since then, it has become dominant in some regions of India and in the UK, and has spread to many other countries[6]. The lineage includes three main subtypes (B1.617.1, B.1.617.2 and B.1.617.3), which contain diverse mutations in the N-terminal domain (NTD) and the receptor-binding domain (RBD) of the SARS-CoV-2 spike protein that may increase the immune evasion potential of these variants. B.1.617.2—also termed the Delta variant—is believed to spread faster than other variants. Here we isolated an infectious strain of the Delta variant from an individual with COVID-19 who had returned to France from India. We examined the sensitivity of this strain to monoclonal antibodies and to antibodies present in sera from individuals who had recovered from COVID-19 (hereafter referred to as convalescent individuals) or who had received a COVID-19 vaccine, and then compared this strain with other strains of SARS-CoV-2. The Delta variant was resistant to neutralization by some anti-NTD and anti-RBD monoclonal antibodies, including bamlanivimab, and these antibodies showed impaired binding to the spike protein. Sera collected from convalescent individuals up to 12 months after the onset of symptoms were fourfold less potent against the Delta variant relative to the Alpha variant (B.1.1.7). Sera from individuals who had received one dose of the Pfizer or the AstraZeneca vaccine had a barely discernible inhibitory effect on the Delta variant. Administration of two doses of the vaccine generated a neutralizing response in 95% of individuals, with titres three- to fivefold lower against the Delta variant than against the Alpha variant. Thus, the spread of the Delta variant is associated with an escape from antibodies that target non-RBD and RBD epitopes of the spike protein.

The SARS-CoV-2 Delta variant (B.1.617.2) has been detected in many countries. It has become predominant in the Indian state of Maharashtra and probably other Indian regions[4], and represented 77% of the sequenced viruses circulating in the UK between 2 June and 9 June 2021[6]. It has been classified as a variant of concern (VOC) and is believed to be 60% more transmissible than the Alpha variant (B.1.1.7). Little is known about the sensitivity of the Delta variant to the humoral immune response. Recent reports have indicated that members of the B.1.617 lineage exhibit a reduced sensitivity to certain monoclonal and polyclonal antibodies compared to the Alpha variant[1–5,7–9].

Isolation and characterization of the Delta variant

We isolated the Delta variant from a nasopharyngeal swab of a symptomatic individual a few days after his return to France from India. The virus was amplified by two passages on Vero E6 cells. Sequences of the swab and the outgrown virus were identical, and identified the Delta

[1]Virus and Immunity Unit, Department of Virology, Institut Pasteur, CNRS UMR 3569, Paris, France. [2]Vaccine Research Institute, Creteil, France. [3]INSERM, Functional Genomics of Solid Tumors (FunGeST), Centre de Recherche des Cordeliers, Université de Paris and Sorbonne Université, Paris, France. [4]Laboratoire de Virologie, Service de Microbiologie, Hôpital Européen Georges Pompidou, Assistance Publique des Hôpitaux de Paris, Paris, France. [5]G5 Evolutionary Genomics of RNA Viruses, Department of Virology, Institut Pasteur, Paris, France. [6]Université de Paris, Sorbonne Paris Cité, Paris, France. [7]Laboratory of Humoral Immunology, Department of Immunology, Institut Pasteur, INSERM U1222, Paris, France. [8]CHU de Strasbourg, Laboratoire de Virologie, Strasbourg, France. [9]Université de Strasbourg, INSERM, IRM UMR_S 1109, Strasbourg, France. [10]Service de Gériatrie, Hôpital Européen Georges Pompidou, Assistance Publique des Hôpitaux de Paris, Paris, France. [11]Unité d'Hygiène Hospitalière, Service de Microbiologie, Hôpital Européen Georges Pompidou, Assistance Publique des Hôpitaux de Paris, Paris, France. [12]CHR d'Orléans, Service de Maladies Infectieuses, Orléans, France. [13]Structural Virology Unit, Department of Virology, Institut Pasteur, CNRS UMR 3569, Paris, France. [14]These authors contributed equally: Timothée Bruel, Etienne Simon-Lorière, Felix A. Rey, Olivier Schwartz. ✉e-mail: timothee.bruel@pasteur.fr; olivier.schwartz@pasteur.fr

nature medicine

ARTICLES

https://doi.org/10.1038/s41591-021-01318-5

Check for updates

Sensitivity of infectious SARS-CoV-2 B.1.1.7 and B.1.351 variants to neutralizing antibodies

Delphine Planas[1,2,3,22], Timothée Bruel[1,2,3,22], Ludivine Grzelak[1,2,3,4], Florence Guivel-Benhassine[1,2,3], Isabelle Staropoli[1,2,3], Françoise Porrot[1,2,3], Cyril Planchais[5], Julian Buchrieser[1,2,3], Maaran Michael Rajah[1,2,3,4], Elodie Bishop[1,2,3,4], Mélanie Albert[6,7], Flora Donati[6,7], Matthieu Prot[8], Sylvie Behillil[6,7], Vincent Enouf[6,7], Marianne Maquart[9], Mounira Smati-Lafarge[10], Emmanuelle Varon[10], Frédérique Schortgen[11], Layla Yahyaoui[12], Maria Gonzalez[13], Jérôme De Sèze[14,15], Hélène Péré[16], David Veyer[16,17], Aymeric Sève[18], Etienne Simon-Lorière[8], Samira Fafi-Kremer[19,20], Karl Stefic[9,21], Hugo Mouquet[5], Laurent Hocqueloux[18], Sylvie van der Werf[6,7,23], Thierry Prazuck[18,23] and Olivier Schwartz[1,2,3,23] ✉

Severe acute respiratory syndrome coronavirus 2 (SARS-CoV-2) B.1.1.7 and B.1.351 variants were first identified in the United Kingdom and South Africa, respectively, and have since spread to many countries. These variants harboring diverse mutations in the gene encoding the spike protein raise important concerns about their immune evasion potential. Here, we isolated infectious B.1.1.7 and B.1.351 strains from acutely infected individuals. We examined sensitivity of the two variants to SARS-CoV-2 antibodies present in sera and nasal swabs from individuals infected with previously circulating strains or who were recently vaccinated, in comparison with a D614G reference virus. We utilized a new rapid neutralization assay, based on reporter cells that become positive for GFP after overnight infection. Sera from 58 convalescent individuals collected up to 9 months after symptoms, similarly neutralized B.1.1.7 and D614G. In contrast, after 9 months, convalescent sera had a mean sixfold reduction in neutralizing titers, and 40% of the samples lacked any activity against B.1.351. Sera from 19 individuals vaccinated twice with Pfizer Cominarty, longitudinally tested up to 6 weeks after vaccination, were similarly potent against B.1.1.7 but less efficacious against B.1.351, when compared to D614G. Neutralizing titers increased after the second vaccine dose, but remained 14-fold lower against B.1.351. In contrast, sera from convalescent or vaccinated individuals similarly bound the three spike proteins in a flow cytometry-based serological assay. Neutralizing antibodies were rarely detected in nasal swabs from vaccinees. Thus, faster-spreading SARS-CoV-2 variants acquired a partial resistance to neutralizing antibodies generated by natural infection or vaccination, which was most frequently detected in individuals with low antibody levels. Our results indicate that B1.351, but not B.1.1.7, may increase the risk of infection in immunized individuals.

SARS-CoV-2 variants have rapidly emerged in humans and supplanted ancestral strains[1–5]. Their proposed increased rates of interindividual transmission conferred a replication advantage at the population level. One of the first identified variants includes the D614G mutation in the gene encoding the spike (S) protein, which enhances viral infectivity and shifts S protein conformation toward an angiotensin-converting enzyme 2 (ACE2)-binding fusion-competent state, without significantly modifying sensitivity to antibody neutralization[1,6–8]. More recently, novel variants have appeared in multiple countries, with combinations of mutations and deletions in the receptor-binding domain (RBD) and N-terminal domain of S protein, as well as in other proteins. The B.1.1.7 variant emerged in the United Kingdom, the B.1.351 variant (also termed 501Y.V2) in South Africa and the P.1 and P.2 lineages in Brazil[2,3,5,9–12]. Although distinct, the variants share common characteristics, including known escape mutations that were previously identified under antibody pressure selection in vitro[2,3,13–17]. Some of the mutations or deletions were also identified in immunocompromised individuals with prolonged infectious viral shedding and treated with convalescent plasma or S-protein

[1]Virus & Immunity Unit, Department of Virology, Institut Pasteur, Paris, France. [2]CNRS UMR 3569, Paris, France. [3]Vaccine Research Institute, Créteil, France. [4]Université de Paris, Sorbonne Paris Cité, Paris, France. [5]Laboratory of Humoral Immunology, Department of Immunology, Institut Pasteur, INSERM U1222, Paris, France. [6]Molecular Genetics of RNA Viruses, Department of Virology, Institut Pasteur CNRS UMR 3569, Université de Paris, Paris, France. [7]National Reference Center for Respiratory Viruses, Institut Pasteur, Paris, France. [8]G5 Evolutionary Genomics of RNA Viruses, Institut Pasteur, Paris, France. [9]INSERM U1259, Université de Tours, Tours, France. [10]CHI de Créteil, Service de Biologie Médicale, Créteil, France. [11]CHI de Créteil, Service de Réanimation, Créteil, France. [12]CHI de Créteil, Service des Urgences, Créteil, France. [13]CHU de Strasbourg, Service de Pathologie Professionnelle et Médecine du Travail, Strasbourg, France. [14]Centre d'investigation Clinique INSERM 1434, CHU Strasbourg, France. [15]CHU de Strasbourg, Service de Neurologie, Strasbourg, France. [16]INSERM, Functional Genomics of Solid Tumors (FunGeST), Centre de Recherche des Cordeliers, Université de Paris and Sorbonne Université, Paris, France. [17]Hôpital Européen Georges Pompidou, Service de Virologie, Paris, France. [18]CHR d'Orléans, Service de maladies infectieuses, Orléans, France. [19]CHU de Strasbourg, Laboratoire de Virologie, Strasbourg, France. [20]Université de Strasbourg, INSERM, IRM UMR_S 1109, Strasbourg, France. [21]CHRU de Tours, National Reference Center for HIV-Associated laboratory, Tours, France. [22]These authors contributed equally: Delphine Planas, Timothée Bruel. [23]These authors jointly supervised this work: Sylvie van der Werf, Thierry Prazuck, Olivier Schwartz. ✉e-mail: olivier.schwartz@pasteur.fr

CORONAVIRUS

Copyright © 2020 The Authors, some rights reserved; exclusive licensee American Association for the Advancement of Science. No claim to original U.S. Government Works

A comparison of four serological assays for detecting anti–SARS-CoV-2 antibodies in human serum samples from different populations

Ludivine Grzelak[1,2,3]*, Sarah Temmam[4]*, Cyril Planchais[5]*, Caroline Demeret[6,7]*, Laura Tondeur[8], Christèle Huon[4], Florence Guivel-Benhassine[1,2], Isabelle Staropoli[1,2], Maxime Chazal[9], Jeremy Dufloo[1,2,3], Delphine Planas[1,2], Julian Buchrieser[1,2], Maaran Michael Rajah[1,2,3], Remy Robinot[1,2], Françoise Porrot[1,2], Mélanie Albert[6,7,10], Kuang-Yu Chen[11], Bernadette Crescenzo-Chaigne[6,7], Flora Donati[6,7,10], François Anna[12], Philippe Souque[13], Marion Gransagne[14], Jacques Bellalou[15], Mireille Nowakowski[15], Marija Backovic[16], Lila Bouadma[17,18], Lucie Le Fevre[18], Quentin Le Hingrat[17,19], Diane Descamps[17,19], Annabelle Pourbaix[20], Cédric Laouénan[17,21], Jade Ghosn[17,20], Yazdan Yazdanpanah[17,20], Camille Besombes[8], Nathalie Jolly[22], Sandrine Pellerin-Fernandes[22], Olivia Cheny[22], Marie-Noëlle Ungeheuer[22], Guillaume Mellon[23], Pascal Morel[24], Simon Rolland[25,26], Felix A. Rey[16], Sylvie Behillil[6,7,10], Vincent Enouf[6,7,10], Audrey Lemaitre[27], Marie-Aude Créach[28,29], Stephane Petres[15], Nicolas Escriou[14], Pierre Charneau[12,13], Arnaud Fontanet[8,30], Bruno Hoen[31], Timothée Bruel[1,2], Marc Eloit[4,32†‡], Hugo Mouquet[5†], Olivier Schwartz[1,2†‡], Sylvie van der Werf[6,7,10†]

It is of paramount importance to evaluate the prevalence of both asymptomatic and symptomatic cases of SARS-CoV-2 infection and their differing antibody response profiles. Here, we performed a pilot study of four serological assays to assess the amounts of anti–SARS-CoV-2 antibodies in serum samples obtained from 491 healthy individuals before the SARS-CoV-2 pandemic, 51 individuals hospitalized with COVID-19, 209 suspected cases of COVID-19 with mild symptoms, and 200 healthy blood donors. We used two ELISA assays that recognized the full-length nucleoprotein (N) or trimeric spike (S) protein ectodomain of SARS-CoV-2. In addition, we developed the S-Flow assay that recognized the S protein expressed at the cell surface using flow cytometry, and the luciferase immunoprecipitation system (LIPS) assay that recognized diverse SARS-CoV-2 antigens including the S1 domain and the carboxyl-terminal domain of N by immunoprecipitation. We obtained similar results with the four serological assays. Differences in sensitivity were attributed to the technique and the antigen used. High anti–SARS-CoV-2 antibody titers were associated with neutralization activity, which was assessed using infectious SARS-CoV-2 or lentiviral-S pseudotype virus. In hospitalized patients with COVID-19, seroconversion and virus neutralization occurred between 5 and 14 days after symptom onset, confirming previous studies. Seropositivity was detected in 32% of mildly symptomatic individuals within 15 days of symptom onset and in 3% of healthy blood donors. The four antibody assays that we used enabled a broad evaluation of SARS-CoV-2 seroprevalence and antibody profiling in different subpopulations within one region.

INTRODUCTION

Within a few months of the initial description of atypical pneumonia cases in Wuhan in December 2019, coronavirus disease 2019 (COVID-19) became a major pandemic threat. As of 8 August 2020, about 20 million infections have been officially diagnosed, with 0.7 million fatalities worldwide. COVID-19 is caused by severe acute

[1]Virus and Immunity Unit, Department of Virology, Institut Pasteur, CNRS UMR 3569, Paris, France. [2]Vaccine Research Institute, Creteil, France. [3]Université de Paris, Sorbonne Paris Cité, Paris, France. [4]Pathogen Discovery Laboratory, Department of Virology, Institut Pasteur, Paris, France. [5]Laboratory of Humoral Immunology, Department of Immunology, Institut Pasteur, INSERM U1222, Paris, France. [6]Molecular Genetics of RNA Viruses, Department of Virology, Institut Pasteur, CNRS UMR 3569, Paris, France. [7]Université de Paris, Paris, France. [8]Emerging Diseases Epidemiology Unit, Department of Global Health, Institut Pasteur, Paris, France. [9]Department of Virology, Institut Pasteur, Paris, France. [10]National Reference Center for Respiratory Viruses, Institut Pasteur, Paris, France. [11]RNA Biology of Influenza Virus, Department of Virology, Institut Pasteur, Paris, France. [12]Pasteur-TheraVectys joined unit, Institut Pasteur, Paris, France. [13]Molecular Virology and Vaccinology Unit, Department of Virology, Institut Pasteur, Paris, France. [14]Innovation lab: Vaccines, Institut Pasteur, Paris, France. [15]Plate-Forme Technologique Production et Purification de Protéines Recombinantes, Institut Pasteur, Paris, France. [16]Structural Virology Unit, Department of Virology, Institut Pasteur, CNRS UMR 3569, Paris, France. [17]Université of Paris, INSERM UMR 1137 IAME, Paris, France. [18]Medical and Infectious Diseases Intensive Care Unit, Assistance Publique-Hôpitaux de Paris, Bichat–Claude-Bernard University Hospital, Paris, France. [19]Department of Virology, Assistance Publique-Hôpitaux de Paris, Bichat–Claude-Bernard University Hospital, Paris, France. [20]Department of Infectious Diseases, Assistance Publique-Hôpitaux de Paris, Bichat–Claude-Bernard University Hospital, Paris, France. [21]Department of Epidemiology, Biostatistics and Clinical Research, Assistance Publique-Hôpitaux de Paris, Bichat–Claude-Bernard University Hospital, INSERM CIC-EC 1425, Paris, France. [22]Investigation Clinique et Accès aux Ressources Biologiques (ICAReB), Center for Translational Research, Institut Pasteur, Paris, France. [23]Unité Coordination du Risque Epidémique et Biologique, AP-HP, Hôpital Necker, Paris, France. [24]Etablissement Français du Sang (EFS), Paris, France. [25]Service de maladies infectieuses, hôpital universitaire Cavale Blanche, Brest, France. [26]CIC 1417, CIC de vaccinologie Cochin-Pasteur, AP-HP, Hôpital Cochin, Paris, France. [27]Direction alerte et crises, réserve sanitaire, Santé publique France, Saint-Maurice, France. [28]Centre d'épidémiologie et de santé publique des armées, Marseille, France. [29]Direction Générale de la Santé, Paris, France. [30]PACRI Unit, Conservatoire National des Arts et Métiers, Paris, France. [31]Direction de la recherche médicale, Institut Pasteur, Paris, France. [32]National Veterinary School of Alfort, Maisons-Alfort, France.
*These authors contributed equally as co-first authors.
†These authors contributed equally as co-last authors.
‡Corresponding author. Email: marc.eloit@pasteur.fr (M.E.); schwartz@pasteur.fr (O.S.)

Downloaded from https://www.science.org on October 10, 2021

INSTITUT PASTEUR

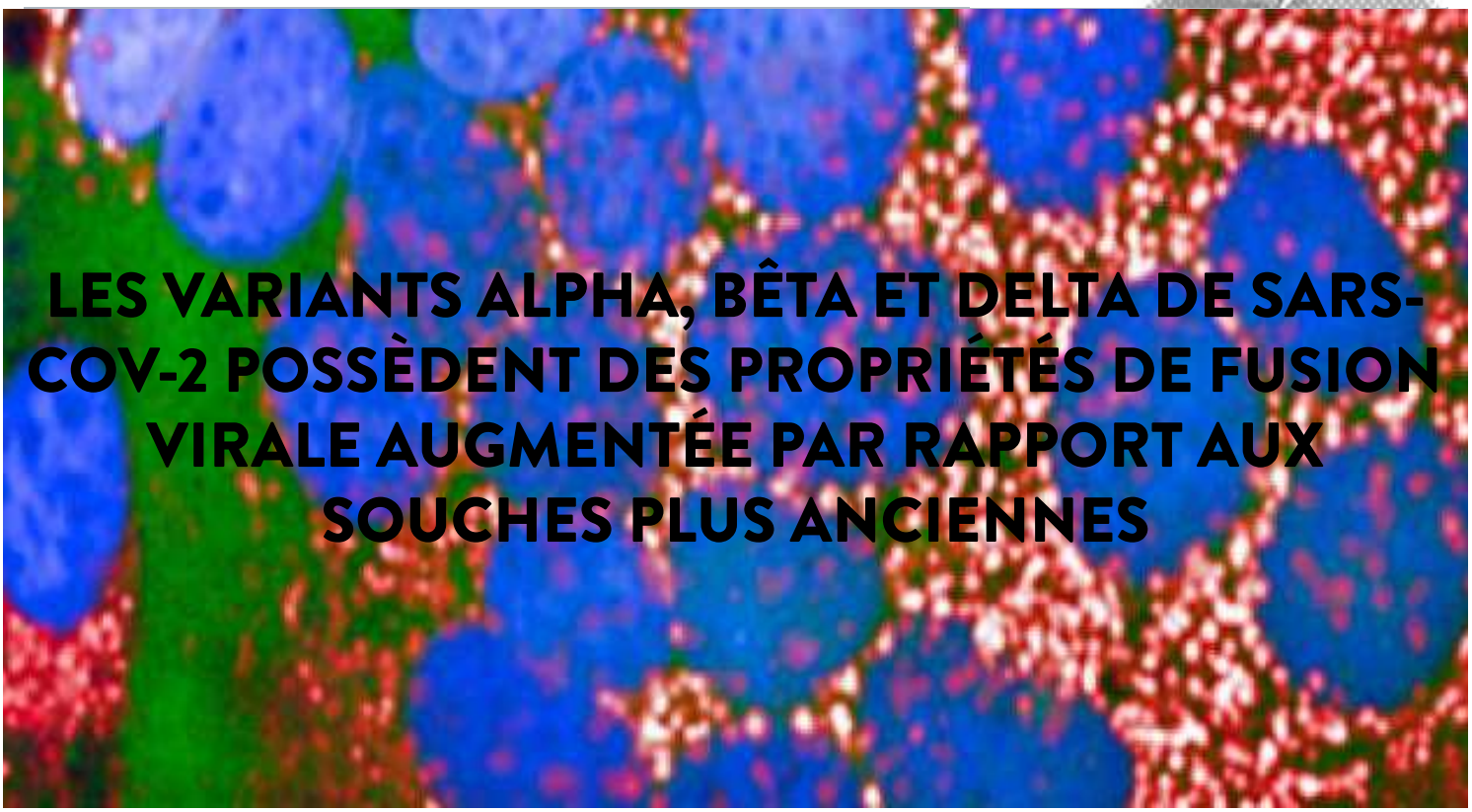

LES VARIANTS ALPHA, BÊTA ET DELTA DE SARS-COV-2 POSSÈDENT DES PROPRIÉTÉS DE FUSION VIRALE AUGMENTÉE PAR RAPPORT AUX SOUCHES PLUS ANCIENNES

COMMUNIQUÉ DE PRESSE | 11.10.2021

Dans une nouvelle étude publiée dans *EMBO Journal* le 2 octobre 2021, des chercheurs et des chercheuses de l'Institut Pasteur, du CNRS, d'Université de Paris, du *Vaccine Research Institute* et de Sorbonne Université ont étudié les mécanismes de fusion de différents variants de SARS-CoV-2 : Alpha (initialement identifié en Grande-Bretagne), Bêta (initialement identifié en Afrique du Sud) et Delta (initialement identifié en Inde). Le variant Delta est désormais le variant prédominant au niveau mondial, et représente 99 % des séquences virales dans de nombreux pays.

La fusion virale est un mécanisme ayant lieu à deux moments du cycle de multiplication du virus. La première étape commence lors de l'entrée des particules virales dans de nouvelles cellules hôtes. La deuxième étape se produit lorsque la cellule infectée va produire la protéine Spike à sa surface, et fusionner avec les cellules avoisinantes, formant ainsi des cellules géantes appelées syncytia.

Ces syncytia sont localisés dans les poumons des personnes présentant des formes critiques de Covid-19, mais leur rôle reste aujourd'hui encore peu compris. L'une des hypothèses est que ces syncytia pourraient faciliter la propagation virale ou permettre au virus d'échapper aux anticorps.

Les principaux résultats de l'étude montrent que les variants Alpha, Bêta et Delta forment plus de syncytia en culture cellulaire que les souches plus anciennes du virus SARS-CoV-2. Le variant Delta est celui qui possède le caractère le plus « fusogène », ce qui pourrait expliquer pourquoi ce variant est plus transmissible que les autres.

Les variants possèdent en effet différentes mutations sur la protéine de Spike. Les scientifiques ont donc étudié le rôle de chacune des mutations et montrent que ces mutations peuvent être de trois catégories :

1. Les mutations facilitant la liaison de la Spike au récepteur (attachement du virus à la cellule) ;
2. Les mutations augmentant la fusion (entrée du virus dans la cellule) ;
3. Les mutations permettant un échappement aux anticorps neutralisants.

Chaque variant possède donc une combinaison particulière de ces mutations améliorant la propagation virale.

Cette étude permet de mieux comprendre pourquoi certains variants, en particulier le variant Delta, sont plus transmissibles que la souche originale du SARS-CoV-2 ayant provoqué la pandémie.

Source

SARS-CoV-2 Alpha, Beta and Delta variants display enhanced Spike-mediated Syncytia Formation, *EMBO Journal*, 2 octobre 2021

Maaran Michael Rajah1,2, Mathieu Hubert1,3,#, Elodie Bishop1,4,#, Nell Saunders1,#, Remy Robinot1, Ludivine Grzelak1,2, Delphine Planas1,3, Jérémy Dufloo1,2, Stacy Gellenoncourt1,2, Alice Bongers1,2, Marija Zivaljic5,6, Cyril Planchais7, Florence Guivel-Benhassine1, Françoise Porrot1, Hugo Mouquet7, Lisa A Chakrabarti1 , Julian Buchrieser1* Olivier Schwartz1,2*.

1 Virus & Immunity Unit, Department of Virology, Institut Pasteur; CNRS UMR 3569, Paris, France
2 Université de Paris, Sorbonne Paris Cité, Paris, France
3 Vaccine Research Institute, Creteil, France

4 Sorbonne Université, Paris F-75005, France

5 Integrative Neurobiology of Cholinergic Systems, Department of Neuroscience, Institut Pasteur; CNRS UMR 3571, Paris, France

6 Sorbonne Université, ED3C “Brain, cognition, behavior”, Paris, France

7 Laboratory of Humoral Immunology, Department of Immunology, Institut Pasteur, INSERM U1222, Paris, France

Second co-authors

*Last co-authors